

*3-2-94  
E8201*  
NASA Conference Publication 10130  
ICOMP-93-46; CMOTT-93-17

# Workshop on Computational Turbulence Modeling

*Proceedings of a workshop  
sponsored by the Institute for  
Computational Mechanics in Propulsion  
and Center for Modeling of Turbulence  
and Transition  
NASA Lewis Research Center  
Cleveland, Ohio  
September 15-16, 1993*



NASA

NASA Conference Publication 10130  
ICOMP-93-46: CMOTT-93-17

# Workshop on Computational Turbulence Modeling

*Proceedings of a workshop  
sponsored by the Institute for  
Computational Mechanics in Propulsion  
and Center for Modeling of Turbulence  
and Transition  
NASA Lewis Research Center  
Cleveland, Ohio  
September 15-16, 1993*



National Aeronautics and  
Space Administration  
Office of Management  
**Scientific and Technical  
Information Program**

1994



**Page intentionally left blank**

# 1993 Lewis Workshop

## on

### Computational Turbulence Modeling

#### 1. Objectives

The purpose of this meeting was to discuss the current status and future development of turbulence modeling in computational fluid dynamics for aerospace propulsion systems. Various turbulence models have been developed and applied to different turbulent flows over the past several decades and it is becoming more and more urgent to assess their performance in various complex situations. In order to help users in selecting and implementing appropriate models in their engineering calculations, it is important to identify the capabilities as well as the deficiencies of these models. This also benefits turbulence modelers by permitting them to further improve upon the existing models.

This workshop was designed for exchanging ideas and enhancing collaboration between different groups in the Lewis community who are using turbulence models in propulsion related CFD. In this respect this workshop will help the Lewis goal of excelling in propulsion related research.

This meeting had seven sessions for presentations and one panel discussion over a period of 2 days. Each presentation session was assigned to one or two branches (or groups) to present their turbulence related research work. Each group was asked to address at least the following points: current status of turbulence model applications and developments in the research; progress and existing problems; requests about turbulence modeling. The panel discussion session was designed for organizing committee members to answer management and technical questions from the audience and to make concluding remarks.

#### Organizing Committee

L.A. Povinelli (Chairman)  
J.M. Abbott  
P.G. Batterton  
R.E. Gaugler

T. Keith  
R. Mankbadi  
E.J. Mularz  
D.R. Reddy

R.J. Shaw  
R.J. Simoneau  
R.M. Stubbs  
A. Shabbir  
T.-H. Shih

**Page intentionally left blank**

## TABLE OF CONTENTS

	Page
Main issues raised in the workshop . . . . .	1
<b>Session I</b>	
<b>Turbulence Modeling Activities at CMOTT</b>	
CMOTT Research Activities	
T.-H. Shih . . . . .	5
Research on two equation models	
Z. Yang . . . . .	27
A Reynolds stress algebraic equation model	
J. Zhu . . . . .	37
Assessment and development of second order turbulence models	
A. Shabbir . . . . .	55
A multiple-scale model for compressible turbulent flows	
W. Liou and B. Duncan (CFD Branch) . . . . .	69
PDF models	
A. Hsu (CFD Branch) and A. Norris . . . . .	79
Analytical theories of turbulence applied to turbulence modeling	
R. Rubenstein . . . . .	93
DNS of turbulence, transition and effect of rotation	
A. Hsu (CFD Branch) and J. Van der Vegt . . . . .	99
<b>Session II</b>	
<b>Heat Transfer and Turbomachinery Flow Physics Branches</b>	
Modeling of by-pass transition	
F. Simon . . . . .	107
Algebraic models for turbine blade heat transfer	
R. Boyle . . . . .	119
Two-equation models for turbine blade heat transfer	
A. Ameri . . . . .	129
Thermal turbulence models for turbine blade heat transfer	
J. Schwab . . . . .	141

**Session III****Aerothermochemistry and Computational Methods for Space Branches**

- A coupled implicit solution for turbulent spray combustion in propulsion systems  
K.-H. Chen and J.-S. Shuen ..... 147

- On turbulent transport of chemical species in compressible reacting flows and Unsteady transitional flows over forced oscillatory surfaces  
S.-W. Kim ..... 163

- On the accuracy of compact differencing schemes for DNS  
S.-T. Yu ..... 179

**Session IV****Computational Fluid Dynamics Branch and Lewis Research Academy**

- Turbulent back-facing step flow and the  $k - \epsilon$  model: A critical comparison  
C. Steffen ..... 195

- Analysis of supersonic flows using the  $k - \epsilon$  models and the RPLUS code  
J. Lee ..... 203

- Validation of a  $k - \epsilon$  model in RPLUS2D code for non-reacting/reacting subsonic shear layers  
H. Lai ..... 215

- Computational aeroacoustics as a branch of turbulence research  
R. Mankbadi ..... 223

- Jet noise prediction using  $k - \epsilon$  turbulence model  
A. Khavaran ..... 231

- Numerical simulation of supersonic flow using  $k - \epsilon$  model  
S.H. Shih ..... 243

- Implementation of a  $k - \epsilon$  model in spectral element code  
W.M. To ..... 255

**Session V****Propulsion Systems Division**

- Subsonic inlet flows with transition  
D. Hwang and K. Ahn ..... 261

- A comparative study of turbulence models in predicting hypersonic inlet flows  
K. Kapoor ..... 269

- Turbomachinery flows  
R. Chima ..... 279

**Session VI**  
**Propulsion Systems Division**

Low emission combustors J. Deur . . . . .	293
Development of a reliable algebraic turbulence model giving engineering accuracy at reasonable cost B.P. Leonard and J.E. Drummond (University of Akron) . . . . .	305
Application of algebraic and two-equation turbulence models to HSR nozzle flow calculations J. DeBonis and N. Georgiadis . . . . .	321
Aircraft icing M. Potapczuk . . . . .	343
Applied RNG turbulence model for 3-D turbomachinery flows K. Kirtley . . . . .	355

Applied $k - \epsilon$ and Baldwin-Lomax turbulence models for S-ducts G. Harloff . . . . .	367
--	-----

**Session VII**  
**Inlet, Duct, and Nozzle Flow Physics Branch**

PROTEUS experience with the modified MML turbulence model J. Conley . . . . .	377
Turbulence model experiences for a round-to-rectangular transition duct C. Towne . . . . .	389
PROTEUS experience with three different turbulence models T. Bui . . . . .	403
Several examples where turbulence models fail in inlet flow field analysis B.H. Anderson . . . . .	413

# Main Issues Raised in the Workshop

(summarized by workshop committee)

A total of thirty five papers were presented at the workshop covering a wide spectrum of work related to propulsion systems as is evident from the contents of this proceedings. Several problems and issues related to the turbulence and transition modeling were raised in these presentations as well as in the panel discussion. These issues are briefly summarized below.

## 1. Transition

Flow over a turbine blade very often undergoes a transition from laminar to turbulent and accurate modeling of this phenomenon is very important. The transition in propulsion systems (named as bypass transition) has its own features and is caused by elevated free stream turbulence, surface roughness, etc. Current work at Lewis shows that turbulence models are not being modified for their use in transitional flows. Current work at Lewis using turbulence models to capture the transition have only limited success. Bypass transition models developed at CMOTT, which take into account the effect of intermittency, account for the effect of free-stream turbulence. The development of transition models which account for both the free stream turbulence and surface roughness effects is a pacing item for transitional flow calculations for propulsion systems. Much work still needs to be done in this area.

## 2. Heat transfer

Currently, most turbulent heat transfer calculations at Lewis use Reynolds analogy (i.e. constant turbulent Prandtl number) coupled with the zero-equation or two-equation models for the velocity field. The turbulent Prandtl number, in general, is not constant for complex flows. Therefore, improvement in the heat transfer calculations requires a more accurate approach for calculating the turbulent thermal diffusivity. One such approach is to use the transport equations for the temperature fluctuations and its dissipation rate. Some work in this direction is in progress at CMOTT.

Since, as noted above, transition occurs on turbine blades quite often, part of the reason for the poor predictions of heat transfer is the inability of current models to capture this transition. There is a need to improve the modeling of this type of transitional flow.

## 3. Turbulent chemical reaction interactions

In this workshop, two approaches were presented for the calculation of turbulent flows with finite rate chemical reactions. One is the pdf method for species in which the chemical production rate of species can be exactly treated without modeling.

The other is the conventional moment closure scheme in which the averaged chemical production rate of species is estimated by the mean temperature of the flow field. Further studies are needed for clarifying and understanding the effect of chemical reaction on turbulence and vice versa. DNS of simple turbulent reacting flows could be very helpful to sort out this issue.

Studies on realistic chemical reaction models are also needed for simulating the interactions between turbulence and chemical reaction.

#### **4. Wall bounded flows**

Some presentations at this workshop showed that for high turbulent Reynolds number flows, the use of wall function as a boundary condition often produces reasonable results for even complex flows in-spite of its theoretical in-validity. In addition, this approach can significantly reduce the number of numerical grid points which, sometimes, is critical for complex engineering calculations. It was also pointed out that sometimes a key ingredient of the flow, such as a separation bubble, is under  $y^+ = 40$ . Such flows, therefore, cannot be well simulated with the wall function approach and in such cases turbulence model equations must be integrated to the wall. ( This type of turbulence modeling is usually called low Reynolds number turbulence modeling.)

Most low Reynolds number turbulence models presented in this workshop are not tensorially invariant, i.e. the model equations contain the detailed coordinate parameters which require *ad hoc* treatments in applications to complex flow geometries. In addition, existing  $k-\varepsilon$  models do not respond to the effect of pressure gradient very well. To address these problems, two efforts have been made at CMOTT. For the wall function approach, a modified new wall function is proposed to better account for the effect of pressure gradient. For low Reynolds number  $k-\varepsilon$  models, a Galilean and tensorially invariant realizable  $k-\varepsilon$  model is developed which can also respond to the pressure gradient very well. Further testing of this model in complex flows is needed to find its potential as well as its deficiencies.

#### **5. Inflow condition**

Some calculations showed that results were very much dependent on the inflow conditions chosen for turbulence quantities (say,  $k$  and  $\varepsilon$ ). To obtain a good comparison with experiments, the turbulence inflow conditions had to be adjusted. This raises the uncertainty about correctness of calculations as well as the performance of turbulence models. To resolve this problem, the determination of correct inflow conditions by either experiments or other methods is important. In situations lacking experimental inflow turbulence quantities, methods to establish reasonable inflow conditions are critical and must be further studied. Turbulence model testing should not be based on the flows with unknown inflow conditions except for the situations in which the flows are self preserving.

#### **6. Numerical method**

It was noticed that different turbulence models were built in different codes. It is difficult to compare the performance of different models based on the results

produced by different codes. It is agreed that the validation and comparison of different turbulence models must be based on the grid independent converged solutions produced by one code with the same/similar initial and boundary conditions.

Turbulence equations are much more stiff and complicated than the Navier-Stokes equations. The study of numerical methods to effectively obtain the accurate solution of turbulence equations is also very critical for turbulent CFD calculations. The collaboration between CFD and turbulence model developers will help to resolve this problem.

## 7. Hierarchy of turbulence models and standards

Several different types of turbulence models have been developed over the past several decades. Each of them was proposed for certain type of flows. In CFD calculations, all models are one-point closure schemes which include zero-equation models (or mixing length models), one- and two-equation models, algebraic Reynolds stress models and second order closure models. At each level of these turbulence models, there are several versions (as many as 10 or more) of same type of models. Each later version was developed to improve the performance over its parent-model for the flows of interest.

Engineers were often, and are still, confused by so many levels of turbulence models with so many versions at each level. Do we need all levels of turbulence models? Is there a best model at each level? The possible answer to above questions is yes.

From zero-equation to second order closure models, each level of turbulence models contains a certain degree of turbulence physics which gives each level of models a different degree of potential as well as limitation. For example, the mixing length models have the potential for modeling of attached boundary layer flows. While the good prediction of pressure distribution is often obtained, the predictions of skin friction and heat transfer are often poor, especially for separated flows. This is not surprising because the mixing length models were developed for that kind of flows and contain little turbulence physics. In this workshop, many presentations showed that two-equation isotropic eddy viscosity models perform much better than mixing length models for variety of flows. This is also not surprise because there are two turbulent transport equations involved in this type of models. However, for flows in which the anisotropy of turbulence plays main role, we must use anisotropic turbulence models. In addition, if the evolution of Reynolds stresses, streamline curvature, rotation, etc. are important, the second order closure schemes will be more appropriate.

In principle, the higher level of models (if they were well developed), give better performance in a wider range of turbulent flows and, of course, at the expense of higher computing cost and numerical difficulty. Further studies on the potential as well as deficiencies of each level of models in turbulent flow calculations are needed. Identifying the best model version at each level seems an urgent task for engineering CFD applications. To achieve this goal, systematic model testing for a variety of bench mark flows as well as real flows in propulsion systems is needed.

**Page intentionally left blank**

# Research Activities at the Center for Modeling of Turbulence and Transition

Tsan-Hsing Shih

1. Introduction
2. General developments
  - 2.1 Turbulent constitutive relations
  - 2.2 Mechanical and scalar dissipation equations
  - 2.3 Eddy viscosity transport equation
3. One-point closure schemes
  - 3.1 One-equation eddy viscosity transport equation model
  - 3.2 Galilean and tensorial invariant realizable  $k-\epsilon$  model
  - 3.3 Reynolds stress algebraic equation model
  - 3.4 Scalar flux algebraic equation model
  - 3.5 Reynolds stress transport equation model
  - 3.6 Non-equilibrium multiple-scale model
  - 3.7 Bypass transition model
  - 3.8 Joint scalar PDF model
4. RNG and DIA
5. Numerical simulation

## Abstract

The main research activities at the Center for Modeling of Turbulence and Transition (CMOTT) are described. The research objective of CMOTT is to improve and/or develop turbulence and transition models for propulsion systems. The flows of interest in propulsion systems can be both compressible and incompressible, three dimensional, bounded by complex wall geometries, chemically reacting, and involve "bypass" transition. The most relevant turbulence and transition models for the above flows are one- and two-equation eddy viscosity models, Reynolds stress algebraic- and transport-equation models, pdf models, and multiple-scale models. All these models are classified as one-point closure schemes since only one-point (in time and space) turbulent correlations, such as second moments (Reynolds stresses and turbulent heat fluxes) and third moments ( $\overline{u_i u_j u_k}$ ,  $u_i \theta^2$ ), are involved. In computational fluid dynamics, all turbulent quantities are one-point correlations. Therefore, the study of one-point turbulent closure schemes is the focus of our turbulence research. However, other research, such as the renormalization group theory, the direct interaction approximation method and numerical simulations are also pursued to support the development of turbulence modeling.

## 1. Introduction

The center for modeling of turbulence and transition was established as a special focus group within the Institute for Computational Mechanics in Propulsion at NASA Lewis Research Center in 1990. Its objective is to improve and/or develop turbulence and transition models for computational fluid dynamics (CFD) applied in propulsion systems. With the advance of computer technology and algorithms, accurate turbulence and transition modeling becomes the pacing item for improving flow calculations used in propulsion system design in all its key elements. The flows of interest in propulsion systems are, in general, very complex since there are wall-bounded three-dimensional complex geometries, chemical reactions, compressibility and transition, etc. In order to accurately predict these flows one must correctly model the turbulent stresses and scalar fluxes which are one-point (in time and space) turbulent correlations. For flows with finite rate chemical reactions, accurate modeling of the production rate of species is crucial for turbulent flow calculations. Based on the above considerations, turbulence modeling activities at CMOTT are focused on one-point closure schemes, that is, using the moment closure schemes for the turbulent velocity field and the joint scalar pdf method for the reacting scalar field.

There are various moment closure schemes which have been developed for various engineering applications. However, in practice, one often finds that the existing models need to be improved and/or re-developed in order to reasonably simulate complex flow structures appearing in propulsion systems. For this purpose, CMOTT devotes itself to improving and/or re-developing these moment closure schemes which include eddy viscosity (one- and two-equation) models, second moment algebraic- and transport-equation models, non-equilibrium multiple-scale models, and bypass transition models. In addition, other studies supporting the development of one-point closure schemes have been also carried out (for example, studies on renormalization group theory (RNG), direct interaction approximation (DIA), direct numerical simulation (DNS) and large eddy simulation (LES)).

In this report, we first describe the general development of turbulent constitutive relations, turbulent mechanical and thermal dissipation and a new eddy viscosity equation. Second, we describe the detailed developments on each moment closure scheme and the pdf method. Then the RNG and DIA methods and finally, the numerical simulation of particular turbulence phenomena, such as rotation and bypass transition, etc., are considered.

Each research subject is the joint project of several CMOTT researchers and visitors. In describing research activities, the names of involved researchers will be mentioned for reference.

## 2. General Developments

### 2.1 Turbulent Constitutive Relations

#### Reynolds stress

Using the invariant theory in continuum mechanics and Generalized Cayley-Hamilton formulas for tensor products, a turbulent constitutive relation (or a general turbulence model) for any turbulent correlations can be obtained, in principle. Therefore, this theory provides an avenue to develop better turbulence models than those existing. For example, a commonly used constitutive relation for Reynolds stresses  $\overline{u_i u_j}$  (in terms of the mean deformation rate tensor  $U_{i,j}$  and the turbulent velocity and length scales characterized by the turbulent kinetic energy  $k$  and its dissipation rate  $\varepsilon$ ) is

$$-\overline{u_i u_j} = C_\mu \frac{k^2}{\varepsilon} (U_{i,j} + U_{j,i}) - \frac{2}{3} k \delta_{ij} \quad (2.1.1)$$

The effective eddy viscosity  $\nu_T$  defined as

$$\nu_T = \frac{-\overline{u_i u_j}}{U_{i,j} + U_{j,i}} = C_\mu \frac{k^2}{\varepsilon} \quad \text{for } i \neq j \quad (2.1.2)$$

is isotropic since  $\nu_T$  is a scalar quantity. However, the invariant theory enables us to formulate the following general model (Shih and Lumley<sup>1</sup>, Johansson<sup>2</sup>):

$$\begin{aligned} \overline{u_i u_j} = & \frac{2}{3} k \delta_{ij} + 2a_2 \frac{K^2}{\varepsilon} (U_{i,j} + U_{j,i} - \frac{2}{3} U_{i,i} \delta_{ij}) \\ & + 2a_4 \frac{K^3}{\varepsilon^2} (U_{i,j}^2 + U_{j,i}^2 - \frac{2}{3} \Pi_1 \delta_{ij}) \\ & + 2a_6 \frac{K^3}{\varepsilon^2} (U_{i,k} U_{j,k} - \frac{1}{3} \Pi_2 \delta_{ij}) \\ & + 2a_7 \frac{K^3}{\varepsilon^2} (U_{k,i} U_{k,j} - \frac{1}{3} \Pi_2 \delta_{ij}) \\ & + 2a_8 \frac{K^4}{\varepsilon^3} (U_{i,k} U_{j,k}^2 + U_{i,k}^2 U_{j,k} - \frac{2}{3} \Pi_3 \delta_{ij}) \\ & + 2a_{10} \frac{K^4}{\varepsilon^3} (U_{k,i} U_{k,j}^2 + U_{k,j}^2 U_{k,i} - \frac{2}{3} \Pi_3 \delta_{ij}) \\ & + 2a_{12} \frac{K^5}{\varepsilon^4} (U_{i,k}^2 U_{j,k}^2 - \frac{1}{3} \Pi_4 \delta_{ij}) \\ & + 2a_{13} \frac{K^5}{\varepsilon^4} (U_{k,i}^2 U_{k,j}^2 - \frac{1}{3} \Pi_4 \delta_{ij}) \\ & + 2a_{14} \frac{K^5}{\varepsilon^4} (U_{i,k} U_{l,k} U_{l,j}^2 + U_{j,k} U_{l,k} U_{l,i}^2 - \frac{2}{3} \Pi_5 \delta_{ij}) \\ & + 2a_{16} \frac{K^6}{\varepsilon^5} (U_{i,k} U_{l,k}^2 U_{l,j}^2 + U_{j,k} U_{l,k}^2 U_{l,i}^2 - \frac{2}{3} \Pi_6 \delta_{ij}) \\ & + 2a_{18} \frac{K^7}{\varepsilon^6} (U_{i,k} U_{l,k} U_{l,m}^2 U_{j,m}^2 + U_{j,k} U_{l,k} U_{l,m}^2 U_{i,m}^2 - \frac{2}{3} \Pi_7 \delta_{ij}) \end{aligned} \quad (2.1.3)$$

where

$$\begin{aligned}\Pi_1 &= U_{i,k}U_{k,i}, & \Pi_2 &= U_{i,k}U_{i,k}, & \Pi_3 &= U_{i,k}U_{i,k}^2, & \Pi_4 &= U_{i,k}^2U_{i,k}^2, \\ \Pi_5 &= U_{i,k}U_{l,k}U_{l,i}^2, & \Pi_6 &= U_{i,k}U_{l,k}^2U_{l,i}^2, & \Pi_7 &= U_{i,k}U_{l,k}U_{l,m}^2U_{i,m}^2\end{aligned}\quad (2.1.4)$$

From Eq.(2.1.3), the effective eddy viscosity

$$(\nu_T)_{ij} = \frac{-\bar{u}_i\bar{u}_j}{U_{i,j} + U_{j,i}} \quad (2.1.5)$$

is no longer a scalar and, hence, is an anisotropic eddy viscosity. It is noticed that the first two terms on the right hand side of Eq.(2.1.3) represent the standard  $k-\varepsilon$  eddy viscosity model (2.1.1) and that the first five terms of Eq.(2.1.3) are of the same form as the models derived from both the two-scale DIA approach (Yoshizawa<sup>3</sup>) and the RNG method (Rubinstein and Barton<sup>4</sup>).

Eq.(2.1.3) is a general model for  $\bar{u}_i\bar{u}_j$ . It contains 11 undetermined coefficients which are, in general, scalar functions of various invariants of the tensors in question, such as  $S_{ij}S_{ij}$  (strain rate) and  $\Omega_{ij}\Omega_{ij}$  (rotation rate) which are  $(\Pi_2 + \Pi_1)/2$  and  $(\Pi_2 - \Pi_1)/2$  respectively. The detailed forms of these scalar functions must be determined by other model constraints, for example, realizability, and by experimental data. Eq.(2.1.3) contains 12 terms; however, its quadratic tensorial form may be sufficient for practical applications. We will see later in section 3.3 that the constitutive relation (2.1.3) has a significant impact on the development of Reynolds stress algebraic equation models.

### Turbulent scalar flux $\bar{\theta u_i}$

We assume the following functional form:

$$\bar{\theta u_i} = F_i(U_{i,j}, T_{,i}, k, \varepsilon, \bar{\theta^2}, \varepsilon_\theta) \quad (2.1.6)$$

where  $\bar{\theta^2}$  is the variance of a fluctuating scalar and  $\varepsilon_\theta$  is its dissipation rate. Eq.(2.1.6) indicates that the scalar flux depends on not only the mean scalar gradient  $T_{,i}$ , but also the mean velocity gradient  $U_{i,j}$  and the scales of both velocity and scalar fluctuations characterized by  $k$ ,  $\varepsilon$ ,  $\bar{\theta^2}$ ,  $\varepsilon_\theta$ .

Applying the invariant theory, we may obtain the following general constitutive

relation for  $\overline{\theta u_i}$ :

$$\begin{aligned}
\overline{\theta u_i} = & a_1 k \left( \frac{k}{\varepsilon} \frac{\overline{\theta^2}}{\varepsilon_\theta} \right)^{1/2} T_{,i} + \frac{k^2}{\varepsilon} \left( \frac{k}{\varepsilon} \frac{\overline{\theta^2}}{\varepsilon_\theta} \right)^{1/2} (a_2 U_{i,j} + a_3 U_{j,i}) T_{,j} \\
& + \frac{k^3}{\varepsilon^2} \left( \frac{k}{\varepsilon} \frac{\overline{\theta^2}}{\varepsilon_\theta} \right)^{1/2} (a_4 U_{i,k} U_{k,j} + a_5 U_{j,k} U_{k,i} + a_6 U_{i,k} U_{j,k} + a_7 U_{k,i} U_{k,j}) T_{,j} \\
& + \frac{k^4}{\varepsilon^3} \left( \frac{k}{\varepsilon} \frac{\overline{\theta^2}}{\varepsilon_\theta} \right)^{1/2} (a_8 U_{i,k} U_{j,k}^2 + a_9 U_{i,k}^2 U_{j,k} + a_{10} U_{k,i} U_{k,j}^2 + a_{11} U_{k,i}^2 U_{k,j}) T_{,j} \\
& + \frac{k^5}{\varepsilon^4} \left( \frac{k}{\varepsilon} \frac{\overline{\theta^2}}{\varepsilon_\theta} \right)^{1/2} (a_{12} U_{i,k}^2 U_{j,k}^2 + a_{13} U_{k,i}^2 U_{k,j}^2 \\
& \quad + a_{14} U_{i,k} U_{l,k} U_{l,j}^2 + a_{15} U_{j,k} U_{l,k} U_{l,i}^2) T_{,j} \\
& + \frac{k^6}{\varepsilon^5} \left( \frac{k}{\varepsilon} \frac{\overline{\theta^2}}{\varepsilon_\theta} \right)^{1/2} (a_{16} U_{i,k} U_{l,k}^2 U_{l,j}^2 + a_{17} U_{j,k} U_{l,k}^2 U_{l,i}^2) \\
& + \frac{k^7}{\varepsilon^6} \left( \frac{k}{\varepsilon} \frac{\overline{\theta^2}}{\varepsilon_\theta} \right)^{1/2} a_{18} U_{i,k} U_{l,k} U_{l,m}^2 U_{j,m}^2 T_{,j}
\end{aligned} \tag{2.1.7}$$

The coefficients  $a_1 - a_{18}$  are, in general, functions of the time scale ratio  $\frac{k}{\varepsilon} / \frac{\overline{\theta^2}}{\varepsilon_\theta}$  and the other invariants formed by the tensors in question, for example,  $T_{,k} T_{,k}$ ,  $T_{,i} U_{i,j} T_{,j}$ , etc.. Again, Eq.(2.1.7) implies that the effective eddy diffusivity

$$(\gamma_T)_i = \frac{-\overline{\theta u_i}}{T_{,i}}$$

is not isotropic. It is noticed that the first term on the right hand side of Eq.(2.1.7) is the standard eddy diffusion model, and the models derived from the two-scale DIA (Yoshizawa<sup>5</sup>) and the RNG method (Rubinstein and Barton<sup>6</sup>) are similar to the first two terms of Eq.(2.1.7). In practice, a form containing the first two terms on the right hand side of Eq.(2.1.7) may suffice. Further development of this model for turbulent heat transfer is described in Section 3.4.

The Researchers involved with the subject in this section are T.-H. Shih, J. Zhu, A. Shabbir, J.L. Lumley<sup>†</sup> and A. Johansson.<sup>‡</sup>

## 2.2 Mechanical and Scalar Dissipation Equation

### Mechanical dissipation $\varepsilon$

In turbulence modeling, we often need turbulent characteristic velocity and length scales. While the turbulent kinetic energy  $k$  is used to characterize the velocity scale, the mechanical dissipation rate  $\varepsilon$  and the scalar dissipation rate  $\varepsilon_\theta$  are used to characterize the length scales for mechanical and scalar fields, respectively. Comparing with the turbulent kinetic energy equation, the exact dissipation rate equation is

<sup>†</sup> Professor, Cornell University, Ithaca, NY

<sup>‡</sup> Professor, Royal Institute of Technology, Stockholm, Sweden

very complicated. In this equation, all the terms which represent important turbulence physics (for example, turbulent diffusion, generation and destruction) are unknown and are of complex forms that are all related to small scales of turbulence. Therefore, in the literature, the exact dissipation equation is not considered as a useful equation to work with. Instead, one creates a model equation by assuming an analogy to the turbulent kinetic energy equation, i.e., one assumes that the model dissipation rate equation also has generation and destruction terms which are assumed to be proportional respectively to the production and dissipation terms in the turbulent kinetic energy equation over the period of large eddy turn-over time characterized by  $k/\varepsilon$ . The resulting model dissipation rate equation is written as

$$\begin{aligned} \varepsilon_{,t} + U_i \varepsilon_{,i} &= \nu \varepsilon_{,ii} - (\overline{\epsilon u_i})_{,i} \\ &\quad - C_{\epsilon 1} \frac{\varepsilon}{k} \overline{u_i u_j} U_{i,j} - C_{\epsilon 2} \frac{\varepsilon^2}{k} \end{aligned} \quad (2.2.1)$$

Recently, Lumley<sup>7</sup> proposed a dissipation rate equation based on the concept of spectral energy transfer caused by interactions between eddies of different sizes. This model equation mimics the physics of statistical energy transfer from large eddies to small eddies and is of a different form than equation (2.2.1).

In this study, we explore another rational way to obtain the model dissipation rate equation which contains certain important physics and hope it will work better than the existing one. The idea is that first, there is a relationship between the dissipation rate  $\varepsilon$  and the mean-square vorticity fluctuation  $\overline{\omega_i \omega_i}$  at high Reynolds numbers or in homogeneous turbulence:

$$\varepsilon = \nu \overline{\omega_i \omega_i}$$

and second, all the terms appearing in the  $\overline{\omega_i \omega_i}$  equation have more clear physical meanings than that in the  $\varepsilon$  equation so that the  $\overline{\omega_i \omega_i}$  equation is easier to model. Once the  $\overline{\omega_i \omega_i}$  equation is modeled, a model dissipation rate equation will be readily obtained.

The exact equation for  $\overline{\omega_i \omega_i}$  is

$$\begin{aligned} \left( \frac{\overline{\omega_i \omega_i}}{2} \right)_{,t} + U_j \left( \frac{\overline{\omega_i \omega_i}}{2} \right)_{,j} &= \nu \left( \frac{\overline{\omega_i \omega_i}}{2} \right)_{,jj} - \frac{1}{2} (\overline{u_j \omega_i \omega_i})_{,j} + \overline{\omega_i u_{i,j}} \Omega_j \\ &\quad - \overline{u_j \omega_i} \Omega_{i,j} + \overline{\omega_i \omega_j} U_{i,j} + \overline{\omega_i \omega_j u_{i,j}} - \nu \overline{\omega_{i,j} \omega_{i,j}} \end{aligned} \quad (2.2.2)$$

where  $u_i$  and  $U_i$  are the fluctuating and mean velocities, and  $\omega_i$  and  $\Omega_i$  are the fluctuating and mean vorticity which are defined by

$$\omega_i = \epsilon_{ijk} u_{k,j} \quad \Omega_i = \epsilon_{ijk} U_{k,j} \quad (2.2.3)$$

Tennekes and Lumley<sup>8</sup> clearly described the physical meaning of each term in equation (2.2.2). Order of magnitude analysis shows that the first, third, fourth and fifth terms on the right hand side of Eq.(2.2.2) become small compared with all other

terms in the equation as the turbulent Reynolds number increases. The sixth and seventh terms are the production due to fluctuating vortex stretching and the dissipation due to the viscosity of the fluid. As the turbulent Reynolds number increases these last two terms become dominant and the balance between them determines the evolution of vorticity fluctuations. Neglecting terms  $\overline{\omega_i u_{i,j} \Omega_j}$ ,  $-\overline{u_j \omega_i \Omega_{i,j}}$ ,  $\overline{\omega_i \omega_j U_{i,j}}$  and  $\nu(\frac{\omega_i \omega_i}{2})_{jj}$ , the evolution of  $\overline{\omega_i \omega_i}$  at large Reynolds number will be described by the following equation,

$$(\frac{\overline{\omega_i \omega_i}}{2})_{,t} + U_j (\frac{\overline{\omega_i \omega_i}}{2})_{,j} = -\frac{1}{2} (\overline{u_j \omega_i \omega_i})_{,j} + \overline{\omega_i \omega_j u_{i,j}} - \nu \overline{\omega_{i,j} \omega_{i,j}} \quad (2.2.4)$$

To model  $\overline{\omega_i \omega_j u_{i,j}} - \nu \overline{\omega_{i,j} \omega_{i,j}}$ , let us first estimate  $\overline{\omega_i \omega_j u_{i,j}}$ . we define an anisotropic tensor  $b_{ij}^\omega$ :

$$b_{ij}^\omega = \frac{\omega_i \omega_j}{\omega_k^2} - \frac{1}{3} \delta_{ij} \quad (2.2.5)$$

then  $\overline{\omega_i \omega_j u_{i,j}}$  can be written as

$$\overline{\omega_i \omega_j u_{i,j}} = b_{ij}^\omega \overline{\omega_k^2 u_{i,j}} \quad (2.2.6)$$

We expect that the vortex stretching tends to align vortex lines with the strain rate so that the anisotropy  $b_{ij}^\omega$  would be proportional to the strain rate  $s_{ij}$ , i. e.,

$$b_{ij}^\omega \propto \frac{s_{ij}}{s}, \quad \text{where } s = (2s_{ij}s_{ij})^{1/2}, \quad s_{ij} = (u_{i,j} + u_{j,i})/2 \quad (2.2.7)$$

This leads to the following model:

$$\overline{\omega_i \omega_j u_{i,j}} \propto \overline{\omega_k^2 (2s_{ij}s_{ij})^{1/2}} \propto \overline{\omega_k^2} \sqrt{2s_{ij}s_{ij}} \quad (2.2.8)$$

where we have assumed that  $\omega_k^2$  and  $(2s_{ij}s_{ij})^{1/2}$  are well correlated.

Using the relation,  $\omega_i = \epsilon_{ijk} u_{k,j}$ , it is not difficult to show that at large turbulent Reynolds number,

$$\overline{\omega_i \omega_i} \approx 2s_{ij}s_{ij} \quad (2.2.9)$$

and Eq.(2.2.8) can be also written as

$$\overline{\omega_i \omega_j u_{i,j}} \propto \overline{\omega_k^2} \sqrt{\overline{\omega_i^2}} = \frac{\overline{\omega_k^2} \overline{\omega_i^2}}{\sqrt{\overline{\omega_i^2}}} \quad (2.2.10)$$

Equation (2.2.10) indicates that this term is of the order  $(u^3/l^3)R_t^{3/2}$  as it should be. On the other hand, from eq.(2.2.4) the term  $\overline{\omega_i \omega_j u_{i,j}} - \nu \overline{\omega_{i,j} \omega_{i,j}}$  must be of the order  $(u^3/l^3)R_t$  which is the order of magnitude of all the other terms in Eq.(2.2.4), therefore the term  $-\nu \overline{\omega_{i,j} \omega_{i,j}}$  must cancel the term (2.2.10) or (2.2.8) such that the difference of these two terms is smaller than the term (2.2.10) or (2.2.8) by an order

of  $R_t^{1/2}$ . This suggests that the combination  $\overline{\omega_i \omega_j u_{i,j}} - \nu \overline{\omega_{i,j} \omega_{i,j}}$  can be modeled by the following two terms:

$$\frac{\overline{\omega_k^2} \overline{\omega_i^2}}{\frac{k}{\nu} + \sqrt{\overline{\omega_i^2}}}, \quad \overline{\omega_k^2} S \quad (2.2.11)$$

because the ratio of  $k/\nu$  to  $\sqrt{\overline{\omega_i^2}}$  and the ratio of  $s$  to  $S$  are of order  $R_t^{1/2}$ , where  $k \approx u^2$  is the turbulent kinetic energy and  $S$  is the mean strain rate  $(2S_{ij}S_{ij})^{1/2}$ . Equation (2.2.11) does give the right order of magnitude for  $\overline{\omega_i \omega_j u_{i,j}} - \nu \overline{\omega_{i,j} \omega_{i,j}}$ . Therefore, the dynamical equation for fluctuating vorticity (2.2.4) at large Reynolds number can be modeled as

$$\left(\frac{\overline{\omega_i \omega_i}}{2}\right)_{,t} + U_j \left(\frac{\overline{\omega_i \omega_i}}{2}\right)_{,j} = -\frac{1}{2} (\overline{u_j \omega_i \omega_i})_{,j} + C_{\omega 1} \overline{\omega_k^2} S - C_{\omega 2} \frac{\overline{\omega_k^2} \overline{\omega_i^2}}{\frac{k}{\nu} + \sqrt{\overline{\omega_i^2}}} \quad (2.2.12)$$

Using  $\varepsilon = \nu \overline{\omega_i \omega_i}$ , we readily obtain the following model dissipation rate equation,

$$\varepsilon_{,t} + U_j \varepsilon_{,j} = -(\overline{u_j \epsilon})_{,j} + C_{\omega 1} S \varepsilon - C_{\omega 2} \frac{\varepsilon^2}{k + \sqrt{\nu \varepsilon}} \quad (2.2.13)$$

where  $C_{\omega 1}$  and  $C_{\omega 2}$  are the model coefficients which are expected to be constant at large Reynolds number.

It should be noticed that Eq.(2.2.13) is different from the standard  $\varepsilon$  equation (2.2.1) by both the generation and destruction terms. First, the Reynolds stresses do not appear in the generation term and the new form of the generation term is similar to that proposed by Lumley<sup>7</sup> which is based on the concept of spectral energy transfer. Second, the destruction term is well behaved so that equation (2.2.13) will not have a singularity anywhere in the flow field. We expect that equation (2.2.13) will be numerically much more robust than equation (2.2.1).

Equation (2.2.13) can be applied to any level of turbulence modeling including second order closure models; however the turbulent transport term  $(\overline{\epsilon u_i})_{,i}$  needs to be modeled differently at different levels of turbulence modeling. In an eddy viscosity model, the term  $(\overline{\epsilon u_i})_{,i}$  will be modeled as

$$(\overline{\epsilon u_i})_{,i} = -\left(\frac{\nu_T}{\sigma_\epsilon} \varepsilon_{,i}\right)_{,i} \quad (2.2.14)$$

The coefficients  $C_{\omega 1}$ ,  $C_{\omega 2}$ ,  $\sigma_\epsilon$  and the eddy viscosity  $\nu_T$  must be calibrated using experimental data (Shih *et al.*<sup>9</sup>)

### Scalar dissipation $\varepsilon_\theta$

A similar analysis leads to the following model scalar dissipation rate equation:

$$\varepsilon_{\theta,t} + U_j \varepsilon_{\theta,j} = -(\overline{u_j \varepsilon'_\theta})_{,j} + C_{\theta 1} S \varepsilon_\theta + C_{\theta 2} Pr^{-1/2} \Phi \sqrt{\varepsilon \varepsilon_\theta} - C_{\theta 3} \frac{\varepsilon \varepsilon_\theta}{k + \sqrt{\nu \varepsilon}} \quad (2.2.15)$$

where  $\Phi = \sqrt{T_{,i} T_{,i}}$  and  $T$  is the mean scalar quantity, such as, the mean temperature. Further development of heat transfer model is described in Section 3.4.

The Researchers involved with the subject in this section are T.-H. Shih, W. Liou, A. Shabbir and Z. Yang.

### 2.3 Eddy Viscosity Transport Equation

In eddy viscosity models, one accepts the following simple constitutive relation

$$\overline{u_i u_j} = -2\nu_T S_{ij} + \frac{2}{3}k\delta_{ij} \quad (2.3.1)$$

and assumes that the eddy viscosity is characterized by some kind of velocity and length scales  $u'$  and  $\ell$ :

$$\nu_T \propto u' \ell \quad (2.3.2)$$

In two-equation  $k-\varepsilon$  eddy viscosity models, for example, one specifies that

$$u' \propto k^{\frac{1}{2}}, \quad \ell \propto \frac{k^{\frac{3}{2}}}{\varepsilon} \quad (2.3.3)$$

and, hence, the eddy viscosity is assumed as

$$\nu_T = C_\mu \frac{k^2}{\varepsilon} \quad (2.3.4)$$

The eddy viscosity assumption (2.3.4) is commonly adopted in two-equation models. Eqs.(2.3.1) and (2.3.4) together with appropriate  $k$  and  $\varepsilon$  equations have been widely used in engineering calculations. However, for cases where the mean flow changes quickly or has a strong mean stream-line curvature or rotation, etc., this kind of model does not work very well, since the assumption (2.3.4) is too simple to account for the effect of the above mean flow structure on eddy viscosity.

The main purpose of this study is to drop the assumption (2.3.4) and to derive an exact equation for  $\nu_T$  based on Eq.(2.3.1) and other exact turbulence equations (i.e. first principles). In this way, we hope that some important turbulent physics can be brought into the eddy viscosity and that a physically sound turbulence eddy viscosity can be calculated.

Using Eq.(2.3.1), we may write for incompressible flows

$$\overline{u_i u_j} \overline{u_i u_j} = 2\nu_T^2 S^2 + \frac{4}{3}k^2, \quad \text{where} \quad S^2 = 2S_{ij}S_{ij} \quad (2.3.5)$$

Differentiating both sides, we obtain

$$\frac{D}{Dt}\nu_T = -\frac{S_{ij}}{S^2} \frac{D}{Dt}\overline{u_i u_j} - \frac{\nu_T}{2S^2} \frac{D}{Dt}S^2 \quad (2.3.6)$$

The equation for  $\overline{u_i u_j}$  can be written as

$$\frac{D}{Dt}\overline{u_i u_j} = D_{ij} + P_{ij} + \Pi_{ij} - \varepsilon_{ij} + Co_{ij} \quad (2.3.7)$$

where

$$\begin{aligned}
D_{ij} &= [\nu \bar{u}_i \bar{u}_j - \bar{u}_i \bar{u}_j \bar{u}_k]_{,k} \\
P_{ij} &= -\bar{u}_i \bar{u}_k U_{j,k} - \bar{u}_j \bar{u}_k U_{i,k} \\
\Pi_{ij} &= -\frac{1}{\rho} \bar{p}_{,i} u_j + \bar{p}_{,j} u_i \\
\varepsilon_{ij} &= 2\nu \bar{u}_{i,k} \bar{u}_{j,k} \\
Co_{ij} &= -2\varepsilon_{imk} \Omega_m \bar{u}_k \bar{u}_j - 2\varepsilon_{jm} \Omega_m \bar{u}_k \bar{u}_i
\end{aligned}$$

Inserting Eq.(2.3.7) into Eq.(2.3.6), we obtain an exact transport equation for eddy viscosity

$$\frac{D}{Dt} \nu_T = -\frac{S_{ij}}{S^2} (D_{ij} + P_{ij} + \Pi_{ij} - \varepsilon_{ij} + Co_{ij}) - \frac{\nu_T}{2S^2} \frac{D}{Dt} S^2 \quad (2.3.8)$$

In this equation, all the important turbulence physics in the Reynolds stress equation, such as Reynolds stress diffusion term  $D_{ij}$ , production term  $P_{ij}$ , pressure-velocity gradient correlation term  $\Pi_{ij}$  and dissipation tensor  $\varepsilon_{ij}$ , are involved. Comparing with the standard eddy viscosity assumption (2.3.4), this exact eddy viscosity equation (2.3.8) contains very rich turbulence physics. This equation also implies that a second order closure model will naturally lead to a corresponding eddy viscosity model.

Now, as an example, we use Launder Reece and Rodi's<sup>10</sup> model and a gradient transport model for the triple velocity correlation ( $-\bar{u}_i \bar{u}_j \bar{u}_k = \frac{\nu_T}{\sigma} \bar{u}_i \bar{u}_{j,k}$ ) to derive a model equation for  $\nu_T$ . The resulting equation is

$$\begin{aligned}
\frac{D}{Dt} \nu_T &= [(\nu + \frac{\nu_T}{\sigma}) \nu_{T,k}]_{,k} + (\nu + \frac{3}{2} \frac{\nu_T}{\sigma}) \frac{\nu_{T,k} S_{,k}^2}{S^2} + (\nu + \frac{\nu_T}{\sigma}) \frac{2\nu_T S_{ij} S_{ij,kk}}{S^2} \\
&\quad + \frac{4}{15} k - C_1 \frac{\varepsilon}{k} \nu_T + 2(C_2 - 2) \nu_T \frac{S_{ik} S_{kj} S_{ji}}{S^2} - \frac{\nu_T}{2S^2} \frac{D}{Dt} S^2
\end{aligned} \quad (2.3.9)$$

Note that the Coriolis terms do not explicitly appear in this equation; however the rotation effect on  $\nu_T$  could be carried over through the mean flow field. In addition, we also note that there are no extra model coefficients introduced in Eq.(2.3.9). All model coefficients ( $\sigma$ ,  $C_1$  and  $C_2$ ) are brought in from the second order closure model. The values of these model coefficients may need adjustment in model applications. Note that Eq.(2.3.9) is not a self-consistent equation since the turbulent kinetic energy  $k$  and its dissipation rate  $\varepsilon$  are also involved. Eq.(2.3.9) together with  $k$ - $\varepsilon$  transport equations will provide a new three-equation model which may better represent the effect of mean flow structure as well as mean flow history on the eddy viscosity.

The Researchers involved with the subject in this section are T.-H. Shih, Z Yang, and W. Liou.

### 3. One-Point Closure Schemes

In this section, we describe the developments on each of the moment closure scheme and the pdf method which are of concern at CMOTT. The first two sections

3.1 and 3.2 describe the one- and two-equation isotropic eddy viscosity models. Sections 3.3 and 3.4 describe the new developments on Reynolds stress and scalar flux algebraic equation models. Section 3.5 assesses Reynolds stress transport equation models. Section 3.6 describes a multiple-scale model for non-equilibrium turbulence. Section 3.7 is about transition models. Finally, in Section 3.8 the pdf method for turbulent chemical reaction is described.

### 3.1 One-equation eddy viscosity model

Recently developed one-equation eddy viscosity models are either based on the assumption (Baldwin and Barth<sup>11</sup>):

$$\nu_T = C_\mu \frac{k^2}{\varepsilon} \quad (3.1.1)$$

or created according to computational experience (Spalart and Allmaras<sup>12</sup>). Both of them are successful in some flow calculations. This scheme is quite attractive in CFD because one only needs to solve one scalar  $\nu_T$  equation without bothering about other turbulence quantities. However, comparing with  $k-\varepsilon$  two equation models, the above mentioned one-equation  $\nu_T$  models do not contain any more turbulent physics. In fact, Baldwin and Barth's model is, basically, a change of dependent variable based on Eq.(3.1.1) plus some extra approximations. Therefore, in principle, we should not expect any superior performance over two-equation models. However, if we do not use the assumption (3.1.1), there is the possibility to improve and extend the capability of one-equation eddy viscosity models.

The objective of this study at CMOTT is to derive a physically sound eddy viscosity equation which contains rich turbulent physics and accounts for various effects from mean flow structures.

Note that in Section 2.3 we have already derived an exact equation for the eddy viscosity (2.3.8) and also a model equation (2.3.9) which is based on the Reynolds stress transport equation model of Launder, Reece and Rodi (LRR). All turbulent physics contained in the Reynolds stress equation can be brought into the eddy viscosity equation. Therefore, in principle, the transport equation (2.3.9) should be better than existing one-equation models based on Eq.(3.1.1). However, Eq.(2.3.9) is not self-consistent because  $k$  and  $\varepsilon$  are also involved. To make Eq.(2.3.9) self-consistent, we must model  $k$  and  $k/\varepsilon$  in terms of  $\nu_T$  and  $S$ . In most shear flows, the energy-containing eddy turn-over time  $k/\varepsilon$  is of the same order as the mean flow time scale  $S^{-1}$ , so that  $\varepsilon/k \propto S$  is a reasonable model. In addition, a crude dimensional analysis gives  $k \propto \nu_T S$  and this is, of course, reasonable only for shear flows. After the above considerations, the resulting self-consistent one-equation model is:

$$\begin{aligned} \frac{D}{Dt} \nu_T &= [(\nu + \frac{\nu_T}{\sigma})(\nu_T)_{,k}]_{,k} - \frac{C_{\nu 0}}{\sigma} (\nu_T)_{,k} (\nu_T)_{,k} + C_{\nu 1} S \nu_T \\ &+ 2(C_{\nu 2} - 2)\nu_T \frac{S_{ik} S_{kj} S_{ji}}{S^2} - \frac{\nu_T}{2S^2} \frac{D}{Dt} S^2 \end{aligned} \quad (3.1.2)$$

where the diffusion terms from the Reynolds stress equation (2.3.7) have been manipulated and approximated. Eq.(3.1.2) clearly exhibits the various effects of the mean flow on the eddy viscosity.

The model coefficients  $C_{\nu 1}$ ,  $C_{\nu 2}$  and  $\sigma$  can be determined by using the experimental data of homogeneous shear flows, free shear flows and boundary layer flows as well as the relations in the inertial sublayer. Extensive tests of this model in various flows are carrying out at the CMOTT.

The Researchers involved with the subject in this section are T.-H. Shih, W. Liou, Z. Yang and J. Zhu.

### 3.2 Galilean and tensorial invariant realizable $k-\varepsilon$ model

The two-equation  $k-\varepsilon$  eddy viscosity model is one of the most widely used turbulence models in engineering calculations. The  $k-\varepsilon$  model has versions for high Reynolds numbers and for low Reynolds numbers. For wall bounded turbulent flows, the high Reynolds number  $k-\varepsilon$  model (for example, Launder and Spalding<sup>13</sup>) must be applied together with a wall function as its boundary condition, while the low Reynolds number  $k-\varepsilon$  model (for example, Jones and Launder<sup>14</sup>) can be integrated to the wall. The high Reynolds number  $k-\varepsilon$  model of Launder and Spalding is considered as a standard  $k-\varepsilon$  model. We notice that even though the model dissipation rate equation is created by assuming an analogy with the turbulent kinetic energy, there was not much modification until Lumley<sup>7</sup> and Shih *et al.*<sup>9</sup> For near wall turbulence, in addition to Jones and Launder's model, there are many other versions of low Reynolds number  $k-\varepsilon$  models (such as Chien<sup>15</sup>, Shih and Lumley<sup>16</sup>, Yang and Shih<sup>17</sup>) which have made better performance over Jones and Launder's model.

There are, probably, four or five issues worth mentioning about existing low Reynolds number  $k-\varepsilon$  models: the model constants are not consistent with those in the high Reynolds number  $k-\varepsilon$  model; the wall correction terms and damping functions are related to the wall distance so that models are not tensorial invariant; a nonrealistic dissipation rate near the wall is introduced; they are not always realizable since normal stress could become negative; and finally, they do not work very well for boundary layer flows with various pressure gradients.

The objective of this study at CMOTT is to overcome the above mentioned problems. First, we propose a vorticity dynamics based dissipation rate equation as a part of high Reynolds number  $k-\varepsilon$  base model.<sup>9</sup> Second, based on the invariant theory, inhomogeneous terms for the dissipation rate equation are proposed which enable the model to better respond to the change of pressure gradients (Yang and Shih<sup>18</sup>). Third, the wall distance parameter is removed from the damping function so that the model is tensorially invariant (Yang and Shih<sup>19</sup>). The model constants are consistent with those in the high Reynolds number  $k-\varepsilon$  model. Finally, the non-negativity of normal Reynolds stresses, the realizability condition, is imposed.

The Researchers involved with the subject in this section are Z. Yang, T.-H. Shih and C. Steffen.

### 3.3 Reynolds stress algebraic equation model

All eddy viscosity models including one- and two-equation models are isotropic. For the flows where anisotropy is important, for example, the secondary flows driven by turbulent normal stresses in a square duct or curved duct, eddy viscosity models do not produce correct flow structures. To overcome this intrinsic deficiency of isotropic eddy viscosity models, one proposes a Reynolds stress algebraic equation model which will provide an effective anisotropic eddy viscosity. The first such a model was proposed by Rodi<sup>20</sup> and it achieved some success in the prediction of anisotropic related flow structure. However, Rodi's formulation is a set of algebraic non-linear system equations for Reynolds stresses and it often creates numerical difficulty in obtaining a converged solution. Recently, Taulbee<sup>21</sup> obtained an explicit algebraic expression for the Reynolds stress using Pope's<sup>22</sup> tensor expansion formulation and solved this numerical difficulty. However, in general, Rodi's formulation assumes that the ratio  $\bar{u}_i \bar{u}_j / k$  is constant and, of course, this is not really true for most turbulent flows of interest. Therefore, sometimes, this Reynolds stress algebraic equation model produces even worse results than the isotropic eddy viscosity models for cases where eddy viscosity models are appropriate.

Alternative ways for obtaining effective anisotropic eddy viscosity models have been tried by a few researchers, for example, the DIA method by Yoshizawa<sup>3</sup>, the RNG method by Rubinstein and Barton<sup>4</sup> and invariant theory by Shih and Lumley.<sup>1</sup>. It is interesting to point out that the RNG and DIA methods result in the same formulation and that this formulation is the first five terms of a general constitutive relation Eq.(2.1.3) except that the model coefficients are different.

One of our goals at CMOTT is to search for an effective anisotropic eddy viscosity model for complex turbulent flows where the nonequilibrium of turbulence is not very severe so that the constitutive relation (2.1.3) is more or less valid. We have explored the potential capability of Eq.(2.1.3) and found that a truncation of Eq.(2.1.3) up to the quadratic terms of the mean velocity gradients is sufficient for various flows of interest. The model coefficients are determined such that realizability for the normal stresses is ensured. The detailed analysis is described by Shih *et al.*<sup>23</sup>

The quadratic version of Eq.(2.1.3) together with the standard  $k-\varepsilon$  transport equations, successfully predicts many complex flows as well as simple flows which include backward-facing step flows; confined coflowing jets; confined swirling coaxial jets; flows in 180° curved duct; flows in a diffuser and a nozzle; boundary layer flows with pressure gradient and turbulent free shear flows. See references<sup>23–25</sup> for detailed results.

The Researchers involved with the subject in this section are J. Zhu and T.-H. Shih.

### 3.4 Scalar flux algebraic equation model

In parallel with Reynolds stress algebraic equation model, we have also tried to develop an effective anisotropic scalar eddy diffusivity model for scalar (heat) fluxes based on the new constitutive relation (2.1.7) and the new thermal dissipation rate

equation (2.2.16). We have determined that it seems sufficient to truncate Eq.(2.1.7) up to linear terms of the mean velocity gradient, i.e.,

$$\overline{\theta u_i} = a_1 k \left( \frac{k \overline{\theta^2}}{\varepsilon \varepsilon_\theta} \right)^{1/2} T_{,i} + \frac{k^2}{\varepsilon} \left( \frac{k \overline{\theta^2}}{\varepsilon \varepsilon_\theta} \right)^{1/2} (a_2 U_{i,j} + a_3 U_{j,i}) T_{,j} \quad (3.4.1)$$

This equation indicates that the heat flux and the mean temperature gradient are not necessarily in alignment due to the distortion of the flow field. This means that the effective scalar eddy diffusivity is anisotropic.

Eq.(3.4.1) together with the  $\overline{\theta^2}$  and  $\varepsilon_\theta$  equations will be a closed set of model equations for turbulent heat fluxes. The model coefficients are calibrated from homogeneous flows. Detailed analysis and a few model tests are described in this research briefs by A. Shabbir.

The Researchers involved with the subject in this section are A. Shabbir and T.-H. Shih.

### 3.5 Reynolds stress transport equation model

The Reynolds stress transport equation model is considered as a next generation of advanced turbulence modeling for engineering applications. In principle, the second moment equations describe various effects of the mean flow and external agencies on the evolution of turbulence, hence, are the most attractive way (also the simplest correct way) to study turbulent flows.

Various closure models for second moment equations have been developed. The success of these closures are marginal and vary with each flow. To identify the sources of their deficiencies, one often uses simple flows where the specific model term in the second moment equations can be isolated, hence, the corresponding model can be checked against experimental data or direct numerical simulation (DNS). For example, using pre-distorted anisotropic homogeneous relaxation flows, we may check the return-to-isotropy models with experimental data or DNS. However, for other flows, several model terms, such as, triple velocity correlations, rapid and slow pressure-strain correlations, etc., simultaneously exist and can not be isolated in the experiments. In these cases (for example, in a homogeneous shear flow or a channel flow) only DNS can provide all the information for simultaneously checking various models.

We have examined various existing closure models using experimental data as well as DNS data (Shih *et al.*<sup>26</sup> and Shih and Lumley<sup>27</sup>). Conclusive statements are difficult to draw at this time. However, the following remarks can be made about various closures for the second moment equations, i.e., the triple velocity correlation  $T_{ijk}$ , the rapid and slow pressure related correlations  $\Pi_{ij}^{rp}$ ,  $\Pi_{ij}^{sl}$ , and the dissipation rate tensor  $\varepsilon_{ij}$ :

a)  $T_{ijk}$ . All the existing models, such as Daly and Harlow<sup>28</sup>, LRR<sup>10</sup>, Lumley<sup>29</sup>, etc., are not very satisfactory for highly inhomogeneous flows, such as flow near the wall. However, for flows where the inhomogeneity is not very high, the above closure models become close to each other and also closer to the DNS data. In addition, the triple velocity correlations in these situations are usually small comparing with

other terms in the equation, so that modeling of this term is not as critical as other terms for the results of turbulent flow calculations, except for the flow near the wall. b)  $\Pi_{ij}^{rp}$ . It is very clear from all the available DNS data that nonlinear models, such as, Shih and Lumley<sup>30</sup> are much better than linear models, such as SSG<sup>31</sup>. It seems also that the following constitutive relation

$$\Pi_{ij}^{rp} = F(\bar{u_i u_j}, U_{i,j})$$

is quite appropriate, i.e., its dependence on turbulent Reynolds number and other parameters is quite weak and can be neglected. However, one deficiency of this form observed by Reynolds<sup>32</sup> is that it can not take the rotation effect into account.

c)  $\Pi_{ij}^{sl}$ . This term is usually modeled together with the dissipation tensor  $\varepsilon_{ij}$  and the combination of the two is called the return-to-isotropy term. All existing models are unsatisfactory at the present time. They are far from "universal", i.e., their performance varies from flow to flow. It is noticed that some strange behavior of return-to-isotropy (for example, for some pre-distorted flow relaxation, turbulence evolves toward anisotropy before it returns to isotropy) occurs and cannot be possibly modeled with the following constitutive relation:

$$\Pi_{ij}^{sl} = F(\bar{u_i u_j}, k, \varepsilon)$$

In addition, the behavior of return-to-isotropy was found to depend not only on the Reynolds stresses at the present time but also on their history according to DNS data (Lee<sup>33</sup>). It may be also necessary to include triple velocity correlations into the above constitutive relations from the definition of  $\Pi_{ij}^{sl}$ . The term  $\Pi_{ij}^{sl}$  seems highly dependent on the turbulent Reynolds number and slowly approaches to its asymptote as Reynolds number goes to infinity, so that, in general, one should not exclude its dependence on turbulent Reynolds number even for moderate Reynolds numbers. In addition,  $\Pi_{ij}^{sl}$  is also noticeably affected by the mean strain rate according to the DNS data<sup>34</sup>, so that, in general, the mean strain rate should be also considered in the constitutive relation. In short, much more research is needed for developing a better model of  $\Pi_{ij}^{sl}$ .

The Researchers involved with the subject in this section are T.-H. Shih and A. Shabbir.

### 3.6 Non-equilibrium multiple-scale model

To consider the effect of the nonequilibrium of energy spectrum on turbulent quantities, such as  $k$ ,  $\varepsilon$  and  $\bar{u_i u_j}$ , etc., Hanjelic et al.<sup>35</sup> are the first to propose a partition in the turbulent energy spectrum. Because of the nonequilibrium, the rate that energy enters the low wave number region,  $\varepsilon_p$ , does not equal to the energy transfer rate from low wave numbers to high wave numbers,  $\varepsilon_t$ . Therefore it is reasonable to describe the evolution of the energy contained in low wave number region,  $k_p$ , and high wave number region  $k_t$ , separately. As a result, the time scale or the length scale defined by different energy transfer rates will be different and this multiple-scale concept reflects the nonequilibrium effect of turbulence.

We think that this concept would be more appropriate for compressible flows because the compressibility often creates nonequilibrium interactions between large and small eddies. We first modify Hanjelic et al.'s model, test it in various free shear flows and boundary layer flows and then extend it to compressible flows by consideration of the effects of compressibility on the equations for  $k_p$  and  $\varepsilon_p$ . The proposed model is tested in both compressible free shear flows and boundary layer flows. For detailed analysis and flow calculations see the report by Duncan *et al.*<sup>36</sup> and Liou and Shih<sup>37</sup>.

The Researchers involved with the subject in this section are W. Liou, T.-H. Shih and B. Duncan.

### 3.7 Bypass transition model

The onset of turbulence transition in the propulsion system is often highly influenced by the free stream turbulence. This transition process does not go through the linear instability but is mainly controlled by nonlinear processes. Therefore, it is sometimes called "bypass" transition. Because of this highly nonlinear process of transition, turbulence models may be used to predict it. In fact, many two-equation models, for example,  $k-\varepsilon$  eddy viscosity models of Launder and Sharma<sup>38</sup>, Chien<sup>15</sup>, etc., do mimic bypass transition on a flat plate when the free stream has a certain amount of turbulent intensity. However, to obtain an accurate prediction of bypass transition, the study of the bypass transition process and physics is needed. The conventional turbulence models must be modified to take into account the intermittent phenomena of transitional flows.

We have proposed transition models based on a two-equation turbulence model using an intermittency factor to modify either the eddy viscosity or modeled  $k-\varepsilon$  equations. Successful results for a flat plate boundary layer under various free-stream turbulence intensities are obtained. For details see the report by Yang and Shih<sup>39</sup>.

The Researchers involved with the subject in this section are Z. Yang and T.-H. Shih.

### 3.8 Joint scalar PDF model

One of the critical problems in turbulent combustion is how to treat the interaction between the chemical reaction on the turbulence. The estimation of the production rate of compositions based on the mean flow temperature would be in a very large error for flows with finite rate chemical reactions. The reason is that the production rate of compositions depends not only on the mean values of temperature  $T$  and compositions  $C_i$ , but also very much depends on the detailed fluctuations of temperature  $\theta$  and compositions  $c_i$ . The moment closure scheme of modeling the production rate of compositions in terms of the mean flow temperature, the mean compositions and various correlations consisting of the fluctuating temperature and composition, such as  $\overline{\theta^2}$ ,  $\overline{\theta c_i}$ ,  $\overline{c_i c_j}$ , ..., has not been successful. However, the PDF method allows us to treat chemical reaction exactly without modeling (Pope<sup>40</sup>). Therefore, for the study of turbulent combustion problems, we use the joint scalar PDF transport equation for the scalar field and the moment closure schemes for

the velocity field and develop a hybrid solver consisting of a Monte Carlo scheme and a conventional CFD method. For detailed description of this procedure and its applications see Hsu<sup>41</sup> and Hsu *et al.*<sup>42</sup>

The Researchers involved with the subject in this section are A. Hsu, A.T. Norris and J.Y. Chen<sup>†</sup>

#### 4. RNG and DIA

In developing one point turbulence models, conventional modeling methods can be supplemented by “non-conventional” methods such as renormalization group theory (RNG) and the direct interaction approximation (DIA). These are two point theories formulated in wavevector or fourier space; one point models are derived by integration over wavevectors. This approach provides theoretical support for conventionally derived models and sometimes suggests theoretically derived forms for the empirical elements, whether constants or functions, which appear in these models.

We have applied RNG methods to both the eddy viscosity and Reynolds stress transport equation models. In addition to the  $k - \epsilon$  model proposed by Yakhot and Orszag<sup>43</sup>, it is possible to obtain constitutive relations for Reynolds stress and heat fluxes (Rubinstein and Barton<sup>4,6</sup> which are special cases of the general results Eqs.(2.1.3) and (2.1.7). By applying the perturbation theories of Yakhot and Orszag<sup>43</sup> to the relevant correlations, expansions in powers of the mean velocity gradient are obtained for the stresses and heat fluxes; quadratic truncation of the series leads to a stress model Eq.(2.1.3) with constant  $a_4, a_6, a_7$  and a heat flux model Eq.(2.1.7) with constant  $a_2, a_3$  in which the constants are in good agreement with empirically selected values. The forms derived are also consistent with the DIA analysis of Yoshizawa<sup>3,5</sup>.

The RNG method also provides a formulation for closing the Reynolds stress transport equation (Rubinstein and Barton<sup>44</sup>). Perturbative evaluation of the correlations  $\Pi_{ij}^{tp}$  and  $\Pi_{ij}^{sl}$  leads to series expansions in powers of the mean velocity gradient. These series can be consolidated, or “resumed” using the known perturbation series for the Reynolds stresses by methods analogous to Pade approximation. Systematic lowest order summation leads to a Reynolds stress transport equation with a form identical to the LRR model equation and with constants in reasonable agreement with empirically chosen values. Higher order resummation leading to nonlinear models of the type described in Sec. 3.5 remains an open possibility. The possibility of such resummation in the context of DIA has been discussed by Yoshizawa<sup>45,46</sup>.

Recent work has focussed on nonequilibrium time dependent relations between the Reynolds stress and the mean flow derived from a simplification of the DIA theory of shear turbulence. In this theory, shear turbulence is modeled by a non-Markovian eddy damping acting against the mean shear. The RNG and DIA Reynolds stress transport models and the LRR model all assume Markovian damping; as in the

<sup>†</sup> Professor, University of California, Berkeley, CA

molecular theory of transport coefficients, Markovian damping describes long time behavior and is incorrect at short times. The most important consequence of non-Markovian damping is a *strong suppression of eddy damping at short times*. This leads to closer agreement between the present theory and rapid distortion theory at short time. This is important in modeling oscillating shear flows: recent work of Mankbadi<sup>47</sup> shows that RDT based models best predict such flows. In transient homogeneous shear flow at high strain rates, the LRR model predicts rapid onset of eddy damping leading to excessive growth of turbulence kinetic energy at short times. The suppression of eddy damping at short times in the present model should lead to improved predictions for this flow as well.

Another consequence of this theory is a stress model Eq.(2.1.3) in which the coefficients  $a_2, \dots$  are functions of the mean strain rate. This theory can be described as RDT with a modified total strain determined by the response function of the DIA theory of isotropic turbulence. The introduction of a phenomenological modified total strain has often been advocated in the RDT literature to improve the agreement between RDT and shear flow data; here the modified total strain is deduced as a consequence of the theory. In the special but important case of simple shear flow in which  $\partial U_i / \partial x_j = S \delta_{i1} \delta_{j2}$ , the result can be formulated in terms of Eq.(2.1.3) in which, for example,  $a_2 = a_2(Sk/\varepsilon)$  and the function  $a_3$  is found exactly from RDT. There are analogous results for the coefficients  $a_4, a_6, a_7$ ; in simple shear flow, the remaining terms in Eq.(2.1.3) identically vanish. Extension of this theory to other mean shear tensors depends on the tabulation of the corresponding RDT solution.

The researchers involved with the subject in this section are R. Rubinstein and A. Yoshizawa.<sup>†</sup>

## 5. Numerical Simulation

To obtain a better understanding of the effect of compressibility and rotation on turbulence, numerical simulations of compressible homogeneous shear flows and rotational flows are carried out. The effects of compressibility and rotation on the energy spectrum and energy cascade between turbulent eddies has been analyzed (Hsu and Shih<sup>48</sup>). These simulations support the idea of the multiple-scale model for nonequilibrium compressible turbulent flows (W. Liou and Shih<sup>37</sup>).

Another numerical simulation is the transition subjected to the free stream large disturbances. The objective of this simulation is to obtain some insight into the transition physics and to provide data base for bypass transition modeling. Based on the assumption that the transition process is mainly controlled by large scale motions, we use a high accuracy finite difference Navier-Stokes solver with coarse grids to simulate the large scale motions of transition. A preliminary calculation of bypass transition was carried out. Various statistics of the calculated flow field are under examination.

The Researchers involved with the subject in this section are A. Hsu, C. Liou<sup>‡</sup>, Z. Yang, A. Shabbir, T.-H. Shih.

<sup>†</sup> Professor, Tokyo University, Japan

<sup>‡</sup> Professor, University of Colorado, Denver, CO

## References

- <sup>1</sup> Shih, T.-H. and Lumley, J., "Remarks on turbulent constitutive relations," NASA TM 106116 (1993).
- <sup>2</sup> Johansson, A., Private communication.
- <sup>3</sup> Yoshizawa, A., Phys. Fluids, **27**, 1377-1387 (1984).
- <sup>4</sup> Rubinstein R. and Barton, J. M., "Nonlinear Reynolds stress models and the renormalization group," Phys. Fluids **2**, 1472-1476 (1990).
- <sup>5</sup> A. Yoshizawa, J. Fluid Mech. **195**, 541 (1988).
- <sup>6</sup> Rubinstein, R. and Barton, J. M., "Renormalization group analysis of anisotropic diffusion in turbulent shear flows," Phys. Fluids **3**, 415-421 (1991).
- <sup>7</sup> Lumley, J. L., "Some comments on turbulence," Phys. Fluids, **4** (1992).
- <sup>8</sup> Tennekes, H. and Lumley, J. L., *A First Course in Turbulence* Massachusetts Institute of Technology, 1972.
- <sup>9</sup> Shih, T.-H., Liou, W. W., Shabbir, A., Yang, Z., and Zhu, J., "A vorticity dynamics based model for the turbulent dissipation," NASA TM 107177 (1993).
- <sup>10</sup> Launder, B.E., Reece, G.J., and Rodi, W. , " Progress in the development of a Reynolds-stress turbulence closure," J. Fluid Mech. **68**, 537-566 (1975).
- <sup>11</sup> Baldwin B. S. and Barth, J. T., "A one-equation turbulence transport model for high Reynolds number wall-bounded flows," NASA TM 102847 (1990).
- <sup>12</sup> Spalart, P. R. and Allmaras, S. R., "A one-equation turbulence model for aerodynamic flows," AIAA-92-0439 (1992).
- <sup>13</sup> Launder, B. E. and Spalding, D. B., "The numerical computation of turbulent flow," Computer Methods in Applied Mechanics and Engineering **3**, 269-289 (1974).
- <sup>14</sup> Jones, W. P. and Launder, B. E., "The calculation of low-Reynolds Number phenomena with a two-equation model of turbulence," International Journal of Heat and Mass Transfer, **16**, 1119-1130 (1973).
- <sup>15</sup> Chien, K.-Y., "Predictions of channel and boundary-layer flows with a low-Reynolds-number turbulence model," AIAA Journal, **20**, 33-38, (1982).
- <sup>16</sup> Shih, T.-H. and Lumley, J. L., "Kolmogorov behavior of near-wall turbulence and its application in turbulence modeling," NASA TM 105663 (1992).
- <sup>17</sup> Yang, Z. and Shih, T. -H., "A new time scale based  $k - \epsilon$  Model for Near Wall Turbulence," AIAA J. **31**, 1191-1198 (1993).
- <sup>18</sup> Yang, Z. and Shih, T. -H., NASA TM to appear.
- <sup>19</sup> Yang, Z. and Shih, T. -H., "A Galliean and tensorial invariant  $k - \epsilon$  model for near wall turbulence," AIAA 24th Fluid Dynamics Conference 93-3105, July 6-9 1993/Orlando, FL.

- <sup>20</sup> Rodi, W., "Turbulence models and their application in hydraulics — A state of the art review," Book Publication of the International Association for Hydraulics Research, Delft, Netherlands (1980).
- <sup>21</sup> Taulbee, D. B., "An improved algebraic Reynolds stress model and corresponding nonlinear stress model," *Phys. Fluids* **4**, 2555 (1992).
- <sup>22</sup> S.B. Pope, "A more general effective-viscosity hypothesis," *J. Fluid Mech.*, **72**, 331 (1975)
- <sup>23</sup> Shih, T.-H., Zhu, J., and Lumley, J. L., "A realizable Reynolds stress algebraic equation model," NASA TM 105993 (1992).
- <sup>24</sup> Zhu, J. and Shih, T.-H., "Computations of confined coflowing jets with three turbulence models," AIAA paper 93-3120 (1993).
- <sup>25</sup> Zhu, J. and Shih, T.-H., "A numerical study of confined turbulent jets," NASA TM 106197 (1993).
- <sup>26</sup> Shih, T.-H., Shabbir, A., and Lumley, J. L., "Advances in modeling the pressure correlation term in the second moment equations," NASA TM 104413 (1991).
- <sup>27</sup> Shih, T.-H. and Lumley, J.L., "Critical comparison of second order closures with direct numerical simulation of homogeneous turbulence," *AIAA J.*, **31**, 663-671 (1993)
- <sup>28</sup> Daly, B.J. and Harlow, F.H., "Transport equations of turbulence," *Phys. Fluid*, **13**, 2634 (1970).
- <sup>29</sup> Lumley, J.L., "Computational modeling of turbulent flows," *Adv. Appl. Mech.*, **18**, 123 (1978).
- <sup>30</sup> Shih, T.-H. and Lumley, J. L., "Second-order modeling of boundary-free turbulent shear flows," *AIAA Journal*, **30**, 1553-1561 (1992).
- <sup>31</sup> Speziale, C.G., Sarkar, S. and Gatski, T.B., "Modeling the pressure-strain correlation of turbulence: an invariant dynamical systems approach," *J. Fluid Mech.*, **227**, 245-272 (1991).
- <sup>32</sup> Reynolds, W. C., "Effect of rotation on homogeneous turbulence," Tenth Australian Fluid Mechanics Conference, December 11-15, 1989.
- <sup>33</sup> Lee, M.J. and Reynolds, W.C., "Numerical experiments on structure of homogeneous turbulence," Dept. Mech. Engng. Rep. TF-24, Stanford University: Stanford California (1985).
- <sup>34</sup> Hallberg, M., "Development of Reynolds stress closures of homogeneous turbulence through physical and numerical experiments," Doctoral Thesis, Royal Institute of Technology, Stockholm, 1993.
- <sup>35</sup> Hanjalic, K., Launder, B.E. and Schiestel, R., "Multiple-time-scale concepts in turbulent transport equation," *Turbulent Shear Flow 2* (1980).
- <sup>36</sup> Duncan, B., Liou, W. W. and Shih, T.-H., "A multiple-scale turbulent model for incompressible flow," AIAA 93-0086 (1993).

- <sup>37</sup> Liou, W. W. and Shih, T. H., "A multiple-scale model for compressible turbulent flows," NASA TM 106072 (1993).
- <sup>38</sup> Launder, B. E. and Sharma, B. I., "Application of the energy-dissipation model of turbulence to the calculation of a flow near a spinning disk," Letters in Heat and Mass Transfer, **1**, 131-138 (1974).
- <sup>39</sup> Yang, Z. and Shih, T.-H., "A  $k-\varepsilon$  model for turbulent and transitional boundary layer," Near Wall Turbulent Flows, Elsevier, 165-175 (1993).
- <sup>40</sup> S.B. Pope, "PDF methods for turbulent Reactive Flows," Prog. Energy Combust. Sci., **11**, 119-192 (1985).
- <sup>41</sup> Hsu, A. T., "Study of hydrogen diffusion flames using pdf turbulence model," AIAA paper 91-1780 (1991).
- <sup>42</sup> Hsu, A. T., Tsai, Y. L. T., and Raju, M. S., "A PDF approach for compressible turbulent reacting flows," AIAA-93-0087 (1993).
- <sup>43</sup> V. Yakhot and S.A. Orszag, J. Sci. Comput. **1**, 3 (1986).
- <sup>44</sup> Rubinstein, R. and Barton, J. M., "Renormalizatin group analysis of the Reynolds stress transport equation," Phys. Fluids, **4**, 1759-1766 (1992).
- <sup>45</sup> Yoshizawa, A., "Derivation of a model Reynolds stress transport equation using the renormalization of the eddy-viscosity type representation," Phys. Fluids, **5**, 707-715 (1993).
- <sup>46</sup> Yoshizawa, A., "Bridging between eddy-viscosity type and second order models using a two-scale DIA," 9th Symposium Turbulent Shear Flows Kyoto Japan, 1993.
- <sup>47</sup> Mankbadi, R. R. and Liu, J. T. C., "Near-wall response in turbulent shear flows subjected to imposed unsteadiness," J. Fluid Mech., **238**, 55-71 (1992).
- <sup>48</sup> Hsu, A. T. and Shih, T.-H., "Effect of the coriolis force on compressible turbulence," 9th Symposium on Turbulent Shear Flows, Kyoto, Japan, 1993.

**Page intentionally left blank**

## Research on Two Equation Models

Presented by Z. Yang

NASA Lewis Workshop on Computational Turbulence Modeling

September 15-16, 1993

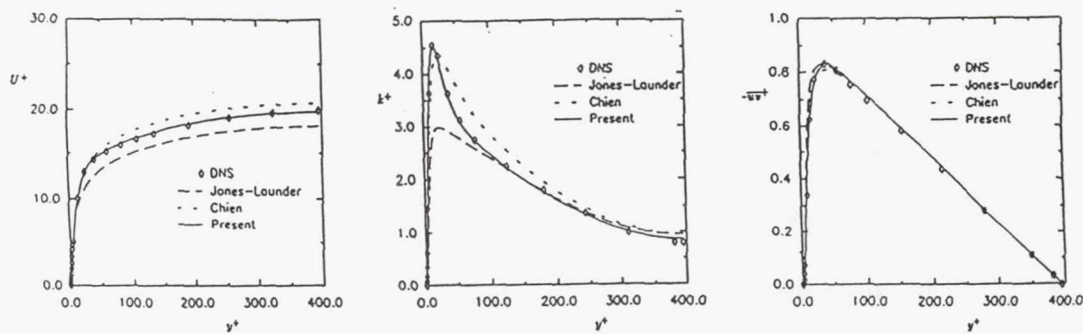
### Motivations and Objectives:

- $k - \epsilon$  model is the most widely used turbulence model in engineering calculations.
- However, the following deficiencies need to be fixed:
  - Currently, most  $k - \epsilon$  models for near wall turbulence contain geometry parameters.
  - The form of the  $\epsilon$  equation lacks a solid theoretical foundation.
  - The  $k - \epsilon$  model performs rather inadequately for flows with adverse pressure gradient.
  - The capability of  $k - \epsilon$  models in predicting bypass transition due to the freestream turbulence needs improving.

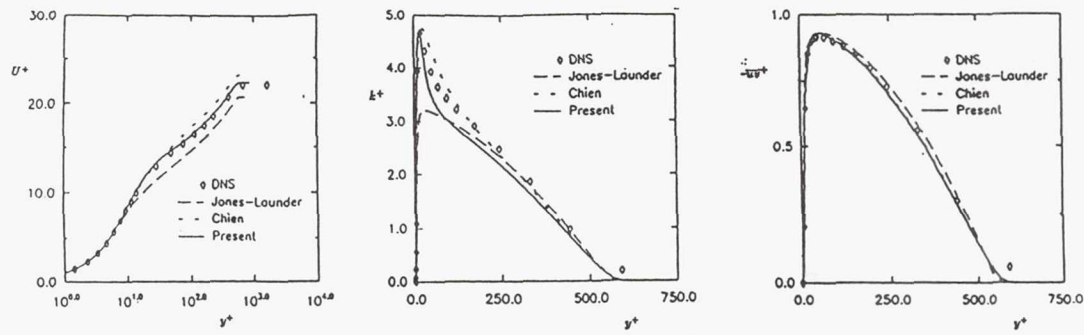
## Modeling of Near Wall Turbulence

- Near wall  $k - \epsilon$  model = Standard  $k - \epsilon$  model + near wall effect.
- The near wall effect:
  - The time scale approaches the Kolmogorov time scale near the wall.
  - The damping function is parametrized by a new parameter which is independent of the coordinate system.
- The resulting model is Galilean and tensorial invariant.
- The resulting model is robust numerically.

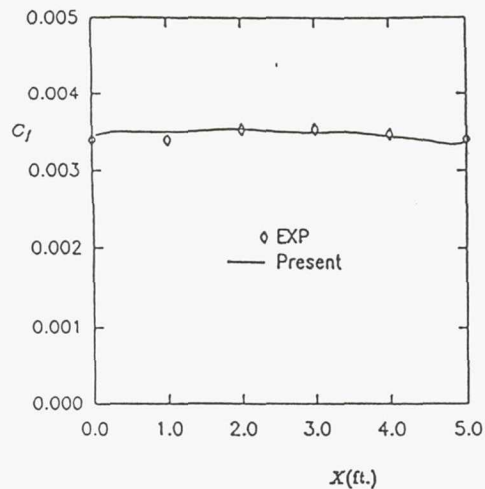
Turbulent Channel Flow at  $Re_\tau = 395$



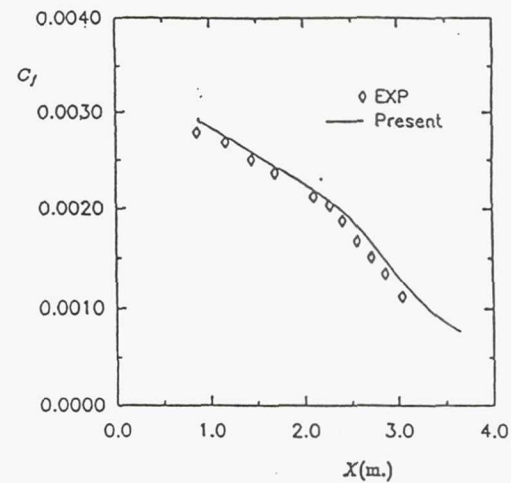
ZPG Turbulent Boundary Layer at  $Re_\theta = 1410$



FPG Boundary Layer

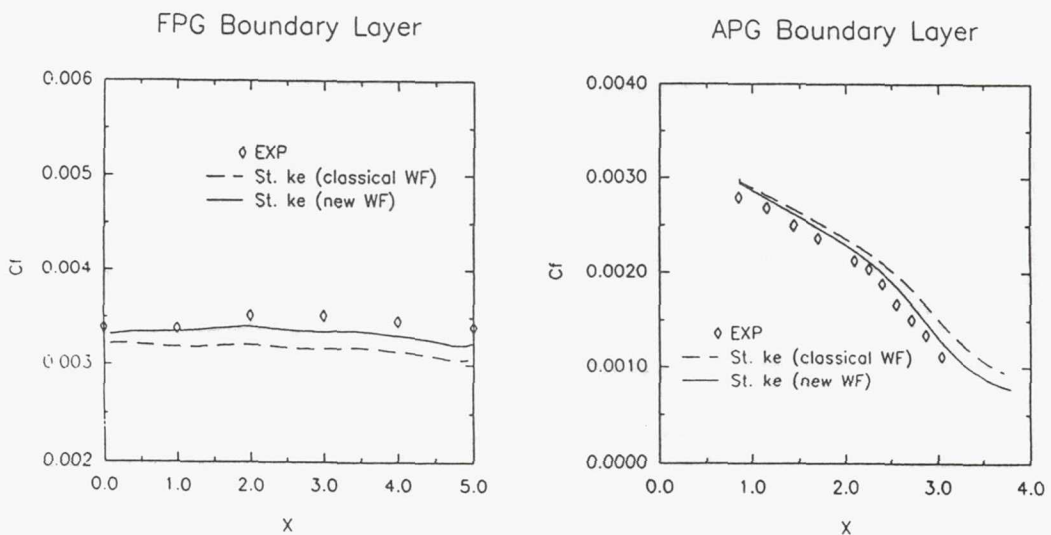


APG Boundary Layer



### On the Wall Functions

- The advantages of the wall function approach:
  - Reduce the number of grid points by half, at least.
  - Reduce the numerical stiffness of the dissipation rate equation, by less grid stretching.
- The limit of wall function approach: the flow is assumed to be attached to the wall.
- Existing wall functions are based on the flat plate BL at zero pressure gradient.  
It is inadequate when the pressure gradient is not zero.
- A new set of wall functions are obtained:
  - They are based on the asymptotic behavior of the governing equations in the log layer.
  - They contain the effect of the pressure gradient.



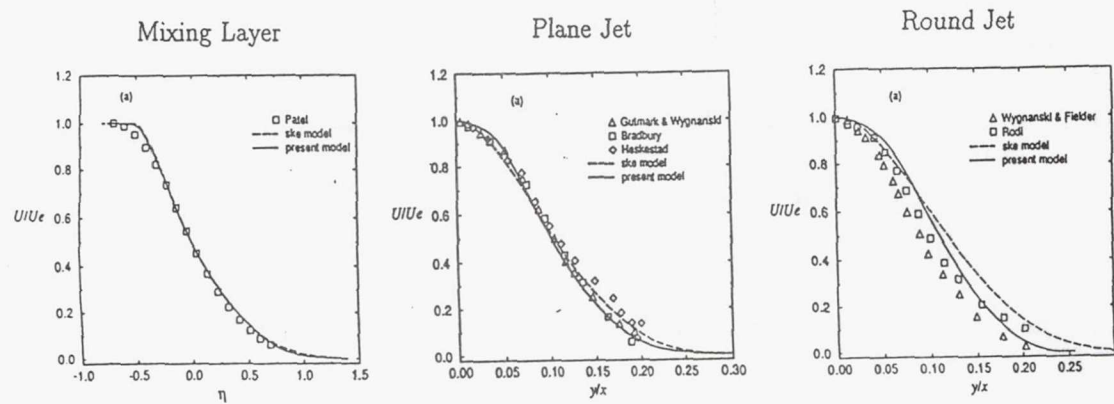
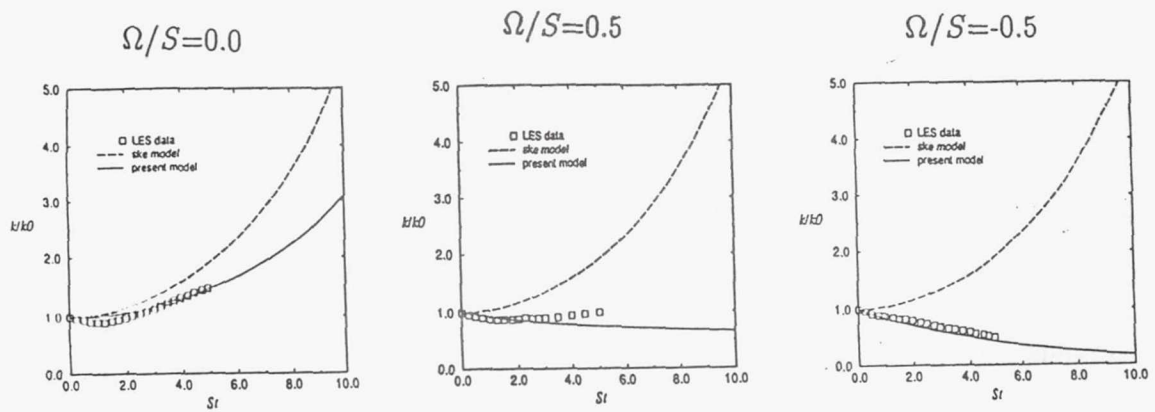
## A Vorticity Dynamics Based Model for the Dissipation Rate Equation

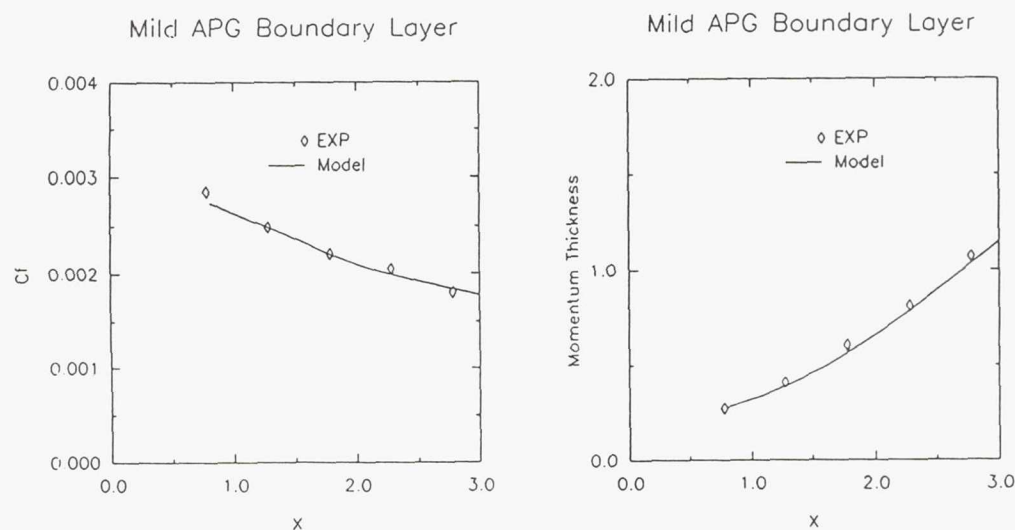
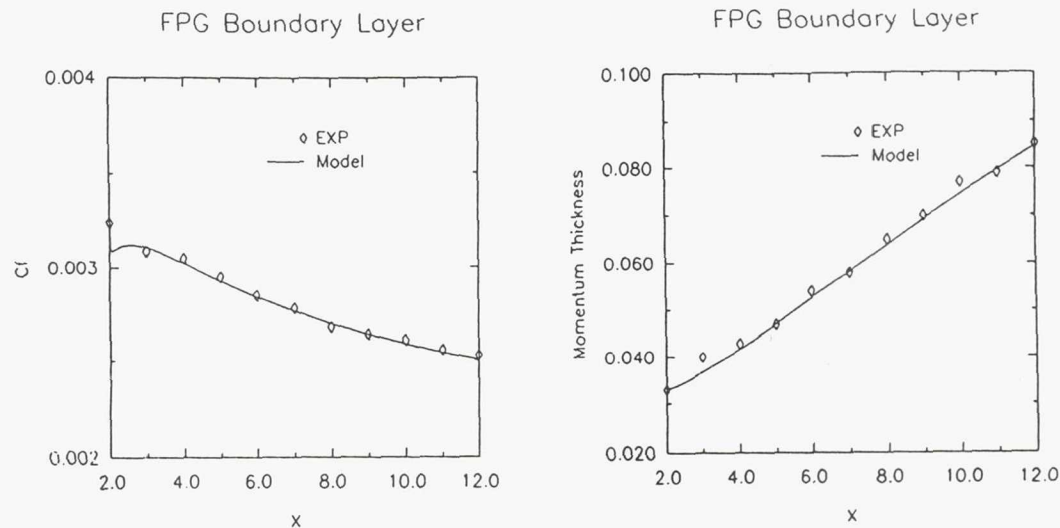
- The dynamic equation for the fluctuating vorticity is analyzed.  
(The terms in the fluctuating vorticity equation have clearer physical meanings than terms in the dissipation rate equation.)
- For large Reynolds numbers,  $\epsilon = \nu \bar{\omega}_i \bar{\omega}_i$ .
- The resulting model equation has a better foundation than the standard  $\epsilon$  equation.
- The resulting model equation always gives a positive production in dissipation rate.
  - The model calculation is expected to be more robust for complex flow calculations.

## Flow Inhomogeneity and the Dissipation Rate Equation

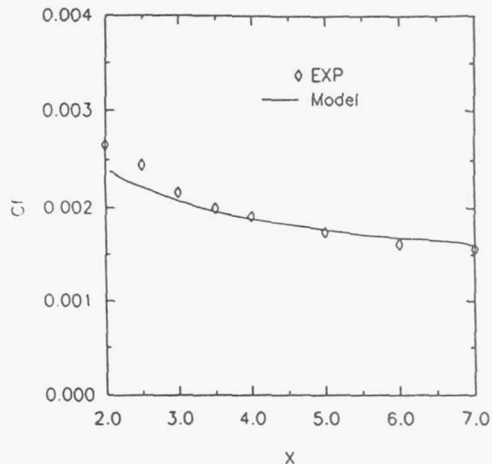
- The exact dissipation rate equation contains source terms due to the flow inhomogeneity.
- However, the existing  $\epsilon$  equations are homogeneous.  
(The source terms are the same for both the homogeneous and inhomogeneous flows.)
- A new model equation for  $\epsilon$  is proposed, which accounts for the inhomogeneity effect:
  - Flow inhomogeneity is represented by  $\nabla S$  and  $\nabla k$ .
  - Invariant theory is used to derive such a model equation.
- The resulting model equation accurately account for the effect of the pressure gradient.

## Rotating homogeneous shear flows

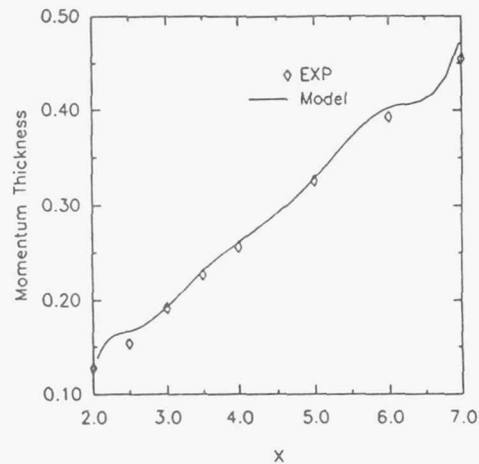




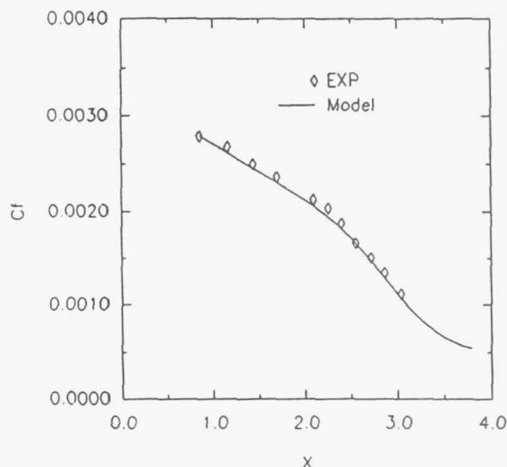
Moderate APG Boundary Layer



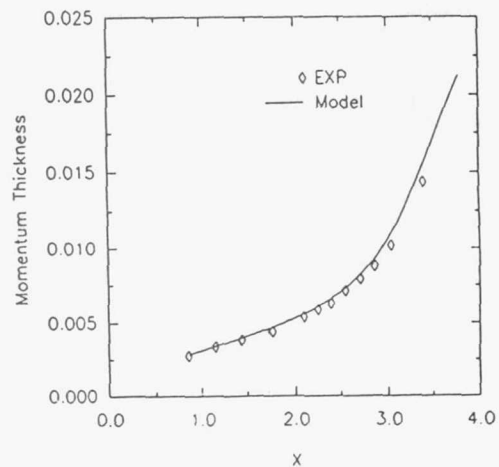
Moderate APG Boundary Layer



Strong APG Boundary Layer

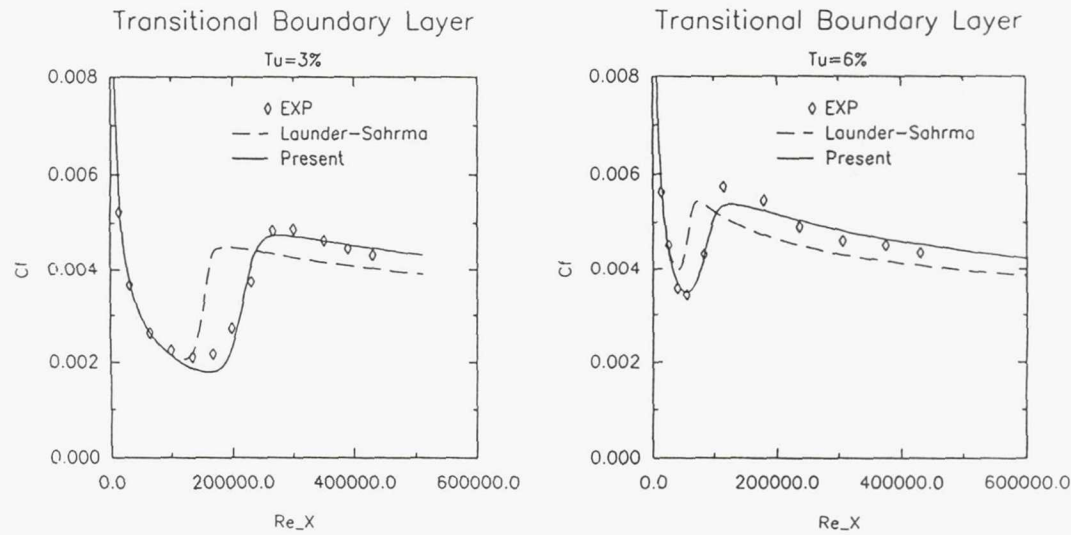


Strong APG Boundary Layer



## Modeling of Bypass Transition

- Low Reynolds number  $k - \epsilon$  models could mimic transition.
  - The predictions are not very good.
  - Among these models, the Launder-Sharma model gives the best prediction.
- New model for bypass transition is proposed by introducing the effect of the intermittency
- The transition model recovers to turbulence model at the end of the transition zone.
- Calculations of the benchmark flows show that the present model gives better predictions compared with the  $k - \epsilon$  models without the intermittency effect.



### Summaries:

The capabilities of  $k - \epsilon$  model are enhanced in the following areas:

- A Galilean and tensorial invariant  $k - \epsilon$  model for near wall turbulence.
- A new set of wall functions for attached flows.
- A new model equation for the dissipation rate:
  - It has a better theoretical basis.
  - It contains the contribution of flow inhomogeneity.
  - It captures the effect of the pressure gradient accurately.
- A better model for bypass transition due to freestream turbulence.

# A REYNOLDS STRESS ALGEBRAIC EQUATION MODEL

Presented by

J. Zhu

## Motivation

- Two-equation turbulence models ( $K-\epsilon$ ,  $K-\omega$ )
  - Simple, robust and computationally inexpensive
  - Isotropic
  - Not realizable.  $\bar{u_i u_i}$  may become negative
- Reynolds stress transport equation models
  - Anisotropic
  - Capable of simulating  $\bar{u_i u_j}$ -transport
  - Difficult to model higher-order correlations
  - Complex and computationally expensive

## Objective

Develop a Reynolds stress algebraic equation model which combines the respective advantages of two-equation models and Reynolds stress transport equation models:

- Simple, robust and efficient
- Anisotropic
- Realizable

## Derivation of Constitutive Relation

- First step: assume some relationship between quantities of interest  $\overline{u_i u_j} = F_{ij}(U_{i,j}, K, \epsilon)$
- Second step: use invariant theory to determine the function  $F_{ij}$ 
  1. An invariant can only be a function of other invariants
  2. If the LHS of an equation is bilinear in arbitrary vectors  $A_i$  and  $B_j$ , the RHS must also be bilinear in  $A_i$  and  $B_j$

- A general constitutive model of  $\bar{u}_i \bar{u}_j$

$$\begin{aligned}
\bar{u}_i \bar{u}_j &= \frac{2}{3} k \delta_{ij} + 2a_2 \frac{K^2}{\epsilon} (U_{i,j} + U_{j,i} - \frac{2}{3} U_{i,i} \delta_{ij}) + 2a_4 \frac{K^3}{\epsilon^2} (U_{i,j}^2 + U_{j,i}^2 - \frac{2}{3} \Pi_1 \delta_{ij}) \\
&\quad + 2a_6 \frac{K^3}{\epsilon^2} (U_{i,k} U_{j,k} - \frac{1}{3} \Pi_2 \delta_{ij}) + 2a_7 \frac{K^3}{\epsilon^2} (U_{k,i} U_{k,j} - \frac{1}{3} \Pi_2 \delta_{ij}) \\
&\quad + 2a_8 \frac{K^4}{\epsilon^3} (U_{i,k} U_{j,k}^2 + U_{i,k}^2 U_{j,k} - \frac{2}{3} \Pi_3 \delta_{ij}) + 2a_{10} \frac{K^4}{\epsilon^3} (U_{k,i} U_{k,j}^2 + U_{k,j} U_{k,i}^2 - \frac{2}{3} \Pi_3 \delta_{ij}) \\
&\quad + 2a_{12} \frac{K^5}{\epsilon^4} (U_{i,k}^2 U_{j,k}^2 - \frac{1}{3} \Pi_4 \delta_{ij}) + 2a_{13} \frac{K^5}{\epsilon^4} (U_{k,i}^2 U_{k,j}^2 - \frac{1}{3} \Pi_4 \delta_{ij}) \\
&\quad + 2a_{14} \frac{K^5}{\epsilon^4} (U_{i,k} U_{l,k} U_{l,j}^2 + U_{j,k} U_{l,k} U_{l,i}^2 - \frac{2}{3} \Pi_5 \delta_{ij}) \\
&\quad + 2a_{16} \frac{K^6}{\epsilon^5} (U_{i,k} U_{l,k}^2 U_{l,j}^2 + U_{j,k} U_{l,k}^2 U_{l,i}^2 - \frac{2}{3} \Pi_6 \delta_{ij}) \\
&\quad + 2a_{18} \frac{K^7}{\epsilon^6} (U_{i,k} U_{l,k} U_{l,m}^2 U_{j,m}^2 + U_{j,k} U_{l,k} U_{l,m}^2 U_{i,m}^2 - \frac{2}{3} \Pi_7 \delta_{ij})
\end{aligned}$$

$\Pi_1 = U_{i,k} U_{k,i}$ ,       $\Pi_2 = U_{i,k} U_{i,k}$ ,       $\Pi_3 = U_{i,k} U_{i,k}^2$ ,       $\Pi_4 = U_{i,k}^2 U_{i,k}^2$ ,  
 $\Pi_5 = U_{i,k} U_{l,k} U_{l,i}^2$ ,       $\Pi_6 = U_{i,k} U_{l,k}^2 U_{l,i}^2$ ,       $\Pi_7 = U_{i,k} U_{l,k} U_{l,m}^2 U_{i,m}^2$

The first five terms are of the same form as that of Yoshizawa (1984) and Rubinstein and Barton (1990).

- Realizable Algebraic Equation Model

$$\begin{aligned}
\bar{u}_i \bar{u}_j &= \frac{2}{3} K \delta_{ij} - \nu_t (U_{i,j} + U_{j,i}) \\
&\quad + \frac{C_{\tau 1}}{A_2 + \eta^3 + \xi^3} \frac{K^3}{\epsilon^2} (U_{i,k} U_{k,j} + U_{j,k} U_{k,i} - \frac{2}{3} \Pi \delta_{ij}) \\
&\quad + \frac{C_{\tau 2}}{A_2 + \eta^3 + \xi^3} \frac{K^3}{\epsilon^2} (U_{i,k} U_{j,k} - \frac{1}{3} \tilde{\Pi} \delta_{ij}) \\
&\quad + \frac{C_{\tau 3}}{A_2 + \eta^3 + \xi^3} \frac{K^3}{\epsilon^2} (U_{k,i} U_{k,j} - \frac{1}{3} \tilde{\Pi} \delta_{ij})
\end{aligned}$$

$$K_{,t} + [U_j K - (\nu + \frac{\nu_t}{\sigma_K}) K_{,j}]_{,j} = -\bar{u}_i \bar{u}_j U_{i,j} - \epsilon$$

$$\epsilon_{,t} + [U_j \epsilon - (\nu + \frac{\nu_t}{\sigma_\epsilon}) \epsilon_{,j}]_{,j} = -C_1 \frac{\epsilon}{K} \bar{u}_i \bar{u}_j U_{i,j} - C_2 \frac{\epsilon^2}{K}$$

where

$$\nu_t = \frac{2/3}{A_1 + \eta + \alpha\xi} \frac{K^2}{\epsilon}$$

$$\eta = \frac{KS}{\epsilon}, \quad S = (2S_{ij}S_{ij})^{1/2}, \quad S_{ij} = \frac{1}{2}(U_{i,j} + U_{j,i})$$

$$\xi = \frac{K\Omega}{\epsilon}, \quad \Omega = (2\Omega_{ij}^*\Omega_{ij}^*)^{1/2}, \quad \Omega_{ij}^* = \frac{1}{2}(U_{i,j} - U_{j,i}) + 4\epsilon_{mji}\omega_m$$

$$C_{\tau 1} = -4, C_{\tau 2} = 13, C_{\tau 3} = -2, A_1 = 5.5, \alpha = 0.1, A_2 = 1000.$$

$$C_1 = 1.44, \quad C_2 = 1.92, \quad \sigma_K = 1, \quad \sigma_\epsilon = 1.3$$

## Solution Procedure

- Conservative finite-volume method
- Non-staggered grids
- Momentum interpolation for velocity-pressure coupling
- Second-order accurate differencing schemes
- Quadratic terms in  $\bar{u}_i u_j$  treated as source
- Strongly implicit solution algorithm of Stone

## Performance in Complex Turbulent Flows

Diffuser flows

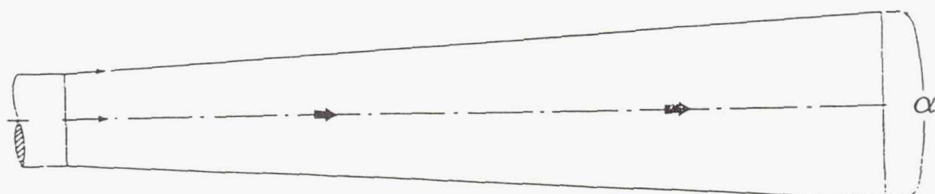
Backward-facing step flows

Confined jets

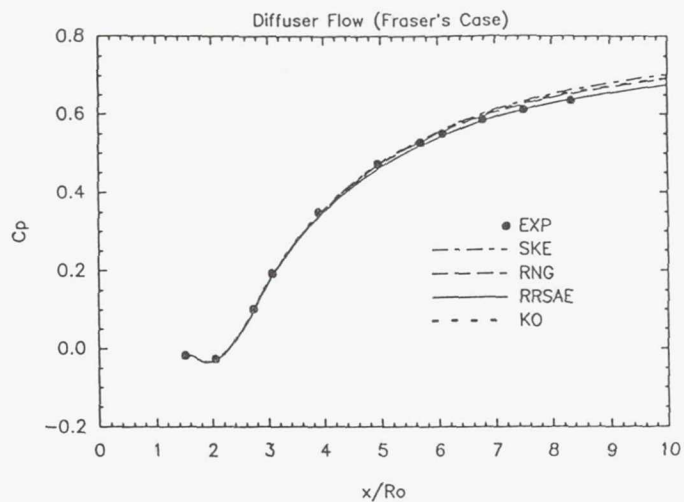
Confined swirling coaxial jets

### Diffuser flows

- Fraser's case,  $\alpha = 10^\circ$
- Trupp, Azad & Kassab's case,  $\alpha = 8^\circ$

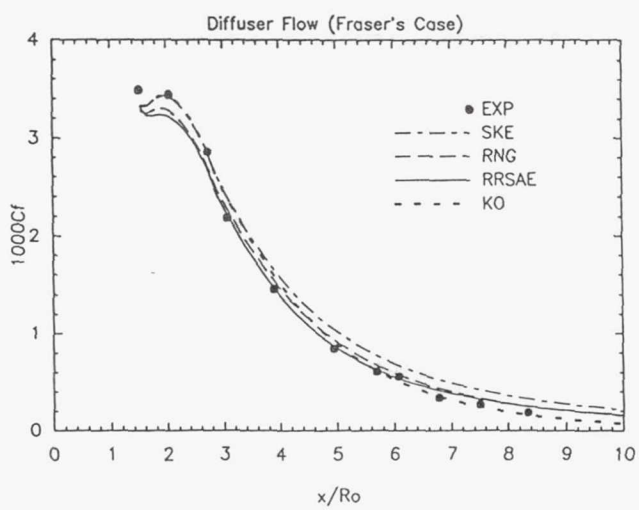


## Wall pressure

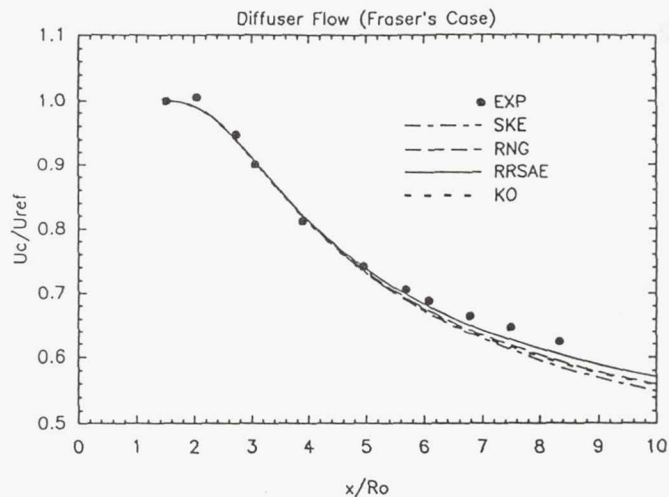


SKE : Standard  $K-\epsilon$  model  
RNG : RNG-based  $K-\epsilon$  model  
RRSAE : Present model  
KO :  $K-\omega$  model

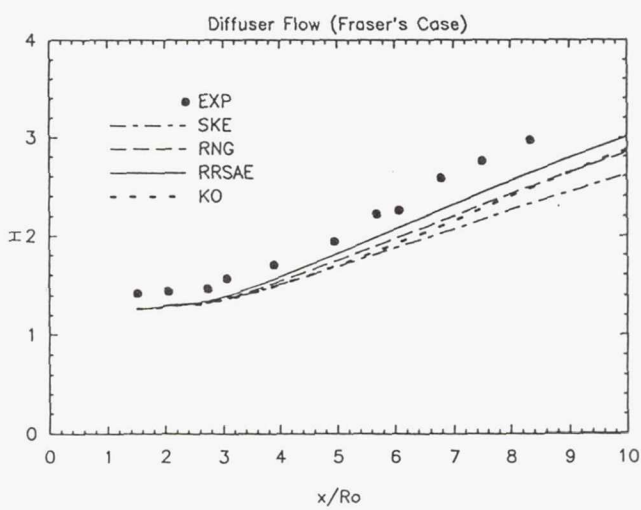
## Skin friction



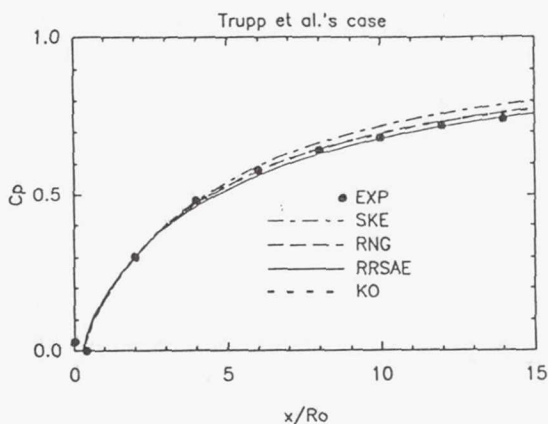
## Centerline velocity



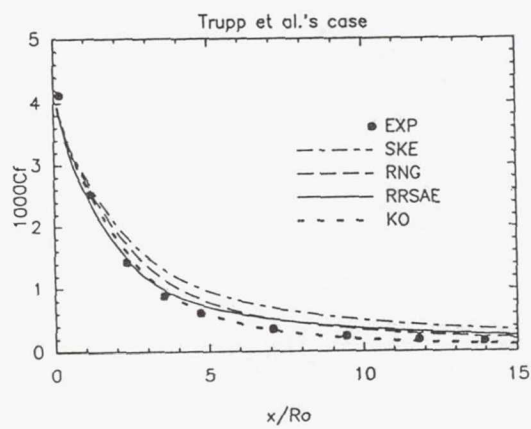
## Shape factor



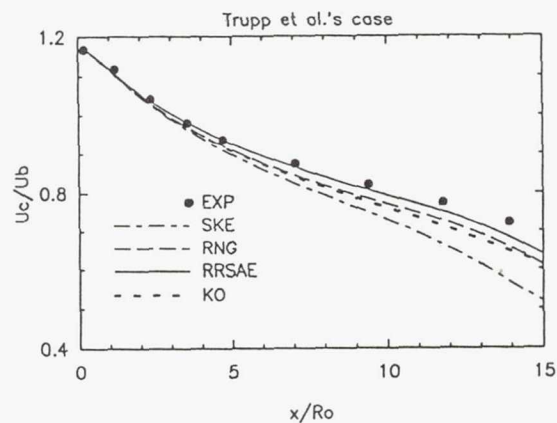
## Wall pressure



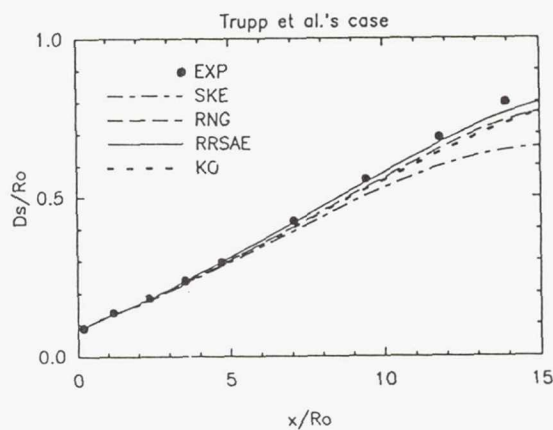
## Skin friction



## Centerline velocity

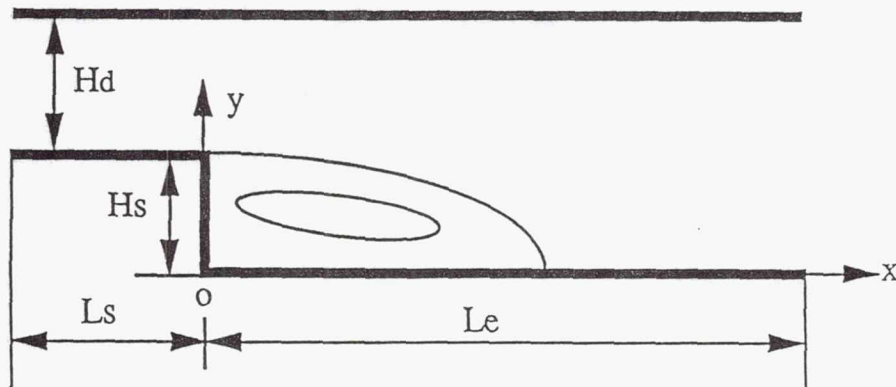


## Displacement thickness



## Backward-facing step flows

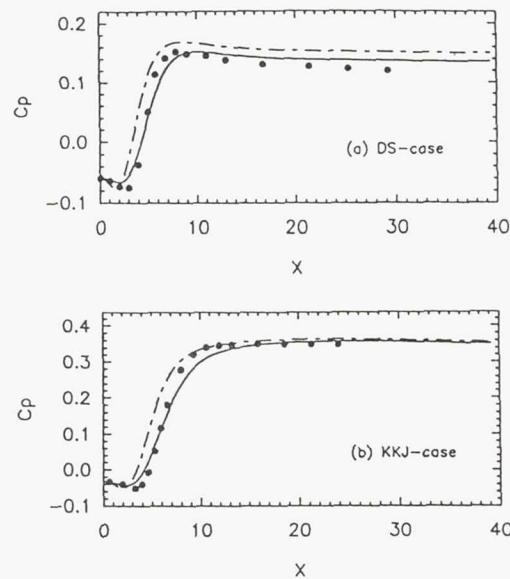
- Driver & Seegmiller's case,  $H_s/H_d = 1/8$
- Kim, Kline & Johnston's case,  $H_s/H_d = 1/2$



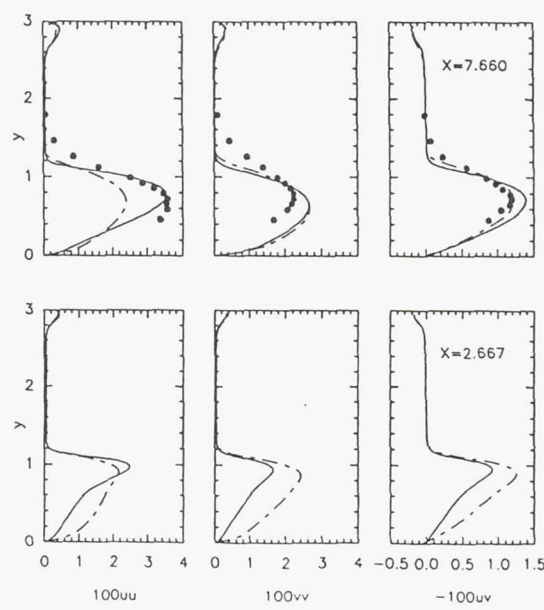
Comparison of reattachment points

case	experiment	K- $\epsilon$	present model	RSM	ASM
DS	6.1	4.99	5.82	-	5.66
KKJ	7 ± 0.5	6.35	7.35	6.44	-

## Wall pressure

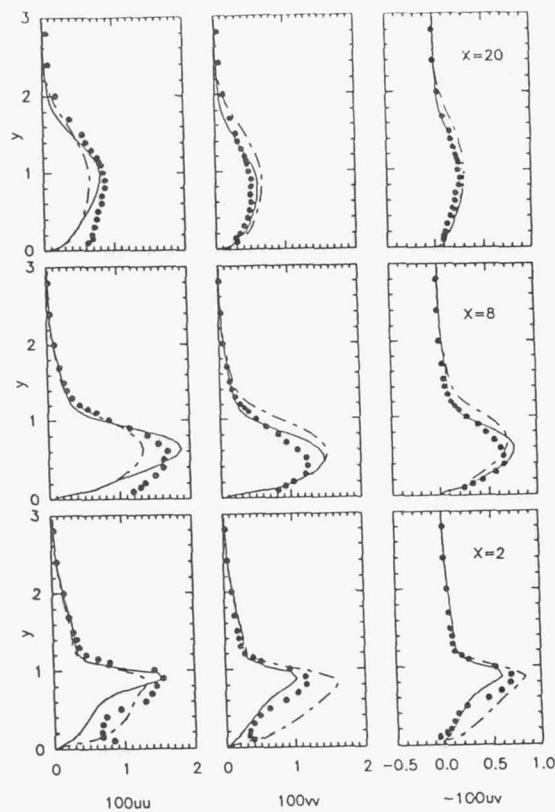


## Reynolds stresses (KKJ-case)



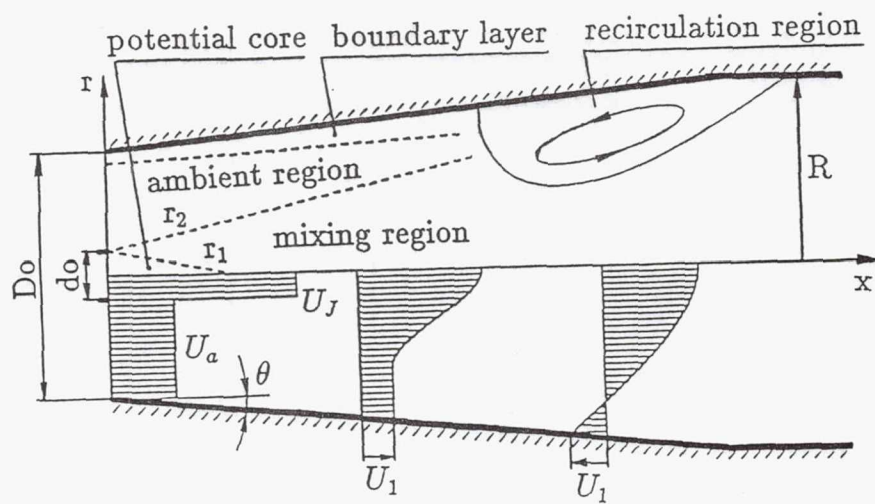
Reynolds stresses

(DS-case)

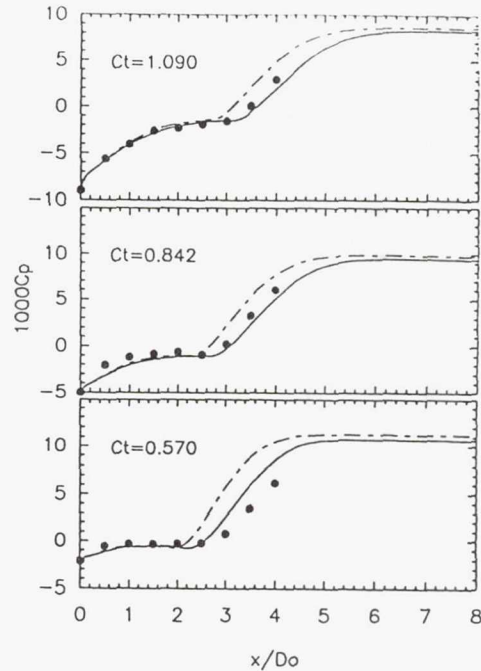
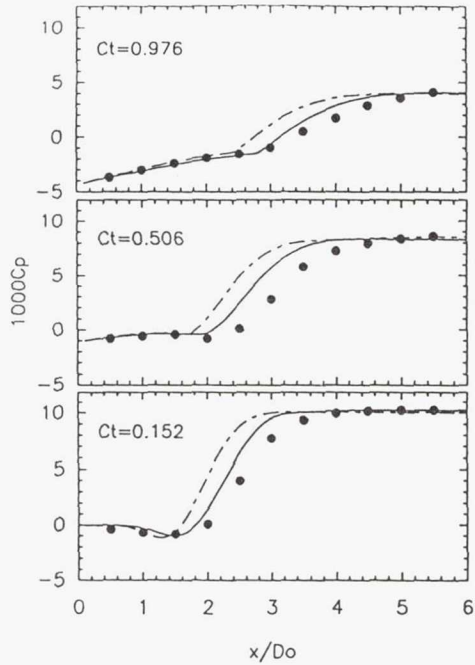


### Confined jets

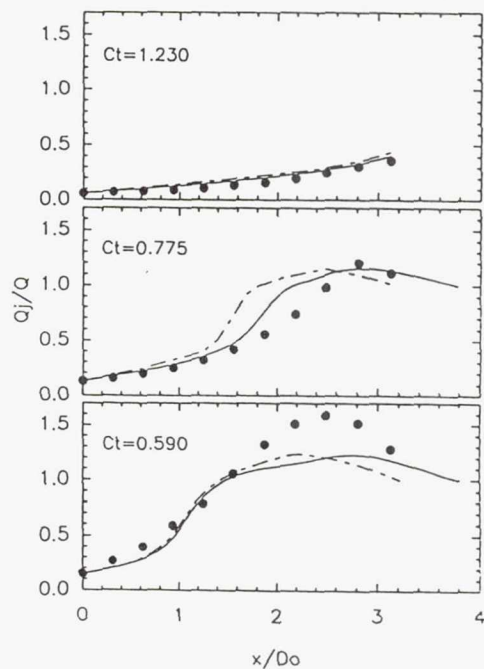
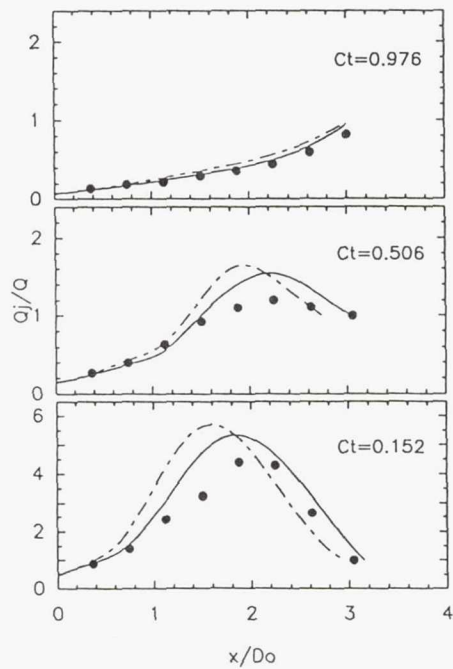
- Barchilon & Curtet's case,  $\theta = 0^\circ$
- Binder & Kian's case,  $\theta = 2.5^\circ$



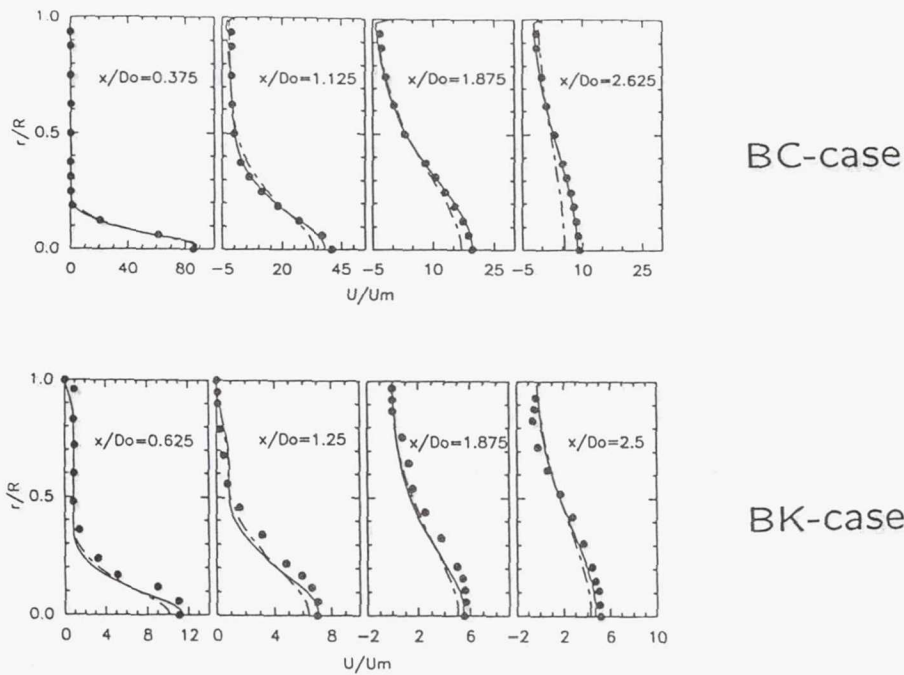
## Wall pressure



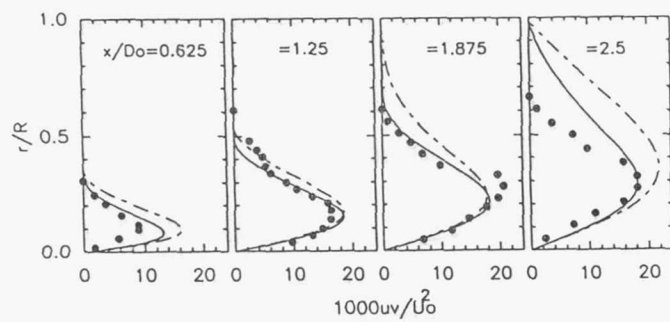
## Jet flow rate



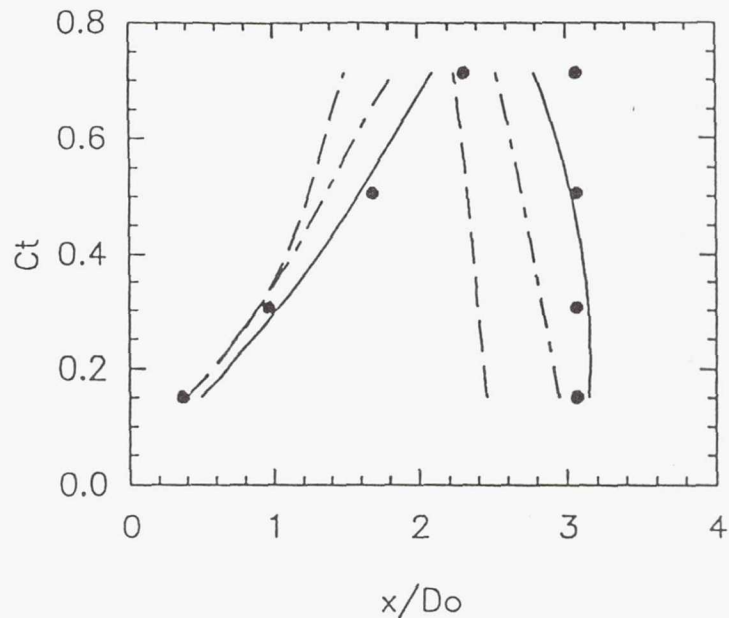
## Axial mean velocity profiles



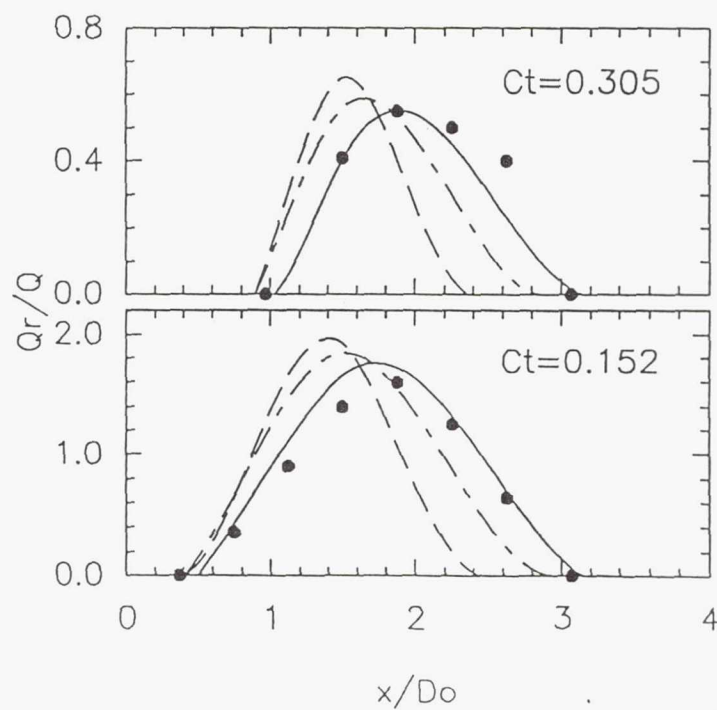
## Turbulent shear stress (BK-case)



Separation and reattachment points (BC-case)

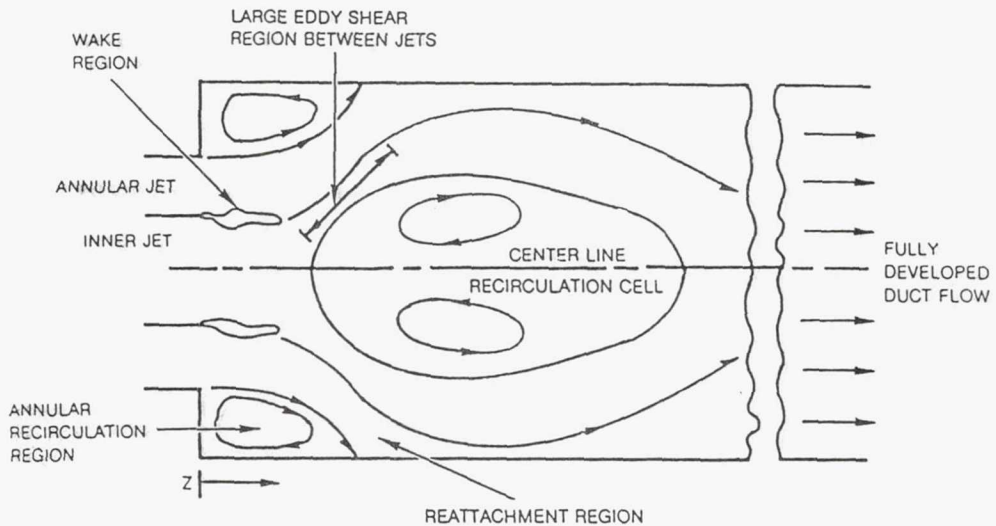


Recirculating flow rate (BC-case)

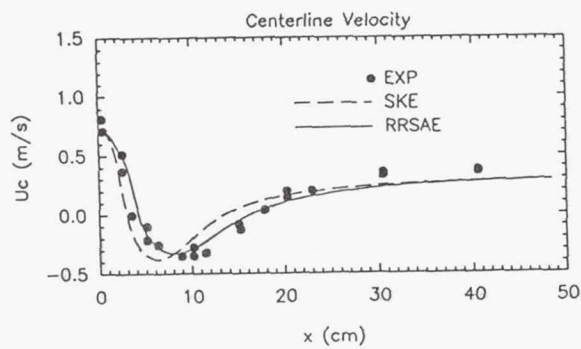


## Confined swirling coaxial jets

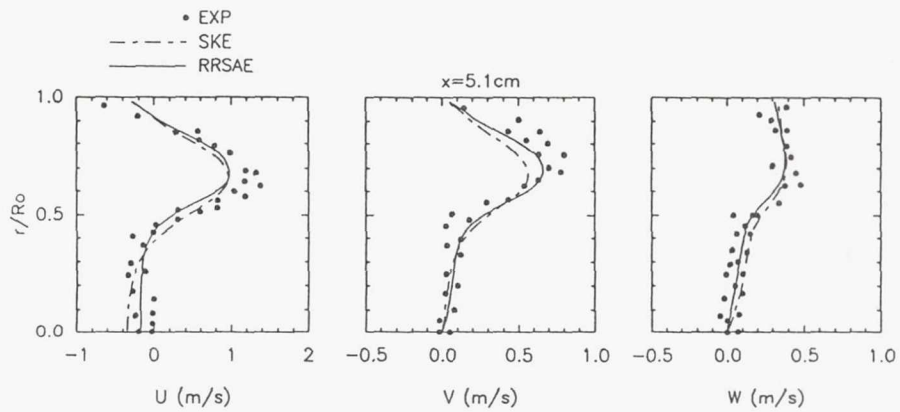
- Roback & Johnson's case



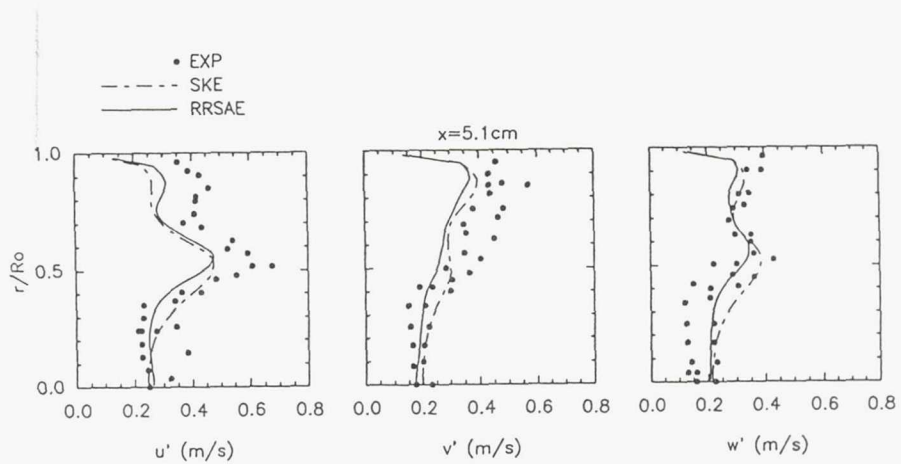
### Centerline velocity



## Mean velocity profiles ( $U$ , $V$ , $W$ )



## Turbulent intensity profiles ( $u'$ , $v'$ , $w'$ )



## Conclusions

- A general constitutive relation for  $\bar{u}_i \bar{u}_j$  has been derived
  1. Its quadratic form seems sufficient
  2. It is realizable
- It significantly improves the performance of  $K-\epsilon$  based models
- Easy to implement
  - No significant increase in computing time
  - Very robust

# ASSESSMENT AND DEVELOPMENT OF SECOND ORDER TURBULENCE MODELS

Presented by  
Aamir Shabbir

## MOTIVATION

- these models describe the effect of mean flow and external agencies (such as buoyancy) on the evolution of turbulence
- therefore, in principle, these models give a more accurate description of complicated flow fields than the two equation models
  - e.g flows with large anisotropy in turbulence (such as near the leading edge of a turbine blade)

## OBJECTIVE

- assess the performance of the various second order turbulence models in benchmark flows
- seek improvements where necessary
  - model for the pressure correlation term in the scalar flux equation
  - model for the scalar dissipation equation

## Transport Equations for Second Moments

$$\begin{aligned}\frac{D\bar{u}_i\bar{u}_j}{Dt} &= P_{ij} + \Pi_{ij} + T_{ij} - D_{ij} \\ \frac{D\bar{u}_i\bar{\theta}}{Dt} &= P_i + \Pi_i + T_i \\ \frac{D\bar{\theta}^2}{Dt} &= P + T - D\end{aligned}$$

These equations have to be closed by providing models for:

- Pressure correlation terms ( $\Pi_{ij}, \Pi_i$ )
- Transport (Diffusion) terms ( $T_{ij}, T_i$ )
- Dissipation terms ( $D_{ij}, D$ )

## HOW TO ASSESS MODELS ?

### Global computation

- Mean and turbulence equations are numerically solved

$$\bullet \quad \frac{D\bar{u}_i u_j}{Dt} = P_{ij} + \dots$$

•  
•  
•

- Results (e.g. Reynolds stresses) are then compared with experiments or DNS data

### Direct comparison

Individual terms in the turbulence equations (such as pressure correlation terms) are directly compared with experiment or DNS data

Note that:

- In experiments pressure correlation terms can not be measured but can only be obtained indirectly through balance of second moment equations
- DNS allows direct computation of these correlations but is limited to low Reynolds number

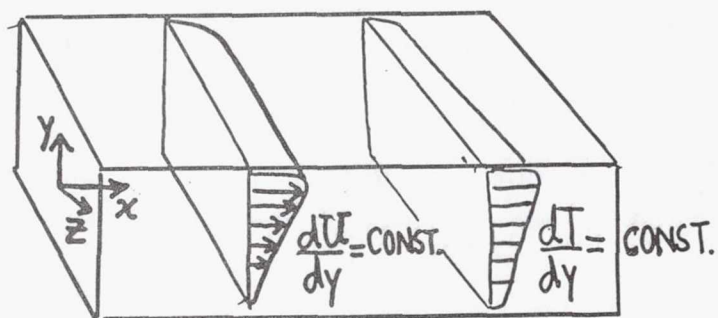
Most of the results to be shown in this presentation are direct comparisons

### Models for pressure correlation term in the scalar flux equation

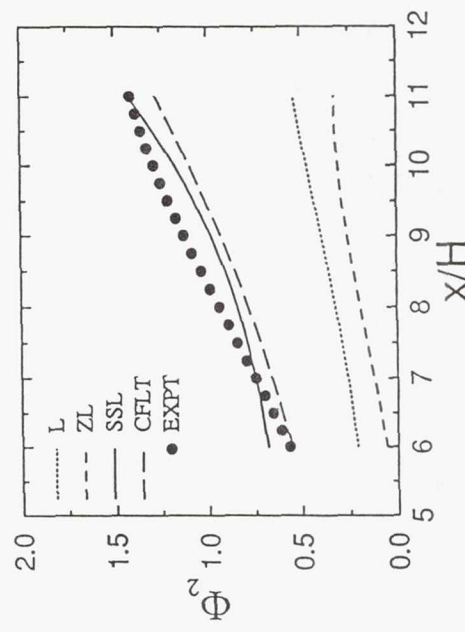
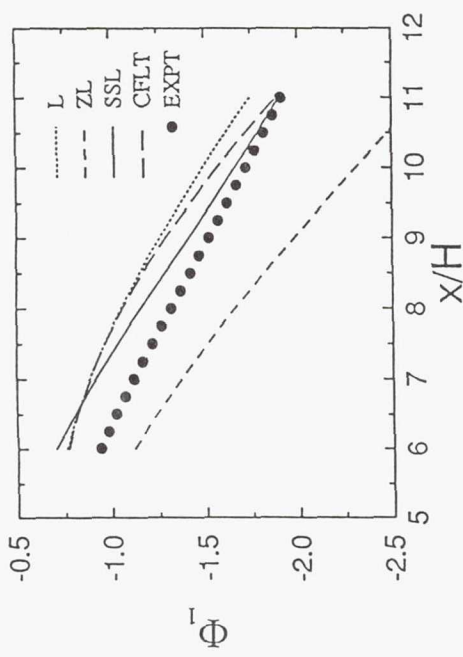
- a. Launder model (1975)
- b. Zeman and Lumley model (1976)
  - linear in scalar flux
  - do not satisfy realizability
- c. Shih, Shabbir and Lumley model (1985,1991)
- d. Craft, Fu, Launder, Tselepidakis model (1989)
  - linear in scalar flux and Reynolds stress
  - satisfy realizability

### Application to Homogeneous Shear Flow

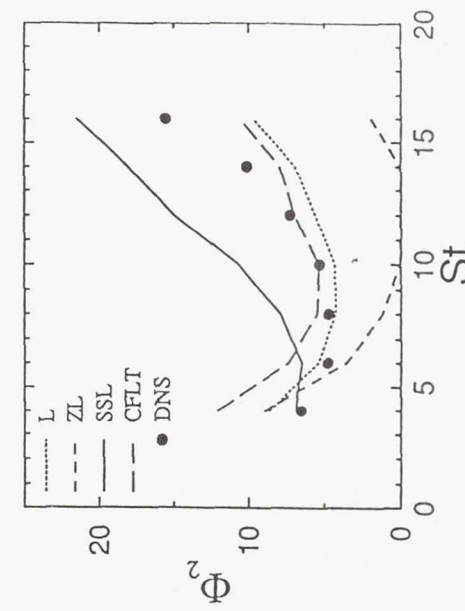
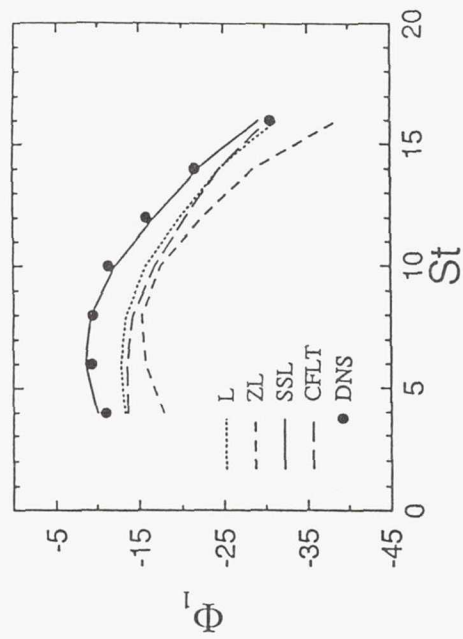
(Experiment as well as DNS data)



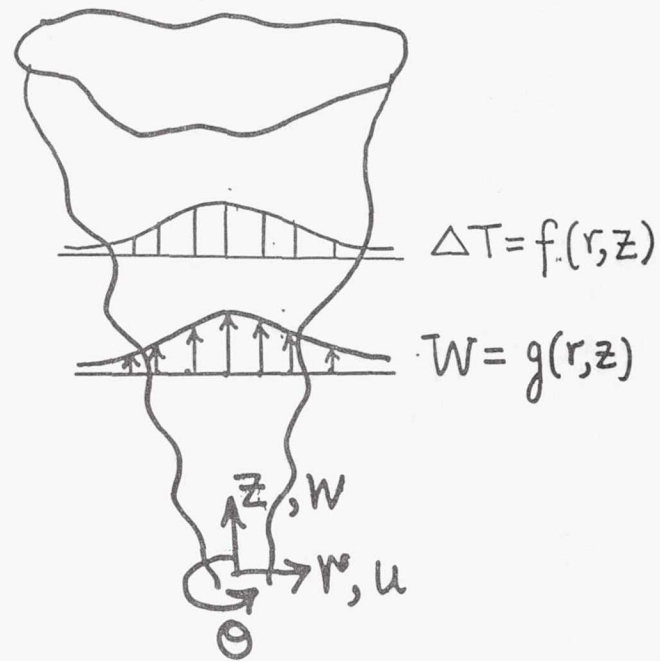
Tavoularis & Corrsin Expt (1981)



DNS Data of Rogers et al. (1986)

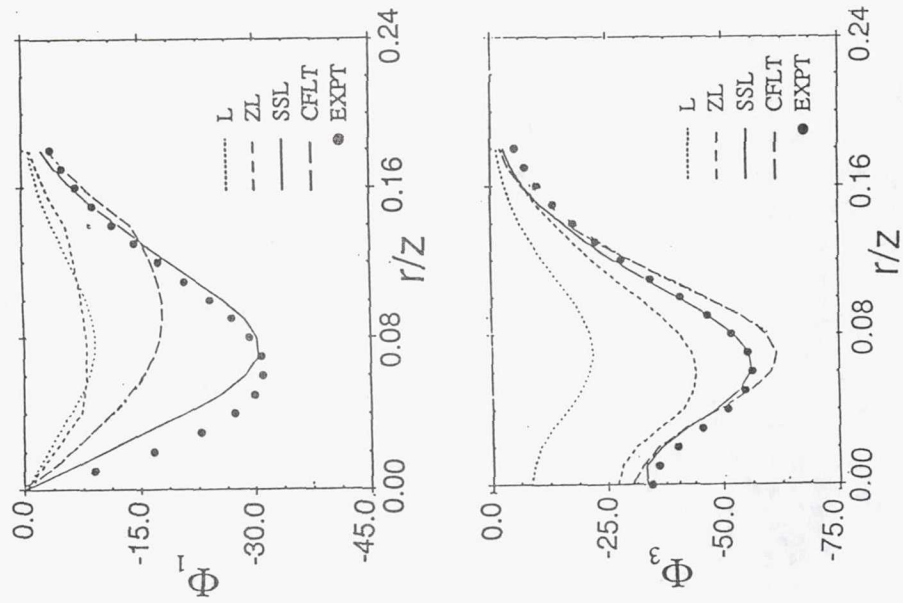


Application to Round Buoyant Plume Flow Experiment



10

Shabbir and George Expt. (1990)



60

## CONCLUSION

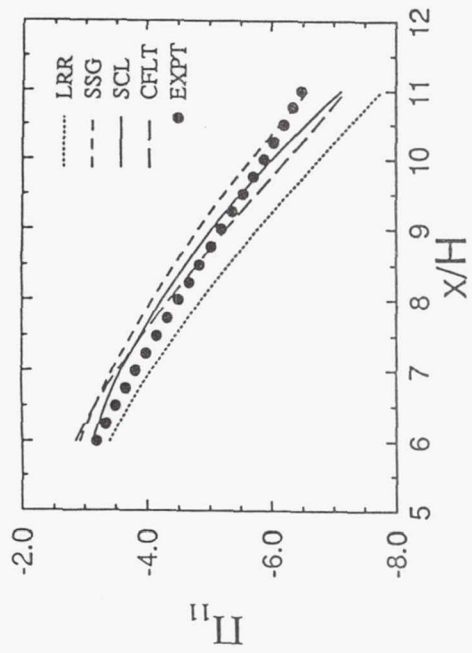
Models for pressure correlation term in scalar flux equation

- Models involving both scalar flux and Reynolds stress give better performance than the models which involve only scalar flux.

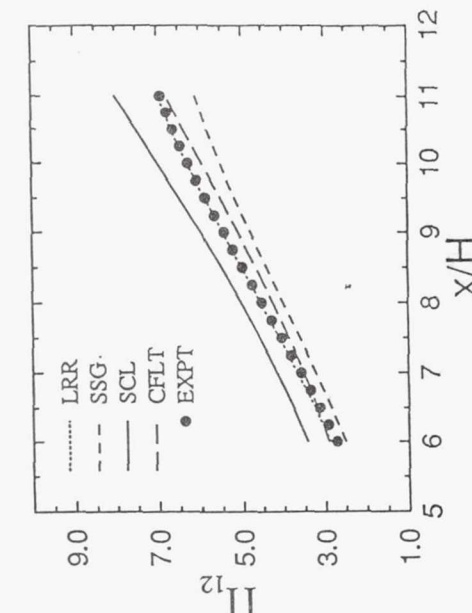
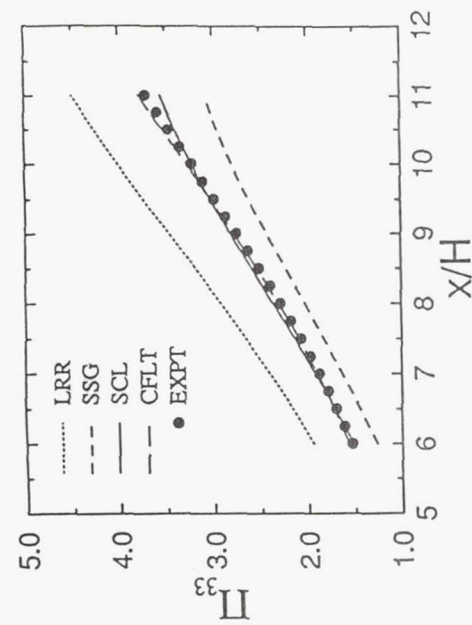
## Models for pressure correlation term in the Reynolds stress equation

- a. Launder, Reece, Rodi model (1975)
- b. Speziale, Sarkar and Gatski model (1991)
  - linear or quasi-linear in Reynolds stress
  - do not satisfy realizability
- c. Shih and Lumley model (1985)
- d. Craft, Fu, Launder, Tselepidakis model (1989)
  - nonlinear in Reynolds stress
  - satisfy realizability

Tavoularis & Corrsin Expt (1981)

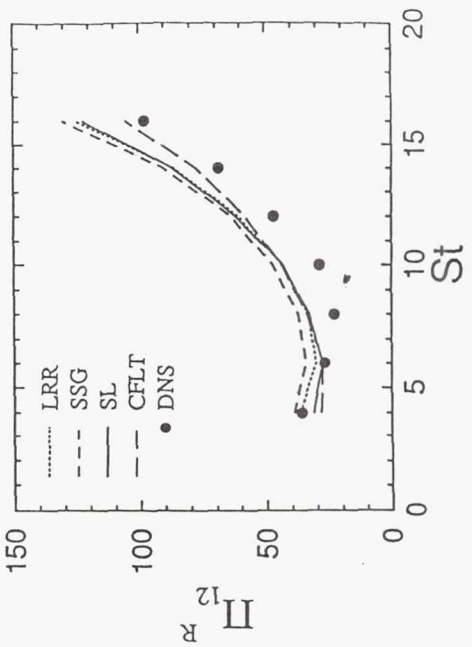
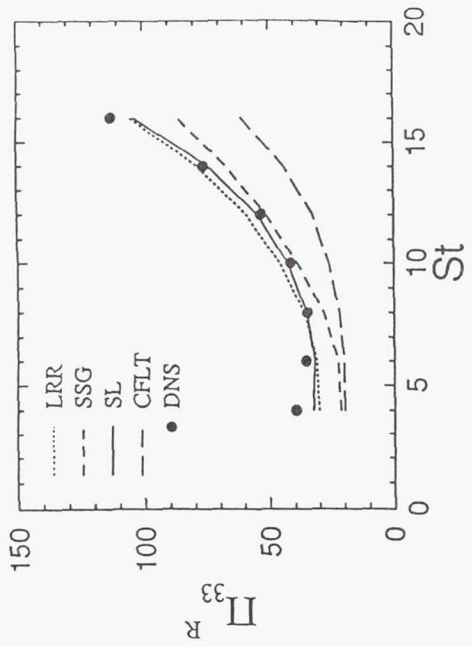
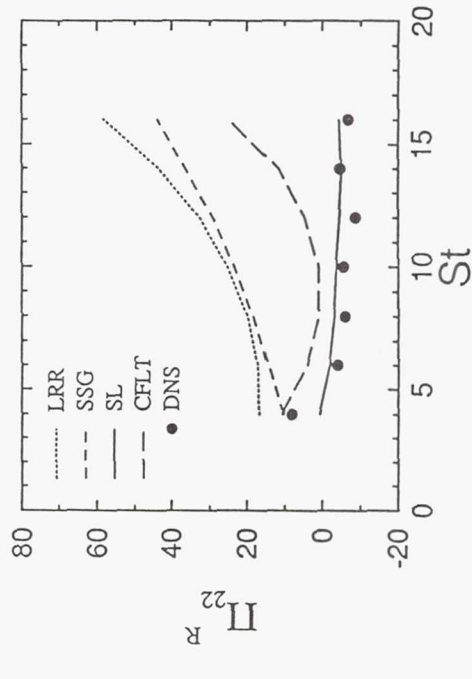
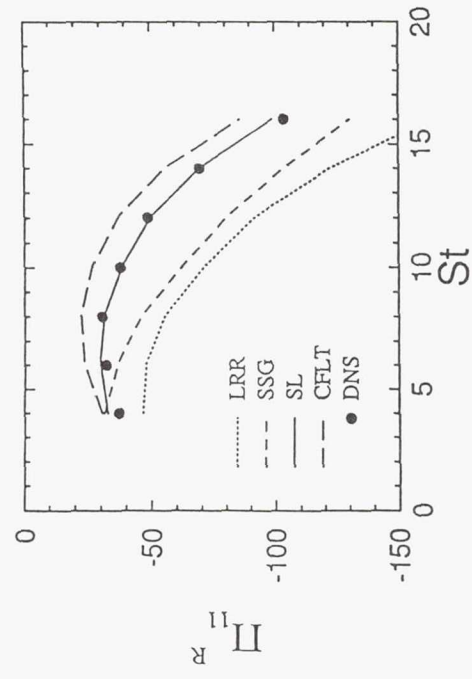


Tavoularis & Corrsin Expt (1981)

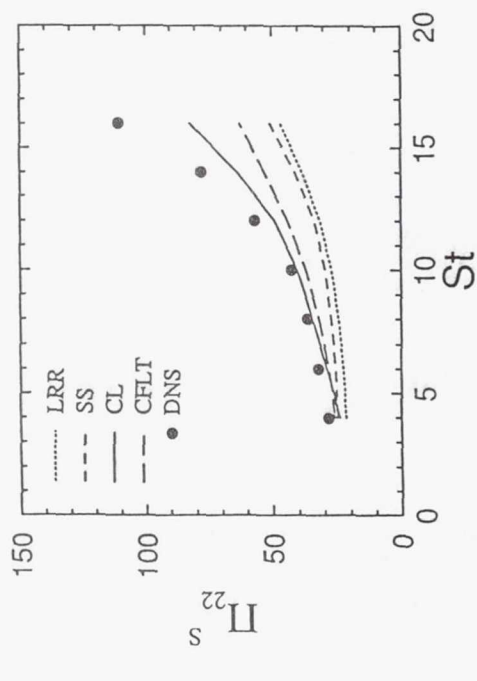
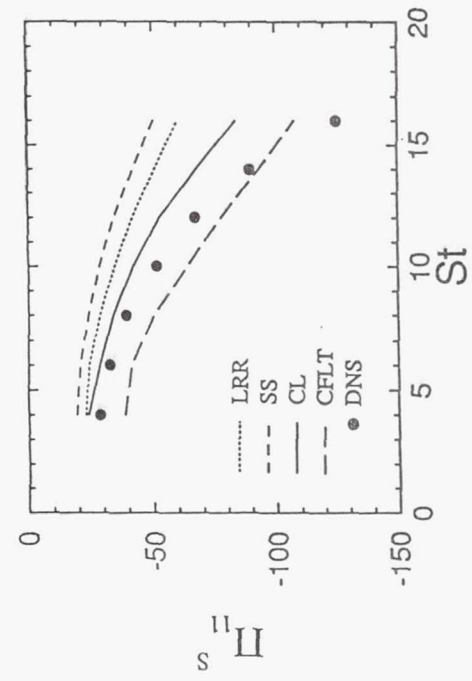


DNS Data of Rogers et al. (1986)

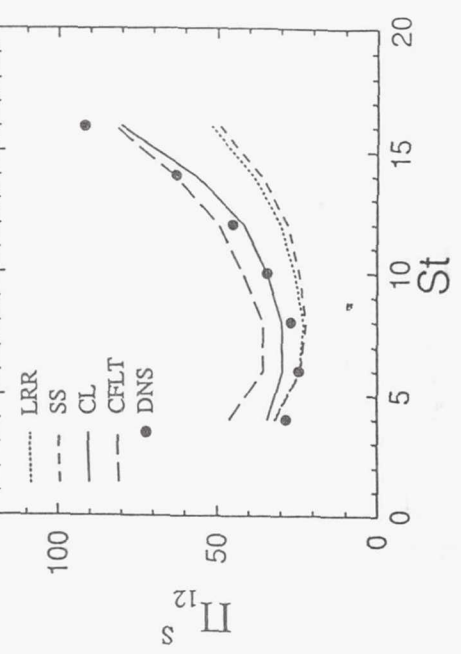
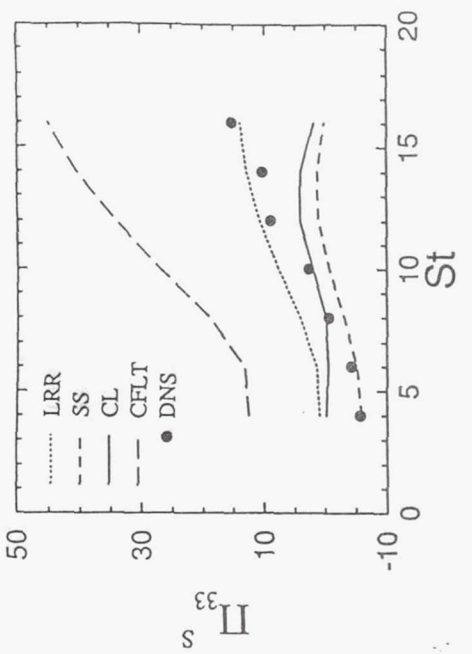
DNS Data of Rogers et al. (1986)



DNS Data of Rogers et al. (1986)



DNS Data of Rogers et al. (1986)



## CONCLUSION

Models for pressure correlation term in Reynolds stress equation

- For the DNS data non-linear models give better performance than linear models. However, for the experiment no single model performs better for all the components
- For the rapid part of the pressure correlation the relation

$$\Pi_{ij}^R = F(\bar{u}_i \bar{u}_j, U_{i,j}) \text{ is found to be adequate}$$

## CONCLUSION (contd.)

- Performance of all the slow pressure correlation models varies from one flow to another.
- Furthermore, the relation  $\Pi_{ij}^S = F(\bar{u}_i \bar{u}_j, k, \epsilon)$ , is inadequate in certain situations
  - DNS shows that  $\Pi_{ij}^S$  is dependent not only on the present time value of Reynolds stress but also on its past history
  - Definition of  $\Pi_{ij}^S$  implies that it is also a function of triple velocity moment  $\bar{u}_i \bar{u}_j \bar{u}_k$
- Therefore, more research is needed before any model for  $\Pi_{ij}^S$  can be recommended for use.

## A New Model Equation for Scalar Dissipation

- Traditional scalar dissipation rate equation is modeled in an analogue fashion to the mechanical dissipation equation
- Equation proposed here is modeled after the exact equation for scalar dissipation
- Its production/destruction mechanisms are different than the traditional model equation

## Application to Homogeneous Benchmark Flows

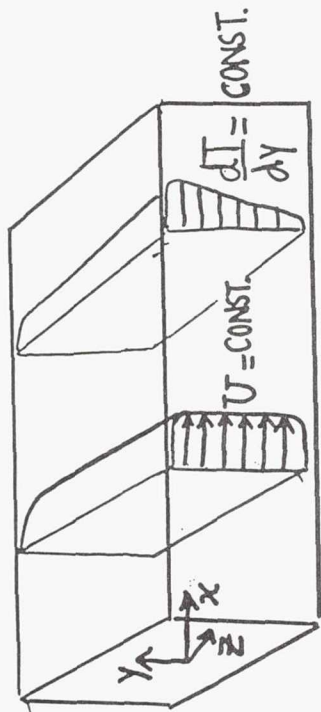
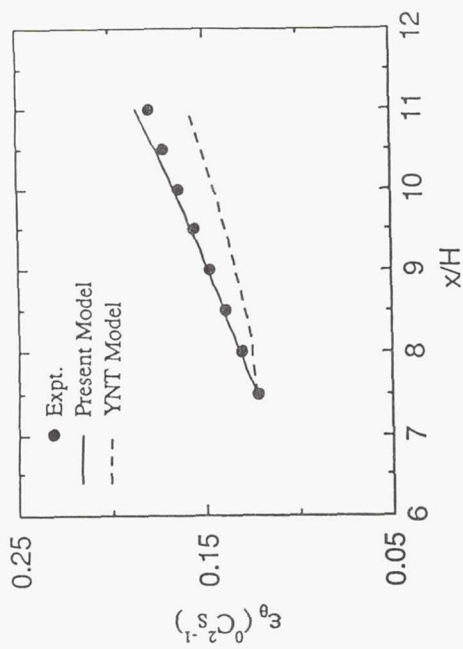
1. Homogeneous turbulence subjected to constant scalar gradient
2. Homogeneous turbulence subjected to constant scalar gradient and constant shear

Global computation of the following two equations

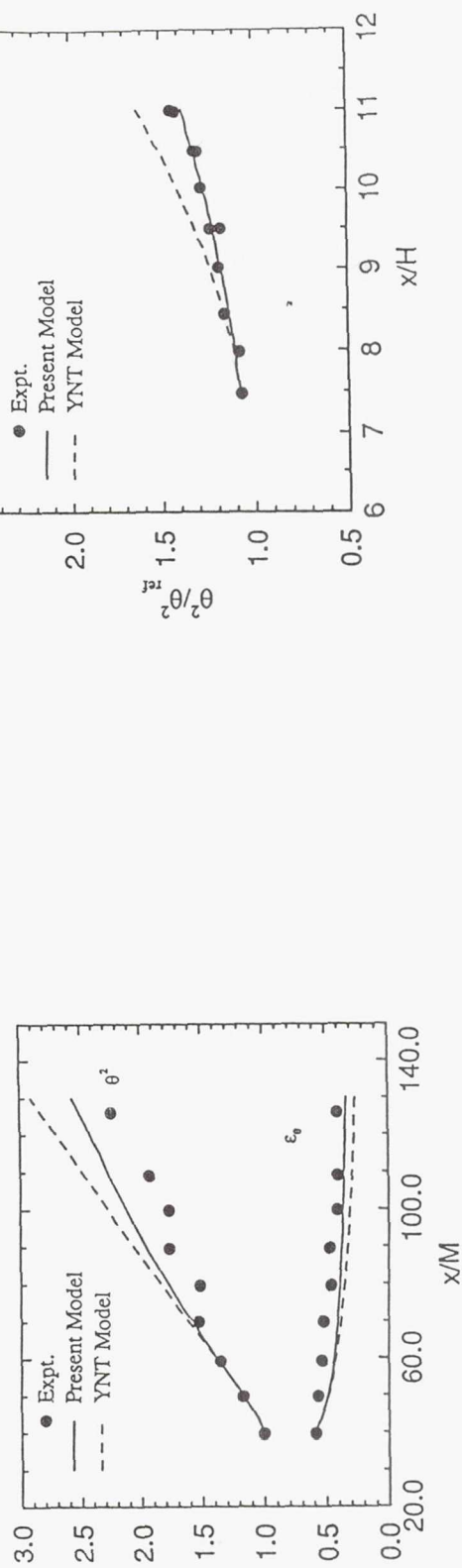
$$U_j \frac{\partial \overline{\theta^2}}{\partial x_j} = - 2\overline{u_i \theta} \frac{\partial T}{\partial x_i} - 2\epsilon_\theta$$
$$U_j \frac{\partial \epsilon_\theta}{\partial x_j} = C_{\theta 1} \epsilon_\theta S + C_{\theta 2} \frac{\sqrt{\epsilon_\theta \epsilon} \Phi}{\sqrt{Pr}} - C_{\theta 3} \frac{\epsilon_\theta \epsilon}{k}$$

Mechanical field (i.e.  $k$ ,  $\epsilon$ , etc.) and scalar flux,  $\overline{u_i \theta}$ , are taken as known. This way performance of the scalar dissipation equation is isolated.

Tavoularis & Corrsin Expt (1981)



Sirivat & Warhaft Expt (1983)



## CONCLUSION

- The transport equation for thermal dissipation rate proposed here gives improvement over the standard equation in at-least all the simpler benchmark flows. Its performance in the wall bounded flows is being assessed

# A Multiple-Scale Model for Compressible Turbulent Flows

presented by

William W. Liou

Workshop on Computational  
Turbulence Modeling

September 15–16, 1993

## Outline

- Motivation
- Model Development
  - formulation and determination of model coefficients
- Model Predictions:
  - compressible shear layer
  - compressible boundary layer
- Concluding Remarks

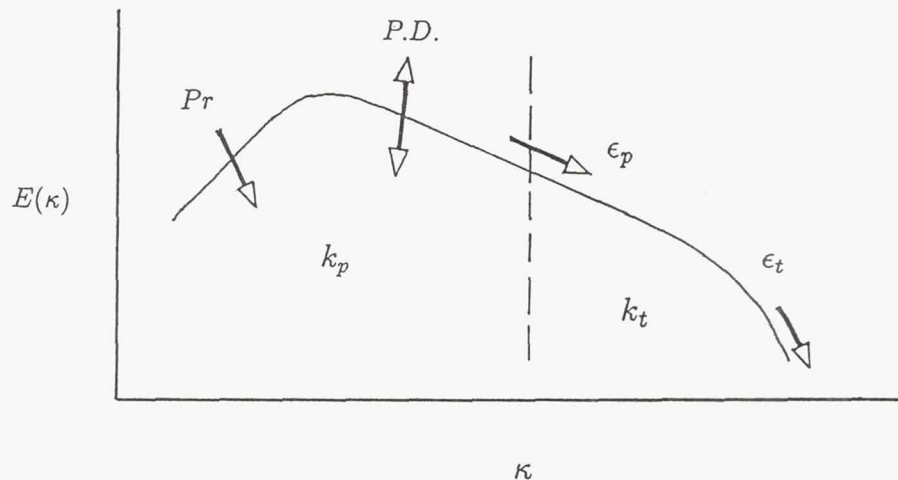
## Motivation

- Incorporate the effects of non-equilibrium energy spectrum of compressible turbulence in computational models

## DNS of Compressible Turbulence

- formation of high gradient regions or eddy shocklets
- enhanced vortex stretching and spectral energy transfer
- non-equilibrium turbulent kinetic energy spectrum due to the flow compressibility

## Multiple-Scale Model



## Model Equations

Large Scale

$$\bar{\rho} \frac{\overline{D}\tilde{k}_p}{\overline{D}t} = \frac{\partial}{\partial y} \left[ (\bar{\mu} + \frac{\mu_T}{\sigma_{\tilde{k}_p}}) \frac{\partial \tilde{k}_p}{\partial y} \right] + \mu_T \left( \frac{\partial \tilde{u}}{\partial y} \right)^2 - \bar{\rho} \tilde{\epsilon}_p + fc_1$$

$$\bar{\rho} \frac{\overline{D}\tilde{\epsilon}_p}{\overline{D}t} = \frac{\partial}{\partial y} \left[ (\bar{\mu} + \frac{\mu_T}{\sigma_{\tilde{\epsilon}_p}}) \frac{\partial \tilde{\epsilon}_p}{\partial y} \right] + C p_1 \frac{\tilde{\epsilon}_p}{\tilde{k}_p} \mu_T \left( \frac{\partial \tilde{u}}{\partial y} \right)^2 - C p_2 \bar{\rho} \frac{\tilde{\epsilon}_p^2}{\tilde{k}_p} + fc_2$$

- $fc_1$  – exchanges between the turbulent kinetic energy and internal energy
- $fc_2$  – increased spectral energy transfer due to eddy-shocklets

## Model Equations (cont.)

### Small Scale

$$\begin{aligned}\bar{\rho} \frac{\overline{D\tilde{k}_t}}{Dt} &= \frac{\partial}{\partial y} [(\bar{\mu} + \frac{\mu_T}{\sigma_{\tilde{k}_t}}) \frac{\partial \tilde{k}_t}{\partial y}] + \bar{\rho} \tilde{\epsilon}_p - \bar{\rho} \tilde{\epsilon}_t \\ \bar{\rho} \frac{\overline{D\tilde{\epsilon}_t}}{Dt} &= \frac{\partial}{\partial y} [(\bar{\mu} + \frac{\mu_T}{\sigma_{\tilde{\epsilon}_t}}) \frac{\partial \tilde{\epsilon}_t}{\partial y}] + Ct_1 \bar{\rho} \frac{\tilde{\epsilon}_t \tilde{\epsilon}_p}{\tilde{k}_t} - Ct_2 \bar{\rho} \frac{\tilde{\epsilon}_t^2}{\tilde{k}_t}\end{aligned}$$

### Eddy Viscosity

$$\mu_T \approx \bar{\rho} u l \approx \bar{\rho} (\tilde{k}_p + \tilde{k}_t)^{\frac{1}{2}} \frac{(\tilde{k}_p + \tilde{k}_t)^{\frac{3}{2}}}{\tilde{\epsilon}_p}$$

## Model Coefficients

### Decaying turbulence and homogeneous turbulence

$$\begin{aligned}Cp_1 &= (1 - \frac{\beta}{\alpha}) + \frac{\beta}{\alpha} Cp_2, \quad Cp_2 = \frac{n+1}{n} \\ Ct_1 &= 1 - \frac{1}{\beta} + \frac{Ct_2}{\beta}, \quad Ct_2 = \frac{\beta - 1 + Cp_2 \beta \frac{\tilde{k}_t}{k_p}}{\beta + \beta \frac{\tilde{k}_t}{k_p} - 1}\end{aligned}$$

$C_\mu$	$\sigma_{\tilde{k}_p}$	$\sigma_{\tilde{k}_t}$	$\sigma_{\tilde{\epsilon}}$	$\sigma_{\tilde{\epsilon}}$	$n$	$\alpha$	$\beta$
0.09	1.0	1.0	1.3	1.3	1.2	2.2	1.05

## Model Equations (cont.)

### □ Large Scale

- $\mathbf{fc}_1$  - Sarkar *et al.* (1992)

$$\mathbf{fc}_1 = -\alpha_2 M_t \mu_T \left( \frac{\partial \tilde{u}}{\partial y} \right)^2 + \alpha_3 M_t^2 \bar{\rho} \tilde{\epsilon}_p$$

- $\mathbf{fc}_2$  - dimensional analysis

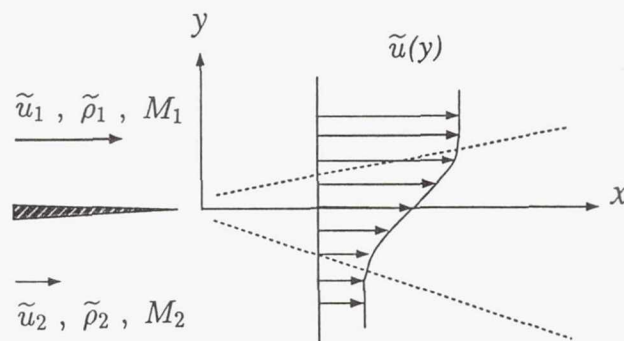
$$\mathbf{fc}_2 \equiv \mathbf{fc}_2(\bar{p}, \bar{\rho}, \tilde{k}, \tilde{\epsilon}, \bar{\mu})$$

$$\Pi_1 = \frac{\bar{p}}{\bar{\rho} \tilde{k}} = \frac{1}{\gamma M_t^2}, \quad \Pi_2 = \frac{\bar{\mu} \tilde{\epsilon}}{\bar{\rho} \tilde{k}^2} = \frac{1}{Re_t}$$

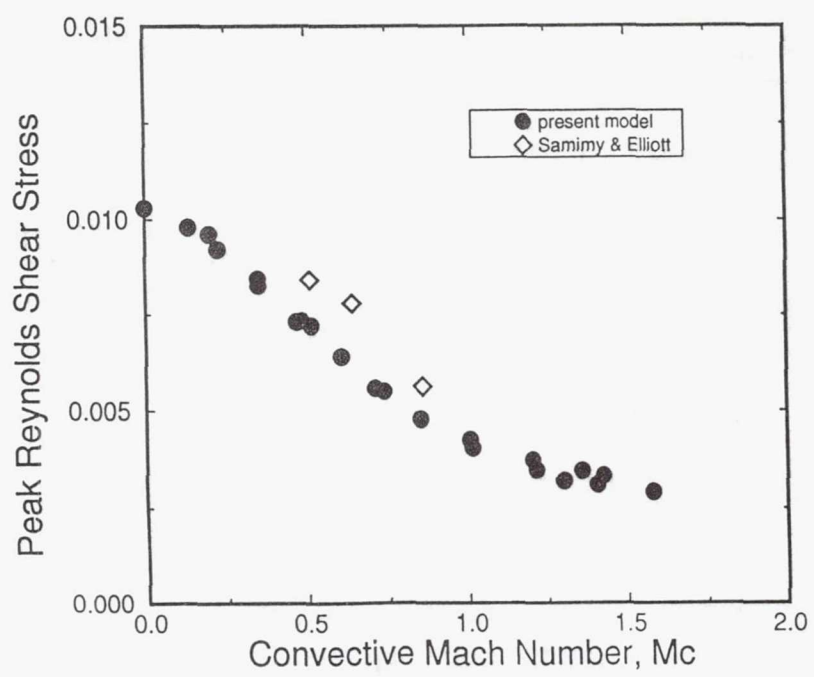
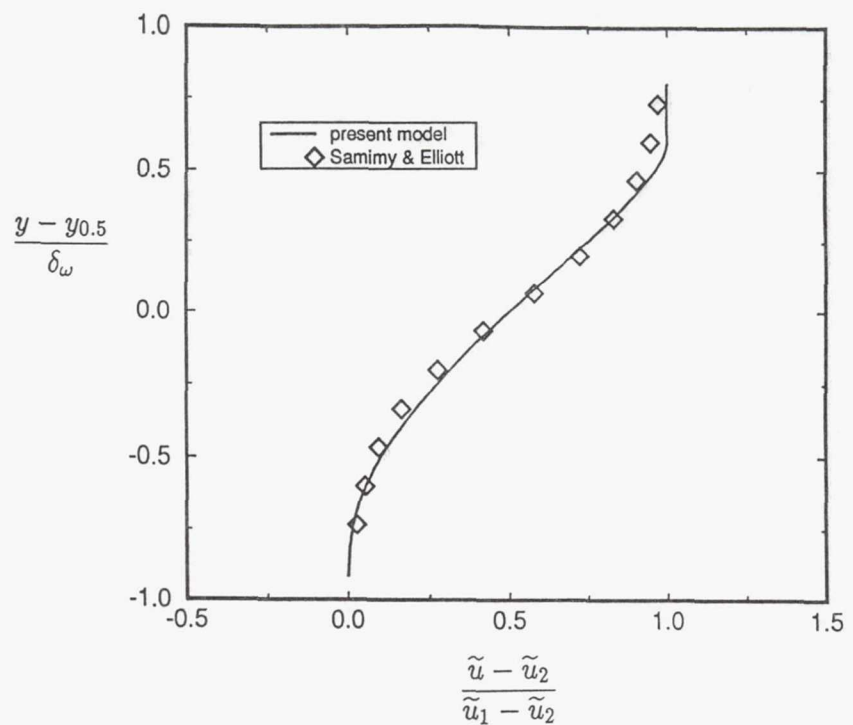
$$\mathbf{fc}_2 = b_1 + b_2 M_t^2 + O(M_t^4)$$

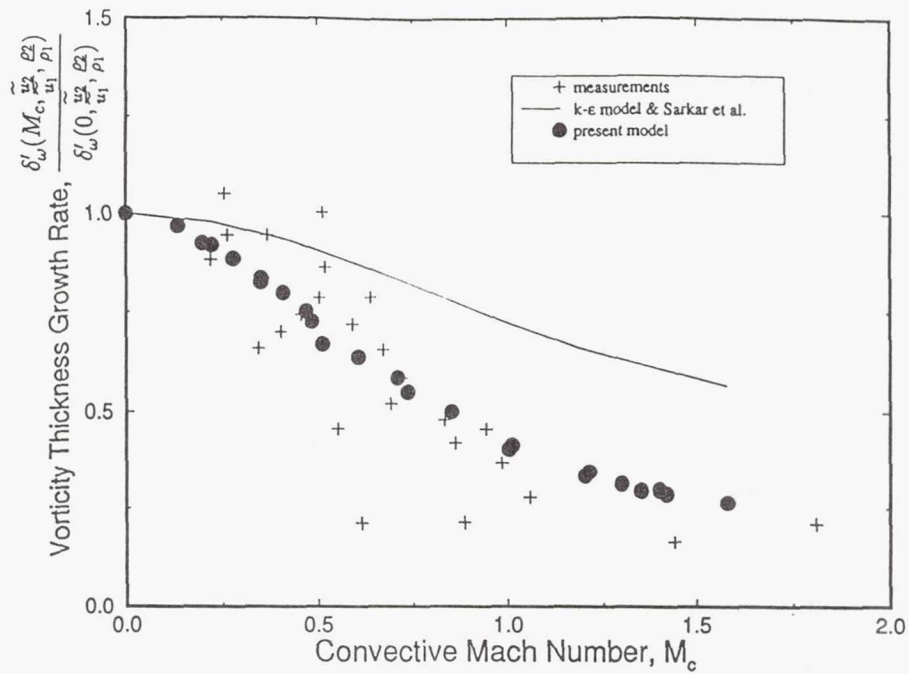
## Model Predictions

### □ Compressible Free Shear Layers



- mean velocity profiles.  $M_c=0.51$
- peak Reynolds shear stresses.  $M_c=0\sim 1.6$
- vorticity thickness growth rates





## Multiple-Scale Model

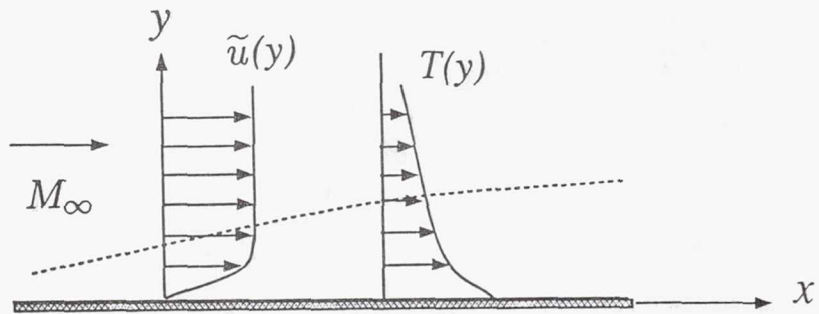
### Wall Function

$$\frac{u_c}{u^+} = \frac{1}{\kappa} \ln (y^+) + 5.2, \quad q_w = -\frac{\mu_t C_p}{Pr_t} \frac{dT}{dy} + u \tau_w$$

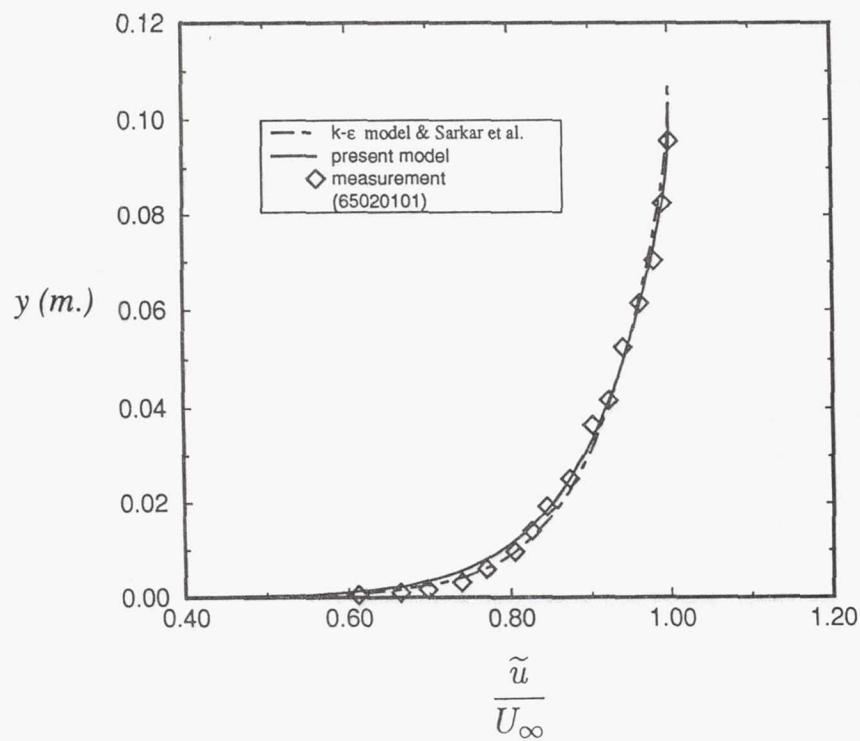
$$\tilde{k} = (\frac{\tau_w}{\rho})/0.3, \quad \tilde{\epsilon} = \frac{(\tau_w/\rho)^{3/2}}{\kappa y}$$

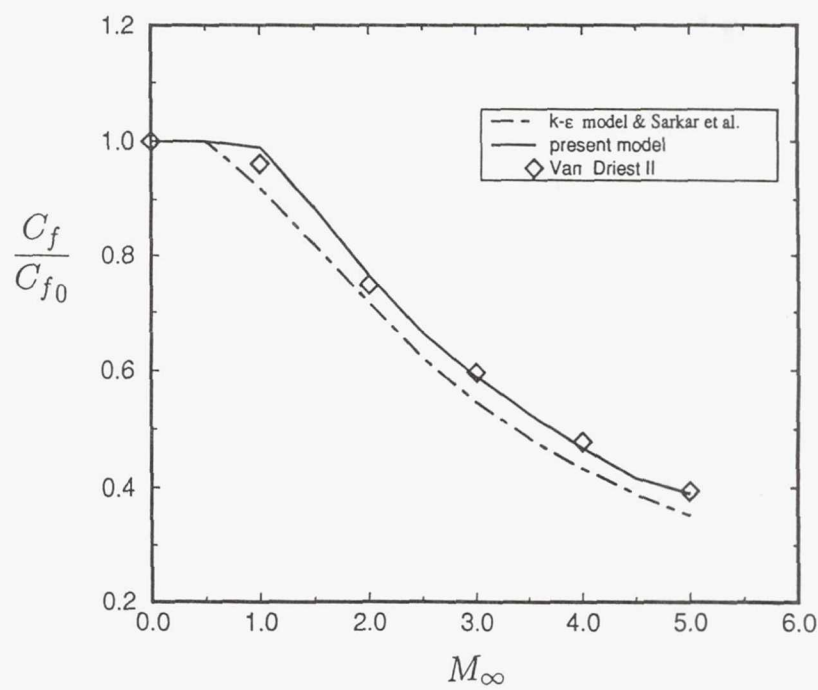
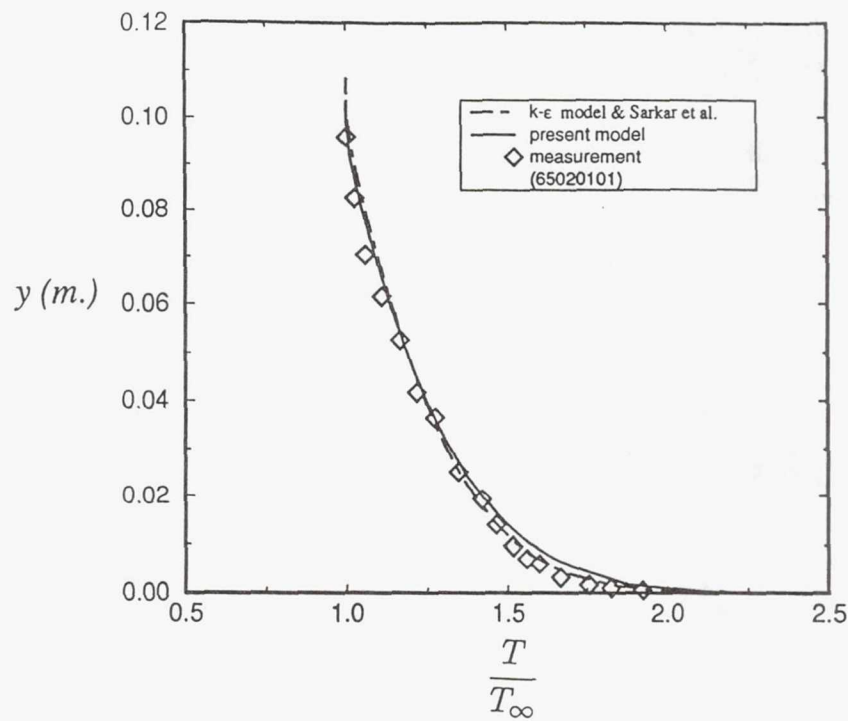
## Model Predictions

### □ Compressible Boundary Layers



- mean velocity profiles.  $M_\infty=2.831$ ,  $Re_\theta=420,700$
- mean temperature profiles.
- skin friction coefficients.  $M_\infty=0\sim 5$ ,  $Re_\theta=10^4$





## Concluding Remarks

- The present compressible multiple-scale model predicts correctly both the spreading rate of compressible shear layers and the skin friction coefficient of compressible boundary layers.
- Need to implement the model into the calculation of more complex compressible turbulent flows.

# PDF TURBULENCE MODELS FOR REACTIVE FLOWS

Presented by

A.T. Hsu

## OUTLINE

1. Motivation: why PDF
2. Works acomplished:
  - . Model development.
  - . Numerical results.
3. Future studies

## CLOSURE PROBLEM:

$$u_i = \bar{u}_i + u'_i,$$

$$Y_i = \bar{Y}_i + Y'_i,$$

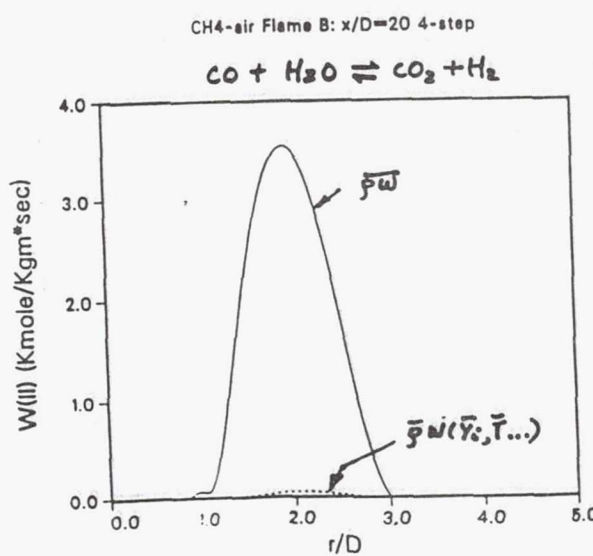
- $\overline{u''_i u''_j}$  — Turbulence Modeling
- $\overline{Y''_i u''_j}$  — Analogy of shear stress: diffusion model.
- $\overline{\rho w_i}$  — ???

$$\rho w_i = \rho w(Y_1, \dots, Y_n, T, \rho)$$

But in general:

$$\overline{\rho w_i} \neq \rho w(\bar{Y}_1, \dots, \bar{Y}_n, \bar{T}, \bar{\rho})$$

## EXAMPLE: REACTION RATE FROM MEAN TEMPERATURE



## PDF Method - Motivation

Avoid Chemical Closure Problem

- Probability Density Function  $P(Y_1, \dots, Y_n, T, \rho)$

$$\overline{\rho w_i} = \int \cdots \int \rho w_i(Y_1, \dots, Y_n, T, \rho) P(Y_1, \dots, Y_n, T, \rho) dY_1 \dots dY_n d\rho$$

$$\overline{Y_i} = \int \cdots \int Y_i P(Y_1, \dots, Y_n, T, \rho) dY_1 \dots dY_n d\rho$$

- Direct Solution of  $P(Y_1, \dots, Y_n, T, \rho)$

## WORK ACCOMPLISHED

Developed continuous mixing model.

Developed compressible flow pdf model that can treat flows with shocks.

Developed 2D and 3D Monte Carlo pdf solvers.

Coupled pdf solver with the RPLUS code and made calculations on realistic combustion problems.

## PDF-CFD COUPLING

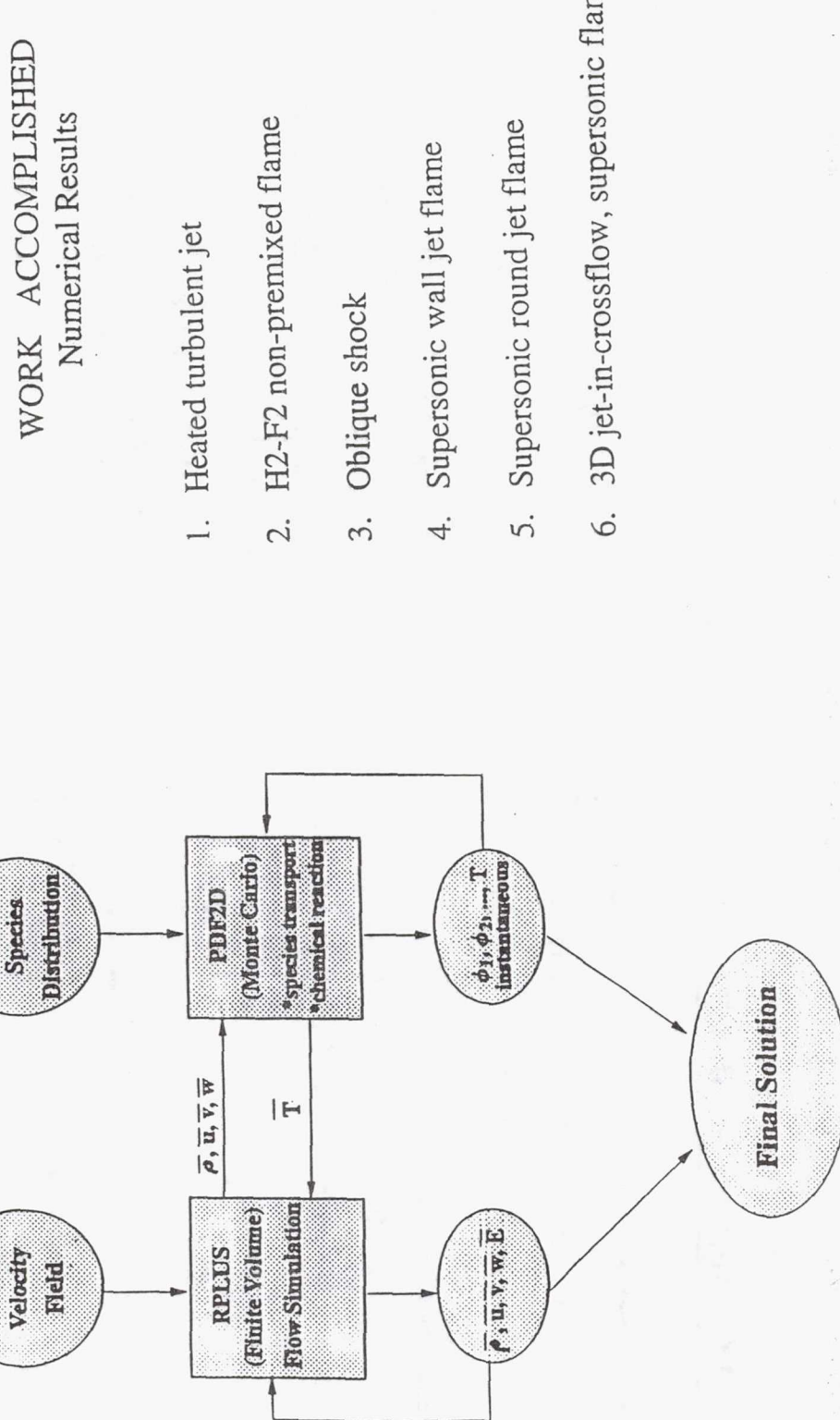
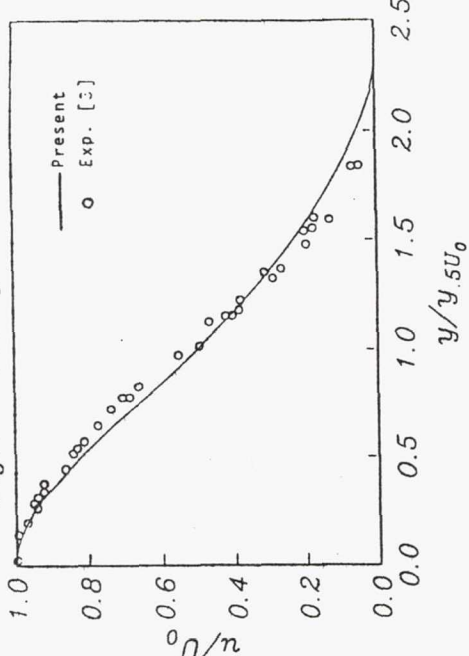


Fig. 4 Velocity distribution



## III. Results

(U) The sketch of a heated plane jet is given on this page. The flow domain is divided into 30 cells in the cross direction, and 100 samples are assigned to each cell. The numerical results from the present study are compared with experimental data in the following figures.

Fig. 5 Turbulent shear stress

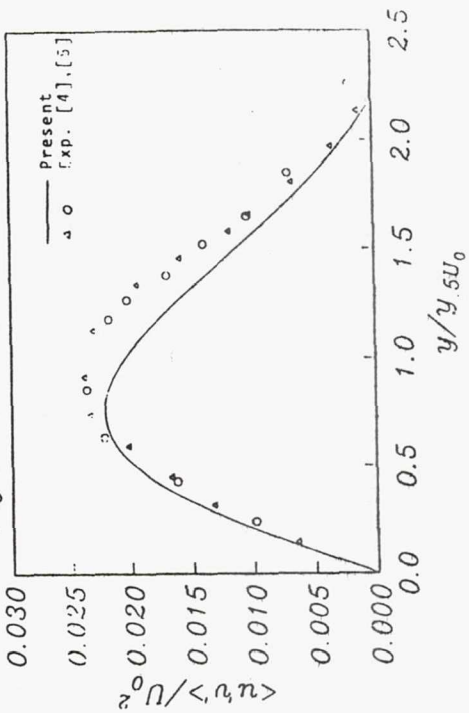
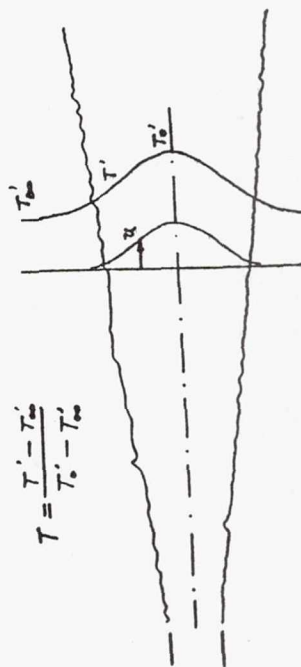


Figure 1. Sketch of a heated turbulent free jet.



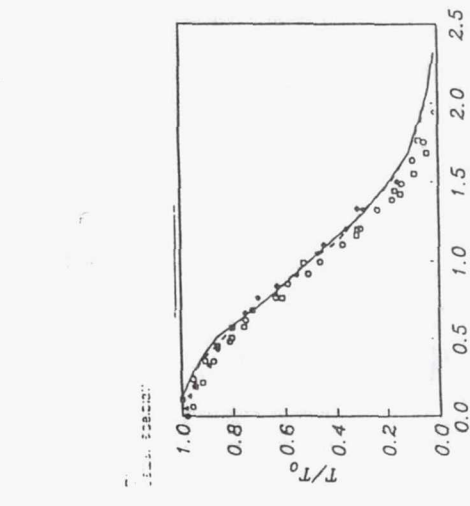


Figure 5. Mean temperature in heated plane jet. — continuous mixing model, - - - modified Curl model,  $\Delta$  Brown et al. (1984),  $\square$  Bashir and Uberoi (1973),  $\circ$  Uberoi and Singh (1975),  $\circ$  Jenkins and Goldschmidt (1973).

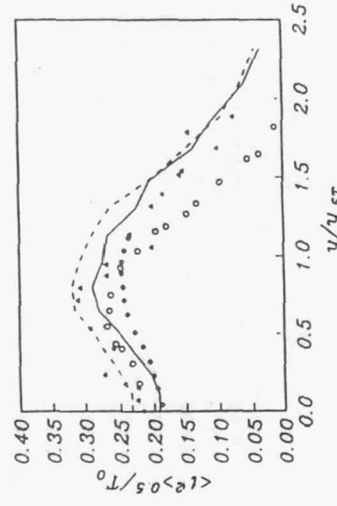
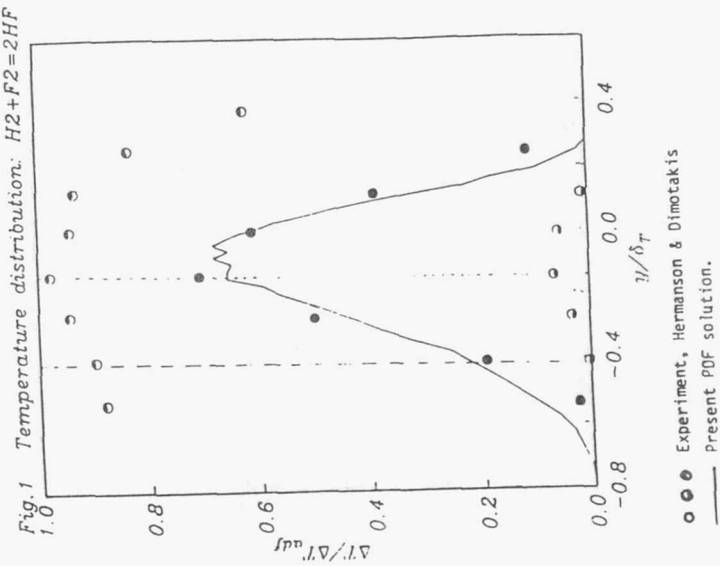
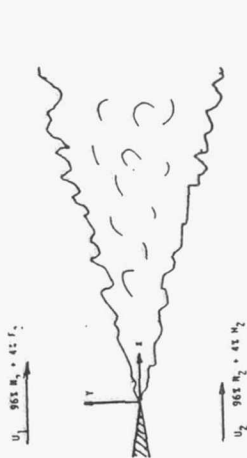
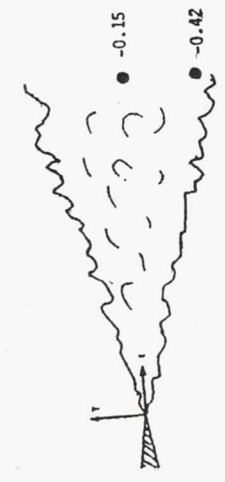


Figure 6. RMS of temperature variance in heated plane jet. — continuous mixing model, - - - modified Curl model,  $\circ$  Antonia et al. (1983),  $\circ$  Bashir and Uberoi (1975),  $\Delta$  Uberoi and Singh (1975).



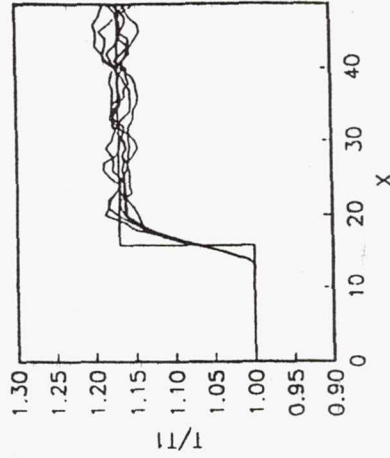
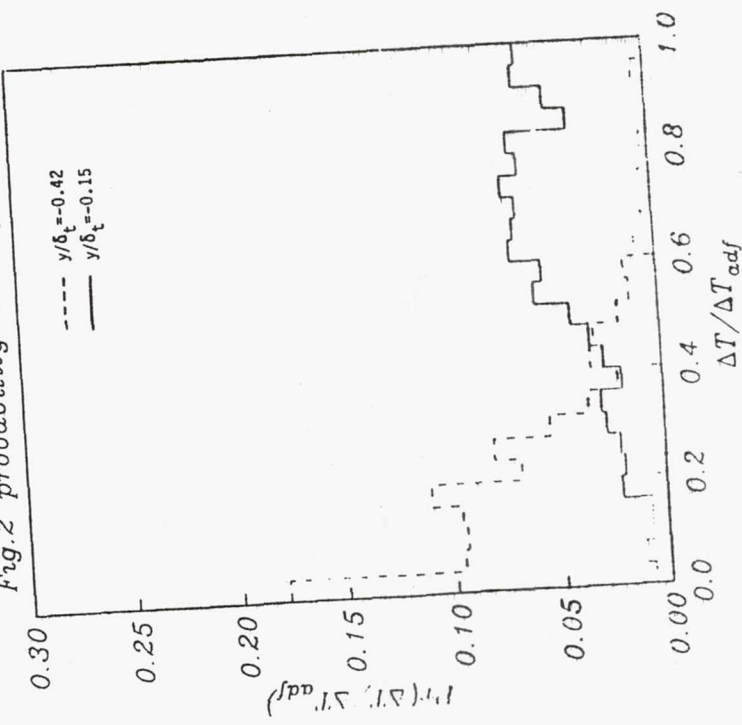
○ ○ Experiment, Hermanson & Dimotakis  
— Present PDF solution.



### COMPRESSIBLE EFFECT

The pdf solution of temperature rise caused by  
an oblique shock:

Fig. 2 probability mass function



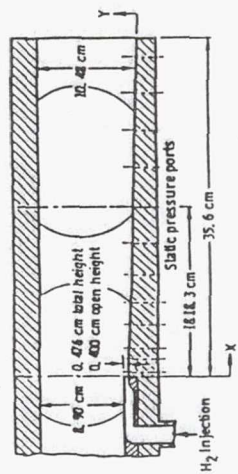


Fig. 6 Flow Configurations of Burrows and Kuchow's Experiment.

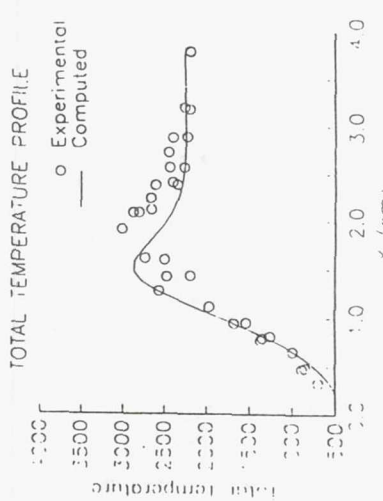
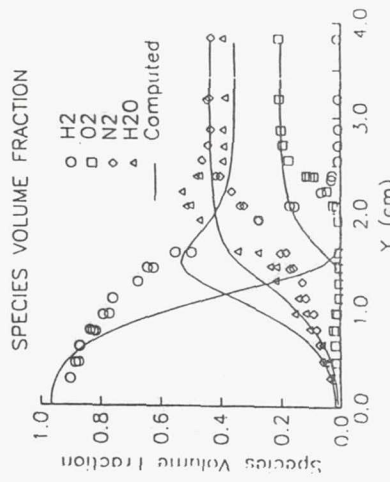


Fig. 7c Oxygen Mass Fraction Contour of Numerical Solution Using PDF.

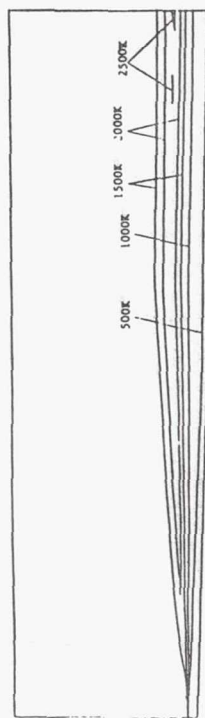


Fig. 7a Temperature Contour of Numerical Solution Using PDF.

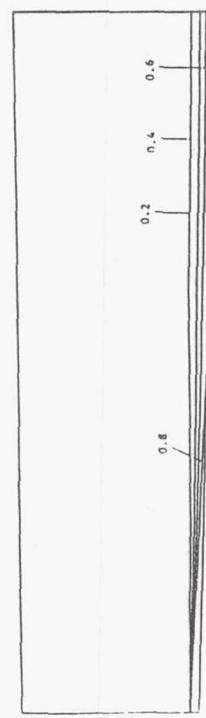
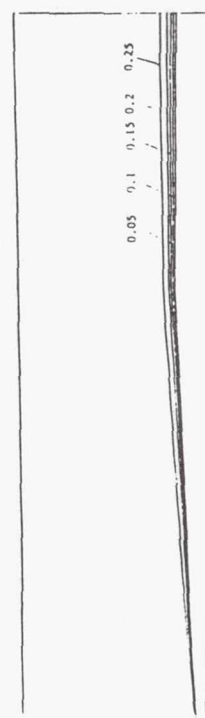
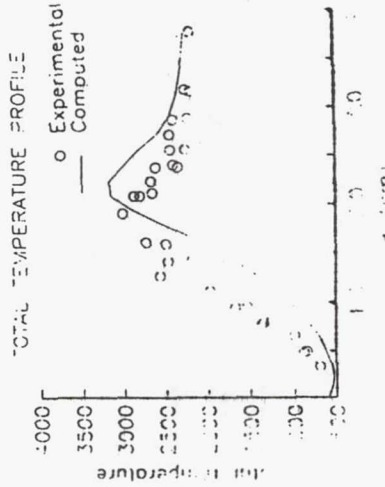
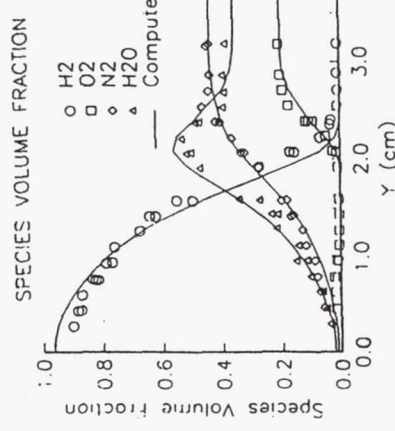


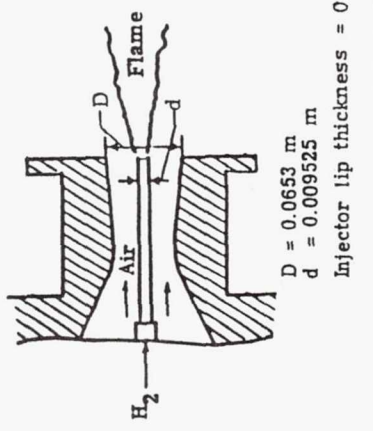
Fig. 7b Hydrogen Mass Fraction Contour of Numerical Solution Using PDF.



## HYDROGEN WALL JET PDF SOLUTION



## COAXIAL HYDROGEN JET (Beach)



	Hydrogen Jet	Free stream
Mach number, $M$	...	2.00
Temperature, $T, \text{ K}$	...	1495
Velocity, $u, \text{ m/s}$	...	2432
Pressure, $p, \text{ MPa}$	0.1	0.1
Mass fraction:		
$a_{\text{H}_2}$	1.00	0.241
$a_{\text{O}_2}$	0	0.478
$a_{\text{N}_2}$	0	0.281
$a_{\text{H}_2\text{O}}$	0	0

## COAXIAL HYDROGEN JET WITHOUT PDF

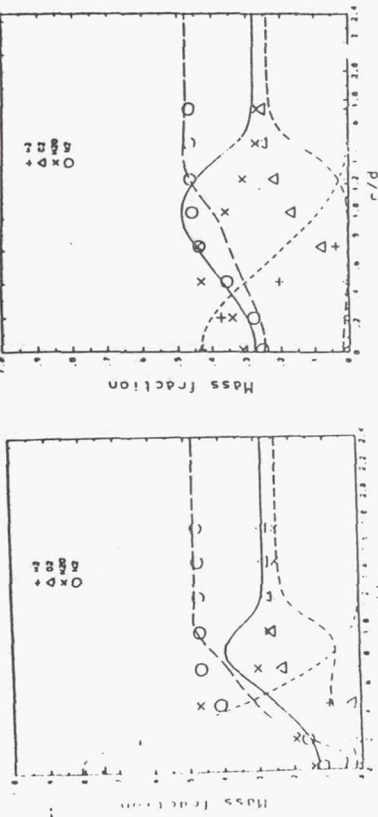


Fig. 5a. Radial profiles of the predicted and measured mass fractions of major species for the CFD solver at  $x/d = 8.26$ .

## COAXIAL HYDROGEN JET WITH PDF SOLUTION

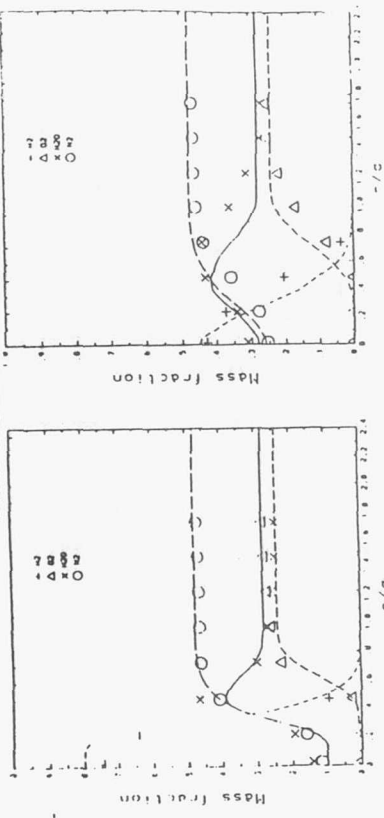


Fig. 4a. Radial profiles of the predicted and measured mass fractions of major species for the pdf-CFD solver at  $x/d = 8.26$ .

Fig. 4c. Radial profiles of the predicted and measured mass fractions of major species for the pdf-CFD solver at  $x/d = 21.7$ .

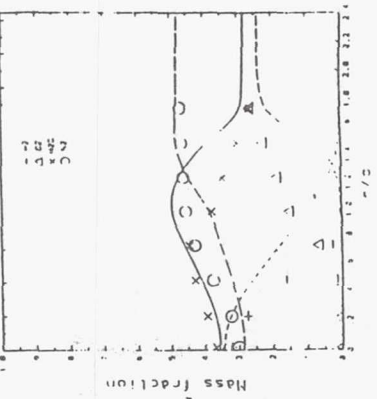


Fig. 4d. Radial profiles of the predicted and measured mass fractions of major species for the pdf-CFD solver at  $x/d = 21.7$ .

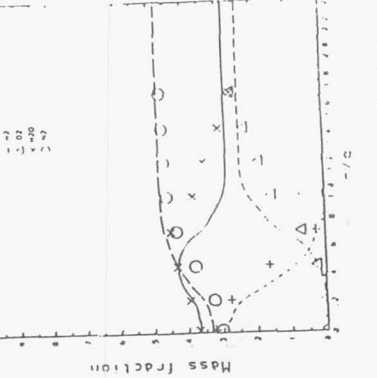


Fig. 4b. Radial profiles of the predicted and measured mass fractions of major species for the pdf-CFD solver at  $x/d = 15.5$ .

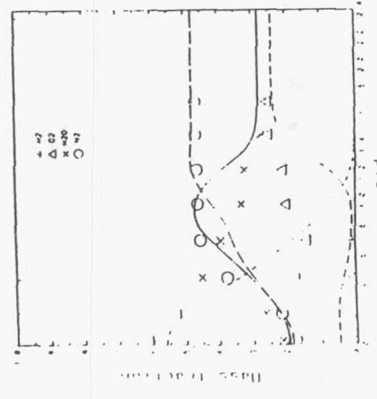
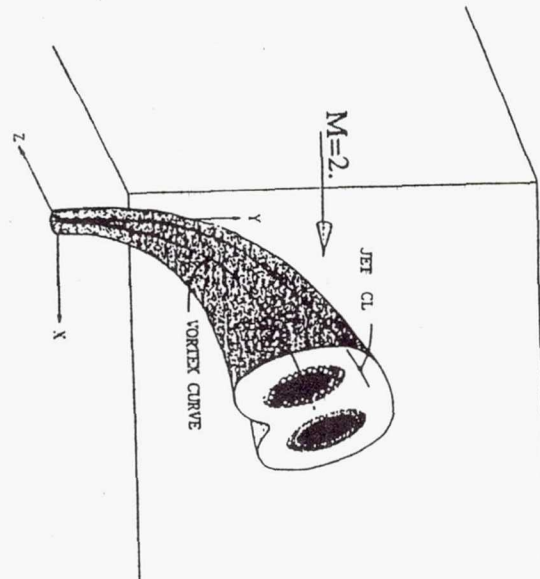
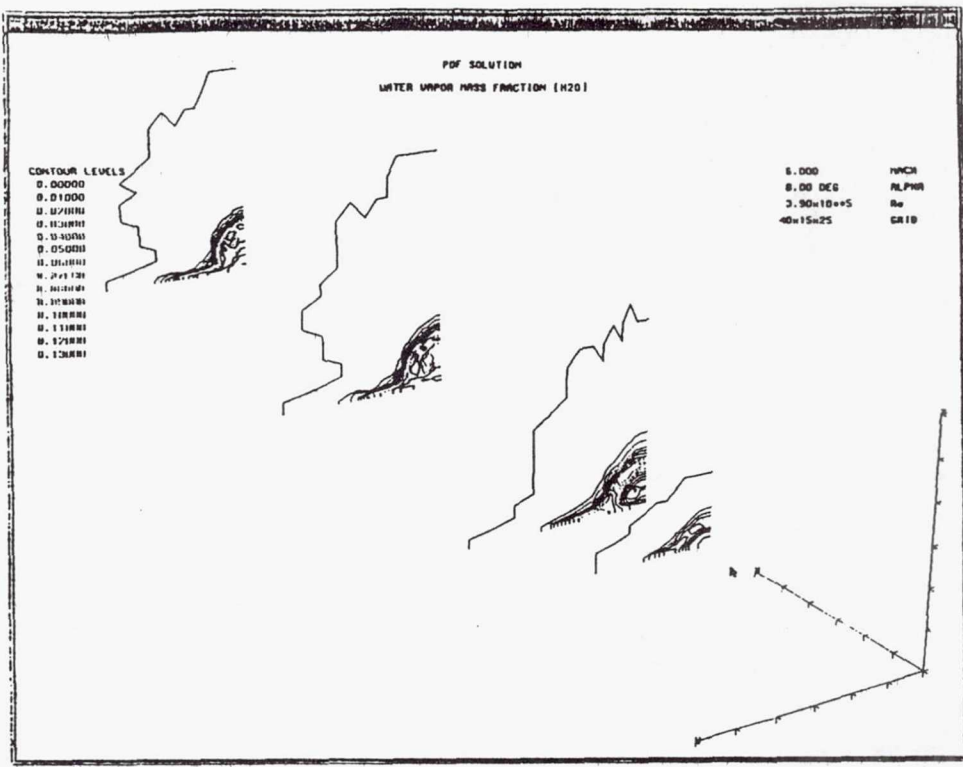


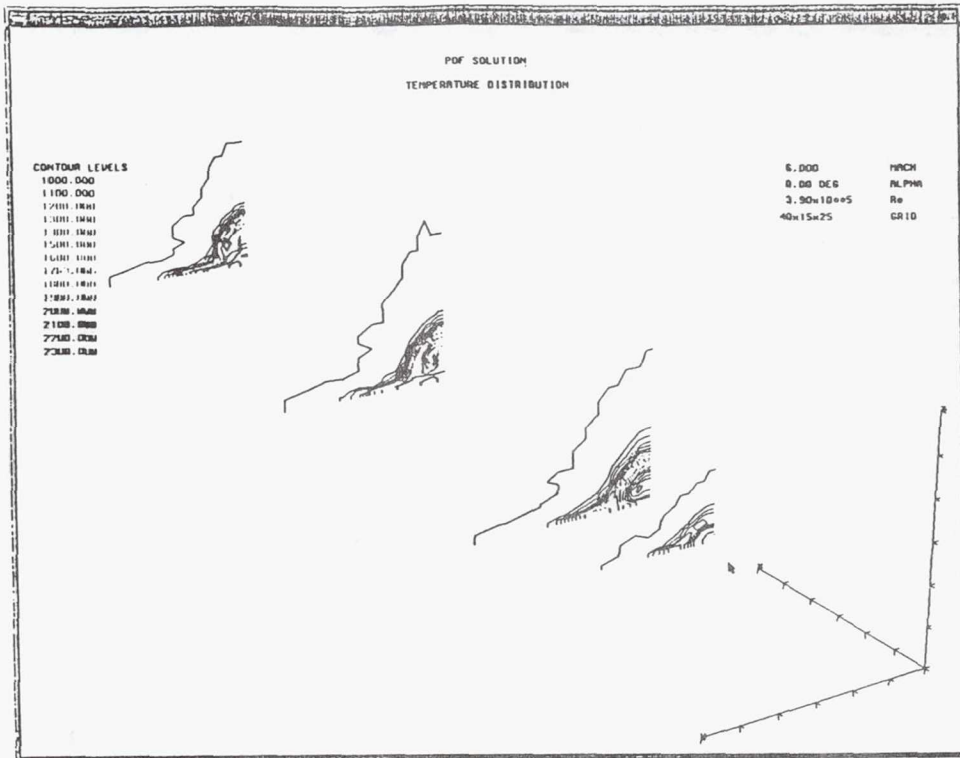
Fig. 5b. Radial profiles of the predicted and measured mass fractions of major species for the CFD solver at  $x/d = 15.5$ .



JET IN CROSS-FLOW

## CONCLUSIONS

- A compressible pdf turbulence model has been developed and implemented.
- A combined time- and ensemble-averaging scheme allows one to use a relatively small sample in the Monte-Carlo computation.
- Efficiency and convergence of the pdf solver is improved, made large scale computation and coupling with CFD solvers feasible.
- The pdf solver can be coupled with any existing CFD flow solvers with equal ease.
- The pdf method performs consistently better than a pure CFD approach for reacting flows.



## Future Research

- Make realistic 3D combustion predictions.
- Develop more accurate pdf models for compressible flames.
- Use DNS data to validate new models.

**Page intentionally left blank**

# **ANALYTICAL THEORIES OF TURBULENCE APPLIED TO TURBULENCE MODELING**

presentation by  
**Robert Rubinstein**  
**CMOTT**

## **MOTIVATION**

**Turbulence models contain undetermined elements**

constants  
functions  
model forms

**Apply analytical theories to determine these elements:**

direct interaction approximation (DIA) (Kraichnan, 1959)  
renormalization group (RNG) (Yakhot and Orszag 1986)

## EXAMPLE 1

Determine constants in nonlinear eddy viscosity (NLEV) (Yoshizawa 1984) and nonlinear eddy diffusivity (Yoshizawa 1987) models

$$\begin{aligned}
 <\mathbf{u}\mathbf{u}> - \frac{2}{3}k\mathbf{I} = & C_\nu \frac{k^2}{\epsilon} (\nabla\mathbf{U} + \nabla\mathbf{U}^T) \\
 & + C_{\tau 1} \frac{k^3}{\epsilon^2} (\nabla\mathbf{U}\nabla\mathbf{U}^T - \frac{1}{3}\nabla\mathbf{U} : \nabla\mathbf{U}^T \mathbf{I}) \\
 & + C_{\tau 2} \frac{k^3}{\epsilon^2} (\nabla\mathbf{U}\nabla\mathbf{U} + \nabla\mathbf{U}^T\nabla\mathbf{U}^T - \frac{2}{3}\nabla\mathbf{U} : \nabla\mathbf{U} \mathbf{I}) \\
 & + C_{\tau 3} \frac{k^3}{\epsilon^2} (\nabla\mathbf{U}^T\nabla\mathbf{U} - \frac{1}{3}\nabla\mathbf{U}^T : \delta\mathbf{U} \mathbf{I}) \\
 <\theta\mathbf{u}> = & C_\kappa \frac{k^2}{\epsilon} \nabla\theta + C_{\kappa 1} \frac{k^3}{\epsilon^2} \nabla\mathbf{U} \cdot \nabla\theta + C_{\kappa 2} \frac{k^3}{\epsilon^2} \nabla\mathbf{U}^T \cdot \nabla\theta
 \end{aligned}$$

Universal inertial range constants for isotropic turbulence:

$$E(k) = C_K \epsilon^{2/3} k^{-5/3}$$

$$\nu(k) = C_D \epsilon^{1/3} k^{-4/3}$$

$$C_K = 1.61 \quad C_D = 0.49 \quad (\text{Yakhot and Orszag 1986})$$

Assume shear is a weak perturbation of isotropic background state. Then (Rubinstein and Barton 1990):

	<i>exact</i>	<i>value</i>	<i>experiment</i>
$C_\nu$	$(\frac{2}{3})^2 C_D / C_K^2$	0.085	$\sim 0.09$
$C_{\tau 1}$	$\frac{5}{105} (\frac{2}{3})^2 / (C_D C_K)^2$	0.034	$\sim 0.04$
$C_{\tau 3}$	$\frac{-2}{105} (\frac{2}{3})^2 / (C_D C_K)^2$	-0.014	$\sim -0.01$

### Passive scalar results

$Pr_T = f(Pr, Re)$  (Yakhot and Orszag 1986)

$f$  is a known function: for  $Re = \infty$ ,  $Pr_T \sim 0.7$

$$C_\kappa = C_\nu / Pr_T$$

Constants of the nonlinear theory are known functions of  $C_D, C_K, Pr_T$  (Rubinstein and Barton 1991)

Diffusivity ratio  $\kappa_{12}/\kappa_{22} = 1.9$  (Tavoularis and Corrsin), 2.3 (theory)

**In principle, higher order nonlinearities in NLEV  
can be computed theoretically**

### EXAMPLE 2

Determine model form for rapid pressure strain correlation  $\Pi$

RNG gives a series for  $\Pi$  in powers of  $\nabla U$ .

The LRR model

$$\Pi = C_{\tau_1} < \mathbf{u} \mathbf{u} > \nabla \mathbf{U} + C_{\tau_2} < \mathbf{u} \mathbf{u} > \nabla \mathbf{U}^T$$

arises from systematic lowest order consolidation (resummation) of this series. (Rubinstein and Barton 1992):

LRR            RNG

$$C_{\tau_1} \quad 0.7636 \quad \frac{16}{21} \sim 0.7619$$

$$C_{\tau_2} \quad 0.1091 \quad \frac{2}{21} \sim 0.0952$$

Second order resummations are possible:

$$\Pi = F(\langle \mathbf{u}\mathbf{u} \rangle) \nabla \mathbf{U} + G(\langle \mathbf{u}\mathbf{u} \rangle) \nabla \mathbf{U}^T$$

$$\Pi = \langle \mathbf{u}\mathbf{u} \rangle [C_1 \nabla \mathbf{U} + C_2 \nabla \mathbf{U} \nabla \mathbf{U} + \dots]$$

These are speculative at this point.

### EXAMPLE 3

Determine unknown functions in generalized nonlinear eddy viscosity representation for simple shear flow

Nonlinear eddy viscosity does not apply at large strain rates: it predicts  $\langle \mathbf{u}\mathbf{u} \rangle / k \rightarrow \infty$ . Introduce the generalization

$$\langle \mathbf{u}\mathbf{u} \rangle - \frac{2}{3}k\mathbf{I} = C_\nu(\eta) \frac{k^2}{\epsilon} (\nabla \mathbf{U} + \nabla \mathbf{U}^T) + \dots$$

where in simple shear flow  $\partial U_i / \partial x_j = S\delta_{i1}\delta_{j2}$ ,  $\eta = Sk/\epsilon$

DIA analysis of shear turbulence leads to

$$\langle u_i u_j \rangle = k F_{ij}(\eta/C_R)$$

where  $F_{ij}$  is known from rapid distortion theory (RDT) (Maxey 1982) and  $C_R$  is a universal constant ( $C_R \sim 1.59$ , Yakhot and Orszag 1986).

### General time dependent theory

$$\langle u_i u_j \rangle(t) = k F_{ij}(\alpha^*(t))$$

where  $\alpha^*$  is a *modified total strain* determined by DIA:

$$\alpha^*(t) = \int_0^t ds G(t-s) S(s)$$

$G$  is the *response function* of DIA.

Homogeneous shear flow at high strain rate

$$\eta = Sk/\epsilon \rightarrow \infty$$

	$b_{12}$	$b_{11}$	$b_{22}$	$b_{33}$
NLEV	$O(\eta)$	$O(\eta^2)$	$O(\eta^2)$	$O(\eta^2)$
LRR	$O(\eta^{-1})$	$f_{11}(c)$	$f_{22}(c)$	$f_{33}(c)$
present	$O(\eta^{-1})$	2/3	-1/3	-1/3
RDT	$O(\eta^{-1})$	2/3	-1/3	-1/3

In LRR,  $f_{ij}(c)$  are model dependent constants. The limiting normal stresses are not necessarily realizable.

DNS (Lee, Kim and Moin) shows that RDT is a good description of these flows even for moderate times.

## CURRENT WORK

Time dependent model for nonequilibrium turbulence based on DIA

New evaluation of NLEV constants

Nonmarkovian damping: short time suppression of eddy damping.

Required for oscillating and highly strained flows.

Two scale theory of shear turbulence:

large scales  $\sim$  RDT,

small scales  $\sim$  Kolmogorov inertial range dynamics

DNS OF TURBULENCE, TRANSITION  
AND EFFECT OF ROTATION

Presented by

A.T. Hsu

MOTIVATION

Provide better understanding of turbulence  
and transition physics.

Provide data base for modeling work; couple  
DNS work with modeling work.

## WORK ACCOMPLISHED

By-pass transition simulated.

Rotation effect on compressible turbulence.

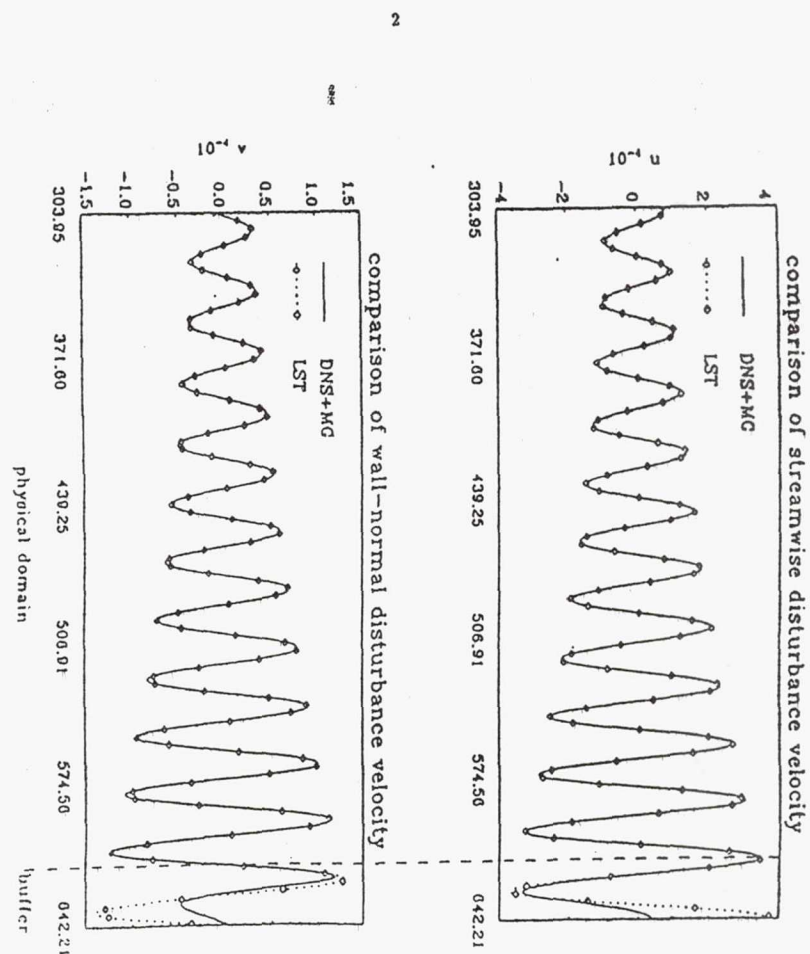
Turbulent reactive flows: effects of chemical reaction on turbulence.

## DNS for Bypass Transition: Numerical Aspects

- Fully implicit, high-order finite difference scheme  
(fourth order in space and second order in time.)
- Acceleration Techniques:
  - Semi-coarsening multigrid
  - Line-box distributive relaxation
- A new buffer outflow boundary condition
- A fine-coarse-fine grid mapping

## DNS for Bypass Transition: Cases Calculated

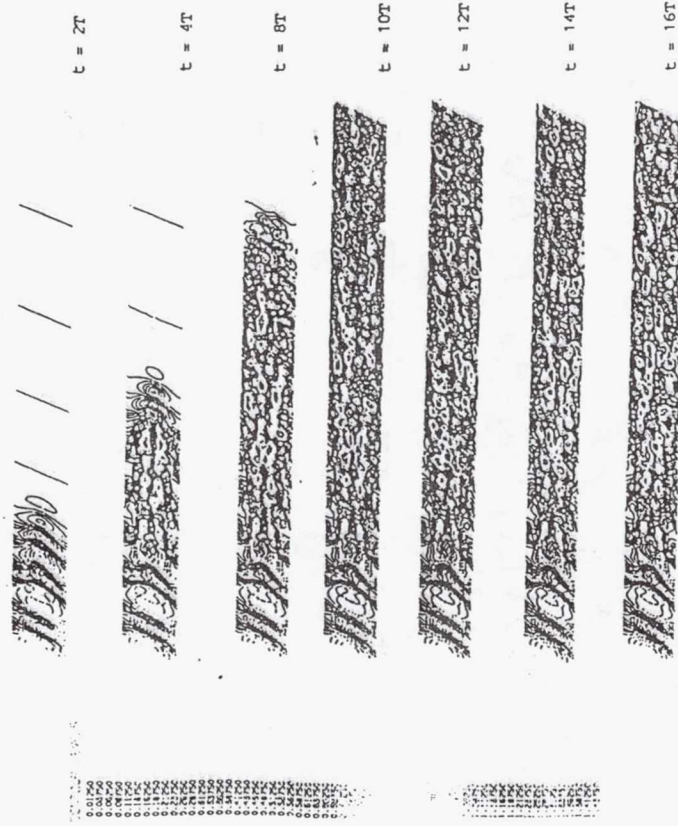
- 2D/3D linear instability stage (temporal simulation)
- 2D/3D linear instability stage (spatial simulation)
- Secondary instability stage (spatial simulation)
- Simulation of the whole transition zone (spatial simulation)



## DNS: Effect of Rotation

### Numerical Method:

- Compressible N-S equations;
- 8th order compact difference scheme;
- 3rd order time marching.



$Re^* = 900, Fr = 86, \beta = 0.1, \epsilon_{21} = 0.04, \epsilon_{24} = 0.015$ . Flow direction is from left to right.

## EQUATIONS FOR ROTATING TURBULENCE

### TRIPLE CORELATION EQUATIONS

The Reynolds stress equations:

$$\begin{aligned} (\overline{u_i u_j}),_t &= -\overline{u_k}(\overline{u_i u_j})_{,k} - \frac{1}{\rho}(\overline{u_i p_{,j}} + \overline{u_j p_{,i}}) + \overline{u_i \tau_{jk,k}} \\ &+ \overline{u_j \tau_{ik,k}} - 2\epsilon_{ilm} \Omega_l \overline{u_m u_j} - 2\epsilon_{ilm} \Omega_l \overline{u_m u_i} \end{aligned}$$

Turbulent kinetic energy:

$$k_{,t} = \frac{1}{2}\overline{u_i u_j u_{j,j}} - \overline{u_i p_{,i}} - \nu \overline{u_i u_{j,j}} - \frac{\nu}{3}\overline{u_i u_{i,j}} -$$

$$(\overline{u_i l u_j l u_{i,j}}),_t = -2\epsilon_{ilm} \Omega_l \overline{u_m u_{i,j}} + OT$$

Incompressible dissipation:

$$\begin{aligned} \epsilon_{,t}^i &= -2\nu \overline{u_i u_j u_{k,j}} - \nu \overline{u_i u_{j,i}} - 2\nu \overline{u_i u_{j,j}} \\ &- 2\nu^2 \overline{u_i u_{j,k}} - \frac{2}{3}\nu^2 \overline{u_i u_{i,j}} \end{aligned}$$

Effects of triple correlations: redistribute energy and dissipation.

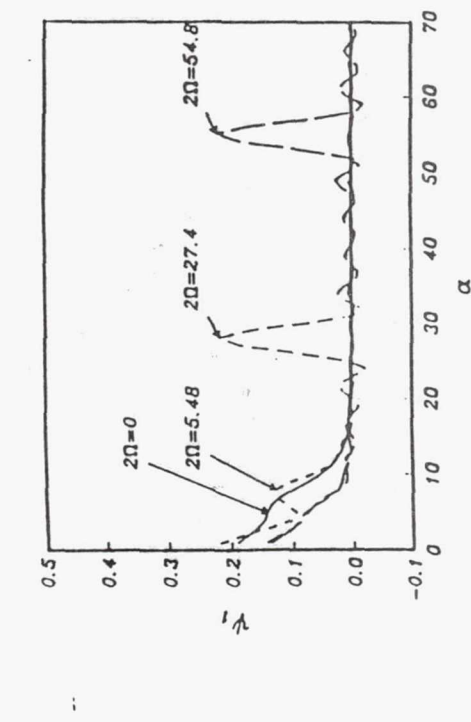


Fig.10 Time spectra of turbulent kinetic energy.

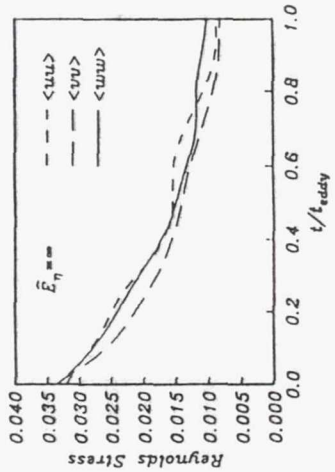


Fig.1 Time history of Reynolds stresses for  $\Omega = 0$ .

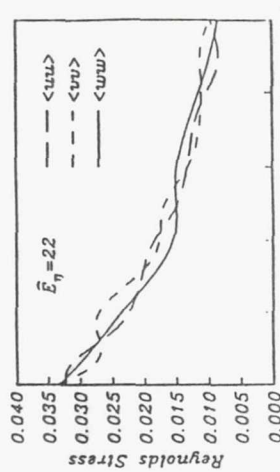


Fig.2 Time history of Reynolds stresses for a moderate rotation rate of  $\Omega = 2.74$ .

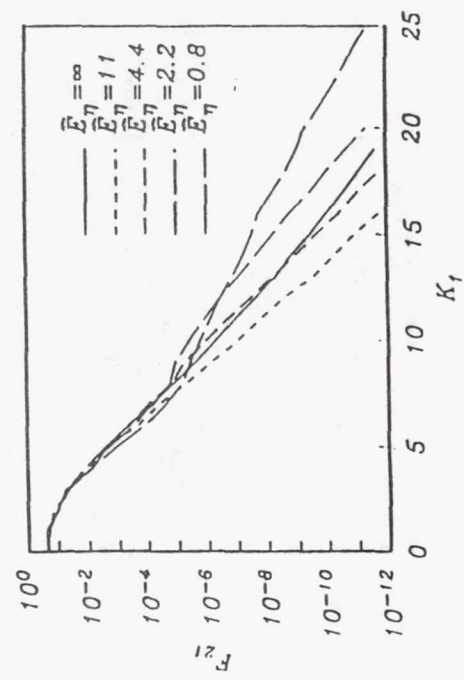


Fig.11 One-dimensional energy spectra for the flow field at  $t/t_{edd} = 1$ .

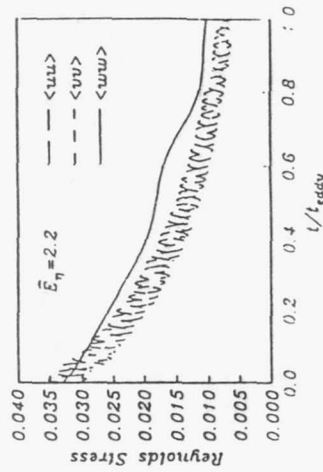


Fig.3 Time history of Reynolds stresses for a high rotation

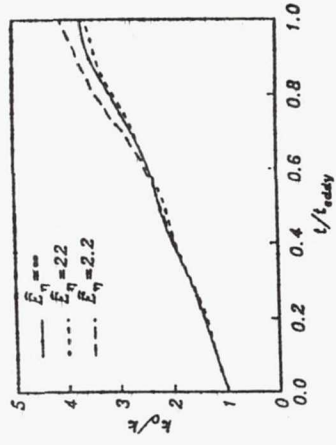


Fig.5 Total turbulent kinetic energy ratio.

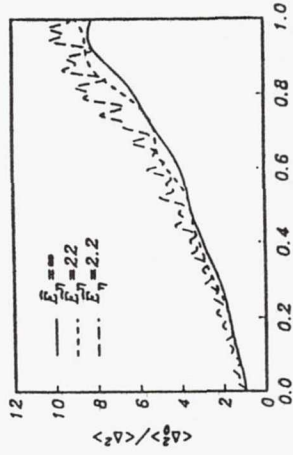


Fig.6 The ratio of velocity divergence square, representing compressible turbulent kinetic energy.

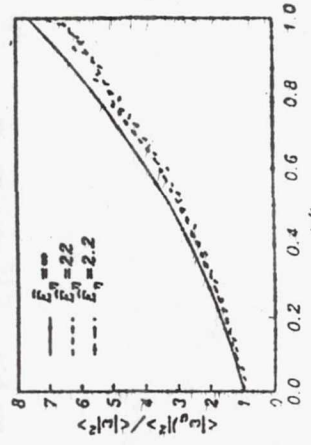


Fig.7 The ratio of vorticity square, representing incompressible turbulent kinetic energy.

DNS: Reactive Flows

### Numerical Method:

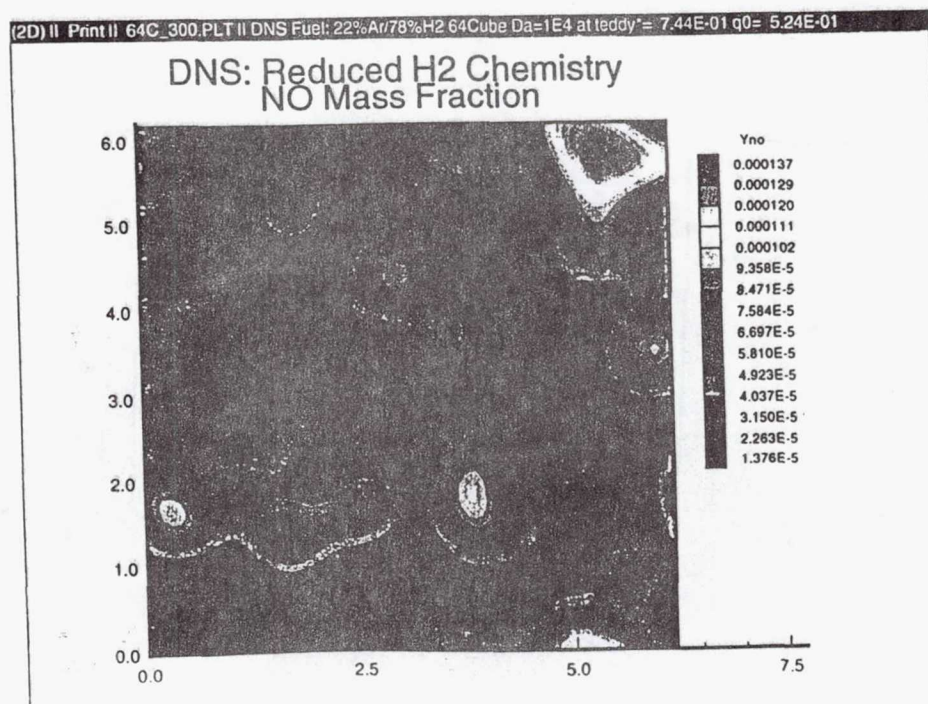
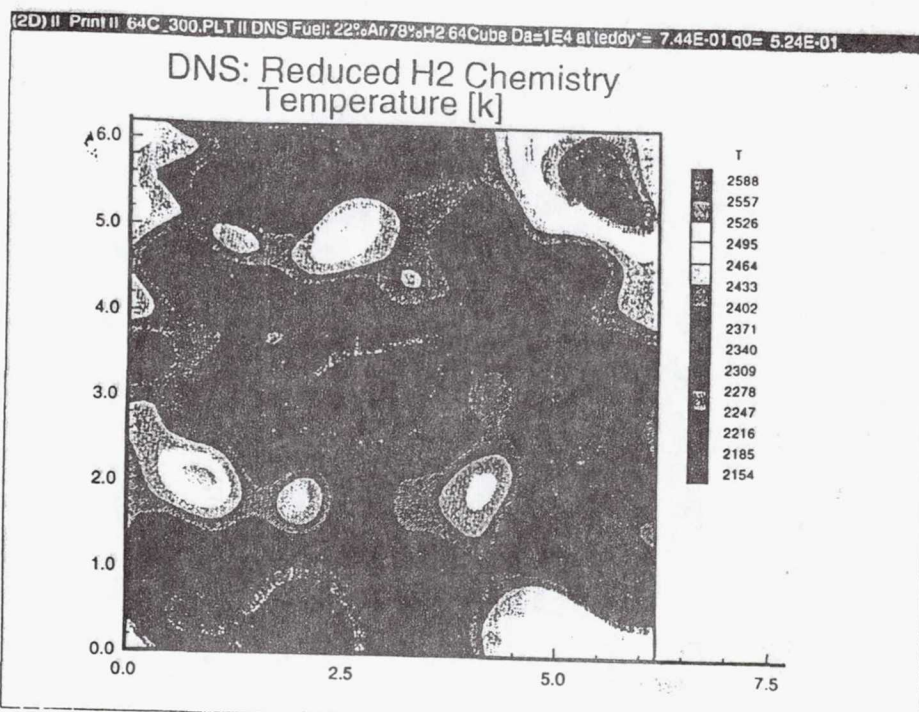
- Compressible N-S equations;
- 8th order compact difference scheme;

• 3rd order time marching;

- finite rate chemistry.

### Results:

- H<sub>2</sub> + Air combustion in homogeneous turbulence with or without shear.





• Presentation of the Problem

Variables

Meaning of Bypass Transition

Physics/Mechanisms to be Modeled

• Modeling of Transition Onset

Use of DNS

Use of k- $\epsilon$  Model

Use of PSE

Summary of Results

• Modeling of the Transition Region

Comment on Linear-Combination Method

Use and Limits of k- $\epsilon$  Methods

Schmidt/Patankar Method

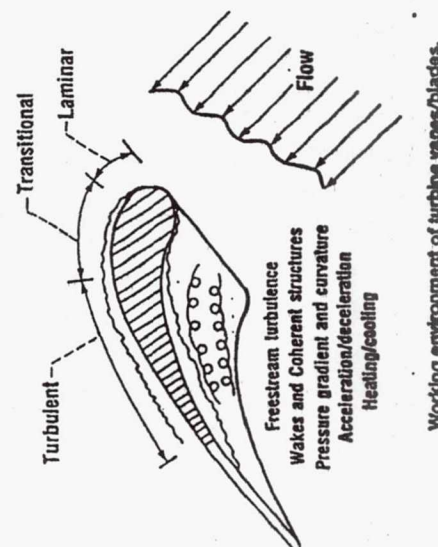
Multi-Time-Scale Method

Intermittency Method

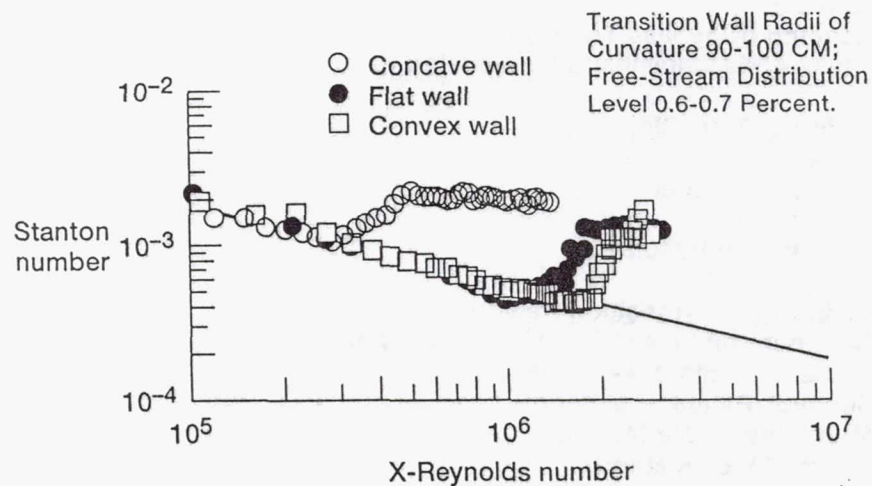
Reynolds Analogy

Summary of Results

• Recommendations

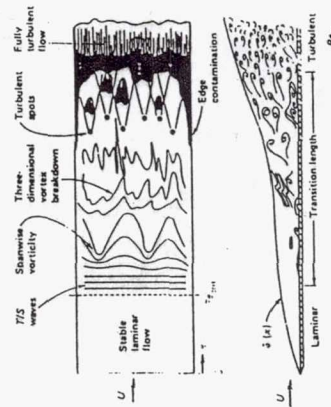


Effect of Streamwise Curvature on Bypass.  
 (Wang, 1984; Kim and Simon, 1991)

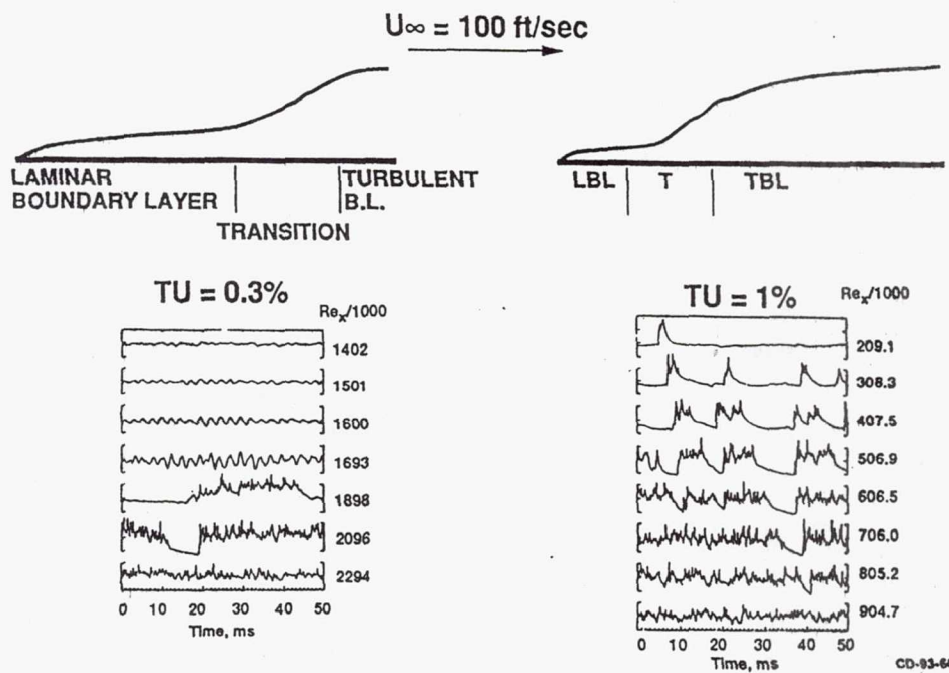


CD-93-66129

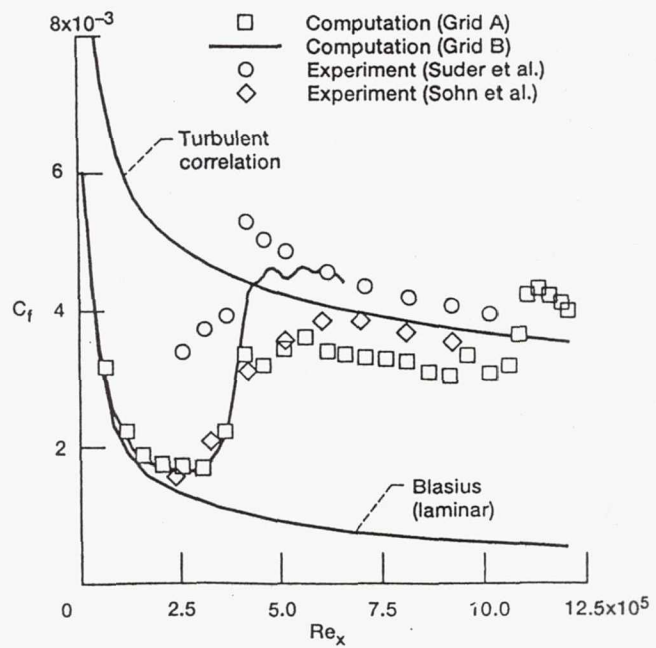
IDEALIZED SKETCH OF TRANSITION  
 PROCESS ON A FLAT PLATE



Linear Versus Bypass Path to Transition, From Suder,  
O'Brien, Reshotko (1988)

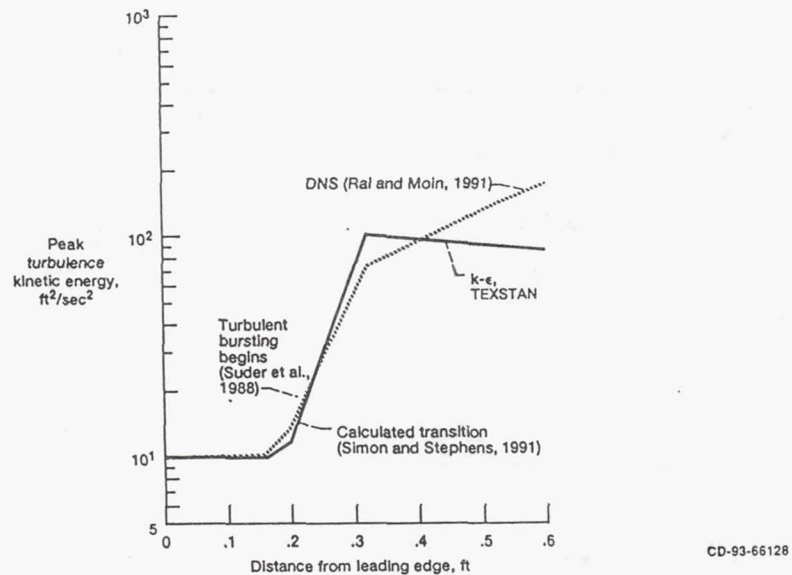


Computed Skin Friction Along the Length of the Flat Plate (Grids A and B), (Rai and Moin, 1991)



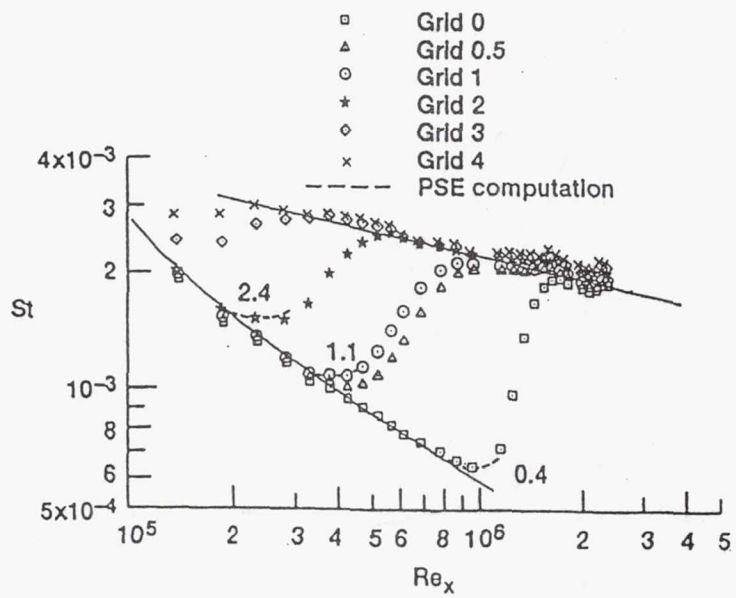
CD-93-66137

Comparison of Computed Disturbance Energy from Computations Based on a  $k-\epsilon$  Model and on Direct Numerical Simulation (DNS) for Bypass Transition (Simoneau and Simon, 1993)

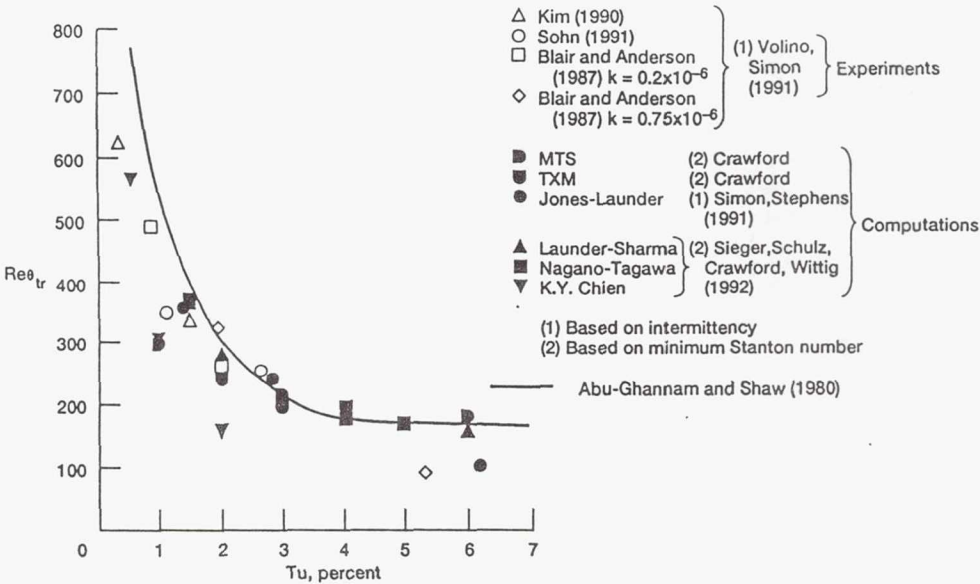


CD-93-66128

Onset Prediction Using PSE Approach  
(Stuckert & Herbert, 1992)  
Data of Sohn & Reshotko(1991)



## Computed and Experimental Momentum Thickness Reynolds Number for transition Onset



CD-93-66127

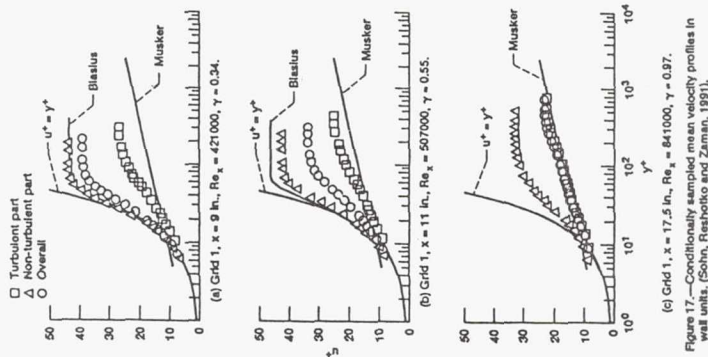


Figure 17—Conditionally sampled mean velocity profiles in wall units. (Sohn, Reshotko and Zeman, 1991).

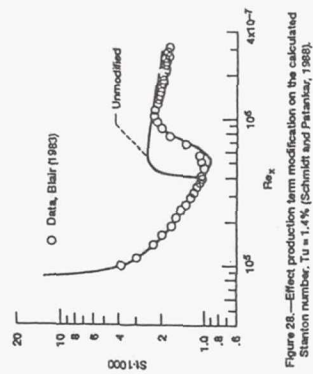
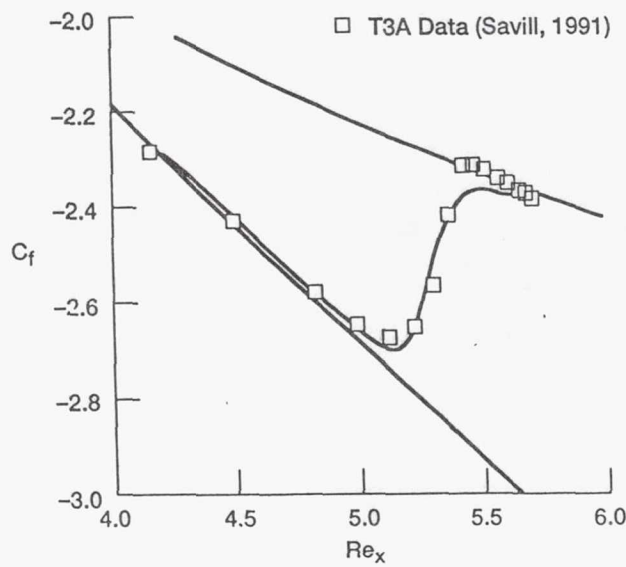


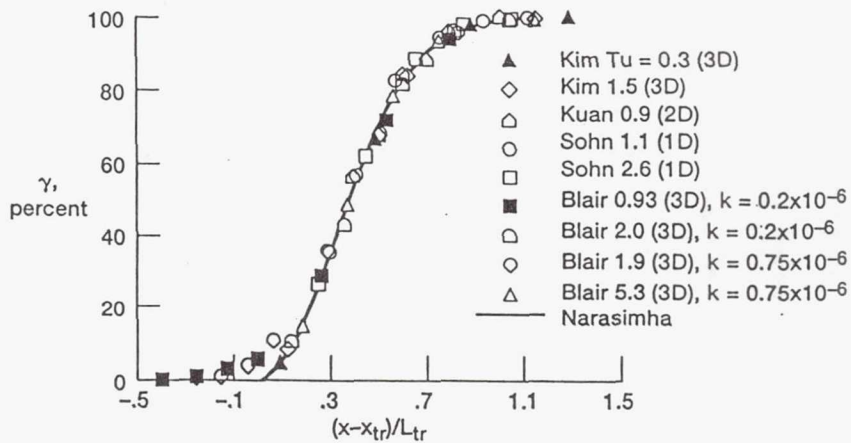
Figure 28—Effect production term modification on the calculated Stanton number,  $T_u = 1.4\%$  (Schmidt and Patankar, 1989).

### The Numerical Prediction of Transition Flow Using MTS Model Compared with Experimental Data of T3A (Crawford, 1993)



CT

## Intermittency (Volino and Simon, 1991)



CD-93-66139

## Transition Length Determination

$$Re_{\epsilon_t} = \frac{2.15}{\sqrt{N}} Re_{\epsilon_t}^{3/2}$$

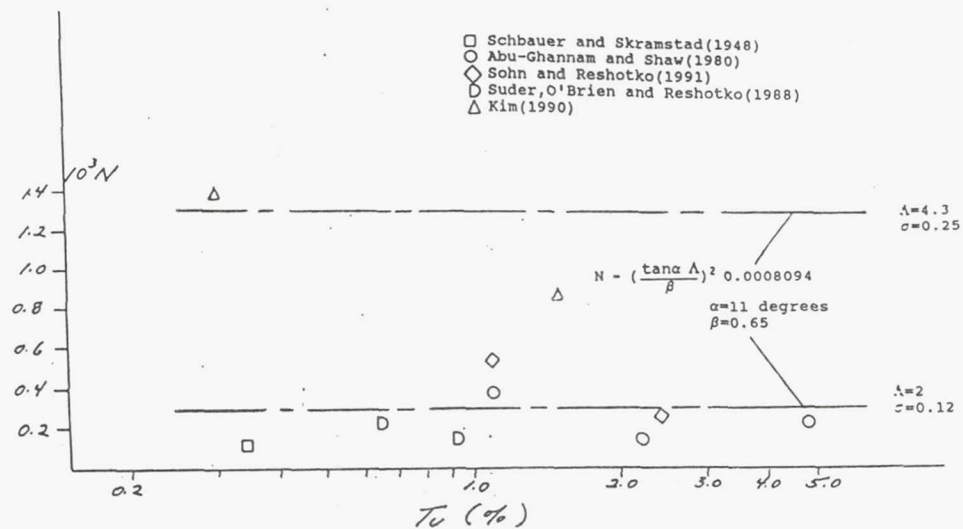
$\gamma = 0 \rightarrow 0.99$

$N$  - non-dimensional / spot  
formation rate

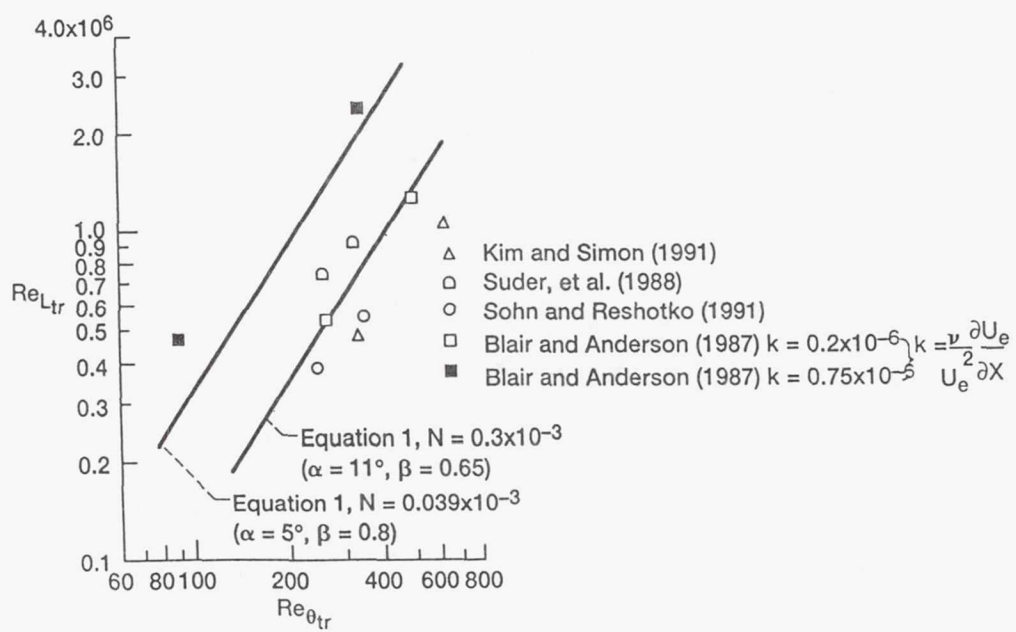
$$= n \delta_t^3 / r$$

$n$  - spot formation rate  
 $s$  - dependence factor  
 $\delta_t$  - momentum thickness

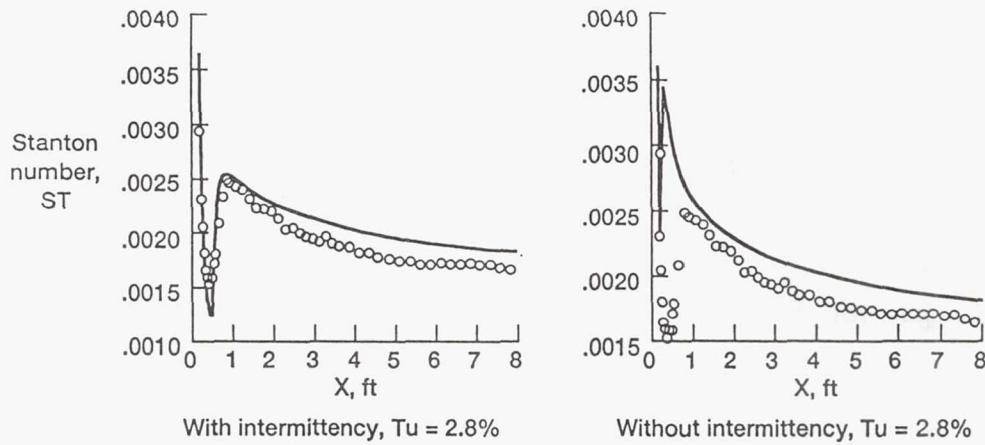
## Variation of Nondimensional Spot Formation Rate with Free-Stream Turbulence (Narasimha(1985)method)



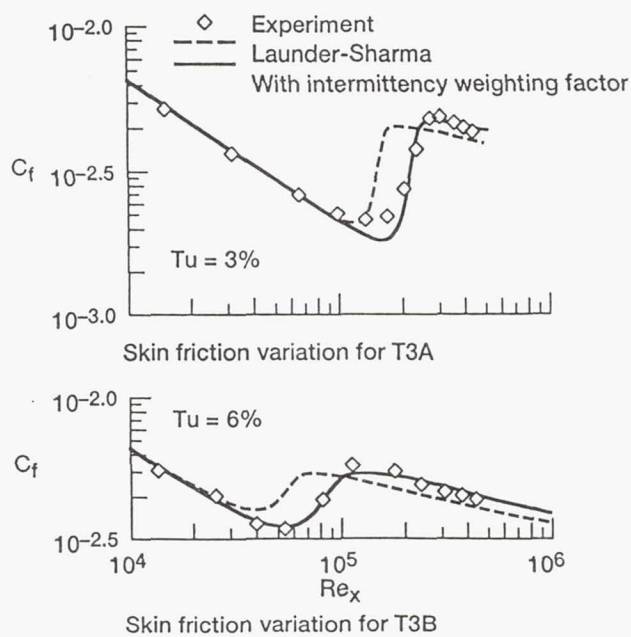
## Transition Length Correlation



## Use of Intermittency to Model Transition Region



## Use of an Intermittency Weighting Factor in Computations (Yang, 1992; Yang and Shih, 1992)



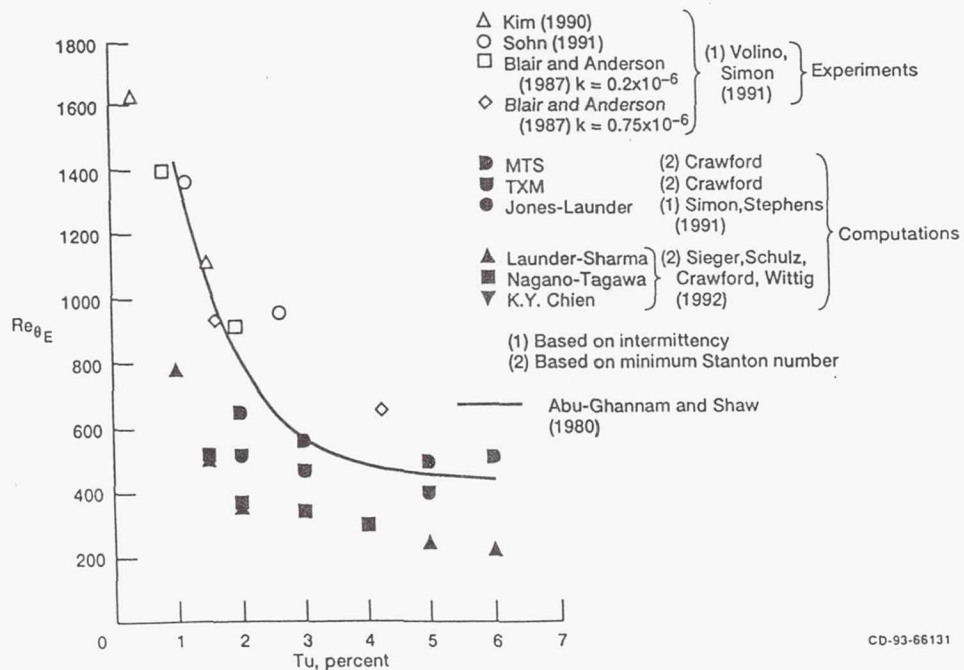


### REYNOLDS ANALOGY EFFECTS

Problem: Reynolds analogy breakdown in flows with pressure gradient

Possible Solution: Use of additional modeled transport equations for the thermal turbulence to predict the turbulent heat flux/turbulent Prandtl number

Computed and Experimental Momentum Thickness  
Reynolds Number for Transition End



CD-93-66131



RECOMMENDATIONS

- Develop a DNS data base with/without heat transfer for turbine blade geometry for (1) understanding physics (2) supporting/guiding experiments (3) developing/testing models
- Continue development of models more faithful to physics
- Continue development of Multi-Time-Scale Model
- Develop Reynolds Stress Turbulence Models
- Initiate an effort in the use of Large Eddy Simulation(LES)
- Develop the PSE approach as design tool
- Develop models for unsteady flows (e.g. wakes)
- Develop capability to predict turbulent Prandtl number
- Test models for turbulence levels found in combustors (6-20%)

**Page intentionally left blank**

LeRC	9/93	Title	1
------	------	-------	---

# ALGEBRAIC MODELS FOR TURBINE BLADE HEAT TRANSFER

R. J. Boyle  
NASA Lewis Research Center

*Workshop on Computational Turbulence Modeling*

LeRC	9/93	Aim and Scope	2
------	------	---------------	---

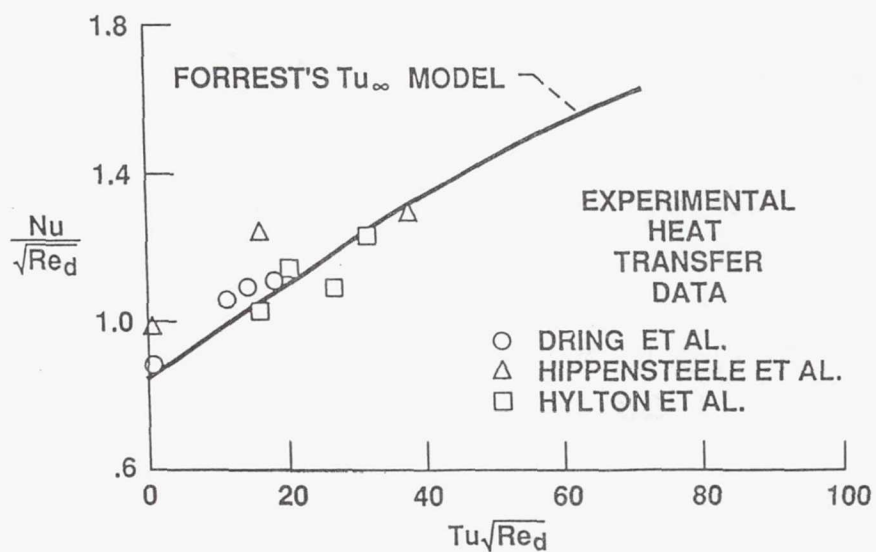
- VALIDATE PREDICTIONS OF TURBINE BLADE HEAT TRANSFER & PRESSURE LOSS SMOOTH AND ROUGH BLADES
- ALGEBRAIC - BALDWIN-LOMAX TYPE MODELS
- IMPLEMENTED IN NAVIER-STOKES CODES - RVC3D & RVCQ3D
- ENGINEERING APPLICATIONS

*Workshop on Computational Turbulence Modeling*

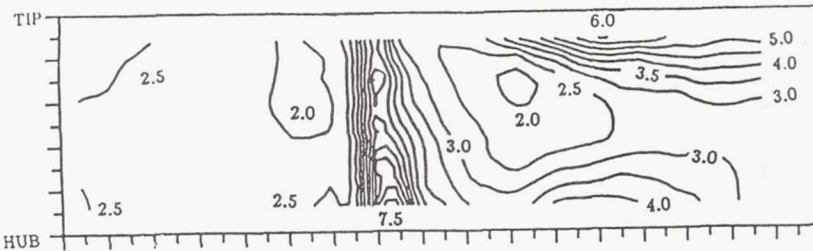
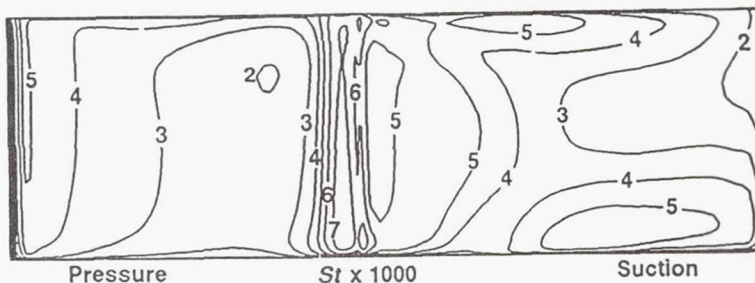
- FREESTREAM TURBULENCE - ex LEADING EDGE
- TRANSITION MODEL - ex MAYLE'S
- ALGEBRAIC - BALDWIN-LOMAX TYPE MODELS

Workshop on Computational Turbulence Modeling

### Tu<sub>∞</sub> EFFECT ON LEADING EDGE HEAT TRANSFER



Workshop on Computational Turbulence Modeling

a) Data of Blair,  $Re = 2.37 \times 10^5$ , Design Flow Angles.

b) Prediction, 1% Clearance.

*Workshop on Computational Turbulence Modeling*

## APPROACHES FOR ROUGH SURFACES

- TAYLOR, COLEMAN, and HODGE
  - EXPLICITLY ACCOUNT FOR BLOCKAGE, DRAG AND HEAT TRANSFER
  - SOURCE TERMS IN NAVIER-STOKES EQUATIONS
  
- CEBEKI and CHANG - USED IN ANALYSIS
  - MODIFY MIXING LENGTH
  - ONLY EDDY VISCOSITY AFFECTED

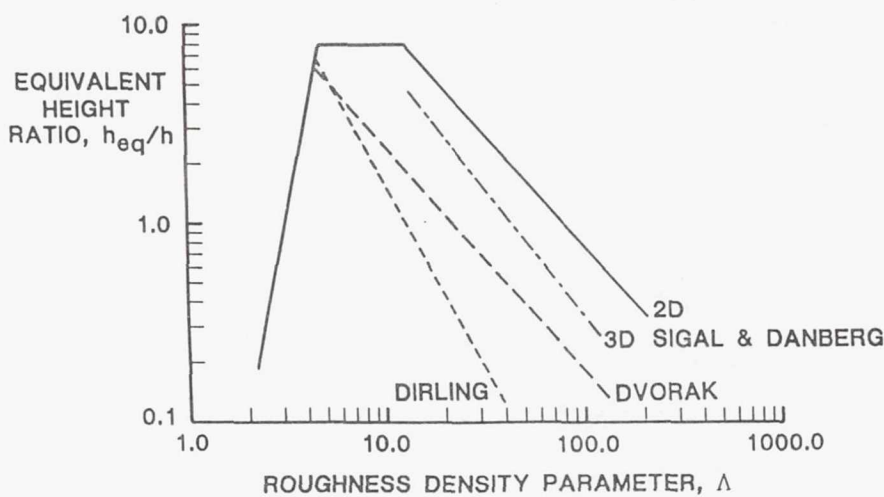
*Workshop on Computational Turbulence Modeling*

## REQUIRED ROUGHNESS PARAMETERS

- *HEIGHT*
- *SPATIAL DENSITY*
- *SHAPE*

*Workshop on Computational Turbulence Modeling*

## CORRELATION FOR EQUIVALENT HEIGHT RATIO FROM SIGAL and DANBERG



*Workshop on Computational Turbulence Modeling*

## EXPERIMENTAL DATA USED FOR COMPARISONS

- HEAT TRANSFER

HOSNI - FLAT PLATE

BLAIR & ANDERSON - LARGE LOW SPEED ROTOR

DUNN & KIM - SSME FUEL TURBINE

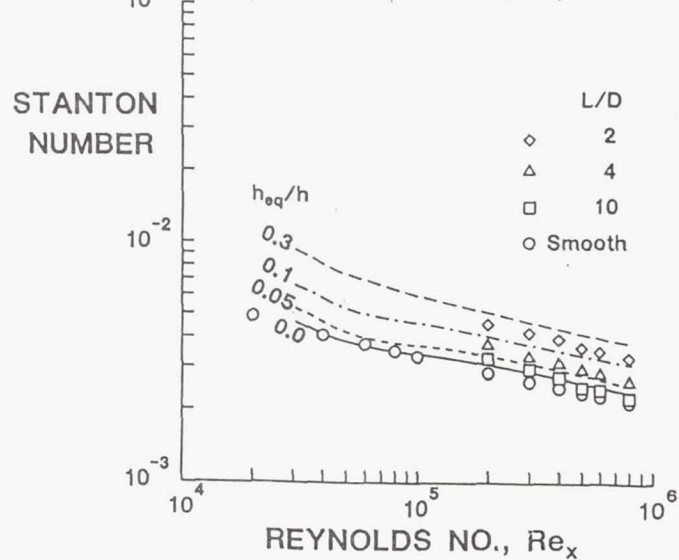
- TURBINE EFFICIENCY

BOYNTON - TWO-STAGE SSME HIGH PRESSURE FUEL TURBINE

*Workshop on Computational Turbulence Modeling*

## ROUGH FLAT PLATE HEAT TRANSFER

(Data of Hosni et al.)



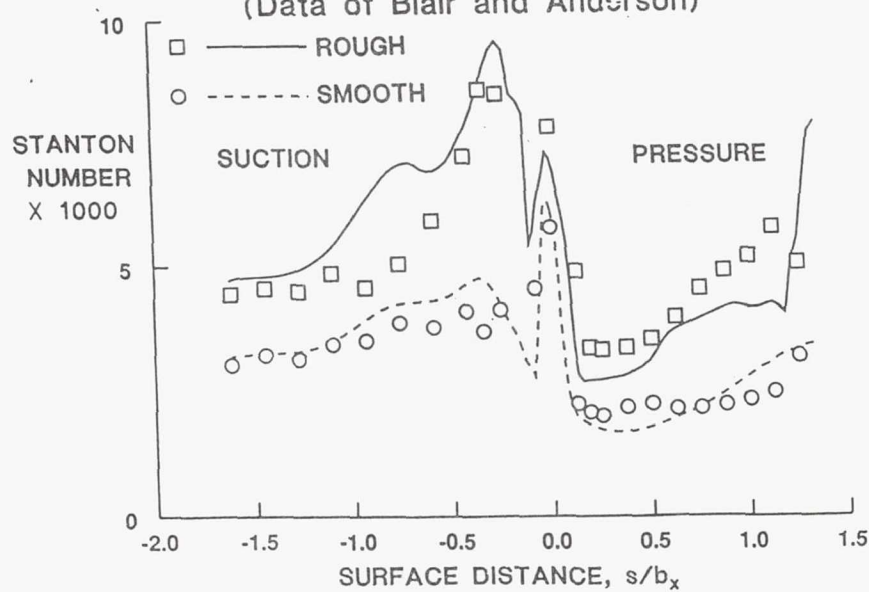
*Workshop on Computational Turbulence Modeling*

RATIO OF PREDICTED TO MEASURED HEAT TRANSFER  
 FOR A FLAT PLATE.  $Re_x = 400,000$ .  
 (DATA OF HOSNI et al.)

L/D	Equivalent Height Correlation					
	Sigal & Danberg		Dvorak		Dirling	
	$h_{eq}/h$	$St_p/St_m$	$h_{eq}/h$	$St_p/St_m$	$h_{eq}/h$	$St_p/St_m$
2	1.58	1.64	2.43	1.85	1.69	1.67
4	0.26	1.36	0.50	1.57	0.45	1.52
10	0.023	1.01	0.061	1.15	0.079	1.22
Smooth		1.10		1.10		1.10

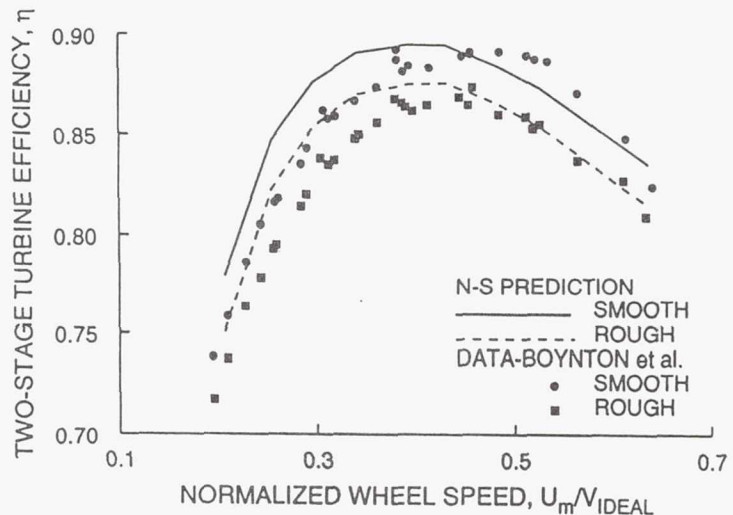
Workshop on Computational Turbulence Modeling

PREDICTED AND MEASURED BLADE HEAT TRANSFER  
 (Data of Blair and Anderson)



Workshop on Computational Turbulence Modeling

## EFFICIENCY FOR SMOOTH AND ROUGH BLADES



Workshop on Computational Turbulence Modeling

Grid	$y^+$	$K$	$A^+$	$\bar{\epsilon}$	$\Delta\eta$
291×54	0.3	0.0	26.0	0.0321	
		0.0	1.0	0.0483	0.011
		0.3	26.0	0.0348	0.002
		0.3	1.0	0.0550	0.015
		1.0	26.0	0.0455	0.009
		1.0	1.0	0.0703	0.026
291×54	0.6	0.0	26.0	0.0423	
		0.0	1.0	0.0570	0.010
		0.3	26.0	0.0449	0.002
		0.3	1.0	0.0654	0.016
		1.0	26.0	0.0546	0.008
		1.0	1.0	0.0767	0.023
291×54	1.2	0.0	26.0	0.0375	
		0.0	1.0	0.0531	0.011
		0.3	26.0	0.0402	0.002
		0.3	1.0	0.0586	0.014
		1.0	26.0	0.0502	0.009
		1.0	1.0	0.0730	0.024
Experimental					0.021

Workshop on Computational Turbulence Modeling

- TEMPERATURE MEASUREMENTS BENEATH ROUGHNESS AFFECT HEAT TRANSFER COEFFICIENT
- $h_{\text{ACTUAL}} / h_{\text{MEASURED}} = 1 + ht/k$   
h - HEAT TRANSFER COEFFICIENT  
t - ROUGHNESS THICKNESS  
k - THERMAL CONDUCTIVITY OF ROUGHNESS
- POSSIBLE REASON FOR HIGHEST AUGMENTATION CORRESPONDING TO LARGEST SCALE

*Workshop on Computational Turbulence Modeling*

## REQUIREMENTS FOR BENCHMARK ROUGHNESS HEAT TRANSFER DATA SETS

- COMPLETE DESCRIPTION OF THE ROUGHNESS CHARACTERISTICS
- SURFACE NOT DISTURBED BY MEASUREMENT TECHNIQUE
- KNOWN TEMPERATURE OF ROUGHNESS ELEMENTS
- VERIFICATION OF ACCURACY BY MEASUREMENTS ON SMOOTH SURFACES

*Workshop on Computational Turbulence Modeling*

- SMOOTH SURFACES  
REASONABLE ACCURACY  
TRANSITION BEHAVIOR GOVERNS  
ACCURACY
- ROUGH SURFACES  
INCONSISTENT ASSUMPTIONS  
NEEDED FOR LOSS AND HEAT  
TRANSFER

*Workshop on Computational Turbulence Modeling*

**Page intentionally left blank**

Internal Fluid Mechanics Division



NAVIER-STOKES TURBINE HEAT TRANSFER

PREDICTIONS USING

TWO-EQUATION TURBULENCE CLOSURES

ALI A. AMERI  
CENTER FOR RESEARCH, INC.  
UNIVERSITY OF KANSAS  
NASA LEWIS RESEARCH CENTER

Internal Fluid Mechanics Division



TURBINE HEAT TRANSFER

OUTLINE

- Brief description of the method of solution
- 2-d examples using various models
- 3-d calculations using algebraic model and  $q-\omega$  model
- Conclusions

TURBINE HEAT TRANSFER

TURBULENCE MODELS

LOW REYNOLDS NUMBER TWO-EQUATION MODELS

- COAKLEY'S  $q$ - $\omega$  MODEL
- CHIEN'S  $K$ - $\epsilon$  MODEL

ALGEBRAIC MODEL

- BALDWIN-LOMAX -- WITHOUT TRANSITION MODEL

TURBINE HEAT TRANSFER

FORMULATION

- MASS AVERAGED COMPRESSIBLE N-S EQUATIONS
- + MODEL EQUATIONS
- NON-PERIODIC C GRID.

**Internal Fluid Mechanics Division**

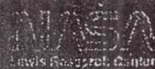


TURBINE HEAT TRANSFER

SOLUTION OF THE NAVIER-STOKES EQUATIONS

- FINITE VOLUME DISCRETIZATION
- 4 STAGE RUNGE-KUTTA SCHEME
- EIGENVALUE SCALING OF ARTIFICIAL DISSIPATION
- VARIABLE COEFFICIENT RESIDUAL SMOOTHING
- MULTIGRIDING

**Internal Fluid Mechanics Division**



TURBINE HEAT TRANSFER

SOLUTION OF THE MODEL EQUATIONS

- FINITE VOLUME DISCRETIZATION
- 4 STAGE RUNGE-KUTTA SCHEME
- VARIABLE COEFFICIENT RESIDUAL SMOOTHING
- MULTIGRIDING

## Internal Fluid Mechanics Division



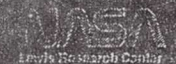
### 2-D CASES

- SSME HIGH-PRESSURE FUEL TURBINE 1ST STAGE VANE
- ALLISON'S C3X VANE DATA OF HYLTON ET AL.

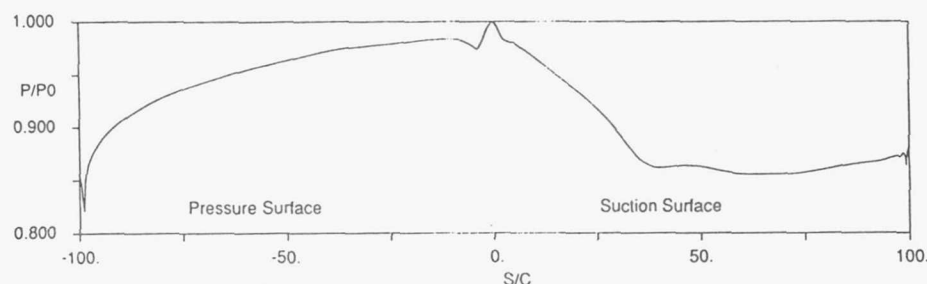
### 3-D CASES

- LANGSTON'S CASCADE, THICK & THIN INLET BOUNDARY LAYERS.

## Internal Fluid Mechanics Division



### TURBINE HEAT TRANSFER

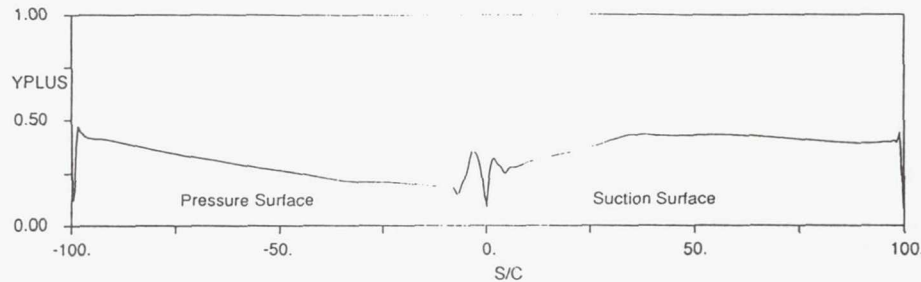


Surface Pressure Distribution- First Stage Stator

## Internal Fluid Mechanics Division



### TURBINE HEAT TRANSFER

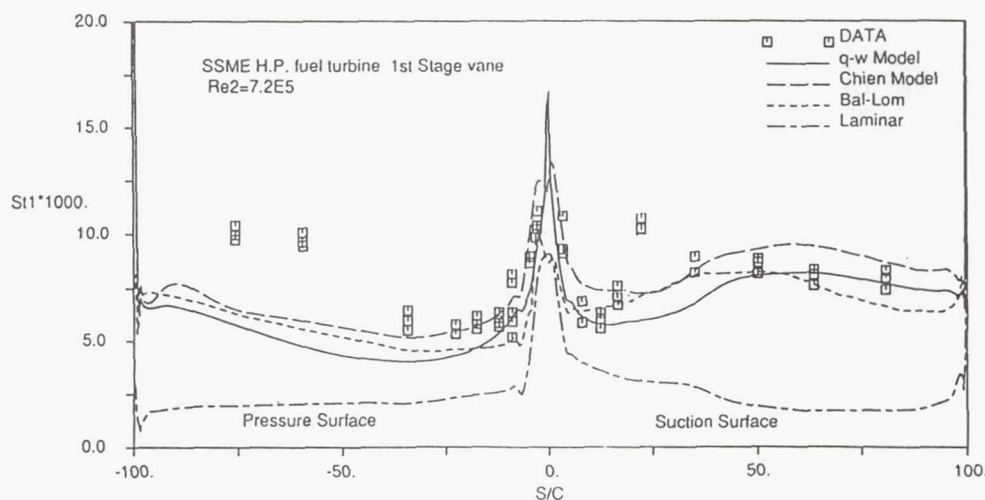


*Grid Spacing from the wall*

## Internal Fluid Mechanics Division



### TURBINE HEAT TRANSFER

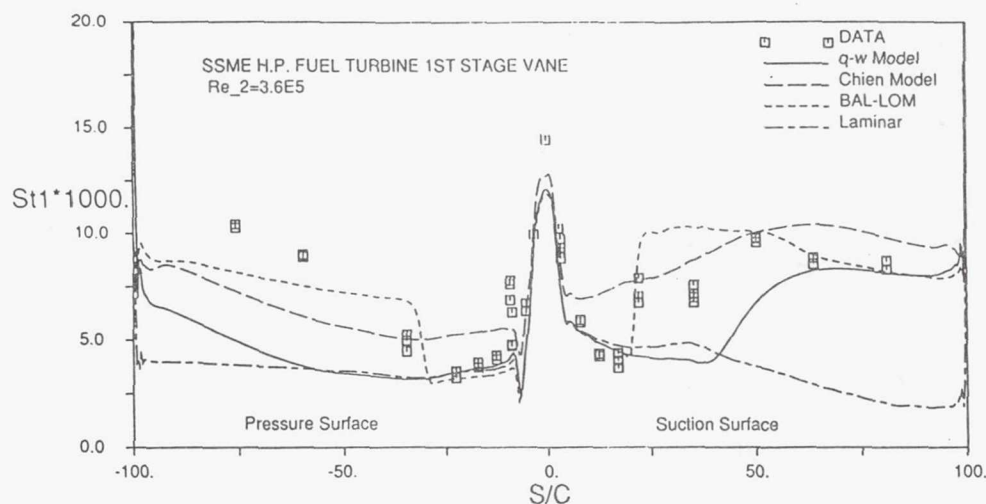


*First Stage Vane, High Reynolds Number*

## Internal Fluid Mechanics Division



### TURBINE HEAT TRANSFER

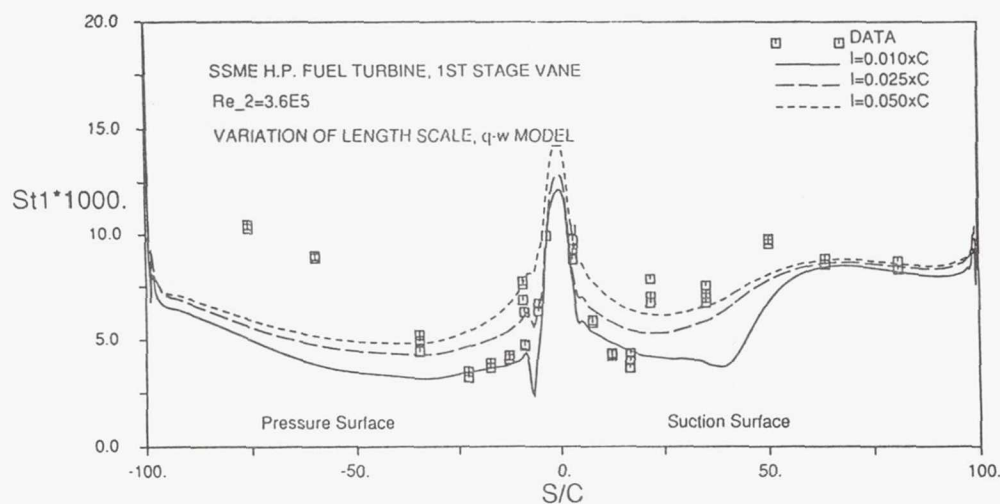


*First Stage Vane, Low Reynolds Number*

## Internal Fluid Mechanics Division

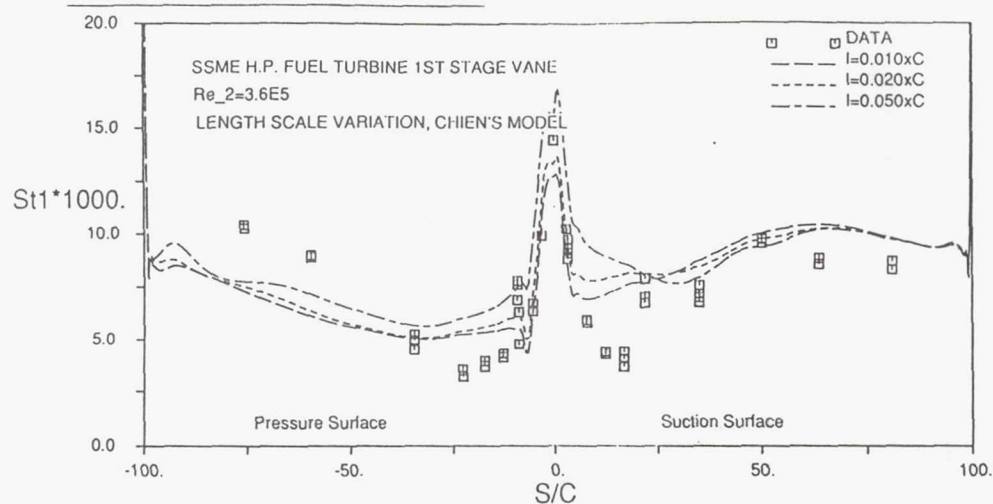


### TURBINE HEAT TRANSFER

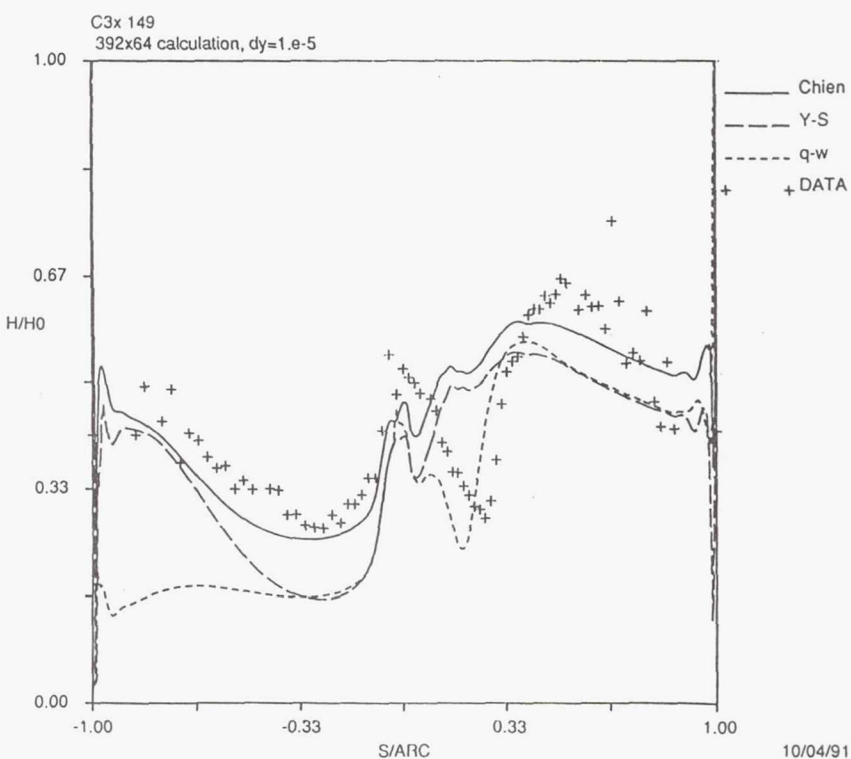


*First Stator, Variation with length scale  
q- $\omega$  Model*

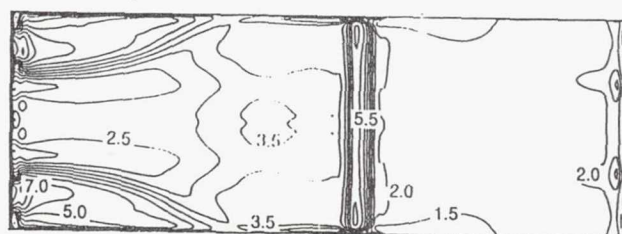
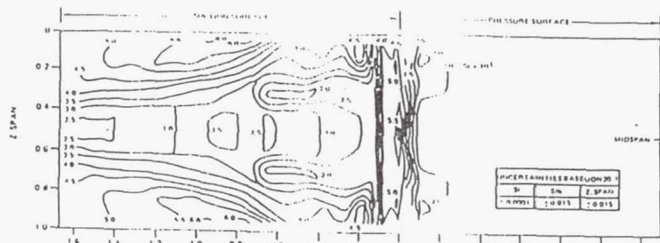
## TURBINE HEAT TRANSFER



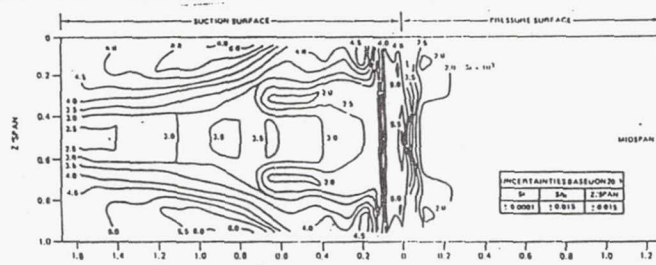
*First Stator, Variation with length scale  
Chien's Model*



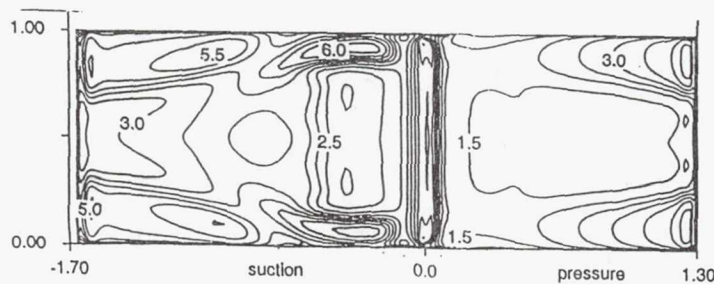
### Thick Inlet Boundary Condition



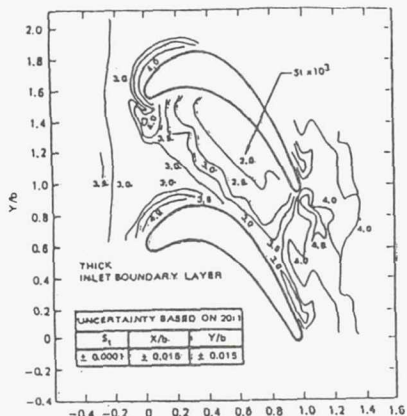
### Surface Stanton Number x 1000. , thick inlet boundary layer



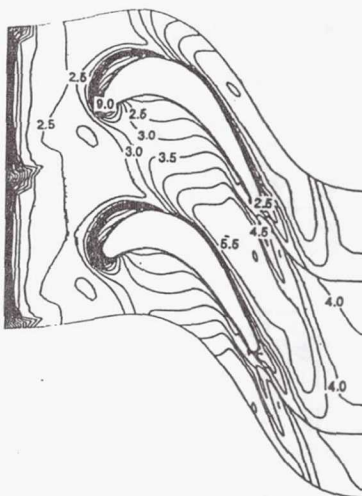
Experiment, Graziani et al.



Langston's Cascade  
Endwall Stanton Number x1000.



Experiment, Graziani et al.



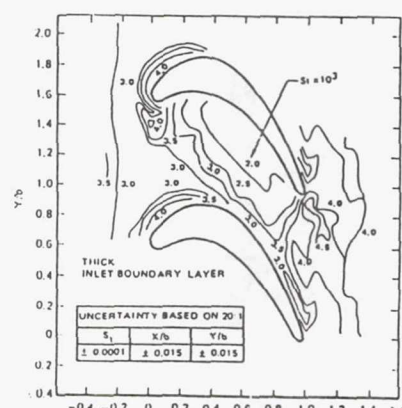
Computation, TRAF3D

Thick inlet boundary layer.

**THICK BOUNDARY LAYER INLET CONDITION**

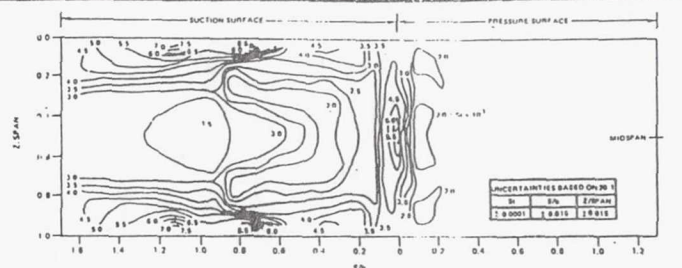


*q-omega Model, 193x49x65*

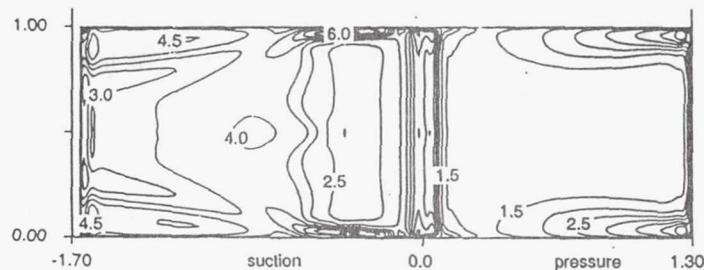


*Experiment Graziani*

Surface Stanton Number  $\times 1000$ . , thin inlet boundary layer

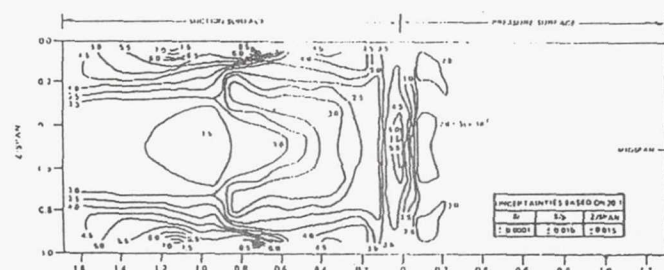


Experiment, Graziani et al.

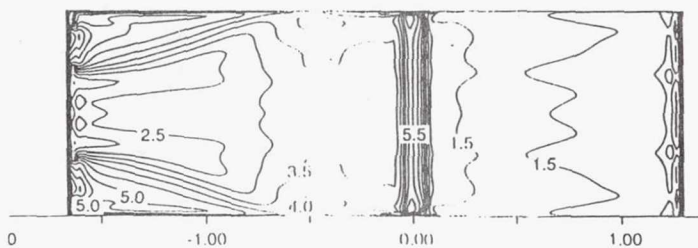


Computation, TRAF3D

SURFACE STANTON NUMBER $\times 1000$ , THIN INLET BOUNDARY LAYER

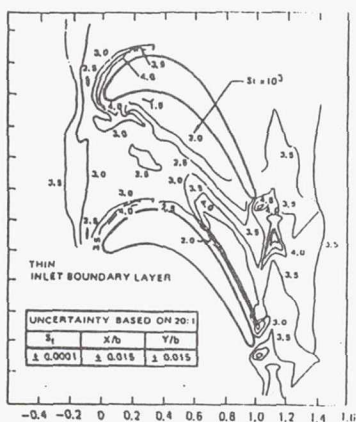


Experiment, Graziani et al.

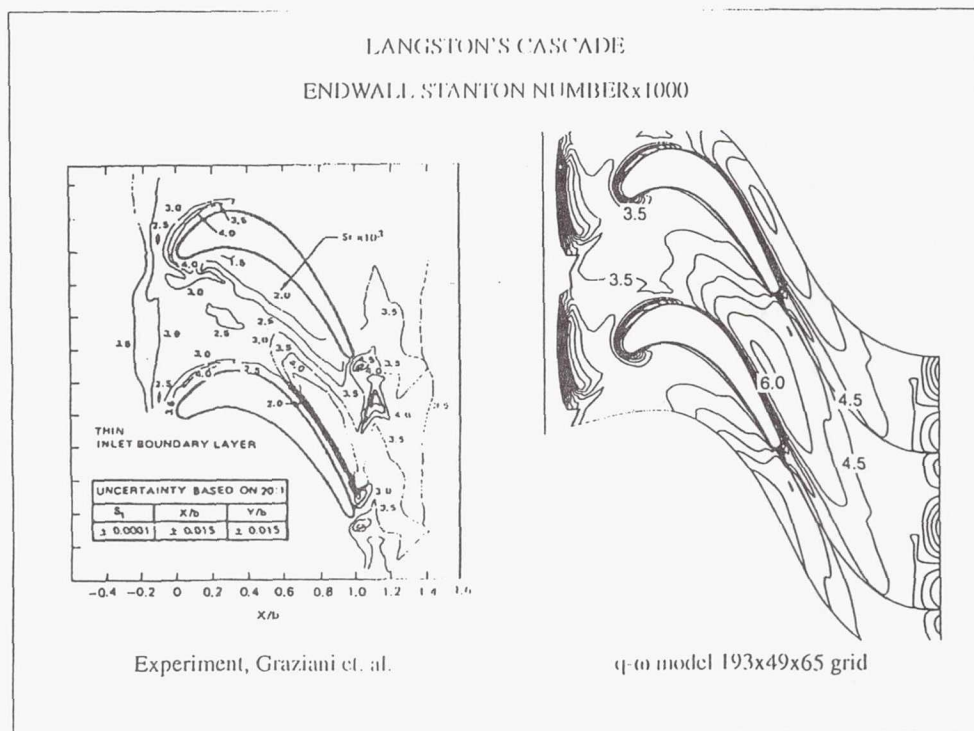


$q-\bar{u}$  model,  $193 \times 49 \times 65$  grid

Langston's Cascade  
Endwall Stanton Number x1000.



Experiment, Graziani et al.      Computation, TRAF3D  
Thin inlet boundary layer.



TURBINE HEAT TRANSFER

CONCLUSIONS

- *Two-equation models perform well in the fully turbulent regime.*
- *The uncertainty re. length scale of turb. needs to be resolved.*
- *Transition modeling is crucial to the success of H-T analysis.*
- *Need further improvements in convergence speed.*

LeRC	9/93		I
------	------	--	---

Thermal Turbulence Models  
for  
Turbine Blade Heat Transfer

John R. Schwab

LeRC	9/93	Objective and Rationale	≥
------	------	-------------------------	---

Objective: Improved prediction of turbine blade surface  
temperature and heat-transfer distributions

Rationale: Existing heat-flux models lack the fundamental  
generality required for complex flows

LeRC	9/93	Approach	3
Fundamental analysis of thermal DNS results			
Detailed evaluation of existing heat-flux models			
Development of thermal time scale model			

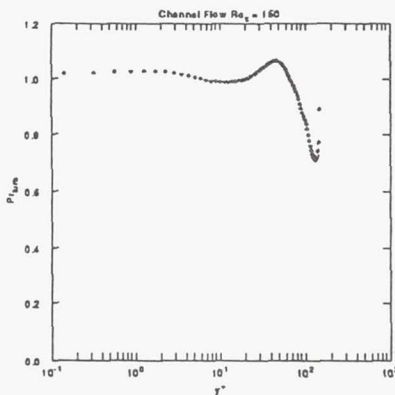
LeRC	9/93	Kasagi, Tomita, and Kuroda DNS	4
fully-developed turbulent channel flow			
constant-heat-flux walls with $Nu = 15.4$			
$Re_\tau = 150$ $Re_{mean} = 4580$ $Pr = 0.71$			
ASME J. Heat Transfer, Vol. 114, August 1992			

LeRC

9/93

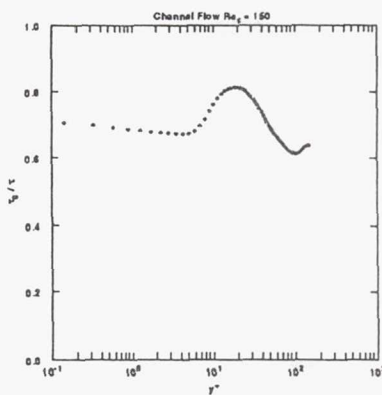
Kasagi, Tomita, and Kuroda DNS

S



$$Pr_{turb} \neq 0.9$$

$$Pr_{turb} \neq \text{constant}$$



$$\tau_\theta / \tau \neq 0.5$$

$$\tau_\theta / \tau \neq \text{constant}$$

LeRC

9/93

Evaluation of existing heat-flux models

lo

Constant  $Pr_t$  models inadequate

Flux-transport models expensive

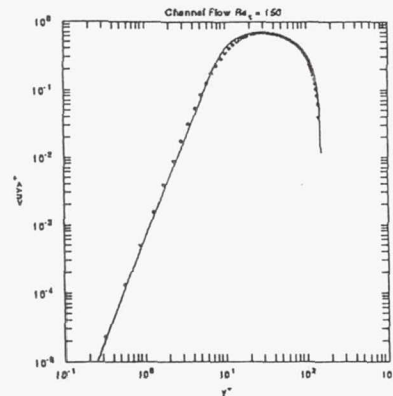
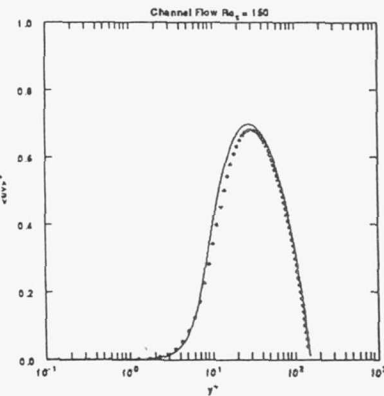
Two-equation thermal models offer affordable improvement

LeRC

9/93

Nagano-Tagawa with  $\Pr_t = 0.86$  vs. Kasagi DNS

7



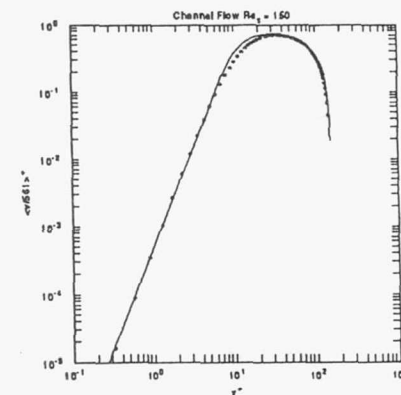
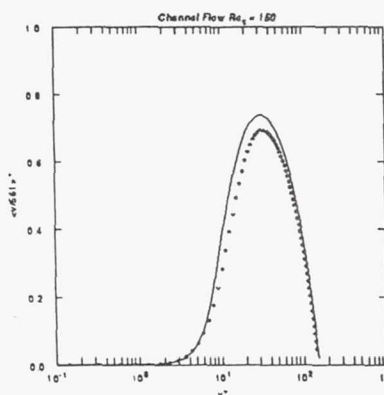
good overall agreement and proper asymptote for  $\langle uv \rangle^+$

LeRC

9/93

Nagano-Tagawa with  $\Pr_t = 0.86$  vs. Kasagi DNS

8



mediocre overall agreement, but proper asymptote for  $\langle v\theta \rangle^+$

Hattori, Nagano, and Tagawa (HNT)

complex damping functions (evaluation in progress)

Sommer, So, and Lai (SSL)

Shima coincidence condition (evaluation in progress)

Thermal time scale model (development in progress)

simple wall boundary condition:  $\tau_\theta = 0$

simple near-wall asymptote:  $\tau_\theta \sim y^2 / 2\alpha$

**Page intentionally left blank**

A COUPLED IMPLICIT SOLUTION METHOD FOR  
TURBULENT SPRAY COMBUSTION IN PROPULSION SYSTEMS

K.-H. CHEN

The University of Toledo, Ohio

and

J.-S. SHUEN

Sverdrup Technology, Inc., Ohio

Aerothermochemistry Branch  
Internal Fluid Mechanics Division  
NASA Lewis Research Center, Cleveland, Ohio

OBJECTIVES

- Develop an efficient and robust algorithm for multi-phase chemically reacting flows at all speeds, with emphasis on low Mach number flows.
- Calculate turbulent spray combustion flow in a gas turbine combustor.

## MOTIVATION

- Many reacting flows in propulsion devices cannot be efficiently calculated by modern compressible flow CFD algorithms, e.g.,
  - rocket motor — wide range of Mach numbers, from near zero velocity at closed end to supersonic at nozzle exit.
  - gas turbine combustor — low subsonic velocity, but large density variation precludes incompressible approach.
- Most low-speed reacting flow codes based on TEACH-type technologies – inefficient and lack of robustness for complex flows.
- Tremendous progress made in high-speed compressible flow CFD in past two decades. Extending application range to low-speed flow regime highly desirable.

## OUTLINES

- GOVERNING EQUATIONS
  - Gas-Phase Equations
  - Liquid-Phase Equations
- NUMERICAL ALGORITHM
- NUMERICAL TEST RESULTS
- CONCLUSION
- FUTURE PLAN FOR ALLSPD CODE

## GOVERNING EQUATIONS

- Gas-Phase Equations

$$\Gamma \frac{\partial \hat{Q}}{\partial \tau^*} + \frac{\partial \tilde{Q}}{\partial \tau} + \frac{\partial (\tilde{E} - \tilde{E}_v)}{\partial \xi} + \frac{\partial (\tilde{F} - \tilde{F}_v)}{\partial \eta} = \tilde{H}_c + \tilde{H}_l, \quad (1)$$

$$\hat{Q} = \frac{y^\delta}{J} \begin{pmatrix} p_g \\ u \\ v \\ h \\ \kappa \\ \epsilon \\ Y_1 \\ Y_2 \\ \cdot \\ \cdot \\ Y_{N-1} \end{pmatrix}, \quad \Gamma = \begin{bmatrix} 1/\beta & 0 & 0 & 0 & 0 & 0 & \cdot & \cdot & \cdot & \cdot & 0 \\ u/\beta & \rho & 0 & 0 & 0 & 0 & \cdot & \cdot & \cdot & \cdot & 0 \\ v/\beta & 0 & \rho & 0 & 0 & 0 & \cdot & \cdot & \cdot & \cdot & 0 \\ h/\beta - 1 & \rho u & \rho v & \rho & 0 & 0 & \cdot & \cdot & \cdot & \cdot & 0 \\ \kappa/\beta & 0 & 0 & \cdot & \rho & \cdot & \cdot & \cdot & 0 & \cdot & 0 \\ \epsilon/\beta & 0 & 0 & \cdot & \cdot & \rho & \cdot & \cdot & \cdot & 0 & 0 \\ Y_1/\beta & 0 & 0 & 0 & \cdot & \cdot & \rho & \cdot & \cdot & \cdot & 0 \\ Y_2/\beta & 0 & 0 & 0 & 0 & \cdot & \cdot & \rho & \cdot & \cdot & 0 \\ \cdot & \cdot & \cdot & \cdot & 0 & \cdot & \cdot & \rho & \cdot & \cdot & 0 \\ \cdot & \cdot & \cdot & \cdot & \cdot & 0 & \cdot & \cdot & \rho & \cdot & 0 \\ Y_{N-1}/\beta & 0 & 0 & \cdot & \cdot & \cdot & 0 & \cdot & \cdot & \rho & 0 \end{bmatrix},$$

$$H_c = \begin{pmatrix} 0 \\ -\frac{2}{3}\delta \frac{\partial(\mu_e v)}{\partial x} \\ \delta[p - \tau_{\theta\theta} - \frac{2}{3}\frac{\partial(\mu_e v)}{\partial y}] \\ -\frac{2}{3}\delta[\frac{\partial(\mu_e u v)}{\partial x} + \frac{\partial(\mu_e v^2)}{\partial y}] \\ y^\delta(\Psi - \rho\epsilon) - \frac{2}{3}\delta\mu_t v(\frac{\partial u}{\partial x} + \frac{\partial v}{\partial y}) \\ y^\delta[(c_1 f_1 \Psi - c_2 f_2 \rho \kappa)\frac{\epsilon}{\kappa} + \Lambda] - \frac{2}{3}\delta\mu_t v(\frac{\partial u}{\partial x} + \frac{\partial v}{\partial y}) c_1 f_1 \frac{\epsilon}{\kappa} \\ y^\delta S_1 \\ \cdot \\ y^\delta S_{N-1} \end{pmatrix},$$

$$H_l = \begin{pmatrix} \sum_p n_p \dot{m}_p \\ \sum_p n_p \dot{m}_p u_p - \frac{4\pi}{3} \rho_p r_p^3 n_p \frac{du_p}{dt} \\ \sum_p n_p \dot{m}_p v_p - \frac{4\pi}{3} \rho_p r_p^3 n_p \frac{dv_p}{dt} \\ \sum_p n_p \dot{m}_p h_{fs} - 4\pi r_p^2 n_p h \Delta T \\ 0 \\ 0 \\ \sum_p n_p \dot{m}_p \\ \cdot \\ 0 \end{pmatrix},$$

## ALLSPD MAIN FEATURES

### Present Capabilities

- 2-D and Axisymmetric geometries
- Second-order central difference for both inviscid and viscous terms
- Fully coupled, fully implicit algorithm
- Efficient convergence for wide range of Mach numbers (from  $M \leq 10^{-10}$  to supersonic)
- Finite-rate chemistry, realistic thermophysical properties
- Multi-block and body-fitted curvilinear coordinates for complex geometries
- $\kappa - \epsilon$  turbulence model
- Stochastic liquid spray model (dilute spray), vortex model for droplet internal circulation and diffusion
- Still a research code, require experience and knowledge of CFD and flow physics to use.

### Future Plans

- Development of a more efficient solver
- Extension to 3-D
- PDF model for turbulence/chemical reaction closure
- Thermal radiation model
- Detailed soot and NOx kinetic models
- Multi-grid and unstructured grid capabilities
- Dense spray and high pressure (near-/super-critical) spray models

## **Difficulties with Compressible Flow Algorithms at Low Mach Numbers**

- Disparities among system's eigenvalues (stiffness),  $u$ ,  $u + c$ ,  $u - c$ , resulting in significant slowdown in convergence rate.
- Singular behavior of pressure gradient term in momentum equations as Mach number approaches zero,

$$\rho^* u^{*2} + \frac{p^*}{\gamma M_r^2}$$

As Mach number is decreased, pressure variation ( $\Delta p^* \propto M^2$ ) becomes of similar magnitude as roundoff error of the large pressure gradient term ( $p^*/\gamma M_r^2$ ).

## METHOD OF APPROACH

### Pressure Singularity Problem

- Pressure decomposed into two parts:

$$p = p_o + p_g$$

$p_g$  replaces  $p$  in momentum equations and retains  $p_g$  as one of the unknowns.

- Employs conservative form of governing equations, but uses primitive variables

$$(p_g, u, v, h, Y_i)$$

as unknowns. Conservation property preserved and pressure field accurately resolved for all Mach numbers.

### Eigenvalue Stiffness Problem

- Pressure rescaled so that all eigenvalues have the same order of magnitude. Physical acoustic waves removed and replaced with pseudo-acoustic waves which travel at speed comparable to fluid convective velocity.

## EIGENVALUES RESCALING

$$\lambda = U, \quad U, \quad \frac{1}{2} \left[ U \left( 1 + \frac{\beta}{c^2} \right) \pm \sqrt{U^2 \left( 1 - \frac{\beta}{c^2} \right)^2 + 4\beta(\alpha_1^2 + \alpha_2^2)} \right], \quad U, \quad U \dots$$

$$\alpha_1 = \xi_z, \quad \alpha_2 = \xi_y, \quad U = \alpha_1 u + \alpha_2 v.$$

For well-conditioned eigenvalues, scaling factor  $\beta$  taken to be

$$\beta = u^2 + v^2 .$$

## LIQUID-PHASE EQUATIONS

### • Droplet Motion Equations

$$\frac{dx_p}{dt} = u_p, \quad (2)$$

$$\frac{dy_p}{dt} = v_p, \quad (3)$$

$$\frac{du_p}{dt} = \frac{3}{16} \frac{C_D \mu_g Re_p}{\rho_p r_p^2} (u_g - u_p), \quad (4)$$

$$\frac{dv_p}{dt} = \frac{3}{16} \frac{C_D \mu_g Re_p}{\rho_p r_p^2} (v_g - v_p), \quad (5)$$

$$Re_p = 2 \frac{r_p \rho_g}{\mu_g} [(u_g - u_p)^2 + (v_g - v_p)^2]^{1/2},$$

$$\frac{24}{Re_p} \left(1 + \frac{Re_p^{2/3}}{6}\right) \quad \text{for } Re_p < 1000,$$

$$C_D = \begin{cases} 0.44 & \text{for } Re_p > 1000. \end{cases}$$

### • Droplet Heat and Mass Transfer Equations

$$\frac{\dot{m}_p'' d_p}{\rho D_f} = 2N_s \ln(1 + B), \quad (6)$$

$$\frac{hd_p}{k} = \frac{2N_p \ln(1 + B)^{Le^{-1}}}{[(1 + B)^{Le^{-1}} - 1]} \quad (7)$$

$$N_s = 1 + \frac{0.276 Re_p^{1/2} Pr^{1/3}}{\left[1 + \frac{1.232}{Re_p Pr^{4/3}}\right]^{1/2}} \quad N_p = 1 + \frac{0.276 Re_p^{1/2} Sc^{1/3}}{\left[1 + \frac{1.232}{Re_p Sc^{4/3}}\right]^{1/2}},$$

$$B = \frac{Y_{fgp} - \bar{Y}_{fg}}{1 - Y_{fgp}} \quad Y_{fgp} = \frac{X_{fgp} W_f}{X_{fgp} W_f + (1 - X_{fgp}) W_a}$$

- Droplet Internal Temperature Equations  
(Vortex Model)

$$\frac{\partial T_p}{\partial t} = 17 \frac{k_l}{C_{pl}\rho_l r_p^2} [\alpha \frac{\partial^2 T_p}{\partial \alpha^2} + (1 + C(t)\alpha) \frac{\partial T_p}{\partial \alpha}] \quad (8)$$

$$C(t) = \frac{3}{17} \left( \frac{C_{pl}\rho_l}{k_l} \right) r_p \frac{dr_p}{dt}$$

$$t = t_{inj}, \quad T_p = T_{inj},$$

$$\alpha = 0, \quad \frac{\partial T_p}{\partial \alpha} = \frac{1}{17} \left( \frac{C_{pl}\rho_l}{k_l} \right) r_p^2 \frac{\partial T_p}{\partial t},$$

$$\alpha = 1, \quad \frac{\partial T_p}{\partial \alpha} = \frac{3}{16} r_p \frac{\partial T_p}{\partial r},$$

### NUMERICAL ALGORITHM

- Gas-Phase - ALLSPD code
- Liquid-Phase
  - Droplet motion equations (ODE) - Runge-Kutta method.
  - Droplet internal equations (PDE) - implicit method (Thomas algorithm).
  - Determination of spray time step for integration.
  - Stochastic separate flow model.
- Interaction Between Two Phases

## SPRAY TIME STEP

- Droplet Velocity Relaxation time ( $t_r$ )

$$t_r = \frac{16}{3} \left( \frac{\rho_l}{\rho_g} \right) \left( \frac{r_p^2}{\nu} \right) (C_D Re_p)^{-1}.$$

- Droplet Life Time ( $t_l$ )

$$t_l = \frac{r_p}{3\dot{m}_p'' \rho_l}.$$

- Droplet Surface Temperature Constraint Time ( $t_s$ )

$$t_s = \ln\left(\frac{1}{1 - \frac{\Delta T_p}{A}}\right)/A'$$

$$\frac{dT_p}{dt} = \frac{6}{\rho_l C_v d_p} [h(\bar{T} - T_p) - \dot{m}_p'' h_{fg}]$$

- Local Grid Time Scale ( $t_g$ )
- Turbulent Eddy-Droplet Interaction Time ( $t_i$ )

$$t_i = t_e, \quad \text{if } L_e > \tau |\vec{u}'' - \vec{u}_p''|$$

$$t_i = \min(t_e, t_t), \quad \text{if } L_e < \tau |\vec{u}'' - \vec{u}_p''|$$

where

$$\begin{aligned} L_e &= C_\mu^{3/4} \kappa^{3/2} / \epsilon \\ t_e &= L_e / (2\kappa/3)^{1/2}. \\ t_t &= -\tau \ln[1 - L_e / (\tau |\vec{u}'' - \vec{u}_p''|)] \end{aligned}$$

- Spray Time step -  $\Delta T_{spr}$

$$\Delta t_{spr} = \alpha \min(t_r, t_l, t_s, t_g, t_i)$$

## INTERACTION BETWEEN TWO PHASES

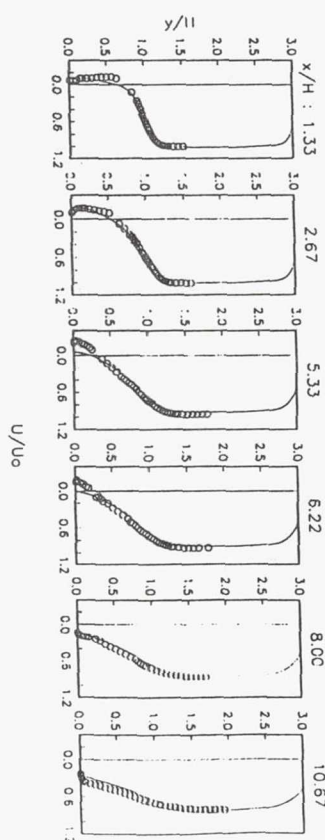
1. Initialize gas and liquid phase variables.
2. Solve liquid-phase equations.
3. Evaluate spray source term,  $H_l$ .
4. Solve gas-phase equations and update gas-phase variables.
5. Update spray source term,  $H_l$  ?  
    No, go to step 4.  
    Yes, go to step 2.

## NUMERICAL TEST RESULTS

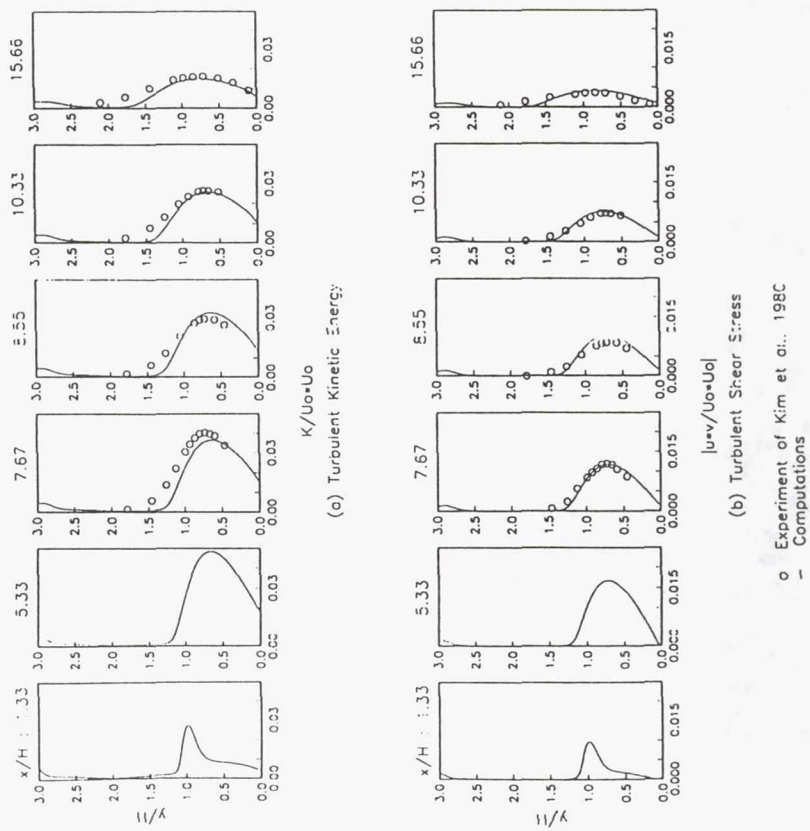
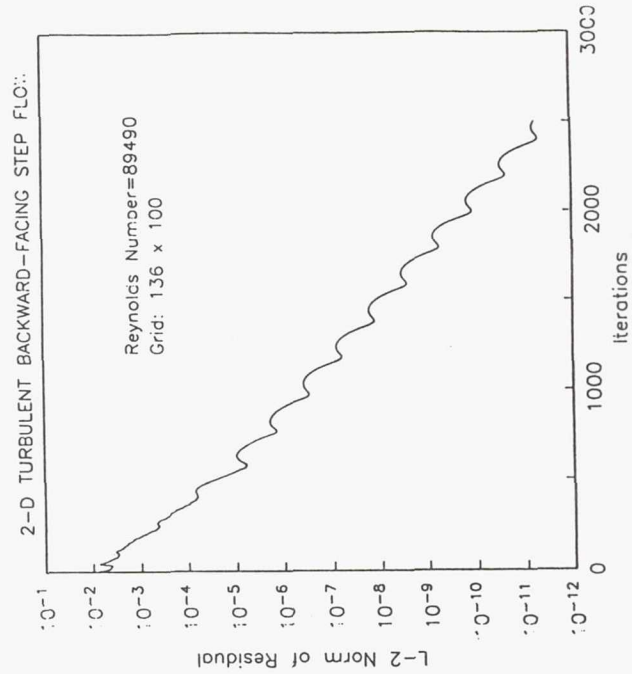
- Turbulent Backward-Facing Step Flow - non-reacting.
- Evaporating Turbulent Spray Flow.
- Gas Turbine Spray Combustion Flow.

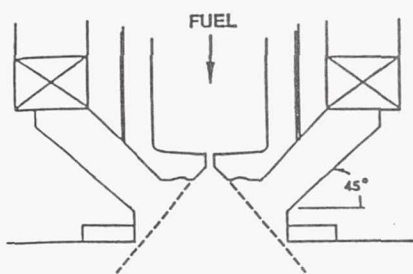
PARTICLE TRACES

0.052  
89490,00 1DEG  
136 x 100 MACH  
ALPHA GRID



○ Experiment of Kim et al., 1980  
— Computations

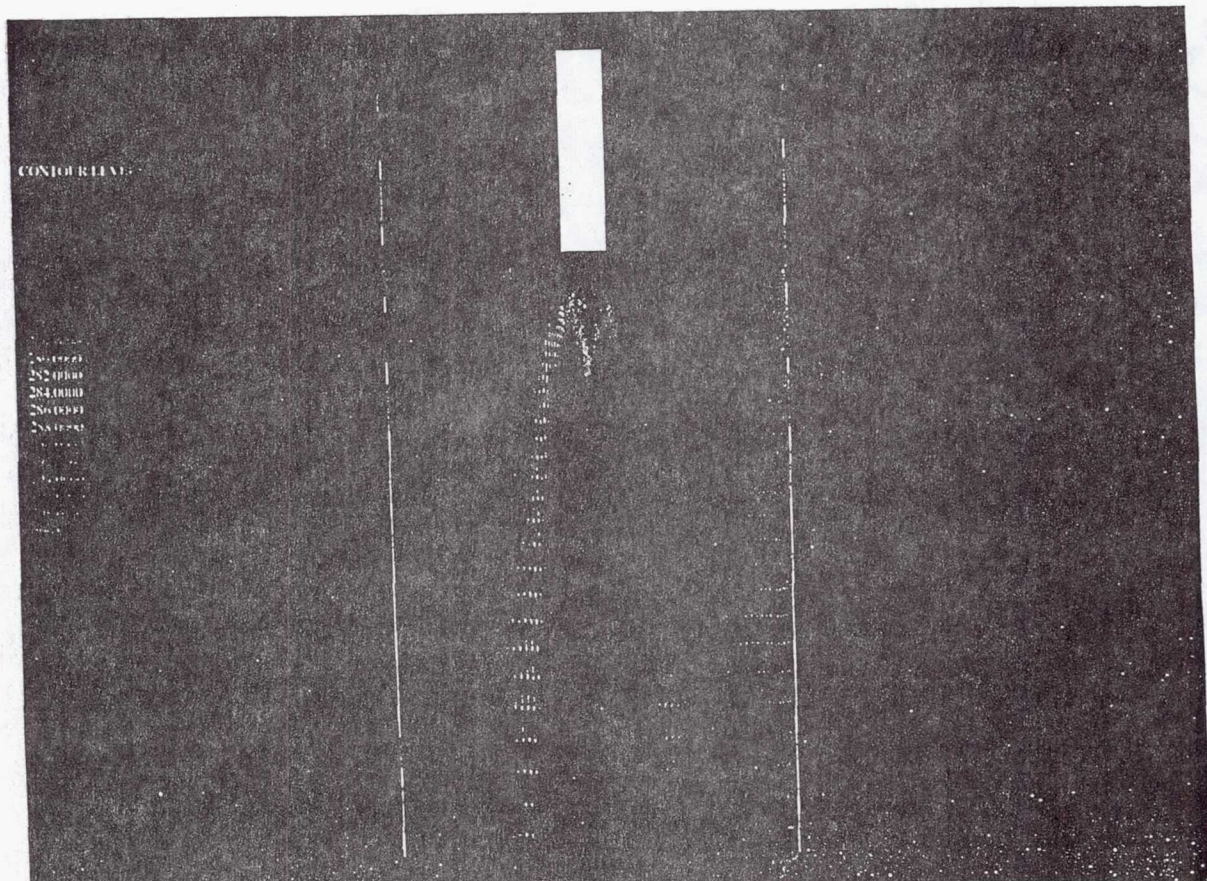


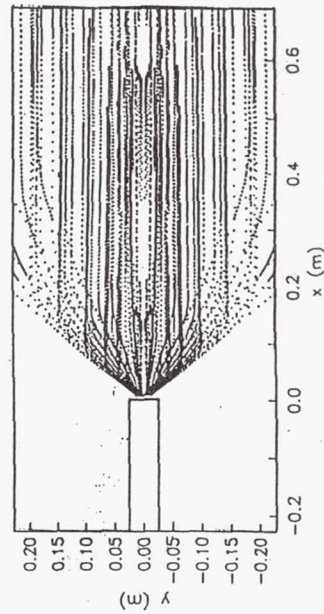
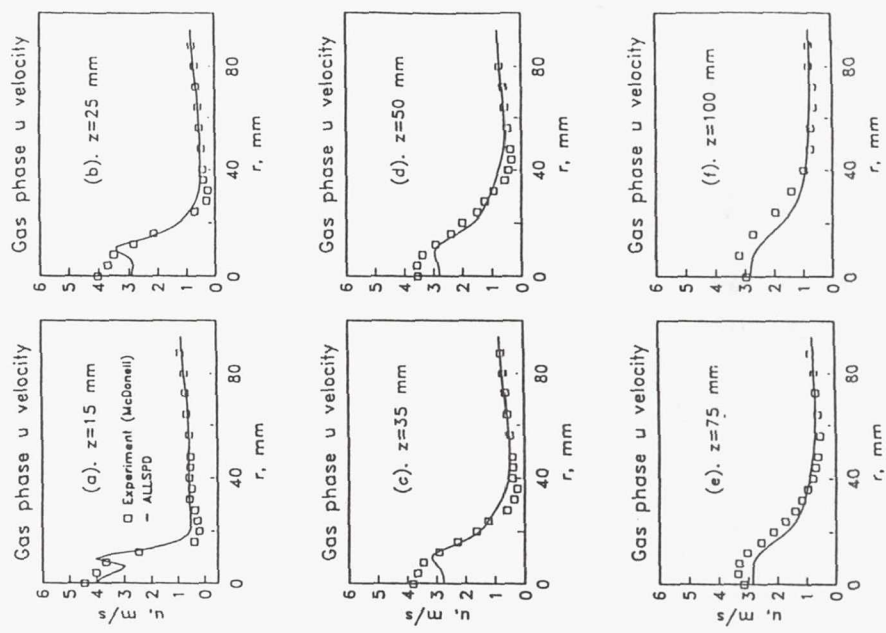


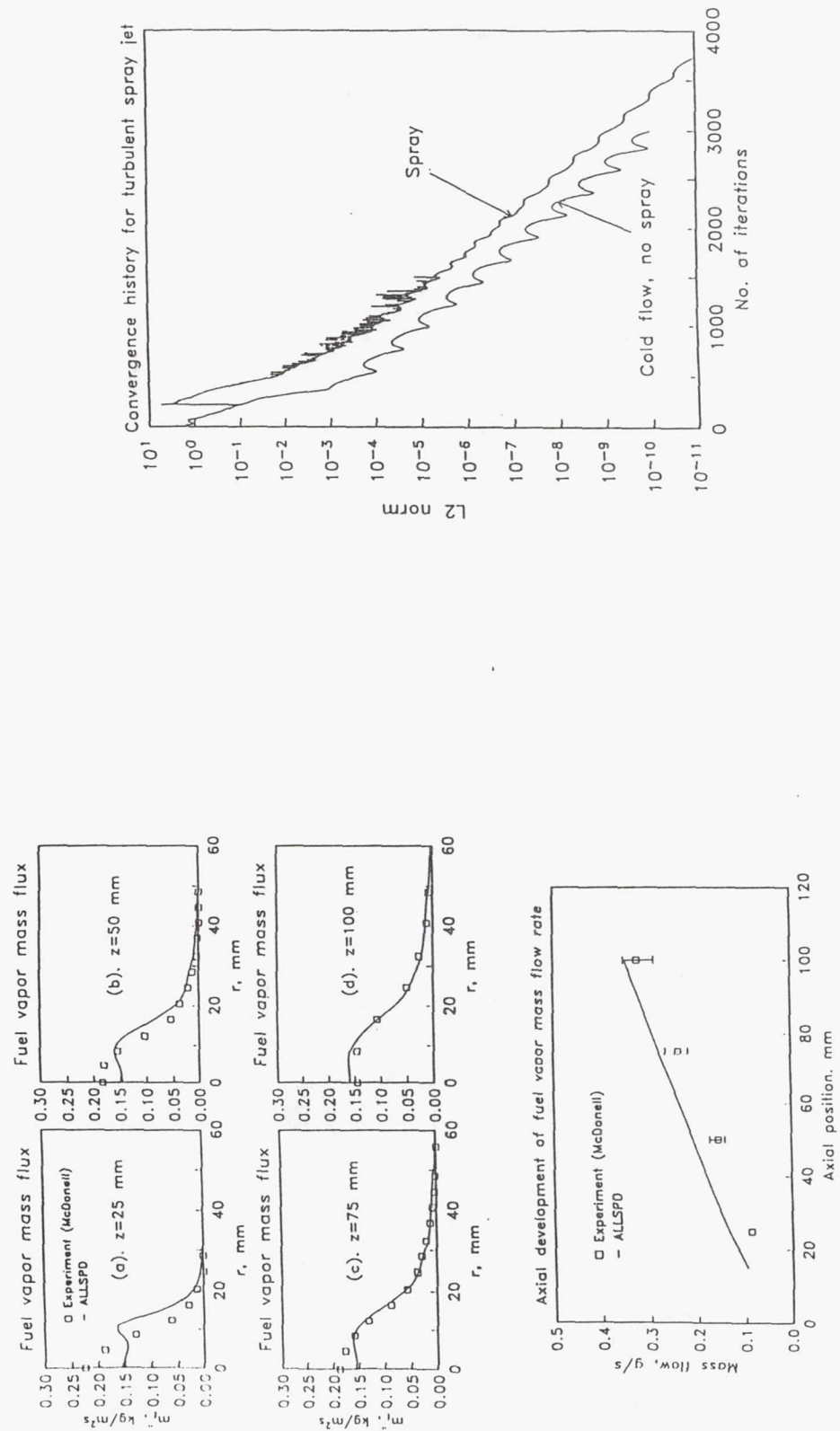
OPERATING MODE 1  
NO ATOMIZING AIR

LIQUID FLOW RATE : 1.26 grams / sec

AIR FLOW RATE : 0.00 grams / sec







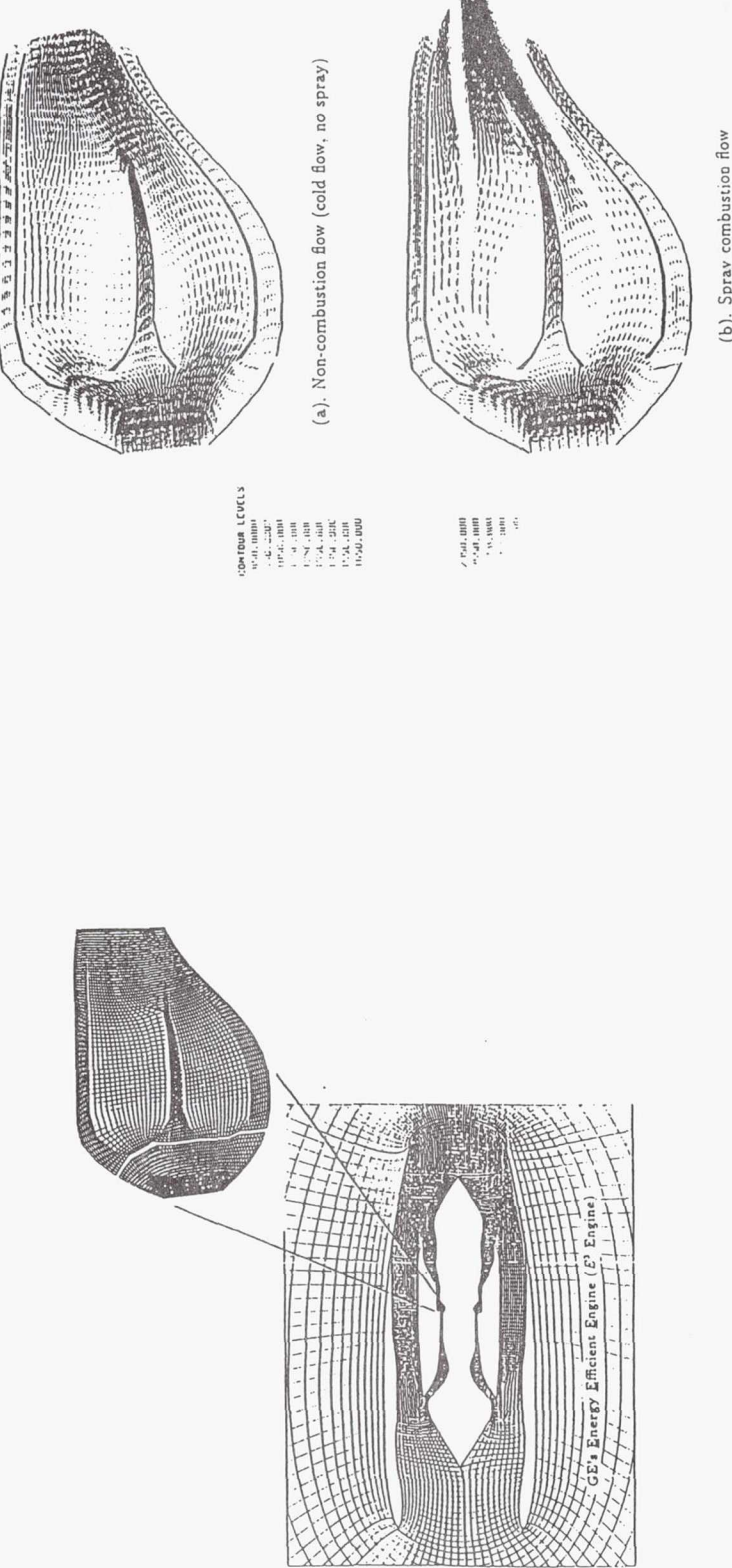


Fig. 9 Center-plane cut for GE's EEE gas turbine engine and the grid for the combustor.

Fig. 11 Velocity vectors (colored by temperature) for (a) non-combustion and (b) spray combustion cases for the gas turbine spray combustion flow.

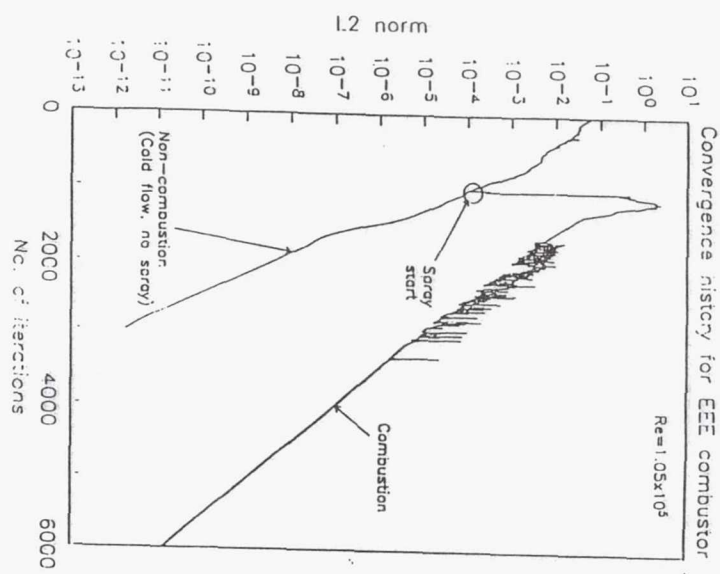


Fig. 13 Convergence history for both non-combustion and spray combustion cases for the gas turbine spray combustion flow.

## CONCLUSION

- ALLSPD code efficiently coupled with the SSF spray model.
- Satisfactory convergence property for flows with and without spray.

## Numerical Investigation of Complex, Transitional, and Chemically Reacting Flows

S.-W. Kim  
Resident Research Associate  
NASA Lewis Research Center  
Cleveland, Ohio 44135

### Part A. On Turbulent Transport of chemical Species in Compressible Reacting Flows

#### Contents

Mixing of chemical species in reacting flows

Analysis

Chemically reacting, turbulent flow equations

Density-weighted, time-averaged Navier-Stokes equations

Multiple-time-scale turbulence equations

Species conservation equations for reacting flows

Numerical Method

Mixing and combustion of hydrogen in vitiated supersonic airstream.

Comparison with measured data and other numerical results obtained using  
k- $\epsilon$  turbulence models and a PDF.

Conclusions and Discussion

## Mixing of chemical species in reacting flows

### Chemically Reacting Laminar Flows

Numerical (or semi-analytical) methods

O.D.E. solvers

1-D Numerical methods

Numerical uncertainty is minimal

### Chemical kinetics

Chemical kinetics (finite rate chemical kinetics & Reduced finite rate chemical kinetics) for certain fuels (hydrogen and some of hydro-carbons) have been tested and validated repeatedly.

Numerical and theoretical analyses yield accurate results.

## Chemically Reacting Turbulent Flows

### Numerical methods

Boundary layer or Navier-Stokes equations solvers  
(Except for semi-analytical analyses of PSR cases)

Uncertainty is caused partly by numerical methods.

### Chemical kinetics

Finite rate chemical kinetics & Reduced finite rate chemical are used.

Uncertainty is caused partly by over-simplified chemical kinetics.

### Turbulence Equations

Numerical analysis yields not so accurate results. Uncertainty caused by turbulence equations is by far greater than that caused by chemical kinetics.\*

The probability density functions are used to improve the predictive capability of turbulent mixing of chemical species. However, some pdf methods yield physically incorrect numerical results.

It is certainly important to better understand the turbulent mixing of chemical species in reacting flows.

\* Westbrook and Dryer, *Prog. Energy Combustion Science*, vol. 10, pp. 1-57, 1984.

## Turbulent Mixing of Chemical Species in Reacting Flows

1. Large eddy mixing
2. Turbulent Mixing
3. Molecular Mixing

The use of accurate chemical kinetics alone can not yield accurate results for numerical analysis of turbulent reacting flows unless turbulent mixing is resolved correctly.

### Large Eddy Mixing

Caused by separated flows, recirculating flows, and organized structures.

The extent of calculated recirculation zone or the organized structures depends on the accuracy of both the numerical method and the turbulence equations since they are nonlinearly coupled with each other.

$$\frac{\partial}{\partial t}(\rho u_i) + \frac{\partial}{\partial x_j}(\rho u_i u_j) - \frac{\partial}{\partial x_j} \left( (\mu + \mu_t) \left( \frac{\partial u_i}{\partial x_j} + \frac{\partial u_j}{\partial x_i} \right) \right) = - \frac{\partial p}{\partial x_i}$$

$$\frac{\partial}{\partial t}(\rho k) + \frac{\partial}{\partial x_j}(\rho u_j k) - \frac{\partial}{\partial x_j} \left( \frac{\mu + \mu_t}{\sigma_t} \frac{\partial k}{\partial x_j} \right) = P_r - \varepsilon_t$$

$$\text{where } \mu_t = \mu_t(k, \varepsilon_t, \dots), \text{ and } P_r = \frac{\mu_t}{\rho} \left\{ 2 \left( \frac{\partial u}{\partial x} \right)^2 + 2 \left( \frac{\partial v}{\partial y} \right)^2 + \left( \frac{\partial u}{\partial y} + \frac{\partial v}{\partial x} \right)^2 \right\}$$

Therefore, the capability to correctly resolve the large eddy mixing depends on the accuracy of the numerical method and the turbulence equations.

Numerical investigations carried out during last decades show that  $k-\varepsilon$ , ARSM, and RSM do not yield accurate results for complex turbulent flows.

On the other hand, the multiple-time-scale turbulence equations\* yield highly improved numerical results for various complex turbulent flows.

\*Kim and Benson, *Int. J. Heat Mass Transfer*, vol.35, pp. 2357-2365, 1992.

### Turbulent Mixing

Caused mostly by energy-containing eddies and partly by fine-scale eddies.

The capability to resolve the turbulent mixing of chemical species depends on the capability of the turbulence equations to correctly describe the turbulent transport of scalar variables (i.e., heat transfer, turbulent kinetic energy, concentrations, and convection-diffusion of species, etc)

Need to be able to describe the chemical reaction-turbulence interaction (i.e., turbulent mixing is enhanced and shear layer thickness is widened by chemical reaction)\*

The multiple-time-scale turbulence equations can resolve the cascade of turbulent kinetic and the nonequilibrium turbulence phenomena.  
(Present numerical results show that the M-S turbulence equations can resolve the chemical reaction-turbulence interaction.)

\* C.T. Chang et al., "Comparison of reacting and non-reacting shear layers at a high subsonic mach number," AIAA paper 93-2381, 1993.

### Molecular Mixing

Caused by molecular diffusivity.

Theoretical and numerical analyses of chemically reacting laminar flows yield accurate results.

Various molecular diffusion equations can accurately describe the molecular diffusion of species.

The Lennard-Jones 12-6 potential law is used in the present study.

Various numerical methods that yield accurate results for laminar flows can resolve the molecular mixing.

### Multiple-time-scale turbulence equations

Energy containing eddies

$$\frac{\partial}{\partial t} (\rho k_p) + \frac{\partial}{\partial x_j} (\rho u_j k_p) - \frac{\partial}{\partial x_j} \left( \left( \mu + \frac{\mu_t}{\sigma_{kp}} \right) \frac{\partial k_p}{\partial x_j} \right) = \rho P_r - \rho \varepsilon_p$$

$$\frac{\partial}{\partial t} (\rho \varepsilon_p) + \frac{\partial}{\partial x_j} (\rho u_j \varepsilon_p) - \frac{\partial}{\partial x_j} \left( \left( \mu + \frac{\mu_t}{\sigma_{\varepsilon p}} \right) \frac{\partial \varepsilon_p}{\partial x_j} \right) = \frac{\rho}{k_p} (c_{p1} P_r^2 + c_{p2} P_r \varepsilon_p - c_{p3} \varepsilon_p^2)$$

Fine Scale Eddies

$$\frac{\partial}{\partial t} (\rho k_t) + \frac{\partial}{\partial x_j} (\rho u_j k_t) - \frac{\partial}{\partial x_j} \left( \left( \mu + \frac{\mu_t}{\sigma_{kt}} \right) \frac{\partial k_t}{\partial x_j} \right) = \rho \varepsilon_p - \rho \varepsilon_t$$

$$\frac{\partial}{\partial t} (\rho \varepsilon_t) + \frac{\partial}{\partial x_j} (\rho u_j \varepsilon_t) - \frac{\partial}{\partial x_j} \left( \left( \mu + \frac{\mu_t}{\sigma_{\varepsilon t}} \right) \frac{\partial \varepsilon_t}{\partial x_j} \right) = \frac{\rho}{k_t} (c_{t1} \varepsilon_p^2 + c_{t2} \varepsilon_p \varepsilon_t - c_{t3} \varepsilon_t^2)$$

Turbulent Eddy Viscosity

$$\mu_t = \rho c_\mu k^2 / \varepsilon_p \text{ where } c_\mu = c_{\mu f} \varepsilon_t / \varepsilon_p$$

**Remark:** Single-time-scale turbulence models can not resolve nonequilibrium turbulence phenomena.

### Species conservation equations for reacting flows

Chemical species concentration equation

$$\frac{\partial}{\partial t} (\rho Y_i) + \nabla \cdot (\rho Y_i (v + V_i)) = \dot{w}_i$$

where the diffusion velocity,  $V_i$ , is approximated using the Fick's law given as

$$Y_i V_i = - (D_{i,l} + D_{i,t}) \nabla Y_i$$

The production rate of the  $i$ -th species,  $\dot{w}_i$ , is given as

$$\dot{w}_i = \sum_{k=1}^{N_r} M_i (n_{i,k}'' - n_{i,k}') w_k$$

where

$$\omega_k = k_{f,k} \prod_{j=1}^{N_s} c_j^{v_{j,k}'} - k_{b,k} \prod_{j=1}^{N_s} c_j^{v_{j,k}''}$$

Chemical reactions for the combustion of H<sub>2</sub> in a vitiated supersonic airstream are described using 9 chemical species (H<sub>2</sub>, O<sub>2</sub>, H<sub>2</sub>O, OH, O, H, HO<sub>2</sub>, H<sub>2</sub>O<sub>2</sub>, and N<sub>2</sub>) and 24 pairs of reaction-steps (Burks and Oran, 1981; Kumar, 1989).

A fast chemistry can not be used to describe the fine details of chemically reacting flows.

A reduced chemical kinetics can not be used confidently due to the uncertainty contained in the reaction mechanisms.

The use of a detailed finite rate chemistry may make it difficult to obtain a fully converged solution due to the coupling between the large number of flow, turbulence, and chemical equations. The numerical method needs to be strongly convergent. Accuracy also depends on the capability of turbulence equations used.

### Numerical Method

The numerical method is a finite volume method that incorporates a pressure-staggered mesh and an incremental pressure equation for the conservation of mass.

Predictor Step: Solve momentum equation.

$$(\rho C_1 + A_i^*) u_i^{**} = \sum_{nb} A_k^* u_k^{**} + S_i^* - \frac{\partial p^*}{\partial x_i} + \rho C_2 u_i^{n-1} - \rho C_3 u_i^{n-2} \quad (1)$$

Corrector Step: Correct the velocity field to be divergence free

Incremental pressure equation

$$\frac{\partial}{\partial x_j} \left( \frac{p'}{RT} u_j^{**} \right) - \frac{\partial}{\partial x_j} \left( \frac{1}{(\rho C_1 + A_j^*)} \frac{\partial p'}{\partial x_j} \right) = - \frac{\partial u_j^{**}}{\partial x_j} \quad (2)$$

Incremental velocity equation

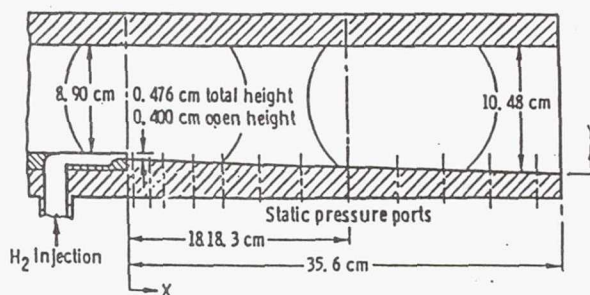
$$u_i' = \frac{1}{(\rho C_1 + A_i^*)} \frac{\partial p'}{\partial x_i} \quad (3)$$

Velocity and pressure corrections

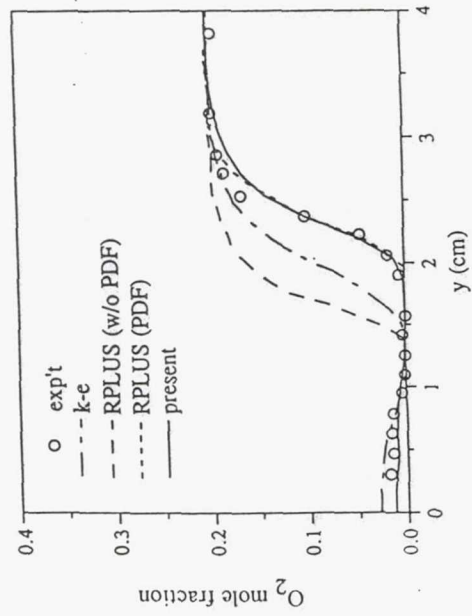
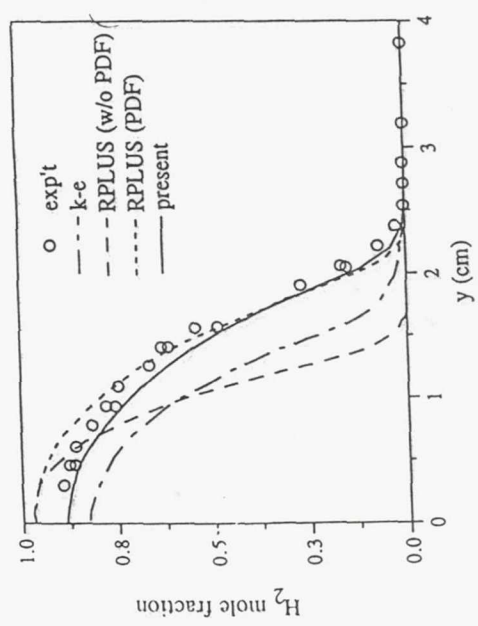
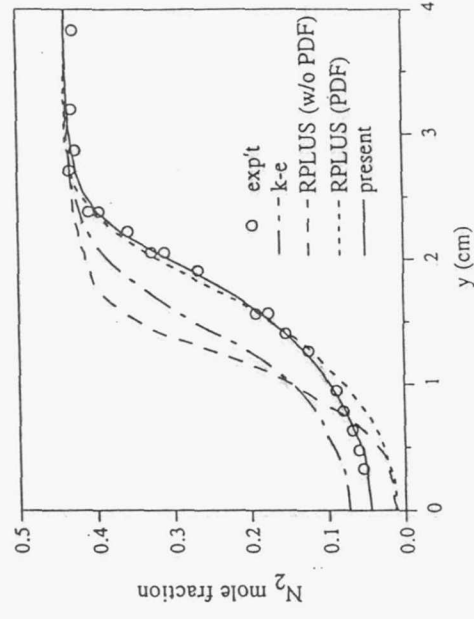
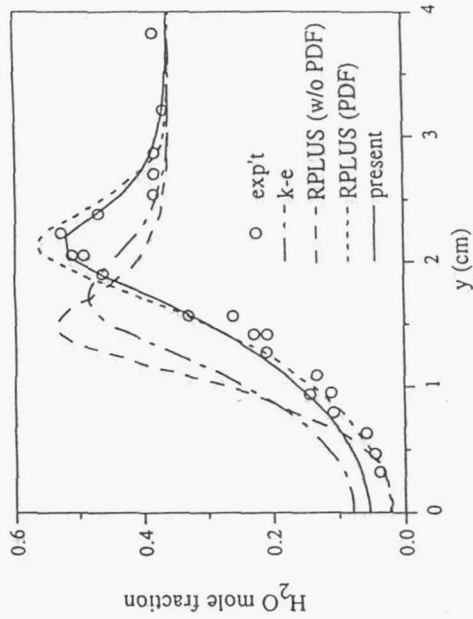
$$u_i^{***} = u_i^{**} + u'_i \quad (4)$$

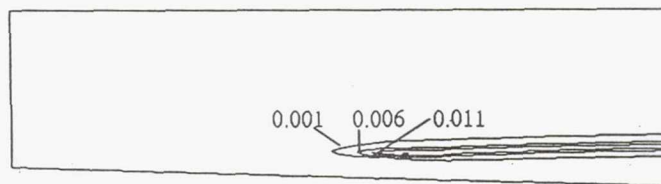
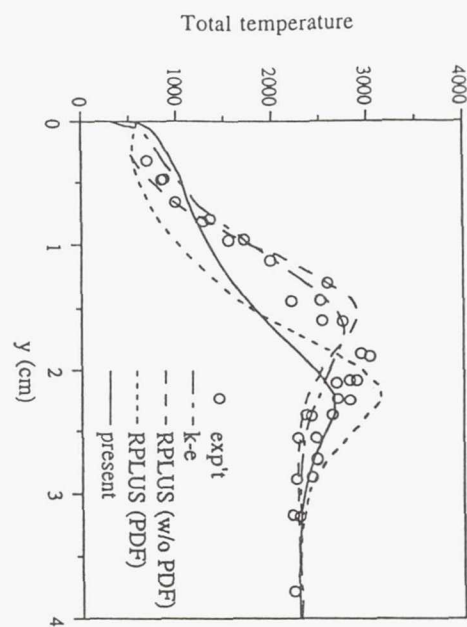
$$p^{**} = p^* + p' \quad (5)$$

Solve eqs. (1-5) iteratively until all flow variables are converged.



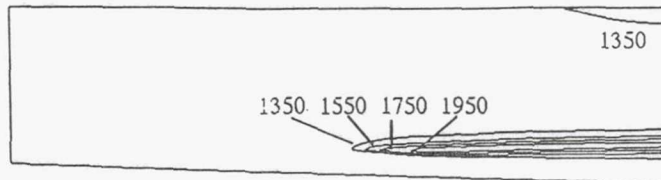
Combustion of H<sub>2</sub> in vitiated supersonic airstream (Burrows and Kurkov, 1973)





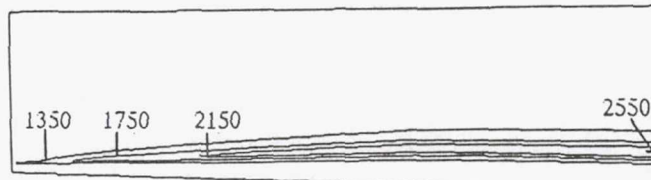
Calculated OH contour.

The numerical result obtained using the M-S turbulence equations indicates that the combustion occurs at approximately middle of the channel. The calculated flame location is in excellent agreement with that observed in the experiment.



Temperature contours obtained using the M-S turbulence equations

It can be seen in the temperature contours that the calculated flame location obtained using the M-S turbulence equations are in correct agreement with the measured data. The contours also indicate that the temperature increases within in a short distance. The trend is in correct agreement with experimental observations that temperature increase occurs within a finite flame thickness.



Temperature contours obtained using the pdf\*

The pdf fails to predict the correct flame location (i.e., ignition delay). The slowly increasing temperature field indicates that the pdf may not be able to predict a correct flame front. The numerical results obtained using the pdf are not in correct agreement with the physics of combustion.

\* A. T. Hsu, Y.-L.P. Tsai, and M. S. Raju, "A PDF approach for compressible turbulent reacting flows," AIAA Paper 93-0087, 1993.

## Conclusions and Discussion

The calculated species concentration profiles are in as good agreement with the measured data as those obtained using the pdf.

The flame location (ignition delay) obtained using the multiple-time-scale turbulence equations is in excellent agreement with the experimentally observed onset of ultraviolet radiation.

Cascade of the turbulence field is influenced by the extra strains caused by chemical reaction.

Both the numerical results and the measured data exhibit enhanced mixing of the hydrogen and vitiated airstream for the reacting case.

The M-S turbulence equations can resolve the chemical reaction-turbulence interaction.

The pdf produces slowly increasing temperature field and it fails to predict the ignition delay. Thus the numerical results obtained using the pdf are not in correct agreement with physics of combustion.

## Part B. Unsteady Transitional Flows over Forced Oscillatory Surfaces\*

### Contents

#### Nomenclature

#### Unsteady turbulent flow equations for flows with moving boundaries

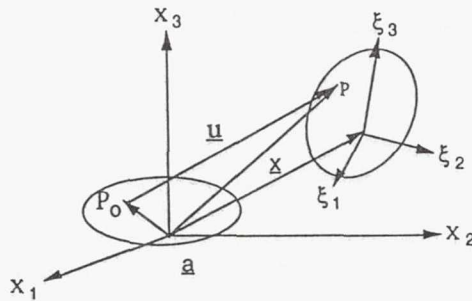
- Navier-Stokes equations defined on Lagrangian-Eulerian coordinates
- Multiple-time-scale turbulence equations

#### Numerical results

#### Unsteady transitional flow field and comparison with measured data.

\* S.-W. Kim, K.B.M.Q. Zaman, and J. Panda, "Calculation of unsteady transitional flow over oscillating airfoil" in *Separated Flows*, eds. J.C. Dutton and L.P. Purtell, Proceeding of ASME Fluid Engineering Conference, Washington D.C., June 20-24, 1993.

### Nomenclature



Lagrangian-Eulerian coordinates

$x$ : fixed reference coordinates

$\xi$ : moving coordinates

$$J = |\partial \xi_j / \partial x_j|$$

### Unsteady transitional flow equations with moving boundaries

Conservation of mass equation

$$\frac{\partial}{\partial t}(\rho J) = J \frac{\partial}{\partial x_j} \left\{ \rho (u_j^g - u_j) \right\} \quad (1)$$

Conservation of linear momentum equation

$$\frac{\partial}{\partial t}(\rho u_i J) = J \frac{\partial}{\partial x_j} \left\{ \rho u_i (u_j^g - u_j) \right\} + J \frac{\partial \tau_{ij}}{\partial x_j} - J \frac{\partial p}{\partial x_i} \quad (2)$$

Convection-diffusion equation for scalar variables (i.e.,  $\phi = \{k_p, \epsilon_p, k_t, \epsilon_t, \text{etc.}\}$ )

$$\frac{\partial}{\partial t}(\rho \phi J) = J \frac{\partial}{\partial x_j} \left\{ \rho \phi (u_j^g - u_j) \right\} + J \left\{ \mu_e \frac{\partial \phi}{\partial x_j} \right\} - J \rho f(\phi)$$

## Numerical Method

The unsteady transitional flow equations are solved using the same finite volume method. Time-integration is made using an iterative-time-advancing scheme.

### Comparison of Unsteady Flow Solution Techniques\*

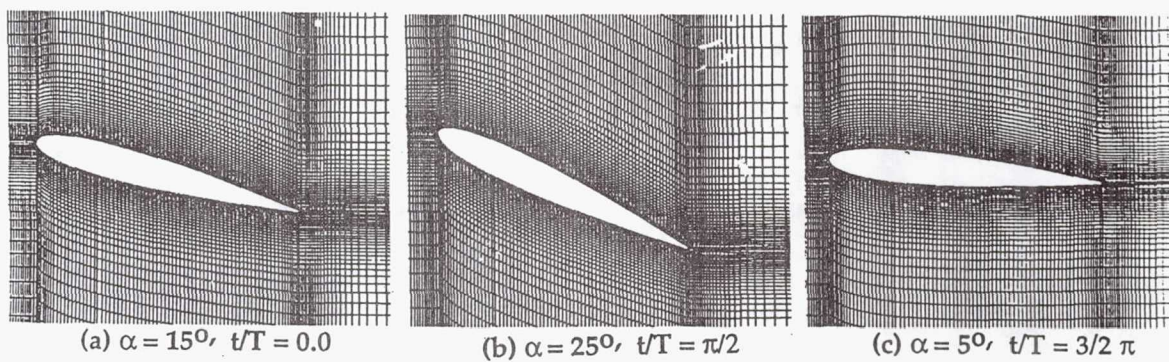
- Iterative Time-Advancing Scheme (ITA).
- Simplified Marker and Cell (SMAC).
- Pressure-Implicit Splitting of Operators (PISO).

The ITA that can best resolve the nonlinearity of the Navier-Stokes equations, and yields the most accurate results.

The SMAC is the most efficient computationally and yields accurate numerical results for laminar flows.

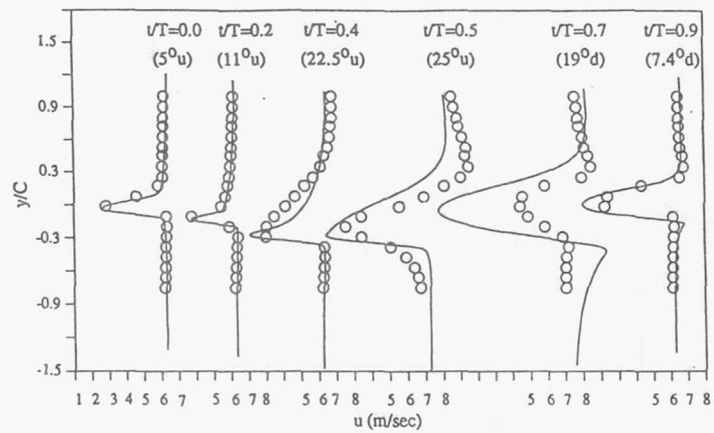
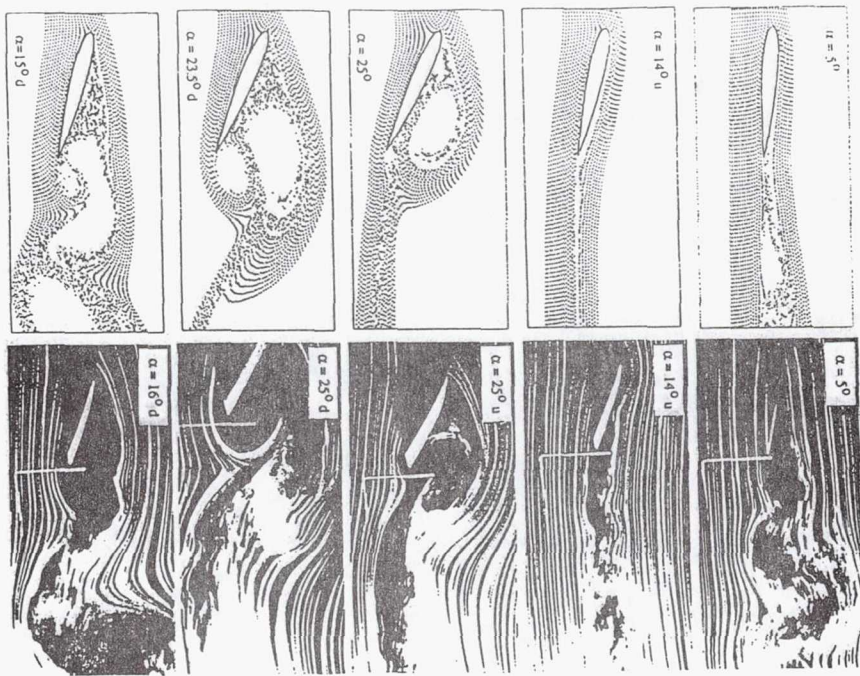
The PISO is the most unstable numerically and yields less accurate results.

\* Kim & Benson, Computers and Fluids, vol. 21, pp. 435-454, 1992



Oscillating airfoil and moving mesh

Comparison of calculated streaklines with smoke picture.

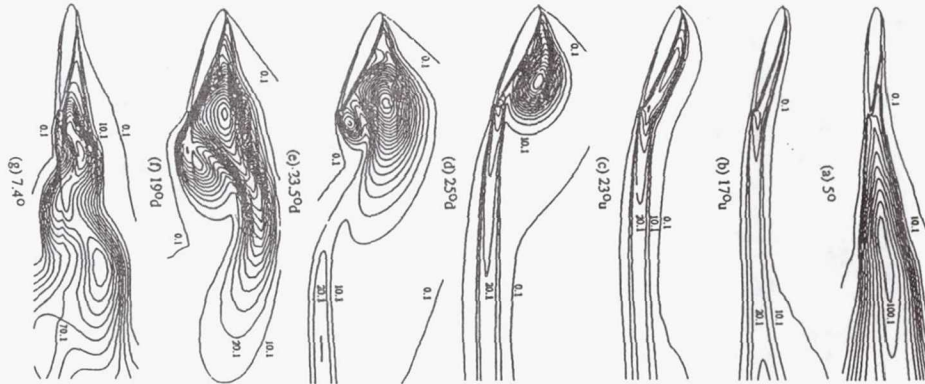


Ensenble-averaged velocity profiles at  $x/c=1.0$

The deteriorated comparison at  $\alpha \approx 19^\circ d$

- (i) The hot wire can not accurately measure the velocity components when the flow is misaligned more than approximately  $30^\circ$  from the hot wire axis.
- (ii) The interaction between the DSV and the TEV occurs in a relatively coarse mesh region and the numerical method yields somewhat deteriorated results.

Turbulent viscosity contour ( $\Delta\mu/\mu_t = 10$ )



## CONCLUSIONS AND DISCUSSION

Numerical method successfully predicts the Dynamic Stall Vortex and the Trailing Edge Vortex.

The calculated ensemble-averaged velocity profiles are in good agreement with the measured data.

Both the numerical results and the measured data show that the transition from laminar to turbulent state and relaminarization occur widely in space and in time.

The good comparison between the numerical results and the experimental data are attributed to the capability of

- (i) the ITA that can best resolve the nonlinearity of the Navier-Stokes equations,
- (ii) the new pressure correction algorithm that can strongly enforce the conservation of mass, and
- (iii) the Multiple-time-scale turbulence equations that can resolve the transitional nonequilibrium turbulence field.

**Page intentionally left blank**

Direct Calculations of Waves in Fluid Flows Using  
A High-Order Compact Difference Scheme

Sheng-Tao Yu

Sverdrup Technology, Inc.  
NASA Lewis Research Center Group  
Brook Park, OH 44142

## APPROACH

- Multiple step Runge-Kutta methods for time marching.
- High-order compact difference schemes for spatial discretization.
- MOC type Nonreflective boundary conditions.
- Fourier analysis for numerical dispersion relations.
- Bench mark testing:
  1. Acoustics admittance of nozzle flow.
  2. Shocked sound wave (N-wave).
  3. A Lamb vortex in an uniform flow.
  4. Vortex pairing

## OBJECTIVES

- To simulate the unsteady flows accurately for:
  - Direct numerical simulations of turbulent flows.
  - Computational aeroacoustics.
  - Flow and/or combustion instability problems.
- Understand numerical dispersion relations of the finite difference schemes.

## FOURIER ANALYSIS

- Time marching methods.
  - 3rd-order Runge-Kutta methods

$$g = 1 + Z + \frac{1}{2}Z^2 + \frac{1}{6}Z^3.$$

- 4th-order Runge-Kutta methods

$$g = 1 + Z + \frac{1}{2}Z^2 + \frac{1}{6}Z^3 + \frac{1}{24}Z^4.$$

- Spatial discretization.

- 4th-order compact difference scheme

$$Z^{(4)} = -\frac{6F \sin(\hat{k})i}{4 + 2\cos(\hat{k})},$$

- 6th-order compact difference scheme

$$Z^{(6)} = -\frac{F[4 \sin(\hat{k}) \cos(\hat{k}) + 56 \sin(\hat{k})]i}{12[2 \cos(\hat{k}) + 3]}.$$

## THE COMPACT DIFFERENCE SCHEMES

- Interior Nodes
  - 4th-order central difference scheme

$$u_{i-1}^{'} + 4u_i^{'} + u_{i+1}^{'} = \frac{3}{\Delta x}(u_{i+1} - u_{i-1})$$

- 6th-order central difference scheme

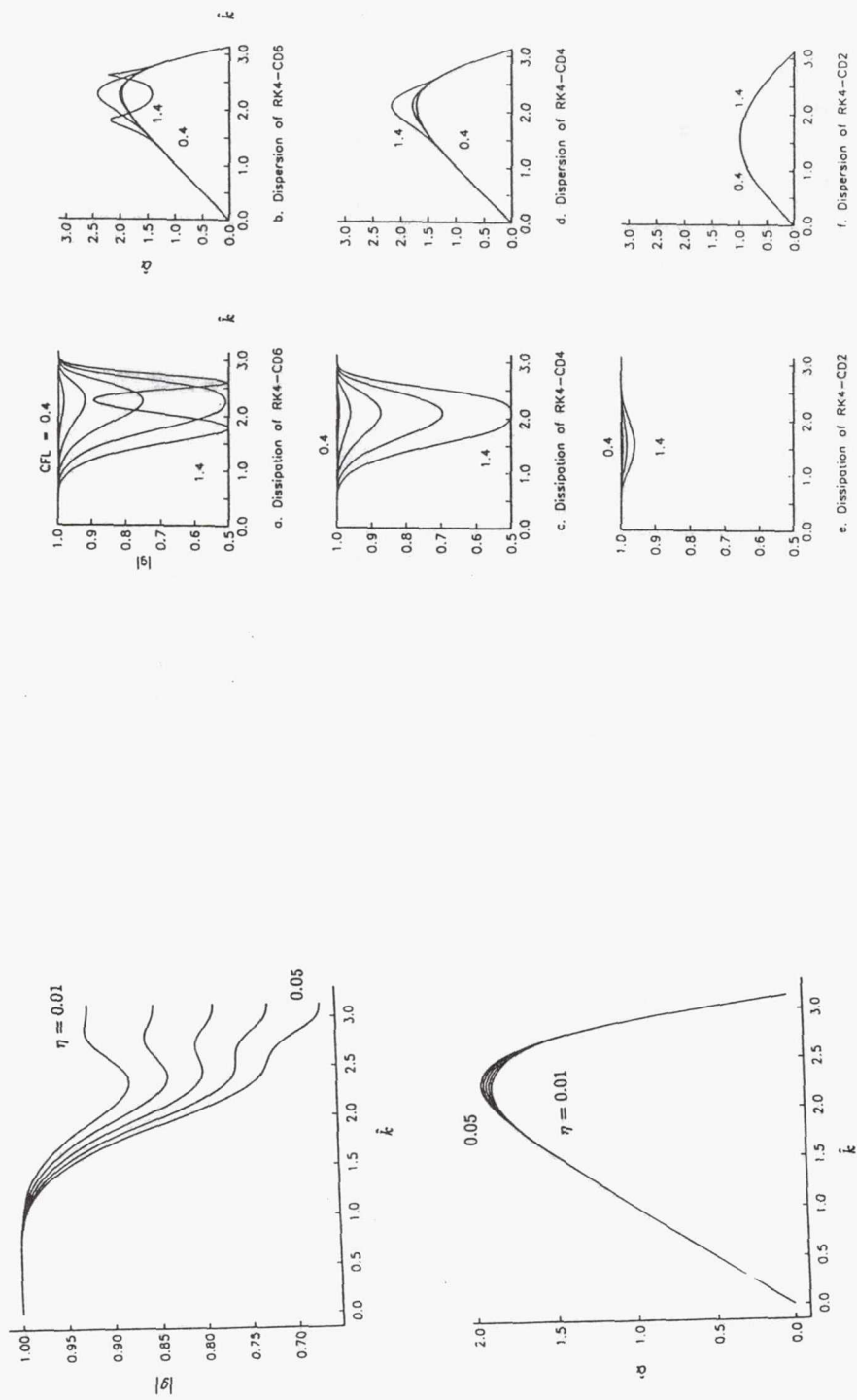
$$u_{i-1}^{'} + 3u_i^{'} + u_{i+1}^{'} = \frac{1}{12\Delta x}(u_{i+2} + 28u_{i+1} - 28u_{i-1} - u_{i-2})$$

- 3rd-order biased difference on boundary Nodes

$$2u_1^{'} + 4u_2^{'} = \frac{1}{\Delta x}(-5u_1 + 4u_2 + u_3)$$

- Implicit methods.

- Require inversion of a scalar tridiagonal matrix.



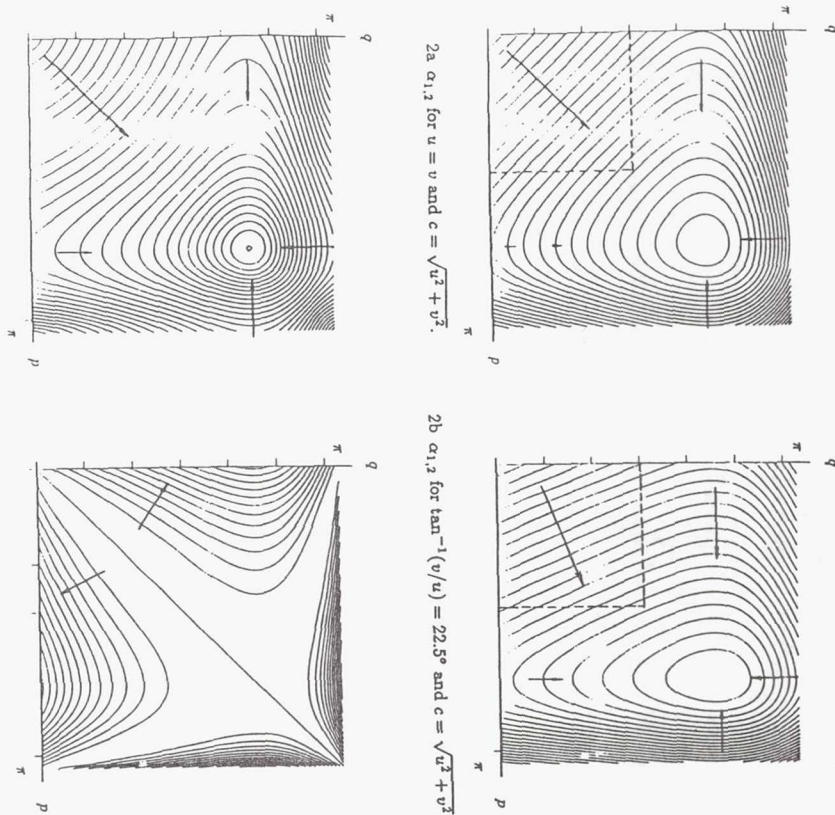


Fig. 2 Dispersion characteristics of the CD6-RK4 scheme for CFL=0.6.

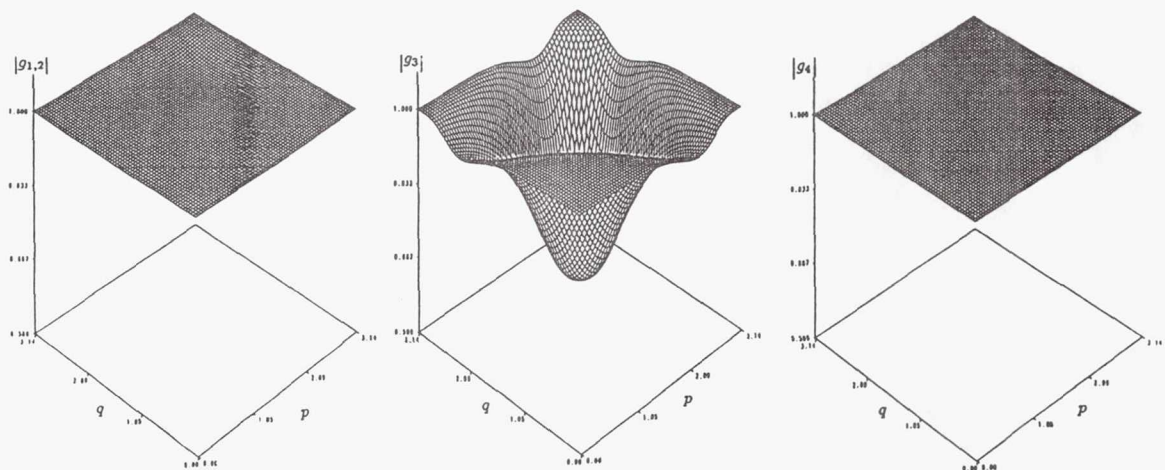


Fig. 1 Dissipation characteristics of the CD6-RK4 scheme for CFL=0.6.

1a  $|g_{1,2}(p, q)|$  for  $u = v$  and  $c = \sqrt{u^2 + v^2}$ .

1b  $|g_3(p, q)|$  for  $u = v$  and  $c = \sqrt{u^2 + v^2}$ .

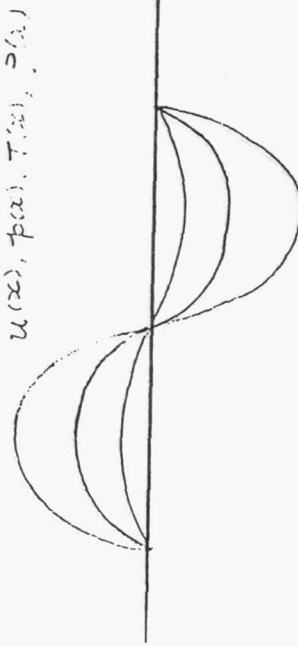
1c  $|g_4(p, q)|$  for  $u = v$  and  $c = \sqrt{u^2 + v^2}$ .

## SHOCKED SOUND WAVES

- Initial condition:
  - Sinusoidal pressure profile.
  - Isentropic conditions to determine  $\rho$  and  $T$  profiles.
  - Simple wave relation,

$$u(x) = \int_{\bar{p}}^{p(x)} \frac{dp}{\rho(x)c(x)}$$

- All flow properties are in phase.
- Straight tube with periodic boundary condition.

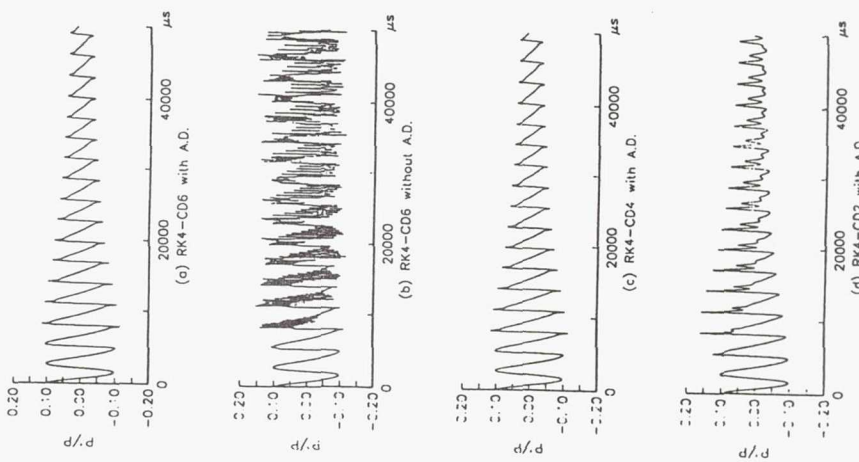


## FOURIER ANALYSIS

- Use high-order spatial differencing to improve dispersive characteristics. ( $CD6 = CD4 \geq CD2$ )
- Use high-order time stepping to enlarge CFL limit.
- No dissipation but high dispersion at the highest wave number mode resolved by a given numerical grid.
- Artificial damping is required.

## SHOCKED SOUND WAVE

- All flow properties are in phase.
- $U+C$
- $U-C$
- $U$



## A LAMB VORTEX IN AN UNIFORM FLOW

- Velocity distribution.

$$u_\theta = \frac{\Gamma}{2\pi} \frac{r}{r^2 + a^2}, \quad (54)$$

– Rigid-body rotation near vortex center.

$$u_\theta \approx r$$

– Irrotational far outside vortex core.

$$u_\theta \approx \frac{1}{r}$$

- Momentum equation.

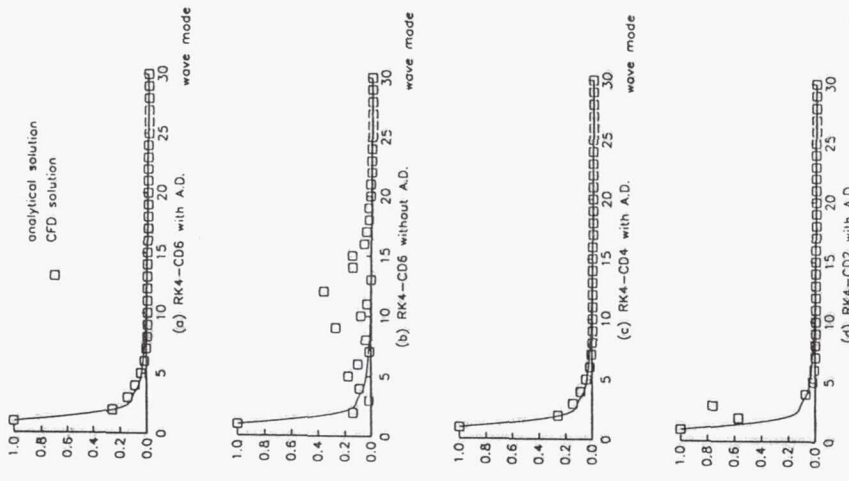
$$\frac{\partial p}{\partial r} = \rho \frac{u_\theta^2}{r}$$

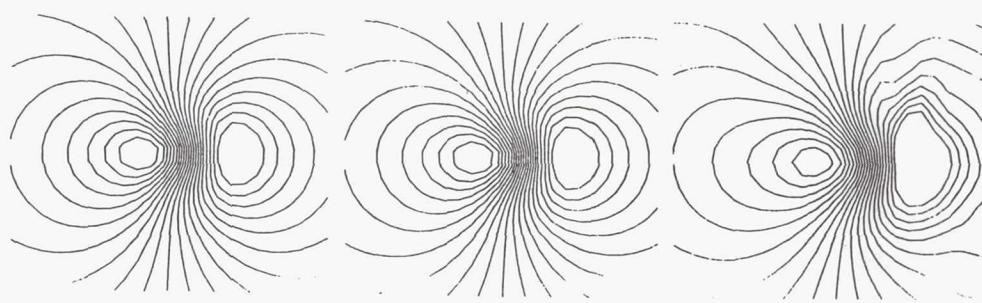
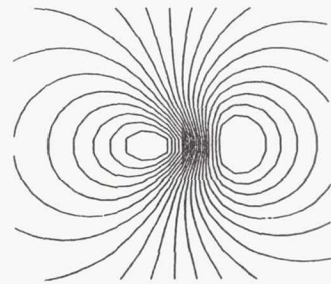
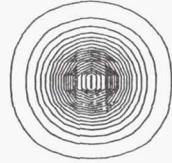
- Energy equation.

$$\frac{\gamma}{\gamma - 1} \frac{p}{\rho} + \frac{u_\theta^2}{2} = h_o$$

- Vortex in an uniform flow.

$$\begin{aligned} u &= \bar{u} + u', \\ v &= \bar{v} + v', \end{aligned}$$





RK4-CD6



RK4-CD4



RK4-CD2

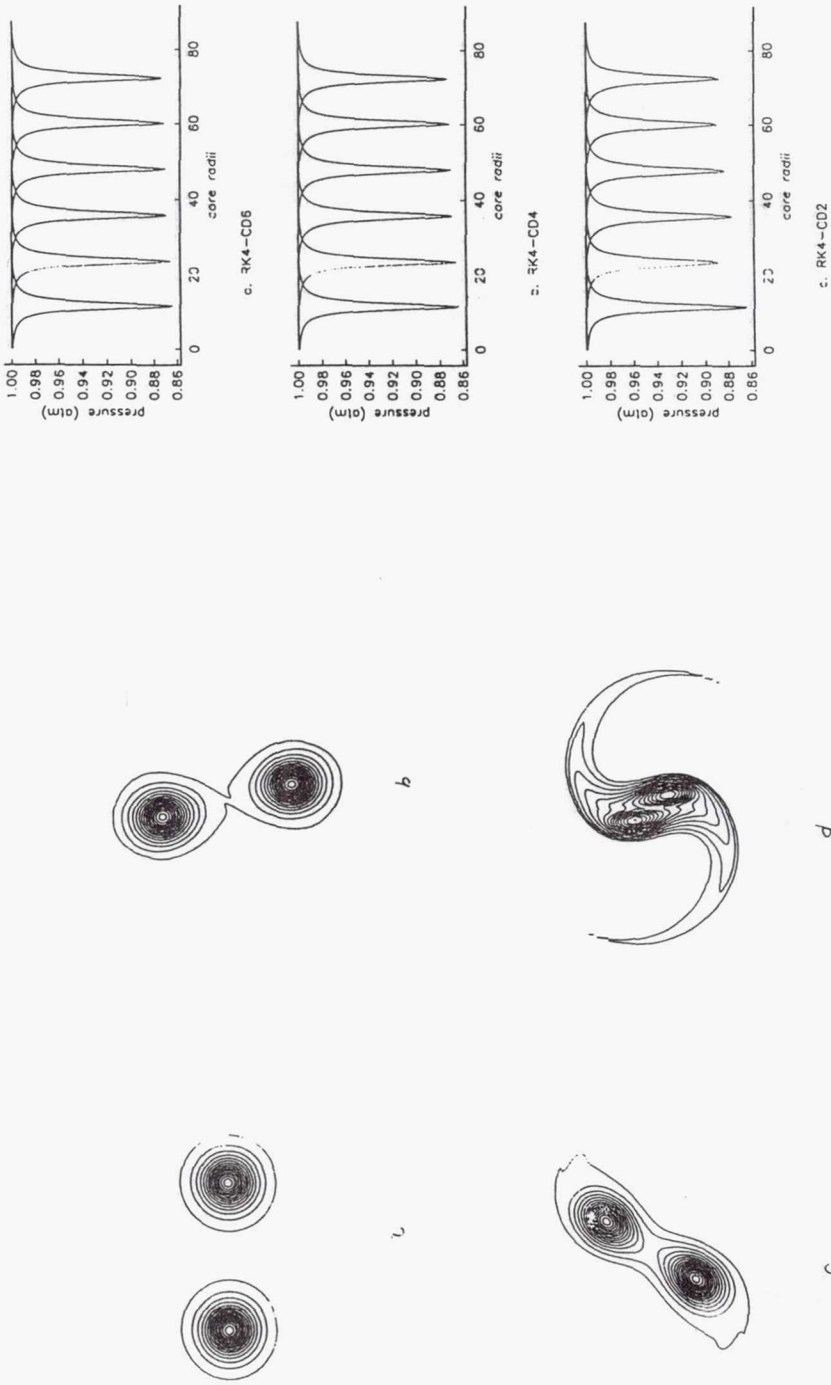


Fig. 11 The vorticity magnitude contours for the vortex pairing.

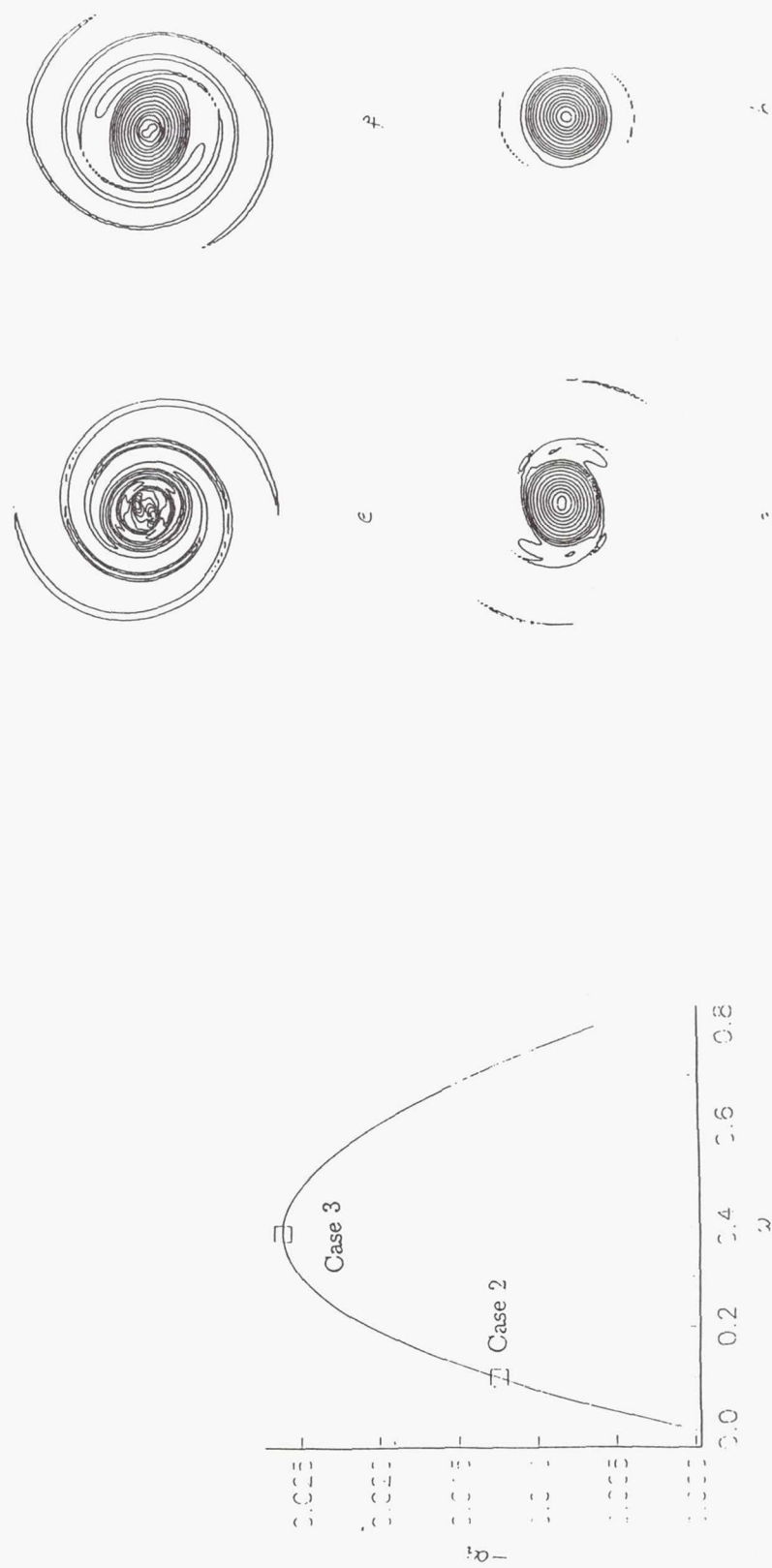


Fig. 8 The spatial growth rate as a function of the angular frequency from linear theory for the compressible free shear layer

Fig. 11 The vorticity magnitude contours for the vortex pairing.

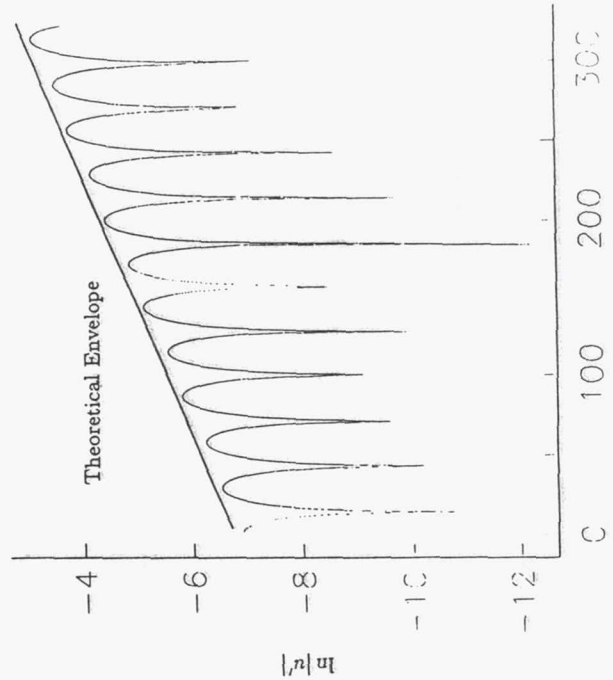


Fig. 11 The Fourier coefficients of the instability waves in a compressible free shear layer perturbed by the most unstable mode at the magnitude of one thousandth,  $\alpha_{max} = 0.0$ .

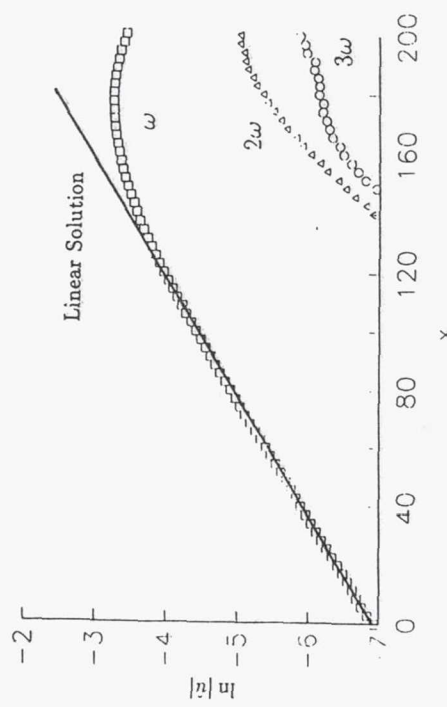


Fig. 9 Instantaneous distribution of  $|u_r'|$  along the center line of the free shear layer.

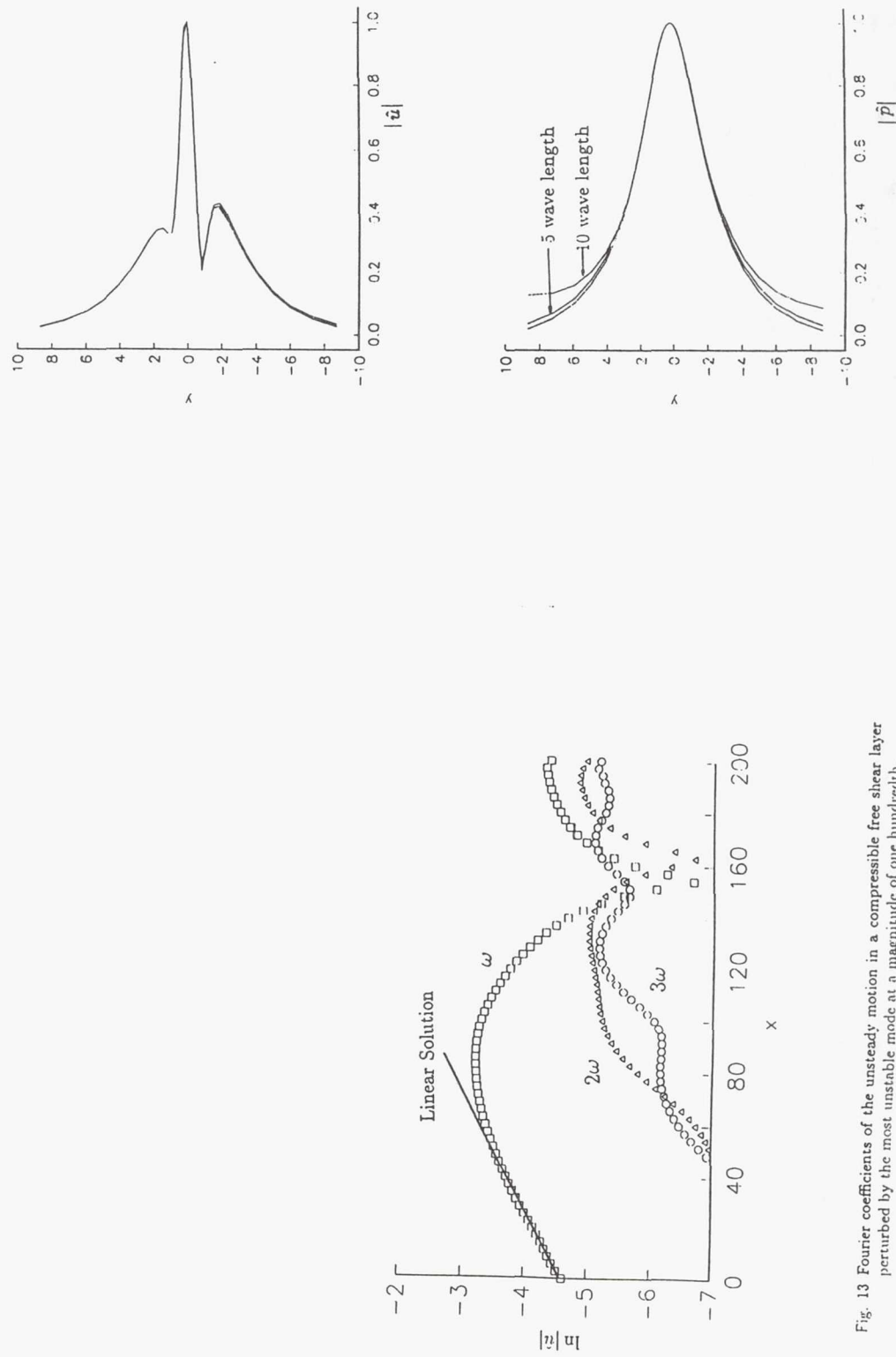


Fig. 13 Fourier coefficients of the unsteady motion in a compressible free shear layer perturbed by the most unstable mode at a magnitude of one hundredth.

Fig. 12 Reconstructed eigenfunction components  $u'$  and  $p'$  from the CFD results for the free shear layer perturbed by the most unstable mode.

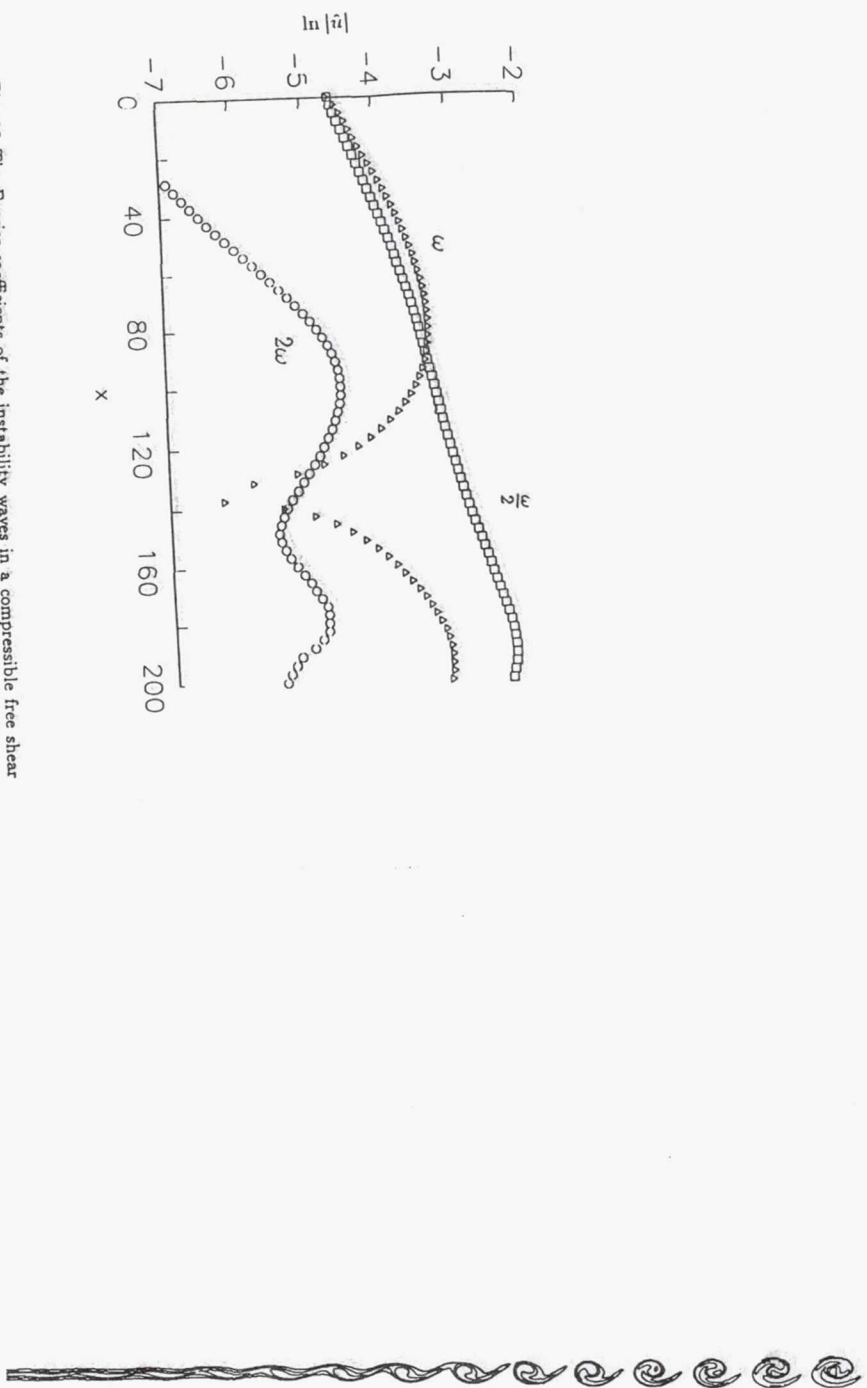


Fig. 15 The Fourier coefficients of the instability waves in a compressible free shear layer perturbed by the most unstable mode and its subharmonic.

Fig. 14 Contours of constant vorticity of the simulated free shear layer perturbed by the most unstable mode at a magnitude of one hundredth.

## CONCLUDING REMARKS

- Successful development of quasi-1-D and 2-D Euler solvers using Runge-Kutta and compact difference methods to simulate unsteady flows.
- Analysis of the Runge-Kutta methods for non-linear equations.

- Fourier analysis to guide the numerical calculations: numerical scheme, CFL number, artificial damping.
- For flows of complex harmonic content, 4th-order central differencing is better than the 2nd central difference.



Fig. 16 Contours of constant vorticity of the simulated free shear layer perturbed by the most unstable mode and its subharmonic.

**Page intentionally left blank**

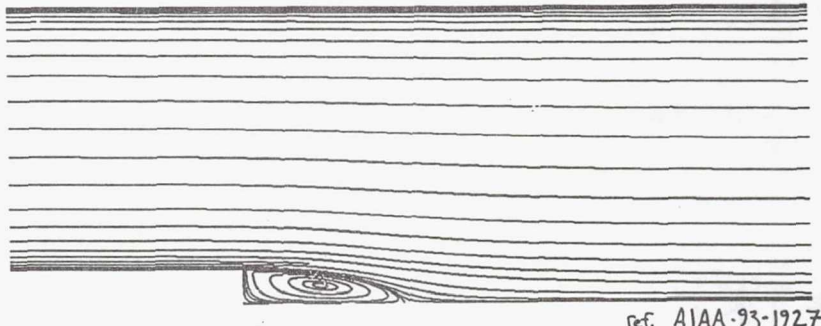


Lewis Research Center

CFD Branch

---

## Turbulent Back-Facing Step Flow and the $k-\epsilon$ model: A Critical Comparison



ref. AIAA-93-1927

Christopher J. Steffen, Jr.

Center for Modeling of Turbulence and Transition (CMOTT)  
NASA Lewis Research Center Cleveland, Ohio



---

Lewis Research Center

CFD Branch

---

### INTRODUCTION

#### CMOTT at NASA Lewis:

to address propulsion related turbulence issues

- assessment of state-of-the-art models
- development of new models
- validation of new techniques

#### Objective of this work:

to assess the performance of several low Reynolds number  $k-\epsilon$  formulations compared to the standard high Reynolds number form for separated flow over a step



Lewis Research Center

CFD Branch

Need to clarify this issue for code developers

Critical comparisons between  $k-\epsilon$  models for:

- Channel flow: Lang & Shih (1991)
- Flow past a hill: Michelassi & Shih (1991)

Avva (1990) compared the high  $Re_t$  and Chien  $k-\epsilon$  models for several flows: noted the deficiency of Chien for step flow skin friction results . . .

Contradicts idea of “more work  $\leftrightarrow$  better result”

Is this a property of all Low Reynolds Number  $k-\epsilon$  models?



Lewis Research Center

CFD Branch

## $k-\epsilon$ TURBULENCE MODEL

Specifically,  $\nu_t = C_\mu f_\mu \left( \frac{k^2}{\epsilon} \right)$

Model transport of  $k$  and  $\epsilon$ :

$$k_{,t} + U_j k_{,j} - \left[ \left( \nu + \frac{\nu_t}{\sigma_k} \right) k_j \right]_j = P - \epsilon + D$$
$$\epsilon_{,t} + U_j \epsilon_{,j} - \left[ \left( \nu + \frac{\nu_t}{\sigma_\epsilon} \right) \epsilon_j \right]_j = C_1 f_1 \frac{\epsilon}{k} P - C_2 f_2 \frac{\epsilon^2}{k} + E$$

where the production of  $k$  is:  $P = -\langle \bar{u}_i \bar{u}_j \rangle \frac{1}{2} (U_{i,j} + U_{j,i})$ .

Primary difference between formulations:  
definition of  $f_\mu, f_1, f_2, D, E$



Low  $Re_t$  forms:

- numerical domain extends to wall
- near wall profiles of  $\vec{U}$ ,  $k$ , and  $\epsilon$  are resolved not assumed
- typically first cell located  $y^+ \approx 1.0$
- damping functions ( $f_1$ ,  $f_2$ , and  $f_\mu$ ) and additional terms (D and E) tuned to specific flows

Generality suffers somewhat . . .

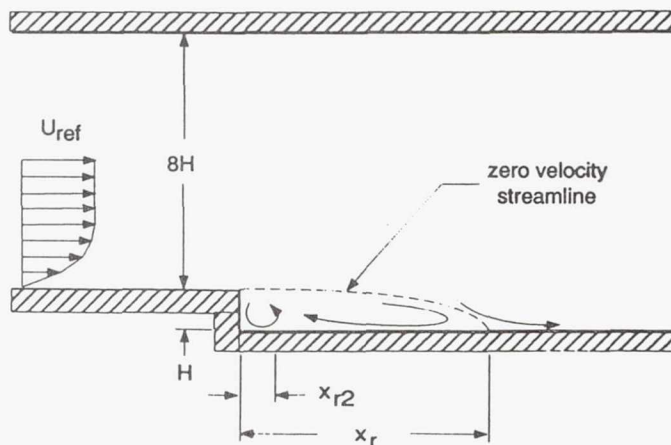
Formulation of above terms can affect the generality as well:

- JL and LS are functions of *dependent variables alone*
- CH and SL are functions of both *dependent and independent variables*



## BACK-FACING STEP (BFS) FLOW

Experiment of Driver and Seegmiller (AIAA J., '85)





Lewis Research Center

*CFD Branch*

---

Configuration:

- $Re_{step}$  of 33420
- inlet Mach Number of 0.128
- inlet tunnel 80H
- exit tunnel 60H

Chosen for:

- LDV data for velocity, turbulent stresses
- wall static  $C_p$  and wall  $C_f$
- reattachment length (time averaged)



Lewis Research Center

*CFD Branch*

---

## **NUMERICAL EXPERIMENT**

Code: modified version of DTNS2D (Gorski '88)

Method:

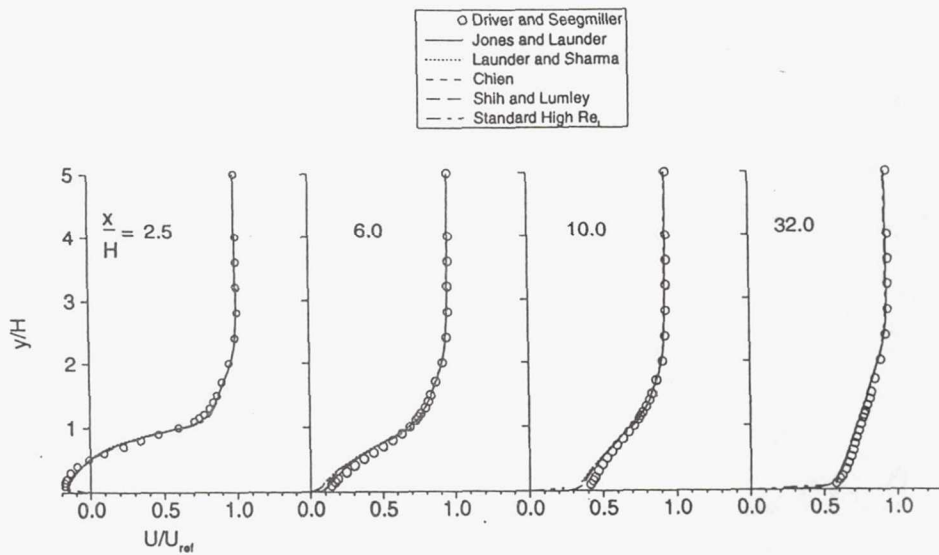
- pseudo-compressibility (Chorin '67)
- upwind differenced, TVD scheme for convective terms  
(Chakravarthy & Osher '85)
- approximate factorization for time integration
- multiblock configuration
- decoupled (lagged) treatment of turbulence equations
- implicit treatment of turbulent source terms



Lewis Research Center

CFD Branch

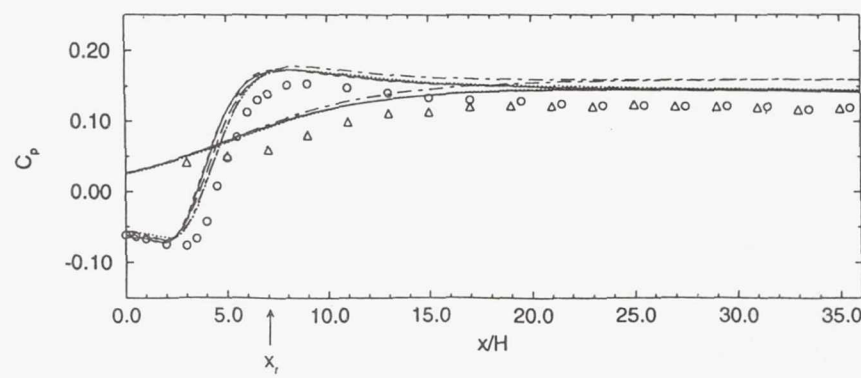
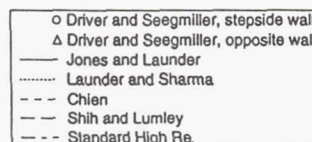
Velocity profiles:



Lewis Research Center

CFD Branch

Wall static pressure coefficient:

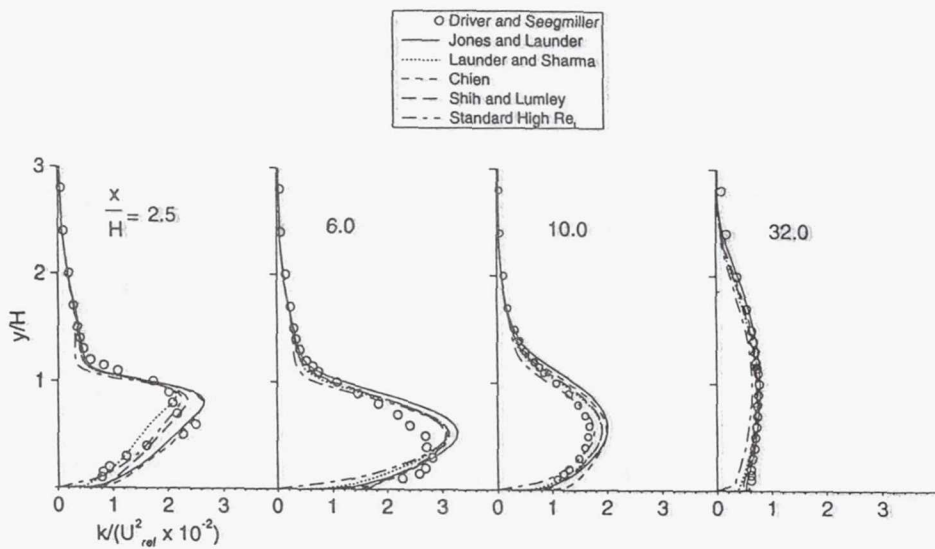




Lewis Research Center

CFD Branch

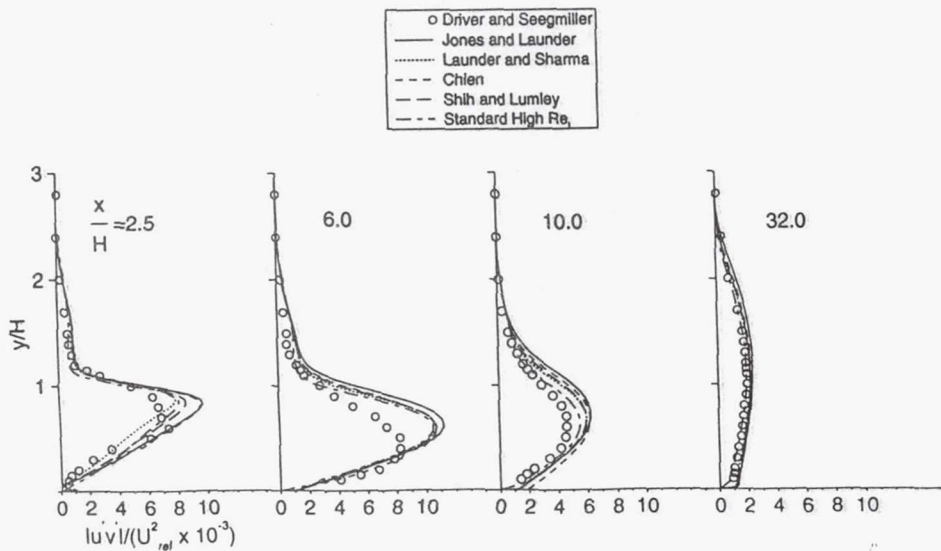
Turbulent kinetic energy profiles:



Lewis Research Center

CFD Branch

Turbulent shear stress profiles:

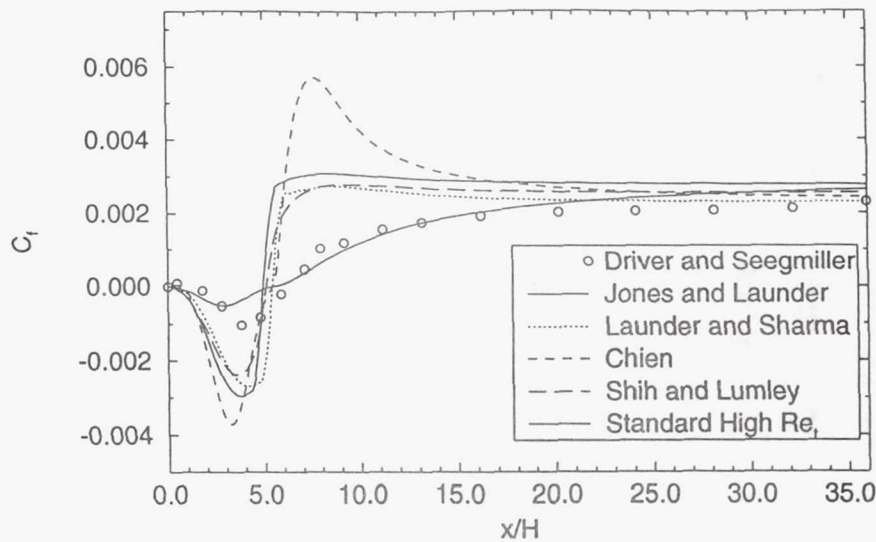




Lewis Research Center

CFD Branch

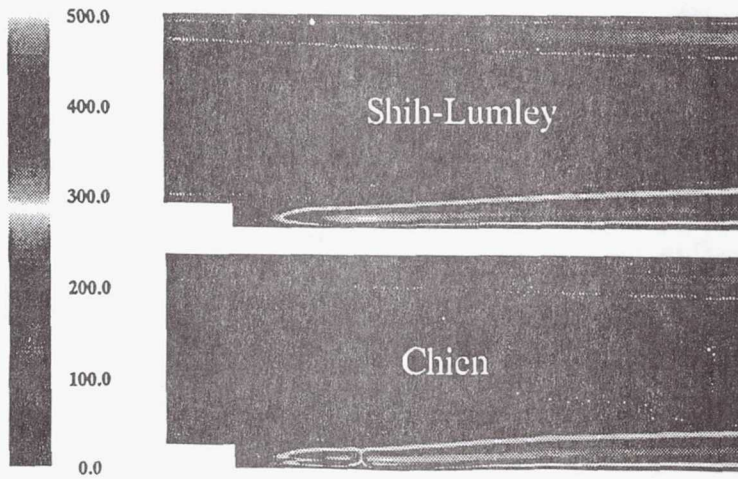
Skin friction coefficient:



Lewis Research Center

CFD Branch

Eddy viscosity field,  $\nu_t$ :





Lewis Research Center

CFD Branch

Primary reattachment length,  $x_r$ :

model	JL	LS	CH	SL	HR
$x_r$	4.9	5.4	5.4	5.1	5.5

Driver & Seegmiller recorded: 6.26H

Secondary reattachment length,  $x_{r2}$ :

model	JL	LS	CH	SL
$x_{r2}$	0.0	0.0	0.8	0.1

Driver & Seegmiller recorded:  $0.5 \leq x_{r2} \leq 1.8$



Lewis Research Center

CFD Branch

## CLOSING COMMENTS

- JL, LS, CH, SL and HR  $k-\epsilon$  models tested for back-step flow
- In general, results very similar between 5 different forms
- All do reasonably well for  $\vec{U}$  and  $C_p$ , albeit LR slightly better
- Turbulence profiles possess misplaced peak values as well as overpredictions in recirculation zone, common to all
- Reattachment length and  $C_f$  are difficult to properly resolve (14% error) especially for LR forms
- Definition of secondary recirculation zone inconclusive on this grid
- Perhaps a sensitivity to pressure gradient would help the LR damping functions . . .

Sverdrup  
Technology Inc.

Internal Fluid Mechanics Division



## **Analysis of Supersonic Flows using k- $\epsilon$ Model and the RPLUS code; Progress towards High Speed Combustor Analysis.**

by J. Lee

Sverdrup Technology Inc./CFD Branch

for Workshop on Computational Turbulence Modeling

Sept. 1993

1



## Outline

- Problem of Interest - High Speed Combustor Flow Fields
  - Parameters need to be Resolved
  - Key Problems of Interest
- k- $\varepsilon$  Model and RPLUS code
  - Numerical Technique
  - Models being Tested
  - Some Results
- Summary

2



## Problem of Interest

- Analysis of Chemically Reacting flow inside of Supersonic RAM jet Combustors-Two Key Parameters need to be determined.
  - Mixing/Combustion Efficiency
  - Kinetic Energy Efficiency (Flow Losses)
  - Inlet, Diffuser, etc..
- In order to do get some ideas on those parameter following (Potential Loss Mechanisms) must be modeled/determined correctly.
  - Mixing, Shear,
  - Turbulence, Vorticity,
  - Shock-waves, Heat Transfer,
  - Fuel Injector Drag, Poor Wall Pressure Integral,
  - Chemical Dissociation.

from 2nd JANNAF workshop on SCRAMjet Combustor performance workshop

3



### Mixing and Injector Design

- At High Mach Number( $M \sim 5.0 +$ ).
  - Doesn't mix well!
  - The Natural diffusion mechanism very INEFFECTIVE.
  - Fuel Residence Time Extremely Small- Even with Fast Fuel Such as  $H_2$
- Geometrical Complexities
  - To induce Favorable mixing and Flame holding features
  - Back-Step/Stream Wise Vorticity/Shock-Wave Interactions
  - Unsteady Mechanism also being Envisioned as mixing enhancement
  - Kumar, Bushnell and Hussani(1987)

4



### Introduction of Externally Generated Mixing Enhancements

- Some External helping hand needed => Modeling Difficulties.
- Externally Generated Vorticity Through Sweep angle of the Ramp injector.
  - Davis(1990), Riggins and McClinton(1990), Drummond(1991).
- Multiple Transverse Injection.
  - Hartfield et. al. (1991)
- Flame holding tricks/ Back-step with Recirculation.
  - Hartfield et. al.(1991)
- Simplified analysis of these features very difficult because of limited database/understanding (Attempts are being made using CFD solutions- JANNAF Combustor Subcommittee).

5

**Sverdrup**

Technology Inc.

**Internal Fluid Mechanics Division**



### Numerical Modeling(CFD) of Combustor Flow Field

- CFD Analysis.
- Numerical Modeling=> Overall Analysis of performance => Difficult
- Overall Laminar Flow Fields with Complex Geometry/Finite Rate Chemistry has been demonstrated.
- Finite Rate Chemistry Model( Yoon and Shuen(1989)
- Multiple Grid Blocks- Moon (1991)
- Analysis of a typical Injector Configuration with Zero Equation Turbulence Model using LU Scheme(RPLUS) code- Lee(1993)

6

**Sverdrup**

Technology Inc.

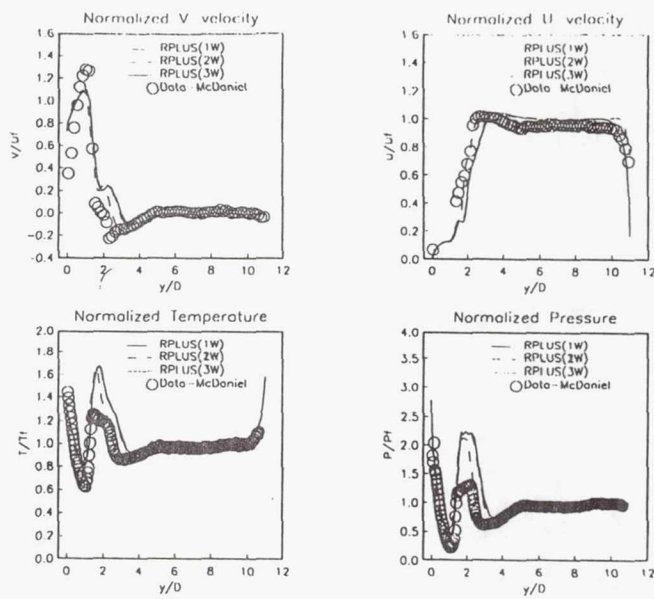
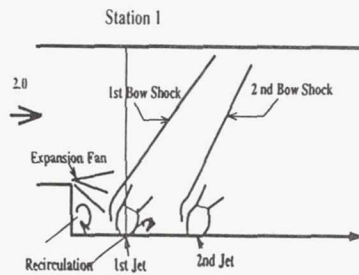
**Internal Fluid Mechanics Division**



**Simple Zero Equation Turbulence model with multiple wall scaling Buleev-Inverse square rule can be used to extend model in to three-dimensional form. (Lee (1993))**

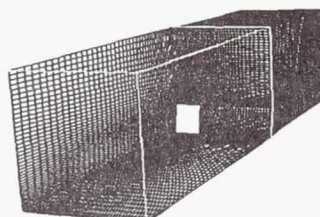
- Good News/Bad News
  - Typical velocity profiles can be reasonably predicted.
  - Over all combustor flow features can be reasonably predicted.
  - Near-wall temperature characteristics near non-equilibrium region around the injector and separated flow were poorly predicted.
  - Overall spreading behavior of shear region poorly predicted.
- 
- Two Equation Transport Turbulence Model has the potential to ease some of these difficulties.

7

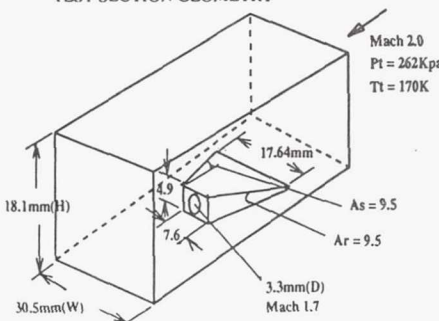


#### THREE-BLOCK GRID SYSTEM

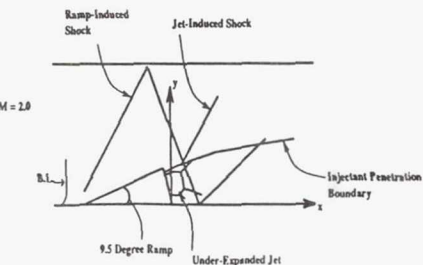
HARTFIELD ET. AL. (1990)

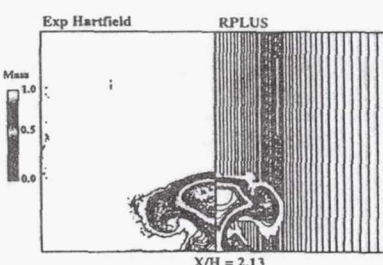
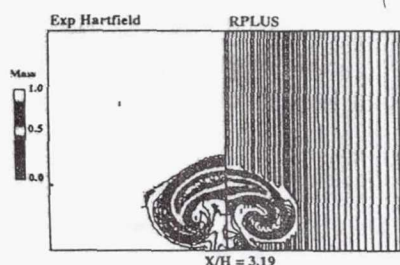
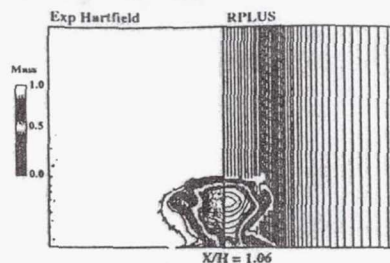


#### TEST SECTION GEOMETRY

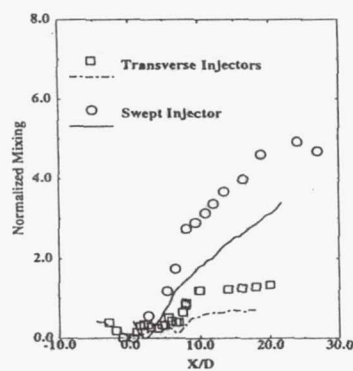


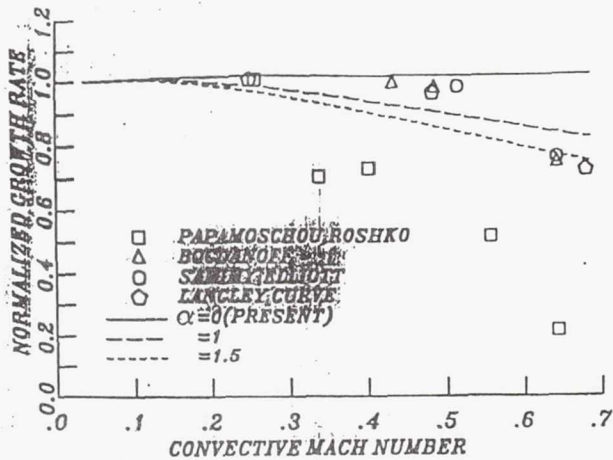
#### FLOW SCHEMATIC





### Mixing Efficiencies





GROWTH RATE VS. COMPRESSIBILITY EFFECT

DR. H. LAI

Sverdrup

Technology Inc.

Internal Fluid Mechanics Division



#### Two Equations Transport Turbulence model are being Analyzed

- High speed turbulence models are somewhat Deficient (The deficiencies are well documented(Marvin(1986), Wilcox(1993)).  
 Effect of Compressibility  
 An-isotropy (Low/High Speed).  
 Non-Equilibrium Flow Features (Low/High Speed).  
 Near-Wall Flow(Low-Reynolds Number Features (Low/High Speed)).  
 Inflexibility of handling Complex Geometry- Invariance Principle  
 (Low/High Speed)  
 Large Dependence in the Numerical Methods Used  
 (especially elliptic Solvers).  
 Appropriate Initial/Boundary Conditions  
 Etc ...



### **K- $\epsilon$ Model-RPLUS Development**

- LU Based k- $\epsilon$  Model Solver-De-coupled Approach.

Mean-Turbulence Transport Equations

LU-SSOR- Yoon and Shuen- Explicit Terms Centrally Differenced

LU-SW -Steger and Warming- Explicit Terms Upwind Differenced

k- $\epsilon$  Models

Convective Terms + Diffusive Terms + Source Terms = 0.0

Model Only differ in Low-Reynolds Number Character.

Models performance are being Evaluated.

Implicit Source Term Handling Strategy also Being Studied

### **k- $\epsilon$ Turbulence Models being studied for potential used in Three Dimensional RPLUS Code.**

- Low-Reynolds Number Model plus Dilatational Terms

Chien (1976)

Launder-Shima(1976)

Shih(1990)

Various CMOTT derivatives of k- $\epsilon$  Model

Realizability

Invariance

Simplified Boundary-Conditions

- Performance of the Low-Reynolds number K-e model in low-Mach number flows have been demonstrated (Patel, Rodi and Scheuerer(1985), Steffen(1993), Launder(1992)).

- Some of the Potential Difficulties in high speed turbulence model are well documented (Marvin(1993), Coakley and Huang(1992)).

Sverdrup

Technology Inc.

Internal Fluid Mechanics Division



### Evaluation and Development of the RPLUS/k- $\epsilon$ Model Solver

- Various 2D-3D problems are being studied to optimize the numerical method and to Evaluate model performance in supersonic flows in context to the LU based numerical Technique.
- Simple 2D k- $\epsilon$  models are also being used to study various components of the flowfield generated by the complex combustor geometry previously shown.
- Studying the Numerical method/Model Behavior/Model Performance.

2D Supersonic Turbulent Boundary-Layer- Skin Fraction/Heat transfer  
(NASA Ames Database).

2D Supersonic Shock-Wave Boundary-Layer Interaction- Skin fraction/Heat  
-Transfer/ Shock-wave(A. Smits (1990's))

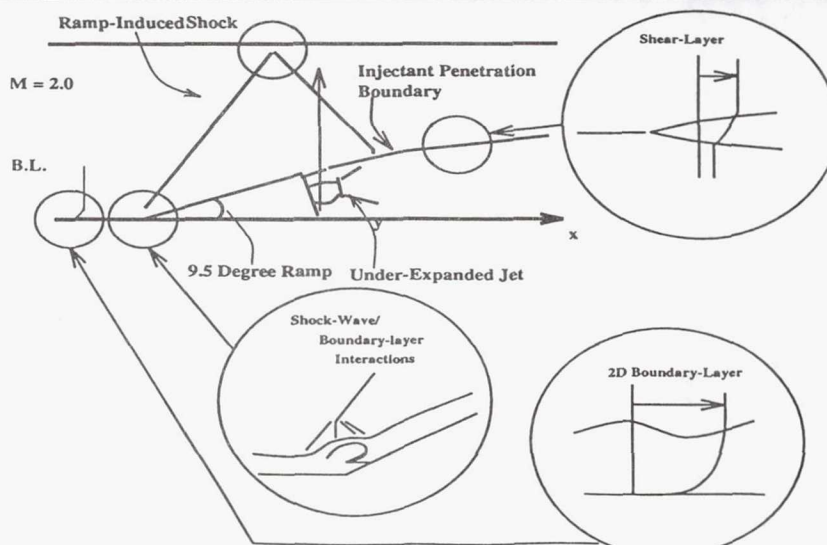
2D Shear-Layer - Mixing (H. Lai(1993))

3D Fin/Flat Plate Interaction- 3D Corner Flows-Interaction Developed through  
a Fin generated Shock-Waves. (D. Davis(1992))

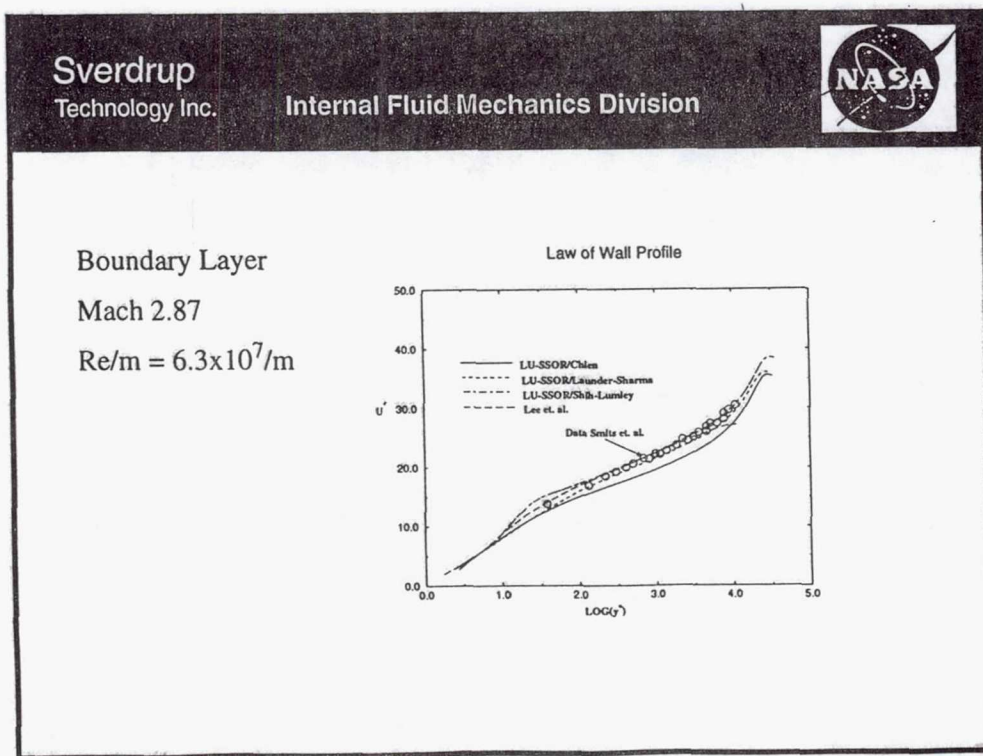
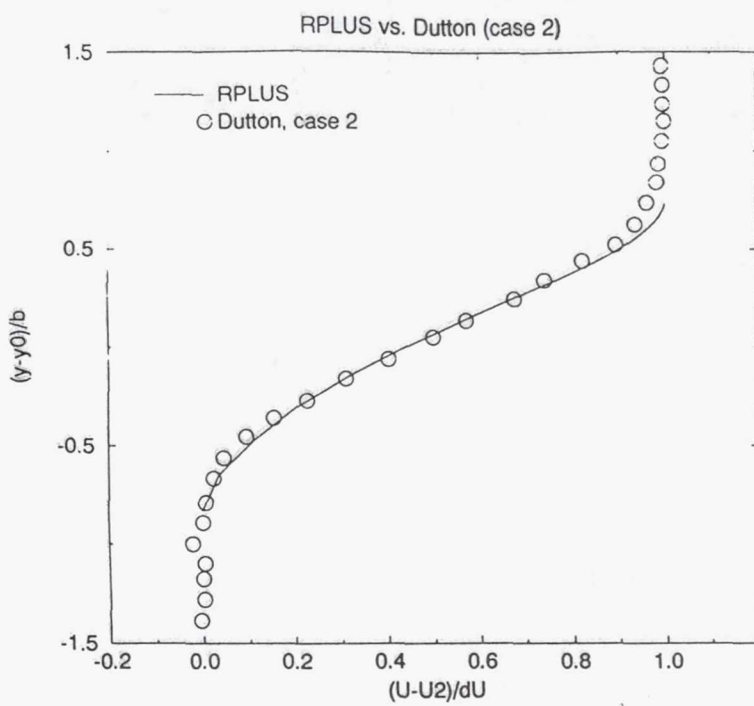
Sverdrup

Technology Inc.

Internal Fluid Mechanics Division



## Supersonic Mixing Layer

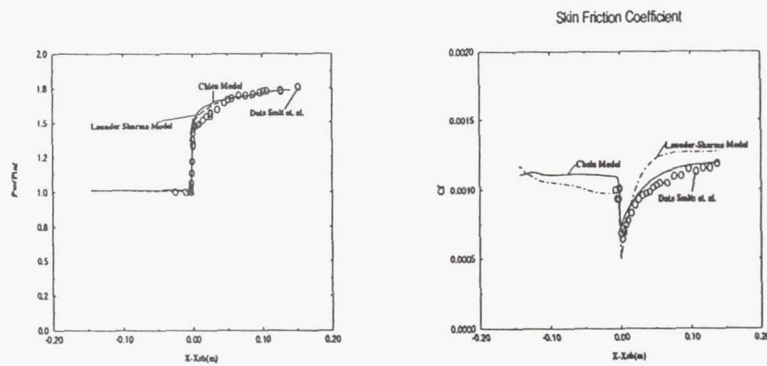




## Turbulent Shock-Wave/Boundary Interactions

Mach 2.87

Ramp Angle = 8.0 degrees



27



## Other Factors

- Optimum Numerical Strategy with in LU frame work.
- Effects of Initial condition.
- Modeling of Compressibility terms/Dilatational terms.
- Modeling of Turbulent terms in the Finite Rate Chemistry Model.  
Anisotropy of Turbulence
- Effects Upstream and Down stream Influences (Inlet(K. Kapoor) and Diffuser(?)).
- Chemistry-Turbulence Model Interactions (A. Hsu-PDF).
- Numerical Robustness(A. Suresh).

28

**Page intentionally left blank**

# Validation of a k-e Model in RPLUS2D Code for Non-reacting/reacting Subsonic Shear layers

H. T. Lai

Workshop on Computational Turbulence Modeling  
September 15-16, 1993

## OVERVIEW

- To simulate an experiment at NASA Lewis by Marek and co-workers for subsonic shear layers
- Computations for nonreacting/reacting flows
- Grid refinement study for nonreacting case
- Compressibility effects in k-e models (nonreacting)
- Torch effects to sustain combustion (reacting)

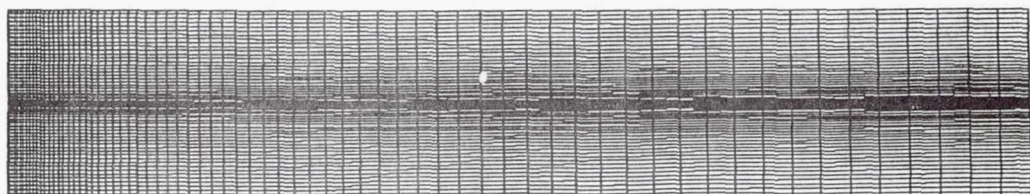
## The RPLUS Code

- Navier-Stokes and species conservation equations
- Finite-volume scheme
- Options for central or upwind differences
- Jameson-type dissipation
- LU-ADI algorithm
- Vectorization on oblique grid lines/planes
- Hydrogen-air chemistry
- Implicit chemical source terms
- High Reynolds number k-e model
- k-e equations uncoupled from other equations

## NONREACTING SHEAR LAYER

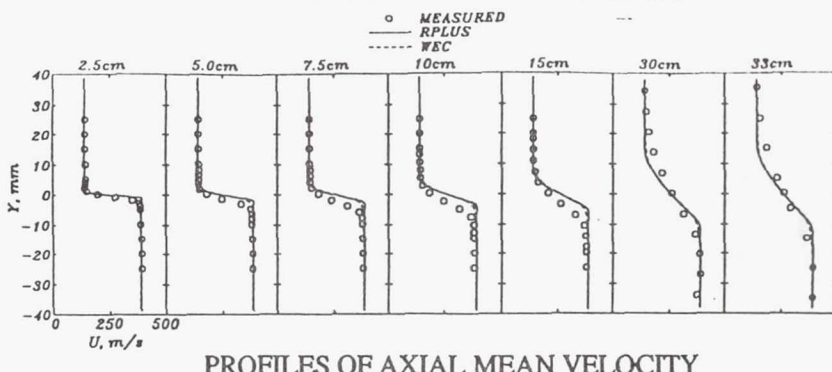
$U=140 \text{ m/s}$ , $T=304.3^\circ\text{K}$ , $P=1.013 \times 10^5 \text{ N/m}^2$ $\dot{\tau}_i=2.25\%$ , AIR	$y=5.08\text{cm}$
$U=390 \text{ m/s}$ , $T=822^\circ\text{K}$ , $P=1.1013 \times 10^5 \text{ N/m}^2$ $\dot{\tau}_i=2.25\%$ , AIR	$y=-5.08\text{cm}$
$x=0$	$x=55.9\text{cm}$

## GEOMETRY AND FLOW CONDITIONS

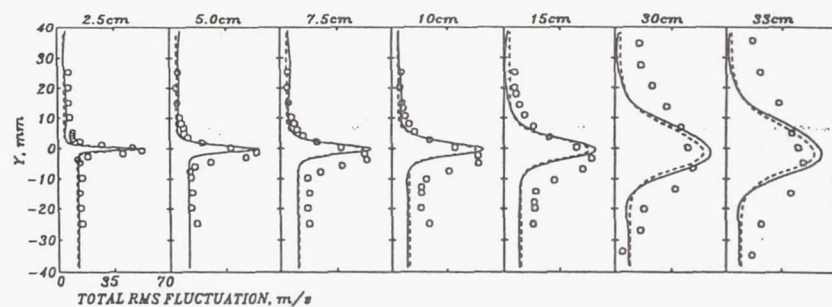


GRID DISTRIBUTION

## NONREACTING SHEAR LAYERS

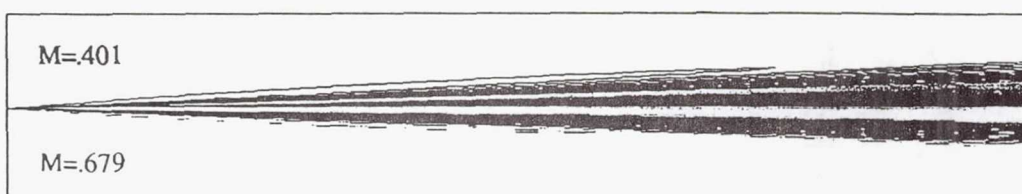


PROFILES OF AXIAL MEAN VELOCITY

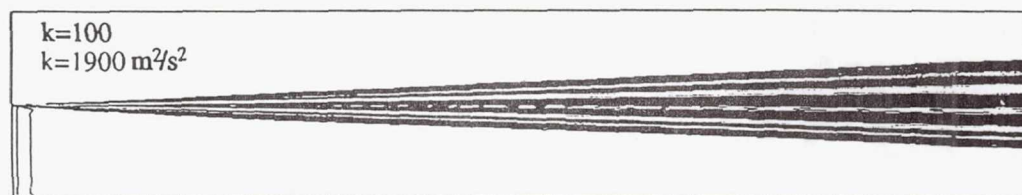


PROFILES OF TOTAL RMS FLUCTUATION

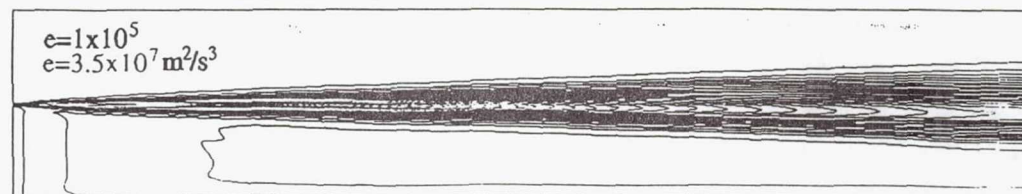
## NONREACTING SHEAR LAYER



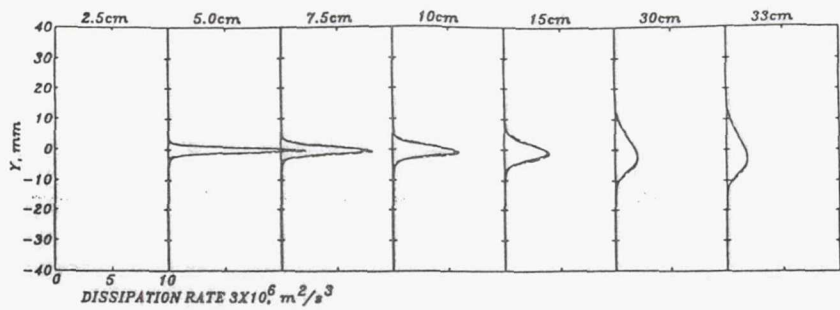
MACH NUMBER CONTOURS



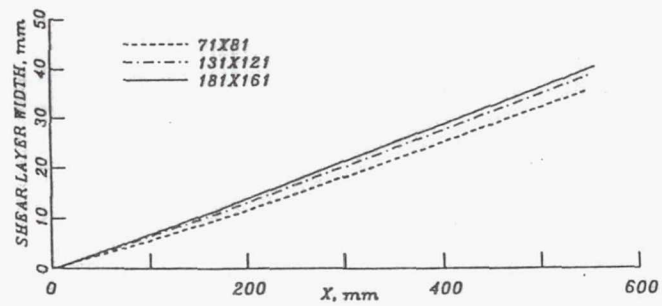
TURBULENT KINETIC ENERGY CONTOURS



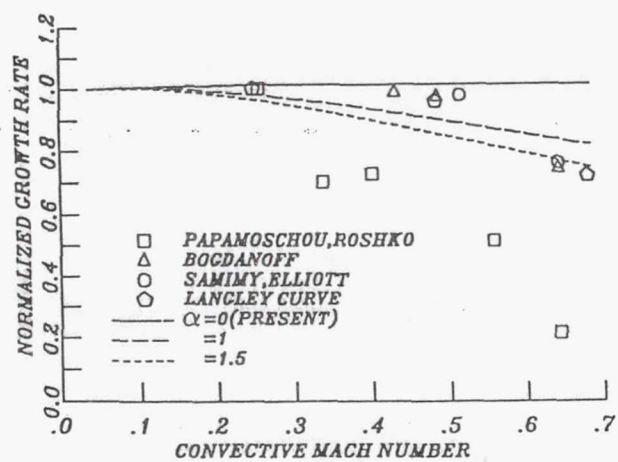
DISSIPATION RATE CONTOURS



PROFILES OF DISSIPATION RATE



SHEAR LAYER THICKNESS VARIATION



GROWTH RATE VS. COMPRESSIBILITY EFFECT

## REACTING SHEAR LAYER

$U=135\text{m/s}$ ,  $T=366.5^\circ\text{K}$ ,  $P=1.013 \times 10^5 \text{N/m}^2$   
 $ti=5\%$ ,  $3.94\% \text{ H}_2$  and  $96.06\% \text{ N}_2$

$U=385\text{m/s}$ ,  $T=810.9^\circ\text{K}$ ,  $P=1.013 \times 10^5 \text{N/m}^2$   
 $ti=6\%$ , AIR

## FLOW CONDITIONS

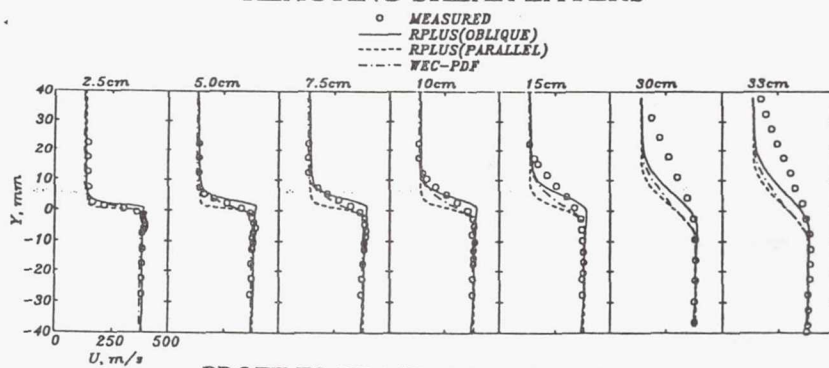
hydrogen torch dimension=1cm  
 $ti=5\%$ ,  $T=1250^\circ\text{K}$ ,  $1.3\% \text{ H}_2 + 21\% \text{ O}_2 + 77.7\% \text{ N}_2$   
 $V=0$  (parallel inflow)

## PARALLEL INFLOW

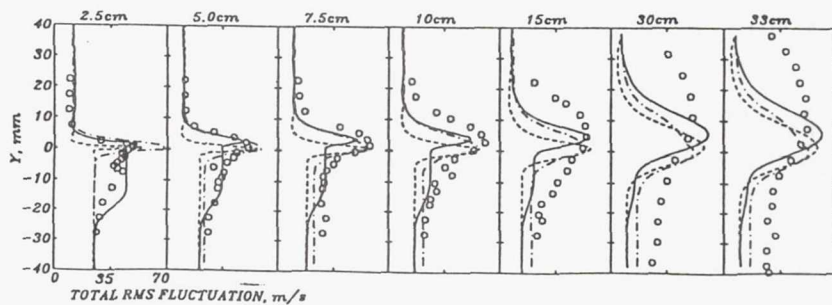
hydrogen torch dimension=2.12cm  
 $ti=11\%$ ,  $T=1250^\circ\text{K}$ ,  $0.1\% \text{ H}_2 + 21\% \text{ O}_2 + 78.9\% \text{ N}_2$   
 $V=50\text{m/s}$  (oblique inflow)

## OBLIQUE INFLOW

## REACTING SHEAR LAYERS

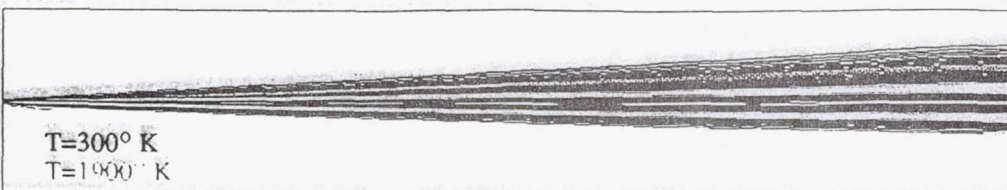


PROFILES OF AXIAL MEAN VELOCITY

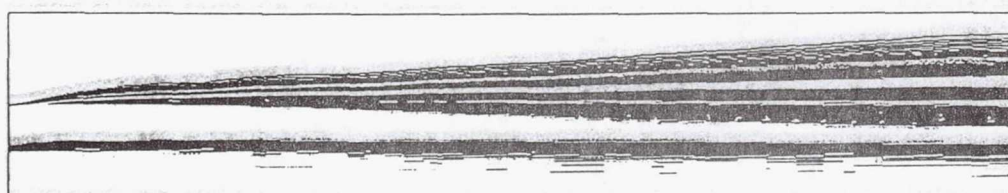


PROFILES OF TOTAL RMS FLUCTUATION

## REACTING SHEAR LAYERS TEMPERATURE CONTOURS

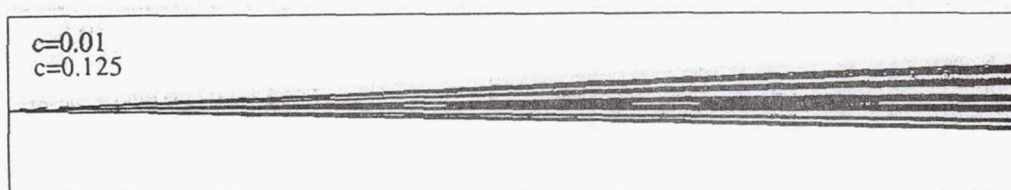


PARALLEL INFLOW

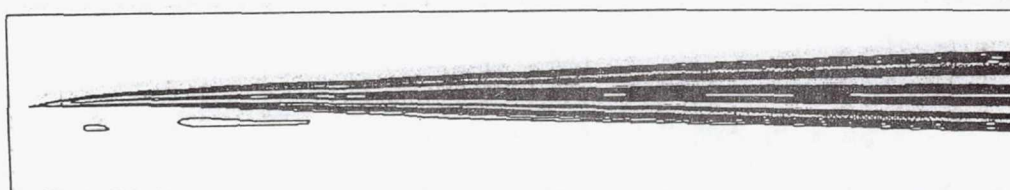


OBLIQUE INFLOW

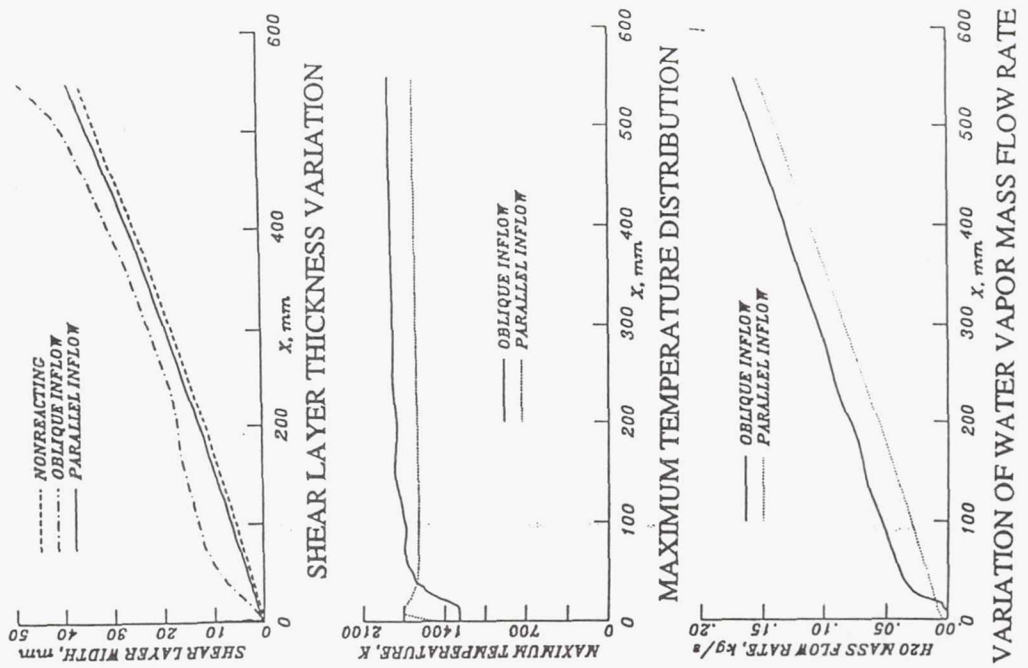
## REACTING SHEAR LAYERS $\text{H}_2\text{O}$ MASS FRACTION CONTOURS



PARALLEL INFLOW



OBLIQUE INFLOW



## CONCLUSIONS

- Growth rate underpredicted, especially reacting
- Large decay of  $k$  near shear layer edges
- Small production of  $k$  or large dissipation rate  $\epsilon$
- But center peaks in  $k$  are constant and overpredicted
- Small improvement with grid refinement
- Inhibition of growth with compressibility effect
- Significant torch effects for reacting flows

**Page intentionally left blank**

Reda R. Mankbadi  
NASA Lewis Research Center  
Cleveland, Ohio

## Noise Produced by Large-Scale Coherent Structure in Subsonic Jets

- The initial region of jet is dominated by large-scale, wave-like coherent structure, which is believed to be the dominant sound source.

- The coherent structure can be calculated by:

Splitting the flow field into three components: time-averaged, coherent, and random. The coherent component is represented by few frequency modes which are taken to resemble a nonlinear instability wave interacting with the mean flow, turbulence, and other coherent components.

Integral equations are then obtained for each scale of motion.

Lighthill theory is used with the stress term given by the coherent structure.

## I. Background

- Acoustic Analogy - Lighthill's Theory:

$$P_s = \frac{1}{4\pi R_o a_*^2} \iiint \frac{\partial^2}{\partial x_i \partial x_j} (\rho u_i u_j) dV \quad (1)$$

$$t_r = t - |\vec{X} - \vec{Y}|/a_o \quad (2)$$

where X and Y are the observer's and the source's locations, respectively.

- Working with time-averaged properties
- Modelled time-dependent sound source
- Noise radiation from linear instability wave
- Noise radiation from large-scale coherent structure

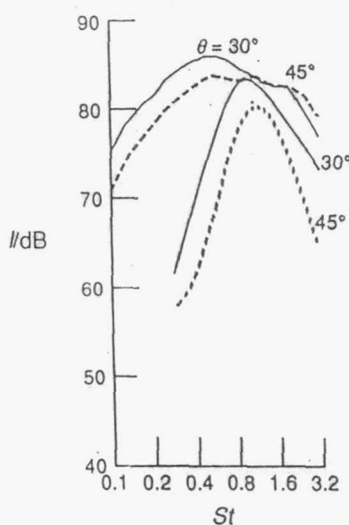
## What is Computational Aero-Acoustics (CAA) ?

CAA is concerned with calculations of the aerodynamically-generated sound source and its propagation:

- The time-dependent flow fluctuations (sound source) are obtained starting from the time-dependent differential equations.
- High-order accurate schemes and appropriate boundary conditions for wave-like solutions are needed.
- Differential or integral techniques for sound propagation.

- I. Background
- II. Prediction of the time-dependent sound source using Large-Eddy Simulations (LES)
- III. Sound propagation to the far-field

Calculated Spectra of Sound Intensity in Decibels Referred to  
 $10^{-12} \text{ W m}^{-2}$  Due to Coherent Structures  
 at Various Emission Angles for  $U_e = 195 \text{ m s}^{-1}$



CD-92-60388

FIGURE 14. Large-scale structure r.m.s. pressure ratio  $(\bar{P})^{1/2}/(\bar{P}_0)^{1/2}$  along the jet centreline: comparison with Moore's (1977) experimental data. (c):  $S_t = 0.18$ ; (d):  $S_t = 0.24$ ; (e):  $S_t = 0.30$ ; (f):  $S_t = 0.35$ ; (g):  $S_t = 0.50$ .

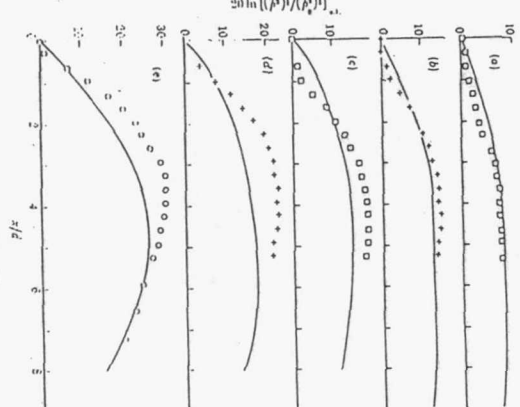


FIGURE 15. Maximum large-scale structure amplification as a function of Strouhal number; comparison with Moore's (1977) experimental data.

## II. Large-Eddy Simulations For Prediction of The Sound Source in a Supersonic Jet

### The Study Indicates:

- The large-scale structure seems to be the dominant sound source.
- Results are sensitive to approximation in the sound source.
- Lighthill's theory predicts some results consistent with observations and some are not.
  - DNS can predict the full spectrum of the sound source...But, the resolution requirements are prohibitive.
  - In large-eddy simulations (LES) the unresolved, small scales are modelled. The acoustically active, larger scales are obtained directly from simulation.

### Harmonic excitation

Inflow disturbances in the form

$$\tilde{u} = \bar{u} + \epsilon e^{-(r-1)^2} \sum_{j=1}^{16} \sin k_j \omega_j t , \quad (5)$$

where  $\omega_j$  was taken  $\pi/8$ . The Gaussian profile of the disturbance was introduced to reduce the adjustment zone.

Discretization:  
 • A fourth order accurate in space and second-order accurate in time MacCormick Scheme is used (2-4, Gottlieb & Turkel).

• An operator splitting is used to maintain the 2-4 accuracy, namely

$$Q^{n+2} = L_x L_y L_z Q^n , \quad (3)$$

where  $L_x$  and  $L_y$  are one-dimensional solution operators corresponding to the scheme applied to the equations

$$Q_r = F_r , \quad Q_t = G_t + S , \quad (4)$$

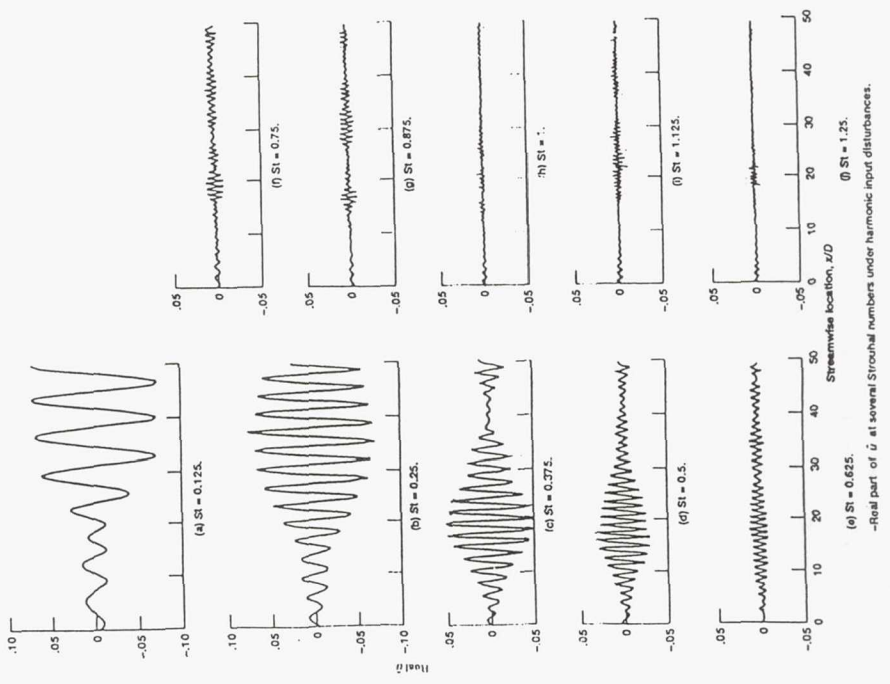
### SGS Model:

• Smagorinsky's model is used for the SGS turbulence.

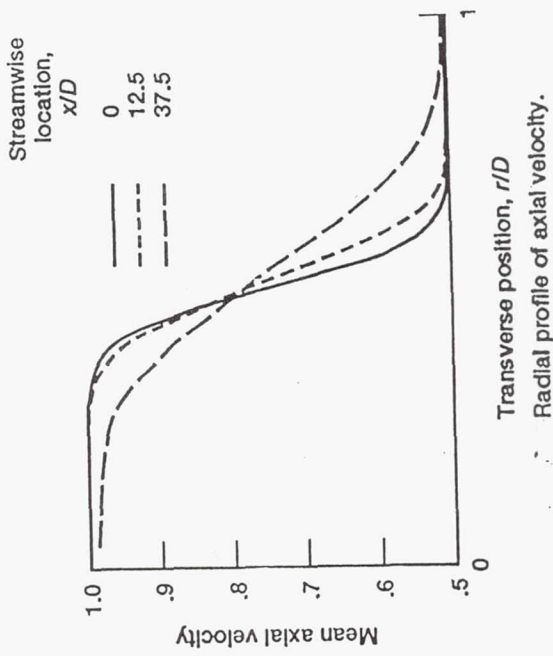
Boundary conditions:

• Objective is to obtain the time-dependent ("wave-like") structure. Boundary conditions could create artificial disturbances or could dampen the physical disturbances. Special attention is needed.

• Several outflow boundary conditions are evaluated.  
 • Linearized characteristics (e.g. Bayless & Turkel) are used to derive the B.C. used herein.



-Real part of  $\hat{u}$  at several Strouhal numbers under harmonic input disturbances.



100%

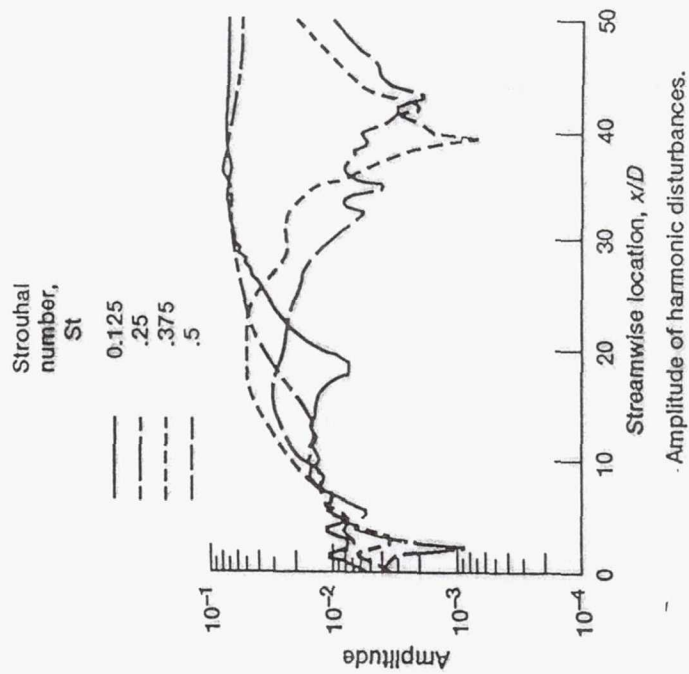
### III. Far-Field Sound

(1) Extend Navier-Stokes computational domain to the far field:  
(a) Prohibitive storage requirements  
(b) acoustic scales are different from fluid scales.

(2) Lighthill's acoustic analogy

(3) Finite-difference of linearized equations

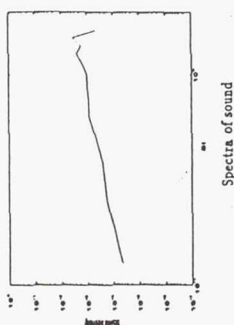
(4) Kirchhoff's method



(2) Prediction of the Far-Field Sound Using Lighthill's Theory

(3) Finite-difference approach --- Linearized Euler equations

- Finite-differencing can be used to solve the linearized Euler equations or other equations (Litay, Phillips) describing the sound propagation to the far-field.
- The problem is that numerical dissipation and dispersion can lead to erroneous results for or the far-field sound.
- Goodrich (1993) developed a new algorithm that seems to be useful for this purpose.  
The scheme is tested for 1D linearized Euler equations and seems to be accurate at very long times with few mesh points



## SUMMARY

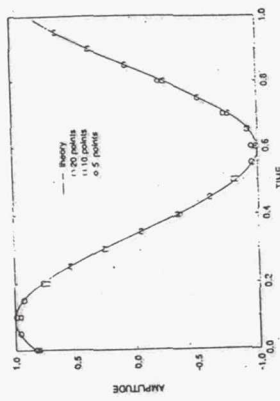
### (4) Kirchhoff's method

- FLOW FIELD:
  - The time-dependent sound source can be predicted via careful large-eddy simulations.
  - For random inflow-disturbances the wave-like nature of the unsteady structure is evident for Strouhal numbers of up to about 1.2.
  - The large-scale structure ( $St < 1.2$ ) could be enhanced via harmonic excitation -- Potential for control.
  - The higher frequency modes peak closer to the jet exit and the lower frequency ones peak farther downstream.

### FAR-FIELD SOUND:

- Lighthill's: Limited success
  - No explicit account for sound-flow interaction
  - Source is assumed to be compact, but it is no-compact for supersonic jets.
- Finite-Difference:
  - A high-accuracy scheme is being evaluated.
- Kirchhoff's method:
  - The predicted pressure on a cylindrical surface enclosing the jet is used to predict the far-field sound -- Most promising.

- Outside the source region the sound transmission is governed by the convective wave equation.
- The sound pressure field is given in terms of a surface integral involving the numerically calculated surface pressure.
- Evaluated for a point source.



- Predicted directivity of jet noise seems to be consistent with observation.

# JET NOISE PREDICTION USING A $k-\epsilon$ TURBULENCE MODEL

A. Khavaran  
Sverdrup Technology, Inc.  
NASA Lewis Research Center

Lewis Internal Workshop  
on  
Computational Turbulence Modeling  
September 15-16, 1993

## MODELING APPROACH

- Source Spectrum Calculations
  - Acoustic Analogy
  - Ribner and Batchelor Assumptions
  - Calculation of the Source Spectrum and its Characteristic Frequency Based on Time-Averaged Flow Calculation (with a  $k-\epsilon$  Turbulence Model)
- Sound/Flow Interaction
  - High Frequency Asymptotic Solution to Lilley's Eq. for Multipole Sources Convecting in an Axisymmetric Parallel Flow (Balsa & Mani)

## GOVERNING EQUATIONS

Lighthill's Equation

$$\frac{\partial^2 \rho}{\partial t^2} - c^2 \nabla^2 \rho = \frac{\partial^2 T_{ij}}{\partial x_i \partial x_j}$$

$$T_{ij} = \rho V_i V_j + \delta_{ij}(p - c^2 \rho) - e_{ij}$$

$$\begin{aligned} e_{ij} &= \mu \left( \frac{\partial V_i}{\partial x_j} + \frac{\partial V_j}{\partial x_i} - \frac{2}{3} \delta_{ij} \frac{\partial V_k}{\partial x_k} \right) \\ \frac{e_{ij}}{\rho V_i V_j} &\sim O\left(\frac{1}{Re}\right), \quad Re = \frac{\rho U L}{\mu} \\ \frac{1}{c^2} dp - d\rho &= \left( \frac{\partial \rho}{\partial s} \right)_p ds \end{aligned}$$

- The effects of source convection and refraction are included in the source term

Lilley's Equation

$$\frac{D}{Dt} \left( \frac{D^2 \sigma}{Dt^2} - \frac{\partial}{\partial x_i} c^2 \frac{\partial \sigma}{\partial x_i} \right) + 2 \frac{\partial V_j}{\partial x_i} \frac{\partial}{\partial x_j} c^2 \frac{\partial \sigma}{\partial x_i} = -2 \frac{\partial V_j}{\partial x_i} \frac{\partial V_k}{\partial x_j} \frac{\partial V_i}{\partial x_k} + \frac{D}{Dt} \left[ \frac{D}{Dt} \left( \frac{1}{c_p} \frac{Ds}{Dt} \right) \right] + \text{viscous terms}$$

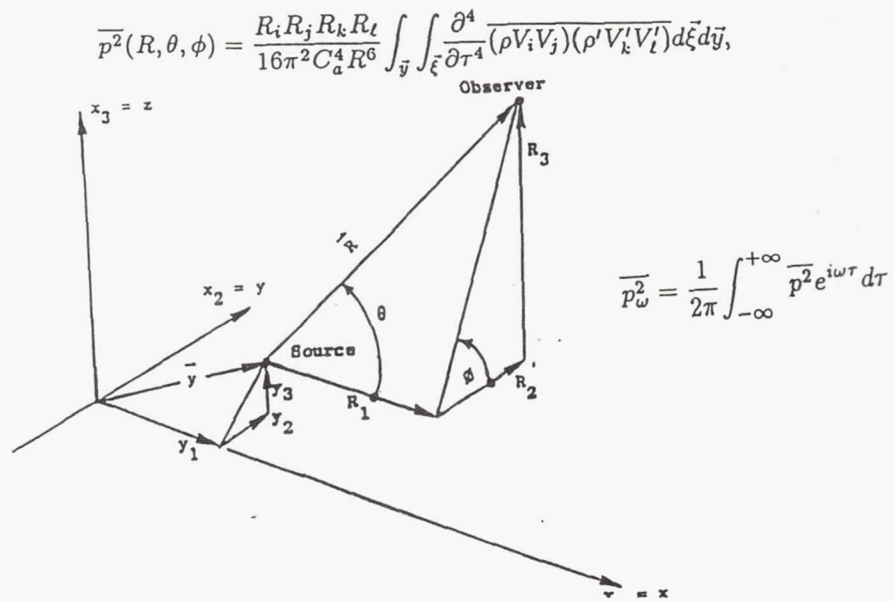
$$\sigma = \frac{1}{\gamma} \ln \frac{p}{p_0}$$

$$\frac{D}{Dt} = \frac{\partial}{\partial t} + V_k \frac{\partial}{\partial x_k}$$

- The effects of source convection and refraction are included in the operator term of Lilley's eq.

### Source Spectrum Calculations

- Mean-square sound pressure autocorrelation in the far field due to a finite volume of turbulence (in absence of convection and fluid shielding)



- Fourth-order velocity correlation tensor

$$S_{ijkl} = \overline{v_i v_j v'_k v'_l} = \int_{-\infty}^{+\infty} (v_i v_j)(v'_k v'_l) dt$$

- Source strength (Quasi-incompressible turbulence)

$$I_{ijkl} = \rho^2 \int_{\vec{\xi}} \frac{\partial^4}{\partial \tau^4} S_{ijkl} d\vec{\xi}$$

- Reduction in order of correlation tensor

$$S_{ijkl} = S_{ik} S_{jl} + S_{il} S_{jk} + S_{ij} S_{kl}$$

$$S_{ij}(\tau, \vec{\xi}) = \int_{-\infty}^{+\infty} v_i v'_j dt$$

- Separable second-order tensors

$$S_{ij}(\tau, \vec{\xi}) = R_{ij}(\vec{\xi})G(\tau)$$

- Isotropic turbulence model of Batchelor

$$R_{ij}(\vec{\xi}) = T e^{-\pi(\xi/L_x)^2} \times \left\{ [1 - \pi(\xi/L_x)^2] \delta_{ij} + \pi \xi_i \xi_j / L_x^2 \right\}$$

$$T = \frac{1}{3} \bar{v_i v_i}, \quad \xi^2 = \xi_1^2 + \xi_2^2 + \xi_3^2$$

- Gaussian correlation time delay

$$G(\tau) = e^{-(\tau/\tau_o)^2}$$

- Source spectrum component

$$I_{1111}(\Omega) \sim \rho^2 k^{\frac{1}{2}} (\Omega \tau_o)^4 e^{\frac{-(\Omega \tau_o)^2}{k}}$$

$$L_x \sim \frac{k^{3/2}}{\epsilon}, \quad \tau_o \sim \frac{L_x}{\sqrt{k}}, \quad k = \frac{1}{2} \bar{v_i v_i}$$

- Characteristic time delay of correlation

$$\tau_o \sim \frac{1}{(\partial U / \partial r)} \quad or \quad \tau_o \sim \frac{k}{\epsilon}$$

- Doppler shifted frequency

$$\Omega = 2\pi f \bar{C}, \quad \bar{C} = \sqrt{(1 - M_c \cos \theta)^2 + (\alpha_c k^5 / C_\infty)^2}$$

$$M_c = .5M + \beta_c M_j$$

## Sound/Flow Interaction

- Mean square pressure in the far field

$$\overline{p^2}(R, \theta, \Omega) = \int_{\vec{y}} \Lambda(a_{xx} + 4a_{xy} + 2a_{yy} + 2a_{yz}) d\vec{y}$$

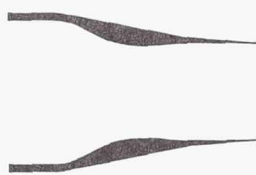
- Source term

$$\Lambda \sim \frac{\left(\frac{\rho_\infty}{\rho}\right)^2 I(\Omega)}{(4\pi R C_\infty C)^2 (1 - M \cos\theta)^2 (1 - M_c \cos\theta)^2}$$

- Shielding function

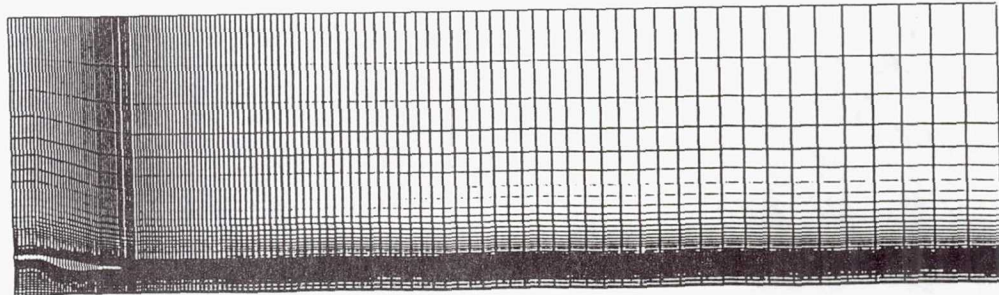
$$g^2(r) = \frac{(1 - M \cos\theta)^2 \left(\frac{C_\infty}{C}\right)^2 - \cos^2\theta}{(1 - M_c \cos\theta)^2}$$

$$M(r) = U(r)/C_\infty \quad M_c = U_c/C_\infty$$



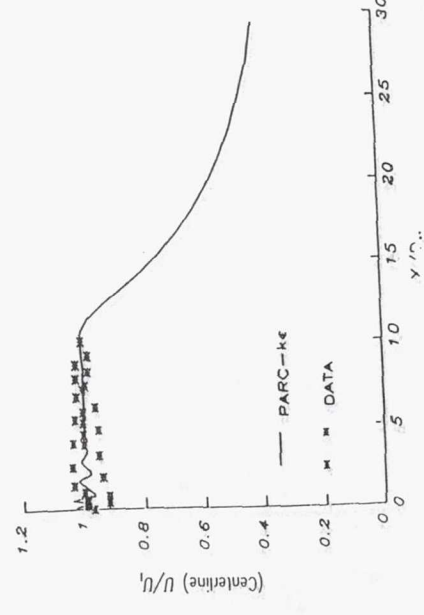
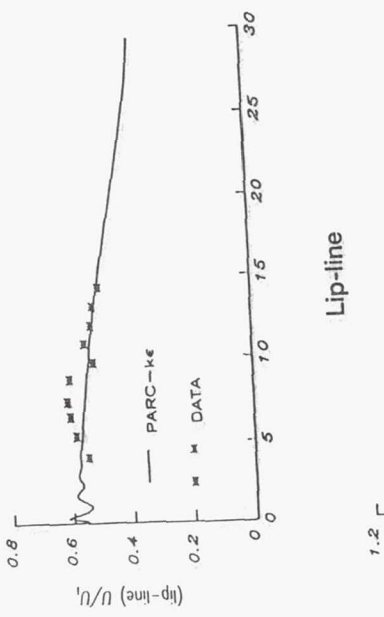
Design Parameters for C-D Nozzle

Throat Diameter	5.1 in.
Exit Diameter	5.395 in.
Distance from Throat to Exit	5.525 in.
Exit Velocity	2409 fps
Ambient Velocity	400 fps
Pressure Ratio	3.121
Stagnation Temp.	1716°R



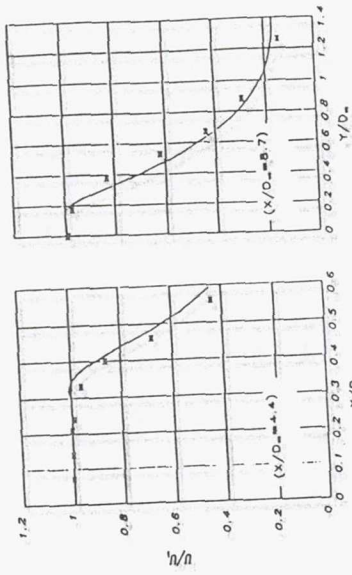
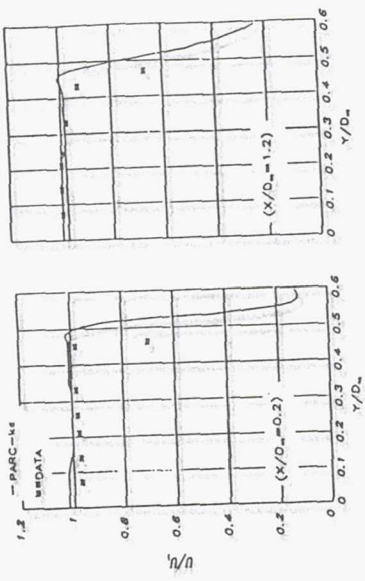
## Comparison of the Velocity Profiles With Data

Centerline



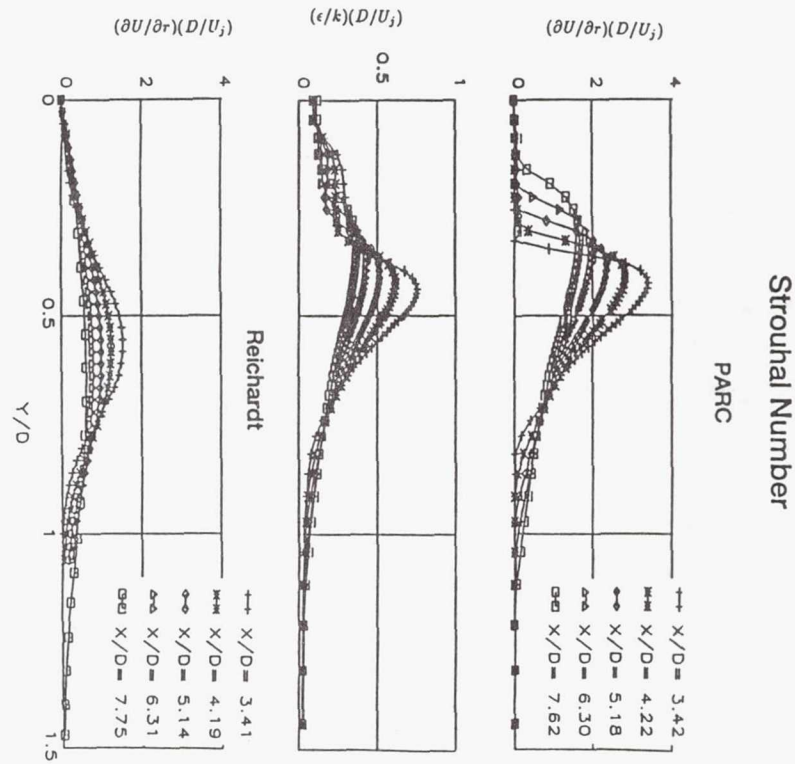
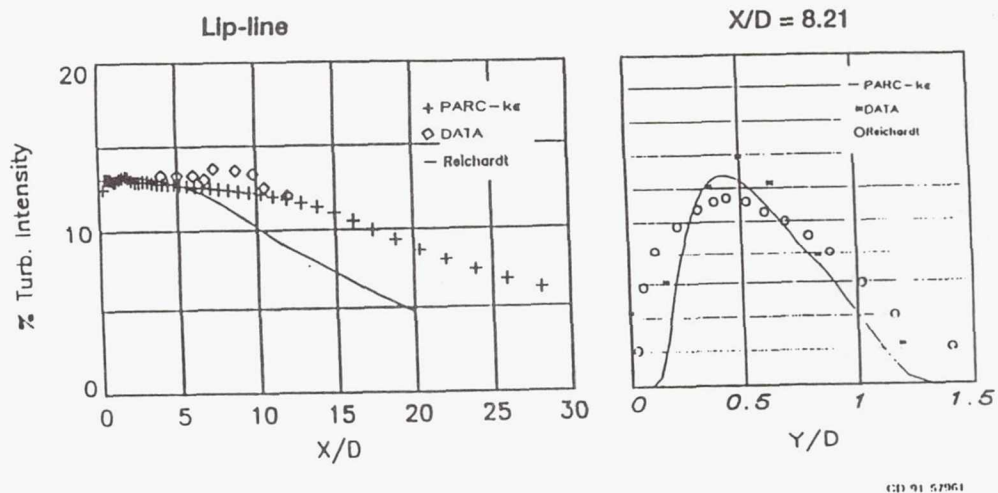
-CD-91-57959

## Comparison of Velocity Profiles With Experimental Data at Four Different Axial Locations

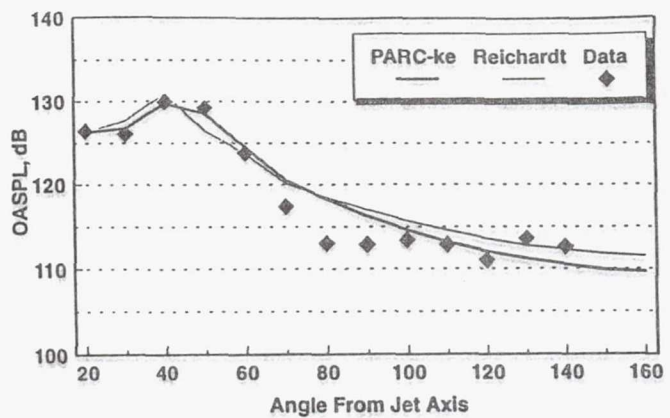


-CD-91-57960

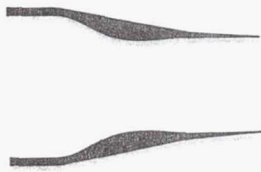
## Comparison of the Turbulent Intensity Profiles With Data



### OASPL DIRECTIVITY (ARC=40 ft)

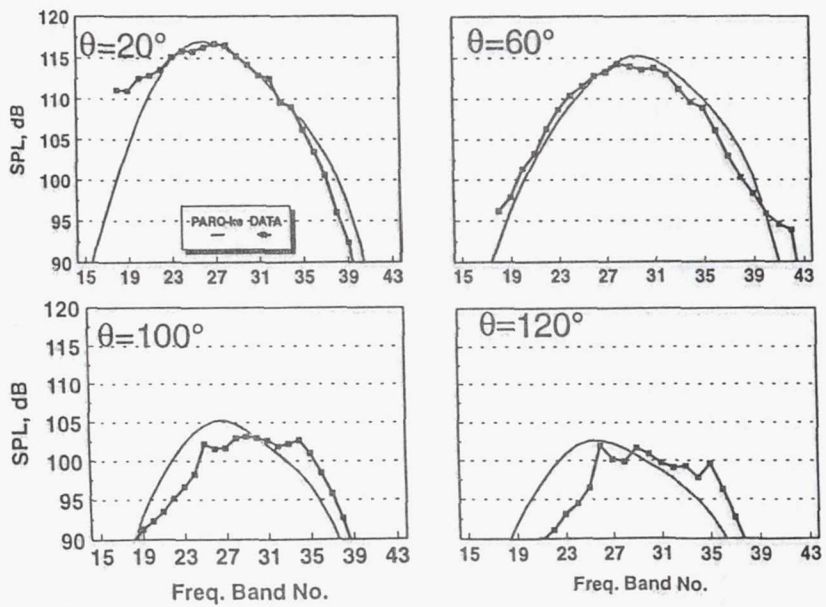


### Design Parameters for C-D Nozzle



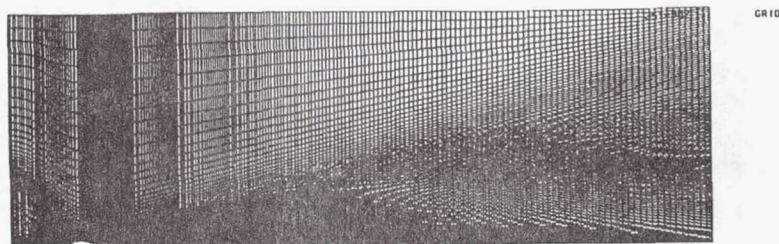
Exit Diameter	5.395 in.
Throat Diameter	5.1 in.
Exit Velocity	2409 fps
Pressure Ratio	3.121
Stagnation Temperature	1716 R

### NOISE SPECTRA (CD Nozzle)



Band 15 is 125 Hz

GRID  
CONTOURED PLUG NOZZLE



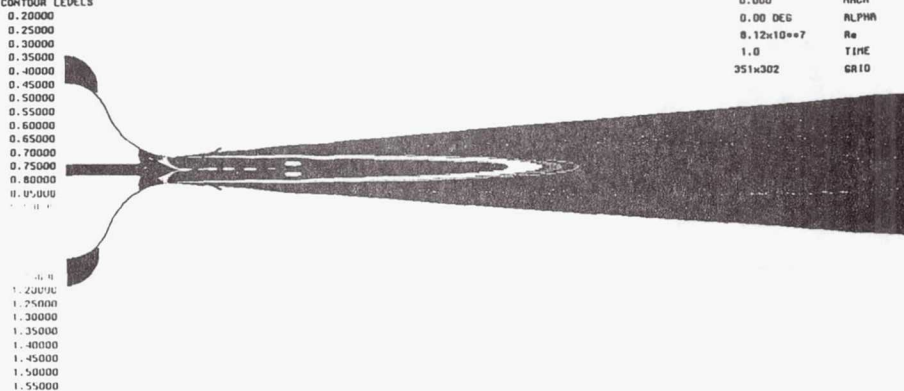
GRID

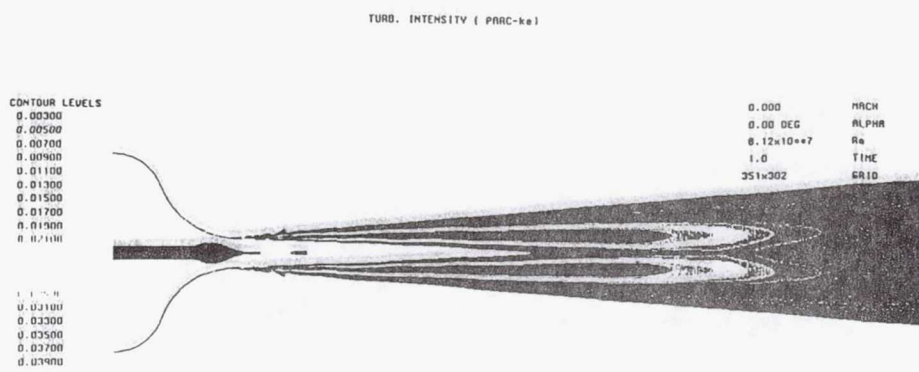
MACH NUMBER  
CPH (PRRC-ka)

CONTOUR LEVELS

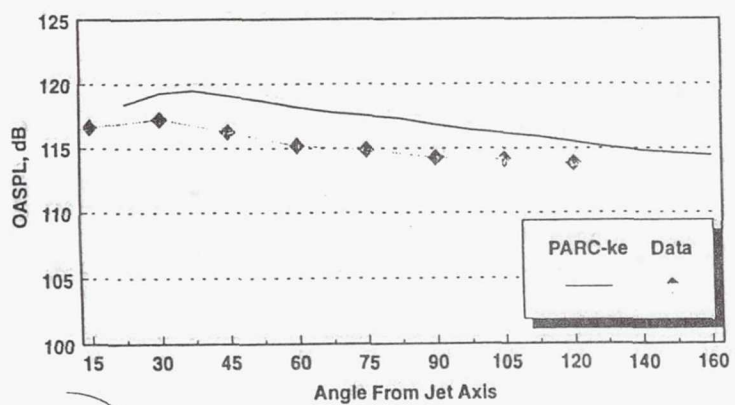
0.20000  
0.25000  
0.30000  
0.35000  
0.40000  
0.45000  
0.50000  
0.55000  
0.60000  
0.65000  
0.70000  
0.75000  
0.80000  
0.85000

0.000  
0.00 DEG  
 $8.12 \times 10^{-7}$   
1.0  
351x302  
MACH  
ALPHA  
Re  
TIME  
GRID

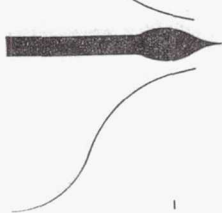




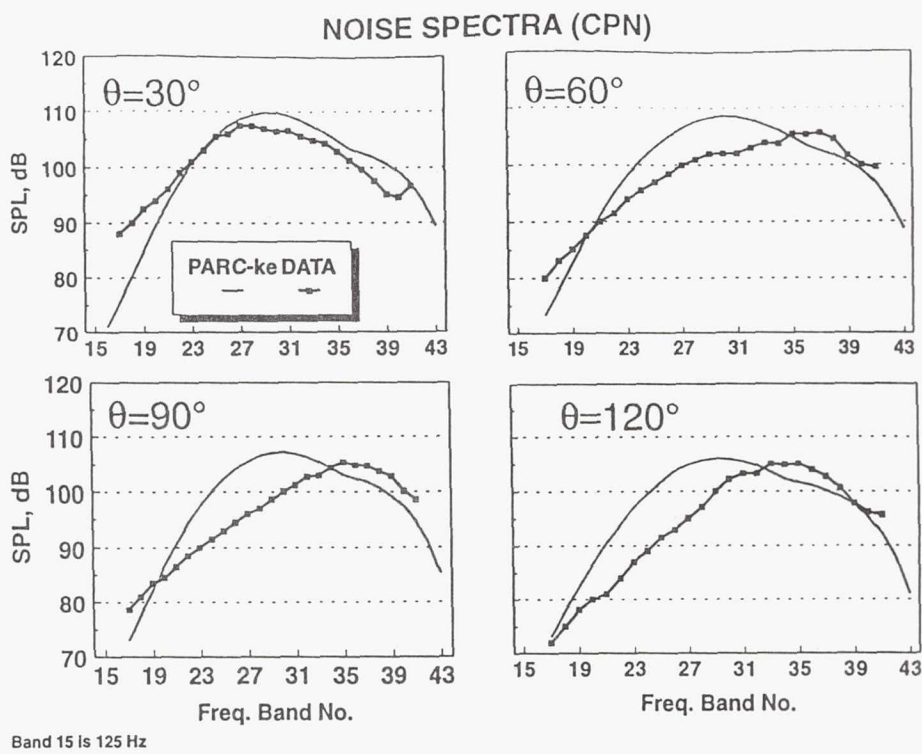
### OASPL DIRECTIVITY (ARC=10 ft)



### Design Parameters for CPN



Exit Inner Diameter .597 in.  
 Exit Outer Diameter 1.77 in.  
 Pressure Ratio 3.61  
 Stagnation Temperature 532 R



## SUMMARY

- Source strength was evaluated using the PARC code with a  $k-\epsilon$  turbulence model
- The characteristic Strouhal no. was obtained from  $k$  and  $\epsilon$  (with an empirical proportionality constant)
- Time-averaged velocity and temperature predictions were used to assess the sound/flow interaction
- Constants used in the supersonic convection factor are determined empirically
- The SPL directivity and spectra demonstrate favorable agreement with data (specially at angles close to the jet axis)
- The empirical constants used in these predictions need to be investigated for other geometries

**Page intentionally left blank**

NUMERICAL SIMULATION OF UNSTEADY SUPERSONIC FLOW USING  
AN IMPLICIT ALGORITHM FOR THE STRONGLY COUPLED  
NAVIER-STOKES AND K-E EQUATIONS

by

S.H. Shih\*, A. Hamed#and J.J. Yeuan#

\* ICOMP, NASA Lewis Research Center  
# Dept. of Aero. Eng. & Eng. Mechanics  
University of Cincinnati, Cincinnati, Ohio

OUTLINE

- \* INTRODUCTION
- \* METHODOLOGY
- \* \* NUMERICAL ALGORITHM
- \* RESULTS
- \* CONCLUSIONS

## METHODOLOGY

- \* MEAN FLOW AND TURBULENCE EQUATIONS ARE INTEGRATED SIMULTANEOUSLY
- \* FULL N-S EQUATIONS IN STRONG CONSERVATION LAW FORM
- \* NICHOLS K-E TURBULENCE MODEL (1990)
- \* BEAM - WARMING SCHEME (1978)
- \* FULLY IMPLICIT TREATMENT OF TURBULENCE SOURCE TERMS
- \* NEWLY PROPOSED 2nd-ORDER DAMPING

## INTRODUCTION

### TWO-EQUATION TURBULENCE MODEL :

- \* TRANSPORT EQUATIONS
- \* CONSIDER FLOW HISTORY, LESS EMPIRICISM.

### PREVIOUS WORKS BY OTHER RESEARCHERS :

- \* UNCOUPLED N-S AND K-E EQUATIONS
- \* STEADY FLOW :
  - TIME LAGGING BETWEEN MEAN FLOW AND TURBULENCE [Huang & Coakley (1992), Sahu & Danberg (1986), PARC Code (1989)]
- \* UNSTEADY FLOW:
  - SUBITERATION TECHNIQUE REQUIRED [Rizzetta & Visbal (1992)]

$$(A.17)$$

$$P_t = C_{t1} PR2 + C_{t3} PRJ - C_{t1} \left( \frac{\partial u}{\partial x} + \frac{\partial v}{\partial y} \right) \left[ \frac{1}{Re} \left( \frac{\partial u}{\partial x} + \frac{\partial v}{\partial y} \right) + \mu k \right]$$

where

$$PRJ = (\tau_{xy})_{\text{loc}} \frac{\partial u}{\partial x} + (\tau_{xy})_{\text{loc}} \frac{\partial v}{\partial y}, \quad PR2 = (\tau_{xy})_{\text{loc}} \left( \frac{\partial u}{\partial x} + \frac{\partial v}{\partial y} \right) \quad (A.18)$$

with the incompressible turbulent stress expressed as

$$(\tau_{xy})_{\text{loc}} = \frac{\mu_i}{Re} \left( \frac{\partial u_i}{\partial x_j} + \frac{\partial u_j}{\partial x_i} \right) \quad (A.19)$$

and the coefficients  $C_{t1}$  and  $C_{t3}$  given as

$$C_{t1} = 1.35, \quad C_{t3} = C_{t1} + 3.0 \exp[-3.5(PRJ/PR2)^{\frac{1}{2}}] \quad (A.20)$$

$$\mu_i = Re C_{\mu} \rho \frac{k^2}{\epsilon} \quad (A.21)$$

The empirical constants for the model are given by [28] as follows:

$$C_{\mu} = 0.09 [1 - \exp(-0.0115y')], \quad C_1 = 1.0, \quad C_2 = 1.3, \quad C_3 = 1.8 [1 - \frac{2}{9} \exp(-\frac{R_i^2}{36})] \quad (A.22)$$

$$C_{\mu} = 0.09 [1 - \exp(-0.0115y')] \quad (A.23)$$

$$R_i = Re \frac{\rho k^2}{\mu \epsilon}, \quad y' = Re \frac{\rho_w u_s y}{\mu_w}, \quad u_s = \left( \frac{\tau_{xy}}{\rho_w} \right)^{1/2} \quad (A.24)$$

## TURBULENCE MODEL

- BASED ON CHIEN'S (1982) LOW REYNOLDS NUMBER TURBULENCE MODEL
- MODIFIED FOR COMPRESSIBILITY EFFECTS AND IRROTATIONAL STRAINS, NICHOLS (1990)
- INTEGRATED TO WALL, WITHOUT THE USE OF WALL FUNCTIONS

(A.11)

$$\frac{\partial U_i}{\partial x} + \frac{\partial E_i}{\partial x} + \frac{\partial F_i}{\partial y} = S_i \quad (A.11)$$

where the turbulent state vector  $U_i$ , flux vectors  $E_i$ ,  $F_i$ , and source vector  $S_i$  are given by:

$$U_i = \begin{bmatrix} \rho k \\ \rho \epsilon \end{bmatrix}, \quad E_i = \begin{bmatrix} \rho \mu k + \frac{1}{Re} \left( \frac{\mu_i + \mu}{\sigma_k} \right) \frac{\partial k}{\partial x} \\ \rho \nu k + \frac{1}{Re} \left( \frac{\mu_i + \mu}{\sigma_k} \right) \frac{\partial \epsilon}{\partial x} \end{bmatrix}, \quad F_i = \begin{bmatrix} \rho \nu k + \frac{1}{Re} \left( \frac{\mu_i + \mu}{\sigma_k} \right) \frac{\partial \epsilon}{\partial y} \\ \rho \mu \epsilon + \frac{1}{Re} \left( \frac{\mu_i + \mu}{\sigma_k} \right) \frac{\partial k}{\partial y} \end{bmatrix} \quad (A.12)$$

$$S_i = \begin{bmatrix} S_{i\#} \\ S_{i\alpha} \end{bmatrix} = \begin{bmatrix} P(1 - C_p) - \rho \epsilon - \frac{1}{Re} \frac{2 \mu k}{Y_n^2} \\ \frac{\epsilon}{k} P_s - C_2 \rho \frac{\epsilon^2}{k} - \frac{1}{Re} \frac{2 \mu \epsilon}{Y_n^2} EXP(-\frac{y'}{2}) \end{bmatrix} \quad (A.13)$$

The turbulence production terms  $P$  is expressed as follows:

$$P = \tau_{xx} \frac{\partial u}{\partial x} + \tau_{yy} \left( \frac{\partial u}{\partial y} + \frac{\partial v}{\partial x} \right) + \tau_{xy} \frac{\partial v}{\partial y} \quad (A.13)$$

$$\tau_{xy} = \frac{\mu_i}{Re} \left( \frac{\partial u_i}{\partial x_j} + \frac{\partial u_j}{\partial x_i} \right) - \frac{2}{3} \delta_{ij} \left( \frac{\mu_i}{Re} \frac{\partial u_i}{\partial x_i} + \mu k \right) \quad (A.14)$$

$$C_p = C_{p1} (\gamma - 1) M M_k^2, \quad M_k = \frac{k^{1/2}}{a}, \quad a : \text{sonic velocity}, \quad C_{p2} = 4.0 \quad (A.15)$$

## NUMERICAL ALGORITHM

$$A = \begin{bmatrix} 0 & \xi_x & \xi_y & 0 & 0 & 0 \\ \frac{\gamma_1 \phi \xi_x - u \bar{u}}{2} & \bar{u} - (\gamma - 2)u \xi_x & -\gamma_1 \gamma \xi_x + u \xi_y & \gamma_1 \xi_x & (\frac{2}{3} - \gamma_1) \xi_x & 0 \\ -\bar{u}v + \frac{\gamma_1}{2} \phi \xi_y & v \xi_x - \gamma_1 u \xi_y & \bar{u} - (\gamma - 2)v \xi_y & \gamma_1 \xi_y & (\frac{2}{3} - \gamma_1) \xi_y & 0 \\ -\bar{u} \bar{u} & a_{41} & a_{42} & a_{43} & \bar{u} & 0 \\ -v \bar{u} & k \xi_x & k \xi_y & 0 & \bar{u} & 0 \\ -v \xi_x & v \xi_y & v \xi_x & 0 & 0 & \bar{u} \end{bmatrix} \quad (4.7)$$

■ GOVERNING EQUATION

■ BEAM-WARMING SCHEME

$$\begin{aligned} \Delta^* U &= \frac{\theta_1 \Delta t}{1 - \theta_2} \left[ \frac{\partial}{\partial \xi} (-\Delta^* E - \Delta^* V_1 + \Delta^* V_2) + \frac{\partial}{\partial \eta} (-\Delta^* F + \Delta^* W_1 + \Delta^* W_2) + \Delta^* H \right] \\ &\quad + \frac{\Delta t}{1 + \theta_2} \left[ \frac{\partial}{\partial \xi} (-E^n + V_1^n + V_2^n) + \frac{\partial}{\partial \eta} (-F^n + W_1^n + W_2^n) + H^n \right] \\ &\quad + \frac{\theta_2}{1 - \theta_2} \Delta^{n+1} U + O[(\theta_1 - \frac{1}{2} - \theta_2)(\Delta x)^2 - (\Delta t)^3] \end{aligned}$$

- THE N.S AND K-E EQUATIONS ARE INTEGRATED SIMULTANEOUSLY
- SOURCE TERMS ARE TREATED FULLY IMPLICIT

where the Jacobian matrices are written as:

$$[F] = \frac{\partial V}{\partial U}, \quad [R] = \frac{\partial V}{\partial U_i}$$

If the viscosity is assumed locally constant, then

$$[F] - [R_i] = 0$$

The viscous Jacobian matrix R is given by:

$$R = \frac{1}{\rho} \begin{bmatrix} 0 & 0 & 0 & 0 & 0 & 0 \\ -\lambda(b_1 u + b_2 v) & \lambda b_1 & \lambda b_2 & 0 & 0 & 0 \\ -\lambda(b_2 u + b_1 v) & \lambda b_2 & \lambda b_3 & 0 & 0 & 0 \\ r_{41} & r_{42} & r_{43} & r_{44} & r_{45} & 0 \\ -\lambda_1 b_1 c & 0 & 0 & 0 & \lambda_1 b_4 & 0 \\ -\lambda_2 b_2 c & 0 & 0 & 0 & 0 & \lambda_2 b_4 \end{bmatrix}$$

$$E^{n+1} = E^n + \left( \frac{\partial E}{\partial U} \right)^n (U^{n+1} - U^n) + O[(\Delta t)^2]$$

$$\Delta^* E = A^* \Delta^* U + O[(\Delta t)^2]$$

$$A = \frac{\partial E}{\partial U}$$

where

- LINEARIZATION
- INVISCID TERMS

The viscous delta term  $\Delta^* V_1(U, U_i)$  is linearized as follows:

$$\begin{aligned} \Delta^* V_1 &= \left( \frac{\partial V_1}{\partial U} \right)^n \Delta^* U - \left( \frac{\partial V_1}{\partial U_i} \right)^n \Delta^* U_i + O[(\Delta t)^2] \\ &= [P]^n \Delta^* U + [R]^n \Delta^* U_i + O[(\Delta t)^2] \\ &= [(P - R_i)P] \Delta^* U + \frac{\partial}{\partial \xi} [(P \nabla \Delta^* U) + O[(\Delta t)^2]] \end{aligned}$$

- SOURCE TERMS

### ARTIFICIAL DISSIPATION

Step 1:

$$\begin{aligned} & \left( I + \frac{\theta_1 \Delta t}{1+\theta_2} \left[ \frac{\partial A^n}{\partial \xi} - \frac{\partial^2 R^n}{\partial \xi^2} - D^n - e_n \delta_{\xi}^n \right] \right) \Delta^n U^n \\ & = RHS[\text{Eq.(4.5)}] - \frac{\Delta t}{1+\theta_2} [e_{it} (\delta_i^4 + \delta_i^2) + e_{it} (D_i \delta_i^2 + D_n \delta_n^2)] U^n \end{aligned}$$

Step 2:

$$\begin{aligned} & \left( I + \frac{\theta_1 \Delta t}{1+\theta_2} \left[ \frac{\partial B^n}{\partial \eta} - \frac{\partial^2 S^n}{\partial \eta^2} - e_n \delta_{\eta}^n \right] \right) \Delta^n U^n \\ & = \Delta^n U^n + \frac{\theta_1 \Delta t}{1+\theta_2} \left[ \frac{\partial B^n}{\partial \eta} - \frac{\partial^2 S^n}{\partial \eta^2} - e_n \delta_{\eta}^n \right] \Delta^n U^n \end{aligned}$$

Step 3:

$$U^{n+1} = U^n + \Delta^n U$$

where

$$e_{it} = e_{it} + e_{it} D_i \quad , \quad e_{in} = e_{in} + e_{in} D_n$$

$$\begin{aligned} D_i &= \frac{1}{4p} \left| \frac{\partial^2 P}{\partial \xi^2} \right| + \frac{1}{4k} \left| \frac{\partial^2 k}{\partial \xi^2} \right| \\ D_n &= \frac{1}{4p} \left| \frac{\partial^2 P}{\partial \eta^2} \right| + \frac{1}{4k} \left| \frac{\partial^2 k}{\partial \eta^2} \right| \end{aligned}$$

- THE FINAL DIFFERENCE FORMULA

$$\begin{aligned} U &= \frac{\theta_1 \Delta t}{1+\theta_2} \left[ \frac{\partial A^n}{\partial \xi} - \frac{\partial^2 R^n}{\partial \xi^2} - \frac{\partial^2 S^n}{\partial \eta^2} - D^n \right] \Delta^n U \\ &= \frac{\Delta t}{1+\theta_2} \left[ \frac{\hat{\partial}}{\partial \xi} (-E^n + V_1^n + V_2^n) + \frac{\hat{\partial}}{\partial \eta} (-F^n + W_1^n + W_2^n) - H^n \right] \\ &\quad + \frac{\theta_1 \Delta t}{1+\theta_2} \left[ \frac{\hat{\partial}}{\partial \xi} (\Delta^{n-1} V_2^n) + \frac{\hat{\partial}}{\partial \eta} (\Delta^{n-1} W_1^n) \right] + \frac{\theta_2}{1+\theta_2} \Delta^{n-1} U \end{aligned}$$

- BLOCK TRIDIAGONAL STRUCTURE
- 6x6 JACOBIAN MATRICES IN 2-D FLOWS

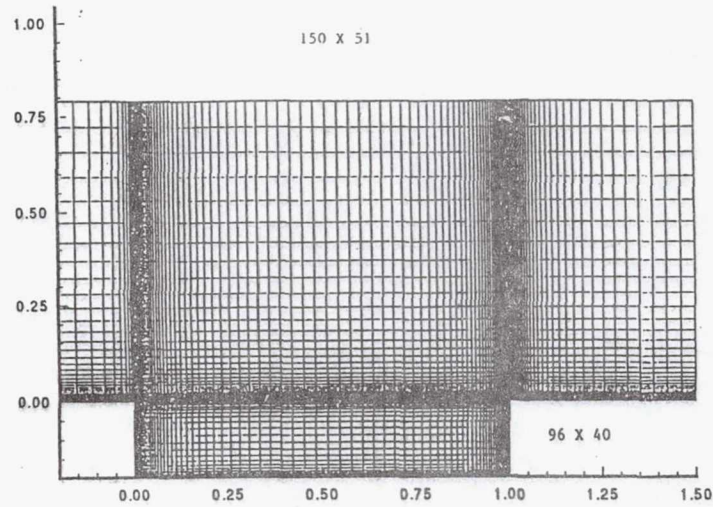


Fig. 41 Computational Grid for Supersonic Flow Over an Open Cavity.

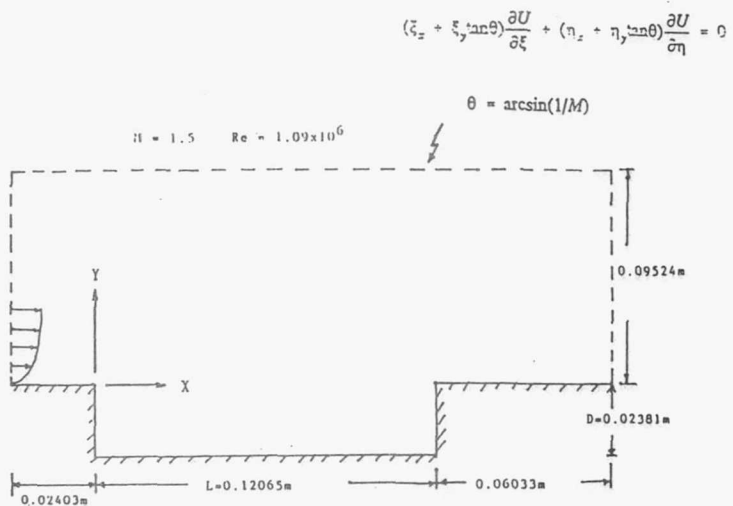


Fig. 40. Schematic of the Solution Domain for Supersonic Flow Over an Open Cavity.

## RIZZETTA & VISBAL (1992)

- BEAM-WARMING ALGORITHM
- LAUNDER & SHARMA (1974) LOW REYNOLDS NUMBER TWO-EQUATION TURBULENCE MODEL
- TURBULENCE EQUATIONS ARE UNCOUPLED FROM THE N-S EQUATIONS AND FROM EACH OTHER
- NEWTON-LIKE SUBITERATION TECHNIQUE

## RESULTS

- SUPERSONIC FLOW OVER AN OPEN CAVITY.
- COMPARISONS WITH EXPERIMENTAL DATA (BY KAUFMAN et al., 1983) AND RESULTS OBTAINED USING RIZZETTA AND VISBAL CODE (1992).

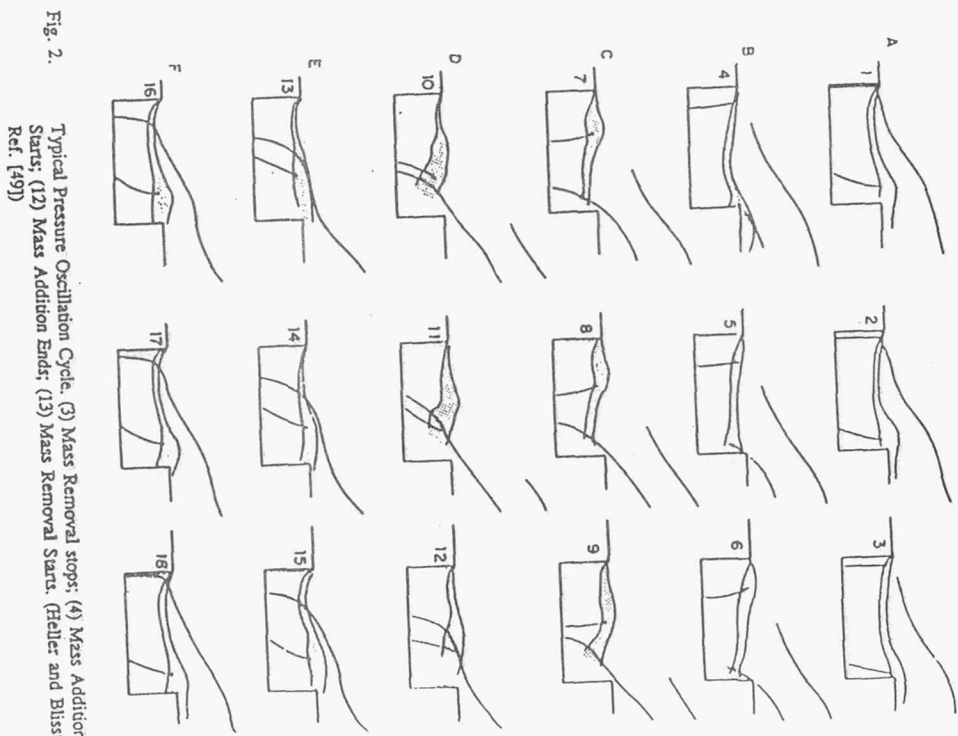
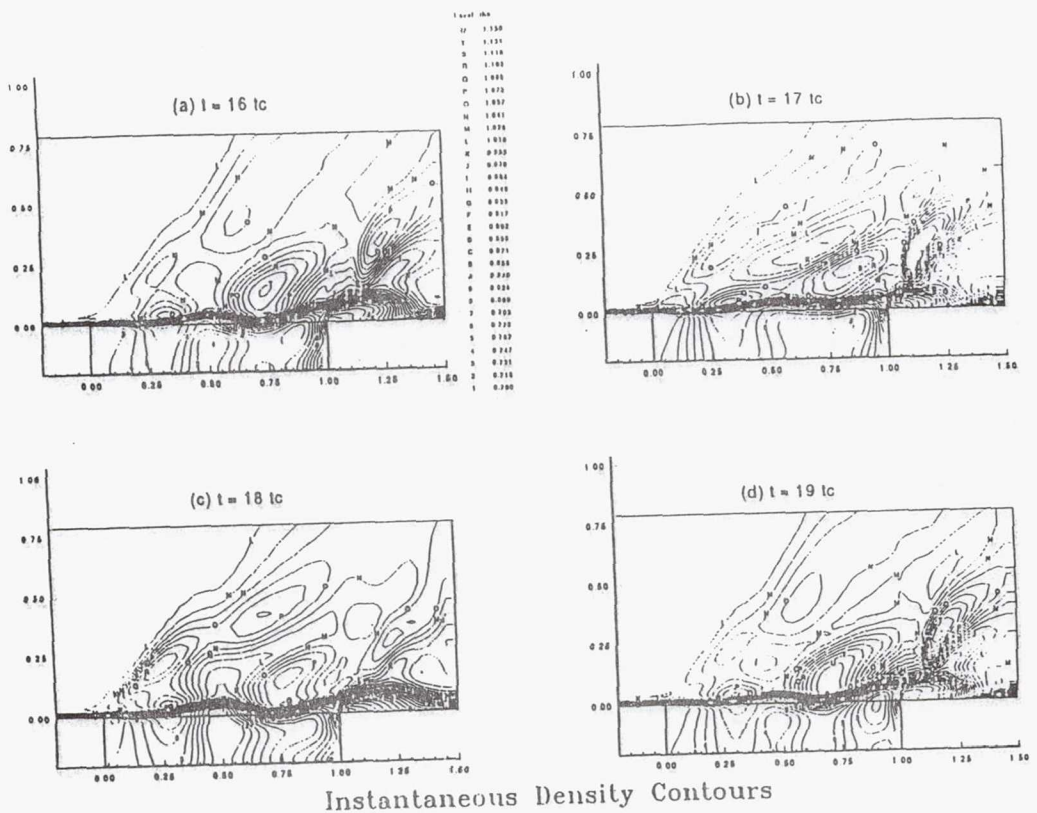
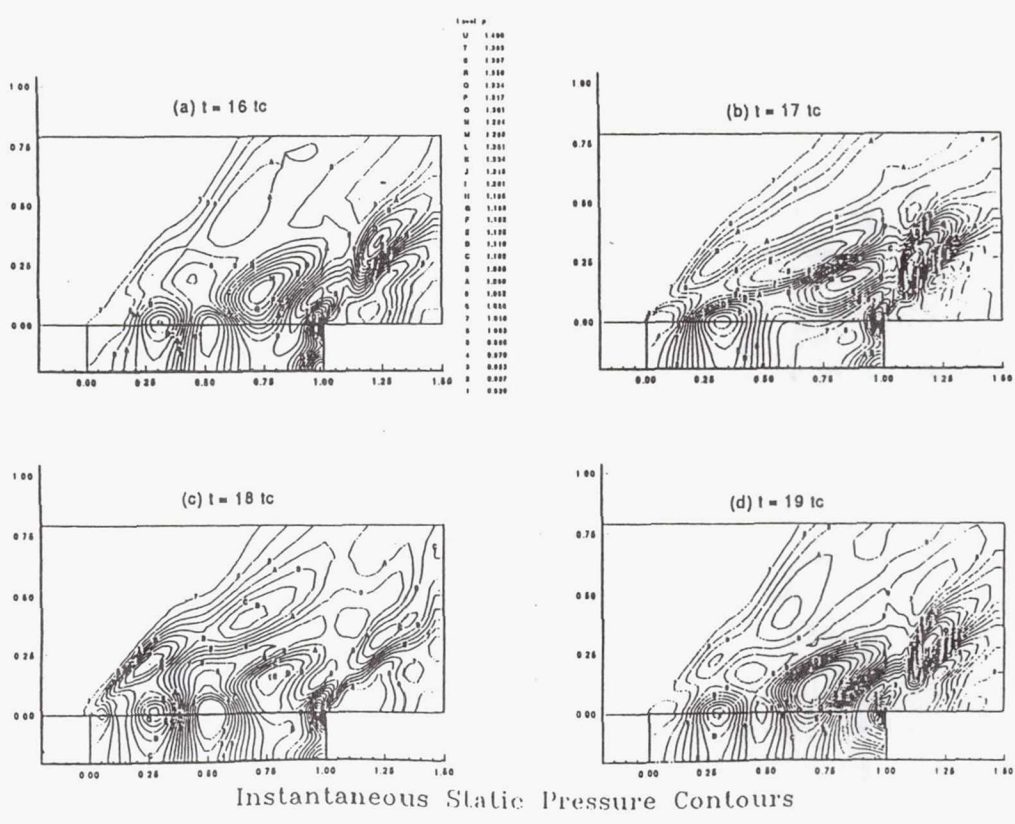
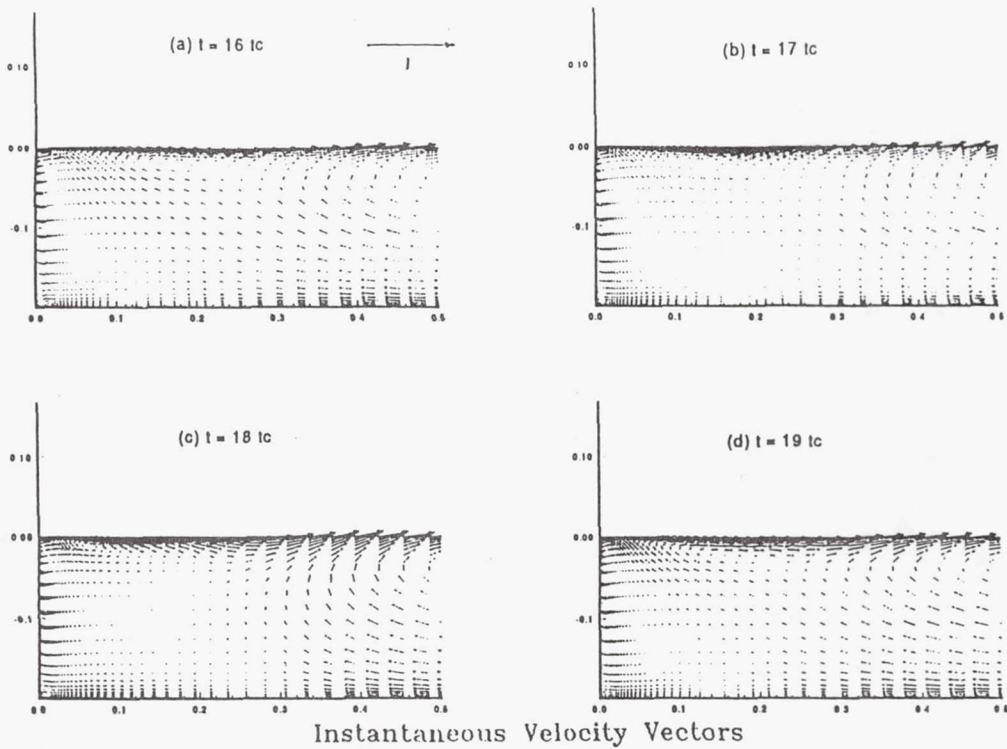


Fig. 2.  
Typical Pressure Oscillation Cycle. (3) Mass Removal stops; (4) Mass Addition Starts; (12) Mass Addition Ends; (13) Mass Removal Starts. (Heller and Bliss; Ref. [9])



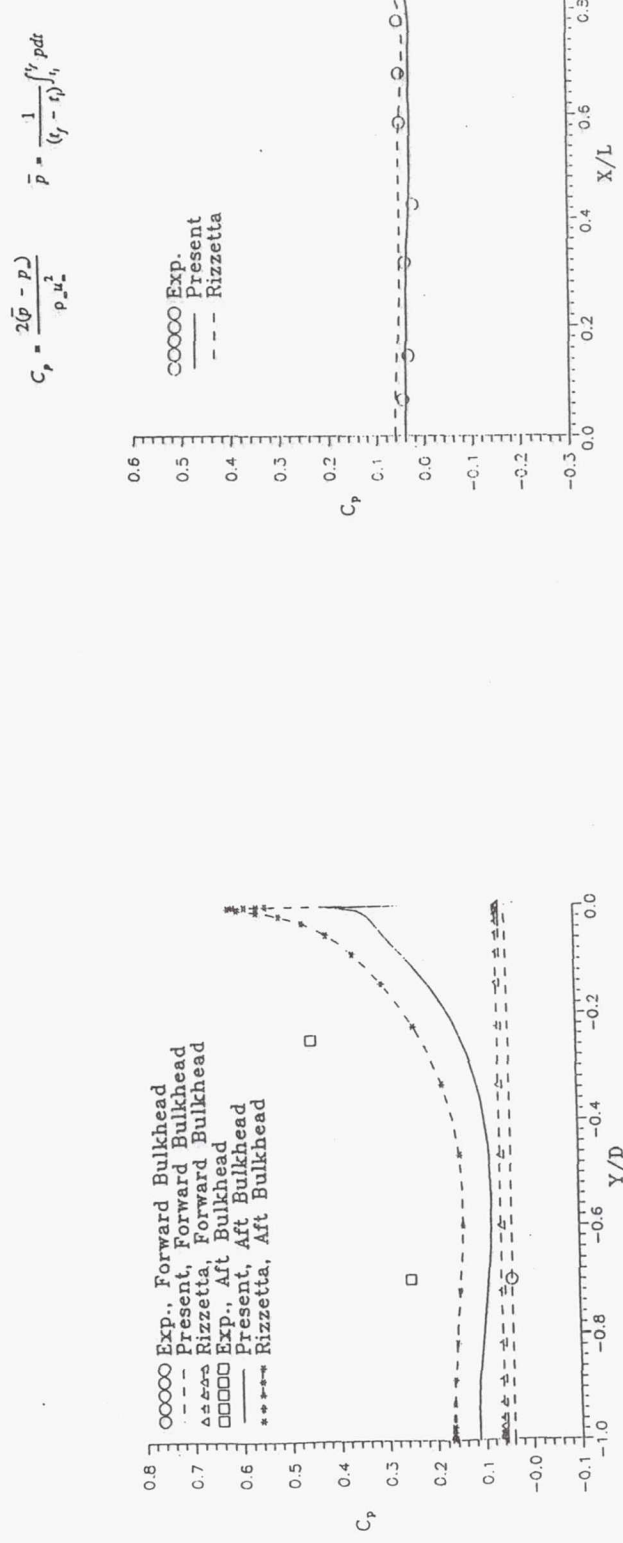


Fig. 46.

Mean Static Pressure Distribution Along the Forward and Aft Bulkheads

Fig. 47. Mean Static Pressure Distribution Along the Cavity Floor.

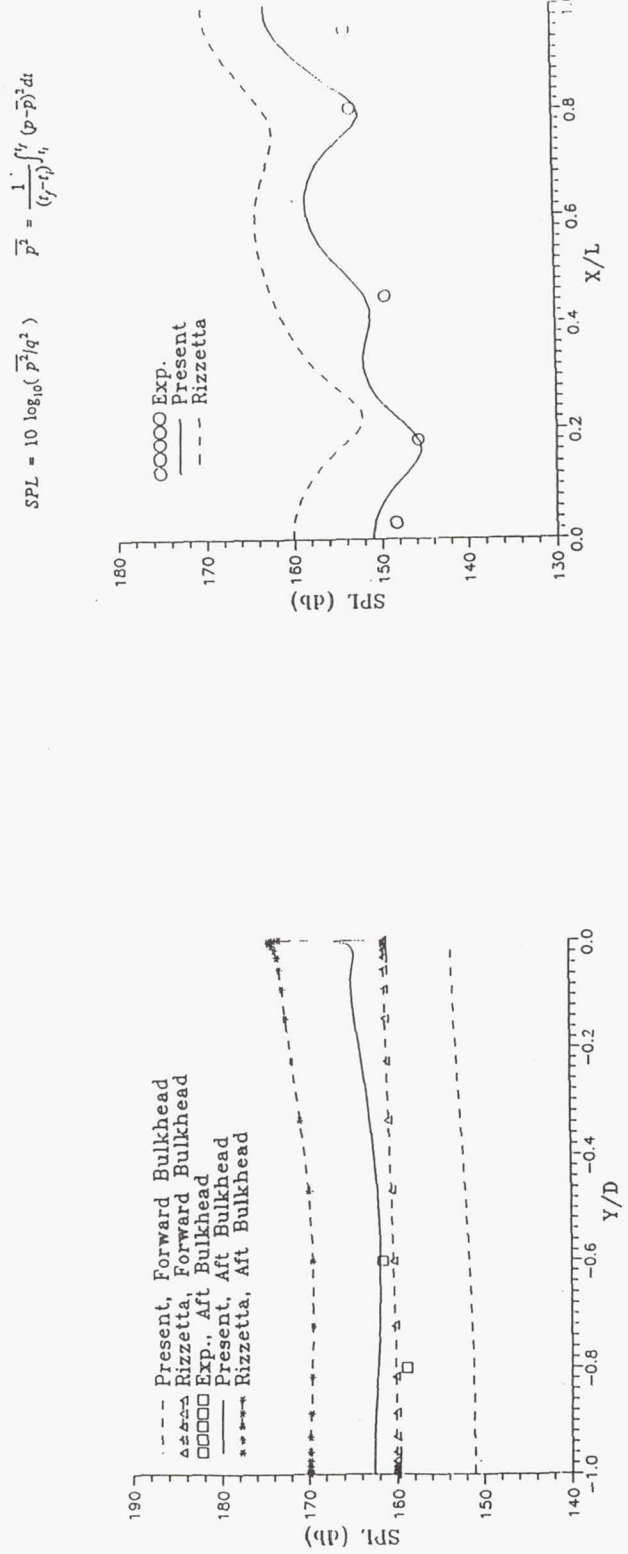


Fig. 48. Overall Sound Pressure Level Distribution Along the Cavity Floor.

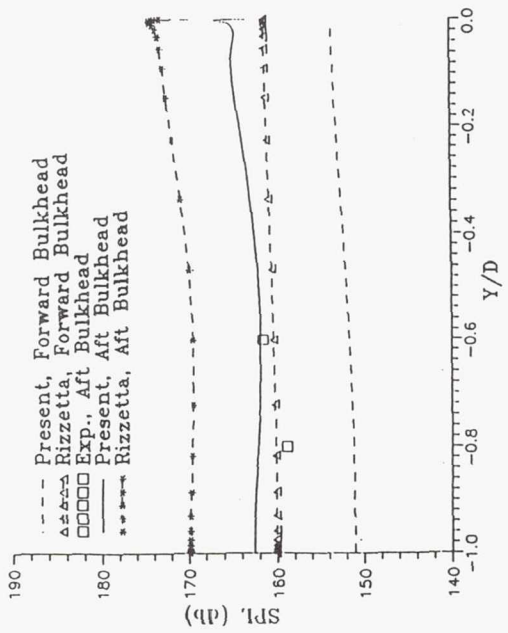


Fig. 49. Overall Sound Pressure Level Distribution Along the Forward and Aft Bulkheads.

## CONCLUSIONS

A NUMERICAL PROCEDURE WAS DEVELOPED FOR THE SIMULTANEOUS IMPLICIT SOLUTION OF THE COUPLED NAVIER-STOKES AND K-E EQUATIONS

### THE RESULTS DEMONSTRATE :

- SELF-SUSTAINED FLOW OSCILLATION WITHIN THE CAVITY IS SIMULATED
- OVERALL SOUND PRESSURE LEVELS ARE WELL-PREDICTED
- RELIEVE STIFFNESS, ENHANCE STABILITY, AND LARGER CFL NUMBER
- 20 CPU HOURS ON CRAY-YMP

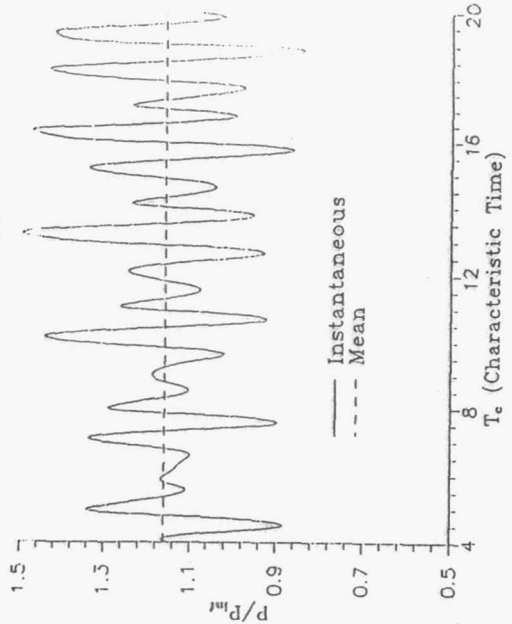


Fig. 49. Pressure Time History on the Aft Bulkhead at  $y/D = -0.4$ .

# **IMPLEMENTATION OF A $k-\varepsilon$ MODEL IN SPECTRAL ELEMENT CODE**

**Wai-Ming To**

**Sverdrup Technology, Inc.**

## **OBJECTIVES**

- Study the flow physics in problems that are generic to turbomachinery flows.
- Assess accuracy of turbulence models.

## EQUATIONS OF MOTION

$$\frac{\partial u_i}{\partial x_i} = 0$$

$$\frac{\partial u_i}{\partial t} = N_i - \frac{\partial p}{\partial x_i} + \frac{\partial}{\partial x_j} \left[ v_e \left\{ \frac{\partial u_i}{\partial x_j} + \frac{\partial u_j}{\partial x_i} \right\} \right]$$

where  $v_e = v_l + v_t$

## TIME DISCRETIZATION

- 2nd order predictor-corrector
- Capacitance matrix method to solve for pressure

### TIME DISCRETIZATION (cont.)

$$u_i^{(1)} = u_i^n + \Delta t f_i - \Delta t \frac{\partial p^{(1)}}{\partial x_i} + \Delta t \frac{\partial}{\partial x_j} \left[ v_e \left\{ \frac{\partial u_i^n}{\partial x_j} + \frac{\partial u_j^n}{\partial x_i} \right\} \right]$$

$$\frac{\partial u_i^{(1)}}{\partial x_i} = 0$$

$$u_i^{(2)} = u_i^n + \Delta t f_i - \frac{\Delta t}{2} \frac{\partial \bar{p}^{(1)}}{\partial x_i} + \frac{\Delta t}{2} \frac{\partial}{\partial x_j} \left[ v_e \left\{ \frac{\partial u_i^n}{\partial x_j} + \frac{\partial u_j^n}{\partial x_i} \right\} \right]$$

$$+ \frac{\Delta t}{2} \frac{\partial}{\partial x_j} \left[ v_e \left\{ \frac{\partial u_i^{(1)}}{\partial x_j} + \frac{\partial u_j^{(1)}}{\partial x_i} \right\} \right]$$

$$\frac{\partial u_i^{(2)}}{\partial x_i} = 0$$

### TIME DISCRETIZATION (cont.)

$$u_i^{n+1} = u_i^n + \Delta t f_i - \frac{\Delta t}{2} \frac{\partial \bar{p}^{(1)}}{\partial x_i} + \frac{\Delta t}{2} \frac{\partial}{\partial x_j} \left[ v_e \left\{ \frac{\partial u_i^{n+1}}{\partial x_j} + \frac{\partial u_j^{n+1}}{\partial x_i} \right\} \right]$$

$$+ \frac{\Delta t}{2} \frac{\partial}{\partial x_j} \left[ v_e \left\{ \frac{\partial u_i^n}{\partial x_j} + \frac{\partial u_j^n}{\partial x_i} \right\} \right]$$

where  $\bar{p} = p^{(2)} + p^n$

## TURBULENCE MODEL

- Eddy viscosity concept  
subgrid model → 2-equation model
- Zero equation model

$$v_t = \kappa^2 y^2 \left[ 1 - e^{-y^+/26} \right] \left| \frac{\partial u}{\partial y} \right|$$

$$v_t = 0.018 u_\infty \delta^*$$

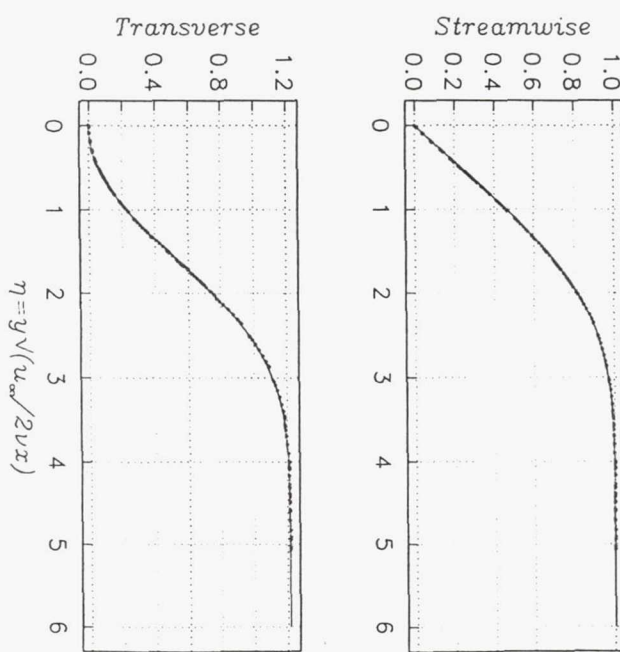
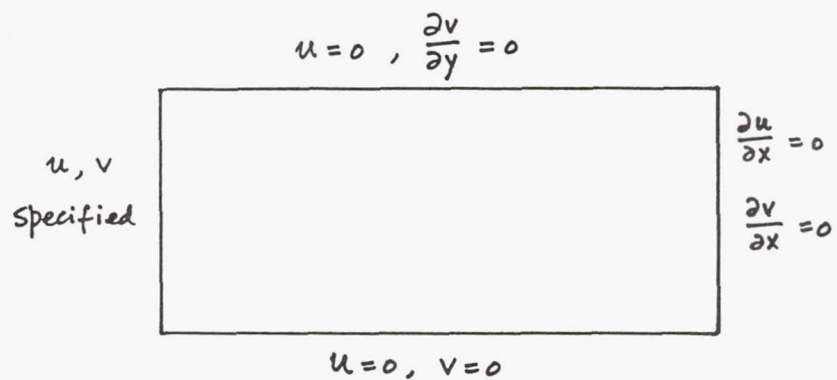
## TURBULENCE MODEL (cont.)

- Wall boundary conditions

$$\frac{\tau_w}{\rho} = \begin{cases} \frac{v_t}{\kappa y} \frac{u}{\frac{1}{\kappa} \ln E y^+} & y^+ > B \\ v_l \frac{u}{y} & y^+ \leq B \end{cases}$$

$$\text{where } y^+ = \frac{y (\tau_w/\rho)^{1/2}}{v_l} = \frac{1}{\kappa} \frac{v_t}{v_l}$$

## NUMERICAL RESULTS (laminar flow)



**Page intentionally left blank**

# **SUBSONIC INLET FLOWS WITH TRANSITION**

**BY**

**Danny Hwang and Kyung Ahn**

September 16, 1993

## **INTRODUCTION**

**Real flow simulation is needed  
(laminar region + turbulent region)**

**for:**

- (1) cruise drag prediction**
- (2) separation angle of attack prediction**

### **Difficulties:**

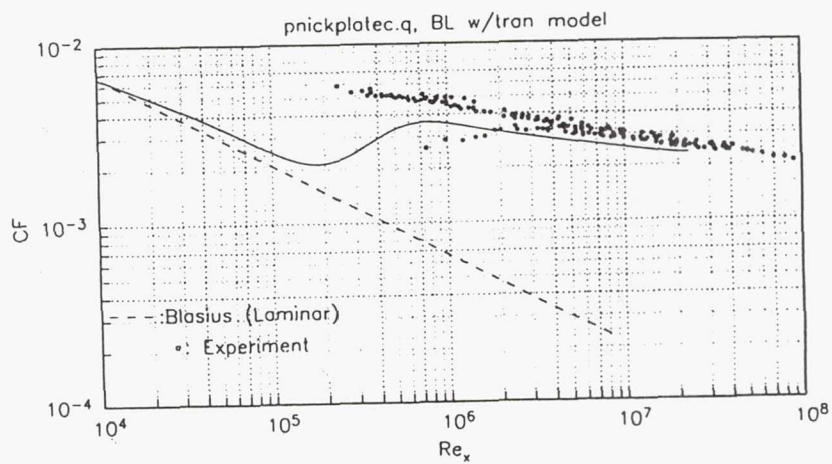
- Transition is a function of many variables
  - free stream turbulence
  - surface roughness
  - streamwise surface curvature
  - pressure gradient
  - etc.
- Skin friction coefficient which is the best transition indicator is difficult to calculate

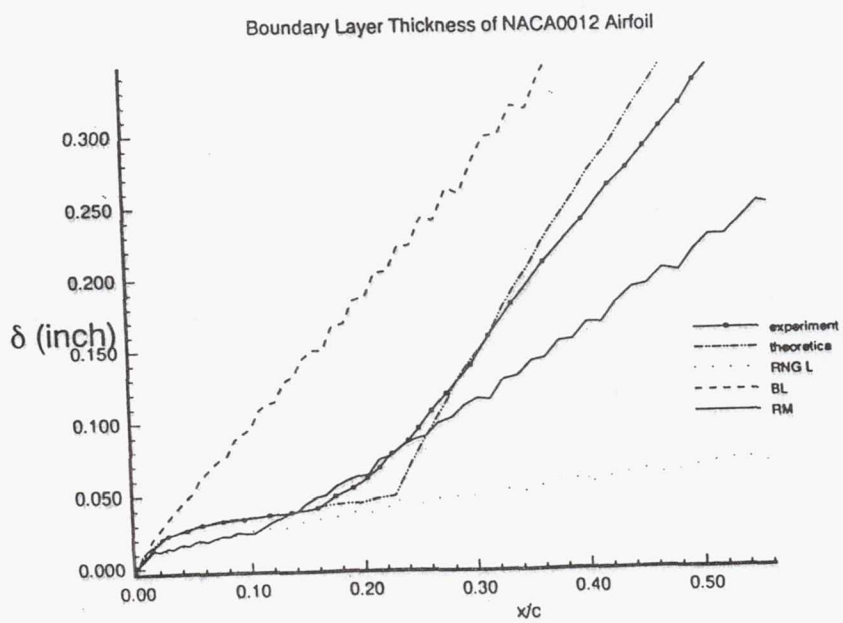
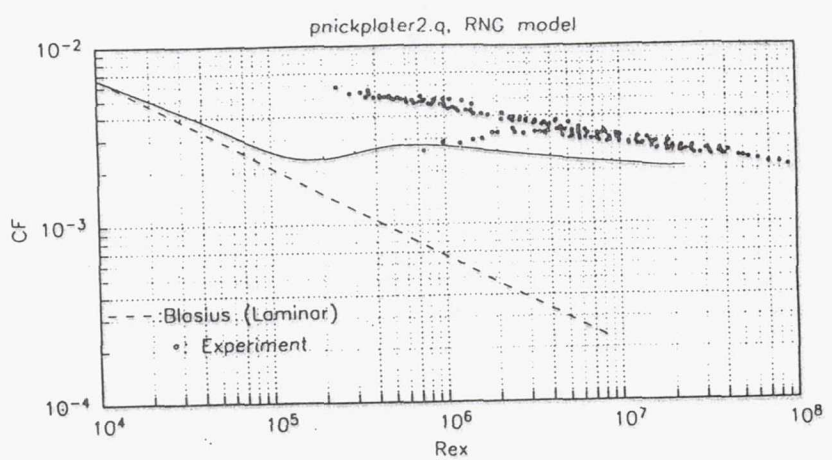
### **METHODS OF TRANSITION PREDICTION**

- Euler/boundary layer approach
- Euler/boundary layer/stability analysis
- Navier–Stokes calculation with turbulence models
  - Baldwin–Lomax with transition
  - RNG turbulence model

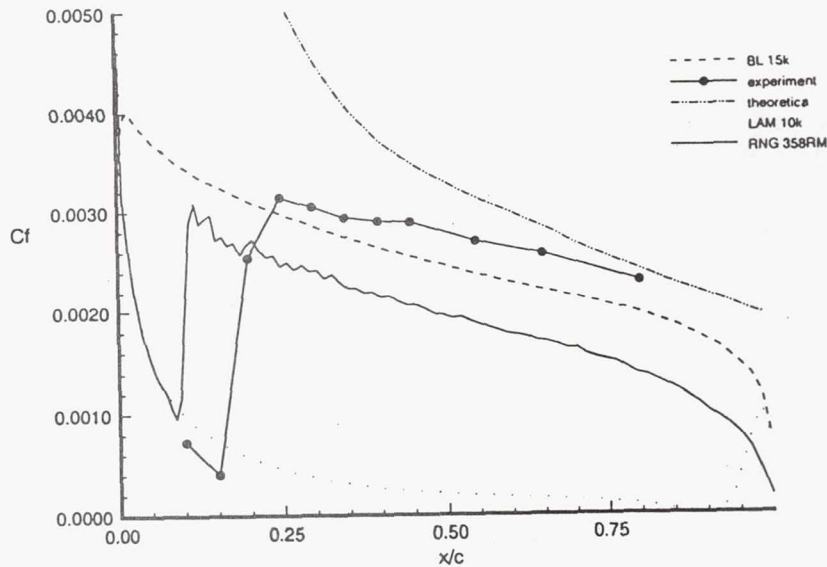
## TRANSITION PREDICTION

- Flat plate
- NACA0012
- ADP inlet

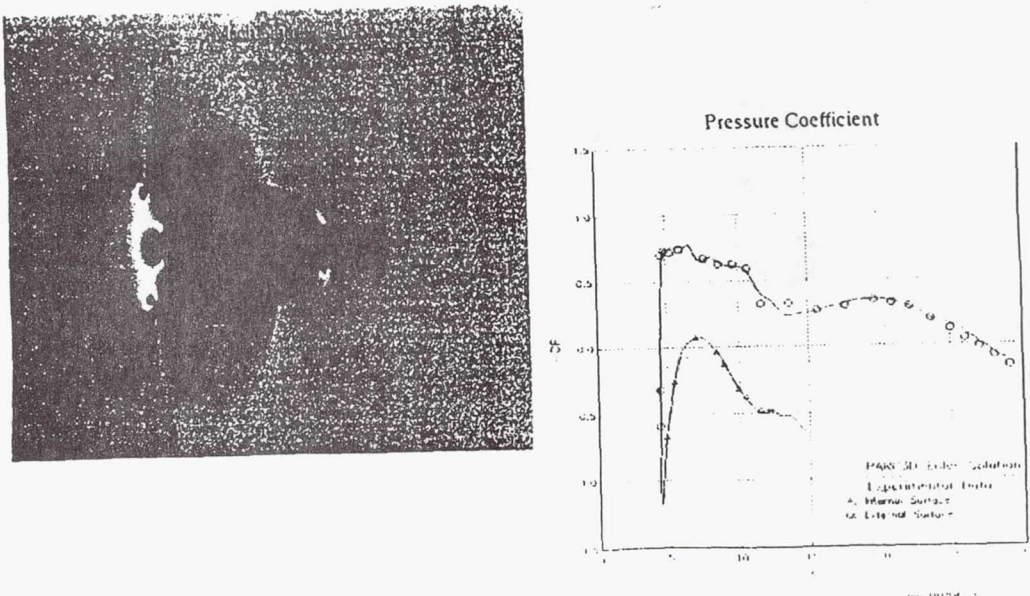




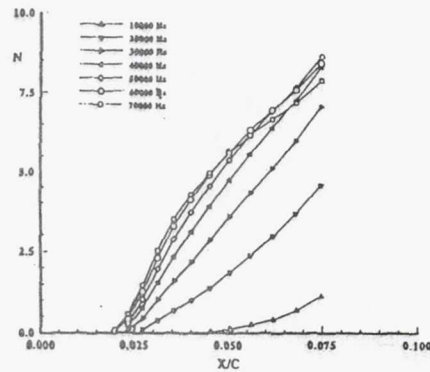
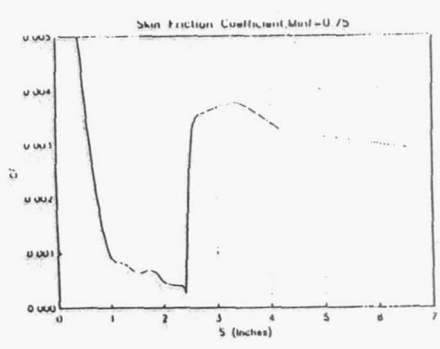
Local Skin Friction Coefficient for NACA0012 Airfoil



### ADP CONVENTIONAL NACELLE AT CRUISE MACH NUMBER



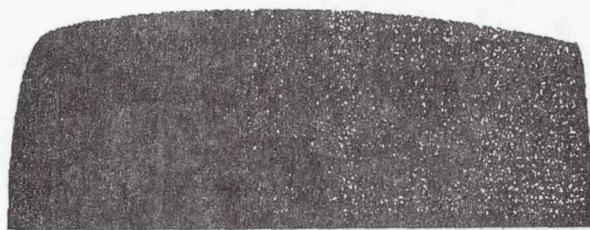
## LAMINAR/TURBULENT TRANSITION



### Laminar/Turbulent Transition

Laminar region

Turbulent region



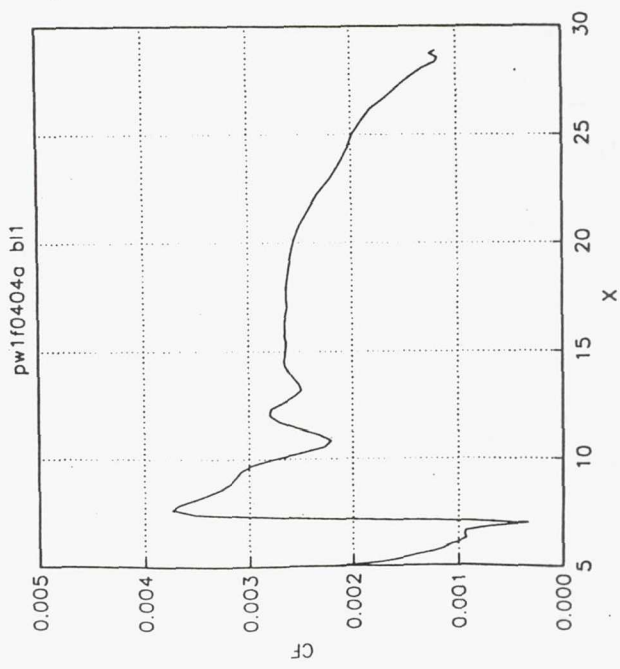
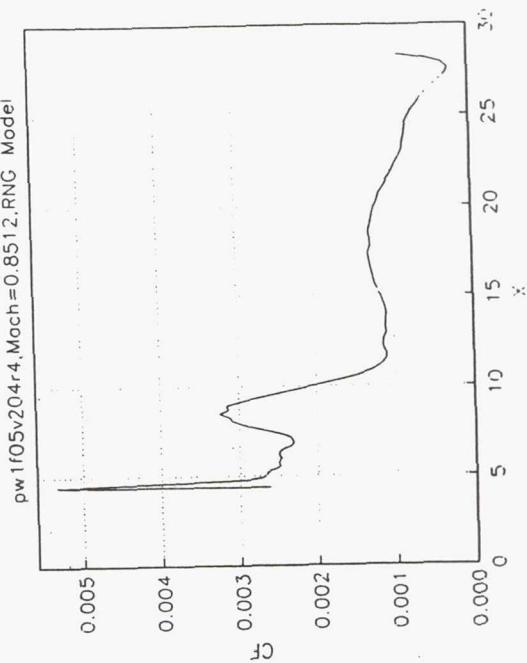
Laminar region prediction:

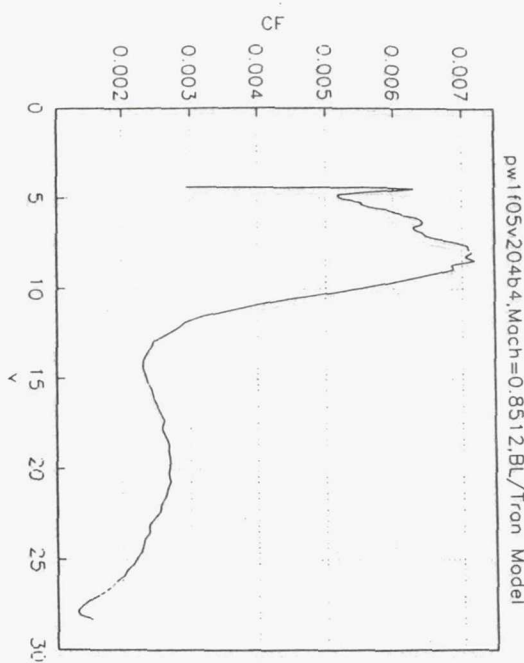
Lewis' s boundary layer analysis : 8.17 % of chord length

Langley's stability analysis : 8.00 % of chord length

On going projects:

RNG turbulence model in PARC3D





## CONCLUDING REMARKS

Several methods have been tested to predict the transition of an ADP inlet. The prediction of the transition at cruise conditions agrees very well among the methods investigated except for the Baldwin-Lomax/Transition model which predicts early transition. The accuracy of prediction methods will be judged by comparing with upcoming laminar flow experiment.

**Workshop on Computational Turbulence Modeling**  
**( Sept. 15-16, 1993 )**

**A Comparative Study of Turbulence Models in Predicting  
Hypersonic Inlet Flows**

by

**Kamlesh Kapoor**

## TEST CASE AND TURBULENCE MODELS CONSIDERED

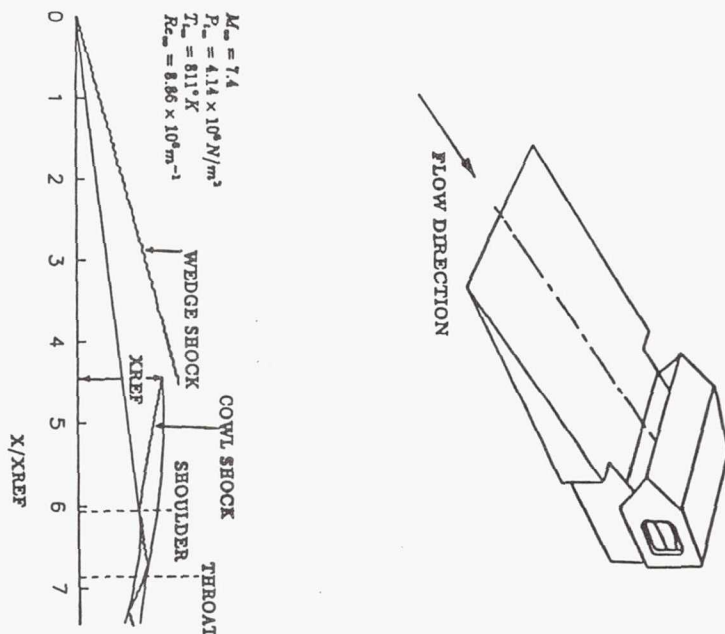
- THE NASA P8 INLET, WHICH REPRESENTS CRUISE CONDITION OF OF A TYPICAL HYPERSONIC AIR-BREATHING VEHICLE, WAS SELECTED AS A TEST CASE FOR PRESENT STUDY.
- PARC2D CODE, WHICH SOLVES THE FULL TWO-DIMENSIONAL REYNOLDS-AVERAGED NAVIER-STOKES EQUATIONS, WAS USED FOR THIS STUDY.
- THE RESULTS ARE PRESENTED FOR A TOTAL OF SIX VERSIONS OF ZERO- AND TWO-EQUATION TURBULENCE MODELS.
  - ZERO-EQUATION MODELS
    - THE BALDWIN-LOMAX MODEL
    - THE THOMAS MODEL
    - A COMBINATION OF THE B.L./THOMAS MODEL
  - TWO-EQUATION MODELS
    - LOW-REYNOLDS NUMBER MODELS
      - THE CHIEN MODEL
      - THE SPEZIALE MODEL
    - HIGH-REYNOLDS NUMBER MODEL
      - THE LAUNDER AND SPALDING MODEL

---

## EXPERIMENTAL BACKGROUND

- THE EXPERIMENTAL INVESTIGATION OF THE P8 INLET WAS CONDUCTED AT NASA AMES' 3.5-FOOT HYPERSONIC WIND TUNNEL.
- THE INLET WAS A MACH 7.4 RECTANGULAR MIXED COMPRESSION (WITH INTERNAL COMPRESSION RATIO OF 8) DESIGN WITH EXITING SUPERSONIC FLOW.
  - INLET COWL HEIGHT = 18.33 CM.
  - OVERALL LENGTH = 136.2 CM.
- TEST CONDITIONS:
  - MACH NO = 7.4
  - TOTAL PRESSURE =  $4.14 \times 10^6$  N/m<sup>2</sup>
  - TOTAL TEMPERATURE = 811°K
  - REYNOLDS NO =  $8.86 \times 10^6$ /m
  - MODEL WAS WATER COOLED AND ISOTHERMAL WALL CONDITIONS WERE MAINTAINED; THE WALLS TEMPERATURE = 302°K
- THE TRANSITION POINTS:
  - CENTERBODY - 40 PERCENT FROM WEDGE L.E. EDGE TO INLET ENTRANCE.
  - COWL - HALFWAY BETWEEN INLET ENTRANCE AND THROAT.

### SCHEMATIC DIAGRAM OF P8 INLET MODEL

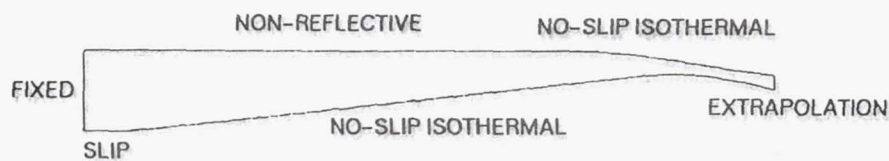


### THE COMPUTATIONAL GRID

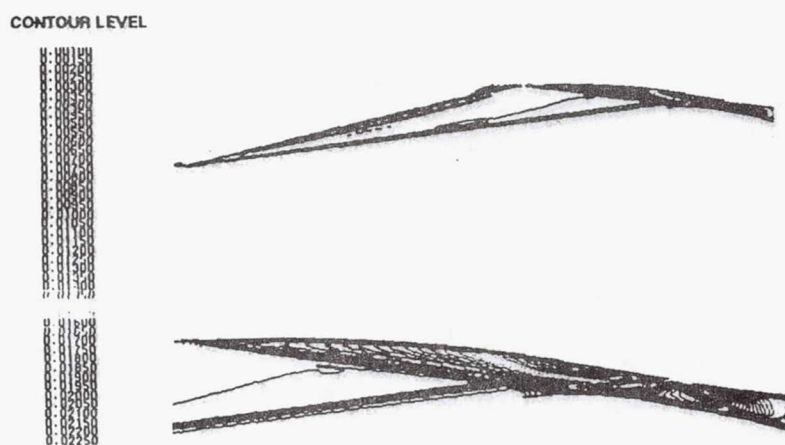


- GRID SIZE WAS  $221 \times 91$ .
- GRID WAS NONUNIFORM IN X DIRECTION:
  - PACKED ON BOTH ENDS FROM THE WEDGE L.E. TO THE COWL L.E.
  - GEOMETRICALLY STRETCHED FROM THE COWL L.E. TO THE EXIT OF THE INLET.
- IN Y DIRECTION, THE GRID WAS PACKED USING HYPERBOLIC TANGENT FUNCTION.  $Y_{PLUS}$  WAS APPROXIMATELY 1 AWAY FROM BOTH WALLS.
- A SEPARATE GRID WAS MADE FOR THE LAUNDER AND SPALDING MODEL AND  $Y_{PLUS}$  OF APPROXIMATELY 30 WAS USED AWAY FROM THE WALLS.

## BOUNDARY CONDITIONS



## DENSITY CONTOURS FOR P8 INLET



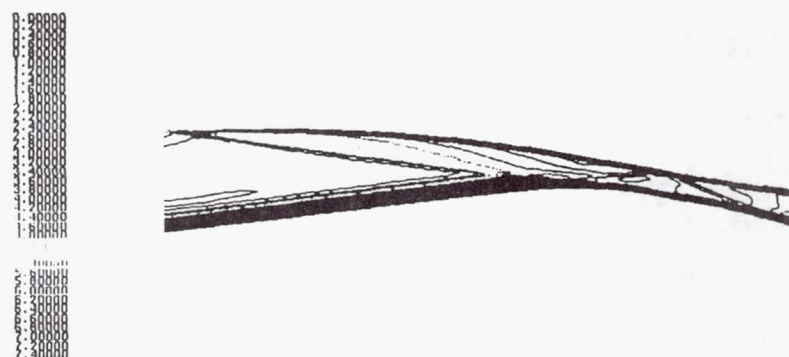
### PRESSURE CONTOURS FOR P8 INLET

CONTOUR LEVEL

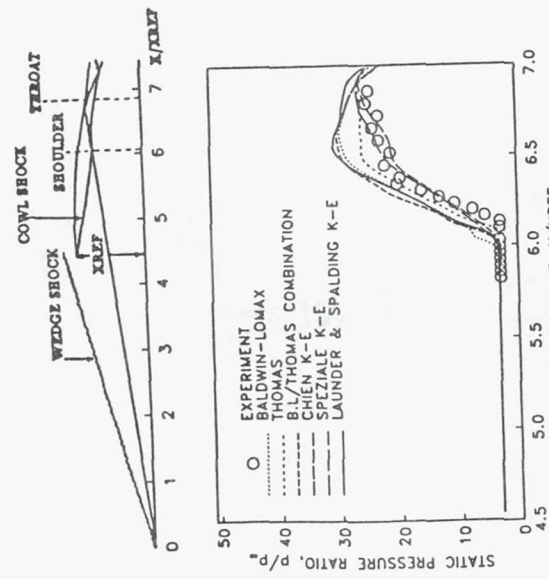


### MACH NUMBER CONTOURS FOR P8 INLET

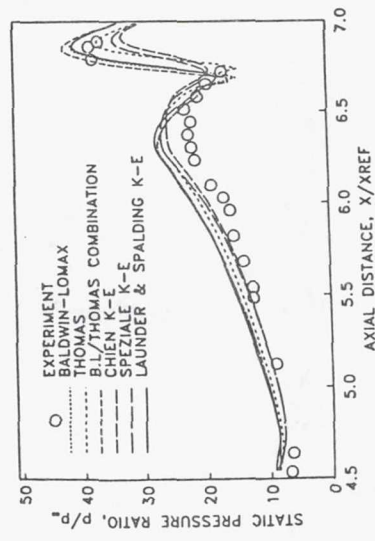
CONTOUR LEVEL



SURFACE PRESSURE DISTRIBUTIONS

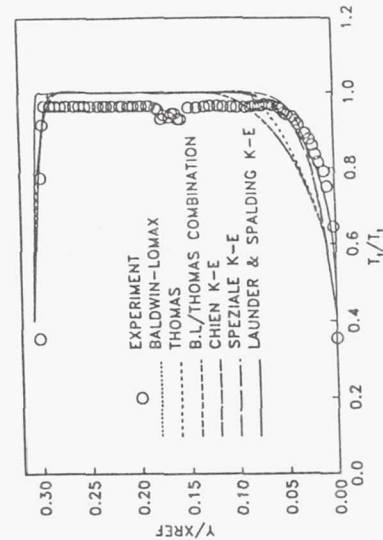
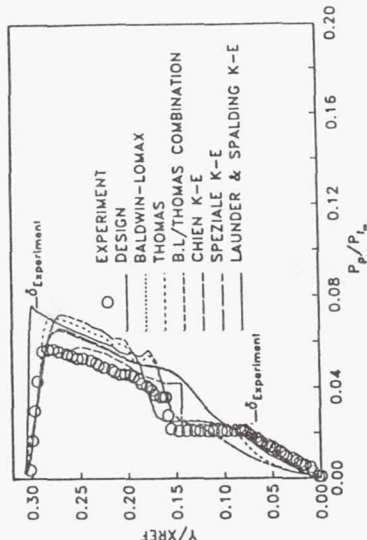
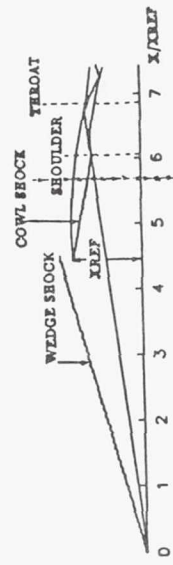


(A) ON THE CENTERBODY

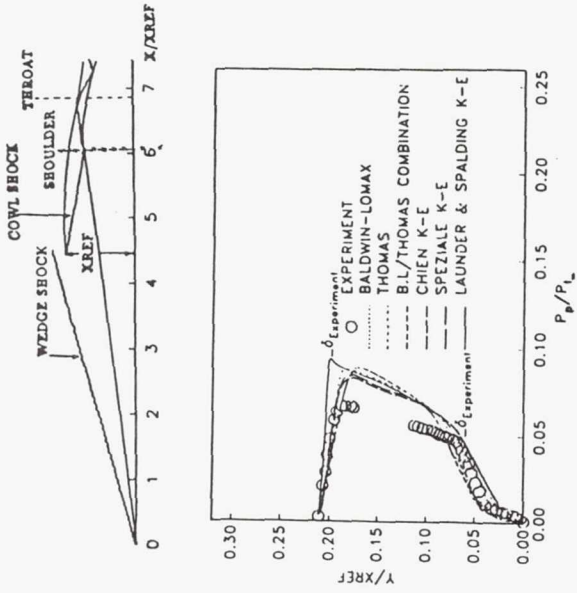


(B) ON THE COULD

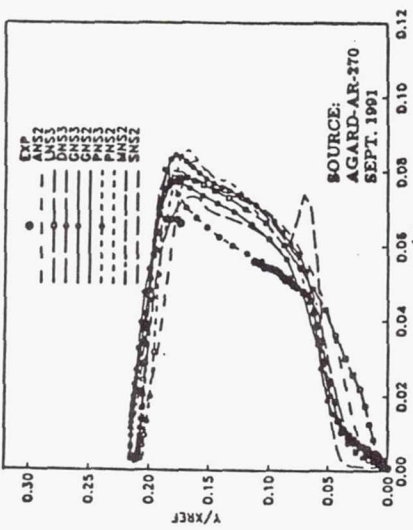
PITOT PRESSURE AND TOTAL TEMPERATURE DISTRIBUTIONS AT  $X/X_{REF} = 5.67$



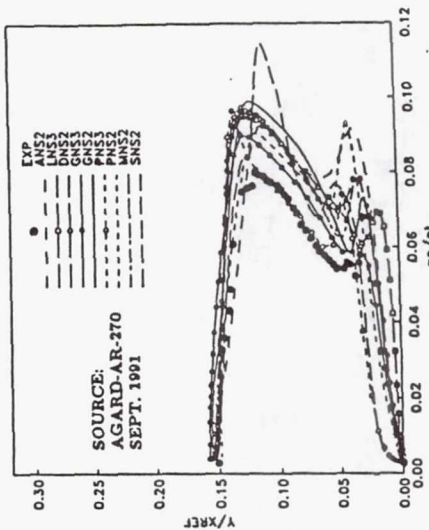
PITOT PRESSURE AND TOTAL TEMPERATURE  
DISTRIBUTIONS AT  $X/X_{REF} = 6.09$



PITOT PRESSURE DISTRIBUTIONS



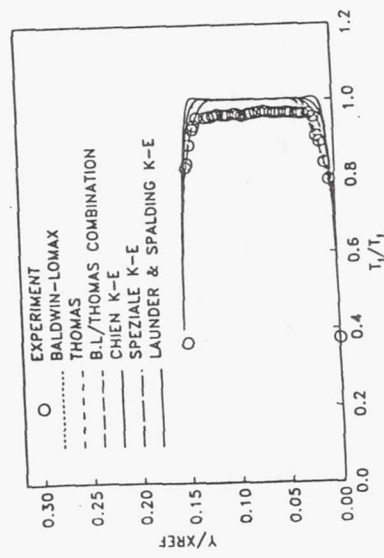
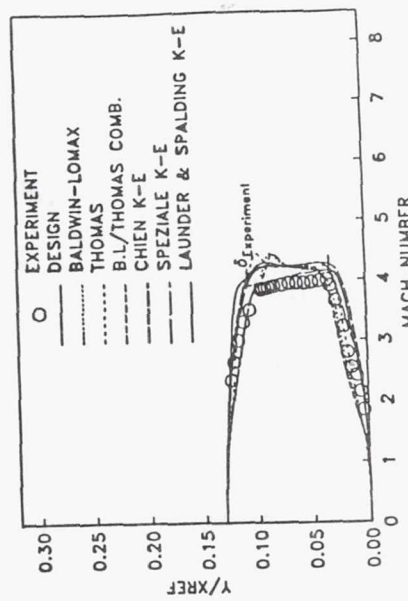
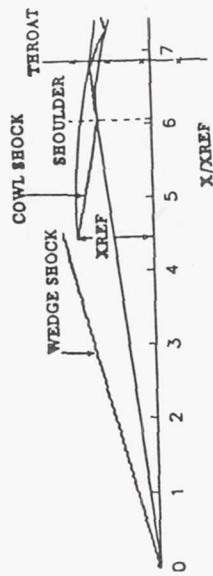
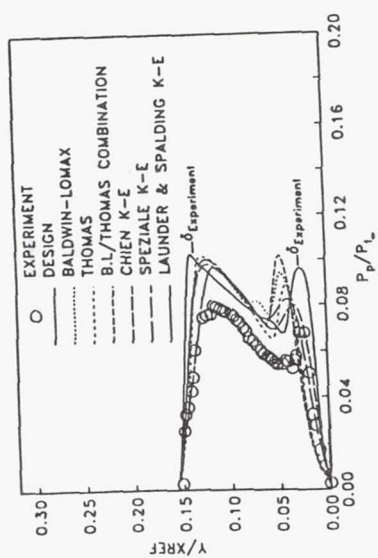
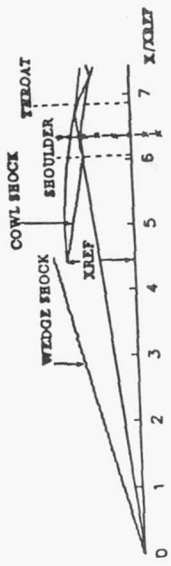
$p_p/p_L$



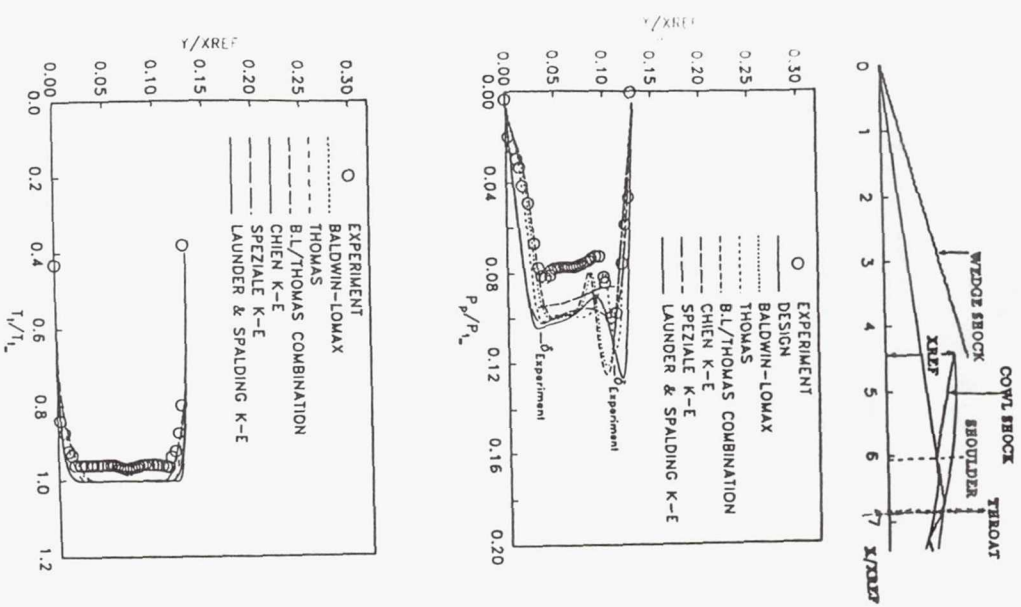
$p_p/p_L$

PITOT PRESSURE AND TOTAL TEMPERATURE  
DISTRIBUTIONS AT  $X/X_{REF} = 6.37$

MACH NUMBER DISTRIBUTIONS AT THE THROAT



## TOT PRESSURE AND TOTAL TEMPERATURE DISTRIBUTIONS AT THE THROAT



## CONCLUSIONS

- A COMPUTATIONAL STUDY HAS BEEN CONDUCTED TO EVALUATE THE PERFORMANCE OF VARIOUS TURBULENCE MODELS.
- THE THOMAS MODEL COMPARES VERY WELL WITH THE EXPERIMENTAL DATA, AND IT PERFORMS BEST AMONG THE ZERO-EQUATION MODELS.
- THE BALDWIN-LOMAX MODEL AND ITS COMBINATION WITH THOMAS MODEL ARE NOT ABLE TO RESOLVE THE PROBLEM OF SHOCK WAVE AND BOUNDARY-LAYER INTERACTION ACCURATELY. THE BALDWIN-LOMAX MODEL PREDICTS SEPARATION NEAR THE INTERACTION OF THE COWL SHOCK WITH THE WEDGE BOUNDARY LAYER, WHERE NONE IS KNOWN TO EXIST IN EXPERIMENTS.
- THE CHIEN AND SPEZIALE MODEL COMPARE VERY WELL WITH THE EXPERIMENTAL DATA, AND PERFORMS BETTER THAN THE THOMAS MODEL, PARTICULARLY NEAR THE WALLS. THE LAUNDER AND SPALDING MODEL DOES NOT PERFORM AS GOOD AS THE CHIEN AND SPEZIALE MODELS.
- AS THE CPU TIME REQUIRED FOR THE THOMAS MODEL IS FAR LESS THAN THE TWO-EQUATION MODELS, IT IS CONCLUDED THAT THE THOMAS MODEL IS BEST SUITED FOR THE PREDICTIONS OF PRESSURE DISTRIBUTIONS, AND THE CHIEN AND SPEZIALE MODELS ARE BEST TO CALCULATE FLOW QUANTITIES NEAR THE WALLS.

**Page intentionally left blank**

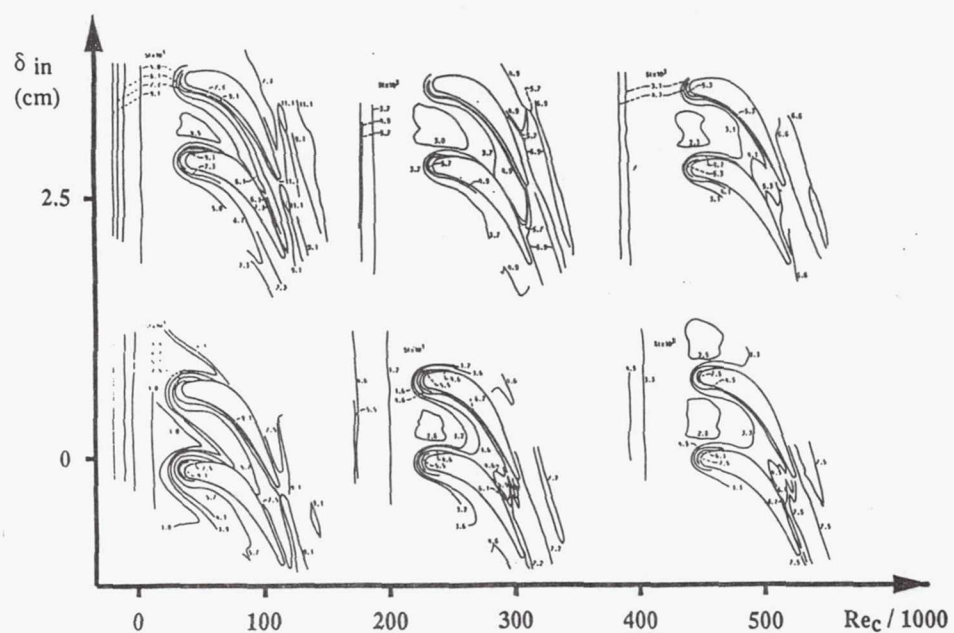
AN ALGEBRAIC TURBULENCE MODEL  
FOR TURBOMACHINERY

by

Rodrick V. Chima  
NASA Lewis Research Center  
Cleveland, Ohio

## OVERVIEW

- MOTIVATION - TURBINE ENDWALL HEAT TRANSFER
- DESCRIPTION OF NEW MODEL
- RESULTS
  - 1. FLAT PLATE
  - 2. ANNULAR TURBINE CASCADE
  - 3. TURBINE ENDWALL HEAT TRANSFER
  - 4. SUPERSONIC COMPRESSOR BLADE
- SUMMARY



EXPERIMENTAL ENDWALL STANTON NUMBER CONTOURS  
AS A FUNCTION OF  $\delta \text{ inlet}$  AND  $\text{Re}_{\text{chord}}$

## RVC3D (ROTOR VISCOUS CODE 3-D)

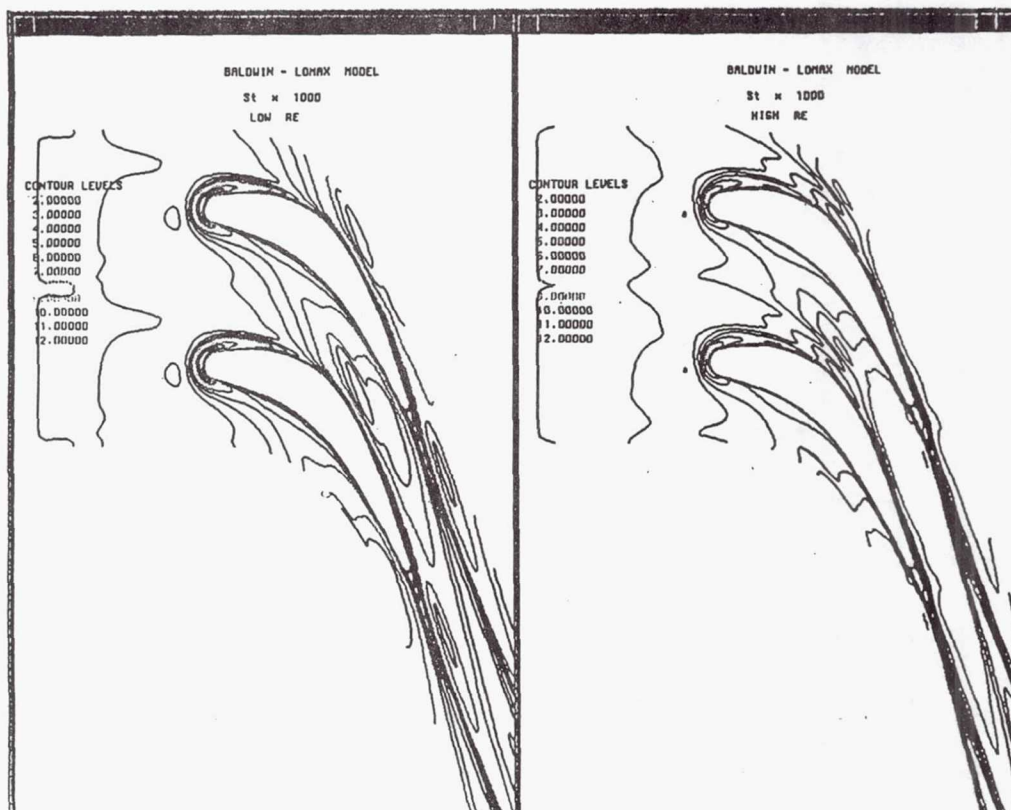
BY R. V. CHIMA

### DESCRIPTION

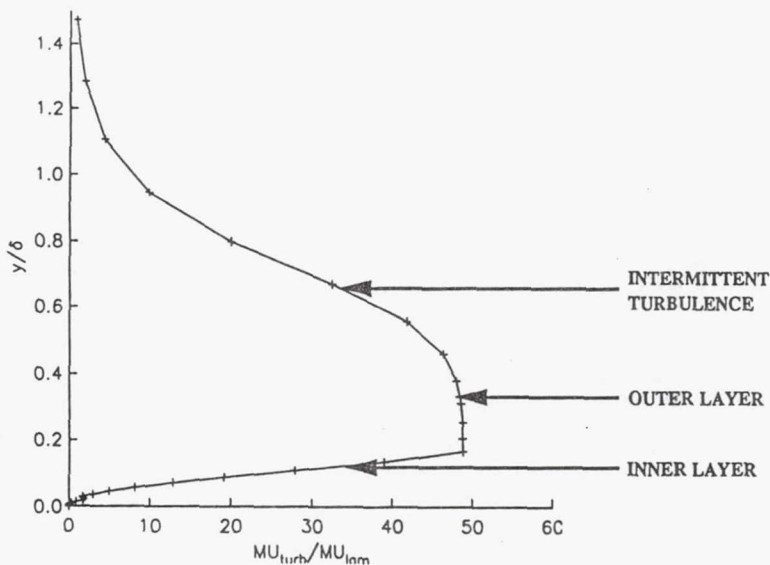
- EULER OR NAVIER-STOKES ANALYSIS  
FOR STEADY 3-D FLOWS IN TURBOMACHINERY

### FEATURES

- CARTESIAN FORMULATION, ROTATION ABOUT X-AXIS  
RECTANGULAR OR ANNULAR GEOMETRIES
- SOLVES NAVIER-STOKES EQUATIONS  
THIN-LAYER FORMULATION, (NO STREAMWISE VISCOSITY TERMS)  
RETAINS HUB-TO-TIP & BLADE-TO-BLADE VISCOSITY TERMS  
BALDWIN-LOMAX OR CEBECI-SMITH TURBULENCE MODEL  
SIMPLE TIP CLEARANCE MODEL
- NODE-CENTERED FINITE-DIFFERENCE FORMULATION  
EXPLICIT 4-STAGE RUNGE-KUTTA TIME-MARCHING SCHEME  
2ND + 4TH ORDER ARTIFICIAL VISCOSITY, EIGENVALUE SCALING  
VARIABLE  $\Delta t_{ij}$  & IMPLICIT RESIDUAL SMOOTHING  
HIGHLY VECTORIZED & AUTOTASKED FOR CRAY Y-MP
- STACKED C-TYPE GRIDS



## TURBULENT VISCOSITY PROFILE



## CEBEKI-SMITH & BALDWIN-LOMAX MODELS

### INNER LAYER: PRANDTL-VAN DRIEST FORMULATION

CEBEKI-SMITH

$$\mu_i = \rho l^2 |\partial u / \partial y|$$

$$l = \kappa y D$$

$$D = 1 - \exp(-y^+/A^+) \quad \text{VAN DRIEST DAMPING}$$

BALDWIN-LOMAX

$$\mu_i = \rho l^2 |\omega|$$

### OUTER LAYER: CLAUSER FORMULATION

CEBEKI-SMITH

$$\mu_o = K \rho \gamma \delta^* u_e$$

$$\gamma = \left[ 1 + 5.5 \left( \frac{y}{\delta} \right)^6 \right]^{-1} \quad \text{KLEBANOFF INTERMITTENCY FUNCTION}$$

BALDWIN-LOMAX

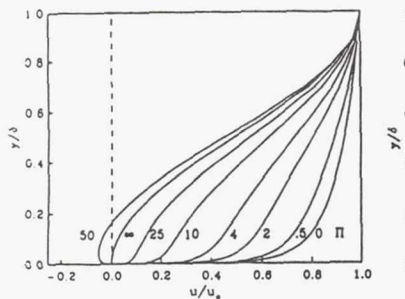
$$\mu_o = K \rho \gamma C_{cp} \min \left\{ \begin{array}{l} y_{max} f_{max} \\ \text{wake option} \end{array} \right.$$

$$f(y) = y |\omega| D$$

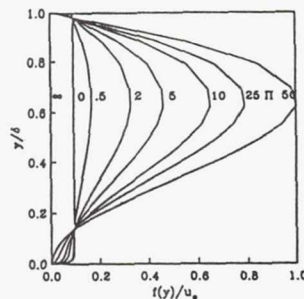
## BALDWIN-LOMAX MODEL ANALYSIS

(SEE PAPER FOR DETAILS)

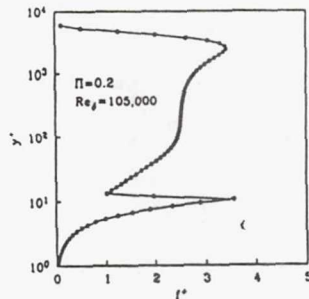
1. ASSUME SUBLAYER-WALL-WAKE VELOCITY PROFILE
2. CALCULATE BALDWIN-LOMAX FUNCTION  $f(y)$   
MAX. OCCURS AT  $y_{max} = .6465$   
INDEPENDENT OF PRESSURE GRADIENT  
NO MAX. FOR INFINITELY FAVORABLE  $\partial p / \partial x$
3. SPURIOUS MAX. CAN OCCUR AT EDGE OF VISCOUS SUBLAYER  
MOST LIKELY AT LOW  $Re$  & FAVORABLE  $\partial p / \partial x$



1. VELOCITY PROFILES,  $Re_\delta = 105,000$



2. B-L FUNCTION  $f(y)$



3. SPURIOUS MAXIMUM IN  $f(y)$

## PROPOSED TURBULENCE MODEL

INNER LAYER (SIMILAR TO BALDWIN-LOMAX)

$$\begin{aligned}\mu_i &= \rho l^2 |\omega| \\ l &= \kappa y D \\ D &= 1 - \exp(-y^+ / A^+) \\ y^+ &= y \frac{u^*}{\nu} \\ u^* &= \sqrt{\frac{\tau_{wall}}{\rho}}\end{aligned}$$

## PROPOSED TURBULENCE MODEL

### PRESSURE GRADIENT EFFECTS

- ACCELERATING FLOWS TEND TO RELAMINARIZE
- MODELLED BY INCREASING  $A^+$  IN FAVORABLE  $\partial p/\partial s$
- CEBECI'S EXPRESSION FOR  $A^+$  USED:

$$A^+ = \frac{26}{\sqrt{1 + 11.8p^+}}$$

$$p^+ = \frac{\nu}{\rho u^{*3}} \frac{\partial p}{\partial s}$$

- PRESSURE GRADIENT EVALUATED USING:

$$\frac{\partial p}{\partial s} \approx \frac{\vec{V}_e}{|\vec{V}_e|} \cdot \nabla p$$

- "EDGE VELOCITY"  $\vec{V}_e$  EVALUATED AT A GRID LINE FAR ENOUGH FROM THE WALL TO GIVE THE GENERAL FLOW DIRECTION
- KAYS-MOFFATT EXPRESSION WAS TESTED, EFFECTS TOO STRONG

## PROPOSED TURBULENCE MODEL

### LOCAL SHEAR MODEL

- IN STRONGLY ACCELERATING FLOWS  $\tau^+$  DECREASES WITH  $y^+$
- MODELLED BY REPLACING  $\tau_{wall}$  WITH  $\tau(y)$  IN  $D$

$$D = 1 - \exp(-y^+/A^+)$$

$$y^+ = y \sqrt{\frac{\rho(\mu_l + \mu_t)}{\mu_l} |\omega|}$$

- ERROR IN ORIGINAL PAPER - USED  $\mu_l |\omega|$  ONLY
- USED BY KAYS, PATANKAR-SPALDING, OTHERS
- ALSO USED TO AVOID PROBLEMS AT SEPARATION WHEN  $\tau_{wall} \rightarrow 0$

## PROPOSED TURBULENCE MODEL

### OUTER LAYER

$$\begin{aligned}\mu_o &= K \rho \gamma \min \left\{ \frac{F}{C_{wk} \bar{y} (|V_{max}| - |V_{min}|)} \right. \\ \gamma &= \left[ 1 + 5.5 \left( \frac{C_{Kletb} y}{\bar{y}} \right)^6 \right]^{-1} \\ C_{wk} &= 0.825 \\ C_{Kletb} &= 0.55\end{aligned}$$

## PROPOSED TURBULENCE MODEL

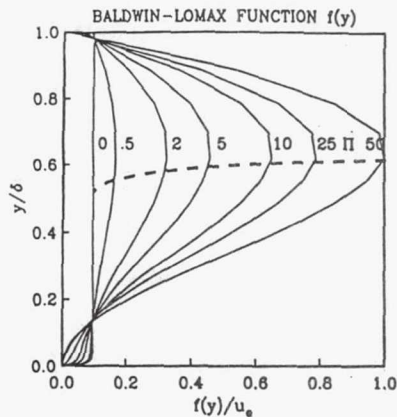
### OUTER LAYER - FUNCTION F

- DEFINE  $F = \int f dy$
- INTEGRATE BY PARTS ASSUMING  $|\omega| \rightarrow 0$  AS  $y \rightarrow \delta$

$$\begin{aligned}F &= \int_0^\infty y |\omega| dy \\ &\approx \int_0^\delta y \frac{\partial u}{\partial y} dy \\ &= uy \Big|_0^\delta - \int_0^\delta u dy \\ &= \int_0^\delta (u_e - u) dy \\ F &= \delta^* u_e\end{aligned}$$

- USE F DIRECTLY IN CEBEKI-SMITH OUTER FORMULATION
- ELIMINATES CONSTANT  $C_{cp}$
- DOES NOT REQUIRE KNOWLEDGE OF  $\delta$  OR  $u_e$
- DISCOVERED INDEPENDENTLY BY D. A. JOHNSON, AIAA 92-0026

## PROPOSED TURBULENCE MODEL



### OUTER LAYER - LENGTH SCALE $\bar{y}$

- $\bar{y}$  IS THE CENTROID OF THE  $f(y)$  CURVE  

$$\int_0^{\bar{y}} f(y) dy = \int_{\bar{y}}^{\delta} f(y) dy$$
- EVALUATE USING COLE'S VELOCITY PROFILES  

II	$\bar{y}/\delta$
0	.5
.5	.55
$\infty$	.606
- USE EQUILIBRIUM VALUE  $C_{Kleb} = \bar{y}/\delta = .55$

## PROPOSED TURBULENCE MODEL

### OUTER LAYER - WAKE MODEL

$$\mu_o = K\rho\gamma \min \left\{ \frac{F}{C_{wk}\bar{y}(|V_{max}| - |V_{min}|)} \right\}$$

- LOWER OPTION IS A CONVENTIONAL WAKE MODEL
- EVALUATE  $C_{wk}$  BY EQUATING TWO OPTIONS, ASSUMING

$$\begin{aligned}\bar{y}_{sep} &= .606 \delta \\ F_{sep} &= u_* \delta / 2 \\ \Delta V/u_* &\approx 1\end{aligned}$$

- GIVES  $C_{wk} = 0.825$

## PROPOSED TURBULENCE MODEL

### 3-D IMPLEMENTATION

- GRANVILLE BLENDING FUNCTION

$$\mu_{eff} = \mu_o \tanh \frac{\mu_i}{\mu_o}$$

- MODEL APPLIED INDEPENDENTLY IN BLADE-TO-BLADE ( $\eta$ ) AND SPANWISE ( $\zeta$ ) DIRECTIONS

- INNER LAYER - USE BULEEV LENGTH SCALE

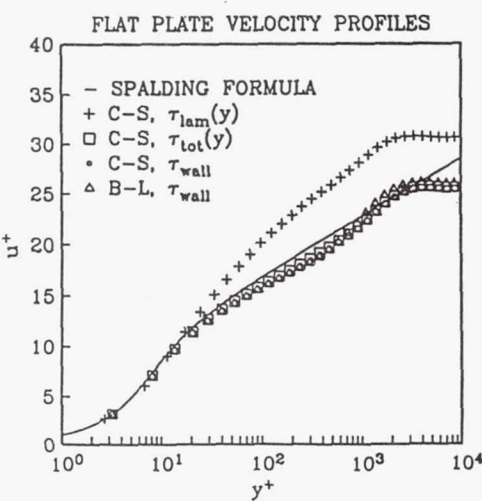
$$y_i = \frac{2s_\eta s_\zeta}{s_\eta + s_\zeta + \sqrt{s_\eta^2 + s_\zeta^2}}$$

- OUTER LAYER - USE ACTUAL DISTANCE ACROSS PROFILE

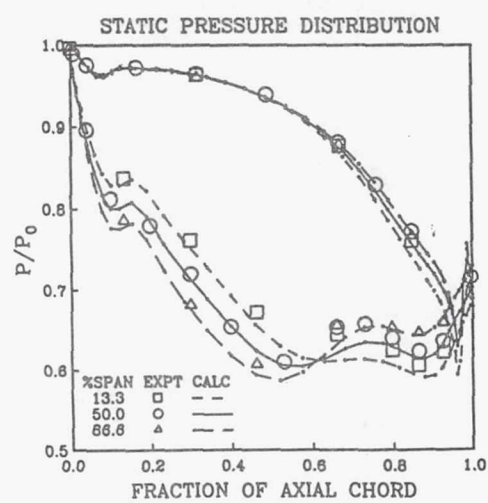
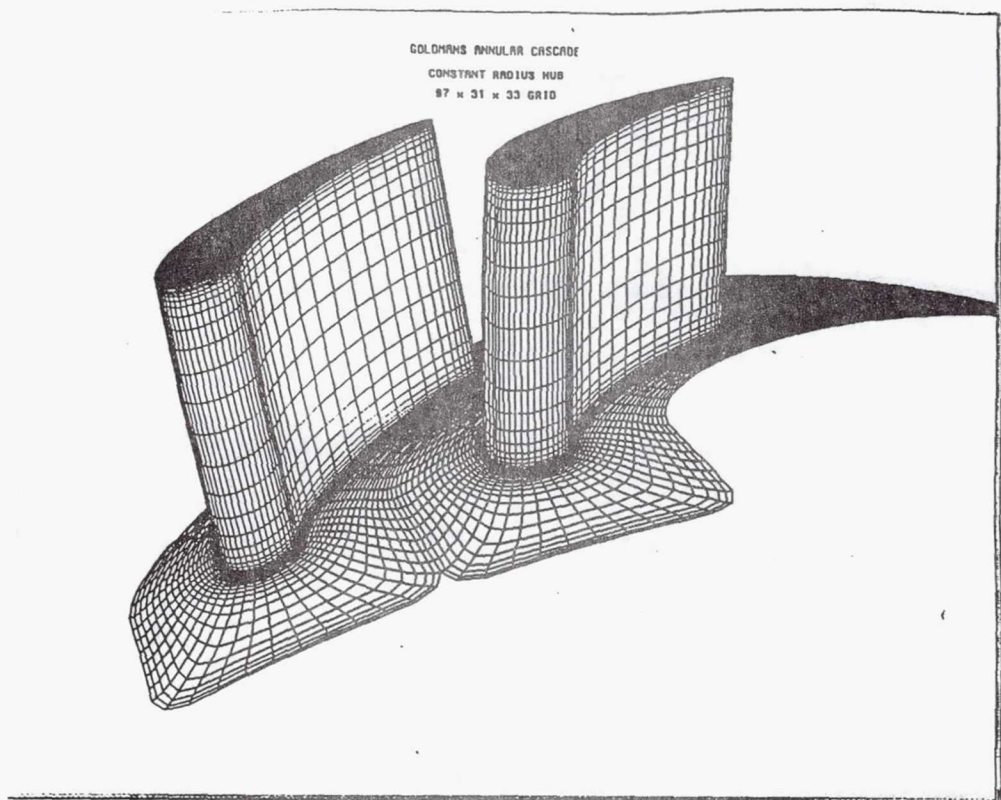
$$y_o = s_\eta \text{ OR } s_\zeta$$

- BLEND  $\eta$  AND  $\zeta$  PROFILES VECTORALLY

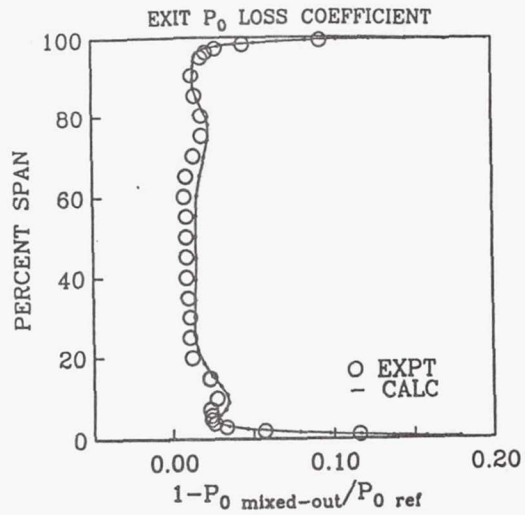
$$\mu_{turb} = \sqrt{\mu_{i\eta}^2 + \mu_{i\zeta}^2}$$



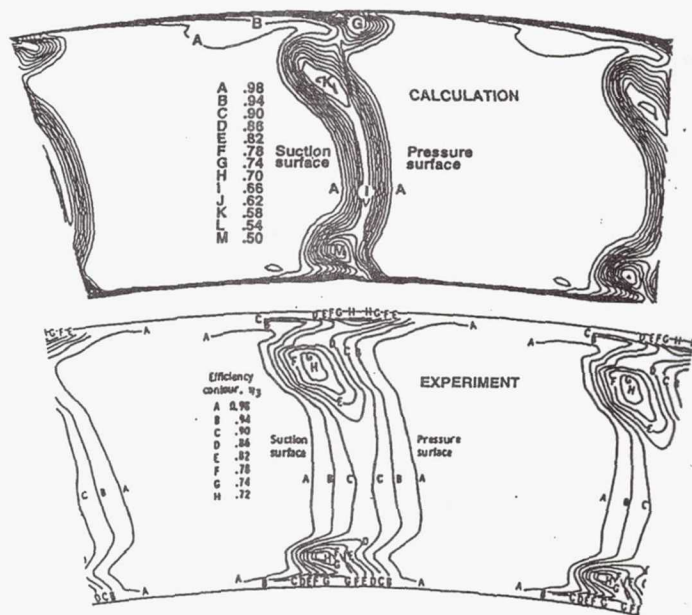
COMPARISON OF FLAT PLATE VELOCITY PROFILES  
TO SPALDING'S COMPOSITE LAW OF THE WALL



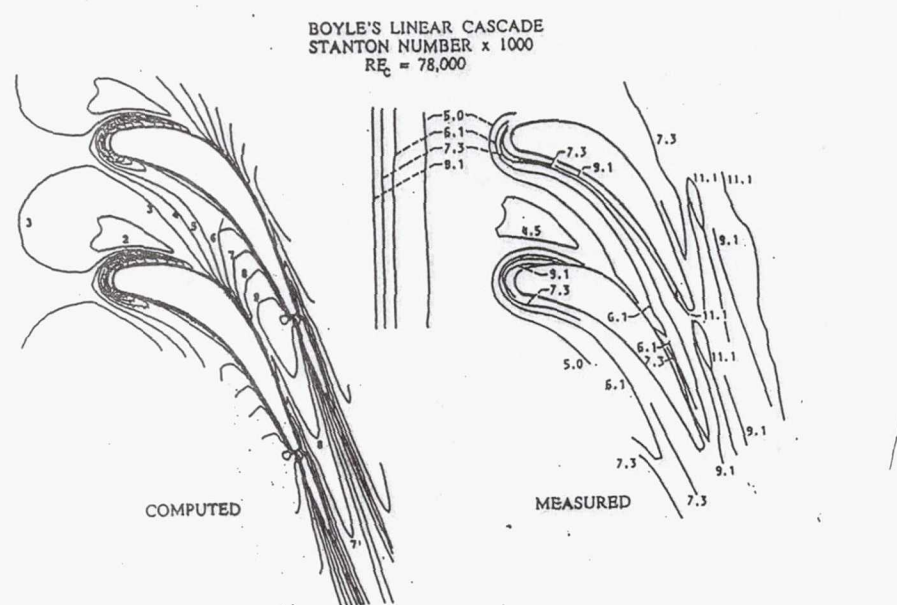
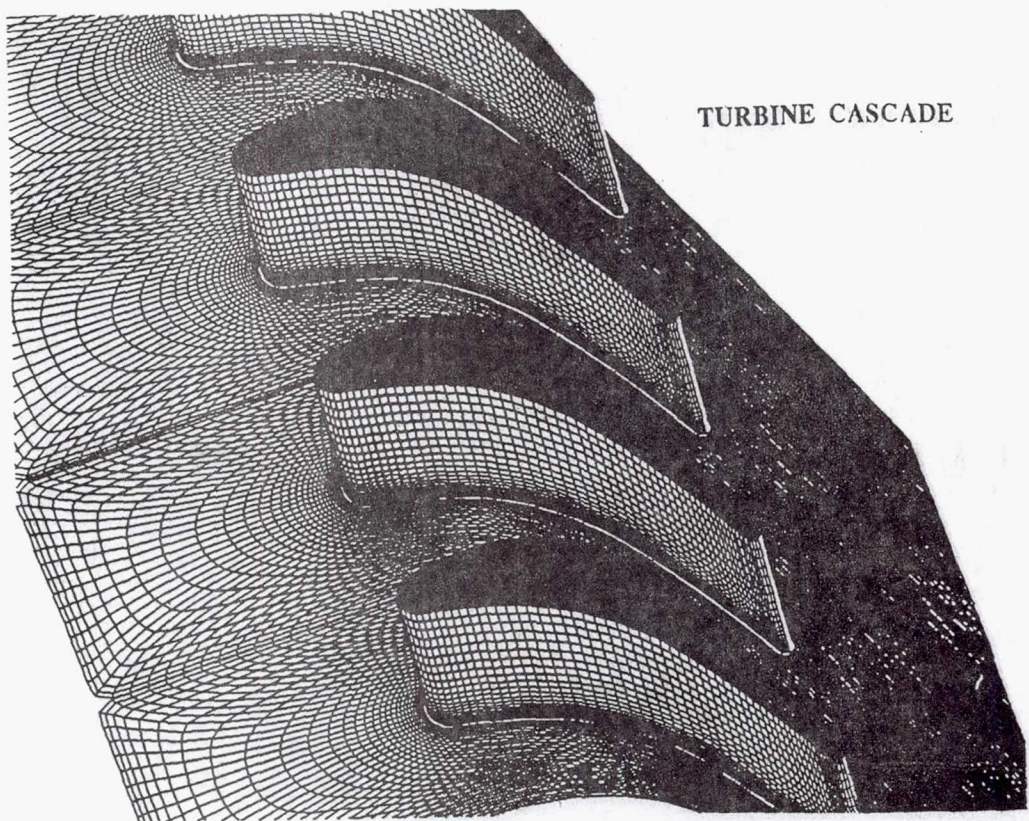
COMPUTED & MEASURED PRESSURE DISTRIBUTIONS  
FOR THE ANNULAR TURBINE CASCADE



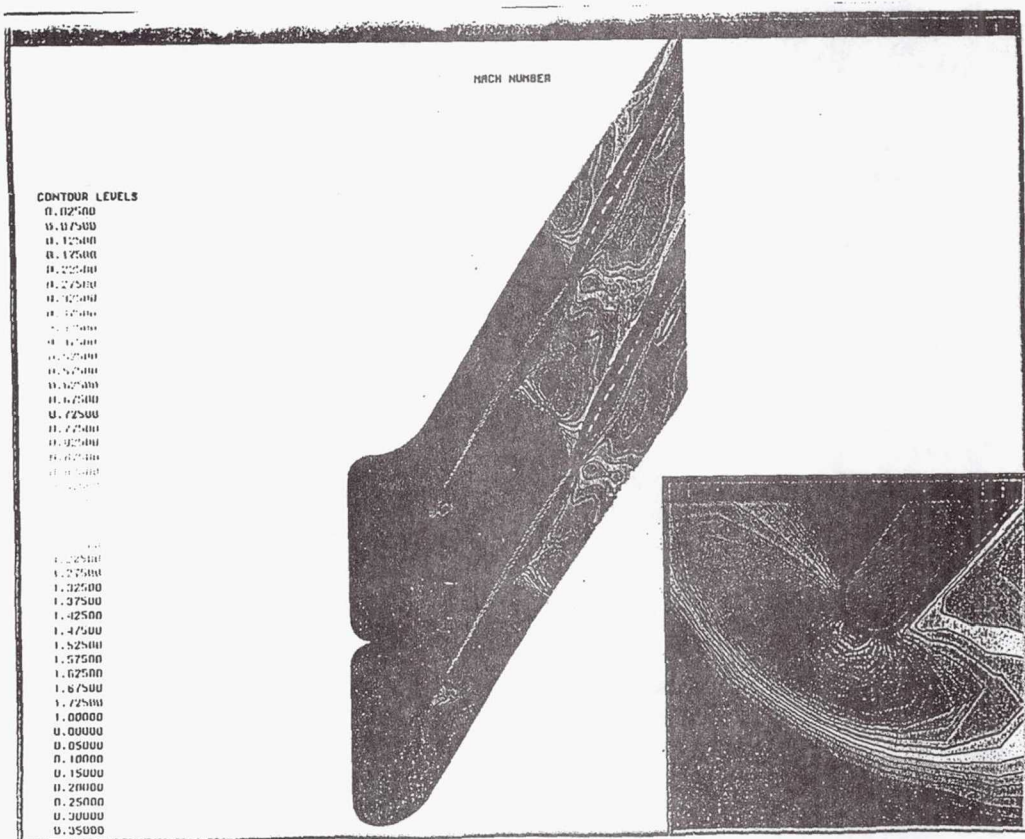
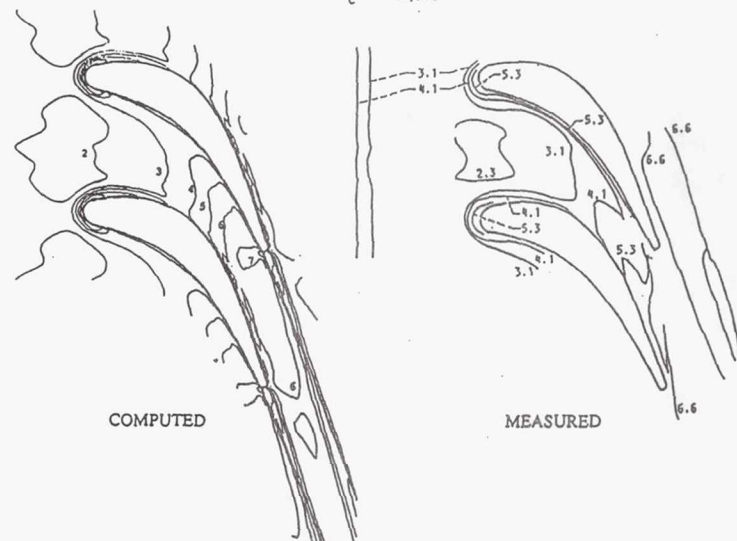
COMPUTED & MEASURED LOSS COEFFICIENT PROFILES  
FOR THE ANNULAR TURBINE CASCADE

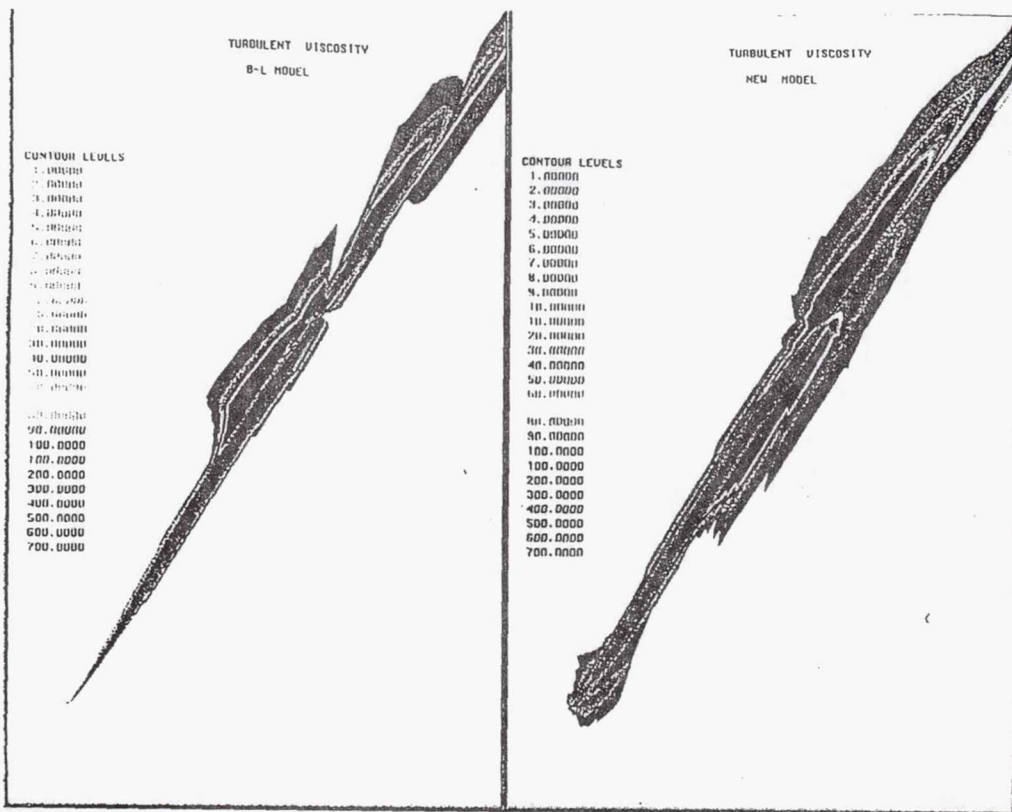


COMPUTED & MEASURED EFFICIENCY CONTOURS  
IN THE WAKE OF THE ANNULAR TURBINE CASCADE



BOYLE'S LINEAR CASCADE  
STANTON NUMBER x. 1000  
 $Re_c = 490,000$





## SUMMARY

- SPURIOUS MAXIMUM IN B-L FUNCTION  $f(y)$  CAN GIVE INCORRECT TURBULENT LENGTH SCALE & ERRATIC  $St$  OR  $C_f$  PATTERNS
  - MOST LIKELY AT LOW  $Re$  AND FAVORABLE  $\partial p/\partial s$
- NEW TURBULENCE MODEL PROPOSED
  - INTEGRAL RELATIONS FOR  $\delta^* u_t$  AND  $\delta$  USED WITH C-S MODEL
  - EFFECTS OF  $\partial p/\partial s$  MODELED
  - WAKE MODEL PROPOSED
- FLAT PLATE
  - B-L & NEW MODEL AGREE WITH LAW OF THE WALL
  - LOCAL SHEAR MOD. DOES NOT AGREE WITH LAW OF THE WALL
- ANNULAR TURBINE
  - GOOD AGREEMENT WITH EXPT. PRESSURE DISTRIBUTION
  - WAKE MIXING UNDER-PREDICTED
- TURBINE ENDWALL HEAT TRANSFER
  - VARIATIONS IN ENDWALL  $St$  WITH  $Re$  PREDICTED WELL
  - EFFECTS OF  $\partial p/\partial s$  IMPORTANT
- TRANSONIC FAN
  - SHEAR LAYER FROM BOW SHOCK ACTS LIKE VISCOUS LAYER
  - NEW MODEL OVERPREDICTS L.E.  $\mu_t$
  - B-L MODEL PREDICTS REASONABLE L.E.  $\mu_t$

Lewis Research Center  
National Aeronautics and  
Space Administration

PROPELLION SYSTEMS DIVISION  
COMBUSTION TECHNOLOGY BRANCH



LOW EMISSIONS COMBUSTORS

J. M. DEUR  
SVERDRUP TECHNOLOGY, INC.  
LEWIS RESEARCH CENTER GROUP  
BROOK PARK, OHIO

Lewis Research Center  
National Aeronautics and  
Space Administration

PROPELLION SYSTEMS DIVISION  
COMBUSTION TECHNOLOGY BRANCH



APPLIED ANALYTICAL COMBUSTION/EMISSIONS RESEARCH

- ANALYZE LOW EMISSIONS COMBUSTORS TO AID IN-HOUSE EXPERIMENTS AND CONTRACTOR COMBUSTOR DEVELOPMENT PROGRAMS.
- PRESENT:
  - UTILIZE EXISTING CODES, PRINCIPALLY KIVA-II.
  - IMPROVE NUMERICS AND PHYSICAL MODELS (E.G., PDF COMBUSTION-TURBULENCE INTERACTION) ON LIMITED BASIS TO SATISFY CRITICAL NEEDS.
- FUTURE:
  - ADOPT 3-D ALLSPD CODE WHEN AVAILABLE.

Lewis Research Center  
National Aeronautics and  
Space Administration

PROPELLION SYSTEMS DIVISION  
COMBUSTION TECHNOLOGY BRANCH



KIVA-II FEATURES

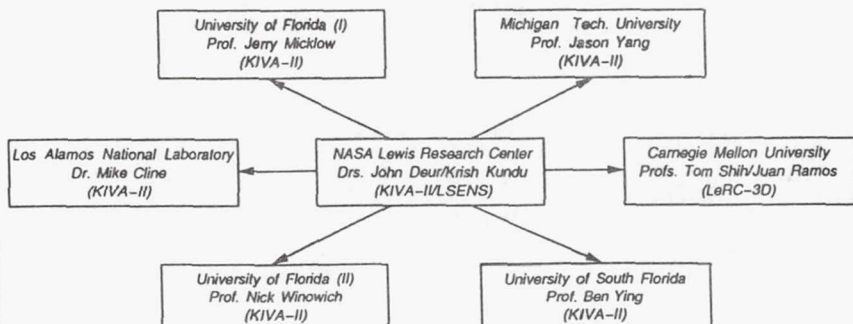
- MULTI-DIMENSIONAL TIME ACCURATE FINITE DIFFERENCE CODE.
- COMPRESSIBLE FLOWS.
- $k-\epsilon$  TURBULENCE MODEL WITH WALL FUNCTIONS OR SUB-GRID SCALE TURBULENCE MODEL.
- LAMINAR KINETICS FOR ARBITRARY REACTION SET WITH QUASI-EQUILIBRIUM OPTION (MIXING CONTROLLED COMBUSTION MODEL ALSO).
- STOCHASTIC SPRAY MODEL WITH VAPORIZATION, AERODYNAMIC BREAKUP, TURBULENT DISPERSION, AND COLLISION SUB-MODELS.
- ADIABATIC OR CONSTANT TEMPERATURE WALL BOUNDARIES.
- ARBITRARY MESH.

Lewis Research Center  
National Aeronautics and  
Space Administration

PROPELLION SYSTEMS DIVISION  
COMBUSTION TECHNOLOGY BRANCH



APPLIED ANALYTICAL COMBUSTION/EMISSIONS RESEARCH TEAM



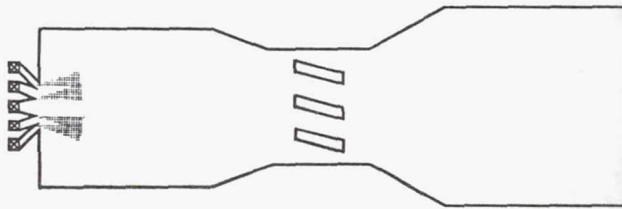
Carnegie Mellon University and University of South Florida leaving program at end of FY93

Lewis Research Center  
National Aeronautics and  
Space Administration

PROPELLION SYSTEMS DIVISION  
COMBUSTION TECHNOLOGY BRANCH



RICH BURN - QUICK MIX - LEAN BURN (RQL) FLAME TUBE



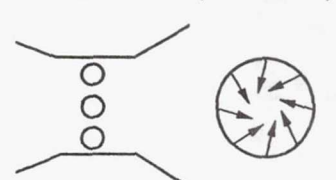
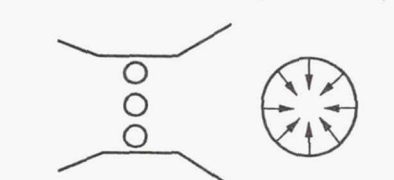
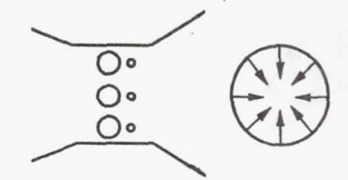
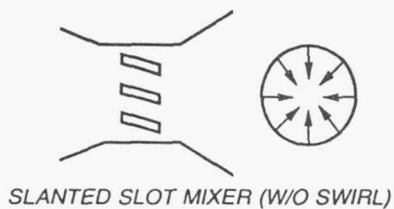
RICH BURN SECTION      MIXER SECTION      LEAN BURN SECTION

Lewis Research Center  
National Aeronautics and  
Space Administration

PROPELLION SYSTEMS DIVISION  
COMBUSTION TECHNOLOGY BRANCH



RQL FLAME TUBE MIXER CONFIGURATION PARAMETRIC STUDY



Lewis Research Center  
National Aeronautics and  
Space Administration

PROPELLION SYSTEMS DIVISION  
COMBUSTION TECHNOLOGY BRANCH



RQL FLAME TUBE WALL TEMPERATURE COMPARISON



SLANTED SLOT MIXER (W/O SWIRL)

TWO HOLE MIXER (W/O SWIRL)



ONE HOLE MIXER (W/O SWIRL)

ONE HOLE MIXER (W/ SWIRL)

MIN

MAX

Lewis Research Center  
National Aeronautics and  
Space Administration

PROPELLION SYSTEMS DIVISION  
COMBUSTION TECHNOLOGY BRANCH



RQL FLAME TUBE TEMPERATURE COMPARISON



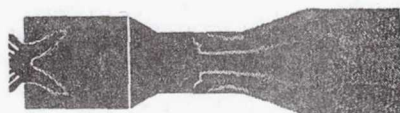
SLANTED SLOT MIXER (W/O SWIRL)



TWO HOLE MIXER (W/O SWIRL)



ONE HOLE MIXER (W/O SWIRL)



ONE HOLE MIXER (W/ SWIRL)

MIN

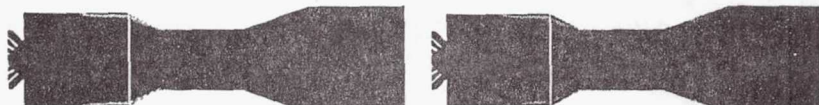
MAX

Lewis Research Center  
National Aeronautics and  
Space Administration

PROPELLION SYSTEMS DIVISION  
COMBUSTION TECHNOLOGY BRANCH

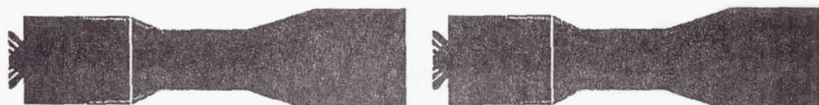


RQL FLAME TUBE NO<sub>x</sub> EMISSION INDEX COMPARISON



SLANTED SLOT MIXER (W/O SWIRL)

TWO HOLE MIXER (W/O SWIRL)



ONE HOLE MIXER (W/O SWIRL)

ONE HOLE MIXER (W/ SWIRL)

MIN

NOTE: CALCULATION CONSIDERS THERMAL NO<sub>x</sub> ONLY.

MAX

Lewis Research Center  
National Aeronautics and  
Space Administration

PROPELLION SYSTEMS DIVISION  
COMBUSTION TECHNOLOGY BRANCH



RQL MIXER CONFIGURATION PARAMETRIC STUDY NO<sub>x</sub> COMPARISON

SLANTED SLOT MIXER W/O SWIRL	1.00
TWO HOLE MIXER W/O SWIRL	1.25
ONE HOLE MIXER W/O SWIRL	1.39
ONE HOLE MIXER W/ SWIRL	0.75

SLANTED SLOT MIXER W/O SWIRL (EXPERIMENTAL) 1.00

NOTE:

- VALUES ARE SPATIAL AVERAGES TAKEN AT SAMPLING LOCATION B.
- VALUES ARE NORMALIZED BY SLANTED SLOT MIXER EXPERIMENTAL READING.

Lewis Research Center  
National Aeronautics and  
Space Administration

PROPELLION SYSTEMS DIVISION  
COMBUSTION TECHNOLOGY BRANCH



THE EFFECTS OF TURBULENCE MODELING ON THE  
NUMERICAL SIMULATION OF CONFINED SWIRLING FLOWS

G. J. MICKLOW AND M. R. HARPER  
UNIVERSITY OF FLORIDA  
GAINESVILLE, FLORIDA

J. M. DEUR  
SVERDRUP TECHNOLOGY, INC.  
BROOK PARK, OHIO

AIAA/SAE/ASME/ASEE 29TH JOINT PROPULSION CONFERENCE  
MONTEREY, CALIFORNIA

Lewis Research Center  
National Aeronautics and  
Space Administration

PROPELLION SYSTEMS DIVISION  
COMBUSTION TECHNOLOGY BRANCH



K - ε TURBULENCE MODEL

$$\frac{DK}{Dt} = \frac{\partial}{\partial x_j} \left( v_t \frac{\partial K}{\partial x_j} \right) + v_t \frac{\partial \bar{u}_i}{\partial x_j} \left( \frac{\partial \bar{u}_i}{\partial x_j} + \frac{\partial \bar{u}_j}{\partial x_i} \right) - \varepsilon$$

$$K = \frac{\overline{u_i u_j}}{2}$$

$$v_t = \frac{C_\mu K^2}{\varepsilon}$$

$$C_\mu = 0.09$$

Lewis Research Center  
National Aeronautics and  
Space Administration

PROPULSION SYSTEMS DIVISION  
COMBUSTION TECHNOLOGY BRANCH



K -  $\varepsilon$  TURBULENCE MODEL

$$\frac{D\varepsilon}{Dt} = \frac{\partial}{\partial x_j} \left( v_t \frac{\partial \varepsilon}{\partial x_j} \right) + C_1 v_t \frac{\varepsilon}{K} \frac{\partial \bar{u}_i}{\partial x_j} \left( \frac{\partial \bar{u}_i}{\partial x_j} + \frac{\partial \bar{u}_j}{\partial x_i} \right) - C_2 \frac{\varepsilon^2}{K}$$

$$C_1 = 1.44$$

$$C_2 = 1.92$$

Lewis Research Center  
National Aeronautics and  
Space Administration

PROPULSION SYSTEMS DIVISION  
COMBUSTION TECHNOLOGY BRANCH



$C_\mu$  MODIFICATIONS TO K -  $\varepsilon$  TURBULENCE MODEL

$$C_\mu = \frac{A u_0}{K^{1/2}}$$

$$A = 0.0083$$

$$C_\mu|_{\text{wall}} = 0.09$$

Lewis Research Center  
National Aeronautics and  
Space Administration

PROPELLION SYSTEMS DIVISION  
COMBUSTION TECHNOLOGY BRANCH



*C<sub>2</sub> MODIFICATIONS TO K - ε TURBULENCE MODEL*

$$C_2 = C_2^* (1 - C_3 \text{Ri}) \quad (0.1 < C_2 < 2.4)$$

$$C_2^* = 1.92$$

$$C_3 = 0.2$$

$$\text{Ri} = \frac{2 v/x^2 \frac{\partial(xv)}{\partial x}}{\left( \frac{\partial w}{\partial x} \right)^2 + \left( x \frac{\partial(v/x)}{\partial x} \right)^2}$$

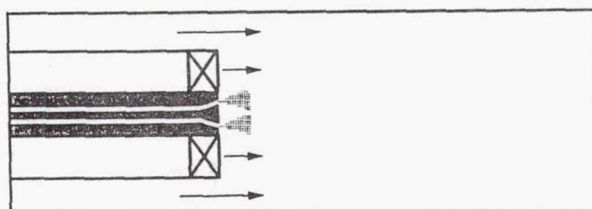
$$C_2|_{\text{wall}} = 1.92$$

Lewis Research Center  
National Aeronautics and  
Space Administration

PROPELLION SYSTEMS DIVISION  
COMBUSTION TECHNOLOGY BRANCH



*UCI AXISYMMETRIC CAN COMBUSTOR*

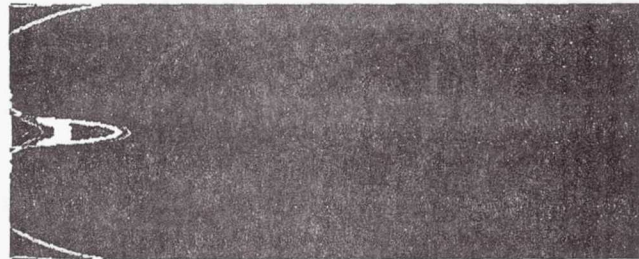


Lewis Research Center  
National Aeronautics and  
Space Administration

PROPULSION SYSTEMS DIVISION  
COMBUSTION TECHNOLOGY BRANCH



$C_\mu$  VARIATION IN UCI AXISYMMETRIC CAN COMBUSTOR



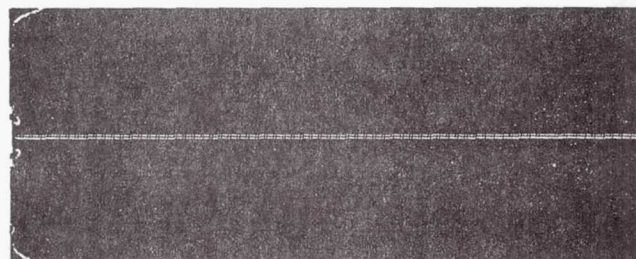
0.0048 [ ] 0.1200

Lewis Research Center  
National Aeronautics and  
Space Administration

PROPULSION SYSTEMS DIVISION  
COMBUSTION TECHNOLOGY BRANCH



$C_2$  VARIATION IN UCI AXISYMMETRIC CAN COMBUSTOR



1.00 [ ] 2.00

Lewis Research Center  
National Aeronautics and  
Space Administration

PROPULSION SYSTEMS DIVISION  
COMBUSTION TECHNOLOGY BRANCH



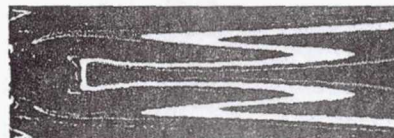
TURBULENT TIME SCALE IN UCI AXISYMMETRIC CAN COMBUSTOR



BASELINE CASE



C<sub>2</sub> CASE



C<sub>μ</sub> CASE

0.0002 s                            0.02 s

Lewis Research Center  
National Aeronautics and  
Space Administration

PROPULSION SYSTEMS DIVISION  
COMBUSTION TECHNOLOGY BRANCH



TURBULENT VISCOSITY IN UCI AXISYMMETRIC CAN COMBUSTOR



BASELINE CASE



C<sub>2</sub> CASE



C<sub>μ</sub> CASE

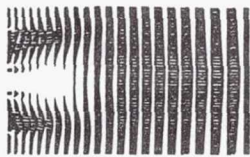
0.0 cm<sup>2</sup>/s                            1.34 cm<sup>2</sup>/s

Lewis Research Center  
National Aeronautics and  
Space Administration

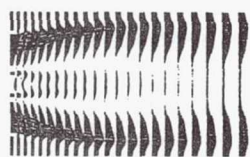
PROPELLION SYSTEMS DIVISION  
COMBUSTION TECHNOLOGY BRANCH



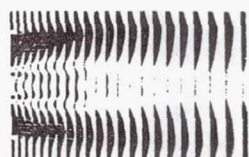
VELOCITY VECTORS IN UCI AXISYMMETRIC CAN COMBUSTOR



BASELINE CASE



$C_\mu$  CASE



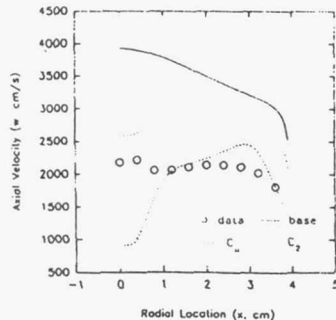
$C_2$  CASE

Lewis Research Center  
National Aeronautics and  
Space Administration

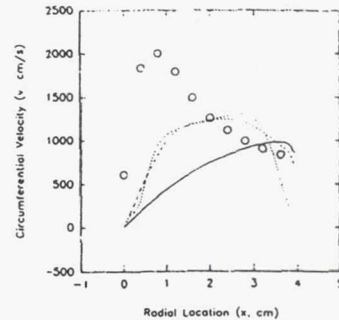
PROPELLION SYSTEMS DIVISION  
COMBUSTION TECHNOLOGY BRANCH



COMPARISONS TO UCI AXISYMMETRIC CAN COMBUSTOR DATA ( $z=24$  cm)



AXIAL VELOCITY



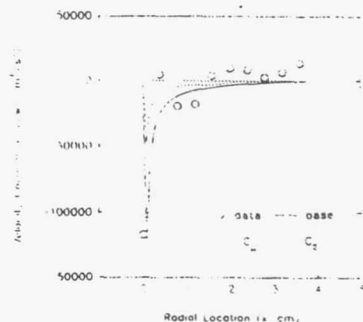
CIRCUMFERENTIAL VELOCITY

Lewis Research Center  
National Aeronautics and  
Space Administration

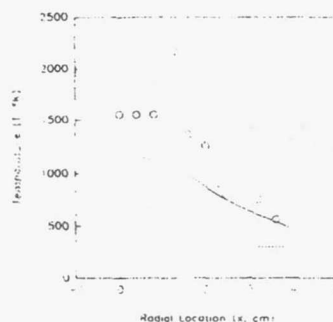
PROPELLION SYSTEMS DIVISION  
COMBUSTION TECHNOLOGY BRANCH



COMPARISONS TO UCI AXISYMMETRIC CAN COMBUSTOR DATA ( $z=24$  cm)



VELOCITY CORRELATION



TEMPERATURE

Lewis Research Center  
National Aeronautics and  
Space Administration

PROPELLION SYSTEMS DIVISION  
COMBUSTION TECHNOLOGY BRANCH



CONCLUSIONS

- INLET VELOCITY IS BEING MODIFIED TO MATCH FIRST INLET STATION.
- PDF COMBUSTION-TURBULENCE MODEL OF HSU, ET AL., IS BEING ADDED.
- MUCH MORE WORK IS REQUIRED.

LeRC CTM WORKSHOP	9/93	TITLE	1
-------------------------	------	-------	---

**DEVELOPMENT OF A  
RELIABLE ALGEBRAIC TURBULENCE  
MODEL GIVING ENGINEERING ACCURACY  
AT REASONABLE COST**

by

**B.P. Leonard and J.E. Drummond**  
**The University of Akron**

LeRC CTM WORKSHOP	9/93	OUTLINE	2
I. CHOICES FOR TURBULENCE MODELLING A. ZERO-EQUATION (ALGEBRAIC MODELS) B. MULTIPLE-EQUATION MODELS II. THE NEED FOR A RELIABLE ALGEBRAIC MODEL A. RELATIVE SIMPLICITY B. ENGINEERING ACCURACY C. COST-EFFECTIVE APPLICATION III. DEVELOPMENT OF THE MODIFIED MIXING LENGTH (MML) MODEL IV. COMPARISON OF MODELS A. MML B. BALDWIN-LOMAX C. TWO-EQUATION ( $k-\epsilon$ ) MODEL V. WHERE DO WE GO FROM HERE?			

LeRC CTM WORKSHOP	9/93	THEORETICAL BASIS OF THE MODEL	3
EFFECTIVE VISCOSITY: $\mu_{eff} = \mu + \mu_t$ (1) TURBULENT VISCOSITY: $\mu_t = \rho \ell^2  \omega $ (2)			
MIXING LENGTH:			
$\ell = \kappa \left( \frac{C_1}{C_2} \right) y^* \left[ 1 - \left( 1 - \frac{y^*}{C_1} \right)^{C_1} \right] \left[ 1 - \exp \left( \frac{-y^*}{A^*} \right) \right]$ for $y^* < C_1$ (3)			
$\ell = \kappa \left( \frac{C_1}{C_2} \right) y^*$ for $y^* > C_1$ (4)			
where: $y^+ = y/y^*$ ; $y^* = \mu/\sqrt{\rho  \tau_w }$			
SHEAR STRESS "FILTER":			
$ \bar{\tau}_i  = 0.1  \tau_{i-2}  + 0.2  \tau_{i-1}  + 0.4  \tau_i  + 0.2  \tau_{i+1}  + 0.1  \tau_{i+2} $ (5)			

OUTER REGION LENGTH SCALE (CAPPING LENGTH):

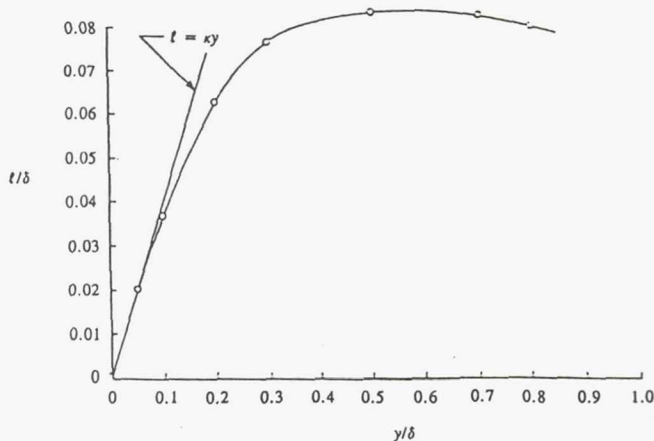
$$\ell = \ell_{\text{CAP}} = \kappa \frac{C_1}{C_2} y^*,$$

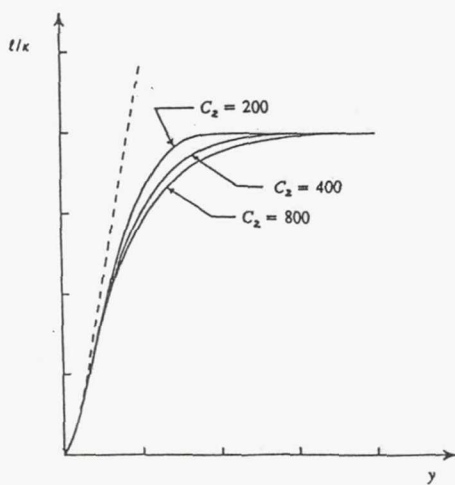
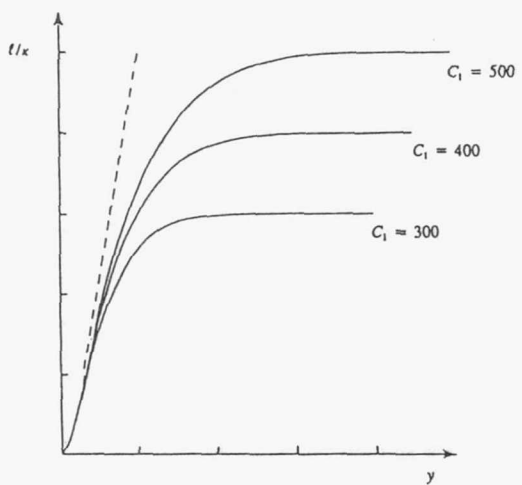
CAPPING LENGTH BASED ON BOUNDARY LAYER THICKNESS:

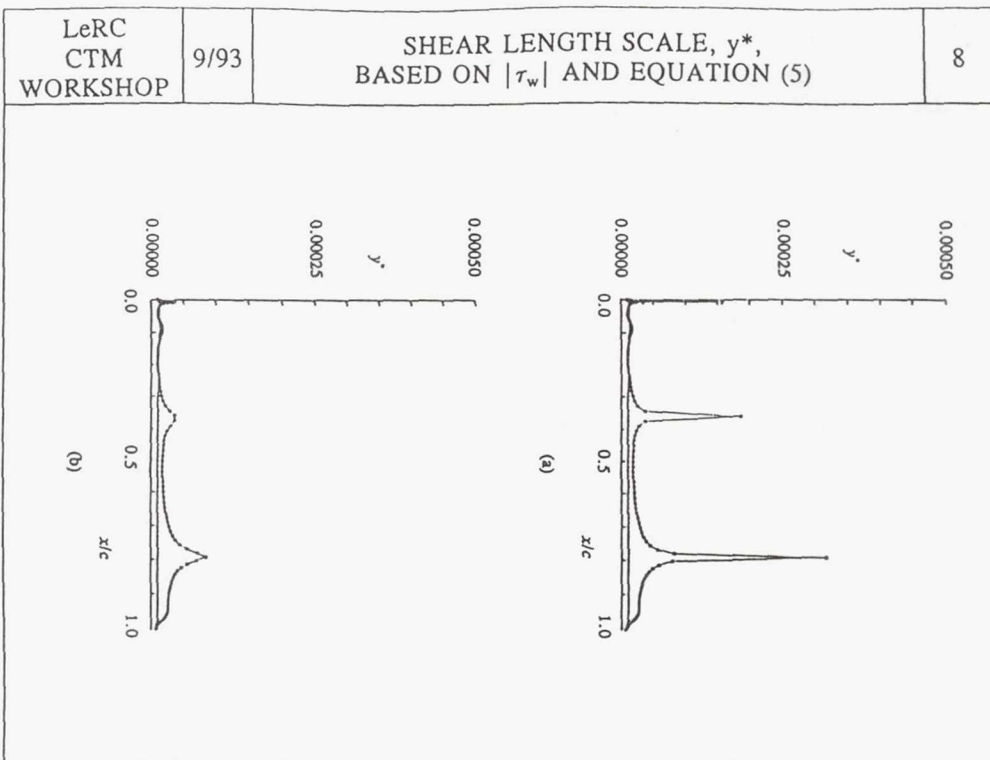
$$\ell_{\text{CAP}} \equiv B \cdot \delta$$

CAPPING LENGTH BASED ON LOCAL SHEAR STRESS:

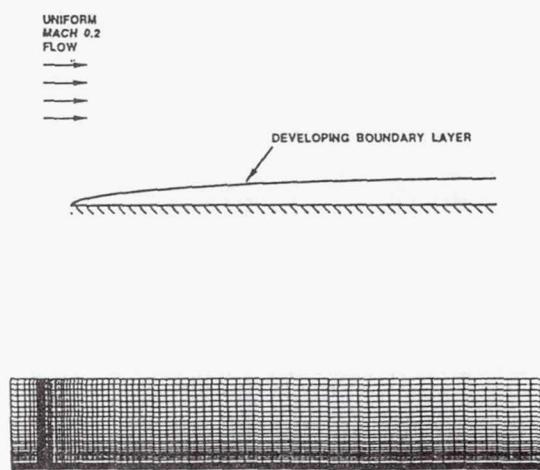
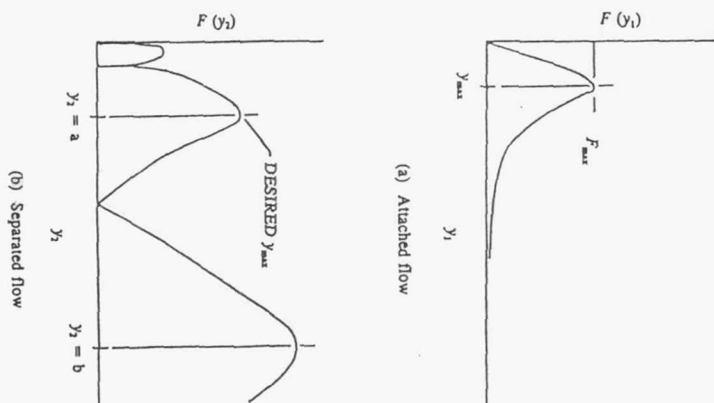
$$\ell_{\text{CAP}} = (3.31 \cdot 10^{-6}) B |C_f|^{-3.5} y^*$$

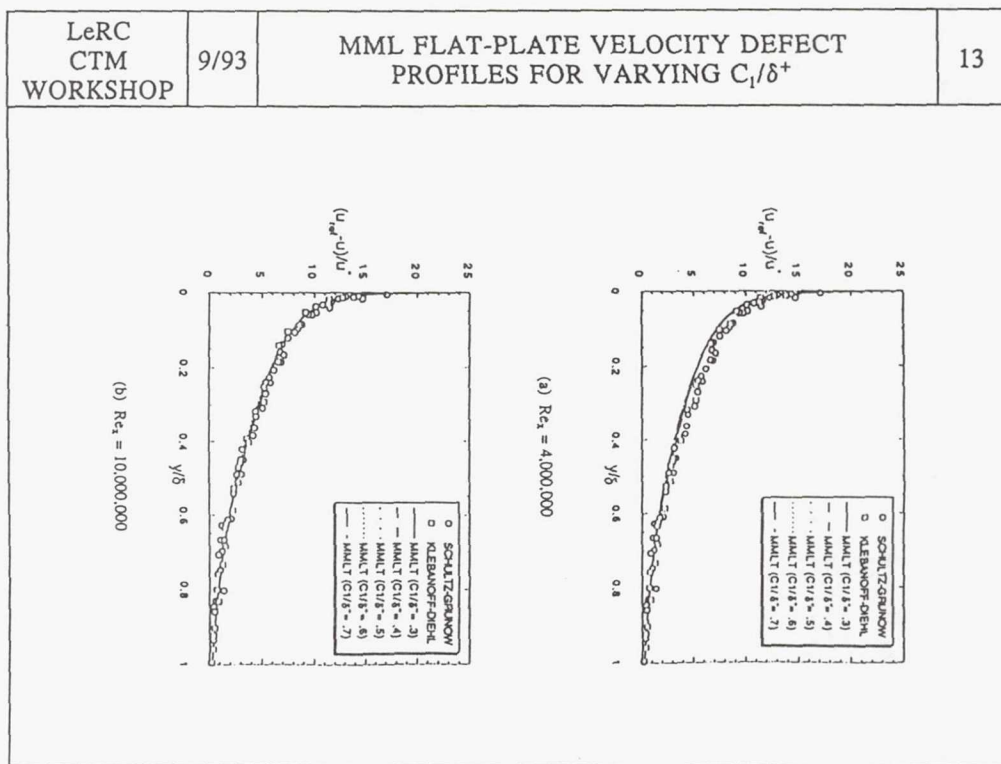
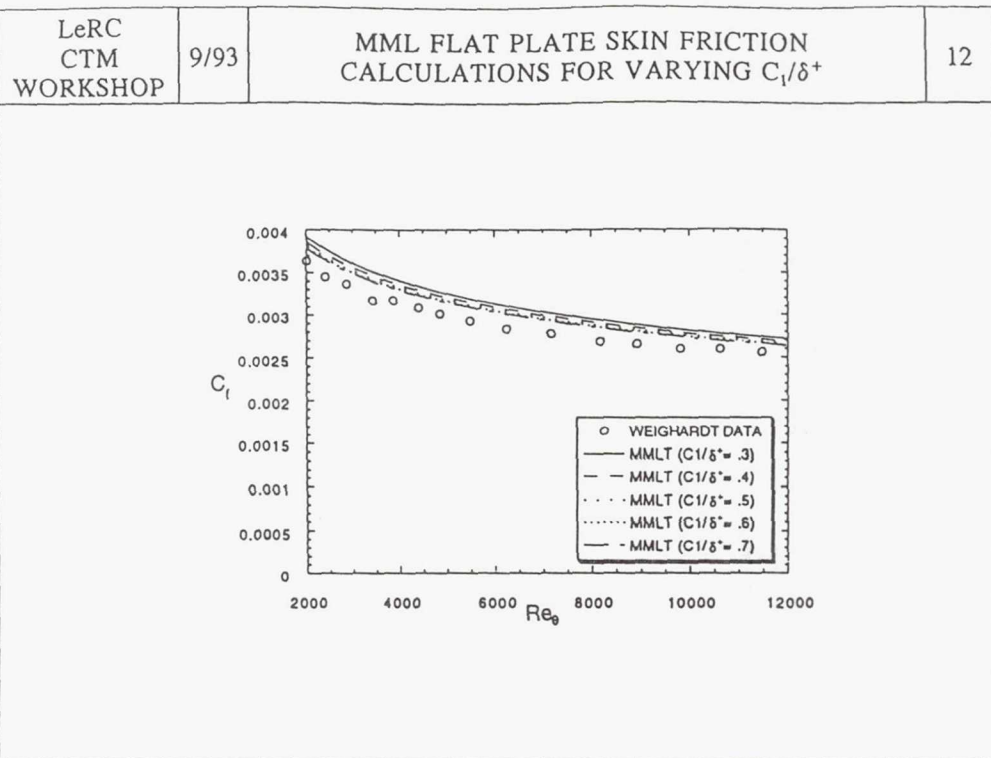




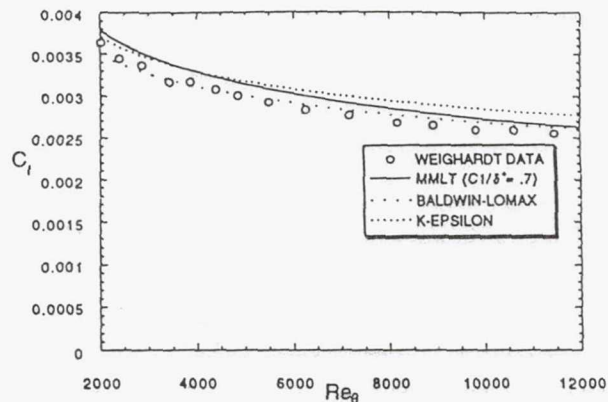


LeRC CTM WORKSHOP	9/93	THEORETICAL BASIS OF BALDWIN-LOMAX MODEL	9
INNER REGION TURBULENT VISCOSITY:			
$\mu_t = \rho \ell^2  \omega $			
WHERE			
$\ell = \kappa y [1 - \exp(-y^+/\Lambda^+)]$			
OUTER REGION TURBULENT VISCOSITY ASSUMES THE SMALLER VALUE OF:			
$\mu_t = \rho K C_{cp} F_k(y) y_{\max} F_{\max}$			
OR			
$\mu_t = 0.25 \rho K C_{cp} U_{\text{diff}}^2 y_{\max} / F_{\max}$			
WHERE			
$F(y) = y  \omega $			
$F_k(y) = \left[ 1 + 5.5 \left( \frac{C_k y}{y_{\max}} \right)^6 \right]^{-1}$			

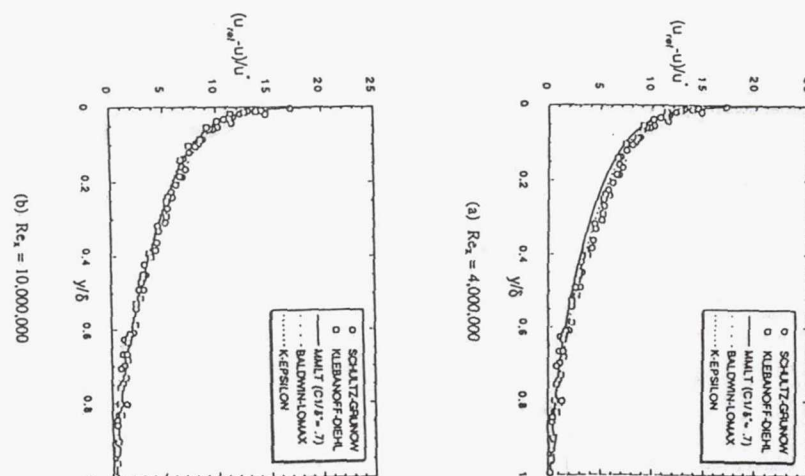




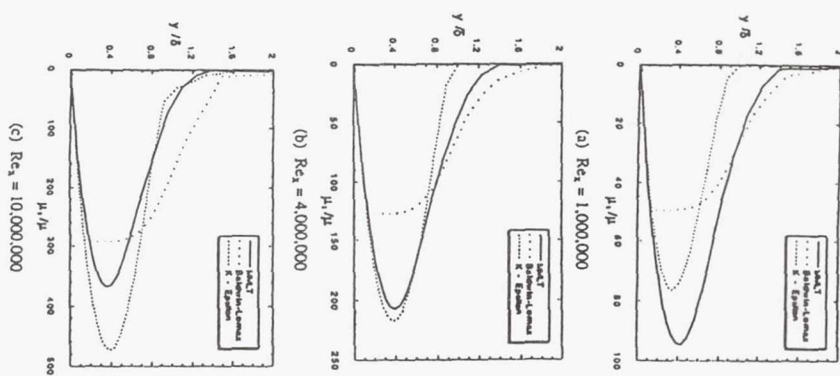
SKIN FRICTION CALCULATIONS FOR  
VARIOUS TURBULENCE MODELS



VELOCITY DEFECT PROFILES FOR  
VARIOUS TURBULENCE MODELS

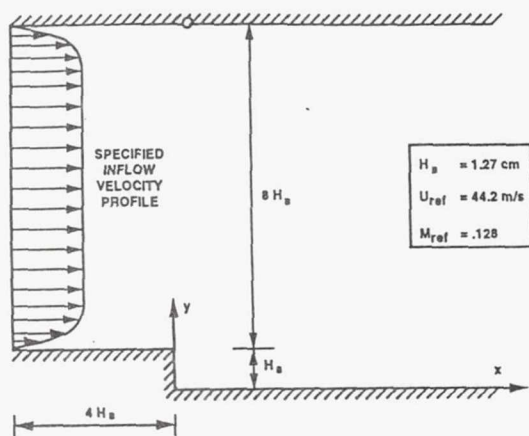


TURBULENT VISCOSITY PROFILES  
FOR VARIOUS MODELS

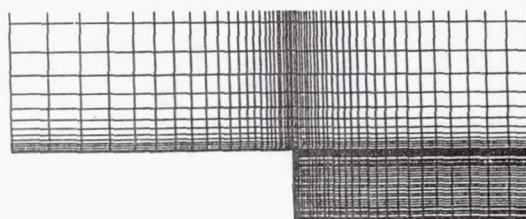


CONVERGENCE CHARACTERISTICS FOR  
FLAT PLATE CALCULATIONS

MODEL	ITERATIONS	CRAY Y/MP CPU TIME (s)
MMLT	4000	500
Baldwin-Lomax	4000	500
Chien k- $\epsilon$	5000	1100



(a) Entire grid



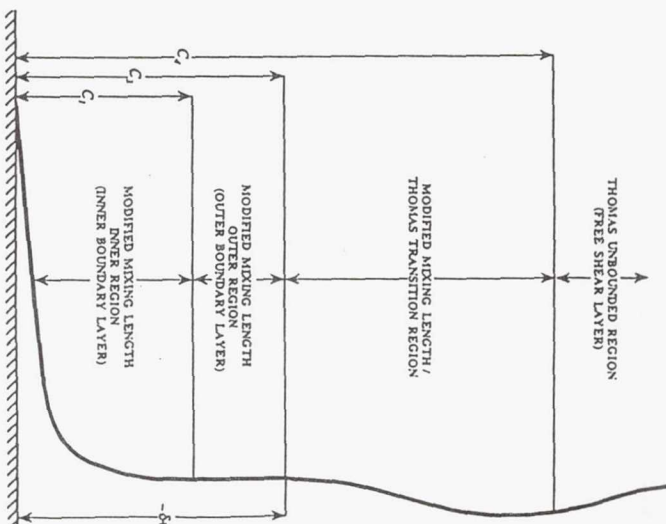
(b) Detail near step

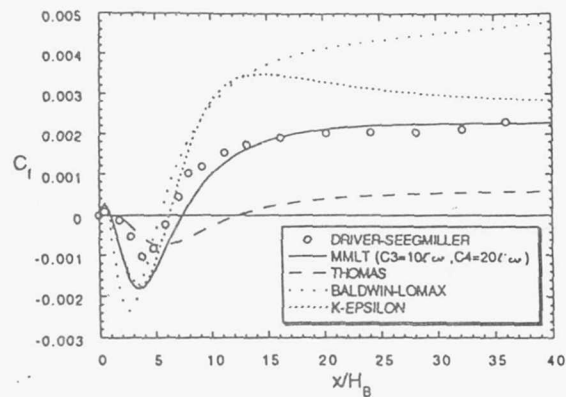
LENGTH SCALE FOR UNBOUNDED REGION FOR THOMAS MODEL:

$$\ell = \frac{\ell_o [\text{Max}(|u_j|) - \text{Min}(|u_j|)]}{\omega_c}$$

TURBULENT VISCOSITY IN TRANSITION REGION BETWEEN  
BOUNDARY LAYER AND UNBOUNDED REGION:

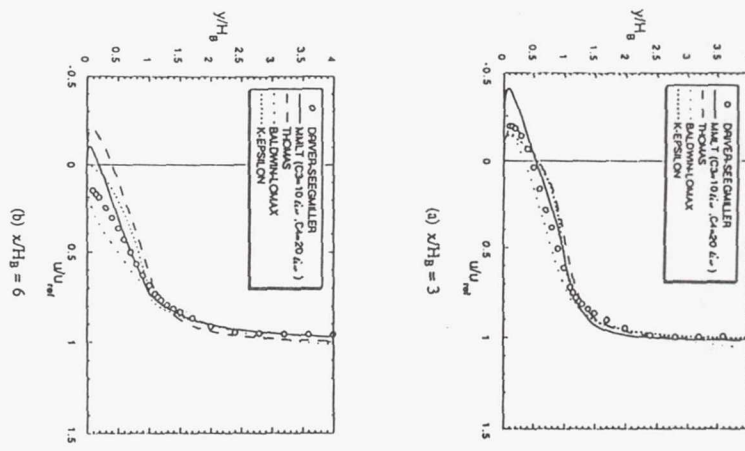
$$\mu_{tr} = \frac{\mu_{MML}(C_4 - y^+) + \mu_{Th}(y^+ - C_3)}{C_4 - C_3}$$



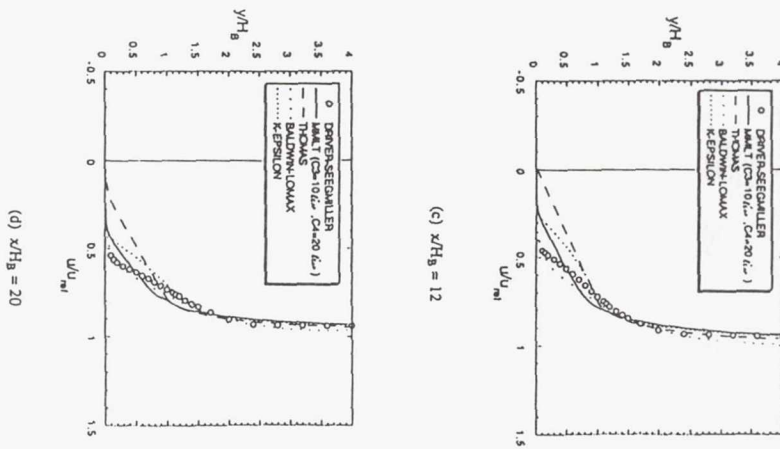


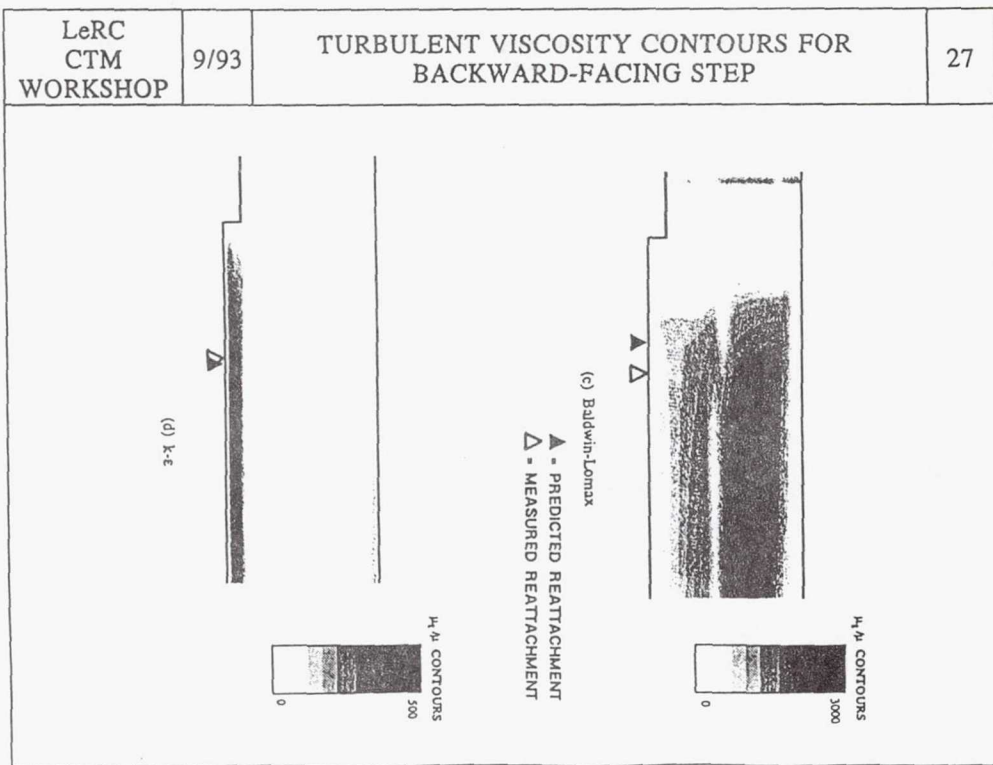
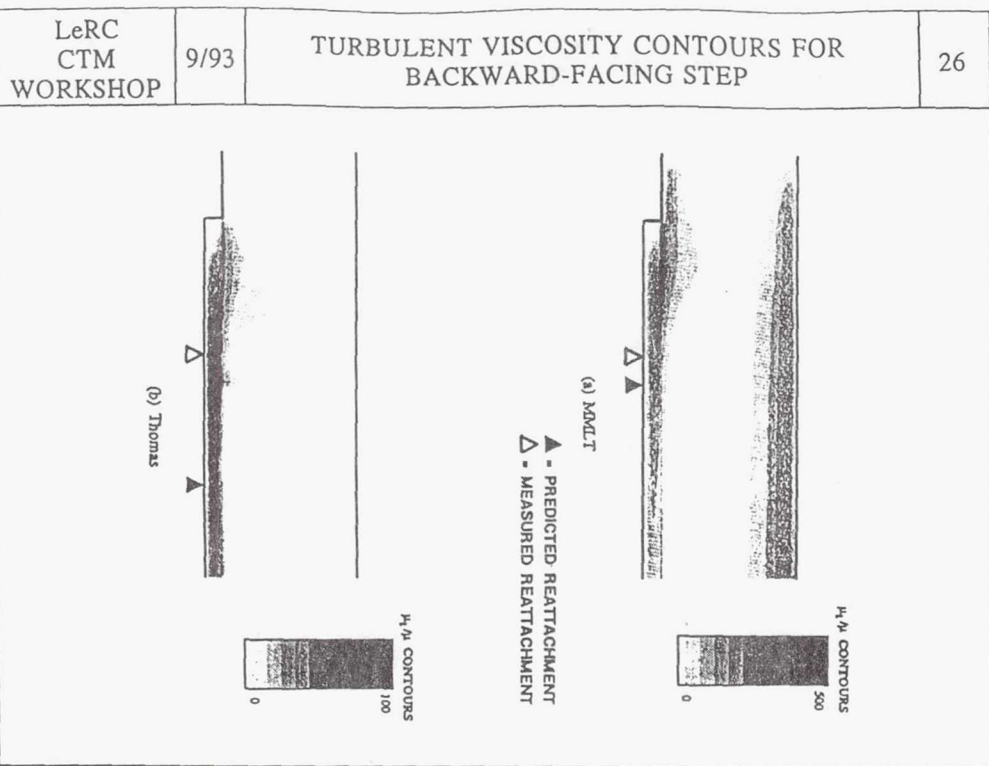
CASE	REATTACHMENT POSITION (STEP HEIGHTS, $H_B$ )
Driver-Seegmiller Data	6.25
MMLT ( $C_1/\delta+ \approx .7$ , $C_3 = 10\ell_{CAP}, C_4 = 20\ell_{CAP}$ )	7.42
Thomas	12.28
Baldwin-Lomax	5.41
Chien k- $\epsilon$	6.27

VELOCITY PROFILE COMPARISON FOR  
VARIOUS TURBULENCE MODELS



VELOCITY PROFILE COMPARISON FOR  
VARIOUS TURBULENCE MODELS





LeRC CTM WORKSHOP	9/93	CONVERGENCE CHARACTERISTICS FOR VARIOUS TURBULENCE MODELS	28
-------------------------	------	--	----

MODEL	ITERATIONS	CRAY Y/MP CPU TIME (s)
MMLT	45,000	7100
Thomas	40,000	6000
Baldwin-Lomax	45,000	7000
Chien k- $\epsilon$	110,000	50,000

LeRC CTM WORKSHOP	9/93	WHERE DO WE GO FROM HERE?	29
-------------------------	------	---------------------------	----

- A. APPLICATION TO MORE COMPLEX FLOWS
  - NOZZLE FLOWS
  - RECIRCULATING INTERNAL FLOWS
  - EXTERNAL FLOWS
- B. COMPARISON WITH OTHER TURBULENT CALCULATIONS
- C. ESTABLISH REASONABLE ALGEBRAIC MODEL AS AN OPTION  
TO GIVE RESULTS WITH ENGINEERING ACCURACY FOR A  
VARIETY OF APPLICATIONS

**Page intentionally left blank**

# **Application of Algebraic and Two-Equation Turbulence Models to HSR Nozzle Flow Calculations**

**N. J. Georgiadis  
and  
J. R. DeBonis**

**Nozzle Technology Branch  
Propulsion Systems Division**

**September 16, 1993**

## **FULL NAVIER-STOKES ANALYSES OF NOZZLES (WITH PARC CODE)**

- OVERVIEW OF PARC CODE AND AVAILABLE TURBULENCE MODELS
- VALIDATION TEST CASES:
  1. AXISYMMETRIC PLUG NOZZLE
  2. EJECTOR NOZZLE
- HIGH-SPEED RESEARCH (HSR) NOZZLES WITH POTENTIAL FOR NOISE REDUCTION:
  1. NASA/GE 2DCD MIXER/EJECTOR NOZZLE
  2. PRATT & WHITNEY 2D MIXER/EJECTOR NOZZLE

## OVERVIEW OF PARC:

- 3D AND 2D/AXISYMMETRIC VERSIONS
- NAVIER-STOKES AND EULER MODES
- CENTRAL DIFFERENCE DISCRETIZATION
- BEAM AND WARMING ALGORITHM
- SEVERAL TURBULENCE MODEL OPTIONS
- CAPABILITY TO HANDLE MULTIPLE GRID BLOCKS  
(NONCONTIGUOUS INTERFACING)
- GENERALIZED BOUNDARY CONDITIONS

### Full Navier-Stokes Equations in PARC

$$\frac{\partial Q}{\partial t} + \frac{\partial F_j}{\partial x_j} = \frac{1}{Re} \frac{\partial G_j}{\partial x_j}$$

$$Q = \begin{bmatrix} \rho \\ \rho u_i \\ E \end{bmatrix} \quad F_j = \begin{bmatrix} \rho u_j \\ \rho u_i u_j + P \delta_{ij} \\ (E + P) u_j \end{bmatrix} \quad G_j = \begin{bmatrix} 0 \\ \tau_{ij} \\ u_k \tau_{jk} - q_j \end{bmatrix}$$

$$\tau_{ij} = \mu \left( \frac{\partial u_i}{\partial x_j} + \frac{\partial u_j}{\partial x_i} \right) - \frac{2}{3} \mu \frac{\partial u_k}{\partial x_k} \delta_{ij}$$

$$q_j = \frac{-K_c}{(\gamma - 1)Pr} \frac{\partial T}{\partial x_j}$$

$$\mu_{eff} = \mu + \mu_t$$

$$K_{c-eff} = K_c + \frac{\mu_t C_p}{Pr_t}$$

## Thomas Model

$$\mu_t = \rho \ell^2 |\omega|$$

Wall bounded flows:

$$\ell = K_y \left( 1 - e^{-y^*/\Lambda^*} \right)$$

Free shear layers:

$$\ell = \frac{\ell_* [ \text{Max}(|u_j|) - \text{Min}(|u_j|) ]}{\omega_c}$$

## Baldwin-Lomax Model

$$\mu_t = \begin{cases} (\mu_t)_{\text{inner}} & , y \leq y_{\text{crossover}} \\ (\mu_t)_{\text{outer}} & , y \geq y_{\text{crossover}} \end{cases}$$

$$(\mu_t)_{\text{outer}} = \rho [\kappa C_{CP} F_{\text{wake}}] F_{\text{kleb}}$$

$$F_{\text{wake}} = \min(y_{\max} F_{\max}, C_{wk} y_{\max} u_{\text{dif}}^2 / F_{\max})$$

$$F(y) = y |\omega| \left( 1 - e^{\frac{-y}{A^*}} \right) \quad F_{\text{kleb}}(y) = \left[ 1 + 5.5 \left( \frac{C_{\text{kleb}} y}{y_{\max}} \right)^6 \right]^{-1}$$

## Chien k-ε Model

$$\mu_t = C_\mu f_\mu \rho k^2 / \varepsilon$$

$$\frac{D(\rho k)}{Dt} = \frac{\partial}{\partial x_i} \left[ \left( \mu + \frac{\mu_t}{\sigma_k} \right) \frac{\partial k}{\partial x_i} \right] + \Pi - \rho \varepsilon - D$$

$$\frac{D(\rho \varepsilon)}{Dt} = \frac{\partial}{\partial x_i} \left[ \left( \mu + \frac{\mu_t}{\sigma_\varepsilon} \right) \frac{\partial \varepsilon}{\partial x_i} \right] + C_{\varepsilon 1} f_1 \Pi \frac{\varepsilon}{k} - C_{\varepsilon 2} f_2 \rho \frac{\varepsilon^2}{k} - 2\mu \frac{\varepsilon}{y^2} e^{(-0.5y^*)}$$

$$\Pi = \mu_t \frac{\partial x_j}{\partial x_i} \left[ \frac{\partial u_j}{\partial x_i} + \frac{\partial u_i}{\partial x_j} \right]$$

$$D = 2\mu k / y^2$$

$$f_\mu = 1 - e^{(-0.0115 y^*)}$$

$$f_1 = 1.0$$

$$f_2 = 1.0 - 0.22 e^{-(R_t/6)^2}$$

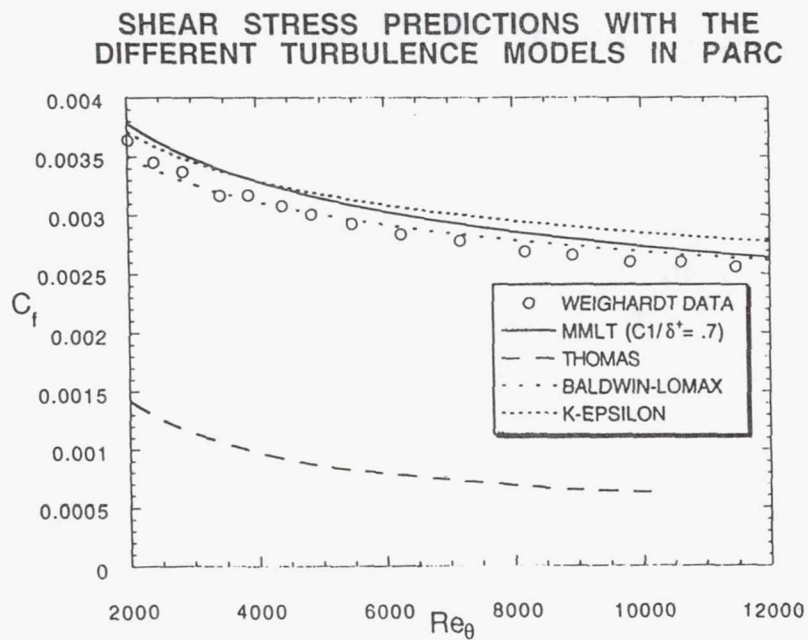
$$Re_t = \frac{\rho k^2}{\mu \epsilon}$$

## TWO-EQUATION MODEL OF SPEZIALE

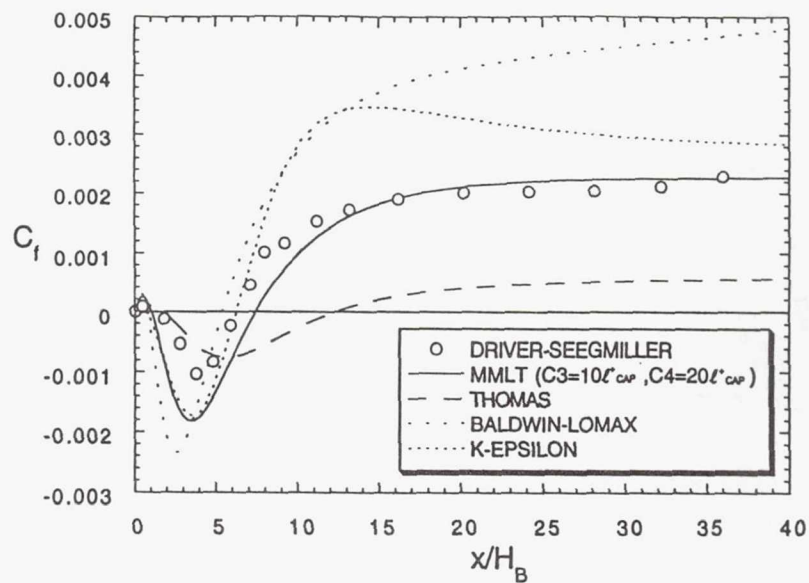
- SOLVED AS A  $k-\epsilon$  MODEL IN PARC
- ORIGINALLY DEVELOPED AS A  $k-\tau$  MODEL  
IN NASA CR-182068
- UPWIND DIFFERENCE DISCRETIZATION  
(MAIN FLOW EQUATIONS IN PARC USE  
CENTRAL DIFFERENCING)

## BENCHMARK VALIDATION CASES

1. Mach 0.2 flat plate
2. Mach 0.128 backward-facing step

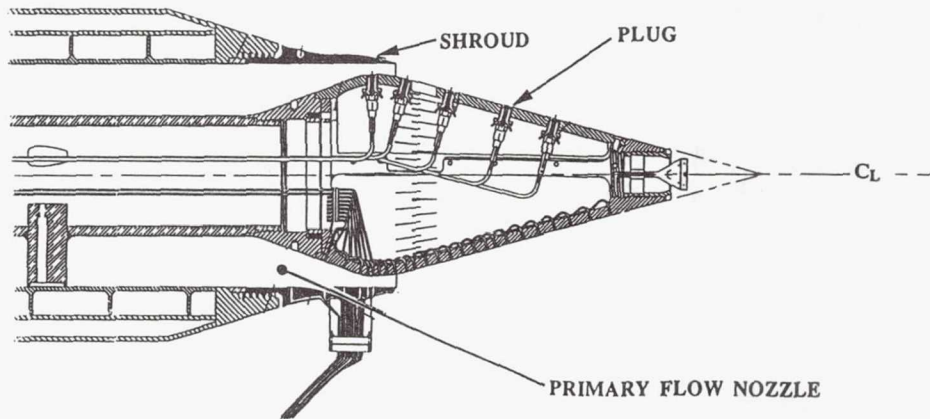


## SHEAR STRESS AFTER THE STEP WITH THE DIFFERENT TURBULENCE MODELS IN PARC

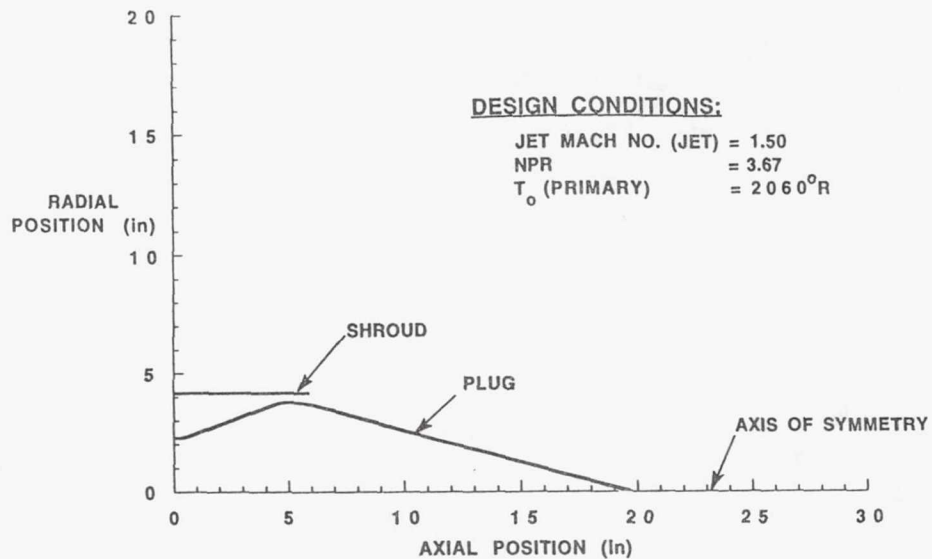


## LANGLEY SINGLE FLOW PLUG NOZZLE

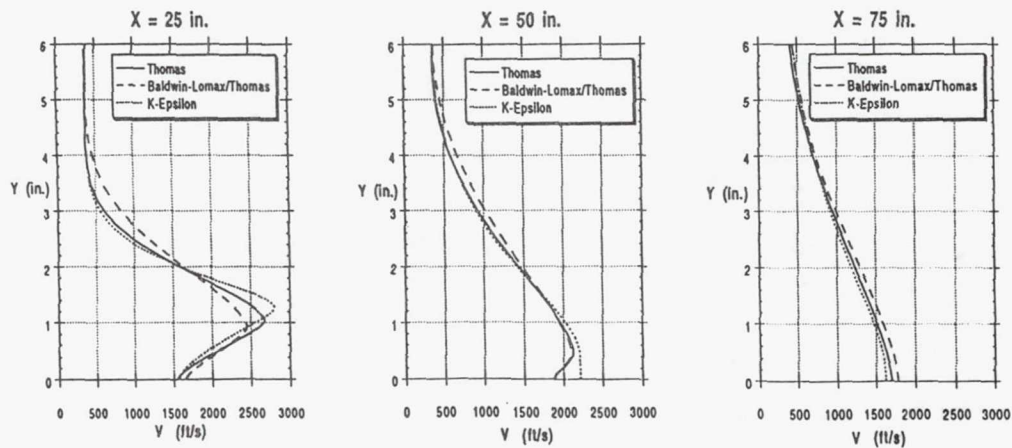
- VENTED AND NON-VENTED PLUGS
- 15° PLUG HALF ANGLE
- HEAVILY INSTRUMENTED TO MEASURE:
  1. PLUG SURFACE TEMPERATURES, PRESSURES, SHEAR STRESS
  2. JET PLUME QUANTITIES ( INCLUDING LDV & FLOW VISUALIZATION)
  3. FLOWFIELD ACOUSTICS



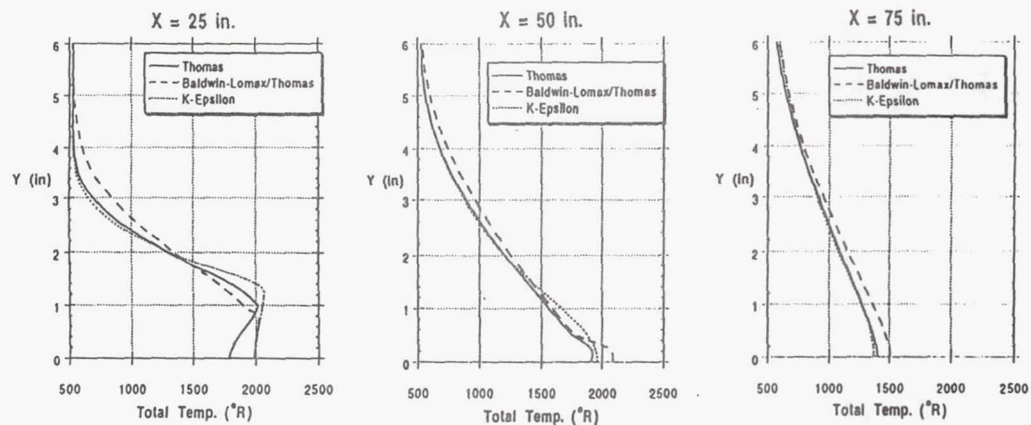
## GEOMETRY FOR GRID GENERATION AND PARC2D CALCULATIONS



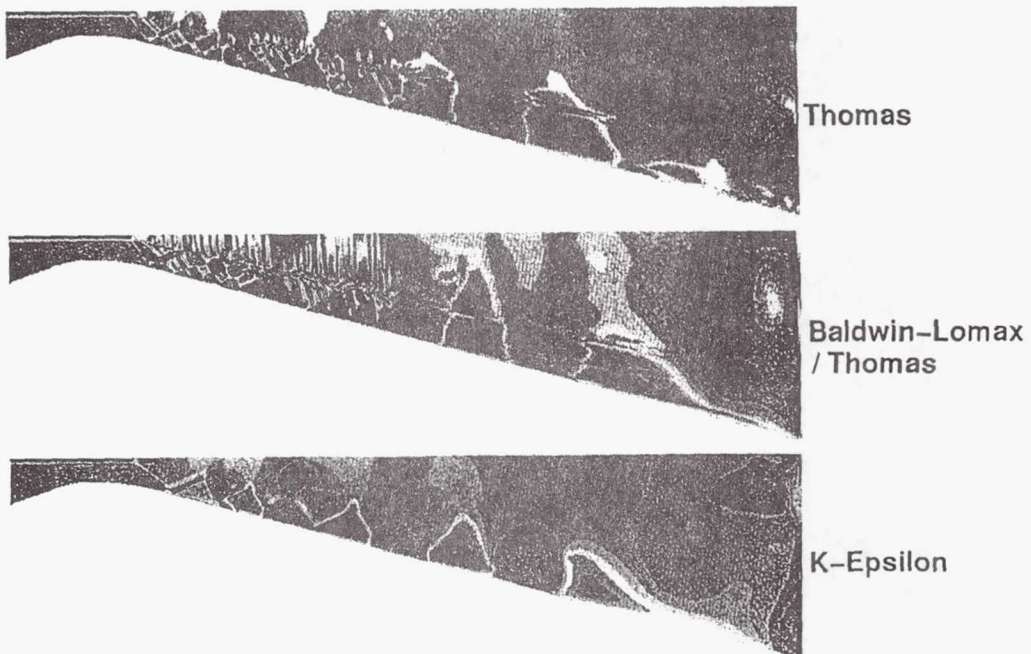
## VELOCITY PROFILES FOR FINE GRID SOLUTIONS



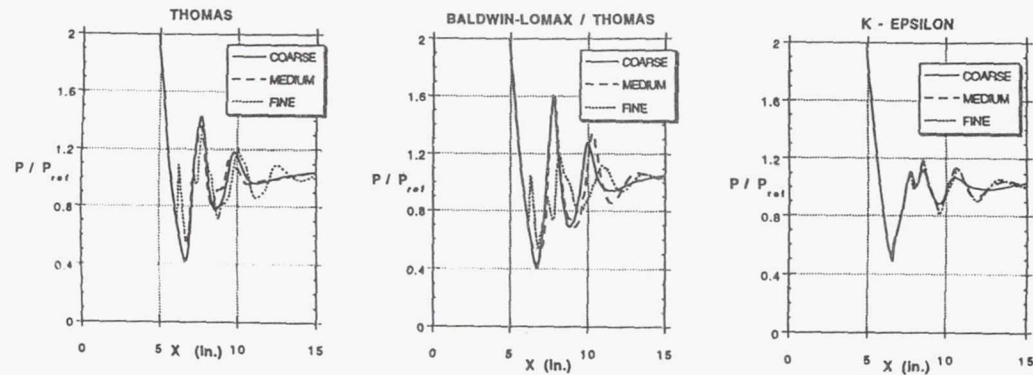
## TOTAL TEMPERATURE PROFILES FOR FINE GRID SOLUTIONS



## SHOCK FUNCTION (BASED ON PRESSURE GRADIENT)



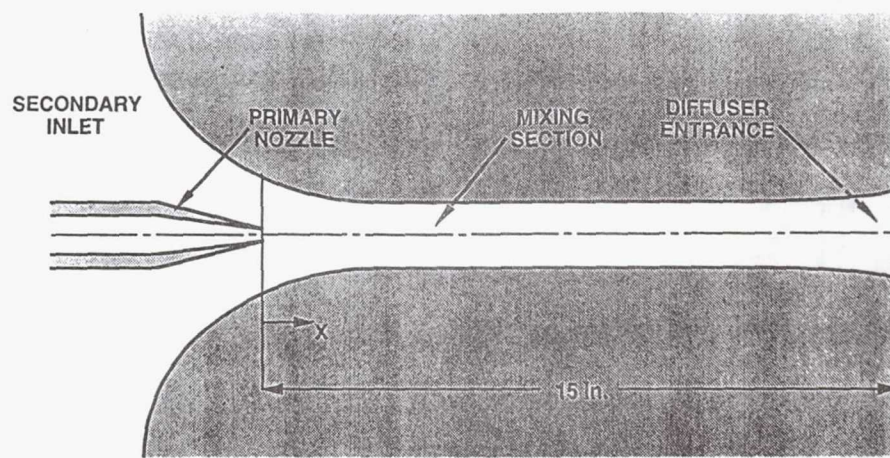
## STATIC PRESSURE DISTRIBUTION ALONG PLUG



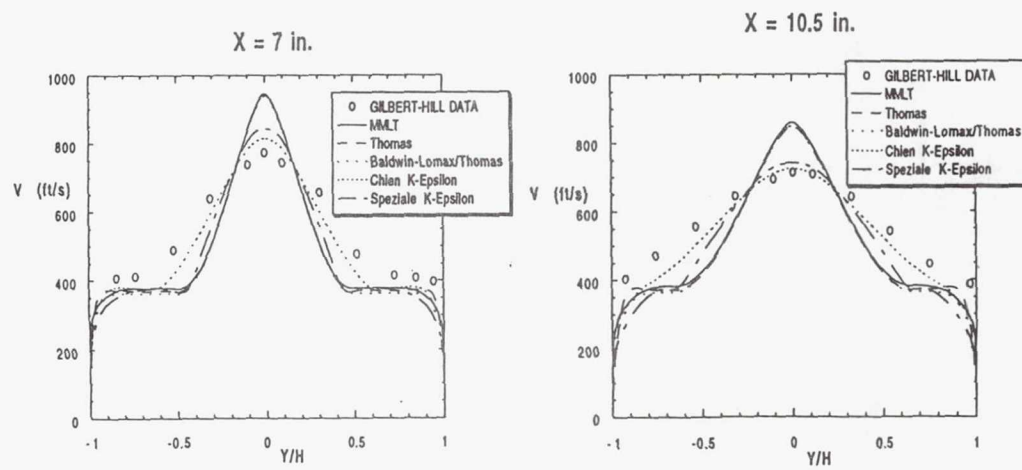
## 2D EJECTOR NOZZLE TEST CASE

- REPRESENTATIVE OF MIXER-EJECTOR NOZZLES THAT ARE BEING CONSIDERED FOR SUPERSONIC TRANSPORT APPLICATION
- FLOW DOMINATED BY TURBULENT MIXING OF A HIGH ENERGY STREAM WITH SECONDARY AIR

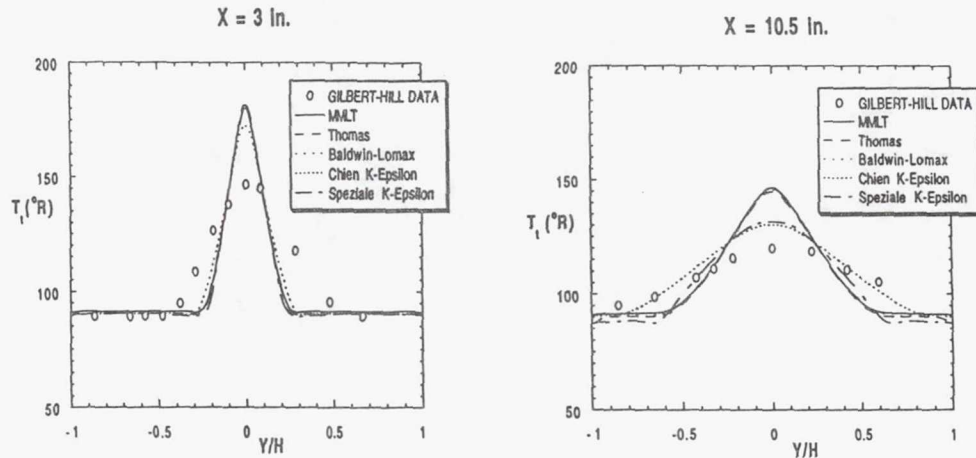
## 2D EJECTOR NOZZLE OF GILBERT AND HILL



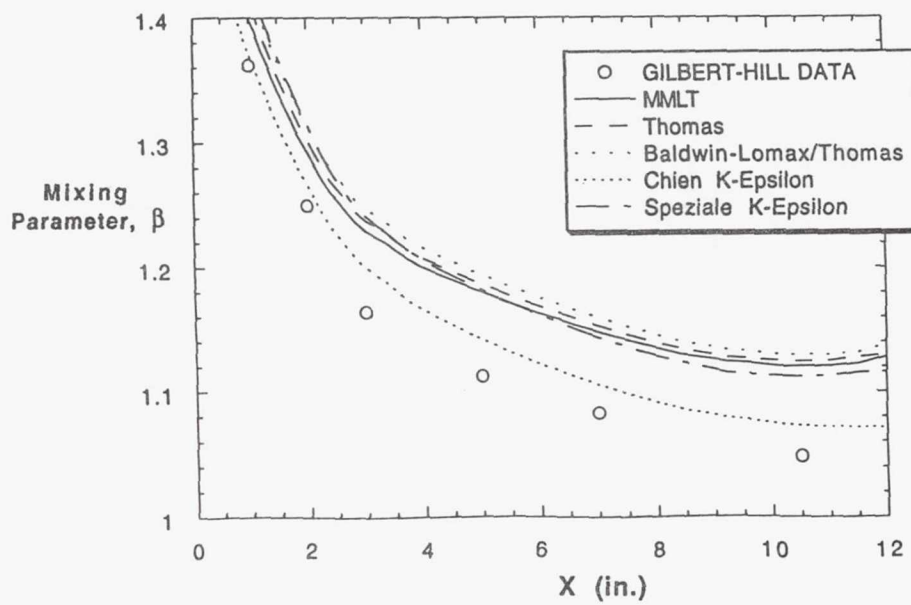
### VELOCITIES IN MIXING SECTION



## TOTAL TEMPERATURES IN MIXING SECTION



## MIXING EFFECTIVENESS



**TURBULENT VISCOSITY CONTOURS  
FOR 2D EJECTOR NOZZLE**

$\mu_t / \mu$

0.00000  
100.0000  
200.0000  
300.0000  
400.0000  
500.0000  
600.0000  
700.0000  
800.0000  
900.0000  
1000.0000  
1100.0000  
1200.0000



Thomas

100.0000  
1000.0000  
2000.0000  
3000.0000  
4000.0000  
5000.0000  
6000.0000  
7000.0000  
8000.0000  
9000.0000  
10000.0000  
11000.0000  
12000.0000

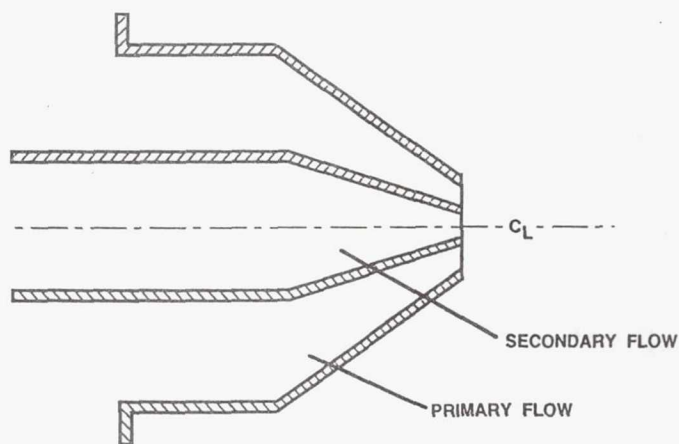


Speziale k- $\epsilon$

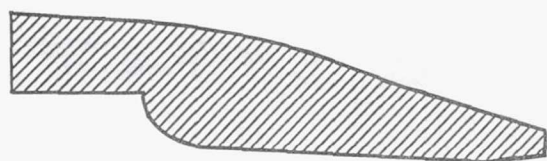
Chien k- $\epsilon$



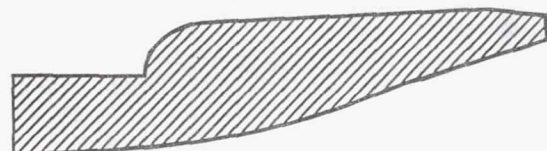
**AXISYMMETRIC INVERTED VELOCITY  
PROFILE NOZZLE OF VON GLAHN,  
GOODYKOONTZ, AND WASSERBAUER**



## AXISYMMETRIC UNDEREXPANDED NOZZLE OF HELSTLEY AND CROSSWY



$M_{jet}$  = 1.56  
 $M_{oo}$  = 0.60  
NSPR = 4.5

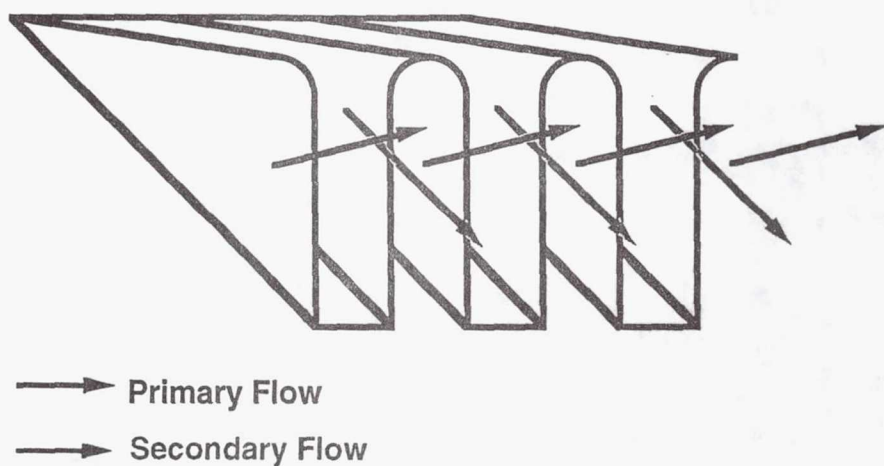


## Mixer/Ejector Nozzles

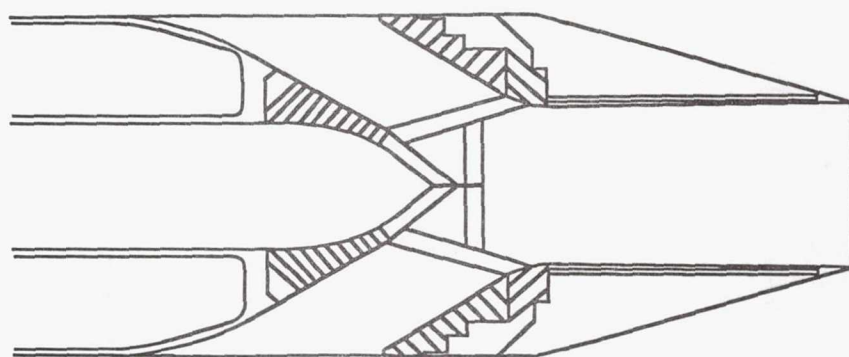
- Entrain large amounts of secondary flow
- Rapidly mix two flows together to lower jet velocity
- Lower jet velocity results in lower noise
- Maintain high thrust due to large mass augmentation

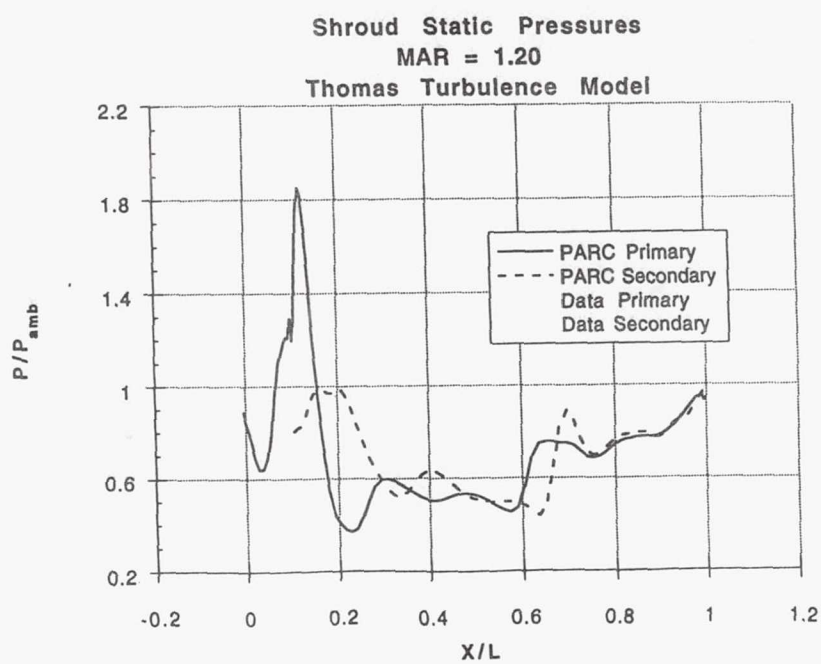
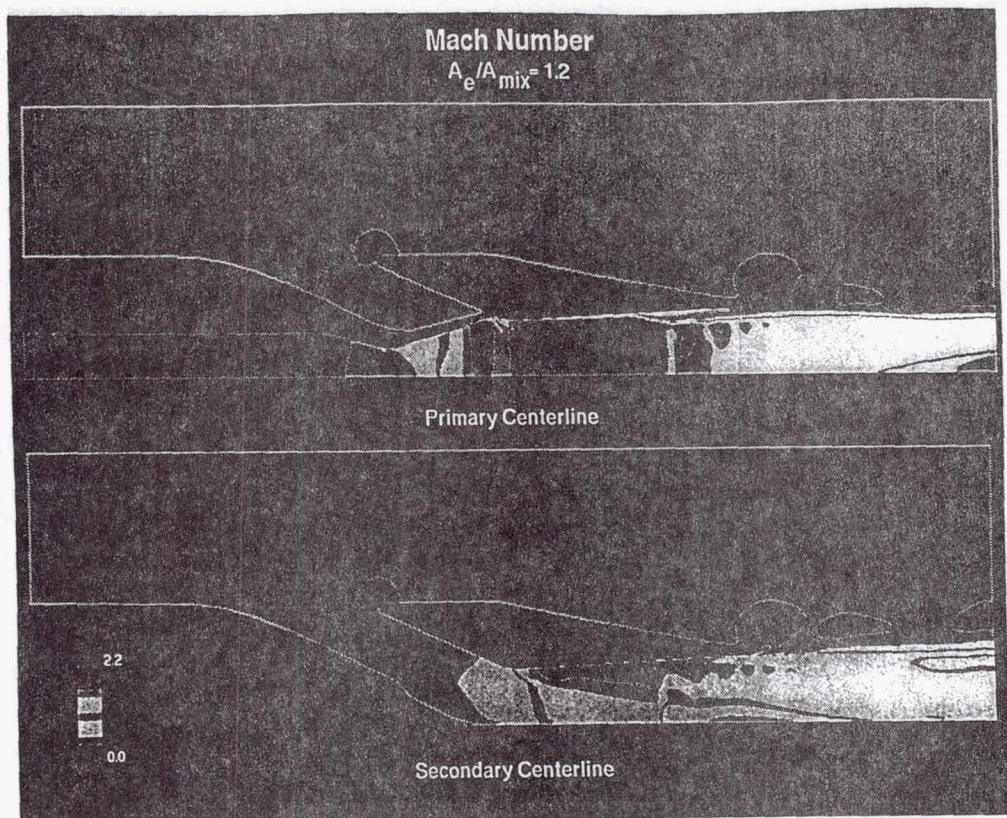
$$F = \dot{m}v$$

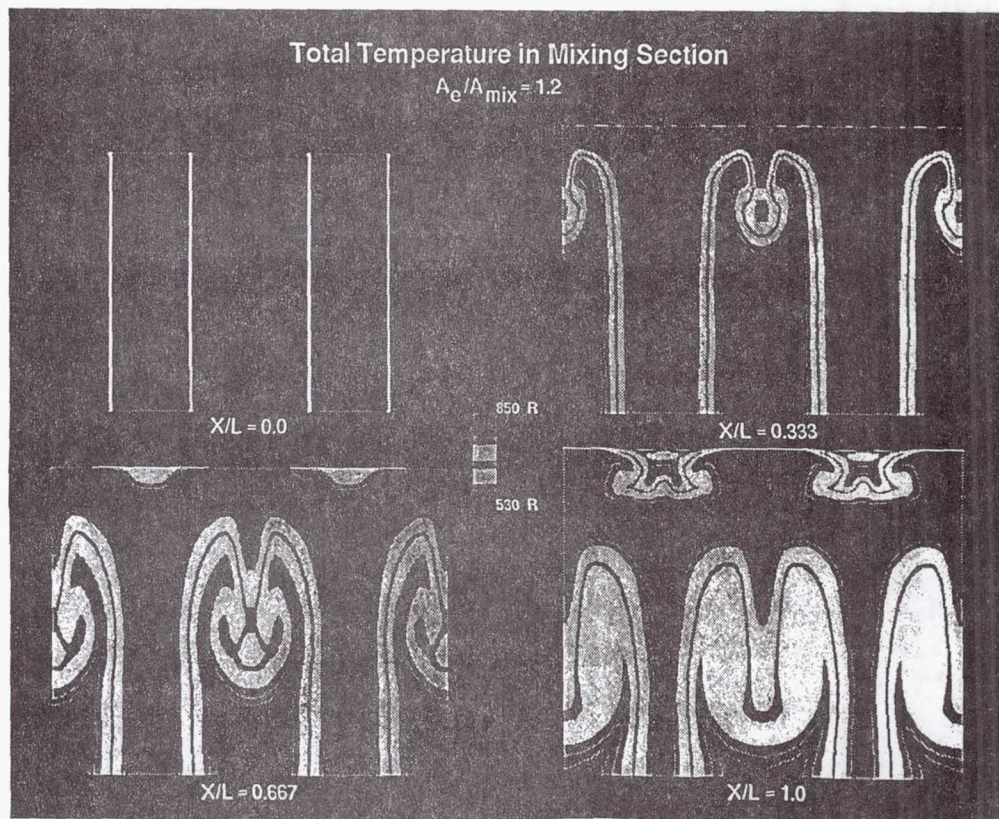
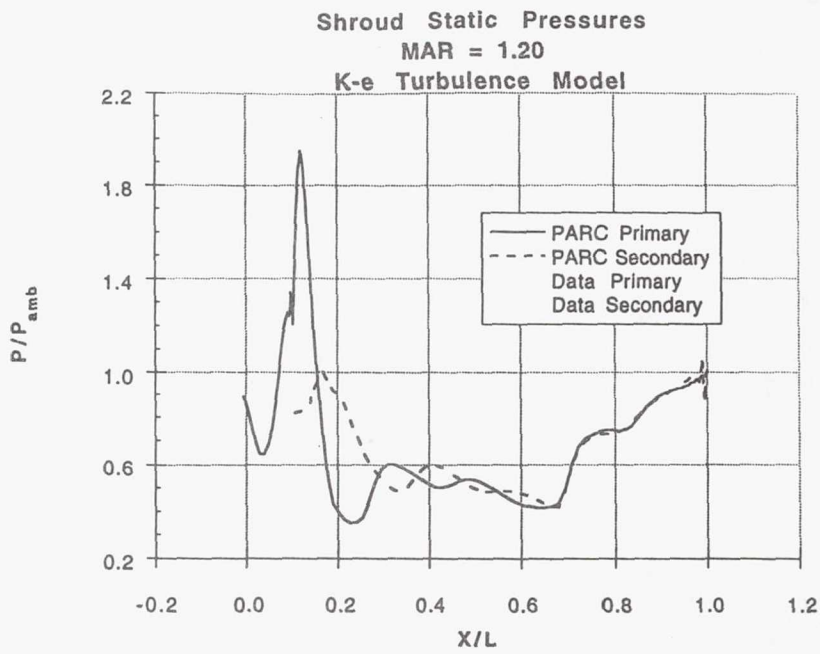
## Typical Mixer/Ejector Nozzle Chute Geometry

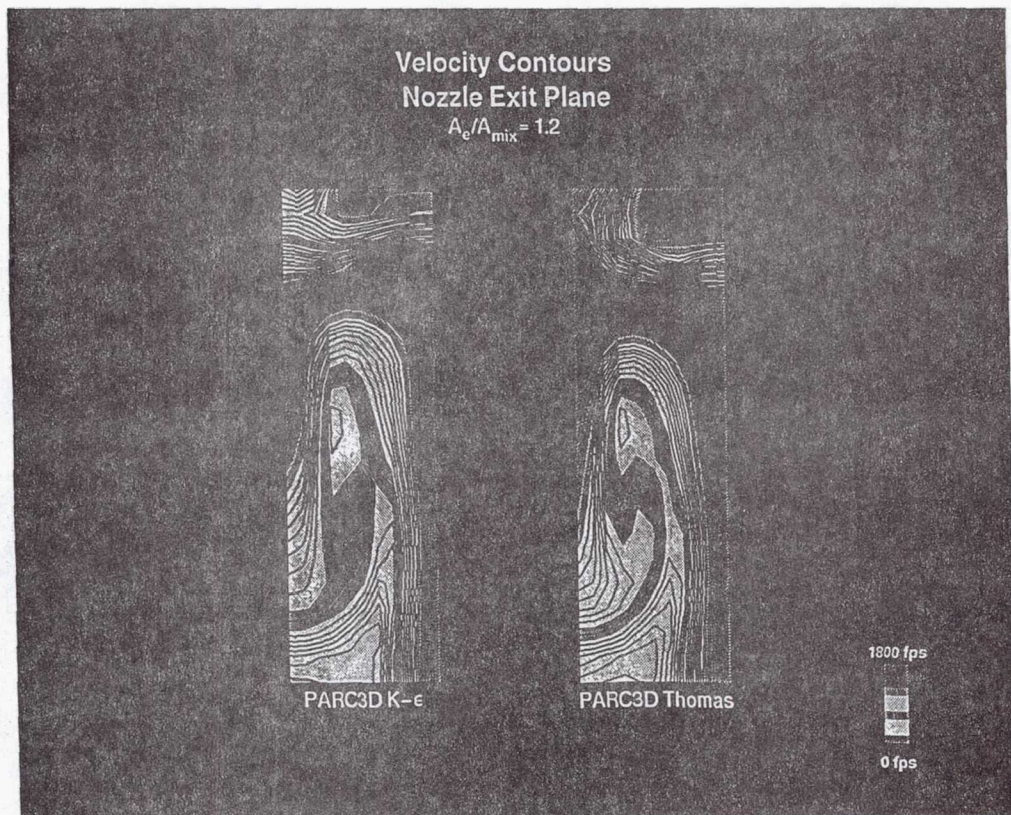
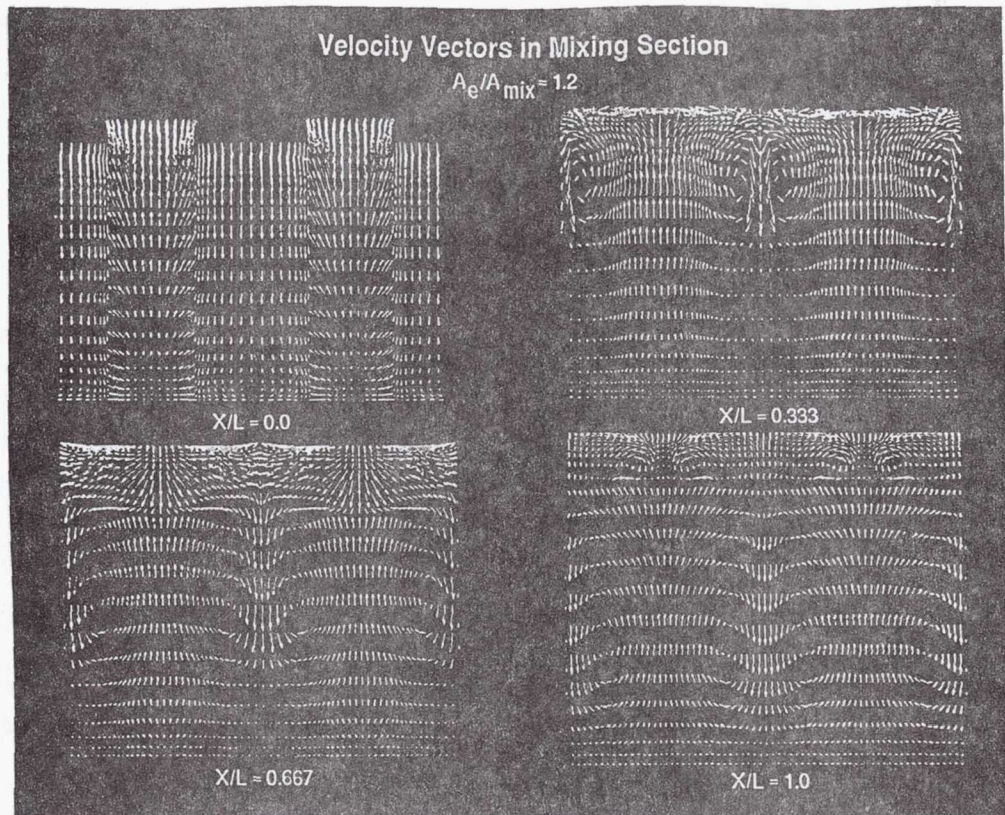


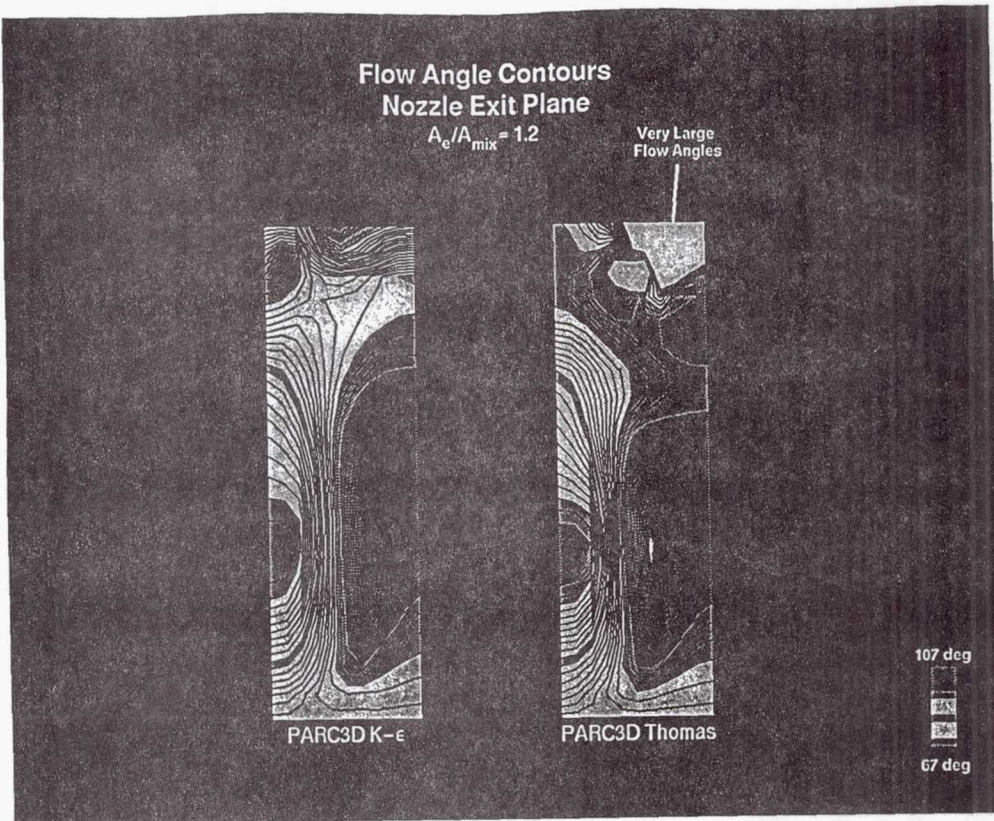
## NASA/GE 2DCD Mixer/Ejector Nozzle







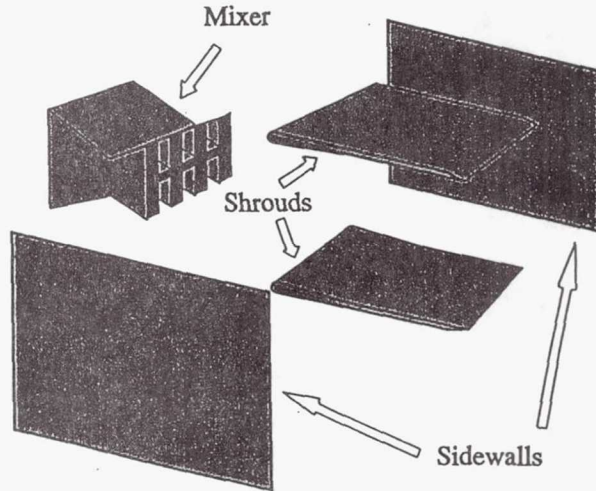




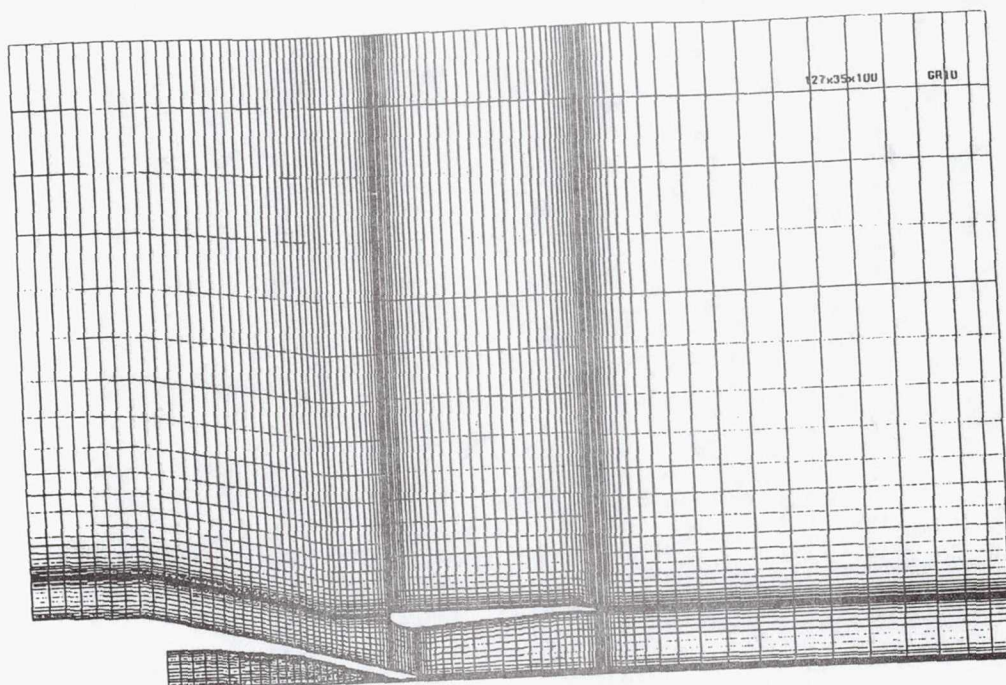
### Anatomy of the HSR P&W 2-D Mixer Ejector Nozzle

#### Inventory:

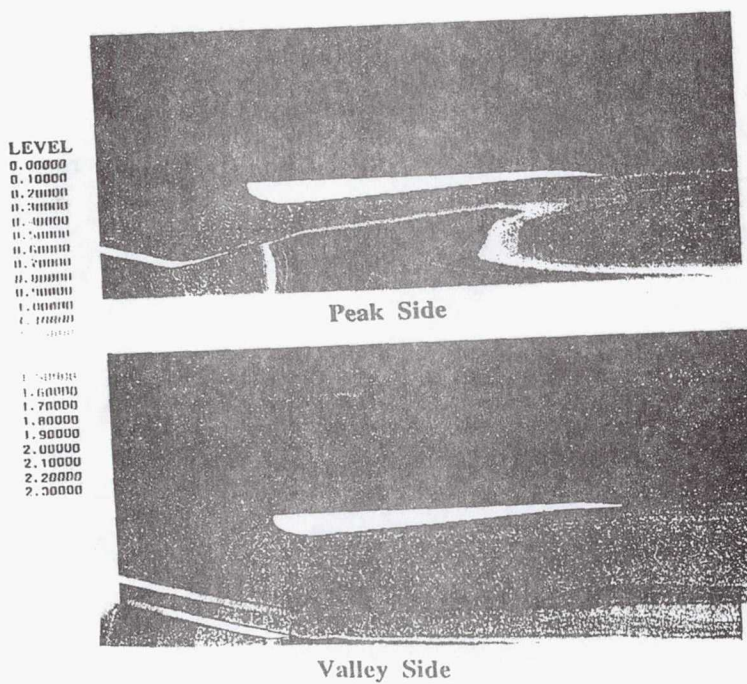
- 2 Mixer Designs
- 3 Shroud Lengths
- 3 Shroud/Sidewall Acoustic Treatments
- Sidewalls with Windows for Flow Visualization



### 3D COMPUTATIONAL GRID FOR NOZZLE FLOWFIELD

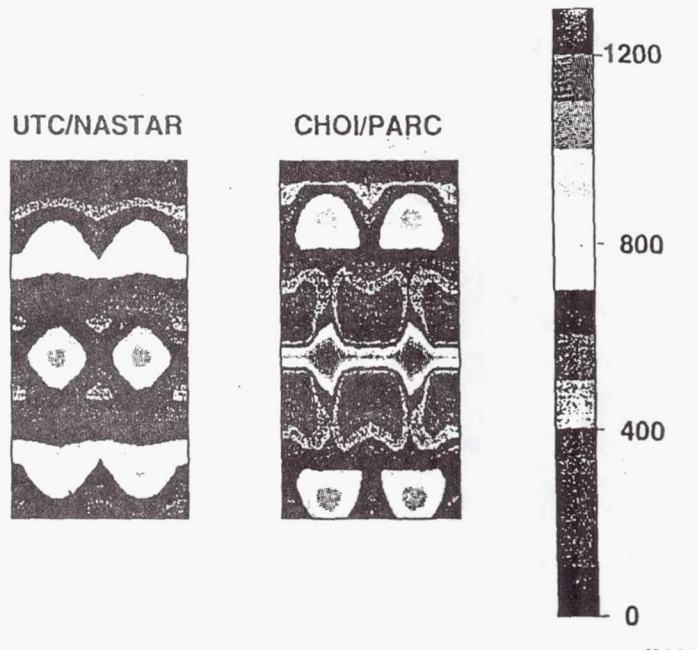


P&W MIXER/EJECTOR NOZZLE  
Mach Number Contours



## 2nd GENERATION MIXER EJECTOR ANALYSIS

Exit Plane Total Temperature



92-3-28-6

## Conclusions

- Algebraic models are inadequate for predicting mixer nozzle flowfields
- Two-equation model available in PARC3D give no improvement over algebraic models
- A reliable two-equation model is required in PARC3D for complex nozzle flows

**Page intentionally left blank**

## **Turbulence Modeling in Aircraft Icing**

**Mark G. Potapczuk  
Icing & Cryogenic Technology Branch**

**Workshop on Computational Turbulence Modeling  
NASA ICOMP  
September 15, 1993**

### **INTRODUCTION**

The Icing and Cryogenic Technology Branch develops computational tools which predict ice growth on aircraft surfaces and uses existing CFD technology to evaluate the aerodynamic changes associated with such accretions.

Surface roughness, transition location, and laminar, transition, or turbulent convective heat transfer all influence the ice growth process on aircraft surfaces.

Turbulence modeling is a critical element within the computational tools used both for ice shape prediction and for performance degradation evaluation.

## CURRENT CODE DEVELOPMENT

### 2D CODES

- LEWICE - POTENTIAL FLOW / INTEGRAL BOUNDARY LAYER
- LEWICE/IBL - POTENTIAL FLOW / INTERACTIVE BOUNDARY LAYER
- LEWICE/NS - NAVIER-STOKES, STRUCTURED GRID
- LEWICE/UNS - NAVIER-STOKES, UNSTRUCTURED GRID

### 3D CODES

- LEWICE3D - PANEL CODE / INTEGRAL BOUNDARY LAYER
- LEWICE3DGR - ANY GRID BASED FLOW SOLUTION

## ICE ACCRETION MODELING

### CURRENT MODEL USED FOR ICE GROWTH

- MASS AND ENERGY BALANCE IN CONTROL VOLUMES ALONG THE SURFACE
- CONVECTIVE HEAT TRANSFER IS MAJOR FACTOR IN ENERGY BALANCE
- INTEGRAL BOUNDARY LAYER FORMULATION USED TO DETERMINE LAMINAR AND TURBULENT HEAT TRANSFER COEFFICIENTS
- SURFACE ROUGHNESS MODELED AS SAND-GRAIN ROUGHNESS; ACTUAL ICE ROUGHNESS VARIES FROM SMALLER TO LARGER THAN BOUNDARY LAYER THICKNESS

## ICE ACCRETION MODELING

CONVECTIVE HEAT TRANSFER MODEL USED FOR ICE GROWTH

### SKIN FRICTION COEFFICIENT

$$\frac{c_f}{2} = 0.1681 \left[ \ln \left( \frac{864.0\theta_t}{k_s} + 2.568 \right) \right]^{-2}$$

WHERE

$$\theta_t(s) = \left[ \frac{0.0156}{V_e^{4.11}} \int_{s_{tr}}^s V_e^{3.86} ds \right]^{0.8} + \theta_l(s_{tr})$$

## ICE ACCRETION MODELING

CONVECTIVE HEAT TRANSFER MODEL USED FOR ICE GROWTH

### LAMINAR

$$h_l(s) = 0.296 \frac{\lambda}{\sqrt{V}} [V_e^{-2.88} \int_0^s V_e^{1.88} ds]^{-1/2}$$

### TURBULENT

$$h_t(s) = St \rho V_e c_p = \left[ \frac{c_f'/2}{Pr_t + \sqrt{c_f'/2} (1/St_k)} \right] \rho V_e c_p$$

## ICE ACCRETION MODELING

CONVECTIVE HEAT TRANSFER MODEL USED FOR ICE GROWTH

### ROUGHNESS STANTON NUMBER

$$St_k = 1.16 \left( \frac{V_r k_s}{V} \right)^{-0.2}$$

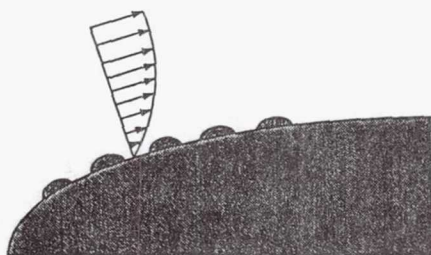
AND

$$V_r = V_e \sqrt{c_f / 2}$$

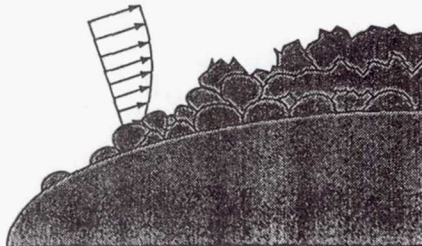
## ICE ACCRETION MODELING

ICE ROUGHNESS CHARACTERIZATION

### SAND-GRAIN ROUGHNESS



ACTUAL ICE ROUGHNESS



## ICE ACCRETION MODELING

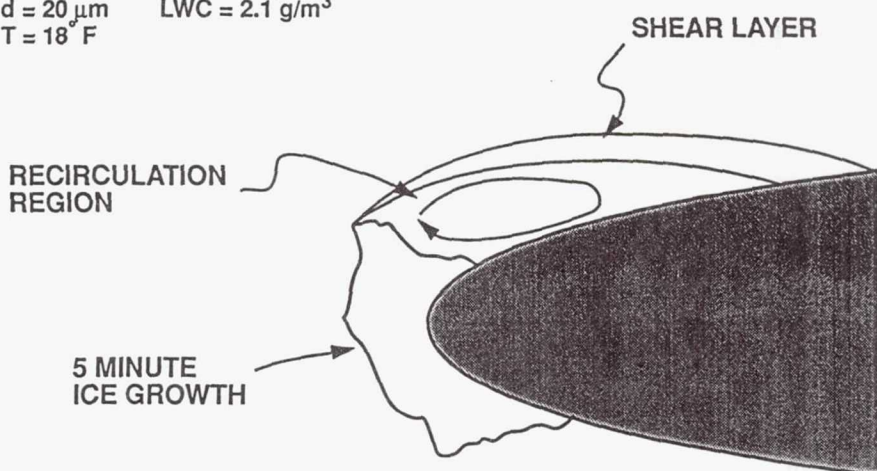
### PLANS

- EXPERIMENTS TO CHARACTERIZE ICE ROUGHNESS GEOMETRIES AT A VARIETY OF ICING CONDITIONS
- EXPERIMENTS TO CHARACTERIZE VELOCITY FIELD OVER REAL AND ARTIFICIAL ICE ROUGHNESS GEOMETRIES
- EXPERIMENTS TO MEASURE HEAT TRANSFER OVER REAL AND ARTIFICIAL ICE ROUGHNESS GEOMETRIES
- DEVELOPMENT OF MODIFIED COMPUTATIONAL MODEL BASED ON THESE EXPERIMENTS

## ICED AIRFOIL AERODYNAMICS

### NACA 0012 ICING CONDITIONS

$\alpha = 4^\circ$        $V = 130 \text{ mph}$   
 $d = 20 \mu\text{m}$        $LWC = 2.1 \text{ g/m}^3$   
 $T = 18^\circ \text{ F}$



## ICED AIRFOIL AERODYNAMICS

### BALDWIN-LOMAX TURBULENCE MODEL

#### Inner Layer

$$\mu_t \sim l^2 |(u_y - v_x)|$$

$l$  = mixing length

#### Outer Layer

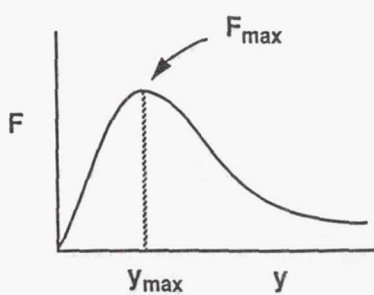
$$\mu_t \sim F_{max} Y_{max}$$

$$F(y) = y|\omega| (1 - \exp((-y^*)/A))$$

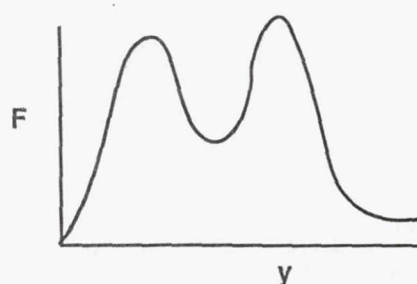
## ICED AIRFOIL AERODYNAMICS

### BALDWIN-LOMAX TURBULENCE MODEL

NORMAL B.L. F PROFILE



RECIRCULATION REGION  
F PROFILE



## ICED AIRFOIL AERODYNAMICS

### MML TURBULENCE MODEL

$$\mu_t = \rho l^2 \omega$$

WHERE

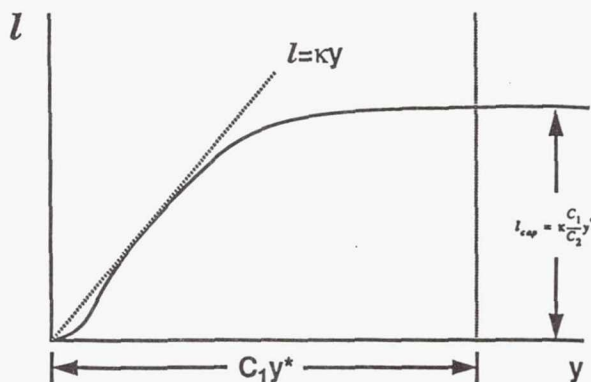
$$\frac{y + \Delta y}{y^*} < C_1 \quad l(y) = \kappa \frac{C_1}{C_2} y^* \left( 1 - \left( 1 - \frac{y^*}{C_1} \right)^{C_2} \right) \left( 1 - e^{-\frac{(y + \Delta y)/A^+}{y^*}} \right)$$

AND WHERE

$$\frac{y + \Delta y}{y^*} > C_1 \quad l(y) = \kappa \frac{C_1}{C_2} y^*$$

## ICED AIRFOIL AERODYNAMICS

### MML TURBULENCE MODEL



$$y^* = \frac{v}{u^*} = \frac{v}{\sqrt{\tau_w / \rho_w}}$$

## ICED AIRFOIL AERODYNAMICS

### MML TURBULENCE MODEL

THE CEBECI-CHANG ROUGHNESS MODEL IS ADDED TO THE TURBULENCE MODEL

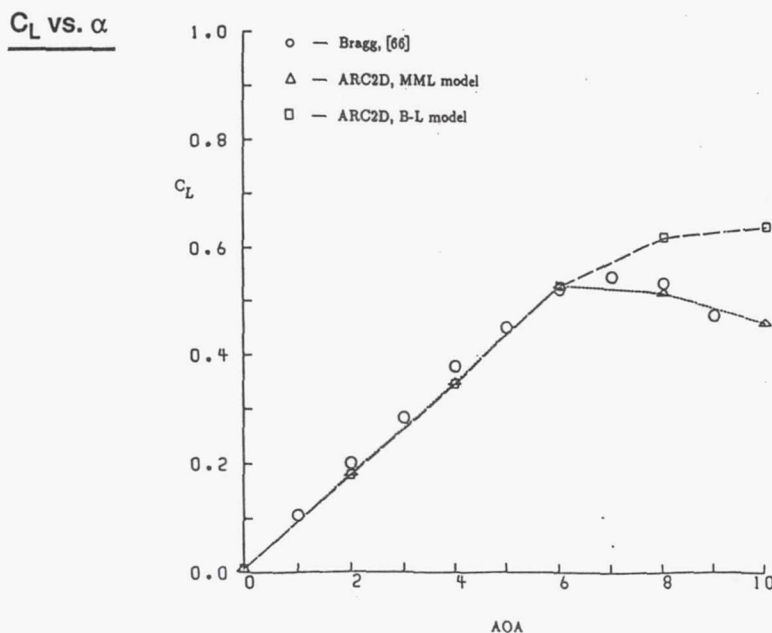
$$\Delta y^+ = \begin{cases} 0.9 \left[ \sqrt{k_s^+} - k_s^+ \exp\left(\frac{-k_s^+}{6}\right) \right] & 5 < k_s^+ \leq 70 \\ 0.7 (k_s^+)^{0.58} & 70 \leq k_s^+ \leq 2000 \end{cases}$$

WHERE,

$$\Delta y^+ = (\Delta y) (u_\tau/v) \quad \text{and} \quad k_s^+ = k_s (u_\tau/v)$$

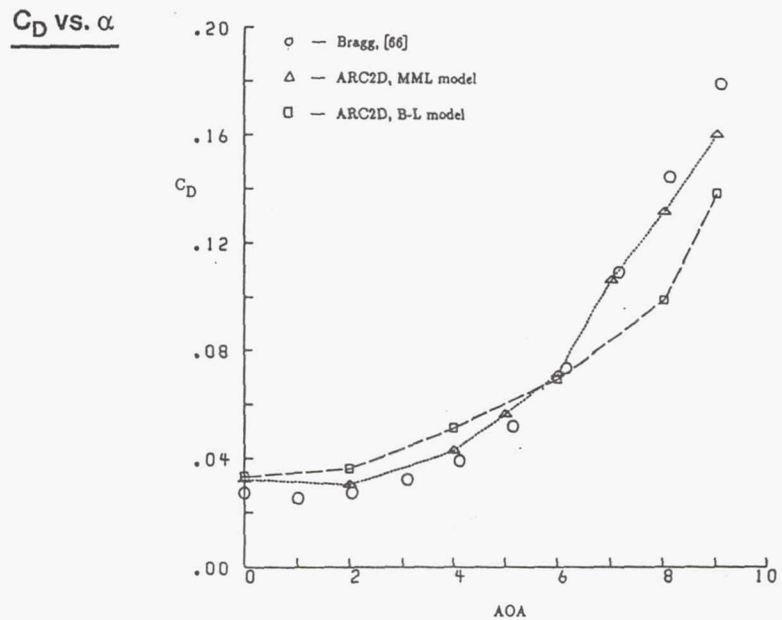
## ICED AIRFOIL AERODYNAMICS

### MML TURBULENCE MODEL



## ICED AIRFOIL AERODYNAMICS

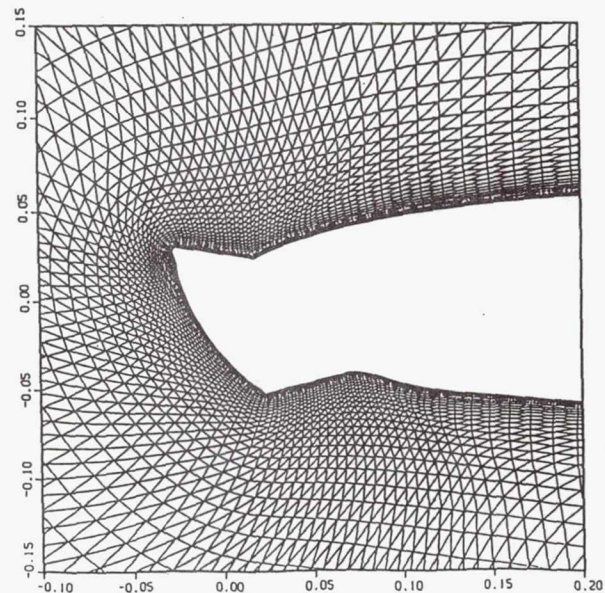
### MML TURBULENCE MODEL



## ICED AIRFOIL AERODYNAMICS

### MML TURBULENCE MODEL

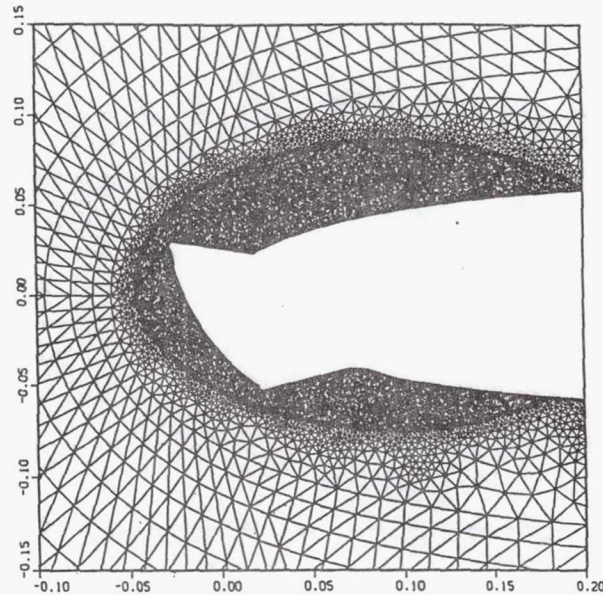
#### STRUCTURED GRID FOR ARTIFICIAL ICE SHAPE



## ICED AIRFOIL AERODYNAMICS

### MML TURBULENCE MODEL

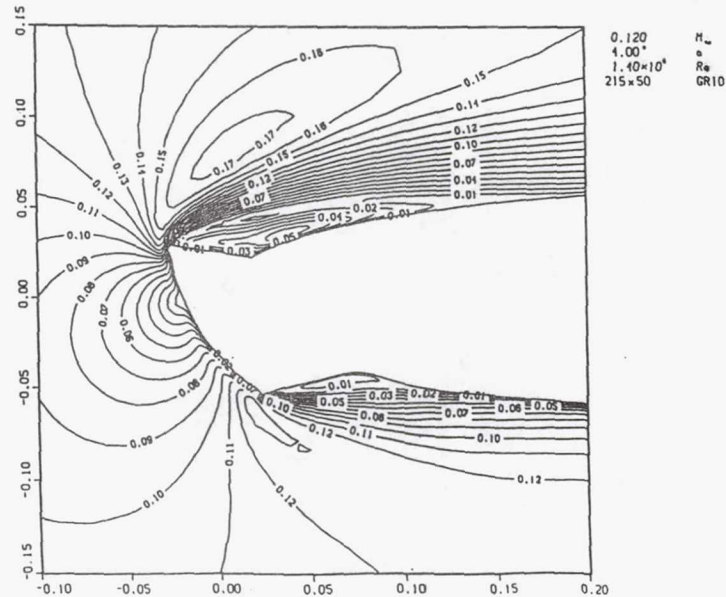
#### UNSTRUCTURED GRID FOR ARTIFICIAL ICE SHAPE



## ICED AIRFOIL AERODYNAMICS

### MML TURBULENCE MODEL

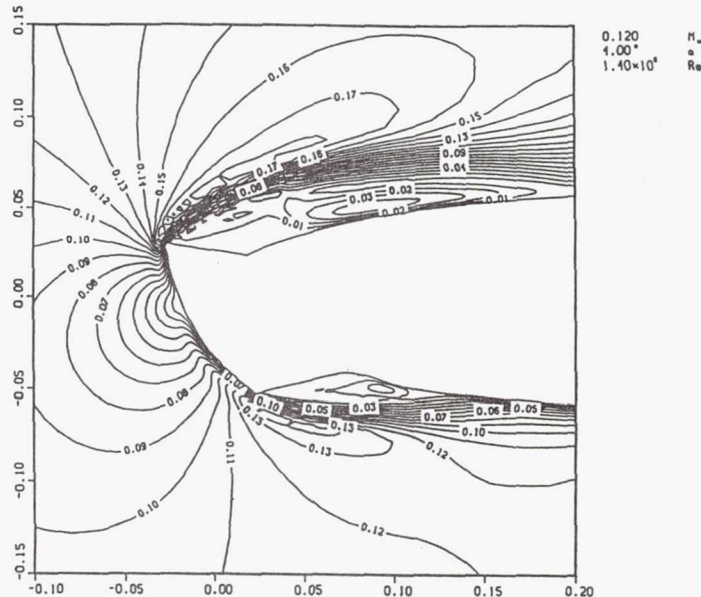
#### STRUCTURED GRID MACH NUMBER CONTOURS



## ICED AIRFOIL AERODYNAMICS

### MML TURBULENCE MODEL

#### UNSTRUCTURED GRID MACH NUMBER CONTOURS



#### CONCLUDING REMARKS

- TURBULENCE MODELING PLAYS A ROLE IN ICE GROWTH PREDICTION AND IN PERFORMANCE EVALUATION
- NEW MODELING IS REQUIRED FOR THE LARGE ROUGHNESS ELEMENTS OF A TYPICAL ICE ACCRETION
- AN EXPERIMENTAL PROGRAM IS CURRENTLY UNDERWAY TO DEVELOP A DATABASE FOR CREATION OF SUCH A MODEL
- AN ALTERNATE ALGEBRAIC TURBULENCE MODEL HAS BEEN USED TO EVALUATE PERFORMANCE DEGRADATION DUE TO ICING
- THE MML MODEL HAS BEEN USED IN AN UNSTRUCTURED GRID NAVIER-STOKES CODE TO CALCULATE FLOW OVER AN ARTIFICIAL ICE SHAPE

**Page intentionally left blank**

**Applied RNG Algebraic Turbulence Model for  
Three-Dimensional Turbomachinery Flows**

**K. R. Kirtley**

Sverdrup Technology, Inc. LeRC Group

and

Cambridge Hydrodynamics, Inc.

## What is RNG ?

Start  $\rightarrow$  Navier-Stokes

### RNG

- 1) Decompose velocity into low and high wave number components
- 2) Use perturbation theory to eliminate high wave number bands then renormalize spectrum and repeat to infrared cutoff
- 3) Correlations disappear through mode elimination procedure
- 4) Closure is automatic
- 5) Evaluate coefficients from high Re limit (fixed point) of perturbation expansion

Self Consistent

### Reynold's Averaging

- 1) Decompose velocity into mean and fluctuating components
- 2) Ensemble (time) average over entire spectrum
- 3) Correlations arise
- 4) Model correlations (Boussinesq)
- 5) Evaluate coefficients from generic flow data, e.g., wake, jet, etc.

Problem Dependent

Result  $\rightarrow$  effective viscosity

## RNG-Based Algebraic Model

$$\nu = \nu_0 \left[ 1 + H \left( \frac{a}{\nu_0^3} \epsilon \Lambda_f^{-4} - C_c \right) \right]^{\frac{1}{3}}$$

$$\epsilon = P = \nu S$$

where

$$S = \left( \frac{\partial u_i}{\partial x_j} + \frac{\partial u_j}{\partial x_i} - \frac{2}{3} \delta_{ij} \frac{\partial u_k}{\partial x_k} \right) \frac{\partial u_i}{\partial x_j}$$

$\Lambda_f$  = Infrared cutoff = top of the inertial range

resolvable  $< \Lambda_f <$  modelled

$a = .1186$  from  $-5/3$  spectral law

$C_c = \frac{200}{70}$  from  $a$  and the ultraviolet dissipation range cutoff

## How do you go from Fourier space to physical space ?

why  $2\pi$  of course.

$$\text{Integral scale, } L_f^i = \frac{2\pi}{\Lambda_f}$$

But we need a mixing length, therefore

$$\text{Assume } E = C_K \epsilon^{\frac{2}{3}} \Lambda^{-\frac{5}{3}} \quad C_K = 1.6075$$

$$\text{Integration from } \Lambda_f \text{ to infinity gives } k = \frac{3}{2} C_K \Lambda_f^{-\frac{2}{3}} \epsilon^{\frac{2}{3}}$$

$$\text{Assume in high Re limit } \nu = L_f^2 S^{\frac{1}{2}} = C_\mu \frac{k^2}{\epsilon}$$

$$\text{Then } L_f = \left( \frac{9}{4} C_\mu C_K^2 \right)^{\frac{3}{4}} \Lambda_f^{-1} = \frac{a^{\frac{1}{4}}}{2\pi} L_f^i$$

$$\text{Giving } \nu = \nu_0 \left[ 1 + H \left( \frac{\epsilon}{\nu_0^3} L_f^4 - C_c \right) \right]^{\frac{1}{3}}$$

## Attributes of the RNG-Based Model

### 1) The Heaviside function mimics:

#### a) Near wall damping

$$\nu = \nu_0 \quad \text{for all } y^+ \leq \frac{C_c^{\frac{1}{4}}}{\kappa} = 9.2$$

#### b) Intermittency

$$\nu = \nu_0 \quad \text{when} \quad \epsilon \leq \frac{C_c \nu_0^3}{L_f^4}$$

$\epsilon \rightarrow 0$  in the outer flow

#### c) Transition

See Next Slide

### 2) Energy-Based $\rightarrow$ Non-equilibrium effects can be included through clever manipulation of the dissipation rate

## A Neat Little Analysis

(following A. Kleut)

Argument of Heaviside is:

$$\frac{\mathcal{E} L_f^4}{\nu_0^3} - C_c$$

For equilibrium turbulence:

$$\mathcal{E} = \frac{C_w k^2}{\nu} = \frac{U_k^4}{\nu}$$

The Heaviside argument is then:

$$\frac{U_k^4 L_f^4}{\nu \nu_0^3} - C_c$$

Let  $L_f = .0845 \delta$  and  $C_c = 200$

If flow is initially laminar then  $\nu = \nu_0$

At what  $Re_x = \frac{U_0 x}{\nu}$  will the Heaviside argument be greater than zero, which is the start of the turbulent region?

$$U_k^2 \equiv U_0^2 \frac{1}{2} C_f$$

$$\text{so } \frac{1}{4} C_f^2 \frac{U_0^4}{\nu_0^4} (.0845 \delta)^4 \stackrel{?}{=} 200$$

$$\text{For laminar flow } C_f = .664 Re_x^{-1/2} \text{ and } \frac{\delta}{x} \approx 5 Re_x^{-1/2}$$

$$\text{Therefore } \frac{1}{4} (.664)^2 Re_x^{-3} Re_x^{-4} (.0845)^4 (\delta)^4 = 200$$

So transition is computed to begin at  $Re_x \approx 6 \times 10^4$ , which is less than two orders from low Tu data for a smooth flat plate. Couette flow calculation showed one order less than stability theory.

→ More work but promising ←

### Cubic vs. Quartic

$$\gamma^3 = \nu_0^3 \left[ 1 + H \left( \frac{\nu S L_f^4}{\nu_0^3} - C_c \right) \right]$$

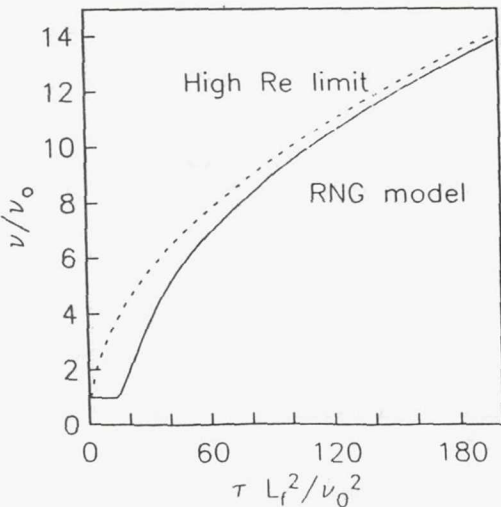
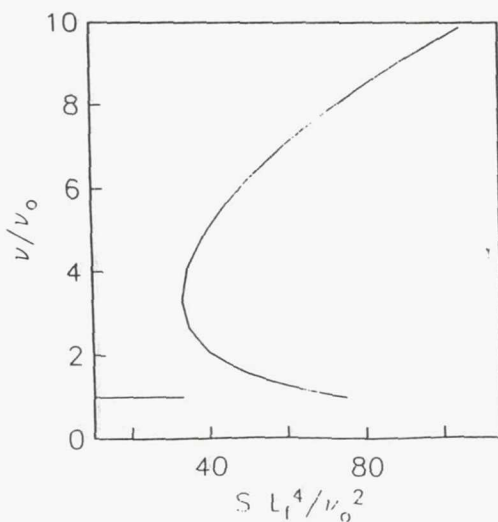
Good: Analytic Solution

Bad: Multivalued

$$\nu^4 - \nu \nu_0^3 - H \left( \tau^2 L_f^4 - \nu C_c \nu_0^3 \right) = 0$$

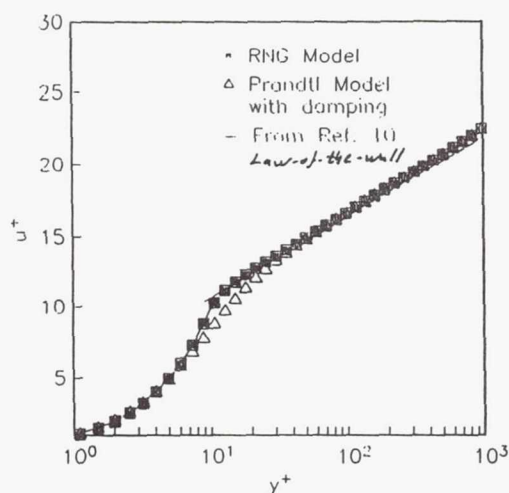
Single Valued

Highly Non-linear

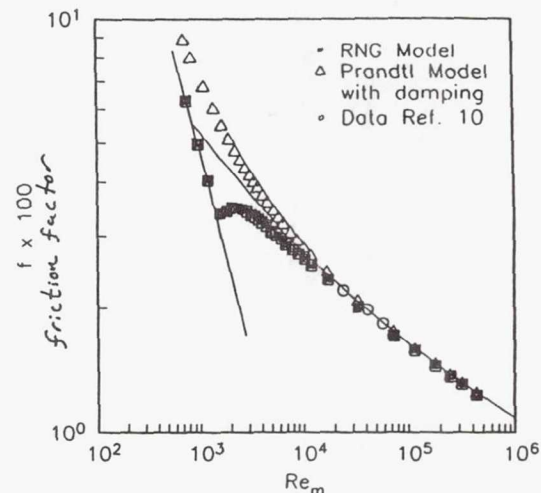


### Couette Flow

#### Near Wall Behavior



#### Friction Factor vs. Reynolds Number



## Turbulence Length Scales

In boundary layers

$$L_f = C_\mu \delta \tanh \left( \frac{\kappa n}{C_\mu \delta} \right)$$

*c. 4.*  
 $\kappa = 0.372$  and  $C_\mu = 0.0845$  from RNG

In wake region use Raj & Lakshminarayana correlation for

cascade wakes

$$L_f = \min(\kappa s, C_w b)$$

$$b = \delta_0 + c C_d^{\frac{1}{2}} 1.35 \left( \frac{s}{c} + 0.02 \right)^{0.58}$$

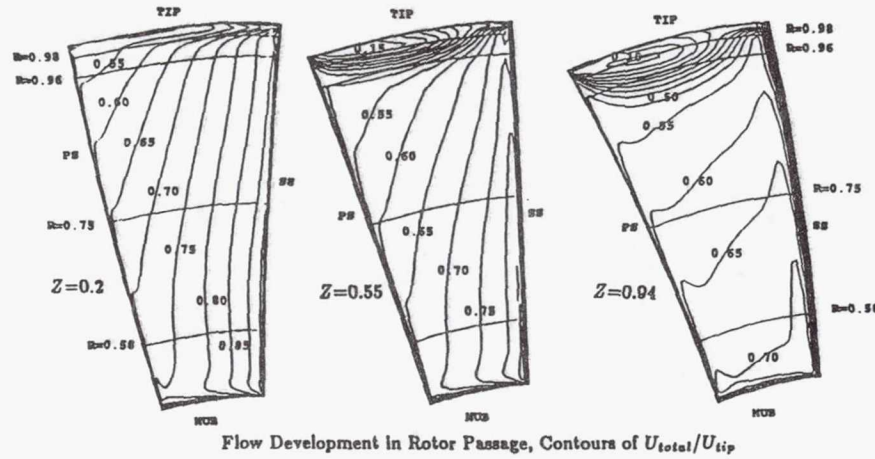
$C_d$  = coefficient of drag (assume 0.015)

$c$  = local chord

$\delta_0$  = ave. of s.s and p.s. trailing edge boundary layer thickness

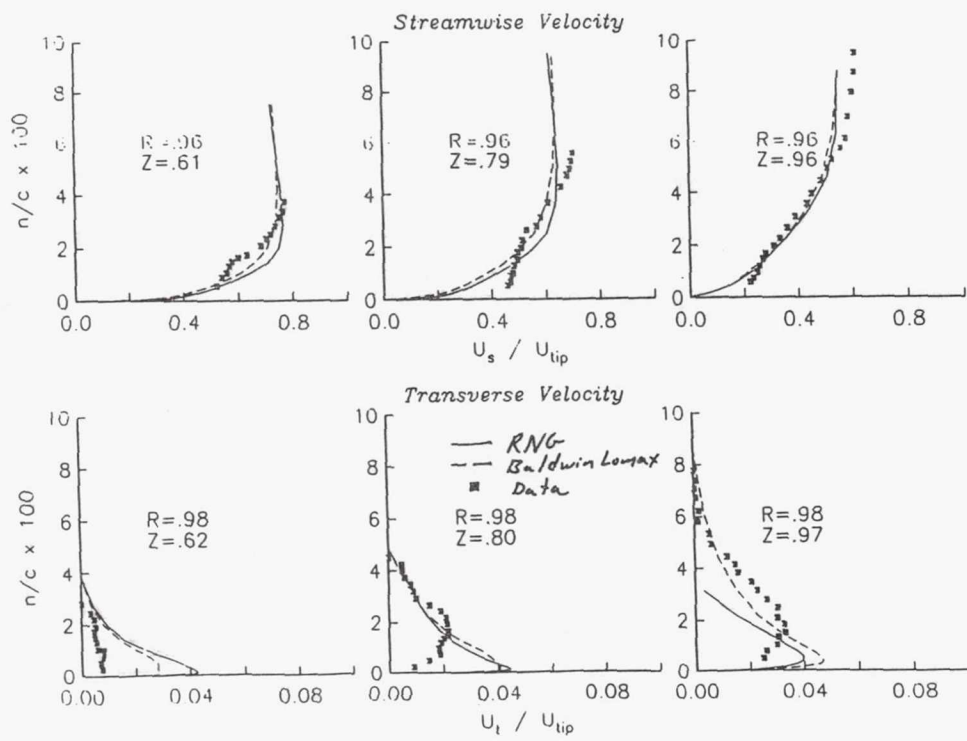
$C_w = 0.169$  from wake behind a circular cylinder

## Flow Development in Rotor Passage



$$\phi = \sqrt{\frac{m}{e}}$$

## PSU Low Speed Compressor



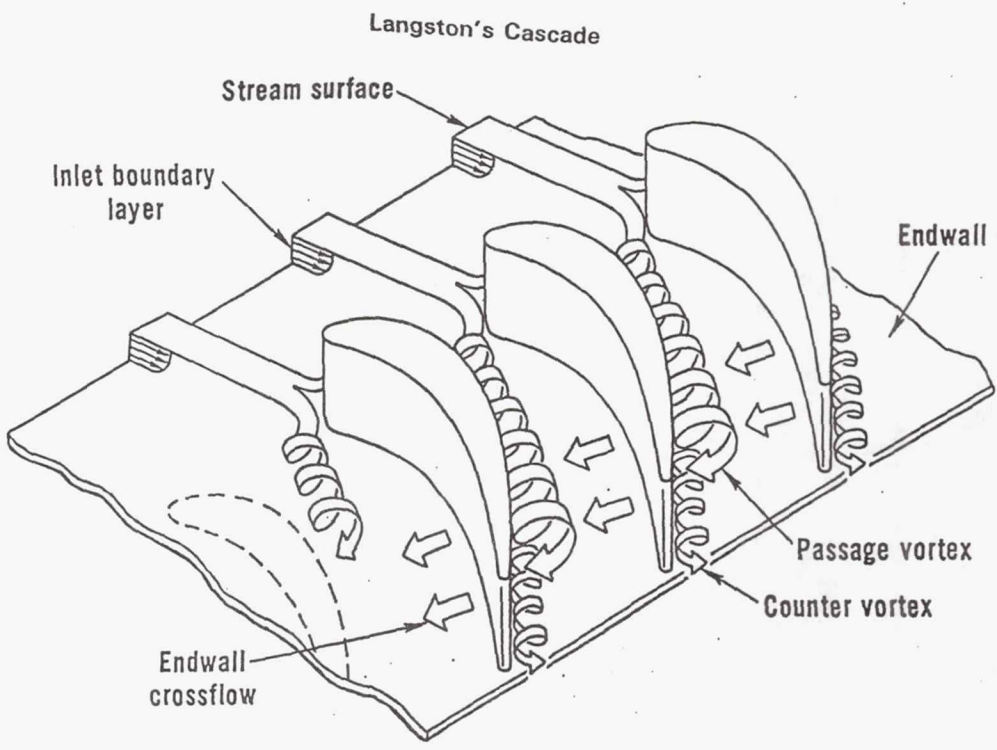
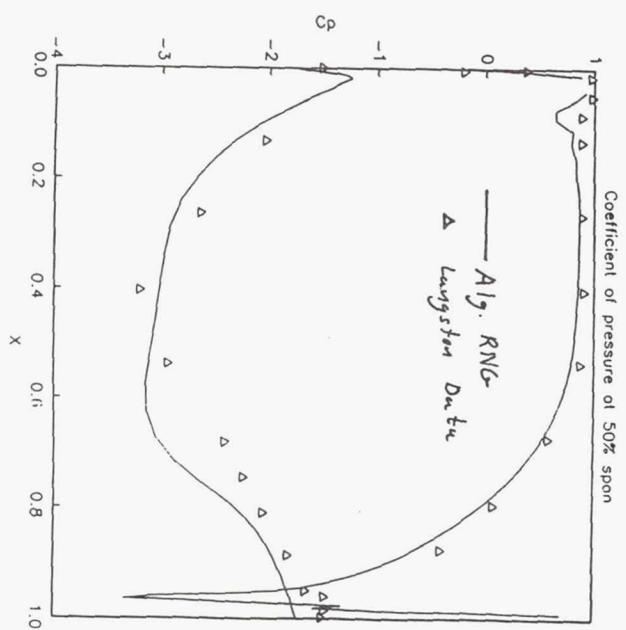
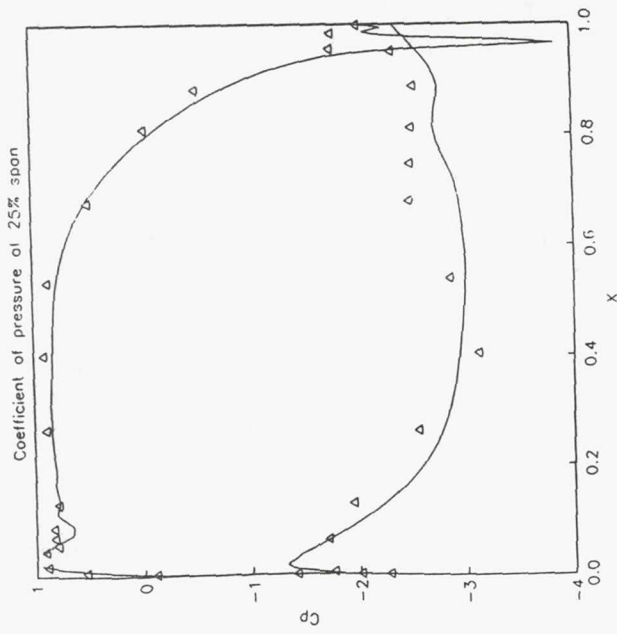
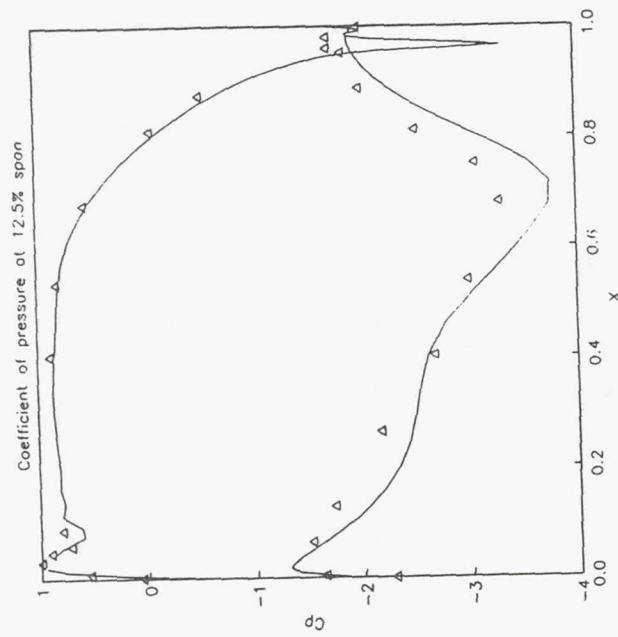
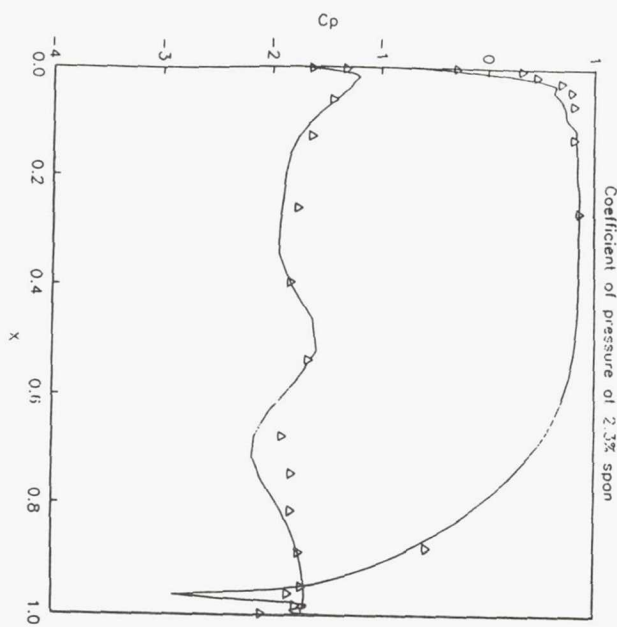


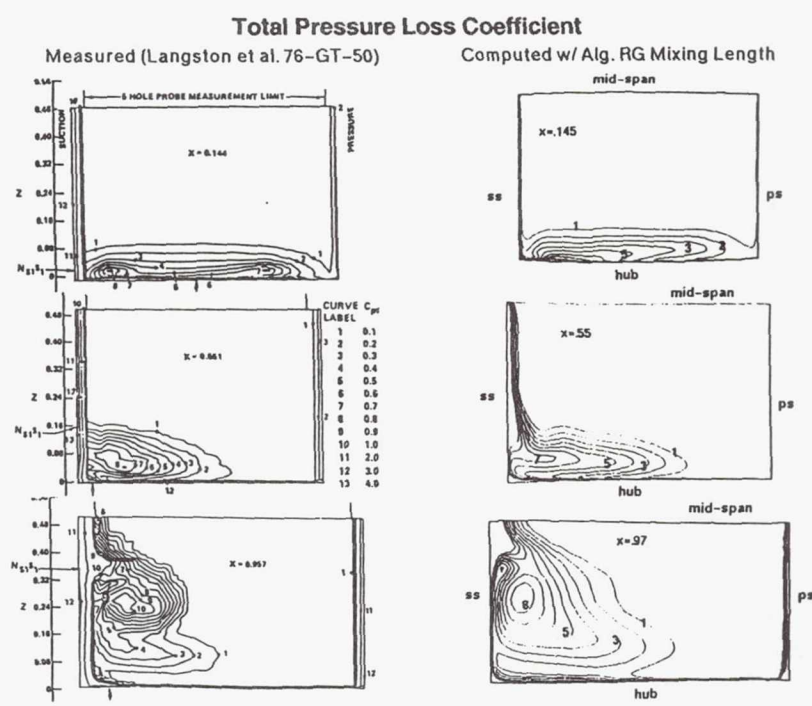
Figure 1







Coefficient of pressure at 2.3% span



### Hub Surface Static Pressure

Measured (Langston et al. 76-GT-50)

Computed w/ Algebraic RG Mixing Length

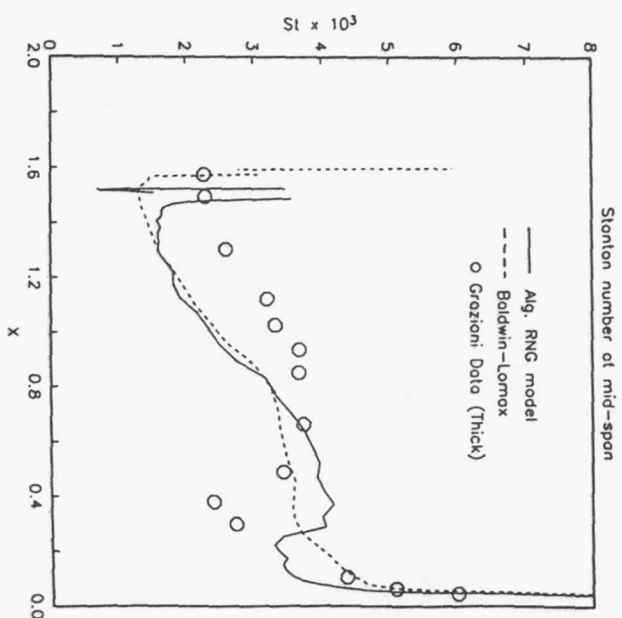
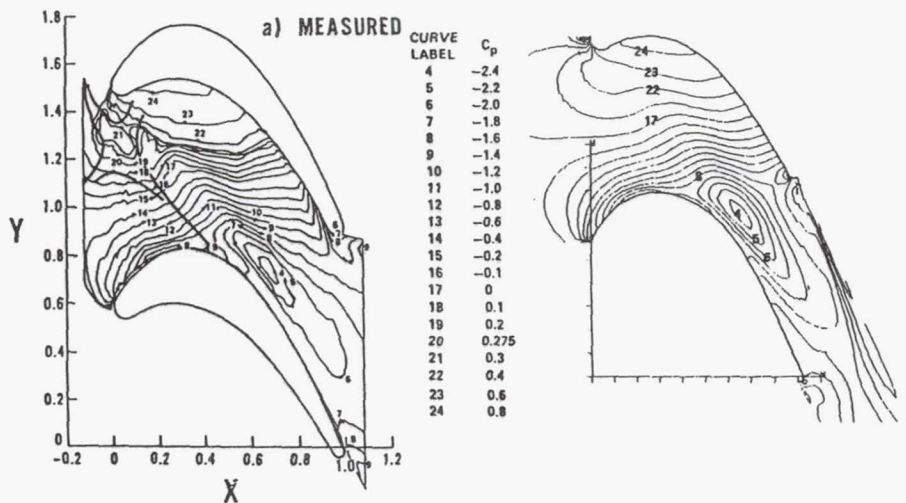


Figure 7

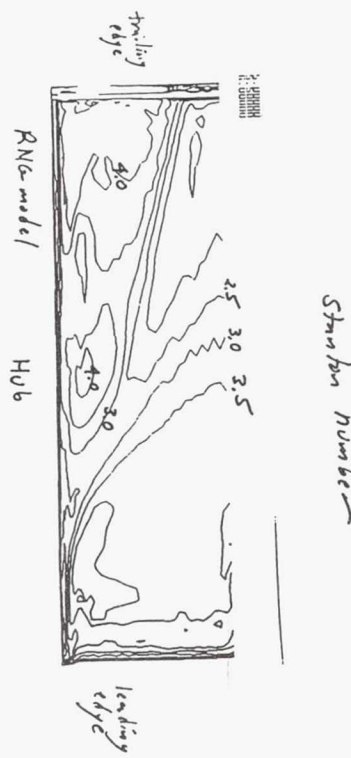
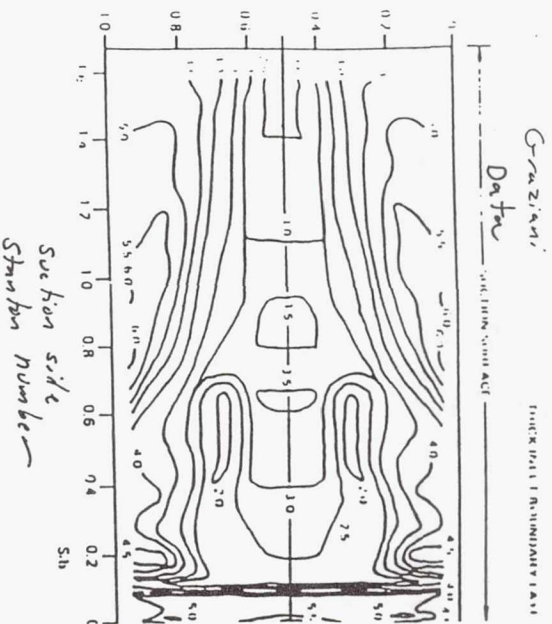


Fig. 8 Endwall Stanton number



## Conclusions

- RNG based algebraic model is a viable alternative to traditional algebraic models for complex flows.
- RNG model mimics transitions and near-wall damping through the Heaviside function
- Good boundary layer profiles, loss profiles, pressure loadings can be achieved for viscous dominated flows
- Stanton number predictions are not yet adequate when using the "plain vanilla" form of the model
- Work is needed to include non-equilibrium effects

**Page intentionally left blank**

**Applied k-e and Baldwin-Lomax Turbulence  
models for S-ducts**

**G.J. Harloff, Sverdrup Technology, Inc.  
LeRC Group, Brook Park, Ohio**

**September 16, 1993**

**Experimental contributions to paper by**

**B.A. Reichert, NASA Lewis Research Center  
Cleveland, Ohio**  
**S.R. Wellborn, Iowa State University  
Ames, Iowa**

## **Objectives**

**Provide CFD validation data with secondary flows**

**Predict and compare with experimental flow fields**

**Assess algebraic turbulence model**

**Compare algebraic and K -  $\varepsilon$  turbulence model results**

## **Introduction**

**Diffusing S-ducts common on aircraft:**

**727, L-1011, F-16, F-18**

**S-duct fabricated and tested**

**CFD: 3-D full Navier-Stokes, two turbulence models**

**Research extends previous PNS and FNS studies**

**Overall features qualitatively correct: total pressure  
velocity vectors, exit vortices**

**Boundary layer separation details generally  
not correct**

**Turbulence models and/or grid resolution usually  
cited for lack of agreement**

## **Code Selected: PARC3D**

**Originally ARC3D - Pulliam and Steger**

**Modified for internal flows - Cooper**

**Full 3-D Navier-Stokes equations in Reynolds (mass)  
average form**

**Beam-Warming approximate factorization**

**Multi-block for computer efficiency**

**Low Reynolds number K -  $\varepsilon$  turbulence model  
of Speziale employed - Nichols**

**Algebraic Baldwin-Lomax turbulence model**

## Boundary Conditions

No slip at wall

Total pressure and temperature specified at inlet

Static pressure specified at exit

Symmetry about x - z plane

$k = 0$  on wall

$$\epsilon = \frac{2\mu}{\rho} \left[ \left. \frac{d\sqrt{k}}{dy} \right|_{wall} \right]^2$$

$k, \epsilon$  : zeroth-order extrapolation at inlet,  
outlet, and centerline

## Nomenclature

$$C_{p_0} = \frac{p_0 - p_{wall}}{p_{0_{cl}} - p_{wall}} \quad C_p = \frac{p - p_{wall}}{p_{0_{cl}} - p_{wall}}$$

$$u^+ = \frac{u}{u^*} \quad y^+ = \frac{u^* y}{v}$$

$$u^* = \sqrt{\frac{T_w}{\rho_w}} \quad c_f = \frac{T_w}{\frac{1}{2} \rho_{cl} U_{cl}^2}$$

## Duct Test Conditions and Geometry

$$Re = 2.6 \times 10^6$$

$$M_1 = 0.6$$

$$D_1, D_2 = 8.04, 9.90 \text{ in}$$

$$\frac{A_2}{A_1} = 1.52$$

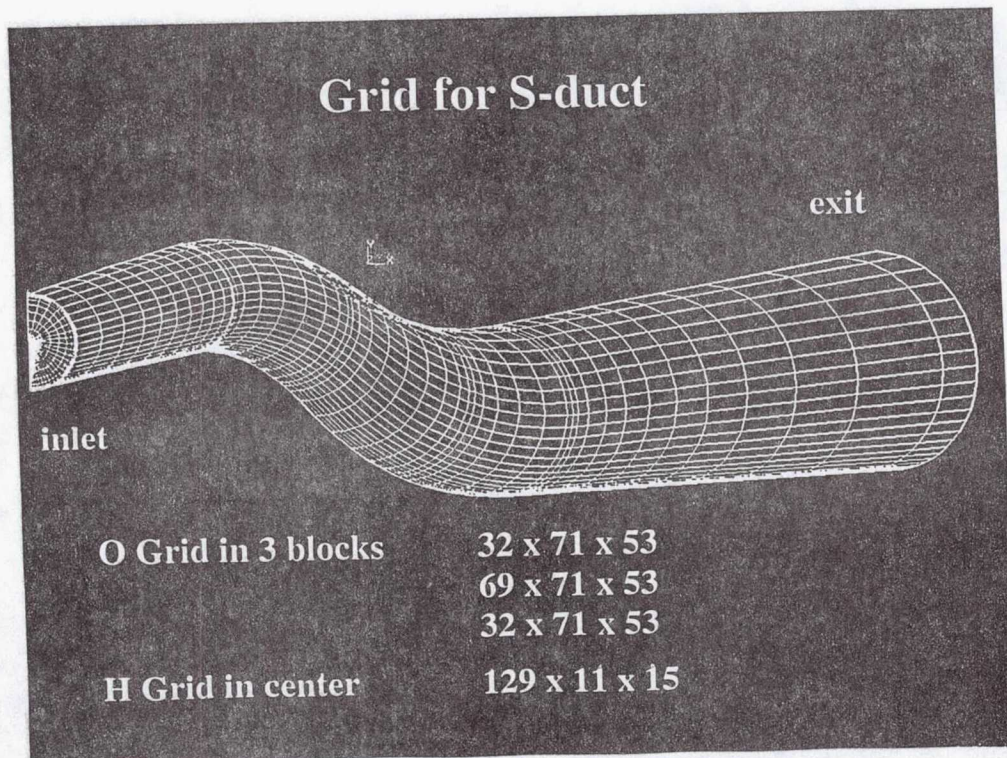
$$R = 40.2 \text{ in}$$

$$\theta_{\max}/2 = 30^\circ$$

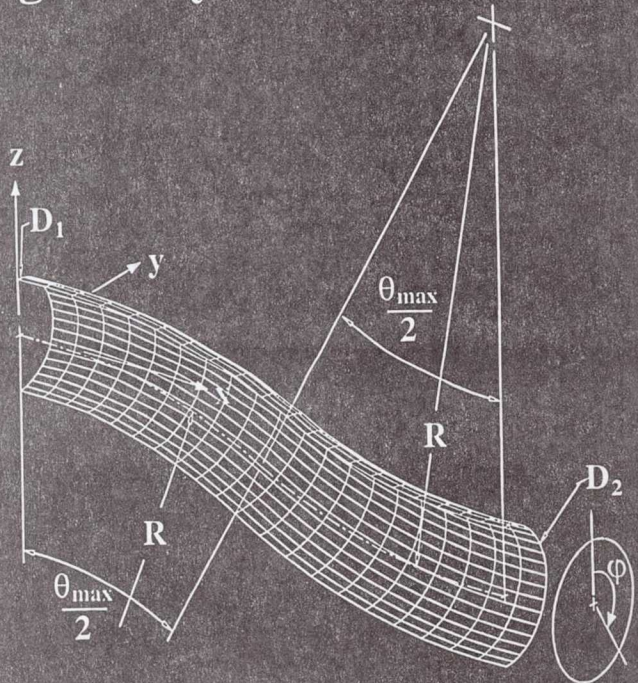
measurement planes S/D<sub>1</sub> = -0.5, 5.73

upstream and downstream pipes = 3.75D<sub>1</sub>

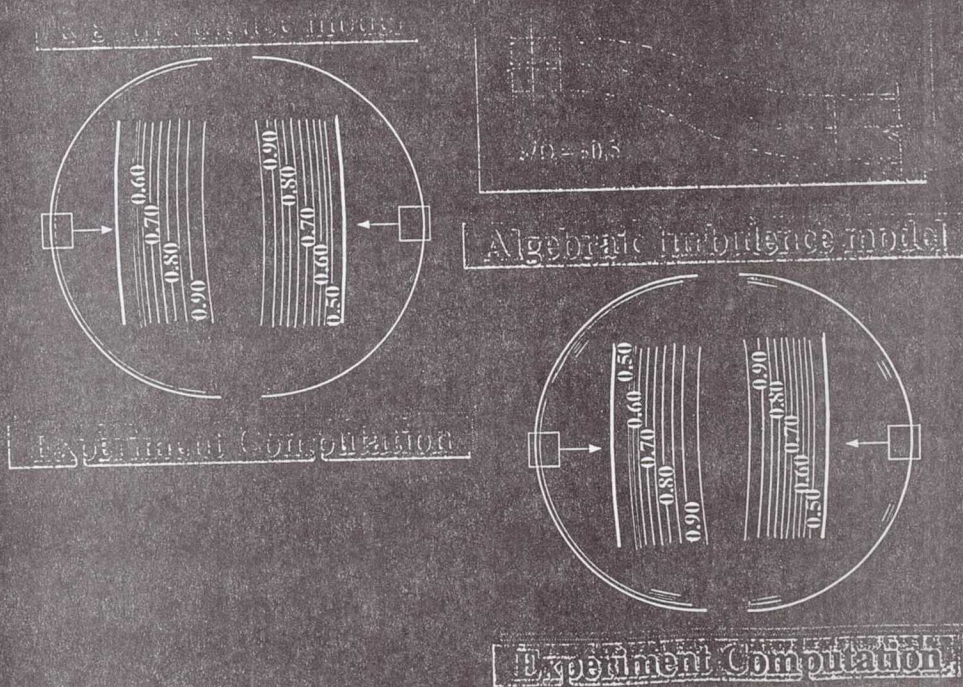
## Grid for S-duct



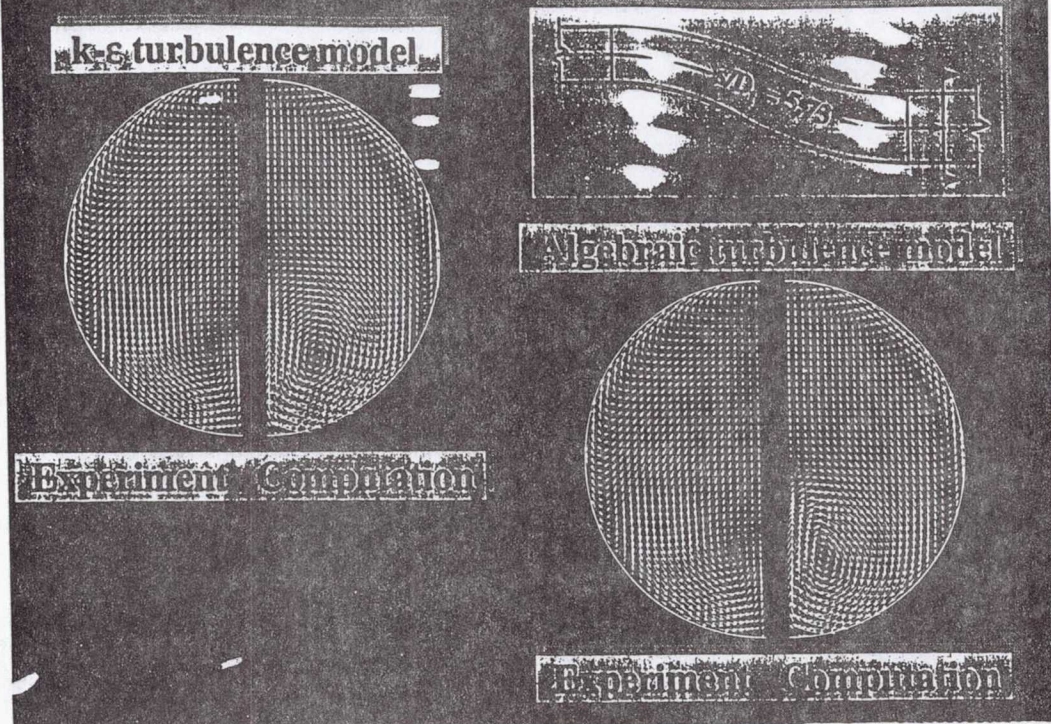
## The geometry of the diffusing S-duct



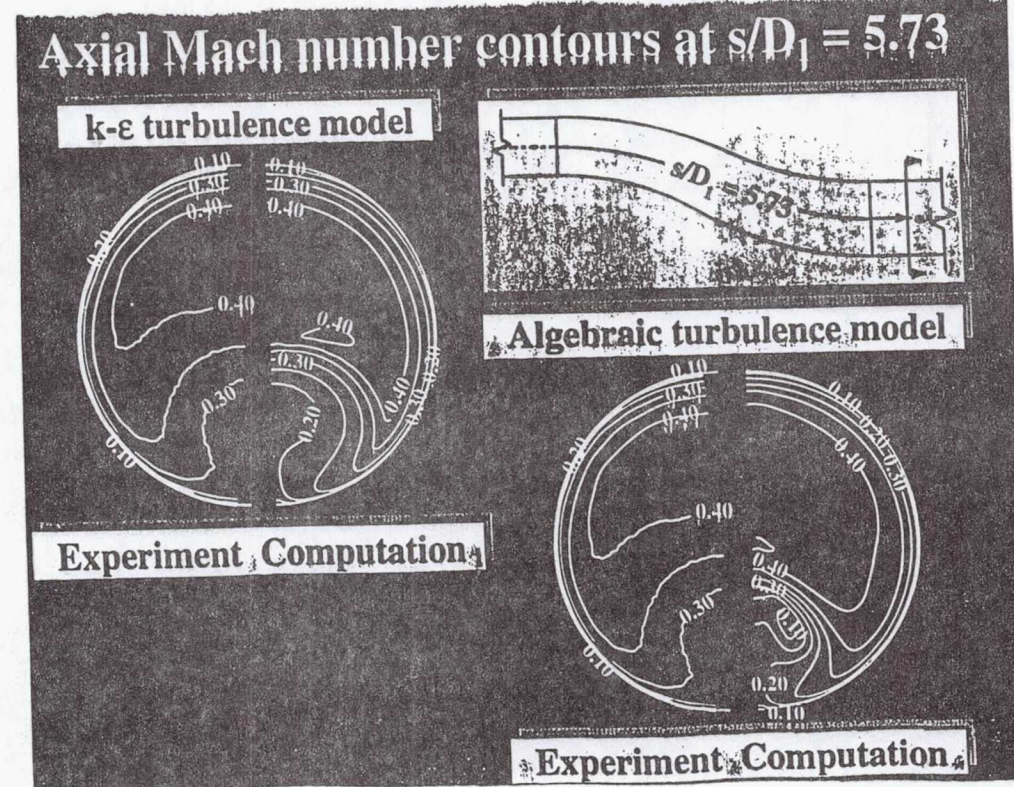
## Total pressure contours at $s/D_1 = -0.5$



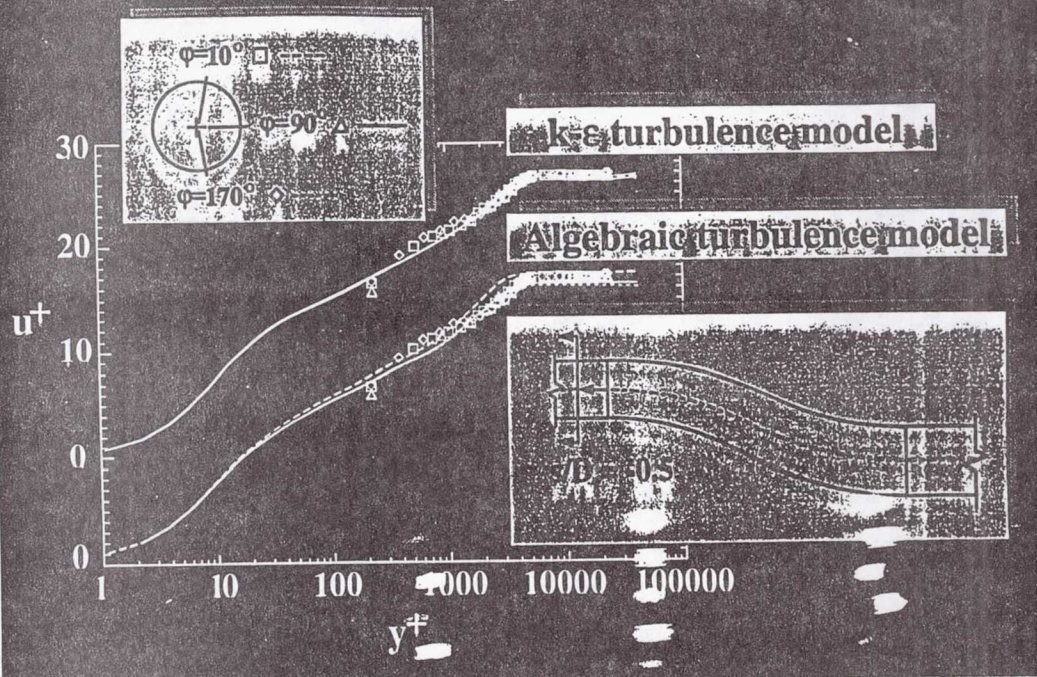
## Transverse velocity components at $s/D_1 = 5.73$



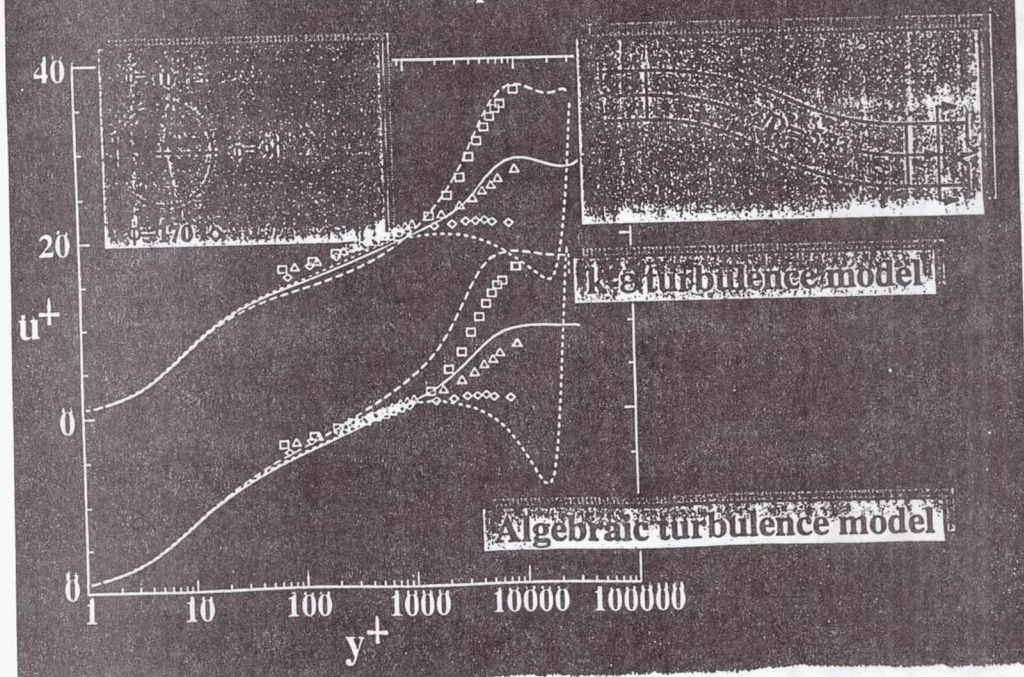
## Axial Mach number contours at $s/D_1 = 5.73$



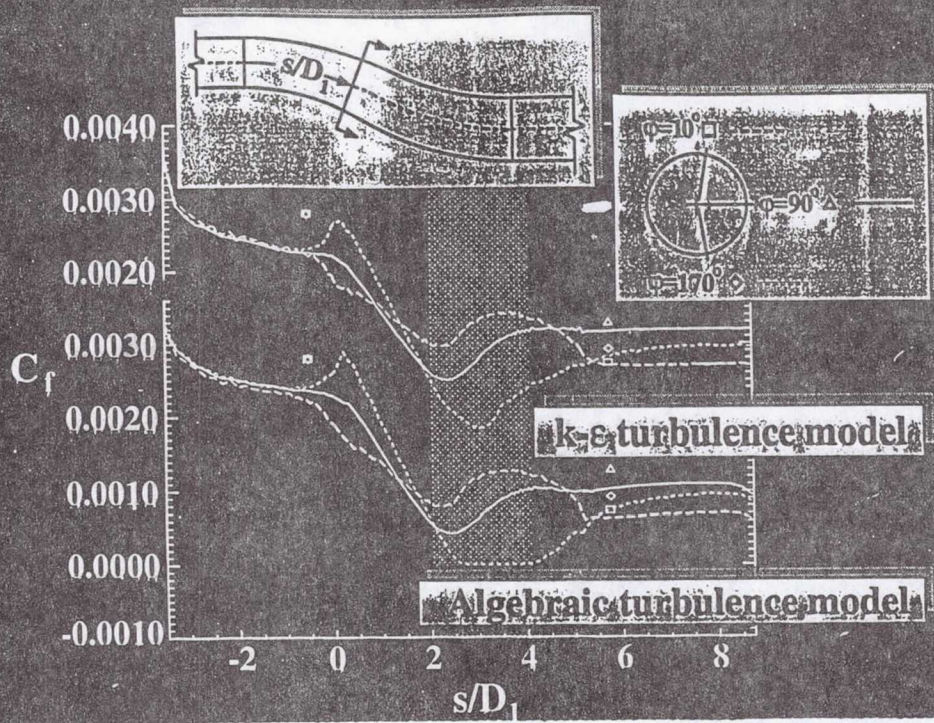
**Boundary layer wall coordinate plots  
at  $s/D_1 = -0.5$**



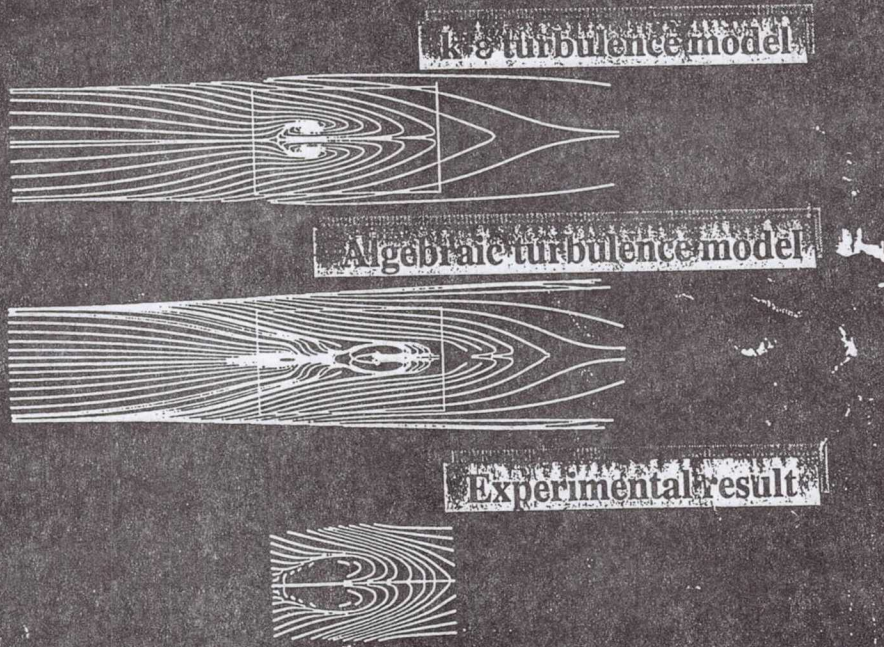
**Boundary layer wall coordinate plots  
at  $s/D_1 = 5.73$**



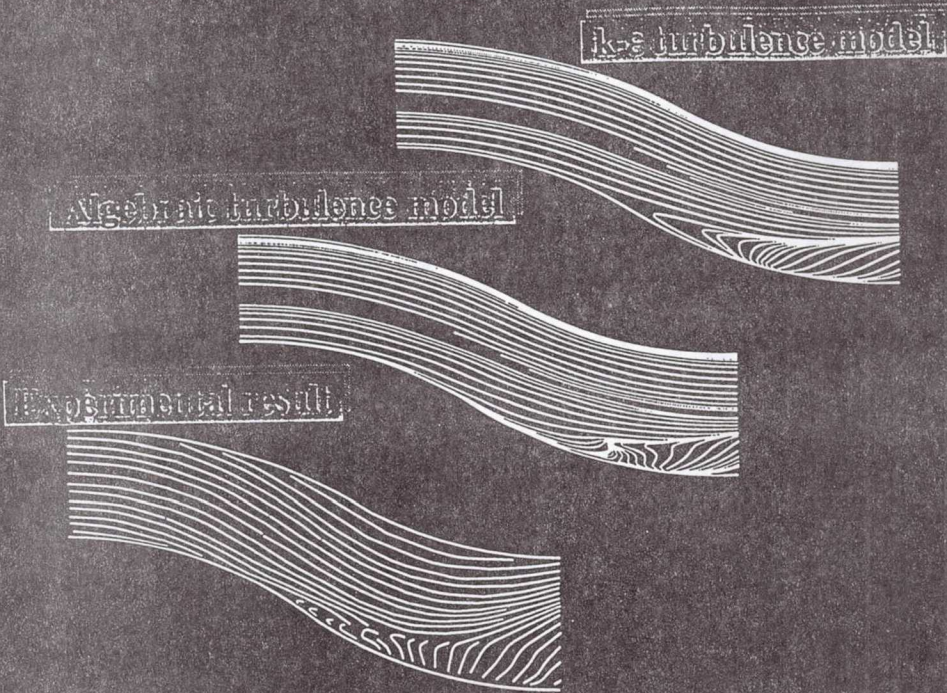
## Axial skin friction coefficient



## Streamlines near the S-duct surface



## Streamlines along S-duct centerline



## Conclusions

Computed flow fields agree reasonably well with  
experimental flow field

K -  $\varepsilon$  turbulence model better predicts pressure field  
than algebraic model

Both models underpredict length, angular extent  
and axial location of boundary layer separation

Possible causes include: inappropriate artificial/  
computed viscosity, especially in separated region

Improvements are needed to account for strong  
secondary flows with separation

**Page intentionally left blank**

## **Proteus Experience with the Modified MML Turbulence Model**

**Julianne Conley  
NASA Lewis Research Center**

*The Workshop on Computational Turbulence Modeling  
NASA Lewis Research Center  
September 15-16, 1993*

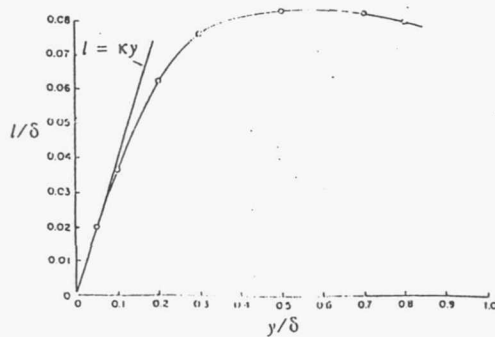
## Overview

- Background
- Modification of MML Turbulence Model
- Test Cases
- Concluding Remarks

## Background

- Based on original MML model of Potapczuk (1989)
- Simple model for flows where Baldwin Lomax model falls short
- Based on Prandtl's mixing length theory:

$$\mu_t = \rho l^2 |\omega|$$



- MML model:

$$l = \kappa \frac{C_1}{C_2} y^* \left( 1 - \left( 1 - \frac{y^+}{C_1} \right)^{C_2} \right) \left( 1 - e^{\left( -\frac{y^+}{A^+} \right)} \right), \quad y^+ < C_1$$

$$l = \kappa \frac{C_1}{C_2} y^*, \quad y^+ > C_1$$

$$y^* = \frac{\mu}{\sqrt{\rho |\tau_w|}}$$

$$y^+ = \frac{y}{y^*}$$

### Modification of the MML Turbulence Model

*Step 1:* Get good estimate of  $\tau_w$

*Step 2:* Evaluate and modify MML for zero pressure gradient boundary layer flows

*Step 3:* Modify model for an adverse pressure gradient flow

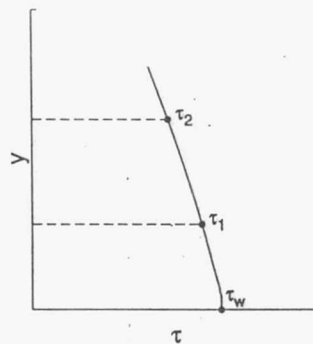
*Step 4:* Combine all features into one general model (MMLPG)

**Step 1: Get good estimate of  $\tau_w$**

$$\tau_w = \mu \frac{\partial u}{\partial y} \Big|_w$$

Global approach -- use momentum equation and 2 interior grid points

$$\frac{\partial \tau}{\partial y} \Big|_w = \frac{\partial p}{\partial x} \Big|_w$$



$$\tau = ay^2 + by + c$$

$$a = \frac{\tau_1 - \tau_2 - b(y_1 - y_2)}{y_1^2 - y_2^2}, \quad b = \frac{\partial p}{\partial x} \Big|_w$$

$$c = \frac{1}{2} (\tau_1 + \tau_2 - a(y_1^2 + y_2^2) - b(y_1 + y_2))$$

$$\Rightarrow \tau_w = c$$

$$\tau = \mu_{total} \left( \frac{\partial u}{\partial y} + \frac{\partial v}{\partial x} \right)$$

Use local average of  $\tau_w$  to avoid large values of  $y^*$  near separated regions:

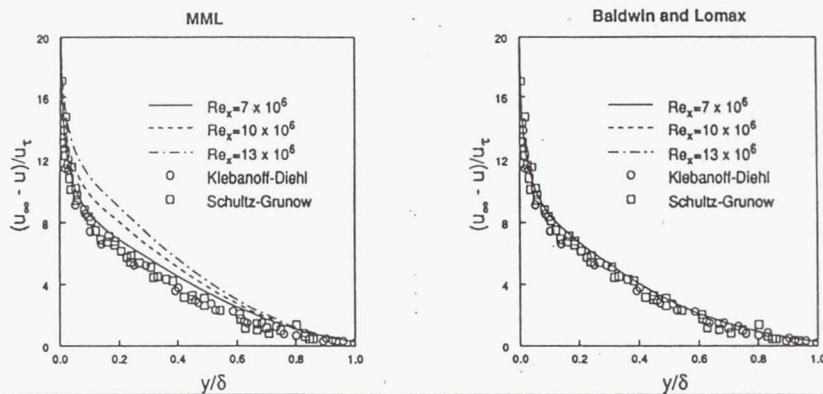
$$|\tau_i| = 0.1|\tau_{i-2}| + 0.2|\tau_{i-1}| + 0.4|\tau_i| + 0.2|\tau_{i+1}| + 0.1|\tau_{i+2}|$$

**Step 2: Evaluate and modify MML for zero pressure gradient boundary layer flows**

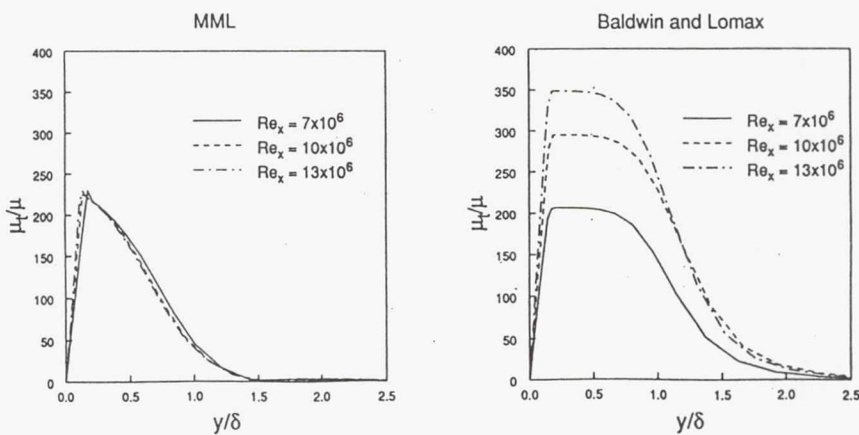
Outer length scale:  $l = \kappa \frac{C_1}{C_2} y^*, \quad y^+ > C_1$

Doesn't allow boundary layer thickness to grow properly.

Velocity Defect Profiles for Flow over a Flat Plate



Turbulent Viscosity for Flow over a Flat Plate



Found optimum  $C_1$  at each  $Re_x$ :

$$l_{inner}^+ = \kappa y^+ \left( 1 - e^{\left( -\frac{y^+}{A^+} \right)} \right), \quad y^+ < C_1$$

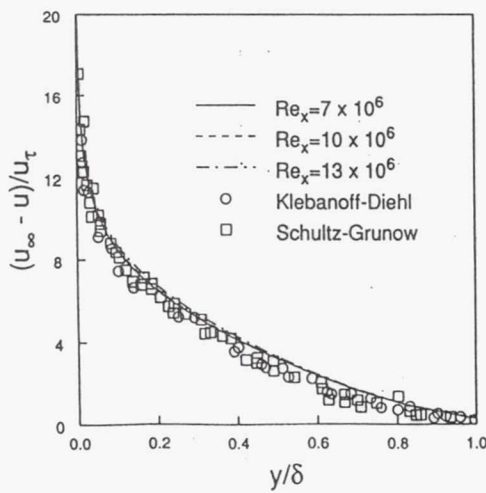
$$l_{cap}^+ = \kappa C_1 \left( 1 - e^{\left( -\frac{C_1}{A^+} \right)} \right), \quad y^+ > C_1$$

Found  $l_{cap}^+ = fcn(c_f)$

$$l_{cap}^+ = 1860 - (6.20 \times 10^5) c_f$$

$$l^+ = \min(l_{inner}^+, l_{cap}^+)$$

#### Velocity Defect for Flow over a Flat Plate



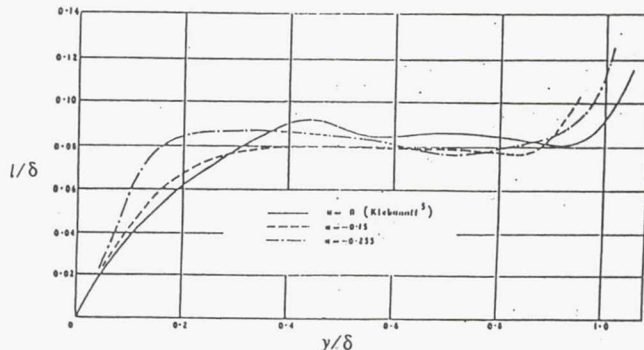
**Step 3: Modifications for adverse pressure gradient flow**

**Benchmark test cases:** Equilibrium boundary layer flows  
(P. Bradshaw, 1966)

$$U_{\infty} \propto x^{\alpha}, \quad \beta = \frac{\delta_1}{\tau_w} \frac{\partial p}{\partial x} = \text{constant}$$

$$\alpha = 0, -0.15, -0.255 \quad \beta = 0, 1, 5$$

Mixing Length



Note:

- $\frac{l_{cap}}{\delta} = 0.08$
- $\frac{C_1}{\delta} = 0.4$
- Slope increases with increasing pressure gradient

Combining with Blending Function:

$$l^+ = \kappa C_3 \frac{C_1}{C_2} \left( 1 - \left( 1 - \frac{y^+}{C_1} \right)^{C_1} \right) \left( 1 - e^{-\left(\frac{y^+}{A^+}\right)} \right), \quad y^+ < C_1$$

$$l^+ = \kappa C_3 \frac{C_1}{C_2} y^+, \quad y^+ > C_1$$

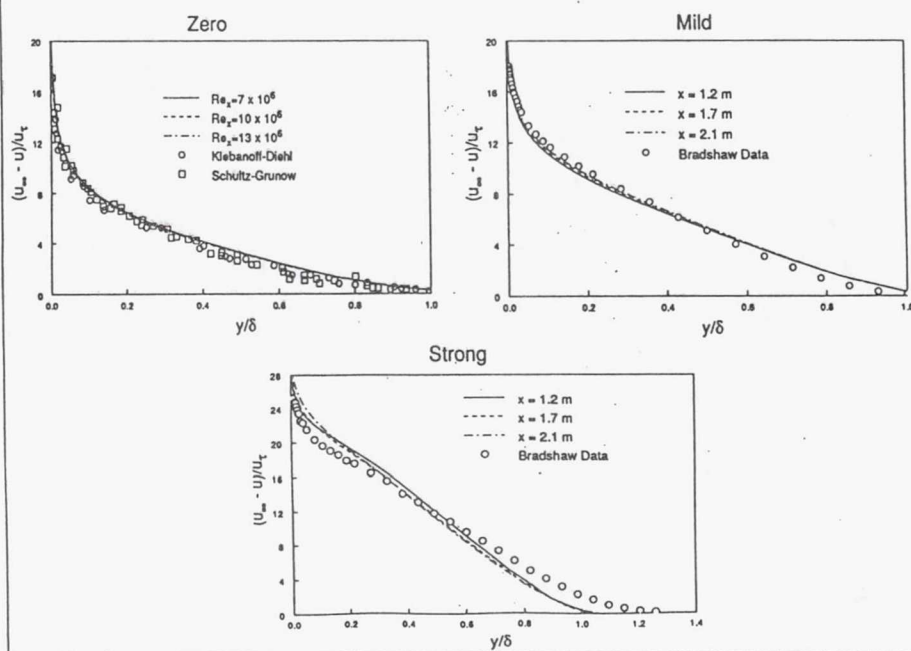
$$C_1 = 0.4 C_4, \quad C_2 = 5 C_3 \kappa$$

$$C_3 = fcn(\beta) \quad C_4 = fcn(\beta, c_f)$$

$$C_4 = C_5 + C_6 c_f$$

Strength of pressure gradient	$\beta$	$C_3$	$C_5$	$C_6$
zero	0	1.00	23,300	-7.75x10 <sup>6</sup>
mild	1	1.25	30,100	-1.16x10 <sup>7</sup>
strong	5	1.53	33,800	-2.09x10 <sup>7</sup>

Velocity Defect Profiles -- Adverse Pressure Gradient Flow



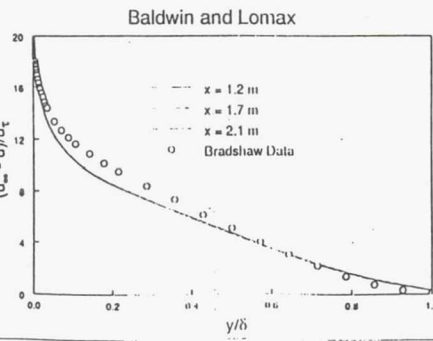
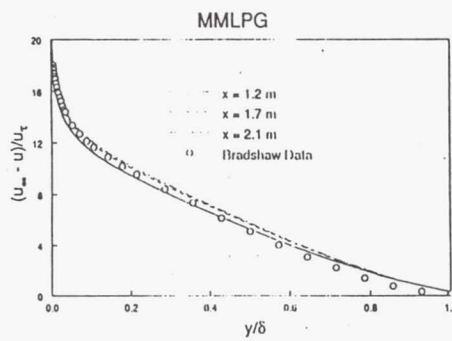
**Step 4:** Combine to get one general model, MMLPG

$$\left. \begin{array}{l}
 C_3 = 1.0 \\
 C_5 = 23, 300 \\
 C_6 = -7.75 \times 10^6
 \end{array} \right\} \beta < 0.0$$
  

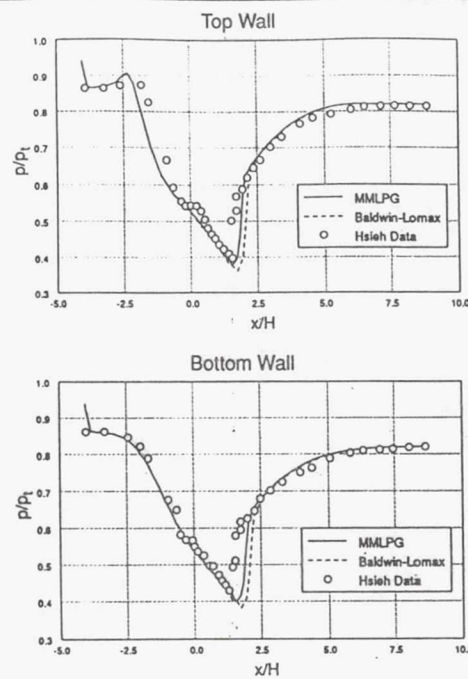
$$\left. \begin{array}{l}
 C_3 = 1.0 + 0.307\beta - 0.0391\beta^2 \\
 C_5 = 23, 200 + 8560\beta - 1230\beta^2 \\
 C_6 = -7.75 \times 10^6 - 4.51 \times 10^6\beta + 386, 000\beta^2
 \end{array} \right\} 0.0 \leq \beta \leq 5.34$$
  

$$\left. \begin{array}{l}
 C_3 = 1.52 \\
 C_5 = 33, 900 \\
 C_6 = -20, 900
 \end{array} \right\} \beta > 5.34$$

Velocity Defect Profiles -- Mild Adverse Pressure Gradient



Static Pressure Distribution -- Weak Shock Case, R=0.82

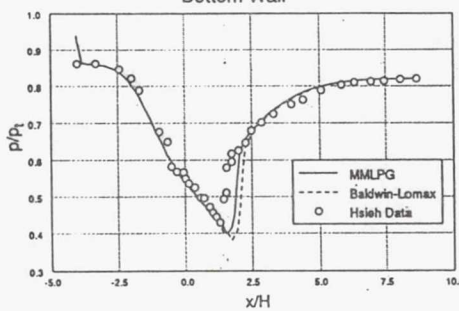


Top Wall

Baldwin-Lomax

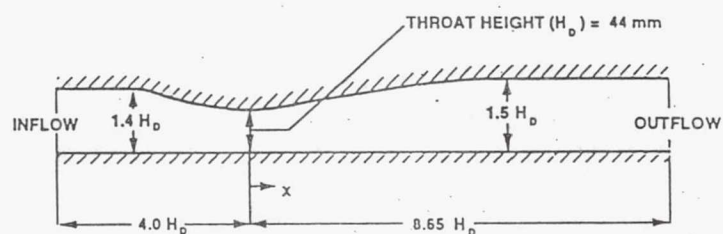
MMLPG  
Hsieh Data

Bottom Wall



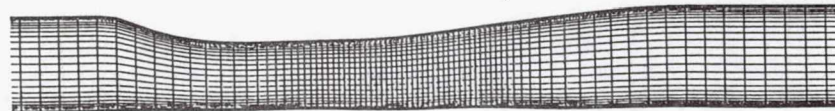
**Test Cases**

Sajben Transonic Diffuser Flows

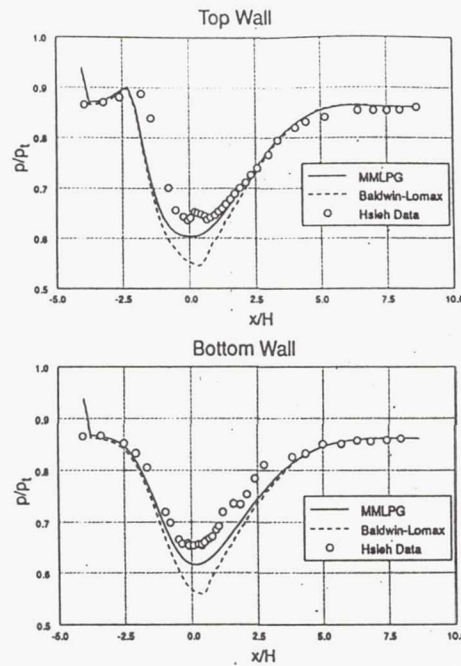


Computational Grid

81x51



Static Pressure Distribution -- No Shock Case, R=0.862



### Concluding Remarks

- Developed MMLPG for adverse pressure gradient flows
- Shown that MMLPG successfully computes boundary layer flows and transonic diffuser flows
- Future work: continue validation  
modifications for separated flow

**Page intentionally left blank**



National Aeronautics and  
Space Administration  
Lewis Research Center

---

## Turbulence Model Experiences for a Round-to-Rectangular Transition Duct

Workshop on Computational  
Turbulence Modeling

September 15–16, 1993

Charles E. Towne

NASA Lewis Research Center  
Cleveland, OH



## TRANSITION DUCT FLOW

National Aeronautics and  
Space Administration  
Lewis Research Center

---

## Outline

- Proteus code description
- Geometry and flow conditions
- Numerical details
- Turbulence model modifications
- Convergence history
- Computed results and  
comparison with experimental data
- Concluding remarks



## TRANSITION DUCT FLOW

National Aeronautics and  
Space Administration  
Lewis Research Center

### Proteus Navier-Stokes Code

- Reynolds-averaged, unsteady, compressible Navier-Stokes equations
- Strong conservation-law form
- Fully-coupled ADI solution procedure, Beam-Warming generalized time differencing
- Second-order central differencing for spatial derivatives
- Implicit steady/unsteady boundary conditions
- Convection and diffusion terms linearized using second-order Taylor series expansion
- Generalized nonorthogonal body-fitted coordinates
- Baldwin-Lomax and Chien  $k-\varepsilon$  turbulence models



## TRANSITION DUCT FLOW

National Aeronautics and  
Space Administration  
Lewis Research Center

### Proteus Navier-Stokes Code

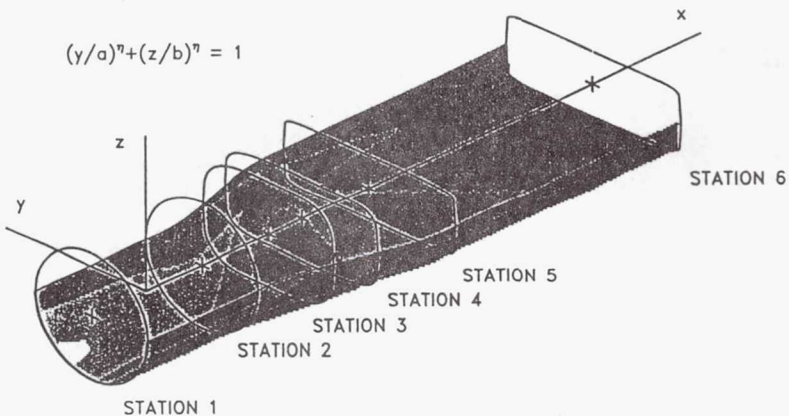
- 2-D, axisymmetric w/wo swirl, or 3-D flow
- Thin-layer and Euler options
- Wide variety of boundary conditions
- Constant stagnation enthalpy option
- Constant-coefficient or adaptive artificial viscosity
- First- or second-order time differencing
- Variety of time step selection methods
- Output files for CONTOUR and PLOT3D
- Highly vectorized for Cray computers
- Extensively commented
- Three-volume documentation set



## TRANSITION DUCT FLOW

National Aeronautics and  
Space Administration  
Lewis Research Center

### Circular-to-Rectangular Transition Duct



## TRANSITION DUCT FLOW

National Aeronautics and  
Space Administration  
Lewis Research Center

### Flow Conditions

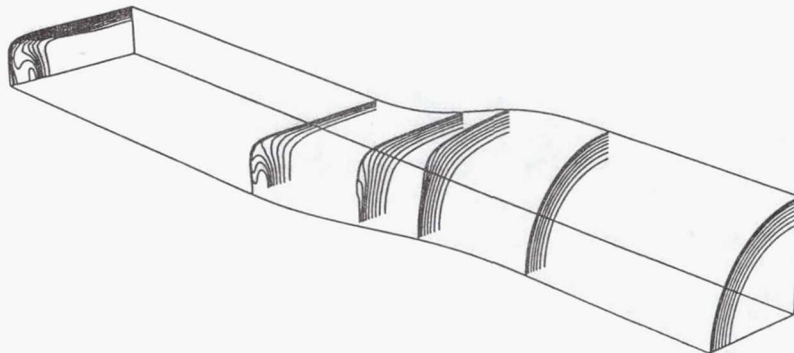
- $M_{ref} = \bar{M}_{inlet} = 0.2$  to simulate incompressible experiment
- $Re_{ref} = (\rho u R / \mu)_{inlet} = 195,000$
- Constant  $c_p$  and  $c_v$ , with  $\gamma = 1.4$
- Constant  $\mu_l$  at  $519^{\circ}\text{R}$
- Constant stagnation enthalpy



## TRANSITION DUCT FLOW

National Aeronautics and  
Space Administration  
Lewis Research Center

### Total Pressure Contours



## TRANSITION DUCT FLOW

National Aeronautics and  
Space Administration  
Lewis Research Center

### Boundary and Initial Conditions

- Boundary conditions

Boundary	Conditions Specified
Inlet	$p_T = (p_T)_{exp}$ , $u_x = 0$ , $v = w = 0$
Exit	$\dot{m} = \dot{m}_{exp}$ , $u_x = v_x = w_x = 0$
Outer wall	$p_r = 0$ , $u = v = w = 0$
Centerline	$(\rho, u, v, w)_{CL} = \text{ave}_{\theta} (\rho, u, v, w)_{CL+1}$
$\theta = 0$	$p_r = u_r = w_r = 0$ , $v = 0$
$\theta = 90$	$p_r = u_r = v_r = 0$ , $w = 0$

- Initial conditions

$$p = p_{\infty}, u = (u_{exp})_{inlet}, v = w = 0$$



## TRANSITION DUCT FLOW

National Aeronautics and  
Space Administration  
Lewis Research Center

### Numerics

- $61(x) \times 31(\theta) \times 50(r)$  and  $61 \times 31 \times 99$  meshes
- Local time step, with:

Mesh	Time Level	CFL
61 $\times$ 31 $\times$ 50	1 – 1001	1
	1001 – 2001	10
	2001 – 3001	10
	3001 – 4001	20
61 $\times$ 31 $\times$ 99	1 – 1501	1
	1501 – 3001	10
	3001 – 4501	10
	4501 – 6001	15
	6001 – 7501	15

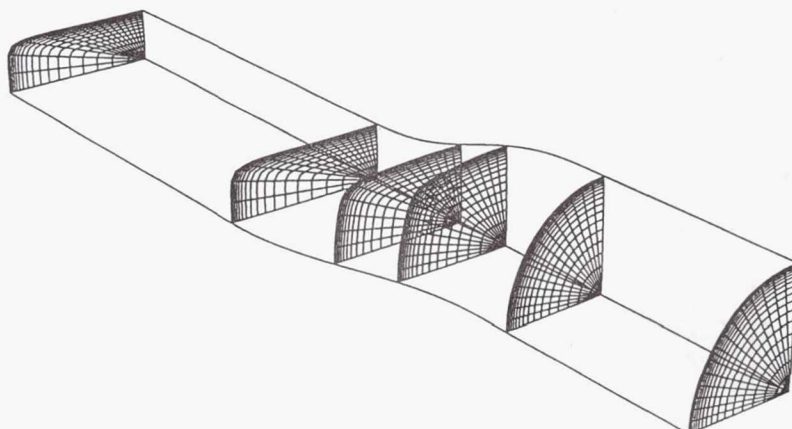
- Cray Y-MP CPU time — just under  $5 \times 10^{-5}$  sec/grid point/time step, or 5.2 and 18.8 hours for the two cases



## TRANSITION DUCT FLOW

National Aeronautics and  
Space Administration  
Lewis Research Center

### Computational Mesh





## TRANSITION DUCT FLOW

National Aeronautics and  
Space Administration  
Lewis Research Center

### Baldwin-Lomax Turbulence Model

#### Inner region

- $\mu_t = \rho l^2 |\vec{\Omega}| Re_{ref}$

#### Outer region

- $\mu_t = KC_{cp} \rho F_{Kleb} F_{wake} Re_{ref}$

where  $F_{wake} = (y_n)_{max} F_{max}$ ,  $F_{max} = \max [y_n |\vec{\Omega}| (1 - e^{-y^*/A^*})]$ ,  
and  $(y_n)_{max}$  is the corresponding  $y_n$

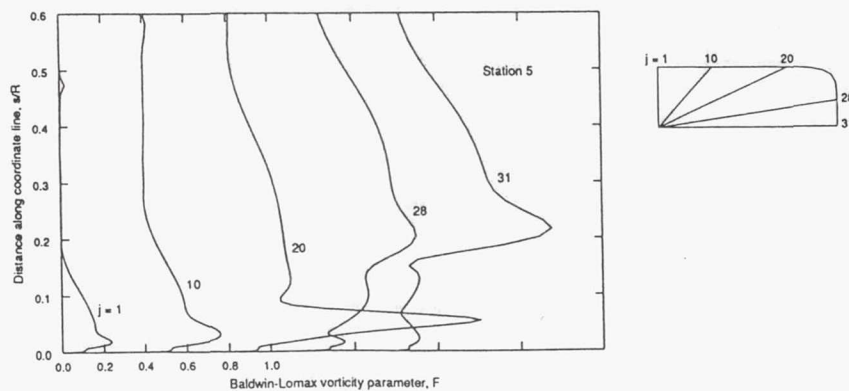
- Model based on boundary layer flows, without accounting for secondary flows and streamwise vorticity
- At each streamwise station, the search region for  $F_{max}$  was limited to the value of  $(y_n)_{max}$  in the  $y = 0$  plane
- Rationale — to prevent the secondary vortices, at the "ends" of the cross-section, from affecting the  $\mu_t$  values



## TRANSITION DUCT FLOW

National Aeronautics and  
Space Administration  
Lewis Research Center

### Effect of Turbulence Model Modification

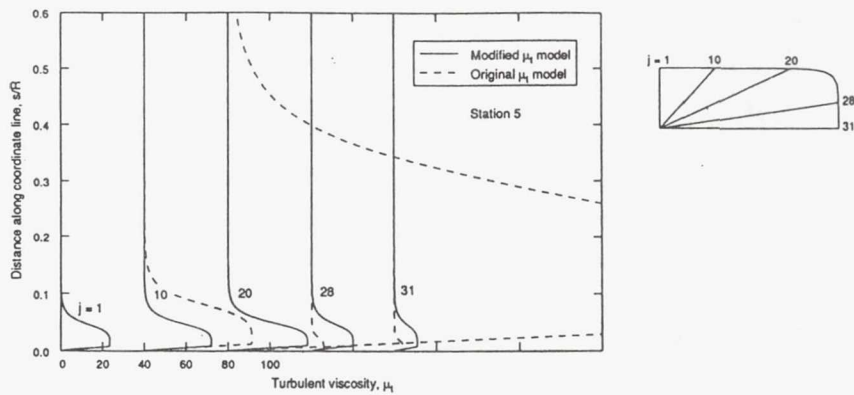




## TRANSITION DUCT FLOW

National Aeronautics and  
Space Administration  
Lewis Research Center

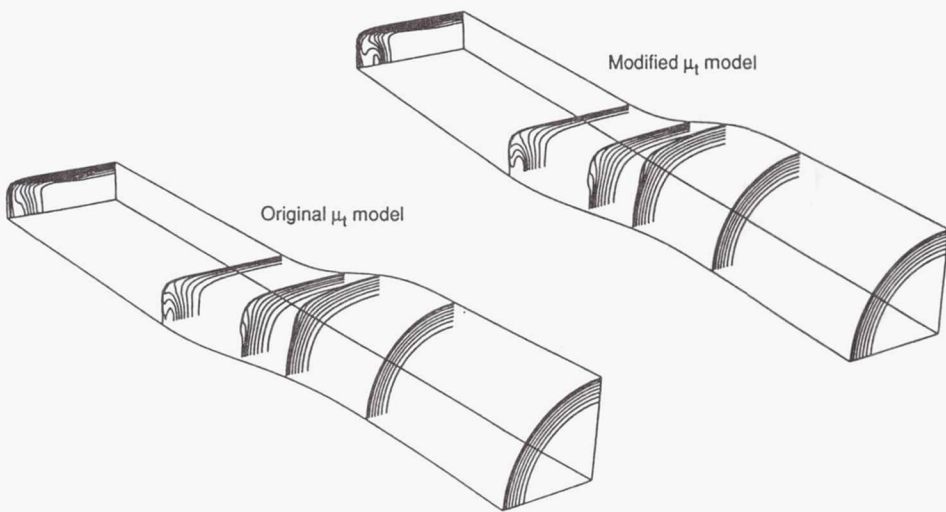
### Effect of Turbulence Model Modification



## TRANSITION DUCT FLOW

National Aeronautics and  
Space Administration  
Lewis Research Center

### Effect of Turbulence Model Modification

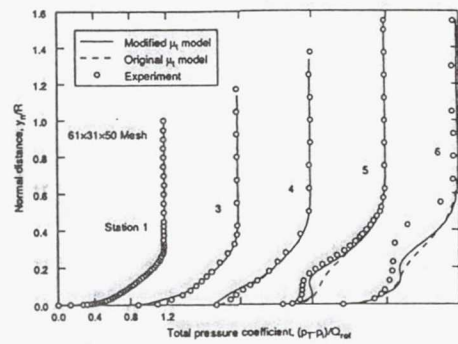
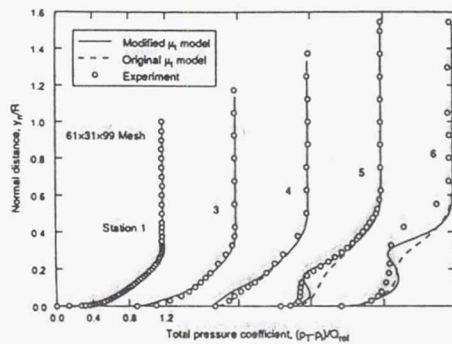




## TRANSITION DUCT FLOW

National Aeronautics and  
Space Administration  
Lewis Research Center

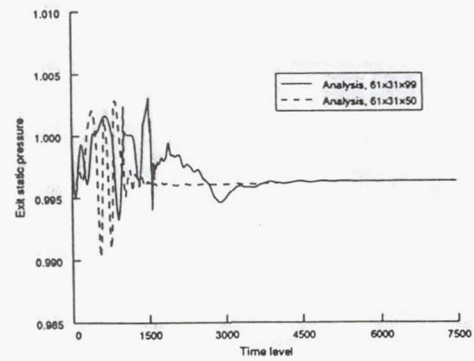
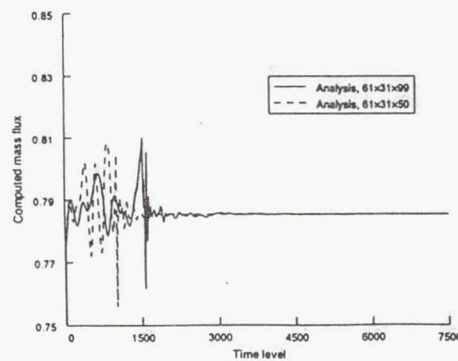
### Effect of Turbulence Model Modification



## TRANSITION DUCT FLOW

National Aeronautics and  
Space Administration  
Lewis Research Center

### Mass Flow Rate Convergence

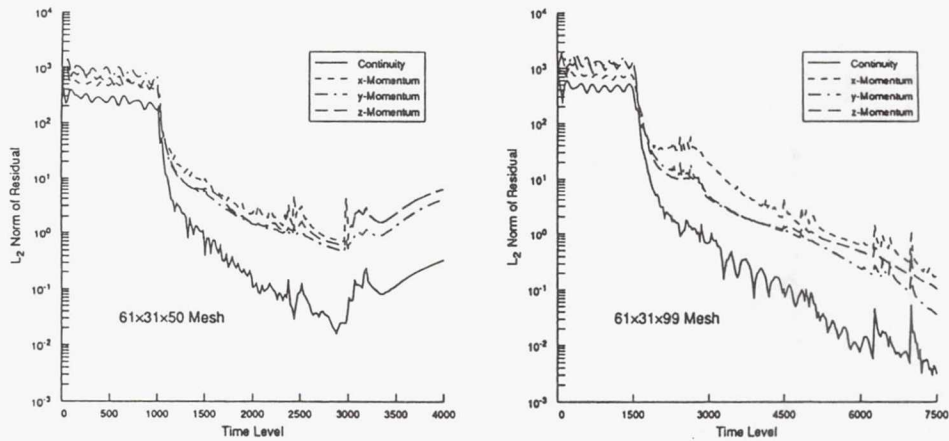




## TRANSITION DUCT FLOW

National Aeronautics and  
Space Administration  
Lewis Research Center

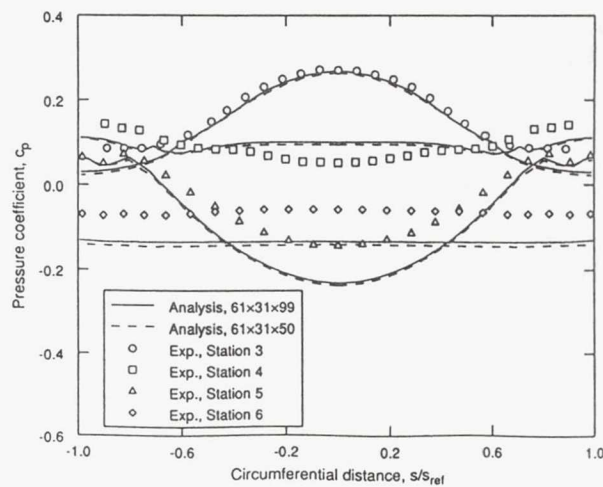
### Convergence History



## TRANSITION DUCT FLOW

National Aeronautics and  
Space Administration  
Lewis Research Center

### Peripheral Static Pressure Distribution

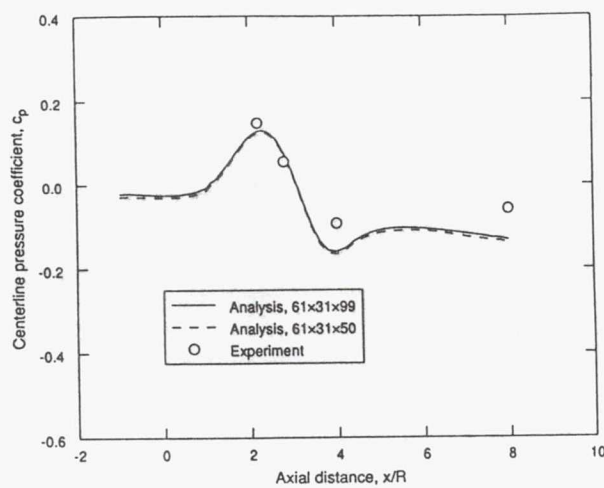




## TRANSITION DUCT FLOW

National Aeronautics and  
Space Administration  
Lewis Research Center

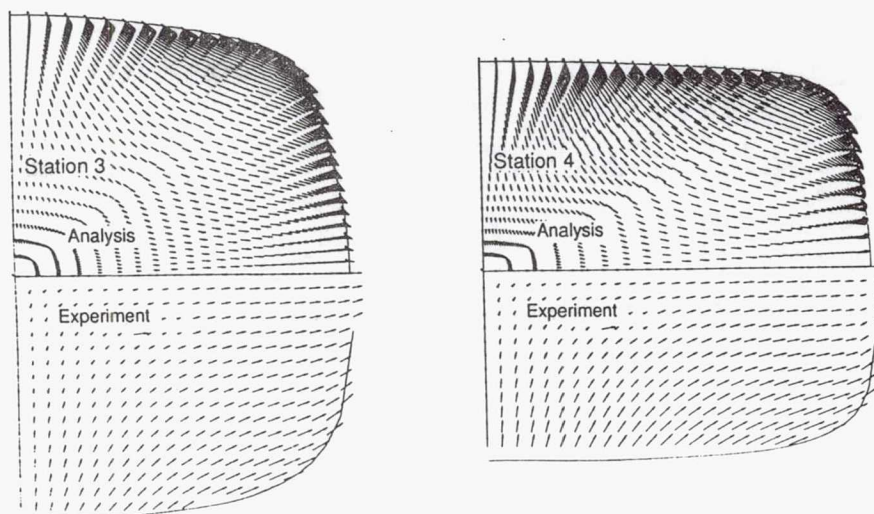
### Centerline Static Pressure Distribution



## TRANSITION DUCT FLOW

National Aeronautics and  
Space Administration  
Lewis Research Center

### Secondary Velocity Vectors

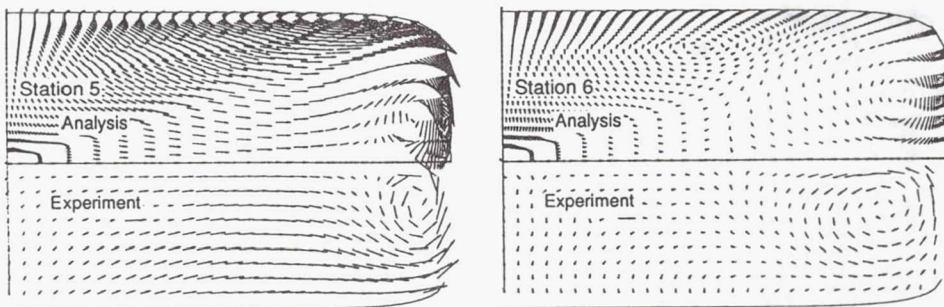




## TRANSITION DUCT FLOW

National Aeronautics and  
Space Administration  
Lewis Research Center

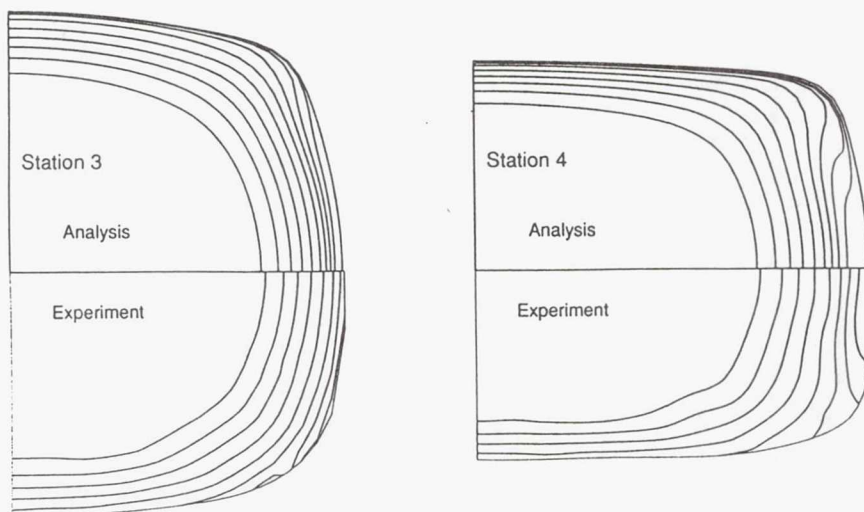
### Secondary Velocity Vectors



## TRANSITION DUCT FLOW

National Aeronautics and  
Space Administration  
Lewis Research Center

### Total Pressure Contours

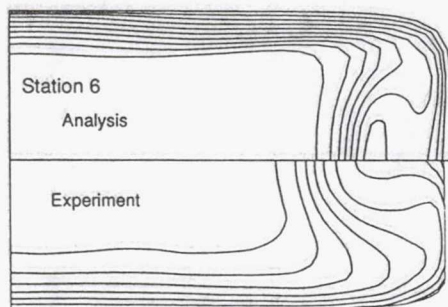
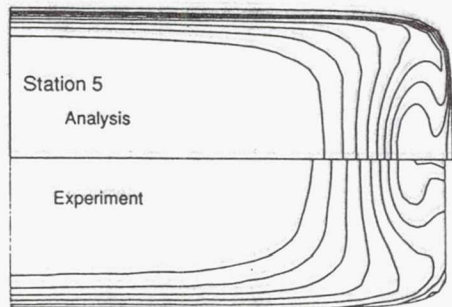




## TRANSITION DUCT FLOW

National Aeronautics and  
Space Administration  
Lewis Research Center

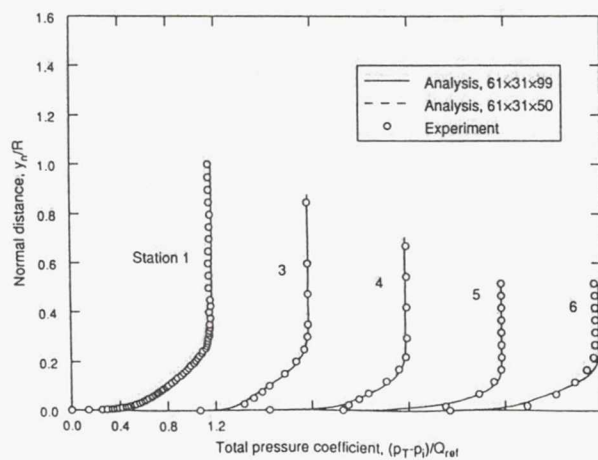
### Total Pressure Contours



## TRANSITION DUCT FLOW

National Aeronautics and  
Space Administration  
Lewis Research Center

### Total Pressure Profiles Along Semi-Minor Axis

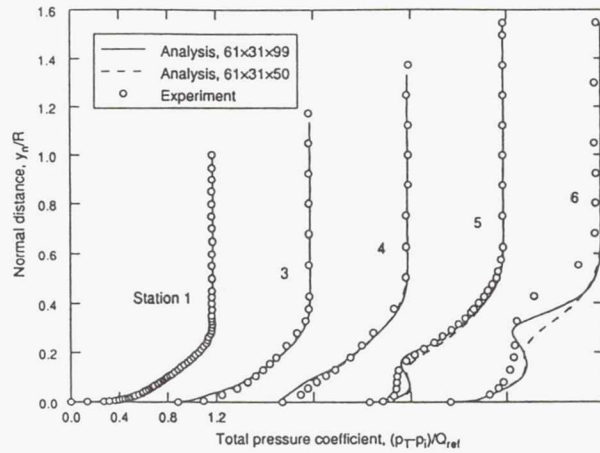




## TRANSITION DUCT FLOW

National Aeronautics and  
Space Administration  
Lewis Research Center

### Total Pressure Profiles Along Semi-Major Axis



## TRANSITION DUCT FLOW

National Aeronautics and  
Space Administration  
Lewis Research Center

### Concluding Remarks

- The Proteus 3-D Navier-Stokes code has been used to compute the flow through a round-to-rectangular transition duct
- The search region for  $F_{max}$  in the Baldwin-Lomax turbulence model was limited to prevent excessively large  $\mu_t$  values
- The code correctly captures the basic physics — the generation of secondary flows and the resulting distortion
- Agreement between computed and experimental results is good through the transition section
- The computed secondary flows are overly damped in the downstream straight section
- Further work is needed to investigate the effects of mesh resolution and turbulence model

**Page intentionally left blank**

# Proteus experience with three different types of turbulence models

Trong T. Bui

NASA Lewis Research Center  
Cleveland, Ohio

---

NASA Lewis Research Center  
Cleveland, Ohio

INTERNAL FLUID MECHANICS DIVISION

## Contents

1. Overview of turbulence models used
2. Practical issues
3. Suggestions

---

NASA Lewis Research Center  
Cleveland, Ohio

INTERNAL FLUID MECHANICS DIVISION

## Overview of turbulence models used

### 1. Algebraic model

- Baldwin-Lomax (BL)

### 2. One-equation model

- Baldwin-Barth one-equation (BB)

### 3. Two-equation models

- Chien k- $\epsilon$  (CH)
- Launder-Sharma k- $\epsilon$  (LS)

---

NASA Lewis Research Center  
Cleveland, Ohio

INTERNAL FLUID MECHANICS DIVISION

## Contents

### 1. Overview of turbulence models used

### 2. Practical issues

- CPU time requirement
- Initialization of multi-equation models
- $y^+$  dependency
- Compressibility corrections
- Where the turbulence models work well, and where they do not work too well

### 3. Comments

---

NASA Lewis Research Center  
Cleveland, Ohio

INTERNAL FLUID MECHANICS DIVISION

## CPU time requirement

Not a major issue in using multi-equation turbulence models:

(CPU time in sec/iter/grid point)

Turbulence models	Incomp. flat plate	Comp. flat plate	S-duct	3-D shock / B.L. inter.
B.- L.	6.031E-5	9.042E-5	5.168E-5	7.888E-5
B.- B.	6.650E-5	9.436E-5	N/A	N/A
Chien	6.822E-5	9.836E-5	6.506E-5	9.757E-5
L.- S.	8.667E-5	11.77E-5	N/A	N/A

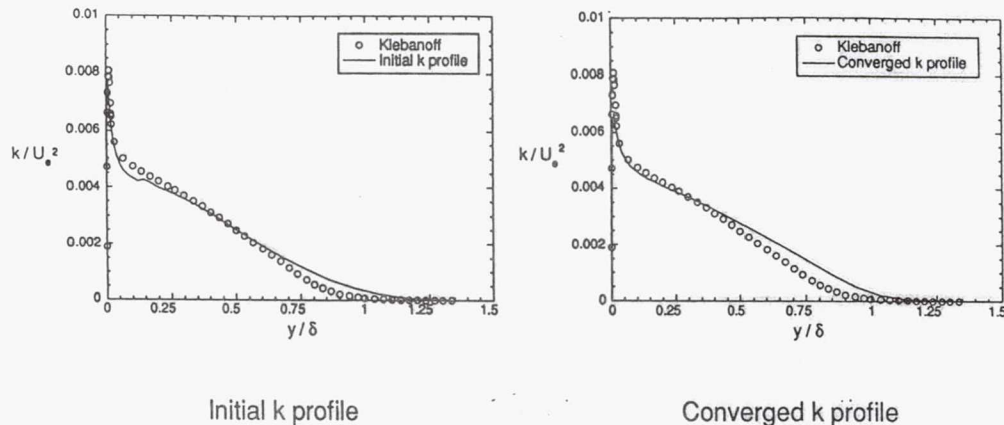
- For flat plates, the Chien k- $\epsilon$  model takes only about 10% more CPU time than the B.- L. model
- For 3-D S-duct and shock/B.L. inter., the Chien k- $\epsilon$  model takes about 25% more CPU time than the B.- L. model

## Initialization of multi-equation models

Initial profiles of turbulence variables are needed to start the time marching process. The following steps have been found to work well:

1.  $\mu_t$  is computed using the BL model.
2. BB model –  $k^2/\epsilon$  is computed using  $\mu_t$  and the BB formula.
3. k- $\epsilon$  models –  $\epsilon$  is calculated from the local equilibrium assumption, and  $k$  is calculated using  $\epsilon$ ,  $\mu_t$ , and the CH damping function  $f_\mu$ .

## Automatic Initial k Profile for Incompressible Flat Plate TBL

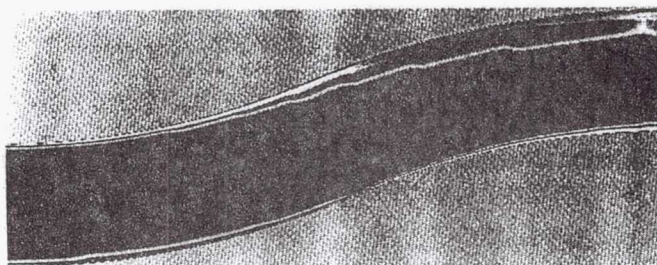


NASA Lewis Research Center  
Cleveland, Ohio

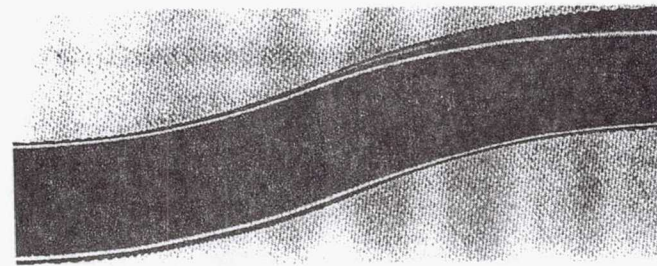
INTERNAL FLUID MECHANICS DIVISION

17

## Initial k Profile for Turbulent S-Duct Flow



Initial k profile

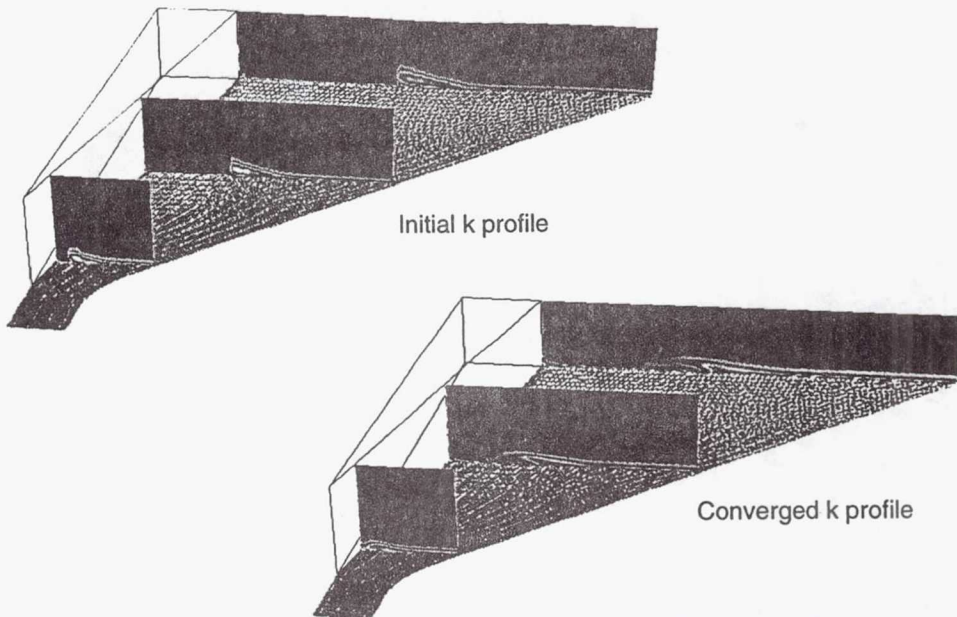


Converged k profile

NASA Lewis Research Center  
Cleveland, Ohio

INTERNAL FLUID MECHANICS DIVISION

## Initial k Profile for Glancing Shock Wave/TBL Interaction



NASA Lewis Research Center  
Cleveland, Ohio

INTERNAL FLUID MECHANICS DIVISION

## $y^+$ dependency

$y^+$  is needed to feed the Van Driest style damping functions in the near wall region. Not desirable for two main reasons:

### 1. Geometrical considerations:

- Need to identify the nearest solid walls. This is difficult for complex 3-D geometries with multiple solid boundaries.
- Need to compute distances to solid walls. This is difficult to do for unstructured grids.
- What is  $y^+$  in base/wake flows?

### 2. Ambiguity in the definition of $y^+$ for variable-property flows:

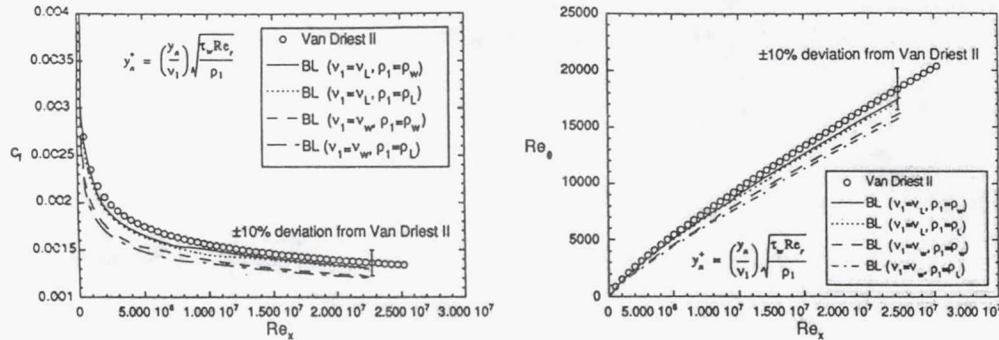
- $y_n^+ = \left( \frac{y_n}{v_1} \right) \sqrt{\frac{\tau_w \text{Re}_r}{\rho_1}}$
- Local or wall values for  $v_1$  and  $\rho_1$ ?

However, models that use  $y^+$  appear to be more stable numerically than the ones that do not.

NASA Lewis Research Center  
Cleveland, Ohio

INTERNAL FLUID MECHANICS DIVISION

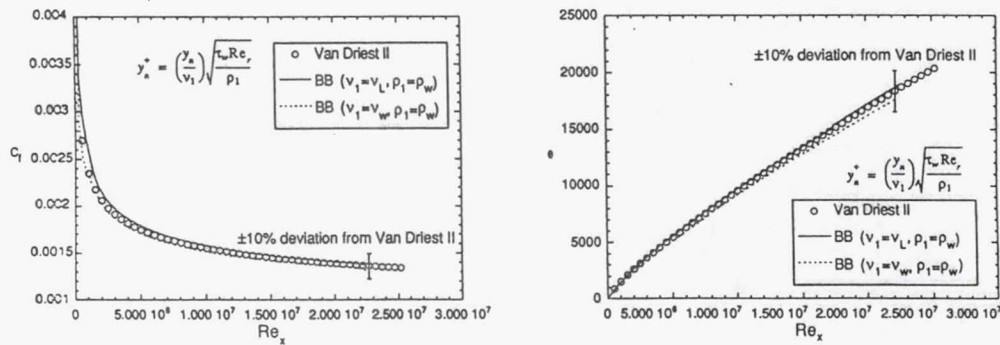
## Effects of $y^+$ Computation, BL



NASA Lewis Research Center  
Cleveland, Ohio

INTERNAL FLUID MECHANICS DIVISION

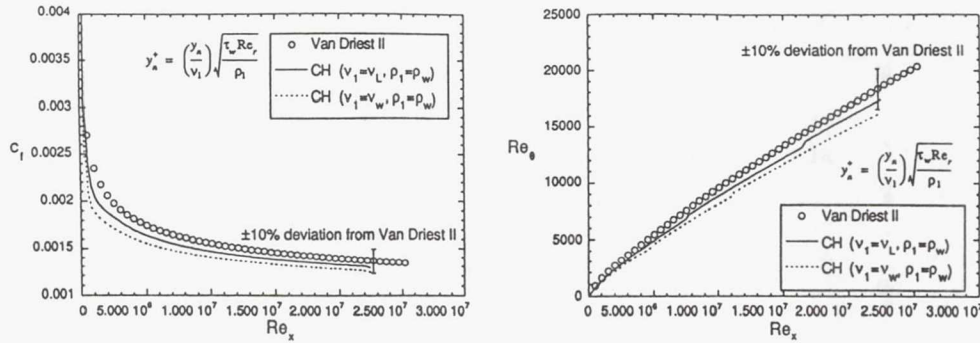
## Effects of $y^+$ Computation, BB



NASA Lewis Research Center  
Cleveland, Ohio

INTERNAL FLUID MECHANICS DIVISION

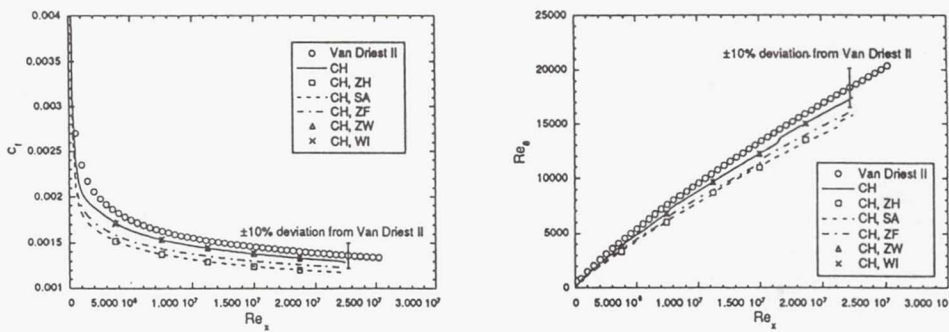
## Effects of $y^+$ Computation, CH



NASA Lewis Research Center  
Cleveland, Ohio

INTERNAL FLUID MECHANICS DIVISION

## Effects of Compressibility Corrections, CH



NASA Lewis Research Center  
Cleveland, Ohio

INTERNAL FLUID MECHANICS DIVISION

## Contents

### 1. Overview of turbulence models used

### 2. Practical issues

- CPU time requirement
- Initialization of multi-equation models
- $y^+$  dependency
- Compressibility corrections
- • Where the turbulence models work well, and where they do not work too well

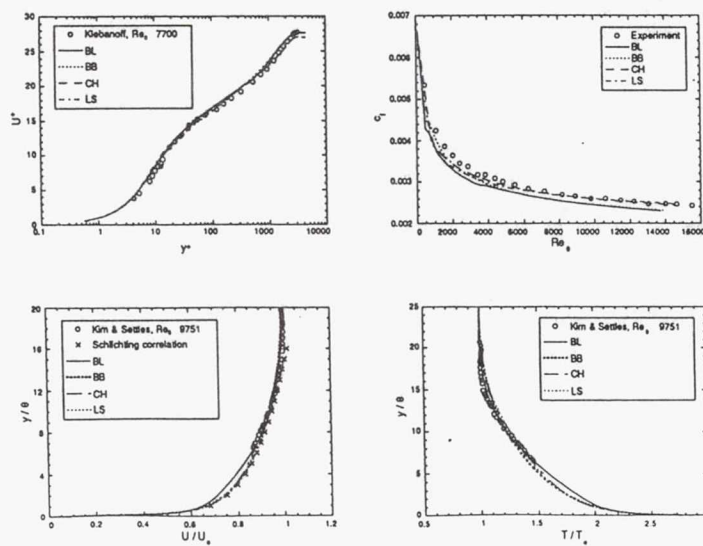
### 3. Comments

NASA Lewis Research Center  
Cleveland, Ohio

INTERNAL FLUID MECHANICS DIVISION

## Where the turbulence models work well

Attached, thin layer flows with little or no pressure gradients

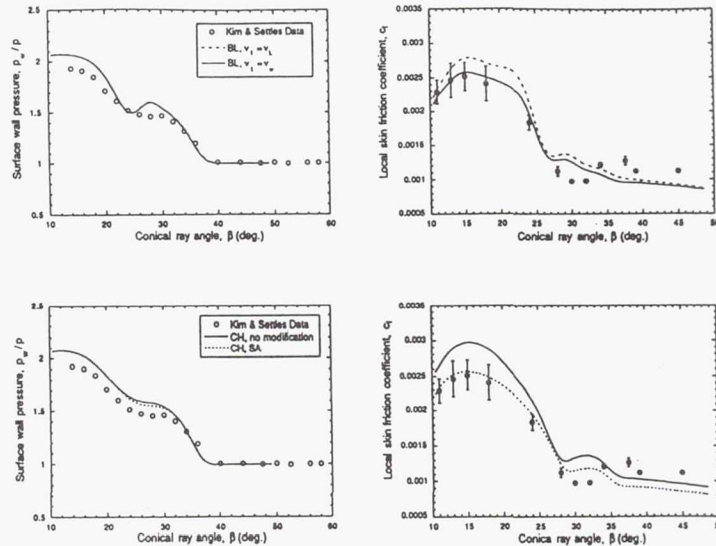


NASA Lewis Research Center  
Cleveland, Ohio

INTERNAL FLUID MECHANICS DIVISION

## Where they don't work too well

Separated/Reattached flows and flows with large pressure gradients



NASA Lewis Research Center  
Cleveland, Ohio

INTERNAL FLUID MECHANICS DIVISION

## Comments

- Two-equation  $k-\epsilon$  models can be used without serious CPU time penalty. However, no real gain in predictive capability compared with algebraic formulations.
- To improve the predictive capability, need to extend the two-equation formulations with algebraic Reynolds stress models or anisotropic  $k-\epsilon$  models.
- $y^+$  dependency limits the generality of turbulence models, and it should be removed if possible (preferably without significant cost in the stability and accuracy of the models).
- Models are needed for the Reynolds heat flux terms.

NASA Lewis Research Center  
Cleveland, Ohio

INTERNAL FLUID MECHANICS DIVISION

**Page intentionally left blank**

---

## **Several Examples Where Turbulence Models Fail in Inlet Flow Field Analysis**

**Bernhard H. Anderson**  
**NASA Lewis Research Center**  
**Cleveland, OH**

---

## **Inlet Flow Field Analysis**

### **Computational Uncertainties**

- Turbulence Modeling for 3D Inlet Flow Fields
  - (1) Flows Approaching Separation
  - (2) Strength of Secondary Flow Field
  - (3) 3D Flow Predictions of Vortex Liftoff
  - (4) Influence of Vortex-Boundary Layer Interactions
- Vortex Generator Modeling
  - (1) Representation of Generator Vorticity Field
  - (2) Relationship Between Generator and Vorticity Field

## **Inlet Flow Field Studies**

### **Goals and Objectives**

To advance the understanding, the prediction, and the control of intake distortion, and to study the basic interactions that influence this design problem.

- To develop an understanding of and predictive capability for the aerodynamic properties of intake distortion and its management.
- To establish a set of design guidelines to maximize the effectiveness of vortex flow control for the management of intake distortion

## Inlet Flow Field Benchmark Data Sets Turbulence and Vortex Generator Modeling

- Fraser Flow A, Stanford Conference 1968
- 727/JT8D-100 S-Duct Confirmation Experiment, 1973
- Univ. Tennessee Diffusing S-Duct Experiments, 1986 & 1992
- Univ. Washington TD410 Transition Duct Experiment, 1990
- M2129 Imperial College Laser-Doppler Experiment, 1990
- DRA-Bedford Experiments on the M2129 Intake S-Duct
  - (2) DRA Surface Pressure and Engine Face Experiment, 1989
  - (3) DRA Phase 1B Hot-Wire Flow Experiment, 1990
  - (4) DRA Phase 2 Yawmeter Flow Experiment, 1991
  - (5) DRA Phase 3 Vortex Generator Experiment, 1992
- TD118 Bi-Furcated Transition Duct Experiment, 1994

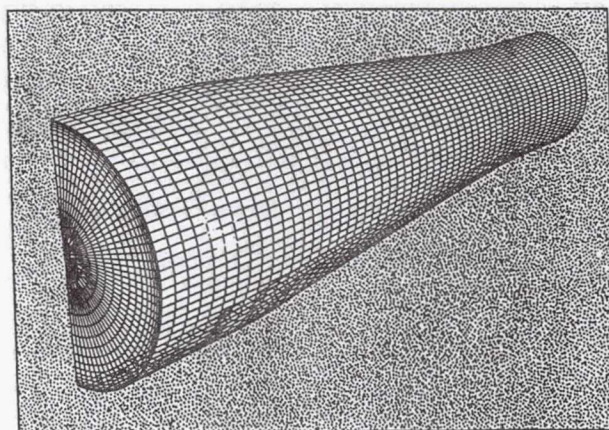
## Reduced Navier-Stokes Analysis RNS3D Computer Code

- Velocity decomposition approach, Briley and McDonald (1979 & 1984)
  - (1) Conservation form of the vorticity transport equation
  - (2) Mass flow conservation,  $\dot{m} = \int_A \rho u_p dA = constant$
- Non-orthogonal coordinate system, Levy, Briley and McDonald (1983)
- Arbitrary geometry gridfile description, Anderson (1990)
  - (1) Recluster existing gridfile mesh distribution
  - (2) Redefine the centerline space curve
  - (3) Alter cross-sectional duct shape
- McDonald Camarata turbulence model

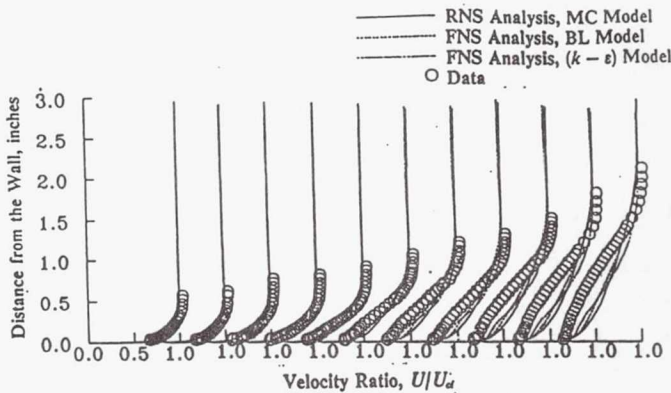
## Full Navier-Stokes Analysis PARC3D Computer Code

- Originally developed by Pulliam & Steger as AIR3D (1980)
  - (1) Conservation form of the governing equations
  - (2) Beam & Warming approximate factorization algorithm
  - (3) Central differencing within a curvilinear system
- Addition of Jameson artificial dissipation by Pulliam, ARC3D (1981)
- Developed for internal flow by Cooper, PARC3D (1987)
  - (1) Baldwin-Lomax turbulence model
  - (2) Diewert approximation to turbulence model in the reverse flow region of flow field

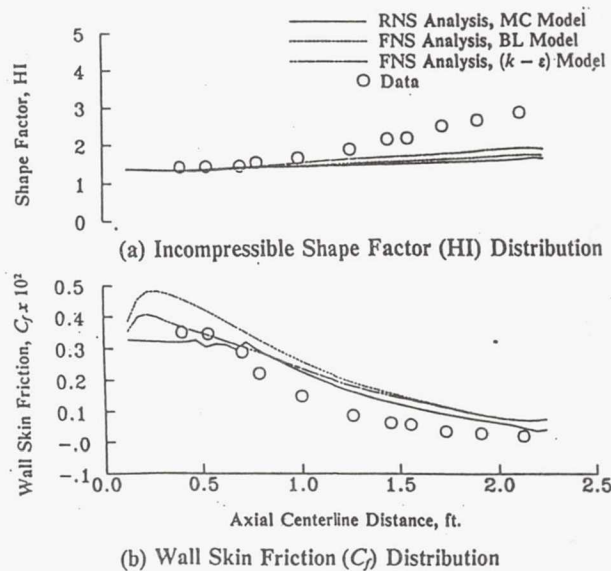
## Fraser Flow A, Stanford Conference 1968 Geometry and Mesh Definition



Fraser Flow A, Stanford Conference 1968  
 Comparison of Turbulence Models  
 $nz = 49, y^+ = 1.17$

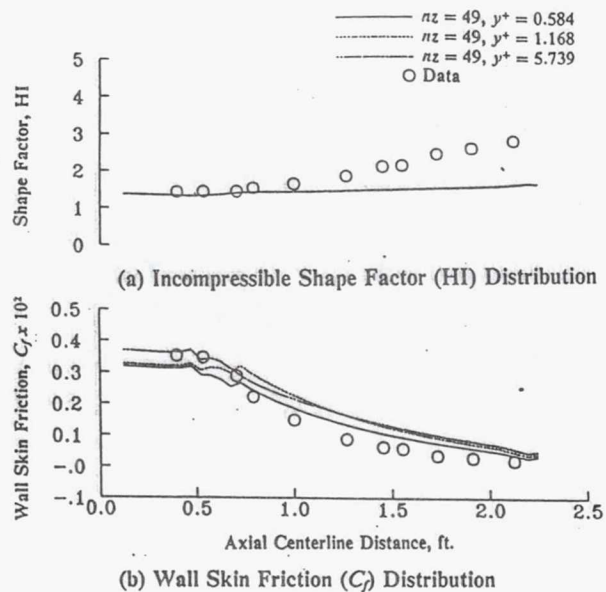


Fraser Flow A, Stanford Conference 1968  
 Comparison of Turbulence Models  
 $nz = 49, y^+ = 1.17$



## Fraser Flow A, Stanford Conference 1968

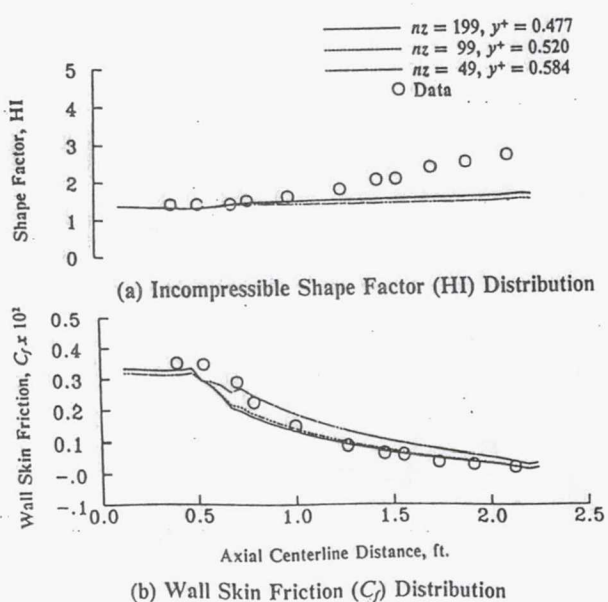
### Effect of $y^+$ on Flow Field Solution



RNS Analysis, McDonald-Camarata Model

## Fraser Flow A, Stanford Conference 1968

### Effect of Mesh Resolution on Flow Field Solution



RNS Analysis, McDonald-Camarata Model

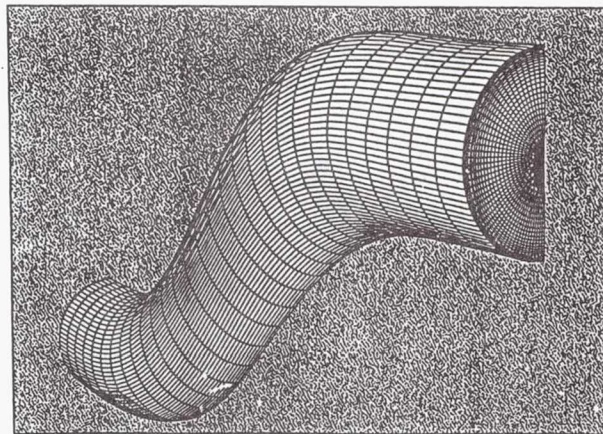
## Fraser Flow A, Stanford Conference 1968

### Conclusions

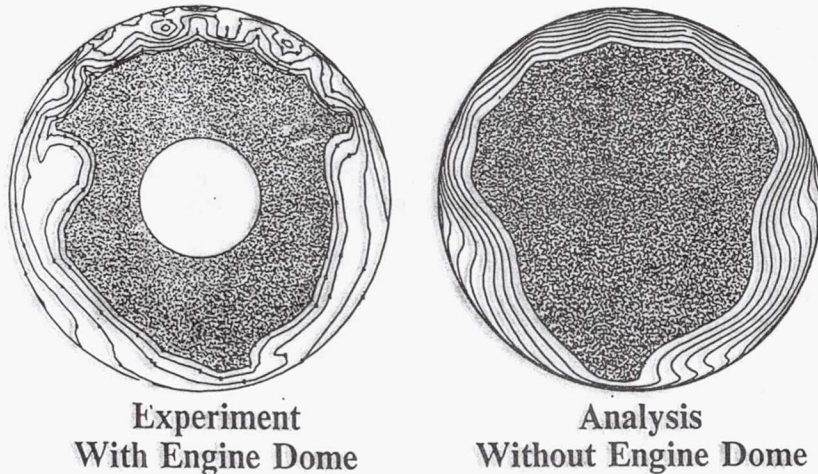
- (1) The current generation of turbulence models were unable to predict the complete state of the diffuser boundary layer approaching flow separation.
- (2) Both near wall and mesh resolution separately played an important role in accurate solutions to wall skin friction distribution in flows characterized as "approaching separation", but had little effect on the solution for the incompressible shape factor development.
- (3) It is important that grid independent solution be demonstrated before judgements about the turbulence models be stated, and that the complete state of the wall boundary layer be considered within this evaluation.

## 727/JT8D-100 Inlet S-Duct

### Geometry and Mesh Definition

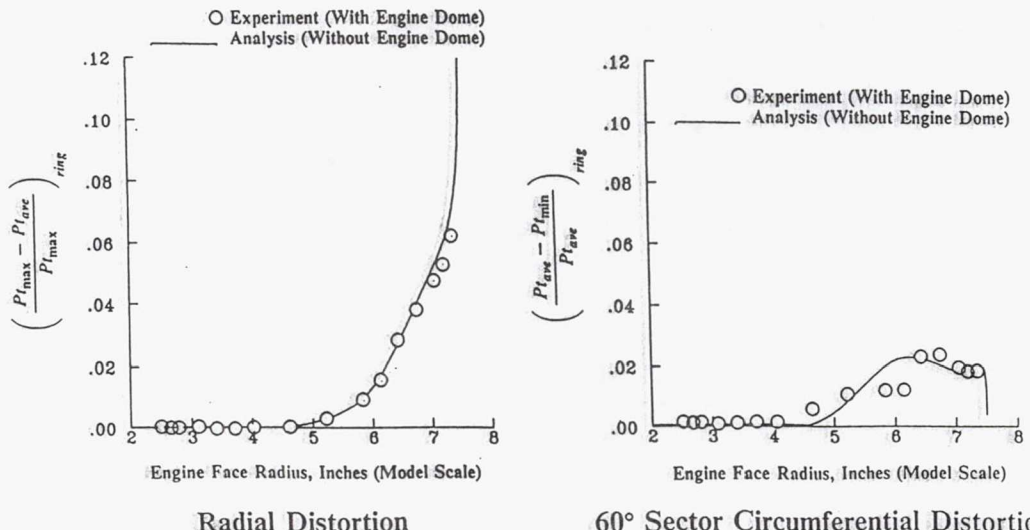


**727/JT8D-100 Inlet S-Duct**  
**Engine Face Flow Field**  
**Generator Config. 12**



RNS Analysis, McDonald-Camarata Model

**727/JT8D-100 Inlet S-Duct**  
**Engine Face Ring Distortion Characteristics**  
**Generator Config. 12**

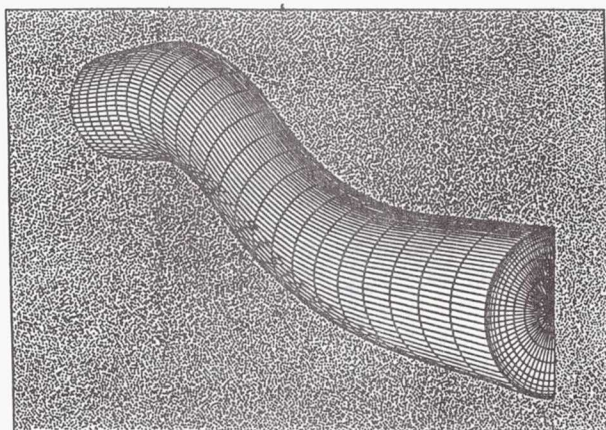


RNS Analysis, McDonald-Camarata Model

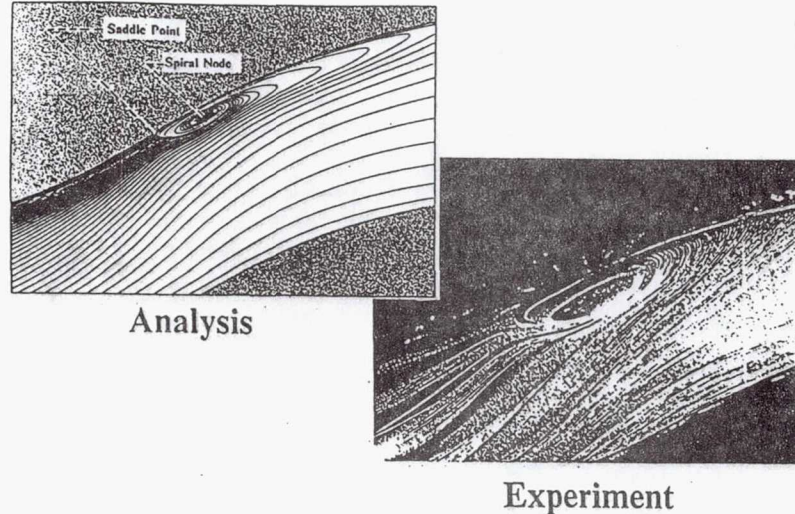
## **727/JT8D-100 Inlet S-Duct Conclusions**

- (1) The current turbulence models predict the overall performance level of vortex generator installation remarkably well, although much of the detailed flow structure was not resolved.
- (2) Turbulence models in 3D inlet flow field analysis can also be evaluated on the basis of standard engine performance parameters, such as radial and circumferential ring distortion descriptors, which provide a sensitive discriminator measuring the state of the overall compressor face flow field.

## **Univ. Tennessee Diffusing S-Duct Geometry and Mesh Definition**

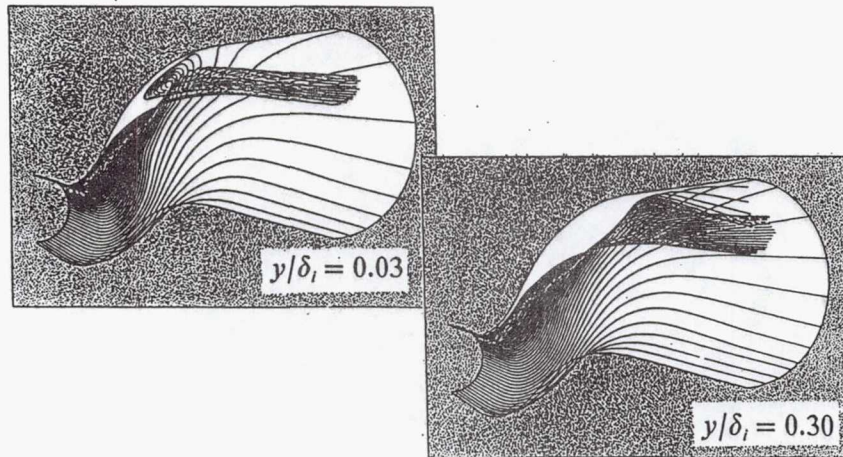


## Univ. Tennessee Diffusing S-Duct Topology of Vortex Liftoff



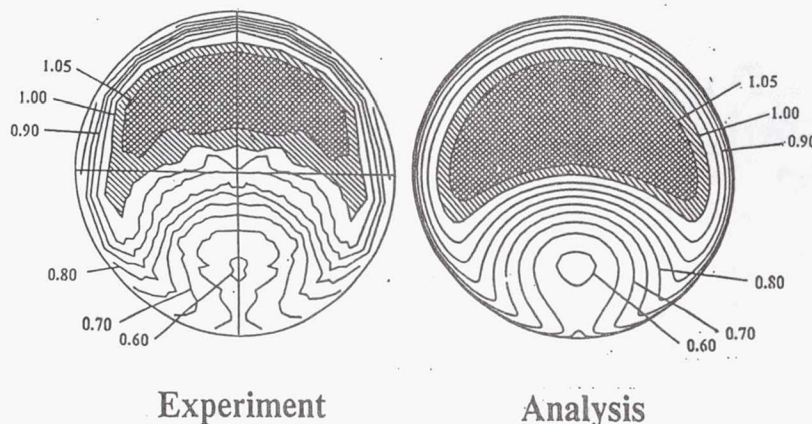
RNS Analysis, McDonald-Camarata Model

## Univ. Tennessee Diffusing S-Duct Topography of Vortex Liftoff



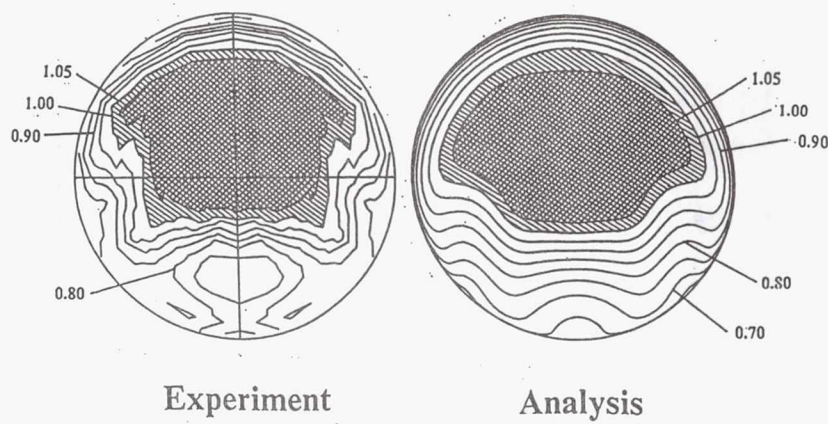
RNS Analysis, McDonald-Camarata Model

**Univ. Tennessee Diffusing S-Duct  
Total Pressure Coefficient Contours  
Without Vortex Generators**



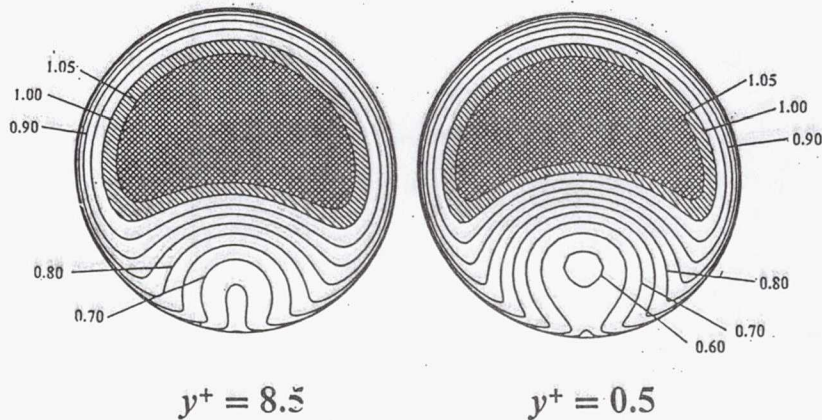
RNS Analysis, McDonald-Camarata Model

**Univ. Tennessee Diffusing S-Duct  
Total Pressure Coefficient Contours  
With Vortex Generators**



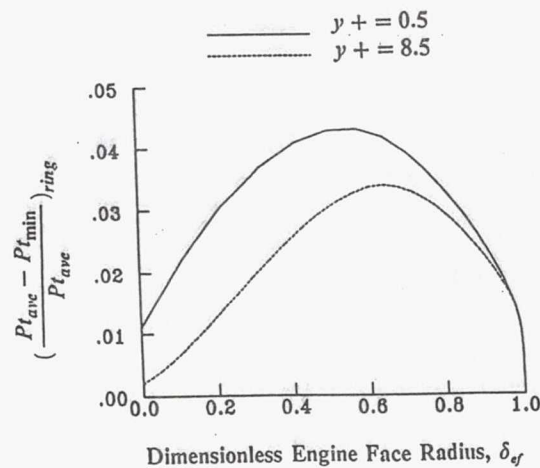
RNS Analysis, McDonald-Camarata Model

**Univ. Tennessee Diffusing S-Duct**  
**Effect of  $y^+$  on Engine Face Flow Field**  
**Total Pressure Coefficient Contours**



RNS Analysis, McDonald-Camarata Model

**Univ. Tennessee Diffusing S-Duct**  
**Effect of  $y^+$  on Circumferential Distortion**

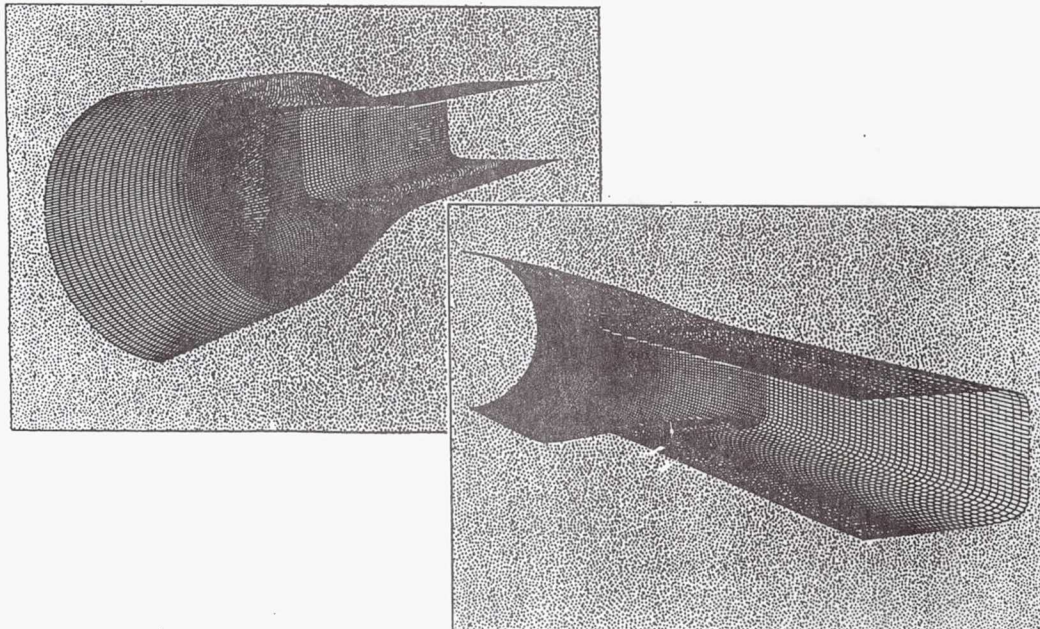


RNS Analysis, McDonald-Camarata Model

## Univ. Tennessee Diffusing S-Duct Conclusions

- (1) Initial value space marching 3D RNS procedures adequately described the topological and topographical features of 3D flow separation associated with vortex liftoff.
- (2) The current turbulence models predicted the overall structure of vortex generator installation remarkably well, although much of the detailed flow structure was not resolved.
- (3) Adequate near wall resolution was necessary to obtain an accurate solution of the phenomena of vortex lift-off.
- (4) Circumferential ring distortion is a sensitive discriminator in measuring the state of the engine face flow field.

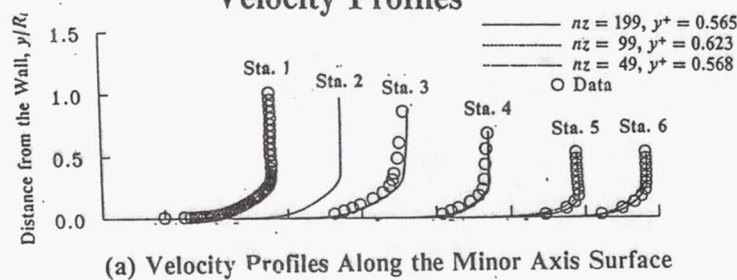
## Univ. Washington TD410 Transition Duct Geometry and Mesh Definition



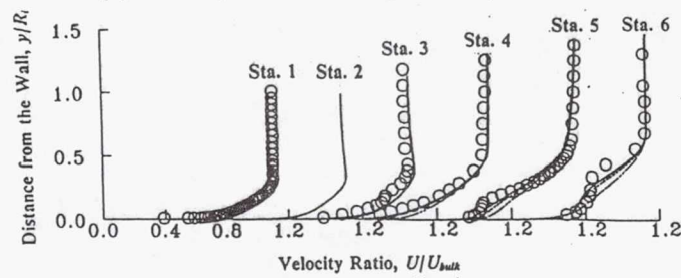
## Univ. Washington TD410 Transition Duct Case Definitions

Case	Grid	Total	CPU (min)	$Y^+$
td410.\$	199 x 121 x 521	12,545,159	149.0	0.565
td410.1	99 x 121 x 521	6,241,059	73.4	0.623
td410.3	49 x 121 x 521	2,851,849	36.0	0.568
td411.1	99 x 91 x 521	4,693,689	57.1	0.623
td412.\$	199 x 61 x 521	6,324,419	72.9	0.565
td412.1	99 x 61 x 521	3,146,319	38.2	0.623
td412.3	49 x 61 x 521	1,557,269	18.7	0.568
td412.4	49 x 61 x 401	1,198,589	14.7	0.568

## Univ. Washington TD410 Transition Duct Effect of Radial Grid Resolution Velocity Profiles

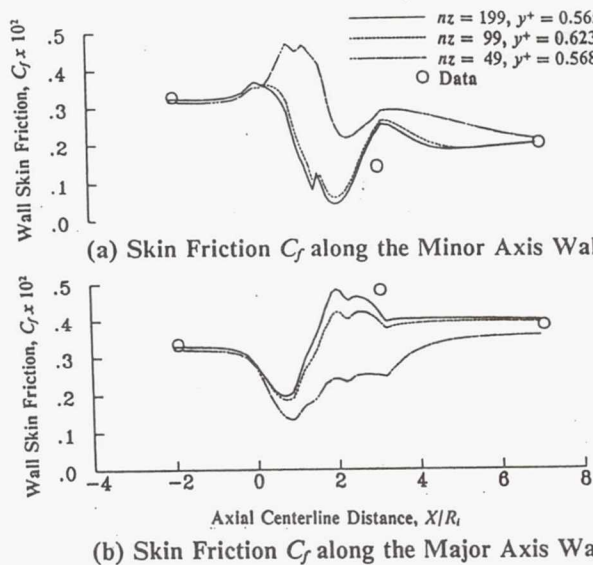


(a) Velocity Profiles Along the Minor Axis Surface



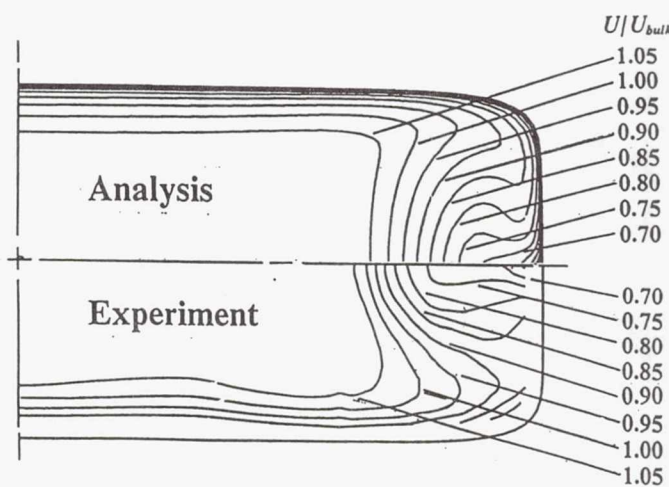
(b) Velocity Profiles Along the Major Axis Surface

**Univ. Washington TD410 Transition Duct**  
**Effect of Radial Grid Resolution**  
**Wall Skin Friction**



RNS Analysis, McDonald-Camarata Model

**Univ. Washington TD410 Transition Duct**  
**Comparison with Experimental Data**  
**Velocity Contours**

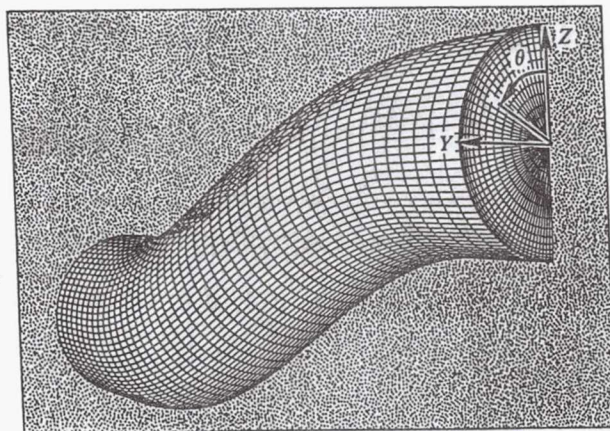


RNS Analysis, McDonald-Camarata Model

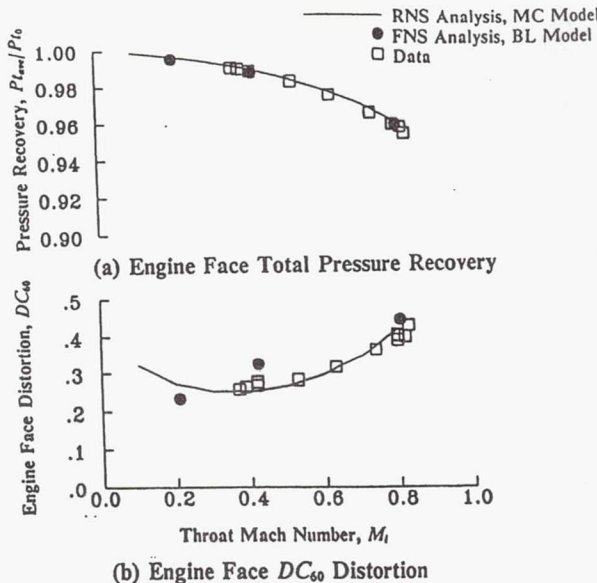
## Univ. Washington TD410 Transition Duct Conclusions

- (1) The current generation of turbulence models predicted the overall development of vortex formation reasonably well, although there were important discrepancies which could not be explained as inadequate near wall or mesh resolution.
- (2) Radial mesh resolution had the largest impact in the region along the major axis where the vortex pair was formed.
- (3) It is important that grid independent solution be demonstrated before judgements about the turbulence models be stated.
- (4) Fully 3D grid independent solutions were achieved with a Reduced Navier-Stokes analysis.

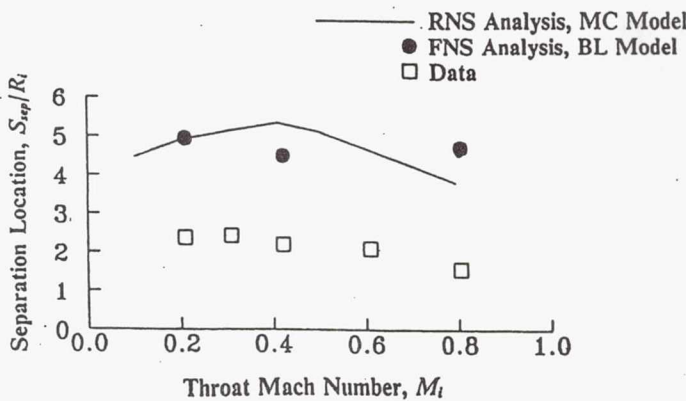
## DRA M2129 Diffusing Inlet S-Duct Geometry and Mesh Definition



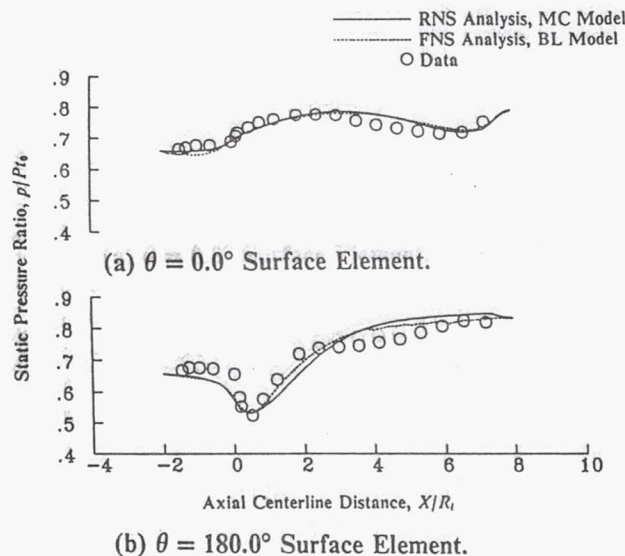
## DRA M2129 Diffusing Inlet S-Duct Performance Characteristics



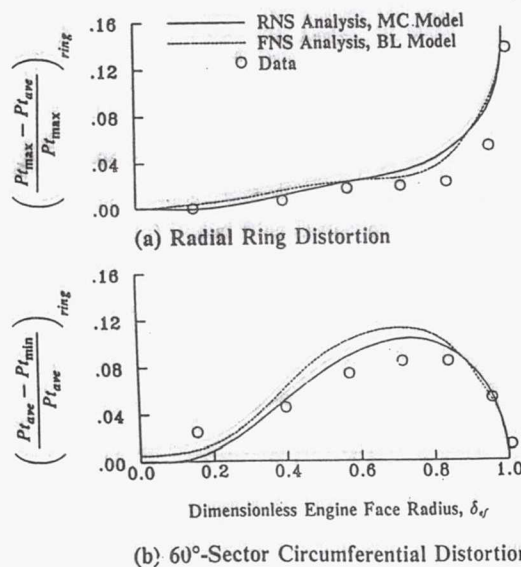
## DRA M2129 Diffusing Inlet S-Duct Separation Characteristics



**DRA M2129 Inlet S-Duct  
Wall Static Pressure Distribution  
AGARD Test Case 3.1**



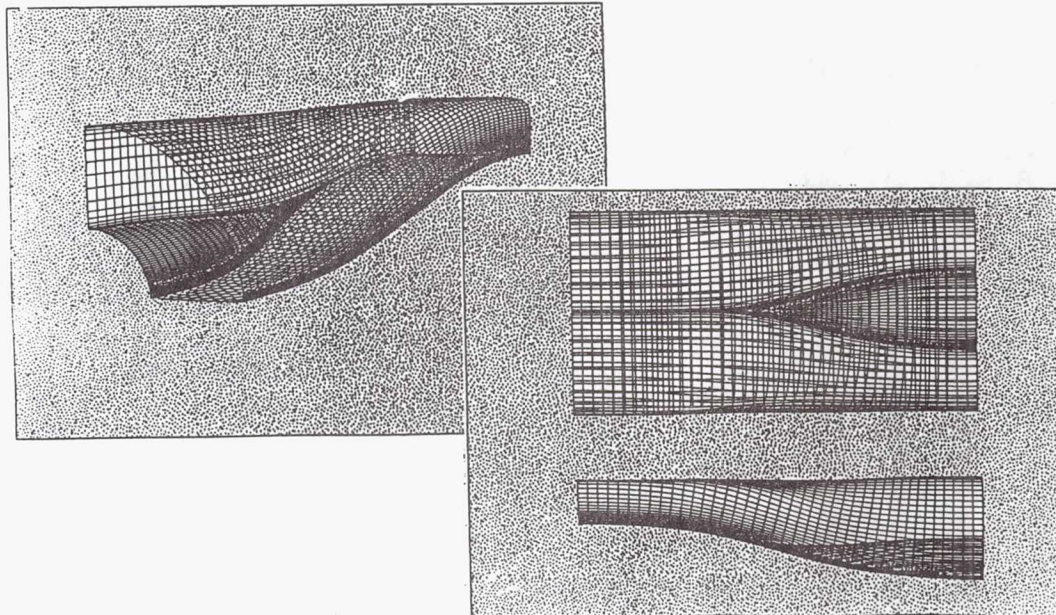
**DRA M2129 Diffusing Inlet S-Duct  
Engine Face Distortion Characteristics  
AGARD Test Case 3.1**



## DRA M2129 Inlet S-Duct Conclusions

- (1) Both Full Navier-Stokes (FNS) and Reduce Navier-Stokes (RNS) analyses adequately describe the overall flow physics of vortex liftoff, but consistently predict the location of liftoff further downstream in the duct inlet than was indicated by data.
- (2) The current generation of turbulence models were unable to described the influence of separation on the main pressure field for "strong" vortex liftoff interactions.
- (3) The current generation of mixing length turbulence models give remarkable good performance results, while the existing discrepancies between data and analysis can be attributed primarily to the over prediction of the liftoff location.

## TD118 Bi-Furcated Transition Duct Geometry and Mesh Definition



## TD118 Bi-Furcated Transition S-Duct Research Objectives

- To demonstrate diffuser duct technology advancement by using CFD to design a "conventionally shorter" transitioning S-duct configuration for application towards high speed inlet systems.
- To develop a computational protocol whereby turbulence model evaluations can be made between different computer codes.
- To develop a benchmark data set to evaluate CFD analysis and turbulence models, which cover fundamental flow phenomena as well as overall flow field physics as determined by standard engine performance parameters.

## TD118 Bi-Furcated Transition S-Duct Effect of Turbulence Model on Inlet Performance

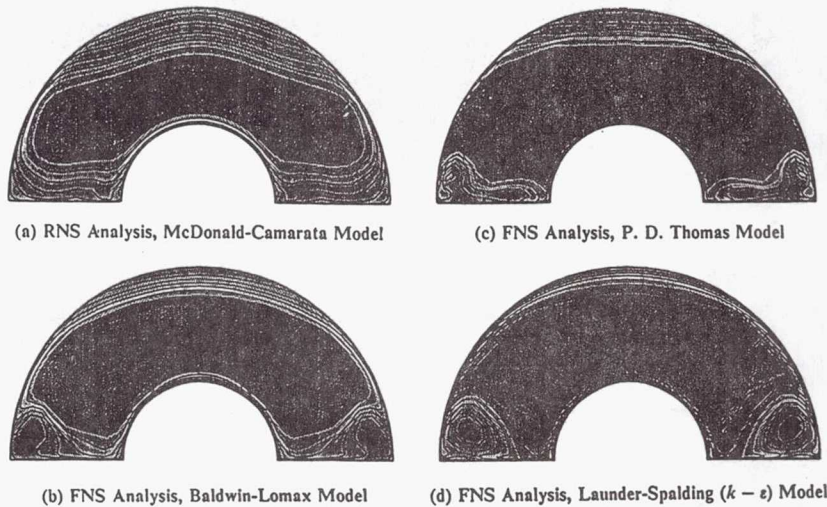
Analysis	Turbulence Model	$Pt_{ave}/Pt_0$	$DH$	$DC_{60}$
RNS3D	McDonald-Camarata	0.955	0.167	0.116
PARC3D	Baldwin-Lomax	0.959	0.163	0.135
PARC3D	P.D. Thomas	0.970	0.153	0.073
PARC3D	Launder-Spaullding	0.975	0.150	0.177

$$DH = (Pt_{max} - Pt_{min})/Pt_{ave}$$

$$DC_{60} = (Pt_{ave} - Pt_{min,60})/q_{ave}$$

## TD118 Bi-Furcated Transition S-Duct

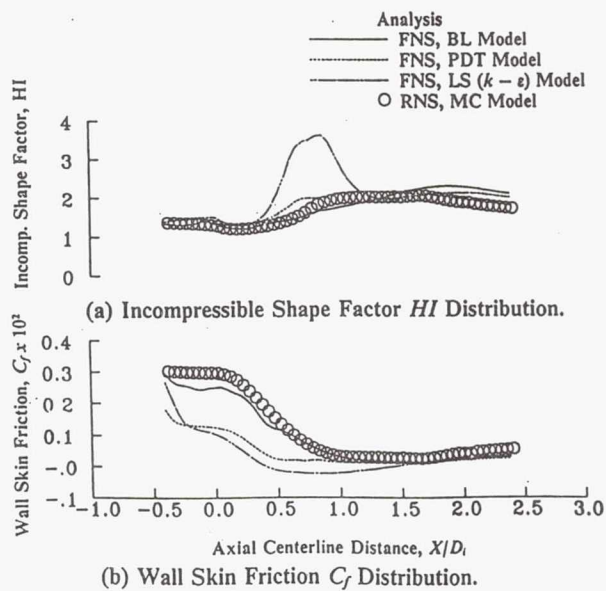
### Effect of Turbulence Model on Engine Face Flow Field



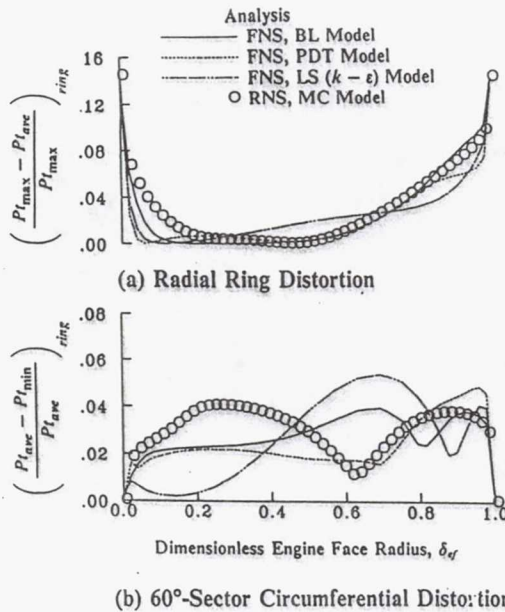
## TD118 Bi-Furcated Transition S-Duct

### Effect of Turbulence Model on Wall Boundary Layer

$\theta = 90.0^\circ$  Surface Element



## TD118 Bi-Furcated Transition Duct Effect of Turbulence Model on Ring Distortion



## Inlet Flow Field Analysis Concluding Remarks

- (1) Difficulties in complex 3D flow fields often arise because fundamental 2D aerodynamic interactions have not been adequately resolved.
- (2) Near wall ( $y^+$ ) and radial mesh resolution ( $nz$ ) play an important role in fundamental 2D and complex 3D flow field analysis.
- (3) Judgements about turbulent models should not be stated until grid independent solutions have been established.
- (4) Adequateness of turbulence models in inlet flow field analysis should also be made on the basis of fundamental performance parameters used to quantify the "goodness" of the flow entering the engine.

REPORT DOCUMENTATION PAGE			Form Approved OMB No. 0704-0188
<p>Public reporting burden for this collection of information is estimated to average 1 hour per response, including the time for reviewing instructions, searching existing data sources, gathering and maintaining the data needed, and completing and reviewing the collection of information. Send comments regarding this burden estimate or any other aspect of this collection of information, including suggestions for reducing this burden, to Washington Headquarters Services, Directorate for Information Operations and Reports, 1215 Jefferson Davis Highway, Suite 1204, Arlington, VA 22202-4302, and to the Office of Management and Budget, Paperwork Reduction Project (0704-0188), Washington, DC 20503.</p>			
1. AGENCY USE ONLY (Leave blank)	2. REPORT DATE	3. REPORT TYPE AND DATES COVERED	
	January 1994	Conference Proceedings	
4. TITLE AND SUBTITLE		5. FUNDING NUMBERS	
Workshop on Computational Turbulence Modeling		WU-505-90-5K	
6. AUTHOR(S)			
A. Shabbir, T.-H. Shih, and L.A. Povinelli, compilers			
7. PERFORMING ORGANIZATION NAME(S) AND ADDRESS(ES)		8. PERFORMING ORGANIZATION REPORT NUMBER	
National Aeronautics and Space Administration Lewis Research Center Cleveland, Ohio 44135-3191		E-8201	
9. SPONSORING/MONITORING AGENCY NAME(S) AND ADDRESS(ES)		10. SPONSORING/MONITORING AGENCY REPORT NUMBER	
National Aeronautics and Space Administration Washington, D.C. 20546-0001		NASA CP-10130 ICOMP-93-46 CMOTT-93-17	
11. SUPPLEMENTARY NOTES			
A. Shabbir and T.-H. Shih, Institute for Computational Mechanics in Propulsion, Lewis Research Center; L.A. Povinelli, Lewis Research Center. Proceedings of a workshop sponsored by the Institute for Computational Mechanics in Propulsion and Center for Modeling of Turbulence and Transition, (work funded by NASA Cooperative Agreement NCC3-233). ICOMP Program Director, L.A. Povinelli, organization code 2540, (216) 433-5818.			
12a. DISTRIBUTION/AVAILABILITY STATEMENT		12b. DISTRIBUTION CODE	
Unclassified - Unlimited Subject Category 34			
13. ABSTRACT (Maximum 200 words)			
<p>The purpose of this meeting was to discuss the current status and future development of turbulence modeling in computational fluid dynamics for aerospace propulsion systems. Various turbulence models have been developed and applied to different turbulent flows over the past several decades and it is becoming more and more urgent to assess their performance in various complex situations. In order to help users in selecting and implementing appropriate models in their engineering calculations, it is important to identify the capabilities as well as the deficiencies of these models. This also benefits turbulence modelers by permitting them to further improve upon the existing models. This workshop was designed for exchanging ideas and enhancing collaboration between different groups in the Lewis community who are using turbulence models in propulsion related CFD. In this respect this workshop will help the Lewis goal of excelling in propulsion related research. This meeting had seven sessions for presentations and one panel discussion over a period of two days. Each presentation session was assigned to one or two branches (or groups) to present their turbulence related research work. Each group was asked to address at least the following points: current status of turbulence model applications and developments in the research; progress and existing problems; requests about turbulence modeling. The panel discussion session was designed for organizing committee members to answer management and technical questions from the audience and to make concluding remarks.</p>			
14. SUBJECT TERMS		15. NUMBER OF PAGES	
Turbulence modeling		448	
17. SECURITY CLASSIFICATION OF REPORT		18. SECURITY CLASSIFICATION OF THIS PAGE	
Unclassified		Unclassified	
19. SECURITY CLASSIFICATION OF ABSTRACT		20. LIMITATION OF ABSTRACT	
Unclassified			